STRUCTURE, VOLCANIC SETTING, HYDROTHERMAL ALTERATION AND GENESIS OF THE THALANGA MASSIVE SULPHIDE DEPOSIT

by

Anthea P. Hill
B.Sc. (Hons), The University of Western Australia

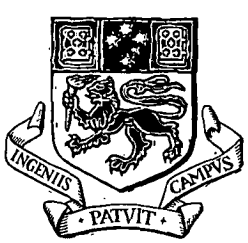

Submitted in fulfilment of the requirements for the degree of
Doctor of Philosophy

University of Tasmania, September 1996

This thesis contains no material which has been accepted for a degree or diploma by the University or any other institution and, to the best of my knowledge and belief, no material previously published or written by another person except where due acknowledgement is made in the text of the thesis.

Anthea Hill

Anthea Hill

Abstract

The Thalanga Zn-Pb-Cu-Ag deposit is located at the contact between the rhyolitic volcanics of the Mount Windsor Volcanics and the overlying dacitic and andesitic volcanic units of the Trooper Creek Formation in the Cambro-Ordovician Mount Windsor subprovince, northern Queensland. The sheet-like massive sulphide lenses and enclosing volcanic units are locally strongly deformed and metamorphosed to upper greenschist facies ($T = 485 \pm 23°C$, $P = 2.5 \pm 1.5$ kbars). Bedding is now subvertical (D_2) and the ore horizon has been offset by two generations of normal faults. Normal faults at a high angle to the stratigraphy separate West and Central Thalanga from the Vomacka Zone and East Thalanga, whereas younger normal faults (D_3), at a low angle to stratigraphy, have repeated and locally structurally thickened the ore lenses.

The pervasive S_2 cleavage has been locally weakly crenulated by S_3. Decussate biotite has overgrown the crenulations, indicating that peak metamorphism at Thalanga was post-S_3. The presence of rare kinked chlorite pseudomorphs of biotite is interpreted to indicate that there was an earlier metamorphic event, which may correlate with regional metamorphism.

The massive sulphides are interpreted to be syn-volcanic in origin because (1) they have been overprinted by the same generations of tectonic structures as the host stratigraphy, (2) the rhyolitic volcanics stratigraphically underlying the massive sulphide lenses contain abundant quartz ± muscovite ± chlorite ± phlogopite ± pyrite assemblages (inferred to be metamorphosed quartz-sericite ± chlorite ± pyrite alteration), whereas the overlying dacite lavas contain metamorphic biotite and local epidote-quartz ± albite-rich assemblages, (3) subvertical pyrite stringer zones (5-40 % pyrite) within the footwall rhyolitic volcanics intersect the ore horizon at the thickest lenses of massive sulphides, and (4) there is a strong stratigraphic control on the location of massive sulphides. The ore lenses at Thalanga occur within and stratigraphically below a poorly-sorted, coarse quartz-bearing, polymict breccia. The internal organisation of this breccia is consistent with transportation to the site of final deposition by subaqueous mass-flows. The breccia has a similar distribution to the massive sulphide lenses and is interpreted to have filled local seafloor depressions. The presence of massive sulphide clasts within the polymict breccia indicates synchronous volcanism and mineralisation. Comagmatic, non-vesicular quartz-feldspar porphyry, with peperitic margins, has locally intruded the polymict breccia.

The main ore minerals are sphalerite, pyrite, chalcopyrite and lesser galena, with minor magnetite, arsenopyrite and tetrahedrite-tennantite. In most places, the sulphides are coarsely recrystallised and preserve no evidence of the deformation history. However, banding in the polymetallic sulphide lenses is interpreted to be tectonic in origin because the

alternating pyrite- and sphalerite-rich bands are subparallel to S_2. Chalcopyrite, sphalerite and galena have been remobilised during deformation and now occupy faults and sites of dilation within the ore horizon, including subhorizontal boudin necks, shallowly-dipping extension veins and piercement structures at the contact between massive sulphides and the overlying dacite. Metal zonation at Thalanga is poorly developed due to widespread sulphide remobilisation, although there is a general zonation from pyrite-chalcopyrite-rich sulphides at the stratigraphic base of ore lenses, to sphalerite-galena ± barite-rich sulphides at the top.

The ore lenses at West and parts of Central Thalanga are composed of massive sulphide veins and disseminations that have cross-cut carbonate (dolomite-calcite) and Mg-rich chlorite assemblages. The Ti/Zr values of the carbonate- and chlorite-rich assemblage are similar to those of the underlying footwall rhyolitic volcanics (Ti/Zr = 2-5), and locally to those of the overlying coarse quartz-bearing polymict breccia (Ti/Zr = 3-10). Carbonate- and chlorite-rich units are therefore interpreted to have formed by the replacement of formerly glassy rhyolitic volcanics and the base of the coarse quartz-bearing polymict breccia by cooler Mg- and HCO_3^- -bearing hydrothermal solutions prior to sulphide deposition. The coarse quartz-bearing polymict breccia may have acted as an impermeable barrier during carbonate-chlorite alteration and trapped the ascending hydrothermal solutions, restricting alteration to a narrow zone at the top of the footwall rhyolitic volcanics. The lack of extensive carbonate-chlorite alteration in the Vomacka Zone and East Thalanga may be due to higher temperature hydrothermal solutions or lack of a capping unit.

The high Mg content of chlorite within the carbonate-chlorite assemblages is consistent with mixing between cold seawater and warm hydrothermal solutions in porous perlitic rhyolite lavas or rhyolitic breccia units in the footwall. HCO_3^- -bearing hydrothermal solutions are interpreted to have been derived from seawater that had circulated through the rhyolitic volcanics of the Mount Windsor Volcanics and possibly some magmatic solutions containing HCO_3^-.

The $\delta^{34}S$ values of sulphides (5.6-17.3 ‰) are consistent with formation from solutions containing dissolved igneous sulphur and Cambro-Ordovician seawater that had been inorganically reduced during hydrothermal convection. The increasing $\delta^{34}S$ of pyrite towards the stratigraphic top of footwall is interpreted to be a consequence of progressive mixing between the hydrothermal solutions and cold seawater. The $\delta^{34}S$ values of barite (27.6-32.4 ‰) are consistent with a Cambro-Ordovician seawater source of sulphur, and support the interpretation that barite was deposited on the seafloor.

The abundance of proximal coherent lavas, domes and syn-volcanic intrusions and associated volcaniclastic facies underlying and overlying Thalanga, and absence of coherent units in the

hangingwall along strike (closest is ~2 km along strike), is interpreted to indicate that the massive sulphide lenses formed within a volcanic centre. Local formation of massive sulphides on the seafloor is inferred to have been interrupted by deposition of the polymict breccia units. The sulphide lenses are interpreted to have formed predominantly by sub-seafloor replacement of the coarse grained bases of polymict breccia units, and local carbonate- and chlorite-rich alteration assemblages, prior to emplacement of the overlying dacite lavas. The presence of coarse quartz-bearing polymict breccia and porphyry units, is interpreted to indicate a long-lived hydrous magma at depth that probably drove hydrothermal convection and may have released volatiles (including CO_2 and potentially metals) to the ascending hydrothermal solutions.

Acknowledgments

My supervisors Professor Ross Large, Dr Ron Berry and Dr Jocelyn McPhie are sincerely thanked for their encouragement, technical advice, critical comments and for tackling the biggest chapters twice. Ron is also thanked for showing me thin section RT-13A. Other people who generously donated their time to read various incarnations of this thesis are Drs David Cooke, Garry Davidson, Bruce Gemmell, David Huston, Paul Kitto, Joe Stolz, and proto-doctor Steve Hunns. Thankyou all for your help and suggestions to improve my science and my writing style. Discussions with others in the geology department are also greatly appreciated and I thank Drs Stuart Bull, Clive Burrett, Tony Crawford, Richard Keele, Peter McGoldrick, Prasada Rao, Michael Roach, Rick Varne and Khin Zaw.

I have enjoyed and will sincerely miss the friendship and geological assistance of my fellow post-grads and their partners, and wish every success to Bruce Anderson, Steve Bodon, Fernando Della Pasqua, Mark Doyle, Mark Duffett, John Dunster, Russell Fulton, Cathryn Gifkins, Massimo Gasparon, Ian Hart, Lachlan Heasman, Kim Hein, Steve Hunns, Marcel Kamperman, Paul Kitto, Ruth Lanyon, Andrew McNeil, Geoff Nichols, Karin Orth, Holger Paulick, Alison Raos, David Rawlings, Peter Rice, Mike Roache, Michael Roach, Jamie Rogers, Anna and Janusz Ryba, David Selley, Michael Seitz, Robina Sharp, Ingvar Sigurdson, Sampan Singharajwarapan, Blackwell Singoyi, Stuart Smith, Andrew Tunks, Alicia Verbeeten, Matt White, Peter Winefield, Rohan Wolfe, Bill Wyman, and Greg Yaxley. Ruth, Alicia, Bear, Russell and Karin are especially thanked for their assistance with that probe. Thanks also to Karin for the great fun while working on carbonate alteration and for your help during the final days of collation.

Simon Stevens, Naomi Deards, Erin McGoldrick and Annette Griggs were patient and extremely helpful in lapidary. Phil Robinson provided accurate XRF analyses, help with chemicals, and an endless supply of little plastic bottles. Fred Koolhof created superb prints and coloured slides at short notice for me. Peter Cornish, Nathan Duhig, Marilyn Feast, Jeanette Harris, Christine Higgins, Sue Hinksman, Nilar Hlang, Katie McGoldrick, June Pongratz and Kathi Stait are thanked for their support and good-humoured advice and assistance on logistical, financial and other stuff. Mike Power and Christine Cook were patient with me in the stable isotope laboratory of the Central Science Laboratory (CSL), as was Wieslaw Jablonski, who instructed me in the careful use of the electron microprobe in the CSL.

The financial and logistical support from Pancontinental Resources (Base Metals) Pty Ltd, and later RGC Exploration and RGC Thalanga Pty Ltd is greatly appreciated. Colin Kendall and previously Andy Purvis were patient with my pestering about rocks, rock transport, travel, finances, drafting and numerous other details. Liz Edmonds, Ann O'Driscoll and

Kathy Hale were helpful in organising my travel to and from Charters Towers, and everyone in the supply department stifled laughter in order to move my rocks safely to Hobart.

Past and present geologists at Thalanga and in the Pancon (and later RGC) exploration office in Charters Towers generously and graciously donated their time, discussed ideas, and have become good friends in the process. I thank Rebecca Askew, John Beeson, Andrew Blair, Haydn Hadlow, Scott Halley, Wally Herrmann, Mel Jones, Colin Kendall, Urpo Kuronen, Craig Miller, Andy Purvis, Rod Sainty, Jarmo Vesanto, Brad Wake, and Ian Warland. In particular, Wally Herrmann, Colin Kendall, Andy Purvis, Rod Sainty and Ian Warland are sincerely thanked for their introduction to geology of Thalanga and the Mount Windsor subprovince, helping me get oriented when underground, and their geological discussions and sharing of interpretations. Andrew Blair, Colin Kendall and Ian Warland were also patient with my computer ability and assisted greatly with generation of drill hole plots, and metal zonation contours. Peter Gregory of BHP-Utah Minerals International, and formerly of Penarroya (Aust) Pty Ltd, for his continued interest and encouragement, information about the exploration mining and for digging up the pre-existing sulphur isotope data.

I appreciate the help of Donna Marr, Dennis Stylianou, Lloyd Lavery and Frank Vomacka, and later help from Kim Burleigh, Krista Davies, Barb Searles, Harold Webber in the core shed, and thank them all for the fun and their friendship. The drafting, surveying, engineering and mining staff at Thalanga and the exploration office are also thanked for their assistance.

My terrific family and friends deserve special thanks for their support, encouragement, understanding and patience. My husband Mark Turkington was a wonderful help with the appendices, organising the colour plates, taking photographs, checking the reference list, collating and all the other tedious jobs. He also kept me sane during the entire process. My running, swimming, cycling, caving, bushwalking, skiing, netball, eating, cooking, shopping, coffee-drinking, gin-and-tonic, dancing, wine tasting and slothing partners from this list, and many not mentioned, know who they are and I look forward to getting back into life with them. Mark, my parents Graham and Lesley Hill, my sisters Narelle and Christine, and my grandmother Freda Hill deserve my utmost gratitude for their support and encouragement and I dedicate this whole story to them.

TABLE OF CONTENTS

VOLUME II

APPENDICES

LIST OF MAPS

LIST OF FIGURES

LIST OF TABLES

CHAPTER 1.

INTRODUCTION

1.1 Preamble

The Thalanga orebody (6.8 Mt @ 12.4% Zn, 2.2%Cu, 3.9% Pb, 0.62 g/t Au, 99 g/t Ag) is the largest massive sulphide deposit in the Mount Windsor subprovince in northern Queensland (Berry *et al.*, 1992). The Mount Windsor subprovince is part of the northern end of the Tasman orogenic belt, comprises a sequence of Cambro-Ordovician subaqueous volcano-sedimentary units, hosts several massive sulphide deposits and prospects, and is considered to be similar in composition to the Mount Read Volcanic belt in Tasmania (Henderson, 1986; Berry *et al.*, 1992). Thalanga is located about 65 km west of Charters Towers in northern Queensland, Australia (at latitude = 20° 20.5' S, and longitude = 145° 46' E), and is connected to port at Townsville by highway and railroad (see Chapter 2 for location map).

Large (1992), and Solomon and Groves (1994) classified Thalanga as a "sheet-style" and "Rosebery-type" VHMS deposit respectively because the massive sulphide lenses have a similar blanket-style morphology to that of Rosebery and are stratigraphically underlain by extensive semi-conformable hydrothermal alteration. The association between sulphide lenses and a distinctive carbonate-rich assemblage at Thalanga (considered to have formed as a hydrothermal exhalative product on the seafloor during sulphide mineralisation; Gregory *et al.*, 1990) is also characteristic of Rosebery. At Rosebery, there is controversy over the origin and timing of sulphide formation, with alternatives including i) deposition from dense saline brines (Green *et al.*, 1981; Green, 1983), ii) formation on the seafloor by coalescing sulphide mounds (Huston, 1988), iii) syn-volcanic sub-seafloor replacement (Allen, 1994), and iv) syn-deformational replacement (Aerden, 1990, 1991, 1994a, 1994b). Potentially, similar alternatives could be proposed to explain the origin of Thalanga. Thalanga is strongly deformed and has been metamorphosed to a higher grade than Rosebery (Laing, 1984, Wills, 1985, Gregory *et al.*, 1990, Berry *et al.*, 1992) and it is important to determine whether the location of massive sulphides is structurally controlled or stratigraphically controlled.

Poorly consolidated, Tertiary sediments unconformably overlie most parts of Thalanga, with up to 80 m of sediments overlying the eastern parts of Thalanga, and prior to mining the only outcrop was the Central Thalanga gossan (Hartley, 1984). Exposure along the Thalanga Range, to the northwest of Thalanga, is excellent and the outcrop extends from the top of the Puddler Creek Formation (at the highway and railway cuttings), includes the Mount Windsor Volcanics (which constitute most of the topographic highs along the Thalanga Range), the

Trooper Creek Formation (typically exposed in creek sections) and parts of the Rollston Range Formation. Recent mining of at Thalanga has opened up significant exposure to allow detailed mapping of structural and stratigraphic relationships in the West, Central and East Thalanga ore lenses.

1.2 Previous Work

Exploration for volcanic-hosted massive sulphide (VHMS) deposits by Penarroya (Aust) Pty Ltd (formerly Le Nickel (Aust) Exploration Pty Ltd) led to the discovery of the Thalanga gossan in 1975 (Douglas-Brown, 1975; Hartley, 1984; Gregory and Hartley, 1982). Exploratory mining began in 1981, but the deposit was not brought into production until purchased by Pancontinental Mining Ltd and Outokumpu Australia Pty Ltd in 1987. Full-scale mining commenced in 1989 under joint venture with Agip Australia Pty Ltd (Purvis, 1989). The initial descriptions of Thalanga were based on the exploration diamond drill holes, and the exploratory decline, cross-cuts and underground drill holes in Central Thalanga, and it was concluded that the massive sulphides at Thalanga were syn-genetic and were deposited onto the seafloor from dense saline solutions (Gregory and Hartley, 1982; Gregory *et al.*, 1990).

Numerous geophysical surveys have been conducted at Thalanga since discovery, and the history of analysis of the geophysical characteristics of Thalanga is reported in Gregory *et al.* (1990) and Bishop and Lewis (1992). Irvine (1987) considered that surface and drill hole mise-a-la-masse and down hole TEM where the most useful in locating massive sulphide lenses. Bishop and Lewis (1992) noted that the poor conductivity of the Zn-rich ore lenses at Thalanga explains the lack of success of EM surveys.

1.3 Aims of this Study

The major objectives of this study were to:

i) describe the composition and textures of the massive sulphide lenses, and document the variation between the four ore lenses Thalanga;

ii) unravel the deformation and metamorphic history of Thalanga, and to determine the effect of deformation and metamorphism on sulphide textures and the distribution of metals within the sulphide lenses;

iii) determine the geometry of the ore horizon, facies architecture of the host stratigraphy, and the relationship between volcanism and sulphide mineralisation;

iv) assess the textures and mineralogy of hydrothermal alteration at Thalanga and relationship of various styles of alteration to sulphide mineralisation;

v) determine whether the massive sulphides at Thalanga are syn-genetic or epigenetic in origin, and to discuss the major controls on ore formation in terms of implications for exploration for massive sulphide deposits in the Mount Windsor subprovince.

1.4 Methods

The objectives of this study have been achieved through the following investigations:

i) detailed logging and sampling of both exploration and production diamond drill holes at Thalanga (Appendix A);

ii) 1:500 scale mapping of the open-pit in Central Thalanga, underground stopes in West, Central and East Thalanga, and 1:5 000 scale mapping of the Thalanga Range along strike from the deposit. Maps and drill hole logs completed by geologists at the Thalanga Mine were also referred to;

iii) detailed petrographic and textural studies on the massive sulphides and host rocks using polished slabs, thin sections, polished thin sections and doubly polished thin sections;

iv) microprobe analysis to determine the composition of sulphides and gangue phases within the ore lenses and alteration assemblages;

v) measurement of the sulphur isotope composition of sulphides and barite within the hydrothermal alteration assemblages and massive sulphide lenses;

vi) cathodoluminescence studies on the carbonate-rich units associated with the massive sulphides;

vii) C and O isotope studies of the carbonate-rich assemblages;

viii) limited whole-rock geochemical analysis of the altered and least-altered host volcanic units.

1.5 Abbreviations

Abbreviations used in this thesis are:

all	allanite
arg	argentite
aug	augite
bis	bismuth
bn	bornite
boul	boulangerite
cb	cubanite
da	dacite
diop	diopside
el	electrum
garn	garnet
kbar	kilo bar
m.y.	million years
ma	marcasite
MS	massive sulphides
mt	magnetite
musc	muscovite
phlog	phlogopite
po	pyrrhotite
py	pyrite
QEV	quartz 'eye' volcaniclastic unit
QFP	quartz-feldspar porphyry
qz	quartz
rhyol	rhyolite
slt	siltstone
sp	sphalerite
sph	sphene
sst	sandstone
stib	stibnite
T	temperature
ta	talc
td	tetrahedrite
tn	tennantite
trem	tremolite
ve	vesuvianite
VHMS	volcanic hosted massive sulphide
zo	zoisite

CHAPTER 2.

REGIONAL GEOLOGY

2.1 Regional Geological Setting

The Thalanga deposit, and other VHMS deposits and prospects including Highway-Reward and Liontown, are situated in Mount Windsor subprovince in north Queensland, which is considered to be part of the northern extent of the Tasman Fold Belt (Henderson, 1986; Murray, 1986, 1990; Berry *et al.*, 1992; Walshe *et al.*, 1995). Volcanic and sedimentary sequences of similar ages have been recognised at Balcooma (in the Georgetown Block north of the Mount Windsor subprovince) in the western part of the Lachlan Fold Belt, and in western Tasmania (Henderson, 1986; Huston, 1990; Withnall *et al.*, 1991). Other components of the Tasman Fold Belt in north Queensland are the Hodgkinson and Broken River Provinces north of the Mount Windsor subprovince, and the New England Fold Belt to the south (Fig. 2.1).

Day *et al.* (1983), Murray (1986, 1990) and Wellman (1995) categorised the Mount Windsor subprovince as the northernmost component of the Thompson Fold Belt, an orogenic belt that underlies the Great Artesian Province in northern Australia and includes the Late-Devonian to Early Carboniferous Drummond Basin and the Anakie Inlier south of the Mount Windsor subprovince (Kirkegaard, 1974; Murray and Kirkegaard, 1978). However, Henderson (1980) argued that there is little evidence of the composition of the basement of the Great Artesian Province, and therefore did not support the presence of the Thompson Fold Belt.

The Mount Windsor subprovince is composed of Late Cambrian to Early Ordovician marine volcanic and sedimentary rocks, and is part of the Charters Towers Province (Henderson, 1980, 1986). The Charters Towers Province was described as the Ravenswood Block by Wyatt *et al.* (1971), but renamed and divided into three subprovinces, the Lolworth-Ravenswood subprovince, the Burdekin subprovince, and the Mount Windsor subprovince (Fig. 2.2), by Henderson (1980).

The Lolworth-Ravenswood subprovince is composed of amphibolite facies metamorphic rocks that are intruded by granitoids of the Ravenswood and Lolworth Batholiths (Henderson, 1980). This subprovince occupies the central part of the Charters Towers Province (Fig. 2.2), and is composed of Proterozoic metamorphic units including the Running River and Argentine Metamorphics in the northern part of the province, the Cape River Beds in the western part of the province, and the Charters Towers Metamorphics in the central region (Henderson, 1980).

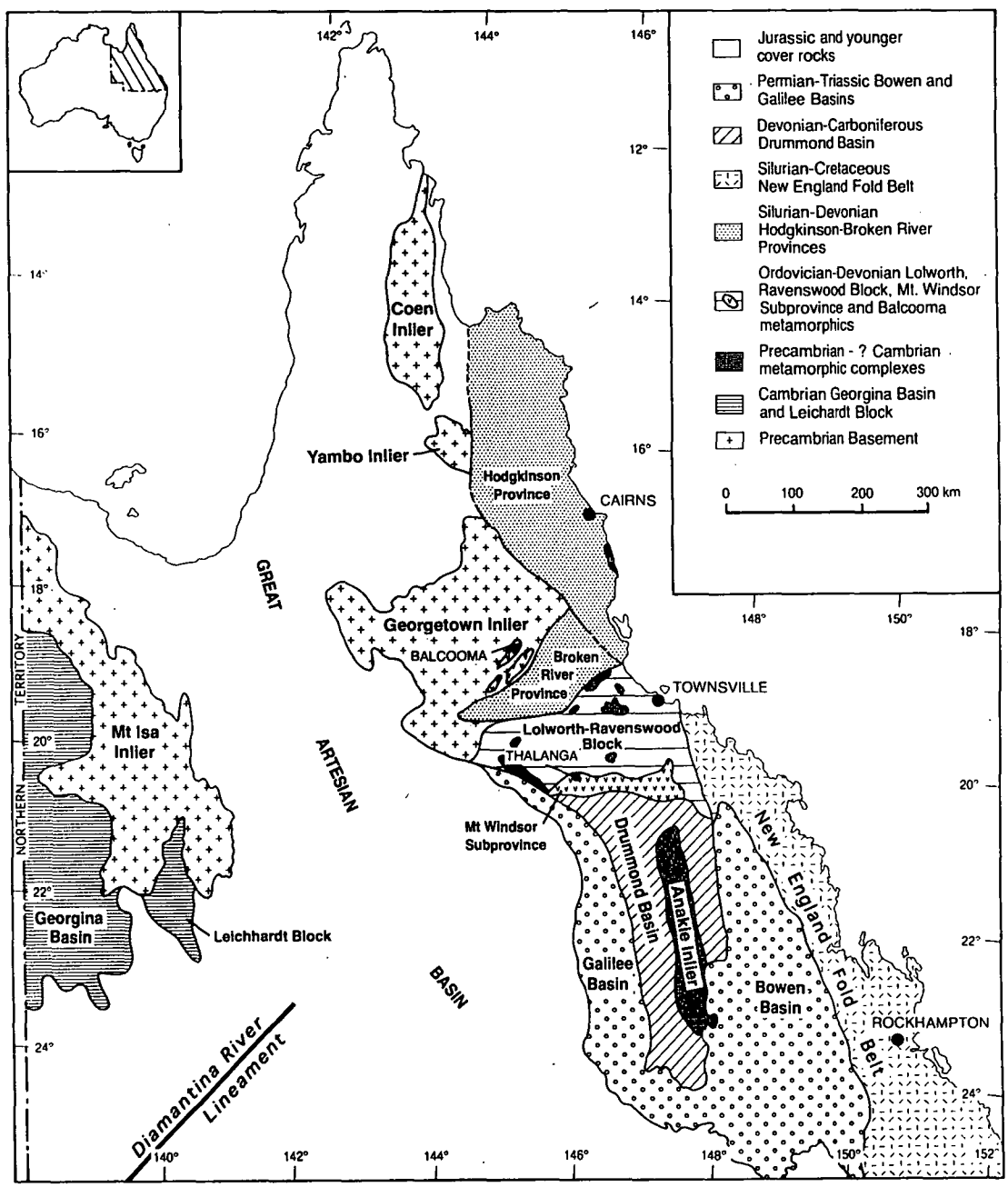

Figure 2.1 Simplified geological map of the distribution of Precambrian basement rocks and major Cambrian to Devonian structural blocks in north Queensland (from Stolz, 1995).

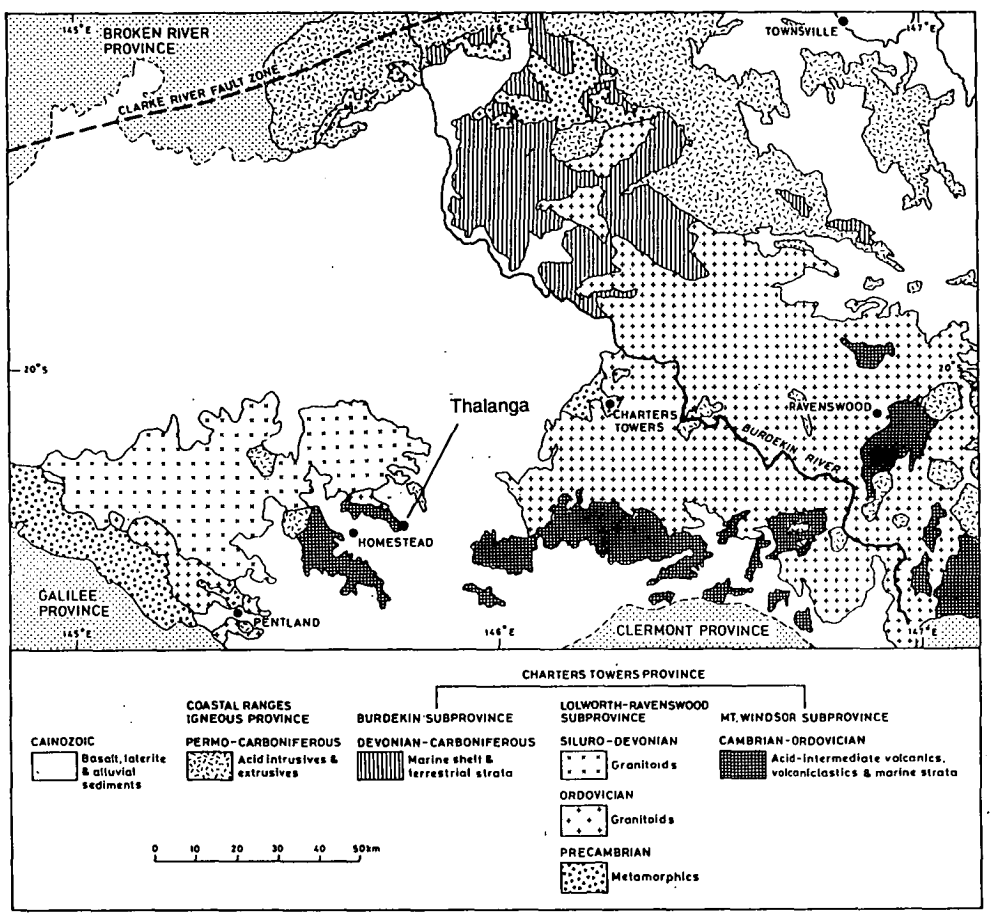

Figure 2.2 Elements of the Charters Towers Province (from Henderson, 1986).

The Burdekin subprovince comprises Devonian to Early Carboniferous marine and continental-derived sediments, and these on-lap the northern parts of Lolworth-Ravenswood subprovince (Fig. 2.2). Henderson (1980) suggests that this subprovince is continuous with felsic to intermediate volcanic units of the Coastal Ranges Igneous Province to the east of the Charters Towers Province.

2.2 The Mount Windsor Subprovince

The Mount Windsor subprovince is an east-west trending volcanic belt (Fig. 2.2), that extends 165 km from the Leichhardt Range, south of Ravenswood in the east, to Pentland in the west (Henderson, 1986). The rocks within the Mount Windsor subprovince were first recognised by Wyatt *et al.* (1971), who identified them as the Cape River Beds, and defined the volcanic component as the Mount Windsor Volcanic Member. Subsequently, Henderson (1980) demonstrated that the Cape River Beds comprise amphibolite grade metamorphic rocks with evidence of polyphase deformation, and concluded that they predate the volcanic rocks and are probably the basement to the Mount Windsor subprovince. Henderson (1980) categorised the Cape River Beds with the other Precambrian metamorphic units in the Charters Towers Province. However, Day *et al.* (1983) and Murray (1986, 1990) agreed with the interpretation of Wyatt *et al.* (1971) that the Cape River Beds are the same age as, and gradational with, the volcanic units in the Mount Windsor subprovince. The interpretation of Henderson (1980) is considered more probable.

The felsic to intermediate volcanic and sedimentary rocks of the Mount Windsor subprovince have been dissected by the Ravenswood and Lolworth granitoids, and are overlain by the middle to upper Carboniferous Drummond subprovince to the south (Henderson, 1980). The northern margin of the Mount Windsor subprovince is separated from the Broken River Province by the Clarke River Fault zone (Fig. 2.2; see also Day *et al.*, 1978; Murray, 1986).

Henderson (1986) correlated the rocks of the Mount Windsor subprovince to the Mount Read Volcanics in western Tasmania based on their similar composition and ages. Recent dating of zircons in the Mount Windsor Volcanics and Trooper Creek Formation has yielded a mean U-Pb age of 475.4±4.7 Ma (Perkins *et al.*, 1993). This is younger than the U-Pb and $^{40}Ar/^{39}Ar$ age of 502.6±3.5 Ma for the Mount Read Volcanics (Perkins and Walshe, 1993).

2.2.1 The Seventy Mile Range Group

The volcanic and sedimentary rocks of the Mount Windsor subprovince are known as the Seventy Mile Range Group, and this group is divided into the Puddler Creek Formation, the Mount Windsor Volcanics, the Trooper Creek Formation, and the Rollston Range Formation

(Henderson, 1986). Bedding in the Seventy Mile Range Group trends east-west in most parts of the volcanic belt (Fig. 2.3). Detailed stratigraphic descriptions of the Seventy Mile Range Group are given in Henderson (1986) and Berry *et al.* (1992), and characteristics of the component formations are summarised in Table 2.1. The volcanic units of the Mount Windsor Volcanics and the Trooper Creek Formation have calc-alkaline affinities (Henderson, 1986; Stolz, 1995; Berry *et al.*, 1992).

Puddler Creek Formation

The Puddler Creek Formation is the oldest unit in the Mount Windsor subprovince, and is composed of continental-derived sandstone, greywacke and siltstone units (Table 2.1; Henderson, 1986; Berry *et al.*, 1992). The Puddler Creek Formation contains both mafic and felsic dykes, although there is disparity in the composition of the mafic dykes (Henderson, 1986; Hartley *et al.*, 1989). Henderson (1986) described dolerite sills and dykes within the Puddler Creek Formation, that are cross cut by the quartz-plagioclase-porphyry dykes. However, microdiorite dykes were identified within the Puddler Creek Formation by Hartley *et al.* (1989) who concluded that the microdiorite and quartz-plagioclase-porphyry dykes within the Puddler Creek Formation are similar in composition to dykes that intrude the Charters Towers Metamorphics. Amygdaloidal andesite lavas in the upper part of the Puddler Creek Formation are interpreted to be the product of intermittent volcanism preceding deposition of the Mount Windsor Volcanics (Stolz, 1991; Berry *et al.*, 1992). The quartz- and quartz-feldspar-porphyritic rhyolite dykes and sills are interpreted to be feeders to the volcanic units within the Mount Windsor Volcanics and Trooper Creek Formation (Berry *et al.*, 1992).

Mount Windsor Volcanics

The Mount Windsor Volcanics are composed of a continuous sequence of rhyolite domes and lavas, commonly 100-150 m thick, with subordinate volcaniclastics (Henderson, 1986; Berry *et al.*, 1992). Stolz (1989) noted that reworked, rhyolitic volcaniclastics are the main component of the Mount Windsor Volcanics in the Trooper Creek region. Berry *et al.* (1992) documented significant stratigraphic thickening of the rhyolitic pile between Highway and Sunrise Spur in the eastern part of the volcanic belt (fig. 2.3), and Henderson (1986) interpreted this thickening to indicate an eastern source for the Mount Windsor Volcanics.

The contact between the Mount Windsor Volcanics and the Trooper Creek Formation is defined as the base of the first dacite or andesite overlying the rhyolites (Henderson, 1986). This change from rhyolitic volcanism to dacitic and andesitic volcanism also corresponds to a decrease in volcanic activity and/or an increase in the rate of sedimentation within the volcanic belt (Stolz, 1991).

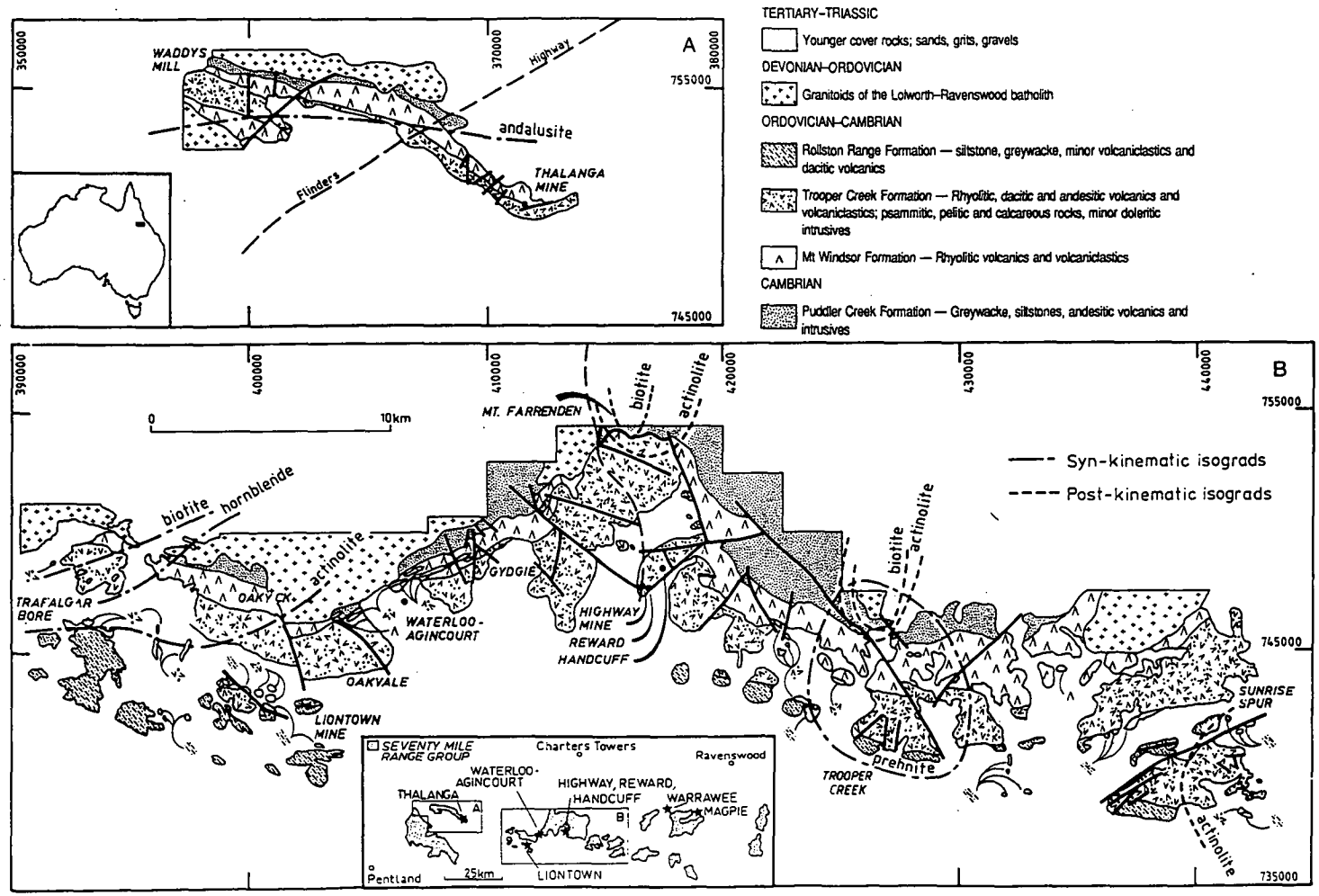

Figure 2.3 Generalised geological map of the Mount Windsor subprovince showing the distribution of the major geologic formations, the location of Thalanga and other massive sulphide deposits, and the location of metamorphic isograds (from Berry *et al.*, 1992).

Table 2.1 Characteristics of formations in the Seventy Mile Range Group (summarised from Henderson, 1980, 1983, 1986; Stolz, 1989; and Berry *et al.*, 1992). Type section locations are presented in Henderson (1986).

Formation	Composition	Thickness	Age
Puddler Creek Formation (PCF)	Continental-derived quartz- and lithic-sandstone, greywacke and interbedded siltstone units. Minor andesite lavas near stratigraphic top.	Maximum thickness ~9000 m with no structural repetition, but stoped out by Ravenswood Granodiorite Complex.	Late Cambrian (no fossils, but age interpreted from relationship with overlying volcanics)
Mount Windsor Volcanics (MWV)	Mainly rhyolite domes, with rhyolitic volcaniclastic units, and minor dacite, and rare andesite.	Maximum thickness ~3500 m at Sunrise Spur, in eastern part of belt, decreases in thickness west of Highway to ~1000 m, and is 300-400 m in thickness at Waddys Mill at the western end of the volcanic belt.	Lower Ordovician. Rb-Sr date of 528 ± 100 Ma (Paine *et al.*, 1971). Pb-U date on zircons (from base of formation) of 474.6 ± 5.1 Ma and 479.1 ± 4.6 Ma (Perkins *et al.*, 1993). Conformably overlies Puddler Creek Formation.
Trooper Creek Formation (TCF)	Coherent and volcaniclastic andesite, dacite and rhyolite, and interbedded epiclastic mudstone and siltstone. Minor basaltic andesite lavas.	Varies from ~4000 m thick at Mount Windsor in the central part, to ~1700 m thick in western part of volcanic belt.	Lower Ordovician (graptolites in siltstones are Lancefieldian in age; Henderson, 1983). Zircons from base of formation yielded Pb-U age of 468.0 ± 5.4 Ma (Perkins *et al.*, 1993). Zircons from either top of TCF, or base of RRF yielded age of 479.7 ± 5.6 Ma (Perkins *et al.*, 1993). Conformably overlies MWV.
Rollston Range Formation (RRF)	Siltstone and sandstone of volcanic origin. Minor dacite lavas.	Minimum thickness is ~1000 m, upper limit is covered by Tertiary alluvium.	Middle Ordovician (graptolites and trilobites are Bendigonian and Chewtonian Stages, with Late Lancefieldian graptolites in western part of belt). Older in west than in eastern part of Mount Windsor volcanic belt. Conformably overlies TCF.

Trooper Creek Formation

Rapid facies and lithological changes are common in the Trooper Creek Formation, with some areas composed of a high proportion of coherent volcanic units, and other areas composed of abundant sedimentary rocks and volcaniclastic units (Table 2.1; Henderson, 1986; Stolz, 1989; Berry *et al.*, 1992). Concentrations of coherent volcanic units within the Trooper Creek Formation, and thickening of the volcanic pile, are interpreted to reflect the location of volcanic centres. A volcanic edifice is preserved between Mount Windsor and Highway (Berry *et al.*, 1992).

Rollston Range Formation

The Rollston Range Formation is composed of volcanic-derived sandstone and siltstone units, with subordinate dacite lavas (Table 2.1; Berry *et al.*, 1992). Graptolites and trilobites from siltstone units within the Rollston Range Formation are Lancefieldian to Bendigonian (Lower Ordovician) in age (Henderson, 1983, 1986).

Depositional Environment

In most parts of the Mount Windsor Volcanics, evidence for the depositional environment during rhyolitic volcanism is inconclusive (Stolz, 1991). However, Berry *et al.* (1992) favoured a subaqueous environment for the passive emplacement of rhyolitic lavas or domes. Possible shards and pumice clasts within the eastern parts of the Mount Windsor Volcanics are interpreted as evidence of subaerial, pyroclastic eruptions (Stolz, 1991).

The sedimentary units, and therefore the volcanic units, in the Trooper Creek and Rollston Range Formations are inferred to have been deposited in a deep marine environment (Henderson, 1986; Stolz, 1991). Pillows associated with andesite lavas in the Trooper Creek Formation support the interpretation of a subaqueous environment of deposition (Berry *et al.*, 1992). Pods and lenses of quartz-hematite or quartz-magnetite are common throughout the Trooper Creek Formation and are interpreted to have formed as low temperature exhalites on the seafloor (Berry *et al.*, 1992; Duhig *et al.*, 1992).

2.3 Lolworth-Ravenswood Batholith

Two important granitoid complexes are present in the northern part of the Mount Windsor subprovince: the Ravenswood Granodiorite Complex, also known as the Ravenswood Batholith, and the Lolworth Igneous Complex. Together these granitoid complexes constitute the Lolworth-Ravenswood Batholith (Fig. 2.2; see also Henderson, 1980, 1986; Richards,

1980). Both the Ravenswood Batholith and the Lolworth Igneous Complex intrude the Precambrian basement and have been intruded by Permian-Carboniferous granitoids (Richards, 1980).

2.3.1 Ravenswood Batholith

The Ravenswood Batholith is composed of multiple plutons of different composition and ages of emplacement (Table 2.2; Clarke, 1971; Wyatt *et al.*, 1971; Levingston, 1981; Rienks, 1991; Hutton and Crouch, 1993; Hutton *et al.*, 1994), and is mainly adamellite to granodiorite in composition. Henderson (1986) noted that the Ravenswood Batholith can be broadly divided into two batholiths, a biotite tonalite west of Charters Towers, and hornblende granodiorite to the east (Fig. 2.2). The hornblende granodiorite was considered the main granodiorite phase by Wyatt *et al.* (1971).

The granitoid batholiths of the Ravenswood Granodiorite Complex contain northwest to east-trending strongly foliated zones (Wyatt *et al.*, 1971; Henderson, 1986), and also contain massive hornblende-bearing granodiorite and tonalite with foliated margins (Hartley *et al.*, 1989). Structural mapping by Berry (1989, 1991) and Berry *et al.* (1992) supported the conclusion of Hartley *et al.* (1989) that both pre- and post-orogenic granitoids are present in the Mount Windsor volcanic belt. Berry (1989, 1991) and Berry *et al.* (1992) interpreted the main deformation event within the Mount Windsor subprovince to be Mid to Late Ordovician or younger in age (Table 2.3), and concluded that the deformed granitoids are Ordovician, and that the undeformed post-orogenic granitoids are Late Devonian in age.

Rb-Sr ages of 454±30 m.y. and 394±30 m.y. determined for the Ravenswood Granodiorite Complex (Webb, 1969, 1970, 1971a,b) were interpreted to indicate that the batholith is composed of multiple granitoids of Late Ordovician to Middle Devonian age (Richards, 1980). More recent mapping and dating of the Ravenswood Batholith shows that emplacement of the batholith occurred in four main episodes (Table 2.2; Hutton *et al.*, 1990; Hutton *et al.*, 1992; Rienks, 1991; Hutton and Crouch, 1993). The majority of the batholith (94 %) was interpreted to have been emplaced between the Early Ordovician and the Early Devonian (Hutton *et al.*, 1993).

The granitoids have intrusive contacts with the Seventy Mile Range Group, with south-trending, elongate apophyses at the margins of the Ravenswood Batholith (Fig. 2.2; and see Henderson, 1986). The Kirk River Beds are interpreted as a block isolated from the Puddler Creek Formation by stoping during granitoid emplacement (Henderson, 1986).

Leucocratic granitoid stocks near the contact between the Ravenswood Granodiorite Complex and the Puddler Creek Formation (Fig. 2.2) were interpreted to be components of the

Table 2.2 Granitoids of the Ravenswood Batholith (summarised from Clarke, 1971; Hutton *et al.*, 1990; Rienks, 1991; Hutton and Crouch, 1993; Hutton *et al.*, 1993).

Age of Emplacement	Composition	Deformation	Comments
Late Cambrian to Early Ordovician (490±6 Ma)	Granodiorite Intruded by microdiorite dykes	Strong foliation (S_2)	Co-magmatic with volcanics of either the Mount Windsor Volcanics or the Trooper Creek Formation
Early to Middle Ordovician	Granite to granodiorite, spatially and temporally associated with mafic intrusives; Peraluminous biotite-muscovite granite, spatially related to migmatites	Medium grained with zones of intense foliation and local mylonites	Contemporaneous felsic and mafic magmatism; Granitoids formed by partial melting near base of crust, mantle derived thoeliitic magmas produced mafic intrusives
Middle Silurian to Early Devonian (426±4 Ma to 406±4 Ma)	Calc-alkaline hornblende-biotite granodiorite to tonalite	Massive with foliated margins; Distribution of some granitoids controlled by NNE trending faults	Isotopically homogeneous, but chemically variable source rocks; Formed by partially melting of thoeliitic underplate, causing partial crustal melting; Some plutons emplaced into NNE trending grabens

Table 2.3 Structural history of the Mount Windsor subprovince (summarised from Berry (1989, 1991) and Berry *et al.* (1992)).

Deformation event	Manifestation	Location	Interpretation	Age
Pre-deformation	Substantial increase in thickness of stratigraphy on one side of fault	Mount Farrendon-Highway-Reward area; Handcuff Fault Windsor Fault CODES Fault	Syn-depositional normal faults, west side down	Late Cambrian
D_1	Variable bedding-cleavage intersection lineations,	Trafalgar Bore, Thalanga Range	Open assymmetric north-south folding (short, steep westerm limb), and related thrust faults with east towards west transport direction	D_1 in the Hodgkinson and Broken River provinces is estimated at 380-385 Ma on the basis of Rb-Sr dates (Bell, 1980)
	South-plunging, north-south trending open folds	Mount Sunrise area		
	Folded faults	Rail-cutting through the Thalanga Range		
D_2	Subvertical east-west cleavage, subvertical east-west trending, south-facing bedding	Entire volcanic belt	Northern limb of upright, east-west syncline, with un-exposed hinge to the south	Mid to Late Ordovician or younger
	Thickened stratigraphy and parasitic fold vergence	Waddys Mill	Hinge region of syncline	
D_3	S_3 cleavage post-dates andalusite porphyroblasts, small-scale folds near granite	North of Thalanga Range, Waddys Mill,	S_3 cleavage spatially associated with unfoliated granites	Silurian-Devonian
	Open F_3 folds, S_3 cleavage	Highway area		
	S_3 parallel to north-dipping NE to ENE-trending normal faults	Entire volcanic belt	Parallel to Mount Leyshon Corridor, and therefore related to post-orogenic granitoids	Carboniferous (Hartley *et al.*, 1993)
Late structures	Long wavelength (~10 km) south-plunging gentle folds	Entire volcanic belt	Late kinking, location of fold hinges possibly related to location of hydrothermal alteration	
	Late faults at high angle to stratigraphy			

Ravenswood Batholith (Levingston, 1981). Henderson (1986) correlated the leucocratic granitoids with quartz-plagioclase porphyry dykes in the Puddler Creek Formation, and suggested that emplacement of the porphyry dykes and leucocratic granitoids coincided with the emplacement of the Mount Windsor Volcanics, and proposed that the leucocratic granitoids are the magmatic equivalent of the Mount Windsor Volcanics.

2.3.2 Lolworth Igneous Province

The Lolworth Igneous Complex is composed of adamellite and granodiorite, with banded pegmatite and garnet-bearing granite, and crops out to the north and west of the Thalanga Range (Fig. 2.2; Levingston, 1981). Granitoids of the Lolworth Igneous Complex have no penetrative foliation (Paine *et al.*, 1971; Richards, 1980).

K-Ar ages and Rb-Sr isochrons produced ages of 390 m.y. to 404 m.y. for the Lolworth Igneous Complex (Webb, 1970, 1971a,b), which is consistent with a Devonian age. Levingston (1981) regarded the Lolworth Igneous Complex as Late Silurian to Early Devonian in age.

2.3.3 Permian-Carboniferous Granitoids

Permian-Carboniferous granitoids are common at the eastern and south eastern margin of the Ravenswood Batholith (Fig. 2.2). These consist largely of biotite and hornblende biotite adamellite, granodiorite and granite that are Late Carboniferous to Early Permian in age (Paine *et al.*, 1974; Levingston, 1981). Henderson (1980) classified these Permian-Carboniferous granitoids as part of the Coastal Ranges Igneous Province, which includes all felsic to intermediate igneous and volcanic rocks in eastern Queensland of Late Devonian-Permian age. Late Permian porphyritic microgranite and leucogranite stocks, of the Mundic Igneous Complex, intrude the Lolworth Igneous Complex west of the Thalanga Range (Fig. 2.1; Levingston, 1981).

Hutton *et al.* (1990) reported that Permian-Carboniferous gabbro to granitic complexes are typically associated with volcanic rocks of the same age, and considered that the emplacement of these complexes was controlled by regional lineaments. The mineralised breccia complex at Mount Leyshon, south of Charters Towers, is associated with Carboniferous to Permian rhyolite and quartz-trachyte plugs (Wormald *et al.*, 1993). Hutton *et al.* (1993) noted that these rhyolitic to trachytic plugs are common at or near the margins of the Ravenswood Batholith.

2.4 Overlying Units

The Seventy Mile Range Group is overlain by the Warang Sandstone, which is Triassic in age and crops out at the western end of the central part of the Mount Windsor volcanic belt. The Warang Sandstone in interpreted to have been deposited in a fluviatile setting (Levingston, 1981). Continental-derived sandstone, pebbly sandstone, and minor mudstone of the Pliocene Campaspe Formation overlie large areas of the Mount Windsor subprovince (Pitt, 1988). In the vicinity of the Thalanga deposit, the Campaspe Formation varies from >102 m to <1 m thick (Pitt, 1988). Pitt (1988) divided the Campaspe Formation into a basal zone with abundant ironstone, interpreted to have been eroded from laterite formations, and a surface zone composed of iron-rich aggregates that are interpreted to have formed by surface weathering after deposition of the Campaspe Formation.

2.5 Structure of the Mount Windsor Subprovince

The structural history of the Mount Windsor subprovince, determined by Berry (1989, 1991) and Berry *et al.* (1992), is summarised in Table 2.3. Three episodes of folding and five generations of faulting were reported by Berry (1989, 1991) and Berry *et al.* (1992).

Berry (1989) assumed a north-south trend for the early folding based on the structural history of the Broken River and Hodgkinson Provinces documented by Bell (1980). Berry (1989) suggested that the early thrust-related folding event is comparable with the early deformation at Dry River South, which is also part of the northern Tasman Fold Belt (Huston, 1990). Berry (1991) and Berry *et al.* (1992) documented south-plunging north-south folds in the Mount Surprise area and interpreted these to be F_1 folds. South-dipping faults with dextral displacement were tentatively interpreted to be D_1 thrusts, with a westward transport direction (Berry, 1990; Berry *at al.*, 1992)

The major deformation event is recognised as strong east-west cleavage (S_2) related to upright folding, and was interpreted as the only deformation event in the subprovince by Laing (1984), Wills (1985), Henderson (1986), and Gregory *et al.* (1990). Berry (1989, 1991) and Berry *et al.* (1992) correlated the upright folding event with folds of Devonian age in the Hodgkinson and Broken River Provinces to the north of the Mount Windsor subprovince. East-west trending fault zones within the Middle Ordovician granitoids of the Ravenswood Batholith are correlated with S_2 in the Seventy Mile Range Group, thus providing an age estimate for D_2 (Table 2.3; Berry *et al.*, 1992). The S_2 cleavage increases in intensity towards the granitoids to the north of the volcanic belt (Berry, 1989).

The hinge region of a regional-scale upright syncline is interpreted to crop out at Waddys Mill, at the northwestern limit of the Thalanga Range (Berry, 1989; Berry *et al.*, 1992). The Trooper Creek Formation is significantly thicker at Waddys Mill compared to elsewhere along the Thalanga Range, and is interpreted to be symmetrical about a fold hinge located within strongly foliated Trooper Creek Formation. Cleavage-bedding relationships suggest north facing stratigraphy, and parasitic fold vergence supports the syncline model (Berry, 1989; Berry *et al.*, 1992).

However, hand specimen characteristics and the geochemical composition of the felsic volcanic units are different from typical rhyolites from the Mount Windsor Volcanics (Stolz, 1991; Hill, 1992). Quartz-muscovite-chlorite schist is present south of dacites, rhyolites, andesites and sandstone of the Trooper Creek Formation at Waddys Mill, and it is this unit that Berry (1989) and Berry *et al.* (1992) interpreted to be strongly foliated rhyolite. Yet, it lacks the quartz phenocrysts that are generally present in the Mount Windsor Volcanics, and has slightly higher P and Ti contents, and Ti/Zr ratios than typical rhyolites from the Mount Windsor Volcanics (Stolz, 1991; Hill, 1992).

The orientations and ages of major lineaments and faults within the Charters Towers region were summarised by Hartley *et al.* (1993). Important NNE-SSW trending lineaments and mylonite zones are present in many parts of the Mount Windsor subprovince (Henderson, 1986), and many of these were interpreted as Pre-Ordovician to Ordovician in age by Hartley *et al.* (1993). Henderson (1986) correlated these faults with the emplacement of the Ravenswood Batholith. This interpretation is supported by Hartley *et al.* (1989, 1993), who also noted that dolerite dykes of Silurian age have similar orientations to the faults, and concluded that regional extension occurred during Silurian-Devonian times.

NE to ENE trending faults, with south side up displacement, are also common throughout the Mount Windsor volcanic belt, and are parallel to S_3, and possibly related to, regional-scale lineaments including the 'Mount Leyshon Corridor' (Berry, 1991; Berry *et al.*, 1992). The Mount Leyshon Corridor is defined as one of the major structures that controlled Carboniferous to Permian magmatism in the Mount Leyshon region, and is interpreted as Carboniferous in age (Morrison, 1988; Hartley *et al.*, 1993; Wormald *et al.*, 1993). However, the close spatial relationship between S_3 and granitoids of Silurian-Devonian age suggests a similar age for D_3 (Berry *et al.*, 1992).

2.6 Regional Metamorphism

Hutton *et al.* (1993) noted that the metamorphic grade of the Seventy Mile Range Group is variable, with widespread greenschist facies assemblages present and local contact

metamorphic aureoles (Henderson, 1986). Metamorphic isograds were mapped by Berry (1989, 1991) and Berry *et al.* (1992), who showed that metamorphic grade increases towards the western parts of the volcanic belt, from prehnite-pumpellyite facies at Trooper Creek, through actinolite, hornblende, biotite and andalusite isograds to a maximum (525°C, 3 kbars) at the Waddys Mill prospect (Fig. 2.3). Andalusite pseudomorphs are aligned in S_2 and have been overprinted by S_3 (Berry, 1991; Berry *et al.*, 1992).

Contact metamorphic aureoles are more prominent in the eastern parts of the volcanic belt where the regional metamorphic grade is lower (Berry *et al.*, 1992). Metamorphic minerals within contact aureoles around post-kinematic granitoids are decussate and overgrow the main cleavage (Berry, 1991; Berry *et al.*, 1992). Such observations were not reported by Henderson (1986).

2.7 Tectonic Setting of the Mount Windsor Subprovince

The composition and distribution of the volcanic units and provenance of the sedimentary rocks within the Seventy Mile Range Group has been used to interpret the tectonic setting of volcanism and the Mount Windsor subprovince (e.g. Henderson, 1986; Stolz, 1989, 1991; Berry *et al.*, 1992; Stolz, 1995). The calc-alkaline volcanic units of the Mount Windsor Volcanics and the Trooper Creek Formation are consistent with convergent margin volcanism generated in an island arc during subduction (Stolz, 1991; Berry *et al.*, 1992; Stolz, 1995).

Large-scale crustal subsidence is required to allow accumulation of the Seventy Mile Range Group, and the north-south trending quartz- and quartz-feldspar-porphyry dykes within the Puddler Creek Formation suggests that the basin developed via east-west extension adjacent to a north-south oriented cratonic margin (Henderson, 1986). Stolz (1995) suggested that the distribution and source of the sedimentary and volcanic components is also consistent with a northeast-southwest oriented Precambrian cratonic margin, interpreted from gravity and magnetic data to be along the Diamantina Lineament. The sedimentary rocks in the Puddler Creek Formation (Table 2.2) are interpreted to have been derived from a basement of continental crust, possibly now represented by the Cape River Beds (Henderson, 1986). Henderson (1986) also regarded the presence of silicic stocks intruding the basal parts of the Seventy Mile range Group as consistent with a basement of continental crust.

The composition of the volcanic units in the Seventy Mile Range Group indicates that the contact between the Puddler Creek Formation and the overlying Mount Windsor Volcanics marks the initiation of a convergent tectonic setting. Henderson (1986) suggested that the increase in stratigraphic thickness towards the eastern parts of the Mount Windsor volcanic belt, was consistent with location of the volcanic arc in the east. The abundance of rhyolitic

volcanic units in the Mount Windsor Volcanics was interpreted to suggest that the depositional basin was developed on stretched continental lithosphere (Henderson, 1986). Nd isotopic data are consistent with the derivation of rhyolite from partial melting of the Precambrian crustal rocks (Stolz, 1995). Volcanic centres at the time of deposition of the Trooper Creek Formation are interpreted to be located in the central and eastern parts of the Mount Windsor volcanic belt (Henderson, 1986; Stolz, 1991).

Geochemical characteristics of the mafic volcanic units in the Mount Windsor volcanic belt have been compared with analyses of lavas with similar compositions in well constrained tectonic settings (Henderson, 1986; Stolz, 1989, 1991, 1995; Berry *et al.*, 1992). Andesites within the uppermost part of the Puddler Creek Formation have geochemical affinities with alkaline intra-plate or rift-related continental thoeliites, and are interpreted to have formed by partial melting of thin, subcontinental lithospheric mantle (Stolz, 1995). Two mafic volcanic suites are present in the overlying Trooper Creek Formation, a low TiO_2 suite and a high TiO_2 suite, both with Nd isotopic ratios that suggest "derivation from a relatively depleted asthenospheric mantle variably modified by subduction processes" (Stolz, 1995). Stolz (1991) showed that basalts within the Trooper Creek Formation are geochemically similar to an average Kuroko basalt and calc-alkaline basalts from the Sunda arc, and interpreted this to indicate formation during the initial stages of back-arc, or intra-arc rifting. The silicic volcanic units within the Trooper Creek Formation were interpreted to be cogenetic with the mafic volcanic units (Stolz, 1995).

The favoured tectonic model for formation of the Mount Windsor volcanic belt involves deposition of the calc-alkaline volcanic units in a back-arc basin at the eastern margin of a Precambrian craton. The back-arc basin formed by extension of continental crust during subduction, and a volcanic chain is interpreted to have been located east of the basin (Henderson, 1986). Stolz (1995) suggested that the Late Proterozoic to Early Cambrian margin of northeastern Australia was an attenuated passive margin, and that rapid deposition of the Puddler Creek Formation occurred as the continental lithosphere extended and subsided. Mafic volcanic units in the uppermost parts of the Puddler Creek Formation represent thinning of the crustal lithosphere, and heat flow during this volcanism may have induced crustal melting and eruption of the Mount Windsor Volcanics (Stolz, 1995).

The interpreted north-south orientation of the back-arc basin is consistent with the north-south trend of the Tasman Fold Belt (Henderson, 1986). Berry *et al.* (1992) proposed that arc volcanism rapidly spread to the west of the back-arc basin, and suggested that this was due to flattening of the subduction zone. Rare volcanic activity followed the emplacement of the Trooper Creek Formation, and volcanic activity returned to the long term arc position east of the Seventy Mile Range Group during the Early Ordovician (Berry *et al.*, 1992; Stolz, 1995).

Volcaniclastic material from the Trooper Creek Formation was then reworked and deposited as the Rollston Range Formation (Stolz, 1995).

The Drummond Basin, to the south of the Mount Windsor subprovince, was formed after compression of the Mount Windsor subprovince during the mid-Ordovician (De Caritat and Braun, 1991; Berry *et al.*, 1992). Stolz, (1995) proposed that oblique plate convergence, rather than a collision event, modified the Mount Windsor volcanic belt into a major transform structure.

2.8 VHMS Deposits in the Mount Windsor Volcanic Belt

There is a strong stratigraphic control on the distribution of mineralisation within the Seventy Mile Range Group (Berry *et al.*, 1992). The Thalanga deposit occurs at the contact between the Mount Windsor Volcanics and the Trooper Creek Formation, and the majority of other massive sulphide deposits are present within the Trooper Creek Formation (Table 2.4; Stolz, 1989; Berry *et al.*, 1992; Hutton *et al.*, 1993). Previous descriptions of the geology of the volcanogenic massive sulphide deposits and prospects within the Mount Windsor subprovince include those by Gregory and Hartley (1982), Gregory *et al.* (1987, 1990), Kay (1987), Beams *et al.* (1989, 1990), Mulholland (1991), Hutton *et al.* (1993). and Huston *et al.* (1995). Berry *et al.* (1992) provide a succinct outline of the important characteristics of deposits in the Mount Windsor volcanic belt, and Table 2.4 summarises their analysis.

Most deposits are stratiform to blanket in style, and are typically zinc-rich and contain low copper and abundant barite (Berry *et al.*, 1992). The pipe-like Reward deposit was interpreted to be syn-deformational in origin (Beams *et al.*, 1989, 1990). However, recent volcanological studies have demonstrated that the mineralisation at Reward was synvolcanic, with sulphides precipitating in a sub-seafloor position (Doyle, 1994).

Carr *et al.* (1995) reported that VHMS deposits in the Mount Windsor subprovince (including Thalanga; G.R. Carr, pers. comm., 1996) have Pb isotopic signatures that are similar to those from VHMS deposits of Silurian age in the Lachlan fold belt. Carr *et al.* (1995) considered that this similarity was coincidental and suggested that their plumbo-tectonic model for the eastern part of the Lachlan fold belt is incorrect for the massive sulphide deposits in the Mount Windsor subprovince.

2.9 Local Geology of Thalanga

The Thalanga Range is composed of volcanic rocks of the Seventy Mile Range Group, and extends WNW from the Thalanga deposit for approximately 13 km to the Waddys Mill

Table 2.4 Massive sulphide deposits in the Mount Windsor volcanic belt.

Deposit	Deposit Style (after Large, 1992)	Grade and Tonnage	Ore Minerals	Stratigraphic Location	Host Lithologies
Thalanga	Sheet-style massive sulphides	Primary: 6.359 m.t. @ 2.2% Cu, 12.3% Zn, 3.9% Pb, 99g/t Ag, and 0.6g/t Au (measured or indicated) Supergene: 0.667 m.t. @ 5.8% Cu, 8.3% Zn, 2.1% Pb, 83g/t Ag, and 0.8g/t Au (proved, probable, or indicated) Oxide: 0.184 m.t. @ 96g/t Ag, and 1.7g/t Au (proved or probable)	Sphalerite, pyrite, galena, chalcopyrite, minor magnetite, tetrahedrite, arsenopyrite	Contact between Mount Windsor Volcanics and the Trooper Creek Formation	Footwall: rhyolitic volcanic units Ore Horizon: Quartz-feldspar-porphyritic rhyolite, and polymict volcaniclastic units Hangingwall: dacite and dacitic volcaniclastic units, minor andesite
Reward	Pipe	Primary: 0.82 m.t @ 11% Pb+Zn, and 1g/t Au (inferred) 1.5 m.t. @ 1.5g/t Au, and 50% Cu (inferred) Supergene: 0.633 m.t. @ 8.1% Cu and 1.7g/t Au (probable) Oxide: 0.216 m.t. @ 4.1g/t Au (probable and inferred)	Pyrite, chalcopyrite, sphalerite, galena, trace of electrum	Trooper Creek Formation	Rhyodacitic to rhyolitic lavas, cryptodomes, and volcaniclastic units
Highway	Pipe	Oxide: 0.05 m.t. @ 5g/t Au (proved or probable)	Pyrite	Trooper Creek Formation	Rhyolitic cryptodomes, lavas, and volcaniclastic units
Handcuff	Sheet, multiple lenses	Primary: 1 m.t. @ 0.6% Cu, 10.0% Zn, 0.4% Pb, 8g/t Ag, and 0.2g/t Au (inferred)	Sphalerite, pyrite, minor chalcopyrite and galena	Trooper Creek Formation	Footwall: Rhyolitic and dacitic to andesitic lavas Hangingwall: Coarse grained rhyolitic to dacitic volcaniclastic units
Liontown	Sheet and disseminated sulphides	Primary: 2 m.t. @ 0.5% Cu, 6.6% Zn, 2.3% Pb, 50g/t Ag, and 0.9g/t Au (inferred)	Sphalerite, pyrite, minor galena and chalcopyrite	Contact between Trooper Creek Formation and Rollston Range Formation	Footwall: Rhyolitic volcanic units Hangingwall: Siltstone, shale, arenite, and crystal-rich dacite
Magpie	Stacked lenses	Primary: 0.25 m.t. @ 2% Cu, 15% Zn, 2% Pb, 30g/t Ag, and 1g/t Au (inferred)	Sphalerite, pyrite, chalcopyrite, galena, minor pyrrhotite, magnetite, and marcasite	Trooper Creek Formation	Footwall: Sediments and intermediate to mafic volcanic units Hangingwall: Dacitic lavas and volcaniclastic units
Waterloo	Sheet	Primary: 0.372 m.t. @ 3.8% Cu, 19.7% Zn, 2.8% Pb, 94g/t Ag, and 2.0g/t Au (inferred)	Sphalerite, pyrite, chalcopyrite, minor galena and tennantite	Trooper Creek Formation	Footwall: Andesitic volcaniclastic units, with lesser felsic volcaniclastic units Hangingwall: Felsic volcaniclastic units, argillite, greywacke
Agincourt	Disseminated		Sphalerite, pyrite, galena, chalcopyrite, minor tennantite	Trooper Creek Formation	Footwall: Felsic volcaniclastic units, with lesser andesitic volcaniclastic units Hangingwall: Felsic volcaniclastic units, with lesser sedimentary rocks
Warrawee	Multiple lenses		Sphalerite, galena, chalcopyrite	Trooper Creek Formation	Footwall: Pyritic, felsic, tuffaceous rocks Hangingwall: Felsic, tuffaceous rocks

Data sourced from Gregory *et al.* (1987, 1990), Kay (1987), Beams *et al.* (1989, 1990), Mulholland (1991), Berry *et al.* (1992), Huston *et al.* (1995a).

prospect (Fig. 2.3). In this location, the Seventy Mile Range Group is enclosed by granitoids and is interpreted to be a roof pendant in the Ravenswood Batholith (Hutton *et al.*, 1993). The contact between the Mount Windsor Volcanics and the Trooper Creek Formation is exposed along the south western side of the Thalanga Range (map M1).

The Thalanga VHMS deposit occurs at the eastern end of the Thalanga Range. The rocks of the Mount Windsor Volcanics and the Trooper Creek Formation are unconformably overlain by the Campaspe Formation in the eastern parts of Thalanga. Bedding at Thalanga is subvertical and has been folded into an open, north-south trending fold, with the deposit centred on the hinge of this fold (Chapter 3). Major faults separate the orebody into four main ore lenses, and these are West, Central and East Thalanga, and the Vomacka Zone (Fig. 2.4). The main stratigraphic units identified at Thalanga are listed in Table 2.5, and are described in Chapter 4. The current resource estimate for each of the four main lenses at Thalanga is:
i) West Thalanga: 1.91 % Cu, 3.14 % Pb, 8.79 % Zn, 80.1 ppm Ag, and 0.3 % Au;
ii) Central Thalanga: 3.17 % Cu, 3.48 % Pb, 10.61 % Zn, 101.8 ppm Ag, and 0.6 % Au;
iii) Vomacka Zone: 1.91 % Cu, 2.87 % Pb, 10.3 % Zn, 66.4 ppm Ag, and 0.7 % Au; and
iv) East Thalanga: 1.2 % Cu, 2.89 % Pb, 9.73 % Zn, 69.9 ppm Ag, and 0.4 % Au (Warland, 1995).

Table 2.5 Stratigraphic units used at the Thalanga mine

Stratigraphic Order	Local Name	Composition	Formation
1 Hangingwall	Andesite	Coherent andesite	Trooper Creek Formation
	Dacite	Coherent dacite and associated volcaniclastic facies	
	Hangingwall fragmental	Siltstone, graded sandy siltstone and dacitic hyaloclastite	
2 Ore horizon	Upper rhyolite breccia	Rhyolite-dominated breccia	uncertain (see Chapter 4)
3 Ore Horizon	Quartz 'eye' volcaniclastic unit	Polymict breccia and sandstone units that contain distinctive large, blue quartz crystals	Trooper Creek Formation
	Quartz-feldspar porphyry	Coarse quartz-feldspar phyric rhyolite, also containing large blue quartz crystals	
4 Footwall	Rhyolitic volcanics	Altered coherent rhyolite and associated volcaniclastic facies	Mount Windsor Volcanics

2.10 Summary

1. The Mount Windsor subprovince is belt of subaqueous volcanic and sedimentary rocks that has been subdivided into four formations (collectively known as the Seventy Mile Range Group) that are, from oldest to youngest, the Puddler Creek Formation, the Mount Windsor Volcanics, the Trooper Creek Formation, and the Rollston Range Formation. These rocks are

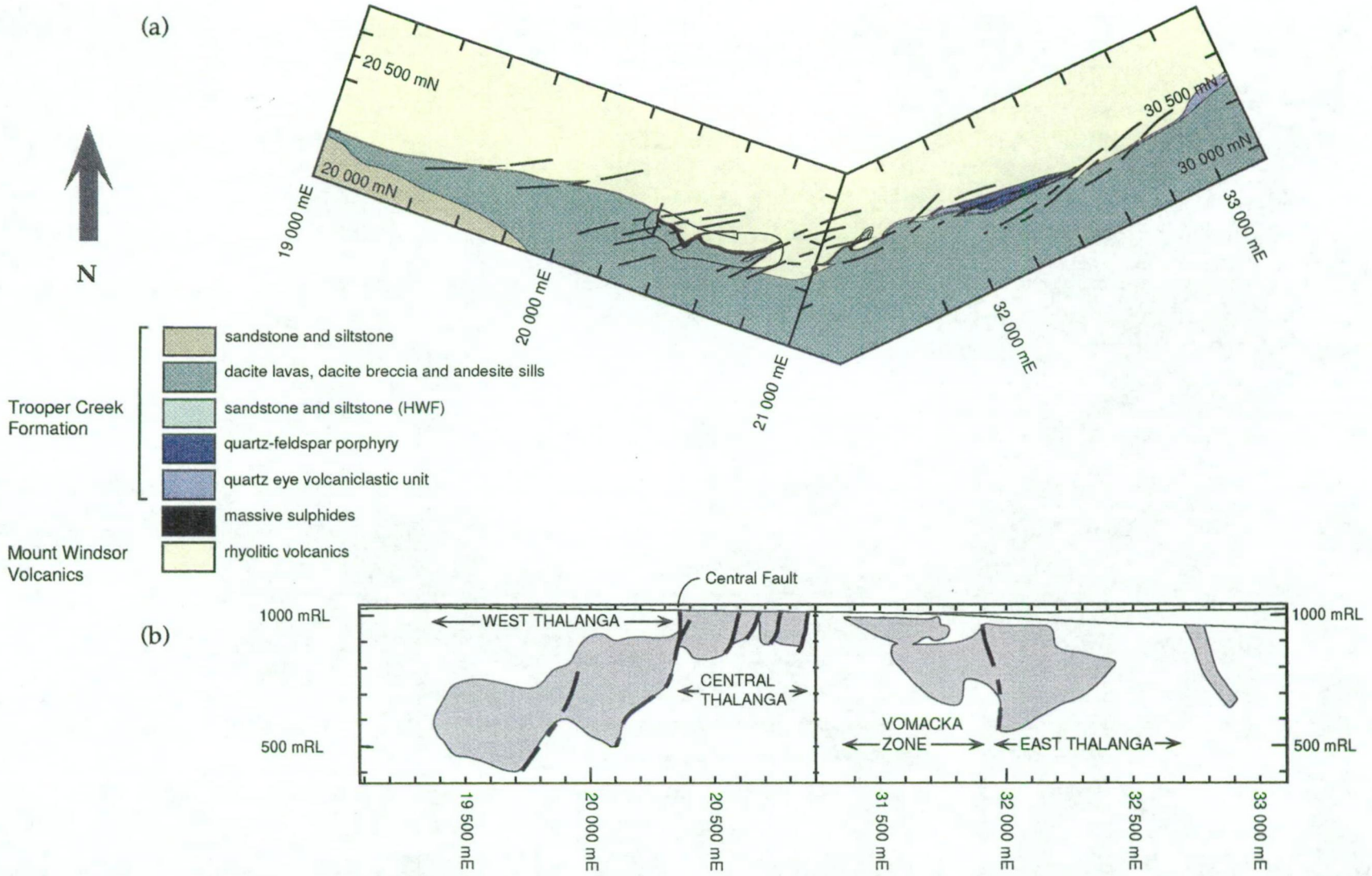

Figure 2.4 Simplified geology of the Thalanga area in (a) plan view, and (b) long section. The plan geology is interpreted from about 950 mRL, and shows cross-cutting ENE-trending normal faults. The ore lenses are projected on to vertical long section, with the interpreted position of the ENE-trending normal faults shown as dashed lines. The Central Fault trends about NNE.

Late Cambrian to Early Ordovician in age (Henderson, 1986), and have been intruded by granitoids of the Lolworth-Ravenswood Batholith, which ranges from Late Cambrian or Early Ordovician to Permian in age. The Mount Windsor subprovince is highly prospective for VHMS deposits, and most of the known deposits and prospects occur at the base and within the Trooper Creek Formation.

2. Prominent subvertical, east-west cleavage (S_2) is associated with regional upright folding during D_2 (Mid-Late Ordovician or younger). The stratigraphy within the Mount Windsor subprovince is now subvertical, faces south and is interpreted to be the northern limb of an upright, east-west syncline (Berry *et al.*, 1992). Regional metamorphism was associated with this deformation event. S_3 cleavage is associated with younger normal faults that may be Carboniferous in age.

3. The regional metamorphic grade varies from high grade (amphibolite facies) in the western part of the belt, to low grade (prehnite-pumpellyite facies) in the eastern parts (Berry *et al.*, 1992). Decussate metamorphic minerals in local contact metamorphic aureoles, around post-kinematic granitoids, have overprinted the earlier metamorphic textures.

CHAPTER 3.

STRUCTURE AND METAMORPHISM OF THALANGA

3.1 Introduction

3.1.1 Previous Structural Investigations and Interpretations

Hall (1981) inferred that the Thalanga massive sulphide deposit occurred on the southern limb of a gently plunging (10-30°), WNW-trending anticline that extended along the Thalanga Range. He correlated the terrigenous siltstone units (now classified as Puddler Creek Formation; Henderson, 1986) north of the rhyolites in the Thalanga Range with the package of dacite lavas, polymict mass flow deposits, sandstone and siltstone units (Trooper Creek Formation; Henderson, 1986) south of the Thalanga Range, and suggested that the hinge of the anticline occurred within the rhyolites of the Mount Windsor Volcanics. Laing (1984) supported the interpretation of Hall (1981) of an anticline in the Mount Windsor Volcanics along the Thalanga Range, but considered it to represent a parasitic fold on the southern limb of a large anticline whose WNW-trending fold axis occurred north of the Thalanga Range.

More recently, Berry (1989) and Berry *et al.* (1992) have shown that an E-W trending syncline (fold hinge south of the Thalanga massive sulphide deposit) is the major regional structure, with the dominant cleavage at Thalanga consistent with a regional, axial planar S_2 cleavage. Berry (1989, 1991) demonstrated that the Thalanga massive sulphide deposit occurs on the northern limb of this syncline, and found no evidence of an anticline within the Mount Windsor Volcanics to the north of Thalanga. He also interpreted the F_2 fold hinge to crop out at Waddys Mill at the north western end of Thalanga Range (see Chapter 2). Regional metamorphism during D_2 deformation is recorded throughout the Mount Windsor subprovince (Henderson ,1986; Berry *et al.*, 1992), and is associated with the intrusion of the Ravenswood Granodiorite during the Middle to Late Ordovician. At Thalanga, previous workers recognised that syn-D_2 metamorphism reached biotite grade, upper greenschist facies (Wills, 1985; Gregory *et al.*, 1990; Berry, 1991; Berry *et al.*, 1992).

Thalanga is divided into four lenses, West, Central, and East Thalanga and the Vomacka Zone, with major structural disruptions of the ore horizon marking the boundaries of each lens (Fig. 2.4). Wills (1985) and Gregory *et al.* (1990) considered that steep, NNE-striking brittle faults controlled the division of the ore horizon into separate lenses. The pronounced bend in the stratigraphy between East and West Thalanga is considered enigmatic, with other

deposits in the region associated with similar structures. Laing (1984) suggested that this "boomerang" structure may represent minor folds formed during regional upright folding. However, Berry (1990) recognised that the "boomerang" structure is post-S_2 in age, and perhaps formed by N-S folding, with the lack of N-S trending cleavage consistent for such open folds.

Early structural interpretations of Thalanga used a syn-depositional growth fault, now subhorizontal, to explain the down-dip termination of the ore horizon (Wills, 1985; Gregory *et al.*, 1990). However, Berry (1989) demonstrated that such horizontal faulting is unlikely at Thalanga. Berry (1989), and Berry *et al.* (1992) proposed that E-W to ENE-striking brittle-ductile normal faults are the main structures truncating the ore horizon at depth.

3.1.2 Aims and Chapter Organisation

This chapter aims to determine the number, timing and style of deformation events and the effect of these processes on the distribution and textures of the massive sulphides and other lithologies at Thalanga. The nature of the structure(s) between West, Central, and East Thalanga, and the Vomacka Zone, and the timing of this deformation is also addressed in this chapter. This chapter is organised so that the structures imposed on Thalanga are examined sequentially and placed within a regional context. Pre-deformation structures are discussed first. The structural history of Thalanga is then compared with the timing of metamorphism, and an estimate of the pressure and temperature conditions of peak metamorphism given. The effect of metamorphism on the microtextures of the ore lenses and hydrothermal alteration assemblages are described in Chapter 6, 10 and 11, and are therefore not treated in this chapter. The compositions of metamorphic minerals were determined using the Cameca SX50 Electron Microprobe facility in the Central Science Laboratory at the University of Tasmania. Analyses are tabled in Appendix B.

3.2 Pre-deformation Structures

3.2.1 Growth Faults

Syn-depositional faulting is common in many volcanic environments within an extensional setting, and such growth faults could have been pathways for ascending hydrothermal solutions (e.g. Large and Both, 1980; Franklin *et al.*, 1981; Gemmell and Large, 1992; Large, 1992). The Reward deposit and Highway and Handcuff prospects, in the central part of the Mount Windsor subprovince, occur within 1 km of a major fault interpreted to be a growth fault, active during deposition of the Trooper Creek Formation, and probably the conduit for the mineralising solutions (Berry, 1990, 1991; Berry *et al.*, 1992). Wills (1985) considered that

the ore horizon at Thalanga was truncated down-dip by a growth fault, and that this fault was now sub-horizontal. However, examination of drill core in the vicinity of the proposed growth fault shows that there is no evidence of a sub-horizontal fault, and no evidence of palaeo-fault scarps as interpreted in Wills' (1985) reconstruction of the depositional environment at Thalanga. In fact, the Thalanga ore horizon is terminated by steeply N-dipping and NE to ENE-striking faults that are interpreted to be D_3 in age (section 3.6.1; Berry *et al.*, 1992).

Unequivocal growth faults are not present at the Thalanga deposit. However, there are two sites whose geometry and alteration patterns are suggestive of focussed fluid flow, possibly associated with syn-depositional faults. The geology in the vicinity of possible growth faults at Thalanga was investigated, in order to determine whether faults were present during mineralisation.

3.2.2 Potential Growth Fault 1: Eastern Margin of West Thalanga

Geology of the Eastern Margin of West Thalanga

The ore horizon of West Thalanga is truncated down-dip by a major ENE-striking fault, with weakly altered footwall rhyolitic volcanics displaced (normal movement) along the fault into the hangingwall (Fig. 3.1; fault B). This fault has early dip-slip kinematic indicators (section 3.6.1), yet the sulphide lens changes from massive and semi massive sulphides (up to 15 m thick), and massive pyrite immediately adjacent to the fault, to thinner (≤5 m) semi massive sulphides and carbonate- and chlorite-rich assemblages with distance up-dip (Fig. 3.1). This decrease in thickness of the ore lens, and presence of carbonate- and chlorite-rich assemblages (interpreted as a low temperature hydrothermal alteration; Chapter 11), may be the result of decreasing temperatures of mineralisation with distance from fault B. Abundant pyrite ± chalcopyrite stringers are present in the footwall rhyolitic volcanics down-dip of the ore lens (Fig. 3.1), suggesting proximity to a hydrothermal feeder zone. The absence of a mineralised ore position overlying the repeated footwall rhyolitic volcanics south of fault B could be a consequence of an abrupt termination of the ore lens against a syn-depositional fault. Mineralising fluids may have been focussed in a zone subparallel to fault B and extended along the ore horizon west and up-dip of the fault, with the massive pyrite deposited adjacent to fault B.

However, if fault B was a growth fault active during deposition of the ore horizon, and utilised by ascending hydrothermal fluids, then volcaniclastic deposits should be thickest directly adjacent to fault B (e.g. Franklin *et al.*, 1981; Ramsay and Huber, 1987; Brown and Taylor, 1988). Both the quartz "eye" volcaniclastic unit (QEV) and the hangingwall fragmental (HWF) were deposited sub-aqueously by mass-flows (lithological descriptions

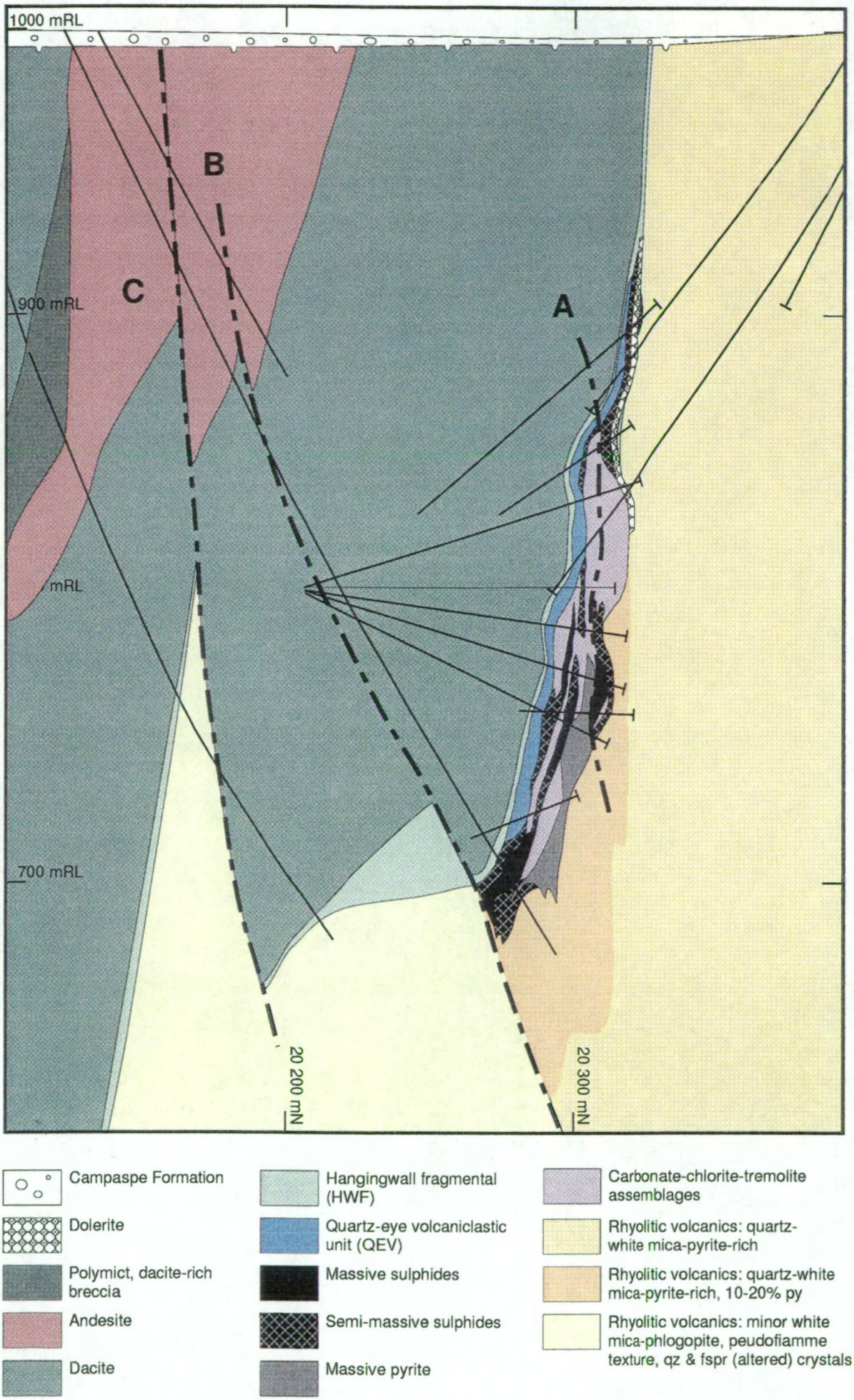

Figure 3.1 Cross-section through West Thalanga along the 20 230 mE section.

and depositional processes are discussed in Chapter 4), thus local basins within the ore-horizon will be represented by thick volcaniclastic deposits. Furthermore, the locations of thick zones of massive pyrite may indicate feeder zones (e.g. Gemmell and Large, 1990; McArthur and Dronseika, 1990; Large, 1992), and the location of these compared to the structure contours of the stratigraphic top of the footwall rhyolitic volcanics will show whether structures in the footwall were utilised by ascending hydrothermal solutions.

Construction of Structure Contour Diagrams

Structure contour diagrams of the stratigraphic top of the footwall rhyolitic volcanics in West Thalanga and the western part of Central Thalanga (Fig. 3.2a), and the stratigraphic base of the hangingwall dacite (Fig. 3.2b), together with isopach maps of the thickness of volcaniclastic units and massive pyrite (Fig. 3.2c-e) within the ore horizon, provide information on the distribution of basins and topographic highs, and also the location of faults in West Thalanga. The structure contour diagrams and isopach maps were constructed, by measurement of cross sections and underground maps, for West and Central Thalanga from 19 910 mE to 20 500 mE. Structure contours were not constructed for the eastern parts of Central Thalanga because of the lack of drilling to depths <900 mRL. Isopachs of units south of fault B were not calculated because of the shallow dip of bedding between faults B and C, and lack of intersections of the stratigraphy south of fault C (Fig. 3.1). The structure contours represent the horizontal distance (positive to the south) from a vertical reference plane at 20 400 mN. All the contour diagrams are in long section and look northeast, as if viewing the stratigraphy from the hangingwall, and mine-grid eastings and RL co-ordinates are used for the location of specific features.

Stratigraphic Top of the Rhyolitic Volcanics and Base of the Dacite

Two main ENE-striking, subvertical faults offset the top of the footwall in West Thalanga (faults A and B; Fig. 3.2a) and these faults are recognised in underground exposures and cross section interpretations (Fig. 3.1; maps M5-10). Fault B separates the West and Central ore lenses below about 780 mRL, whereas above about 780 m RL, a NNE-striking fault (the Central Fault; Fig. 3.2f) defines the western limits of Central Thalanga.

Only one fault in the western part of Central Thalanga is illustrated on Figure 3.2a. However, interpretations of the open pit and underground mapping in Central Thalanga (maps M2-4) suggest that several similarly oriented ENE-striking faults may cross-cut the ore lens in this area. Faults A and B, and the Central Fault are also present in the structure contour diagram of the base of the coherent hangingwall dacite (Fig. 3.2b).

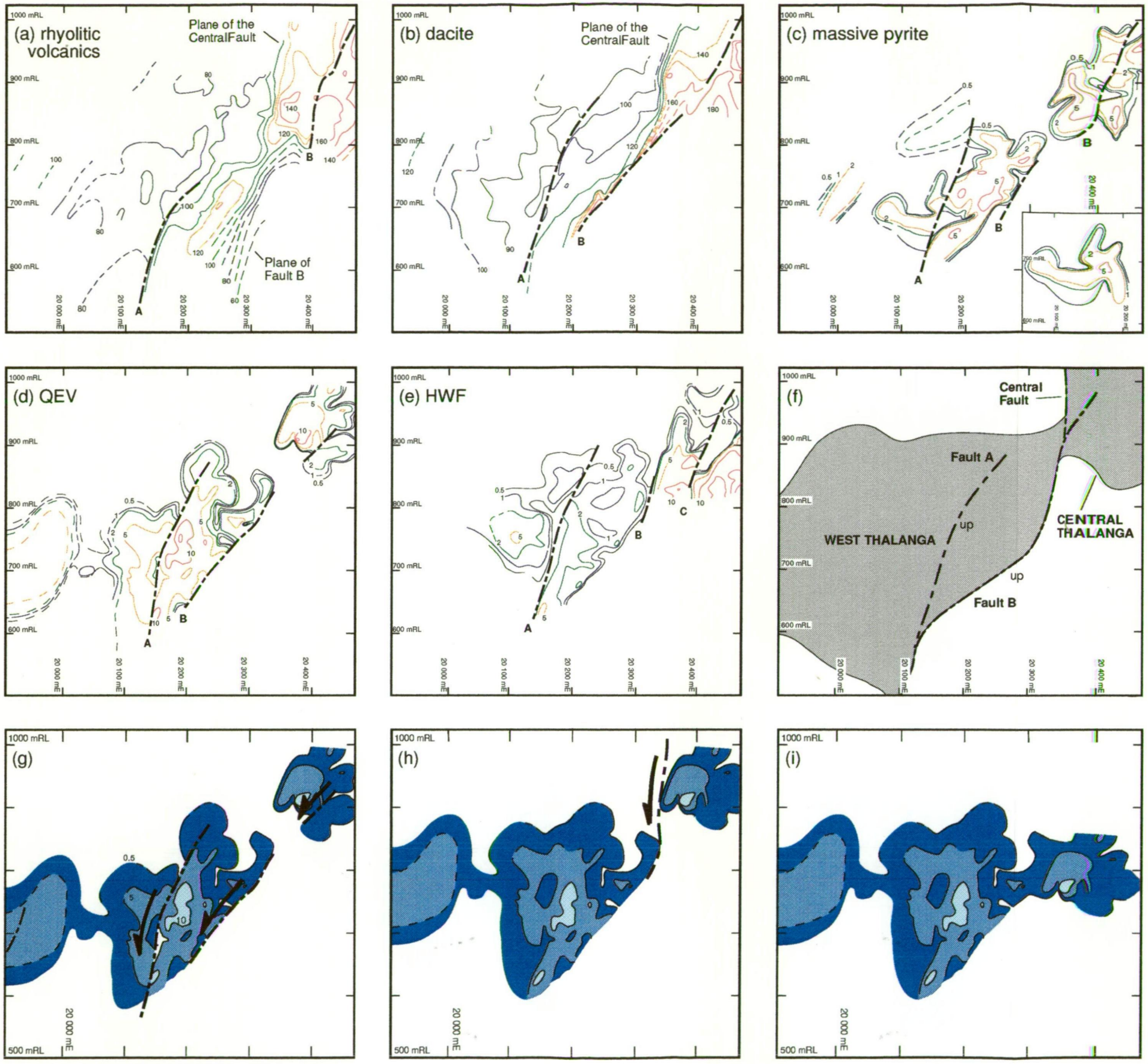

Figure 3.2 Structure contour diagrams and isopach maps of selected units within the ore horizon at the contact between West and Central Thalanga. Structure contours are measured from an arbitrary base line at 20 400 mN, with both structure contours and isopach contours in metres. The coloured contours grade from purple for low values to bright red for the highest values. (a) structure contours of the stratigraphic top of the footwall rhyolitic volcanics, (b) structure contours of the stratigraphic base of the hangingwall dacite, (c) isopach map of the total thickness of massive pyrite within the ore horizon, (d) isopach map of the thickness of the quartz 'eye' volcaniclastic unit (QEV) within the the ore horizon, (e) isopach map of the thickness of the hangingwall fragmental (HWF) that overlies the ore horizon, (f) outline of the economic limits of West Thalanga and Central Thalanga sulphide lenses. The up-thrown side of faults A and B is marked "up", (g) simplified diagram of the QEV isopach map, arrows indicate relative movement along the faults, (h) reconstruction of the distribution of QEV after ENE-striking normal faults (faults A,B and C) removed, and (i) possible distribution of QEV prior to displacement along NNE-trending normal fault (Central Fault).

Thickness of Massive Pyrite

The distribution of thick accumulations of massive pyrite in the ore horizon at West Thalanga, which may overlie feeder zones (Chapter 6 and 10), is shown by an isopach map of pyrite thickness (Fig. 3.2c). Where more than one pyrite lens is present within the ore-horizon, the total thickness of massive pyrite was calculated. In West Thalanga, the thickest regions of massive pyrite are present between faults A and B (Fig. 3.2c). The line of thickest pyrite accumulation pitches subparallel to the traces of fault B, which truncates the massive pyrite on its western margin (Fig. 3.2c).

West of about 20 110 mE the data is not comprehensive, although the few intersections of massive pyrite and areas with no massive pyrite suggest that it is not a continuous sheet. Pyrite thickness on the down thrown block of fault A is contoured separately (Fig. 3.2c(inset)). The elongate nature of the pyrite distribution in this area suggests that there may have been some channelling of hydrothermal solutions, and that perhaps the pyrite occurs in zones of focussed flow of high temperature, hydrothermal fluids.

Thickness and Distribution of the Volcaniclastic Units

The distribution of the QEV indicates the location of topographic lows in West and Central Thalanga at the time of QEV deposition (Fig. 3.2d). Immediately west of the fault A, the QEV has an arcuate distribution, and the thickest QEV corresponds to the lowest structure contours of the footwall map (cf. Fig. 3.2a and d). Between faults A and B, the QEV is thickest at depth, with areas of QEV >10 m thick occur below 780 mRL. The QEV exhibits patchy distribution in the western part of Central Thalanga and is absent from the eastern parts of Central Thalanga. This distribution pattern is interpreted to show that the rhyolitic volcanics in the eastern parts of Central Thalanga were topographically higher than in West Thalanga and the western parts of Central Thalanga prior to QEV deposition. The areas where QEV is >5 m in thickness in Central Thalanga correspond to the location of coherent quartz-feldspar porphyry (QFP) mega-clasts (Chapter 4).

An almost continuous sheet of HWF, which varies between 1-5 m in thickness, occurs in West Thalanga (Fig. 3.2e). The decrease in thickness of both the QEV and HWF up-dip in West Thalanga is interpreted to be a primary depositional feature. The HWF does not occur adjacent to fault B below about 730 mRL, indicating that the ore-horizon was topographically higher in this area at the time of HWF deposition. The HWF is absent immediately east of fault C in Central Thalanga, but exhibits a sharp increase in thickness further east of fault C (Fig. 3.2e). A topographic high on the east side of fault C, prior to faulting and deposition of the HWF, would explain the absence of HWF in this region. In this location, the HWF directly overlies massive sulphides and therefore the lack of HWF

suggests a classic seafloor mound of massive sulphides in the style of Hellyer (cf. McArthur and Dronseika, 1990; Gemmell and Large, 1992).

Interpretation

Isopach contours show that QEV >5 m thick occurs in several parts of the ore horizon in West Thalanga and the distribution of thick QEV is unrelated to the ENE-striking fault B (Fig. 3.2d). Thick QEV and massive sulphide mineralisation also occurs on the eastern side of the fault in Central Thalanga, which is unrealistic for a growth fault model. The absence of stratigraphic thickening close to the fault B, and the repetition of lithologies on the eastern side of fault B, indicates that any fault in this position has not had a significant effect on sedimentary thickness. The coincidence of highly altered footwall and thick massive pyrite in the ore horizon adjacent to the ENE-striking fault B possibly indicates that the orientation of faulting was partly controlled by original lithologies and competency contrasts. Removal of both sets of dip-slip faults , and restoration of the QEV to possible depositional configuration is illustrated in Figure 3.2 (g-i).

3.2.3 Potential Growth Fault II: In the Vomacka Zone

A potential growth fault is interpreted to occur in the footwall of the Vomacka Zone, along a 2-10 m wide zone of actinolite-chlorite ± clinozoisite ± epidote ± carbonate ± diopside at the contact between quartz-muscovite-pyrite-rich footwall rhyolitic volcanics and weakly chloritic rhyolitic volcaniclastic units (Fig. 3.3a). Rare, discontinuous lenses of chlorite schist within the calc-silicate zone may be remnants of a pre-existing chlorite alteration zone. The location of the calc-silicate assemblage, in sharp contact between intensely and weakly altered footwall units, supports the interpretation that it represents a fault exploited by ascending hydrothermal solutions. The calc-silicate assemblage is confined to the footwall and does not continue through the ore horizon or the stratigraphically overlying HWF and dacite, indicating that the fault was formed and active as a fluid conduit before deposition of the hangingwall units. The calc-silicate zone is subvertical and partly folded (Fig. 3.3b), and when the volcanic units are unfolded and restored to depositional geometries, the calc-silicate assemblage occupies a valid orientation for a growth fault (Fig. 3.3c).

In this model (Fig. 3.3c), quartz-sericite-pyrite alteration and pyrite stringer mineralisation were produced in the footwall rhyolitic volcanics overlying the fault as hydrothermal solutions move upwards away from the fault. The weak chlorite alteration of the rhyolitic volcaniclastic units on the footwall side of the fault is probably due to seawater circulation (e.g. Costa *et al.*, 1983; McLeod and Stanton, 1984), and a chlorite-quartz-carbonate assemblage may have been produced by the interaction of seawater with hydrothermal

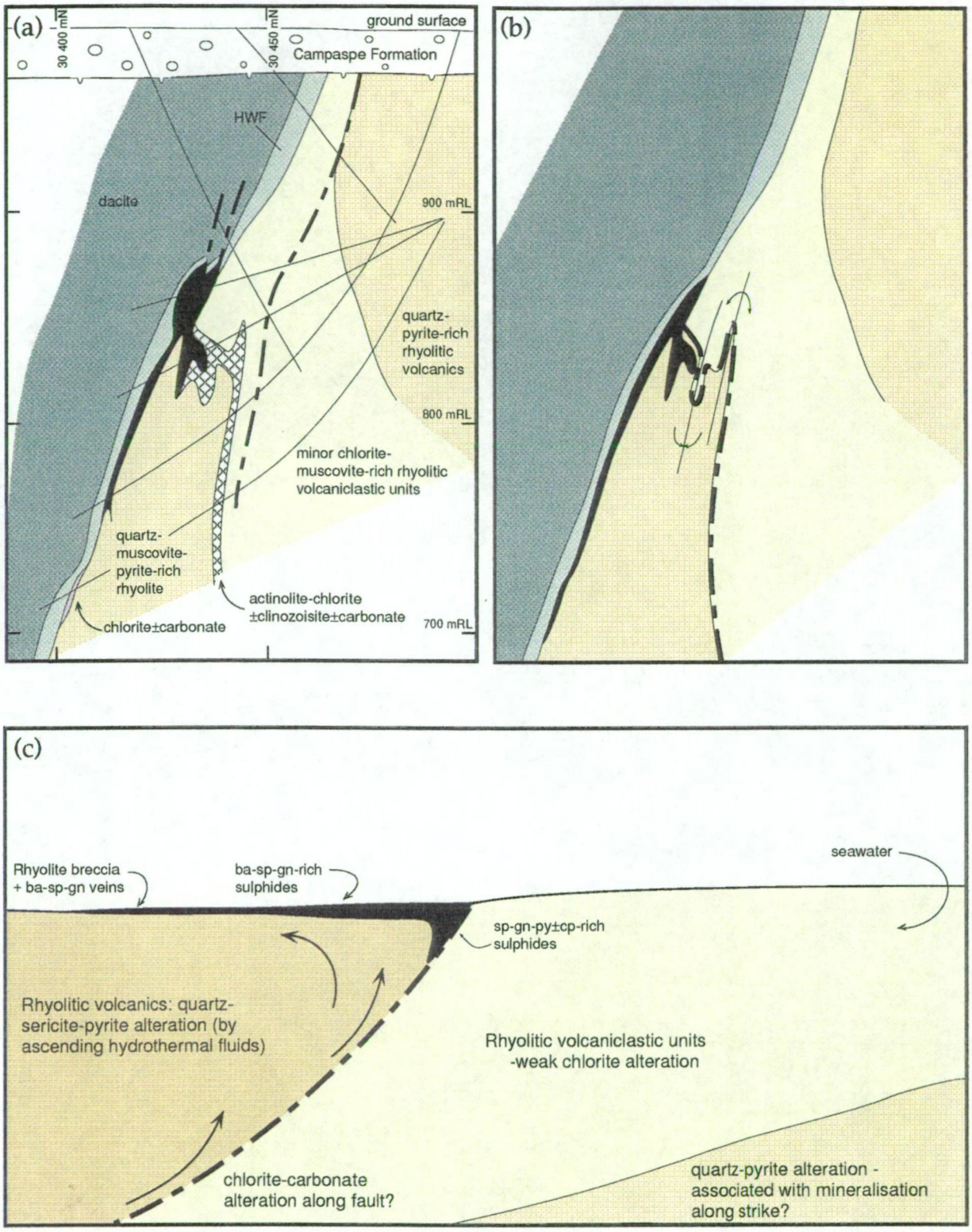

Figure 3.3 Model of the formation of a possible growth fault in the footwall of the Vomacka Zone at the Thalanga deposit. (a) Cross section along 31 840 mE in the Vomacka Zone of the Thalanga deposit. The folded zone of actinolite-chlorite±clinozoisite±carbonate alteration may represent a pre-existing structure used as a pathway by the mineralising fluids. (b) normal faults are removed in intermediate step in the restoration of the cross section. Folding of calc-silicate alteration probably occurred during D_2. The current mineral assemblage is interpreted to be the metamorphic product of a chlorite-carbonate precursor. (c) Schematic diagram of the 31 840 mE section restored to a pre-deformation geometry. Massive sulphides are deposited on the seafloor adjacent to and along strike from the possible growth fault . Abbreviations: ba = barite, cp = chalcopyrite, gn = galena, py = pyrite, sp = sphalerite.

solutions ascending along the fault. Regional metamorphism of the chlorite-quartz-carbonate assemblage would produce the calc-silicate minerals that now define the fault zone.

The ore horizon in the Vomacka Zone is compositionally zoned, and from the fault to the down-dip limit of mineralisation, is composed of;
(i) massive pyrite-galena-sphalerite ± chalcopyrite, or massive to semi massive sphalerite-pyrite-galena adjacent to the fault,
(ii) massive barite with minor vein or disseminated sphalerite-pyrite-galena,
(iii) poorly sorted polymict breccia with veins of barite and sphalerite-galena-pyrite ± barite, or vein-style sphalerite-pyrite-galena in footwall rhyolitic volcanics (Chapter 6). This compositional zonation probably reflects a temperature gradient (cf. Eldridge *et al.*, 1983) and supports the growth fault model, with the pyrite-chalcopyrite-sphalerite-rich sulphides forming proximally to the fault from high temperature solutions emanating directly from the fault, and barite-rich sulphides formed from cooler fluids at distal part of the ore horizon (Fig. 3.3c).

In the absence of growth faults elsewhere at Thalanga, other structures must have channelled hydrothermal fluids to the ore horizon. The distribution of intense alteration in semi-conformable zones within the footwall rhyolitic volcanics suggests that porous volcaniclastic units within the footwall provided pathways for ascending hydrothermal solutions, and this is discussed in detail in Chapter 10.

3.2.4 Pyrite Stringers and Other Sulphide Veins.

Pyrite veins are present within discrete subvertical zones of quartz-muscovite-pyrite ± chlorite-rich assemblages in the footwall rhyolitic volcanics, and in chlorite schist at the stratigraphic top of the rhyolitic volcanics. The footwall stringer zones are subparallel to stratigraphy, strike approximately E-W, and possibly formed along originally porous volcaniclastic units within the footwall (Chapter 10). Pyrite veins are most abundant in zones enriched in quartz, and chalcopyrite is present within some pyrite veins. Sphalerite stringers are rare within the footwall rhyolitic volcanics. Figure 3.4 (a,b) shows the orientation of the pyrite and pyrite-chalcopyrite veins in the footwall of Central Thalanga. Two trends are prominent: a steeply S-dipping, SW- striking vein-set, and a steeply N-dipping, E-W to SE-striking vein set. In parts of Central Thalanga, barite-rich veins, with minor sphalerite-pyrite, cross-cut the pyrite stringer veins. The barite-rich veins vary from steeply to moderately N-dipping and strike E to SE (Fig. 3.4c).

The 1-2 cm wide pyrite stringer veins are cross-cut by S_2, and vary from open to tightly folded, with the axial plane parallel to the cleavage (Fig. 3.5a bottom). The rare sphalerite stringers are typically <0.5 cm wide and are also folded with axial plane parallel to

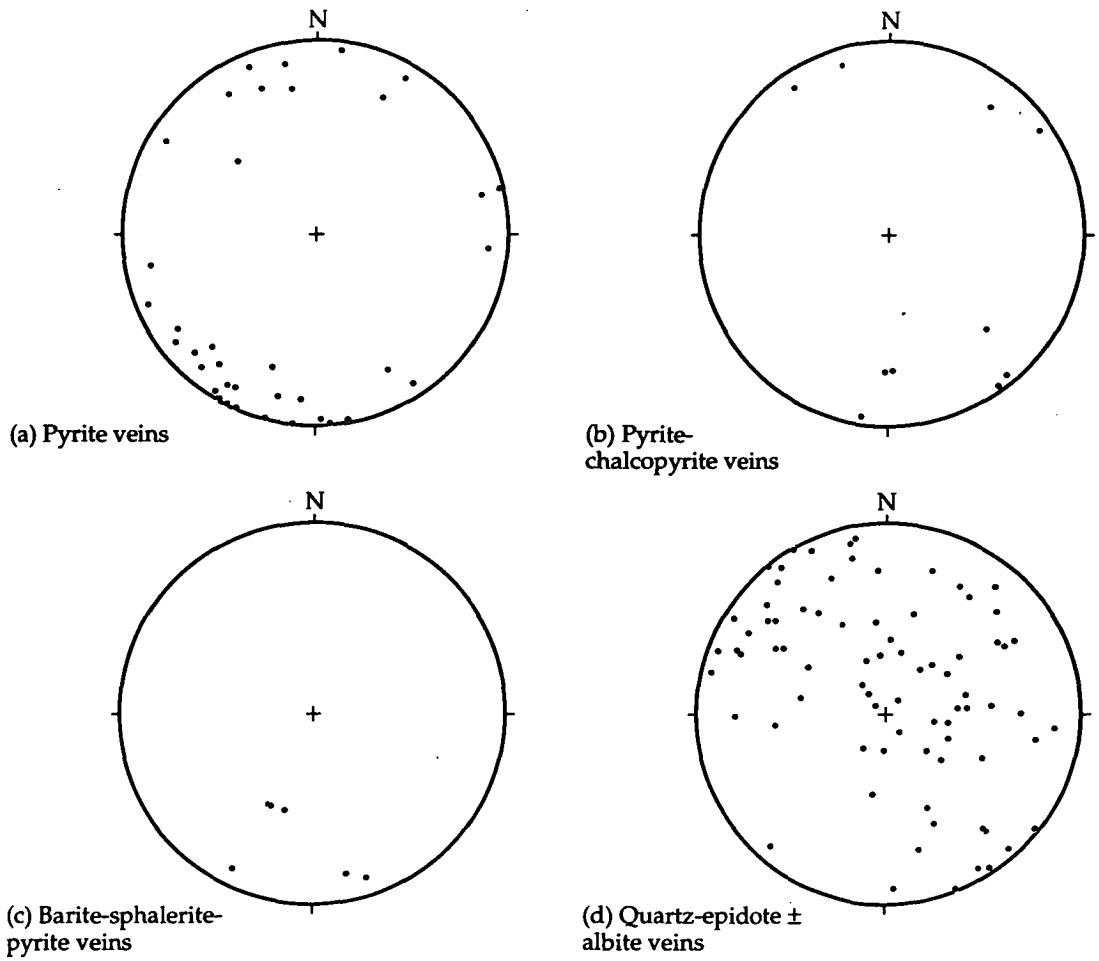

Figure 3.4 Equal area stereonets of: (a-c) poles to sulphide veins in the footwall rhyolitic volcanics in Central Thalanga, (d) poles to quartz-epidote veins in the dacite overlying the Central and West Thalanga ore lenses.

Figure 3.5 Folded and boudinaged veins.

(a) Folded pyrite and sphalerite stringers. Top: folded sphalerite vein from the footwall rhyolitic volcanics. S_2 is parallel to the axial plane. Small (<2 mm) quartz crystals are preserved within the quartz-muscovite-rich rhyolite. Sample E3198SD24-53.7, East Thalanga. Bottom: typical pyrite stringers in quartz-muscovite-pyrite-rich rhyolitic volcanics. Stringers are folded and cross-cut by S_2. Pyrite extends from the fold hinge along the axial plane. Sample E3198SI50-5, East Thalanga.

(b) Folded quartz-epidote veins. Top: irregularly folded quartz-epidote vein, with axial planar S_2 cleavage, in siliceous feldspar-quartz-phyric rhyolite. Sample TH26-303.5, Central Thalanga. Bottom: weakly folded quartz-epidote vein cross-cutting aphyric dacite. S_2 is strongly defined in epidote-rich, vein alteration halo. Sample TH243-397, West Thalanga.

(c) Boudinaged quartz veins subparallel to S_0 in siliceous HWF. Biotite and chalcopyrite blebs are subparallel S_2. Sample TH209-88.7, Central Thalanga. Arrow points to facing direction.

(d) Boudinaged quartz vein in strongly foliated (S_2) QEV. Location: E765 Stope (right), East Thalanga. Pen is approxiamately 14 cm in length. Facing to left.

(e) Asymmetrically folded quartz veins, with subvertical fold hinge, within sandstone of the Trooper Creek Formation near the Waddys Mill area. Small shear bands parallel to S_2 are present along the fold limbs. Location: Thalanga Range; 18 730 mN, 9 600 mE (mine grid). Facing to top.

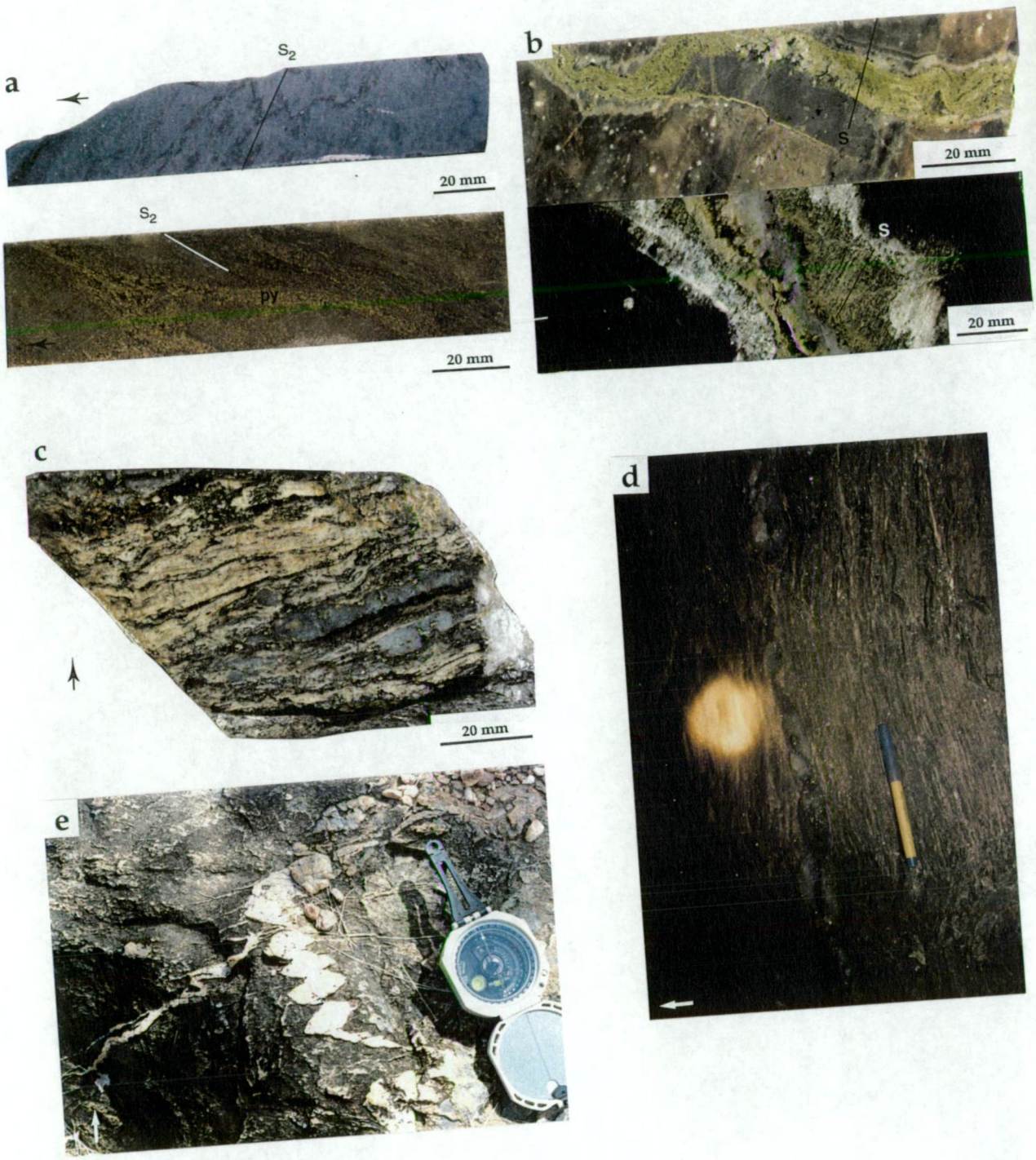
a
S_2
20 mm
S_2
py
20 mm
b
S
20 mm
S
20 mm
c
20 mm
d
e

cleavage (Fig. 3.5a top). The hinge of folded pyrite veins is attenuated and pyrite extends along the axial plane in places (Fig. 3.5a bottom). Although the hinges of folded stringer veins are rarely exposed, some pyrite, pyrite-chalcopyrite, and sphalerite stringer veins have S-vergence, indicating that they have subvertical fold hinges and were formerly perpendicular to the ore horizon. Other stringer veins have N-vergence (e.g. Fig. 3.5a top), subhorizontal fold hinges, and were therefore originally subparallel to the ore horizon. This apparent contradiction in fold vergence is supported in underground exposures, where pyrite veins are both subparallel and perpendicular to the ore lenses.

3.2.5 Quartz-Epidote Veins

Irregularly distributed, fracture-controlled to locally pervasive quartz-epidote alteration is present in the dacite stratigraphically overlying the ore horizon at Thalanga. Quartz-epidote veins are less common in the andesite, QFP and QEV units, and rarely occurs in quartz-feldspar-phyric rhyolite. Fine grained epidote is disseminated through the microdiorite dykes, with quartz-epidote veins overprinting the dykes in a few locations. Stolz (1989) noted that quartz-epidote alteration is confined to 100-150 m above the ore horizon at Thalanga, but is absent from other deposits and prospects in the Mount Windsor subprovince. It is here interpreted, from the spatial association between quartz-epidote veins and carbonate alteration in the underlying ore horizon, that quartz-epidote veins are the metamorphosed equivalents of post-ore formation, hangingwall alteration (Chapter 10).

Most veins are composed of quartz, with lesser epidote and rare albite, and have epidote ± chlorite ± actinolite selvages and quartz (with minor hematite) or epidote alteration halos in the host rock (see Chapter 10). Quartz within the veins is strongly recrystallised or has undulose extinction, indicating overprinting deformation. However, the fine-grained quartz within the alteration halo is completely recrystallised. The random orientation of quartz-epidote veins in the dacite (Fig. 3.4d) suggests that pre-existing structures were exploited and filled by vein material. Perhaps original cooling joints in the dacite provided sites for later quartz-epidote deposition. Locally, the quartz-epidote veins are tightly to irregularly folded, with axial planar cleavage parallel to S_2 (Fig. 3.5b, top). S_2 is typically strong within the alteration halo (Fig. 3.5b, bottom), supporting the interpretation that the quartz-epidote veins formed prior to deformation. However, the presence of quartz-epidote veins in the microdiorite dykes (interpreted to have intruded after deformation; section 3.5.3) indicates that quartz-epidote may have been locally remobilised, or also formed after deformation.

3.3 D_1 Structures

Subvertical quartz veins cross-cut bedding within the HWF at an acute angle, and are boudinaged and subparallel to S_2 (Fig. 3.5c,d). These quartz veins have been strongly recrystallised and have preserved no evidence of their original textures. Locally, parasitic tight to isoclinal folds, with axial plane parallel to S_2, occur in these veins. Similar isoclinally folded quartz veins are common within the volcaniclastic sandstone units in the Trooper Creek Formation along the Thalanga Range (Fig. 3.5e). Clearly the quartz veins predate the D_2 structures, and must have formed during an earlier deformation event. Variable bedding-cleavage (S_2/S_0) intersection lineations (B^0_2) along the Thalanga Range have been interpreted to be consistent with asymmetric folding during D_1 (Berry *et al.*,1992). Perhaps the boudinaged and isoclinally folded quartz veins at Thalanga were formed during D_1. Alternatively, the quartz veins may be related to mineralisation and no evidence of D_1 was found in this study.

3.4 D_2 Structures

3.4.1 E-W Fold

Bedding faces south and is subvertical to steeply south-dipping at the Thalanga massive sulphide deposit. Bedding strikes approximately WNW at West Thalanga, has variable strike in Central Thalanga, and strikes WSW at East Thalanga (Fig. 3.6a-c). The variability of the S_0 orientation in Central Thalanga (Fig. 3.6b) is interpreted to be due to primary irregularities in bedding orientations, and displacement along the numerous ENE-striking normal faults that offset stratigraphy (section 3.6.3). Along the Thalanga Range, bedding dips steeply south and strikes WNW to NW, and is subparallel to S_2 in many places (cf. Fig. 3.6d,e with Fig. 3.7a-c). Near the southern extent of the range, close to the Thalanga deposit, bedding is slightly overturned and dips steeply NW (Fig. 3.6d). However, further NW along the Thalanga Range bedding dips SW (Fig. 3.6e).

Flow banding is prominent in the coherent rhyolites in the Mount Windsor Volcanics and is typically parallel to S_0 along the Thalanga Range (Fig. 3.6f). In places the flow banding is irregularly folded (Chapter 4). Berry (1989) demonstrated that cleavage cross-cuts tight folds in flow-banded rhyolite, and thus discounted the interpretation of Laing (1984) and Hall (1981) of an anticline within the Mount Windsor Volcanics along the Thalanga Range.

At Thalanga and along the Thalanga Range, S_2 is consistently anticlockwise of S_0. This bedding-cleavage relationship, together with asymmetric parasitic folds in finely laminated siltstone units in the HWF, support the interpretation of Berry *et al.* (1992) that

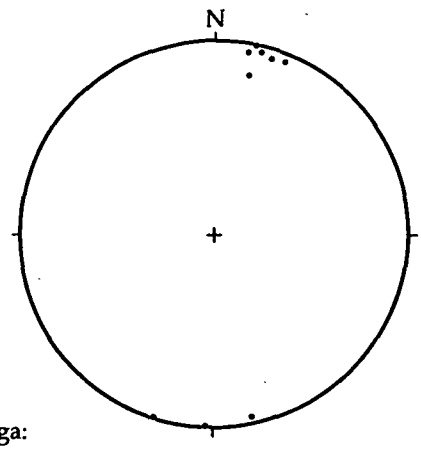

(a) West Thalanga: poles to bedding

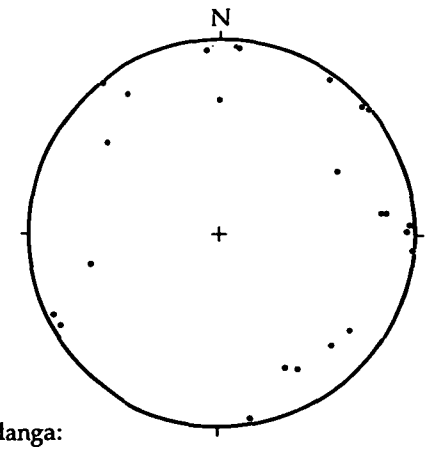

(b) Central Thalanga: poles to bedding

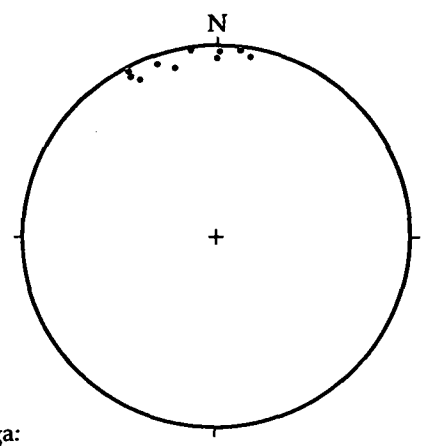

(c) East Thalanga: poles to bedding

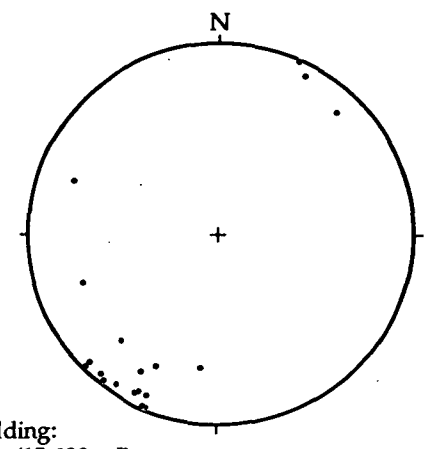

(d) Poles to bedding: Thalanga Range (15 600 mE to 20 000mE; mine grid)

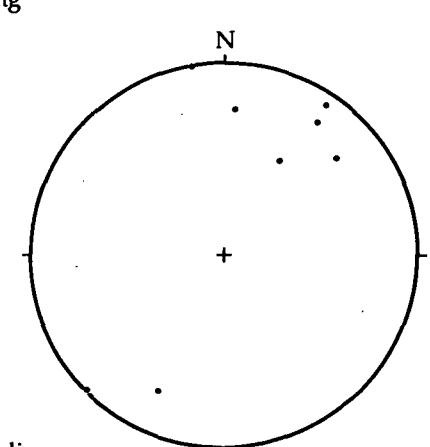

(e) Poles to bedding: Thalanga Range (6 800 mE to 15 600 mE; mine grid)

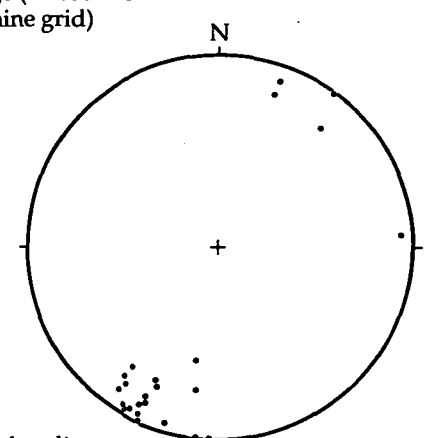

(f) Poles to flow banding from Thalanga Range

Figure 3.6 Equal area stereonets of poles to bedding and flow-banding from the Thalanga massive sulphide deposit and the Thalanga Range.

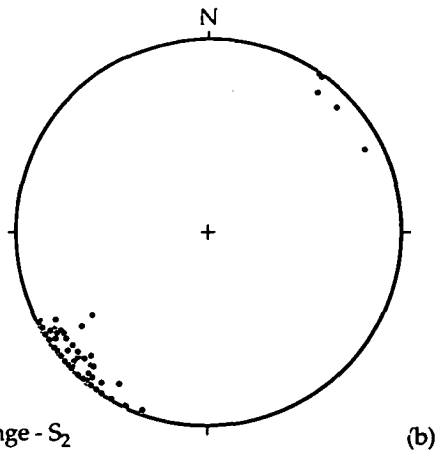

(a) Thalanga Range - S_2

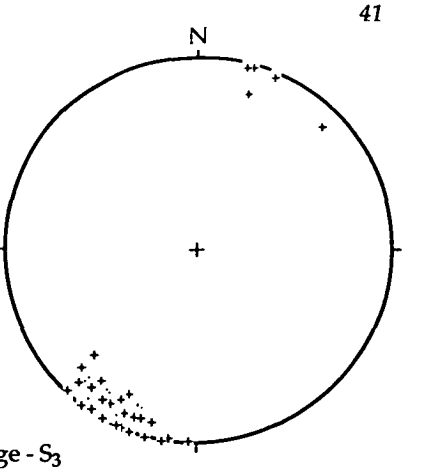

(b) Thalanga Range - S_3

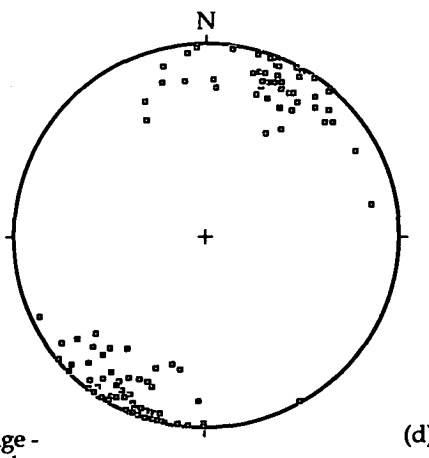

(c) Thalanga Range - undifferentiated cleavage

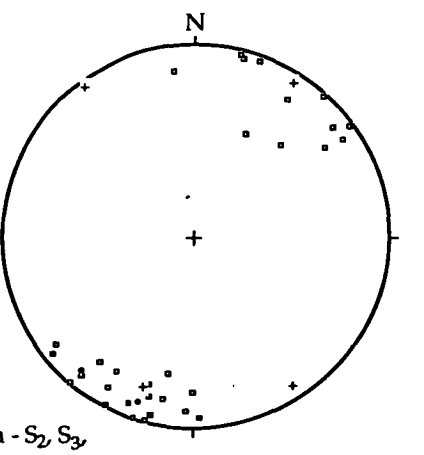

(d) West Thalanga - S_2, S_3, and undifferentiated cleavage

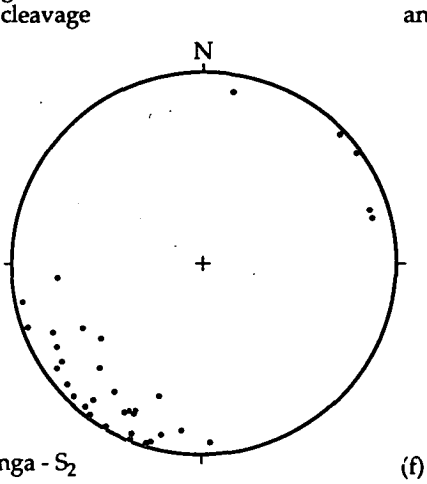

(e) Central Thalanga - S_2

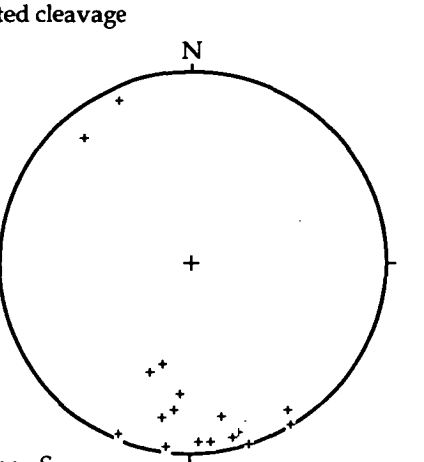

(f) Central Thalanga - S_3

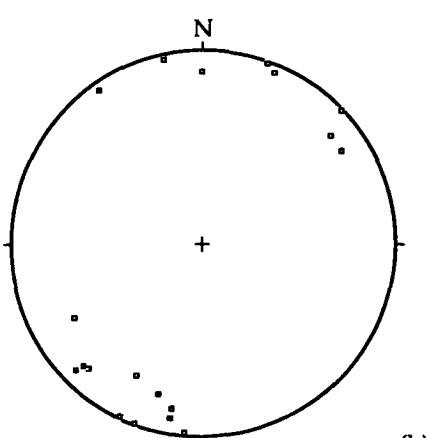

(g) Central Thalanga - undifferentiated cleavage

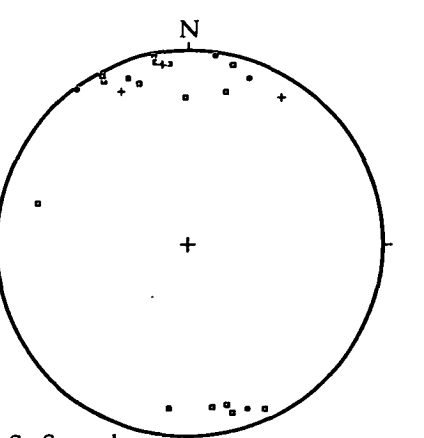

(h) East Thalanga - S_2, S_3, and undifferentiated cleavage

Figure 3.7 Equal area stereonets of poles to cleavages from the Thalanga deposit and the Thalanga Range. (•) S_2, (+) S_3, (•) $S_{undifferentiated}$.

Thalanga occurs on the northern limb of an upright, E-W syncline (F_2) with axial planar S_2. This regional-scale folding, and related metamorphism, is correlated with the intrusion of the Ravenswood Granodiorite to the north of Thalanga (Laing, 1984; Wills, 1985; Gregory *et al.*, 1990; Berry *et al.*, 1992).

A possible large-scale parasitic fold is present in West Thalanga, where bedding dips shallowly south between overprinting normal faults (Fig. 3.1). Upright folds are interpreted to explain the repetition of hangingwall lithologies in the up-dip parts of the Vomacka Zone (Fig. 3.8), with the folds offset along later, E-W trending faults (Fig. 3.9). However, the fold geometry on Figure 3.9, where anticlines occur on the SE side of the faults, only makes sense if the faults were active at the same time as folding. The absence of a sulphide ore lens repeated in the ore horizon position in the syncline (north of the mineralised anticline) is interpreted to be due to an original lack of mineralisation in this part of the Vomacka Zone.

3.4.2 S_2 Cleavage

The prominent slaty cleavage at Thalanga is subparallel to bedding, dips steeply north and strikes between 090° and 140° in West and Central Thalanga and the Thalanga Range (Fig. 3.7a,d,e,h), similar to the regional slaty S_2 cleavage recognised by Berry (1990, 1991) and Berry *et al.* (1992). In East Thalanga, S_2 strikes between 060° and 100° (Fig. 3.7h). S_2 is best developed in fine grained, phyllosilicate-rich rocks at Thalanga. Consequently, the HWF, fine grained tops of QEV units, chlorite-rich units within the ore horizon, and muscovite-, phlogopite- or chlorite-rich footwall rhyolitic volcanics are strongly foliated, whereas the coherent dacite and areas of strong quartz alteration in the rhyolitic volcanics have weak S_2 cleavage.

Microscopically, S_2 cleavage in the quartz-muscovite-pyrite-rich rhyolitic volcanics is defined by the preferred orientation of fine-grained muscovite and phlogopite. Bands of recrystallised elongate quartz parallel to S_2 in the footwall rhyolitic volcanics may have initially formed as quartz ribbons (implying high finite strain during D_2; Ramsay and Huber, 1987), and recrystallised during later metamorphism. Euhedral pyrite disseminated in the hydrothermally altered footwall rhyolitic volcanics is also elongate parallel to S_2 in most places. Chlorite, phlogopite and muscovite gangue, and sulphide banding in places, define S_2 in both the massive sulphide lenses and carbonate-chlorite-tremolite assemblages within the ore horizon. S_2 in dacite in the hangingwall is weakly defined by aligned biotite and minor fine-grained muscovite in the groundmass. Pressure shadows around crystals and phenocrysts have typically been filled with quartz, which was subsequently recrystallised during metamorphism (section 3.10).

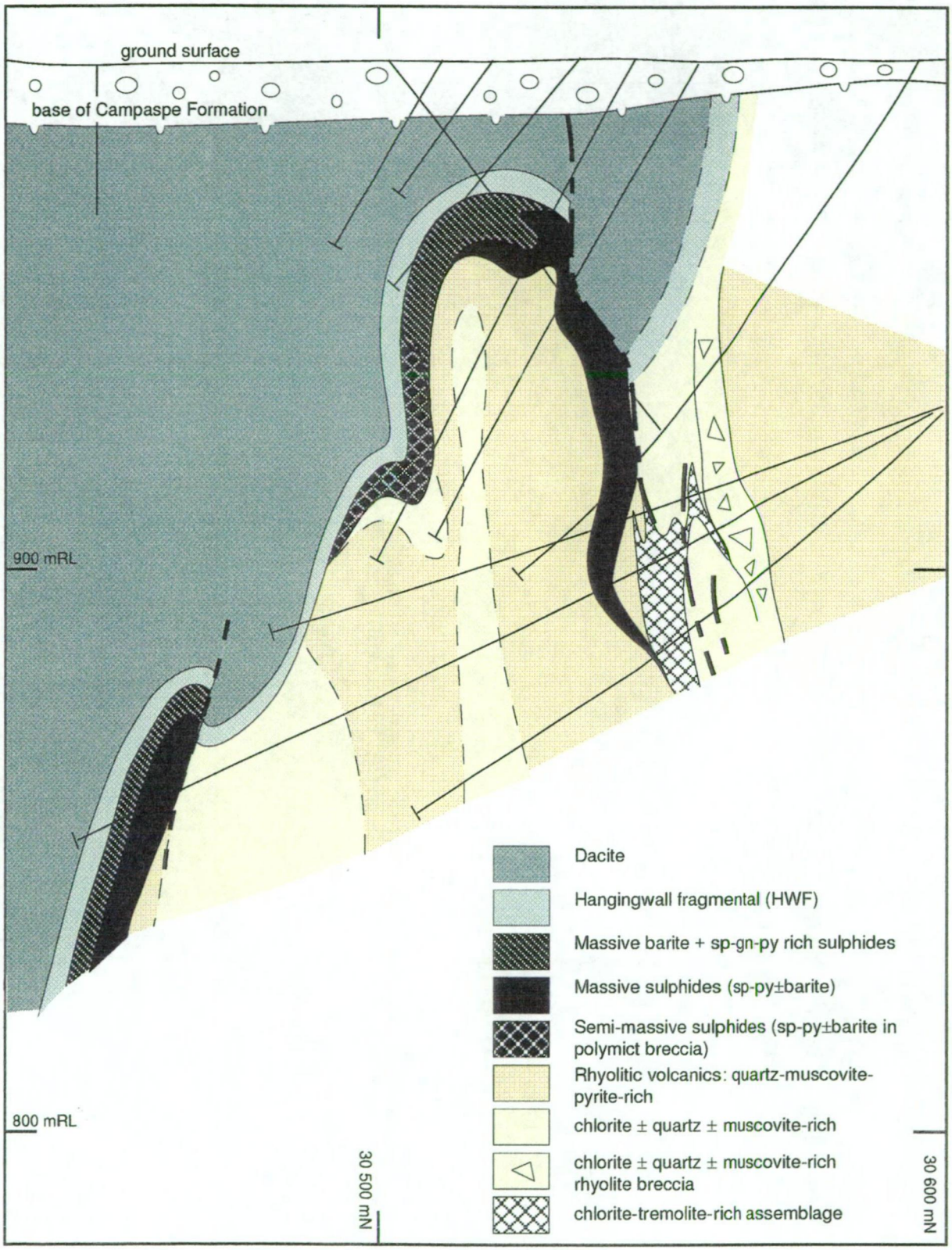

Figure 3.8 Cross section along 31 600 mE in the Vomacka Zone of the Thalanga deposit. See Fig. 3.3 for abbreviations of sulphide minerals.

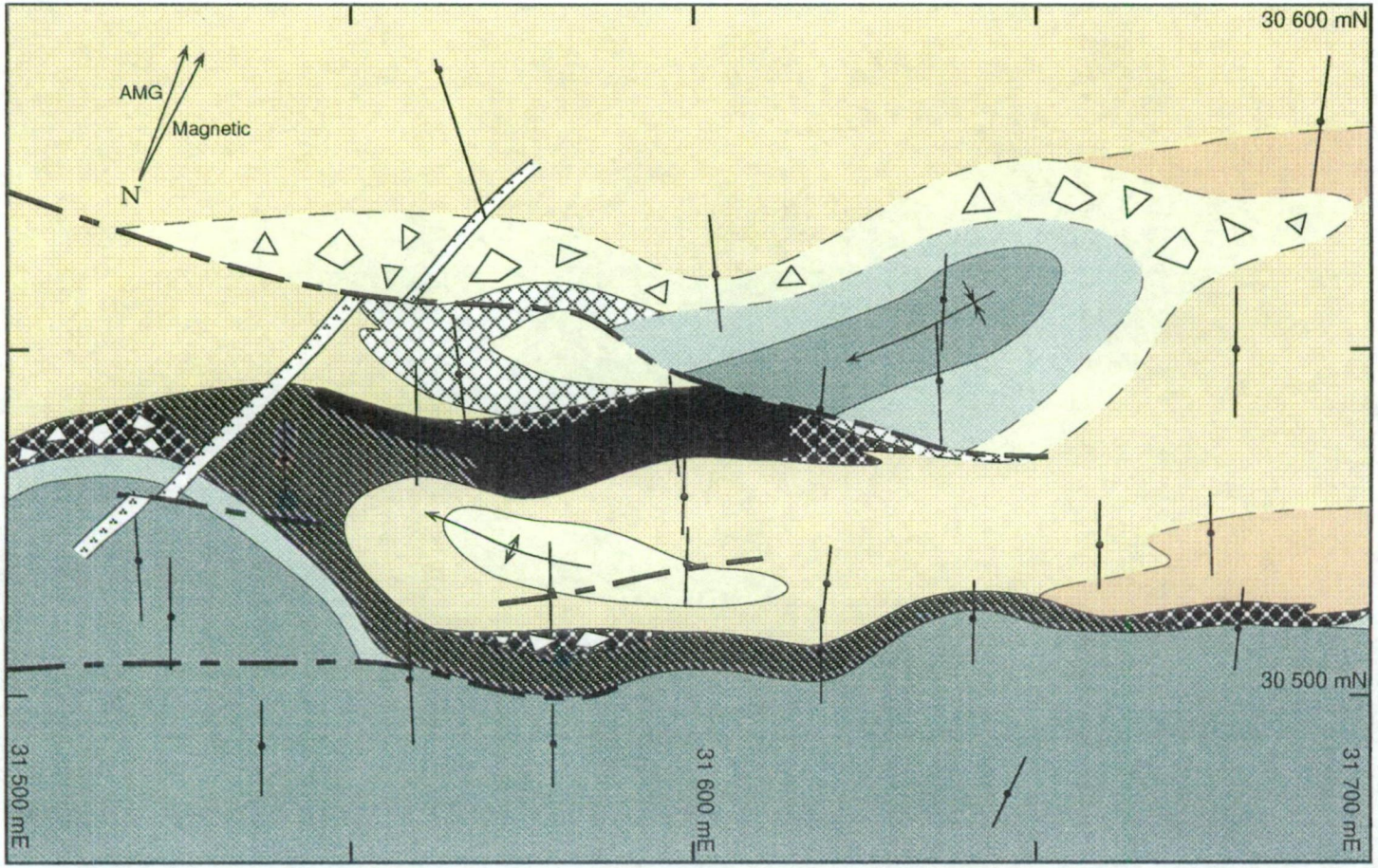

Figure 3.9 Interpretive geology of the Vomacka Zone at the 940 mRL level (based on drill hole logs). Drill holes shown as a single line with a dot marking the location of the intersection with the level plan.

3.4.3 L_2 Mineral Lineations

Mineral stretching lineations (L_2) in the host volcanic units at Thalanga plunge moderately to steeply NE, with L_2 varying from steeply N-plunging in West Thalanga, to moderately-steeply NE to ENE-plunging in Central Thalanga, and steeply ENE to E-plunging in East Thalanga (Fig. 3.10a). This lineation direction is consistent with subvertical extension during D_2.

L_2 is typically defined by elongate clusters of biotite and fine grained Ti-oxides in the groundmass of dacite and weakly altered quartz-feldspar-phyric rhyolites (Fig. 3.11a,b), biotite in S_2 pressure shadows, and by elongated volcanic clasts in the HWF (Fig. 3.11c). Biotite clusters aligned parallel to the S_3 cleavage in some rocks are generally less elongate (than those on S_2) and have decussate texture. Pale sphalerite spots in altered footwall rhyolitic volcanics in Central Thalanga are elongate and plunge steeply ENE to NE, and some pyrite stringers in the rhyolitic volcanics also have a mineral stretching lineation that plunges moderately to steeply ENE (Fig. 3.10a).

3.4.4 Quartz Veins

Shallow-dipping barren quartz veins are common in the competent QFP, QEV and footwall rhyolitic volcanics in Central and East Thalanga. In West Thalanga, similarly oriented quartz-filled tension gashes, <1 m in length, cross-cut banding in the massive sulphides. The quartz veins are perpendicular to L_2, dipping between 20° and 40° towards SW (Fig. 3.10b), and in places the veins occur in conjugate sets 15–45° apart. The quartz veins cross-cut S_2 cleavage, and are truncated by D_3 brittle-ductile faults and terminated at massive sulphide lenses (Fig. 3.11d,e), with vein quartz extending <1 m along the vertical contact between (up-dip) QEV and massive sulphides in East Thalanga. The absence of quartz veins in the adjacent massive sulphides is interpreted to indicate ductile deformation in the massive sulphides, with coeval brittle extension of the QFP and QEV. Similar variation in the style of deformation is reported from the Mobrun massive sulphide deposit, Quebec, where sphalerite-rich sulphides contain no quartz veins, but adjacent pyrite-rich sulphides contains abundant quartz and chalcopyrite veins (Larocque and Hodgson, 1995).

Quartz veins in the QFP and QEV are usually discontinuous and are widest, therefore displaying maximum extension, at their southern edge (Fig. 3.11e). There is usually no alteration halo associated with these quartz veins and tension gashes, and they are interpreted to have resulted from high fluid pressures during continued subvertical extension of the mineralised horizon in the final stages of D_2.

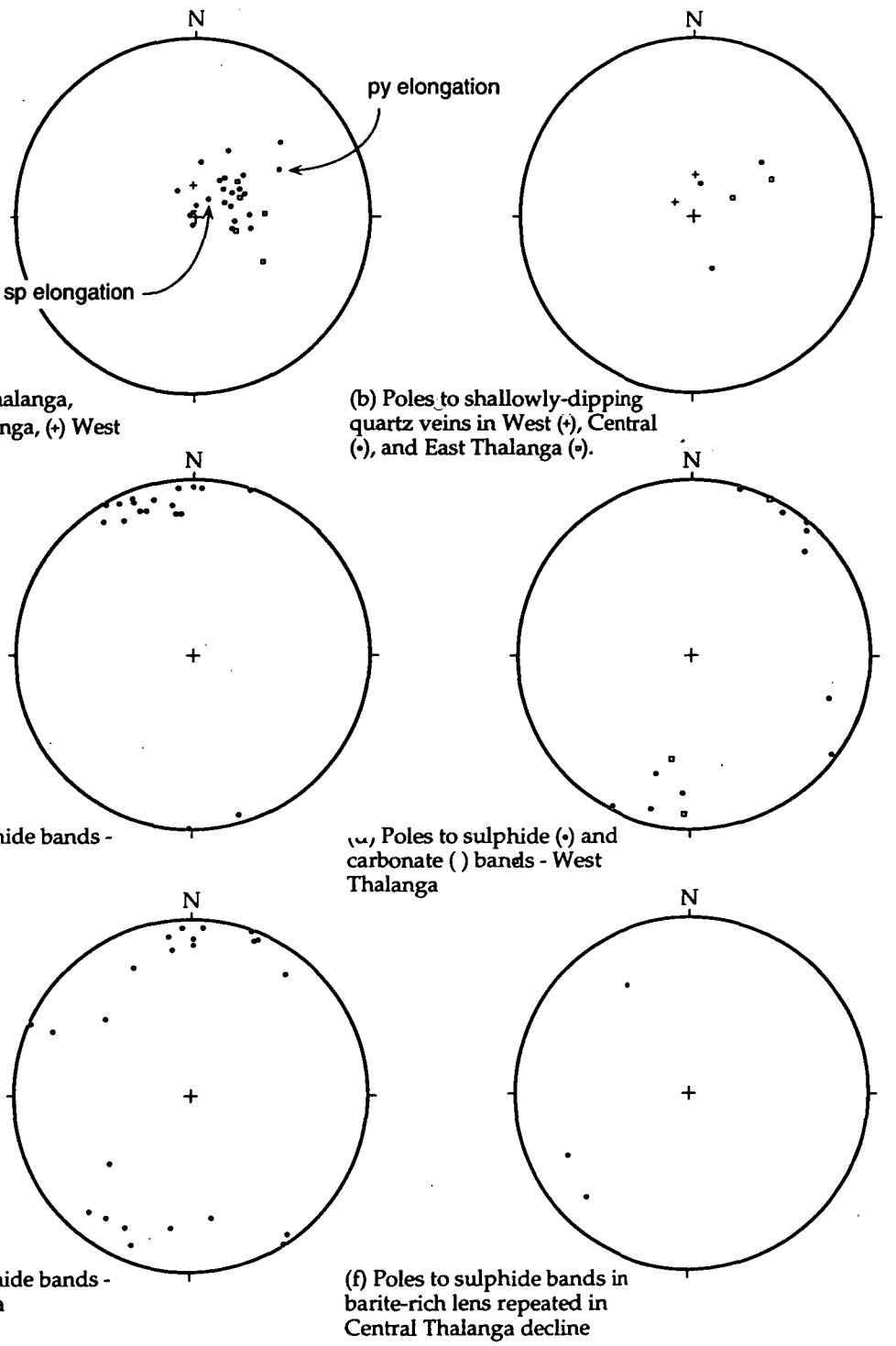

(a) L_2 . (•)East Thalanga, (•) Central Thalanga, (+) West Thalanga.

(b) Poles to shallowly-dipping quartz veins in West (+), Central (•), and East Thalanga (▫).

(c) Poles to sulphide bands - East Thalanga

(d) Poles to sulphide (•) and carbonate ( ) bands - West Thalanga

(e) Poles to sulphide bands - Central Thalanga

(f) Poles to sulphide bands in barite-rich lens repeated in Central Thalanga decline

Figure 3.10 Equal area stereonets of (a) mineral and clast elongation lineations, (b) extension veins, and (c-f) poles to compositional banding in massive sulphide lenses at Thalanga. Abbreviations: py = pyrite, sp = sphalerite.

Figure 3.11 Structures that formed during subvertical extension at Thalanga.

(a) Photomicrograph of anhedral, elongate chlorite (after biotite) grains that define a lineation on S_2. Section is cut parallel to L_2. Sample C2039ND20-48.0: weakly altered rhyolitic sandstone, Central Thalanga. Plane light.

(b) Same sample as (a), cut perpendicular to L_2. Plane light.

(c) Elongated irregular rhyolite and dacite clasts from breccia facies of the HWF . Location: Central Thalanga; 20 200 mN, 20 475 mE, 955 mRL. Pencil is about 14 cm in length. Facing to left.

(d) Shallow-dipping quartz veins in QFP have maximum extension at the hangingwall contact with the banded to massive sulphides. Quartz does not extend into the sulphides. Location: C860 Stope, Central Thalanga; 20 240 mN, 20 425 mE, 860 mRL. Geological hammer at base of photograph is about 30 cm in length. Facing to left.

(e) Close-up of (d).

(f) Boudinage of chlorite-rich band within massive sphalerite-galena-pyrite-tremolite-rich sulphides. Coarse-grained chalcopyrite and dark red-brown sphalerite fill the necks of boudins. Location: 20 305 mN, 20 245 mE, W780 Stope West Thalanga. Magnet is about 12 cm in length. Facing to right.

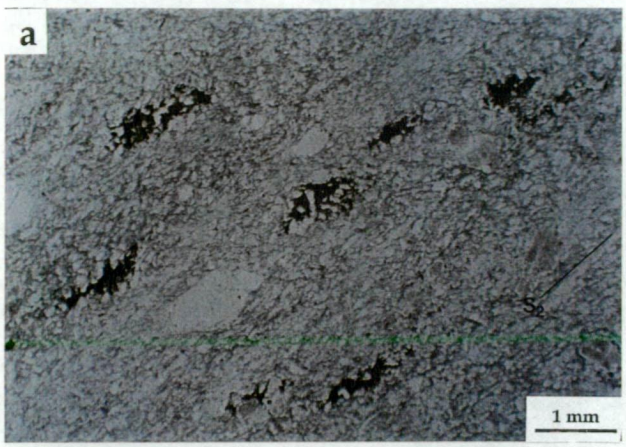
a
1 mm

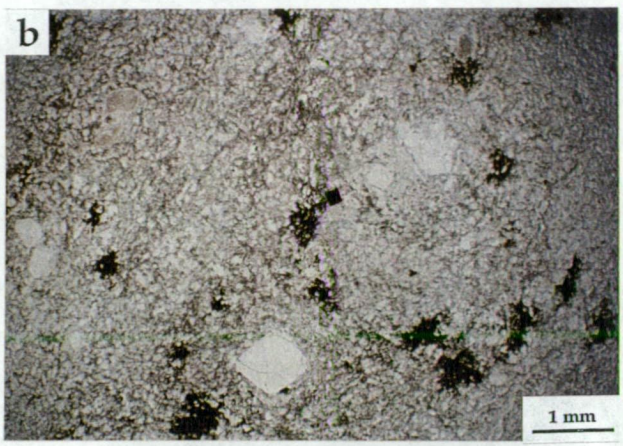
b
1 mm

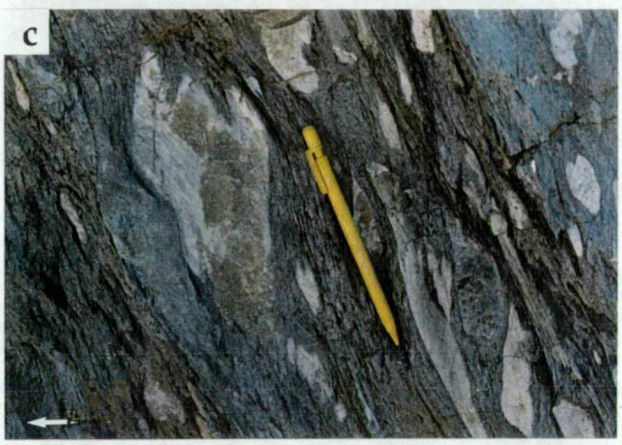
c


d
QFP
sp-py


e
qz


f
chl
cp

3.4.5 Banding in the Massive Sulphides

Compositional banding within the massive sulphide lenses is defined by discontinuous bands of coarsely recrystallized sphalerite-rich and pyrite-rich sulphides. Irregular domains of chalcopyrite has overprinted the banding in places. Sulphide banding varies from subparallel to lithological contacts (suggesting it may be partly depositional in origin) to parallel to the S_2 cleavage and later structures. Isoclinal folds in sulphide bands are rare and, despite an axial plane approximately parallel to S_2, are interpreted to be false folds that resulted from replacement of sphalerite-rich massive sulphides by pyrite (see Chapter 6). In East Thalanga, sulphide bands within the ore lenses commonly dip steeply south and strike 240° to 270° (Fig. 3.10c), and banding in the West Thalanga ore lens is subvertical to steeply north-dipping, and strikes 090° to 130 ° (Fig. 3.10d). In both West and East Thalanga the banding in the sulphide lenses is subparallel to S_2 (cf. Fig. 3.10c,d with Fig. 3.7d,h). Sulphide bands in Central Thalanga commonly strike E-W and dip steeply south (similar to S_2), but in places strike between SE and NE (Fig. 3.10e). This is interpreted to be due to local folding of the ore lens during later deformation (D_3).

Locally sulphide bands within the sulphide lenses are folded towards and become parallel to adjacent faults (e.g. map M7). In the East Thalanga ore lens, banding in massive sulphides adjacent to E-W trending shears (produced during D_3; see section 3.6.1) is oriented E-W, but these shears cross-cut the ore lens and the banded sulphides in places (e.g. map M11), indicating that compositional banding in massive sulphides developed prior to D_3.

3.4.6 Boudinage Structures

Vertical extension of the ore horizon is reflected by boudinage within the massive sulphides and the associated alteration. In all boudinage structures the shallowly W-plunging necks indicate subvertical extension similar to the direction defined by mineral stretching and clast elongation lineations.

Boudinage is common within the carbonate- and chlorite-rich assemblages within the ore horizon at Thalanga, and reflect subtle differences in competency between dolomite-chlorite-tremolite and tremolite-chlorite dominated assemblages (Fig. 3.11f). Rare discrete bands of massive barite within the massive sulphides are more competent than the enveloping sulphides and form boudins, whereas the sulphides behave in a more ductile fashion and fold towards the boudin neck (Fig. 3.12a). Coarse-grained chalcopyrite ± dark brown sphalerite ± galena ± quartz typically have infilled the extensional sites at the necks of the boudins.

Other extensional textures within the ore horizon include the rare *en echelon* boudinage of chlorite-phlogopite bands within massive sulphides (Fig. 3.12b,c). Coarse grained

Figure 3.12 Boudinage and pull-apart structures within the ore lenses, and style of S_3 cleavage.

(a) Boudinaged barite layer from within the banded pyrite-sphalerite-rich part of ore lens. Pyrite-sphalerite bands are folded towards boudin neck, which has been filled with coarse-grained chalcopyrite and dark, red-brown sphalerite. Minor calcite is intergrown with barite. Sample UG-13, location unknown, but either West or Central Thalanga.

(b) *En echelon* brittle boudins of a fine-grained chlorite-phlogopite-rich band within the massive sulphide lens. Coarse-grained chalcopyrite is present between the boudins. Location: W780 Stope, 20 320 mN, 20 335 mE, West Thalanga. Hammer is about 30 cm in length. Facing to right.

(c) Sketch of (b).

(d) Photomicrograph of S_2 (preserved in muscovite-rich possible pumice clast; HWF) crenulated by weak, bifurcating S_3. Sample TH5-279, Central Thalanga. Crossed nicols.

(e) Photomicrograph of S_2 in altered footwall rhyolitic volcanics is locally crenulated by S_3. Both cleavages are defined by muscovite. Sample TH287-196, East Thalanga. Crossed nicols.

(f) S_3 has overprinted banding (alternating chalcopyrite and sphalerite bands), and is defined by preferentially oriented dark brown sphalerite. Banding was subparallel to S_2 and dipped steeply north. Sample (TH1) located at stratigraphic top of ore lens. C860 Stope, 20 225 mN, 20 400 mE, 860 mRL, Central Thalanga. Arrow points to facing direction.

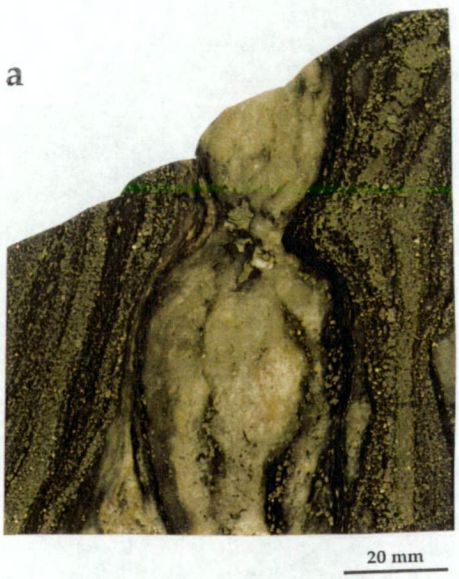
a
20 mm


b

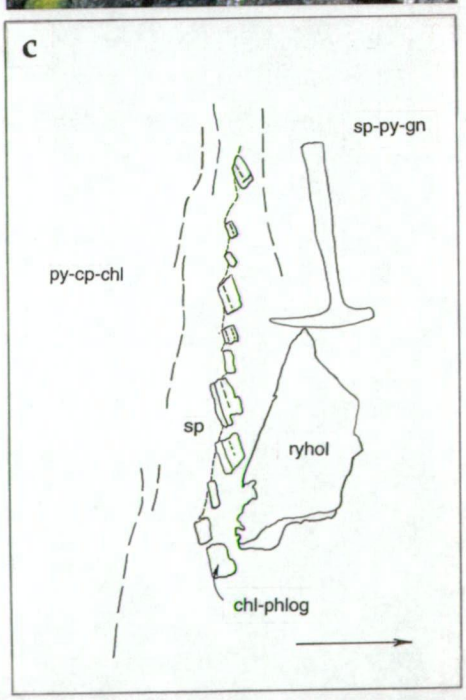
c
sp-py-gn
py-cp-chl
sp
ryhol
chl-phlog

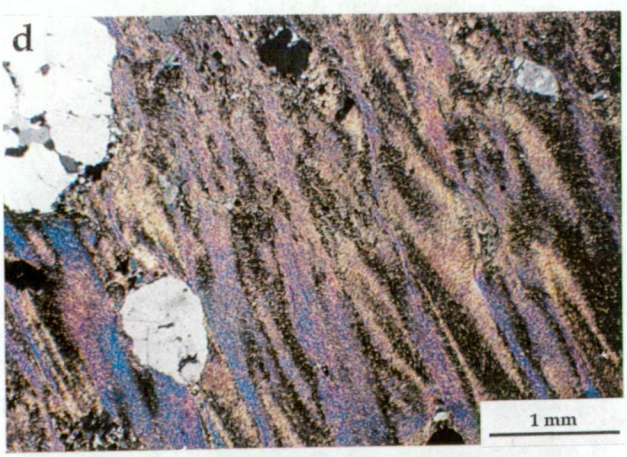
d
1 mm

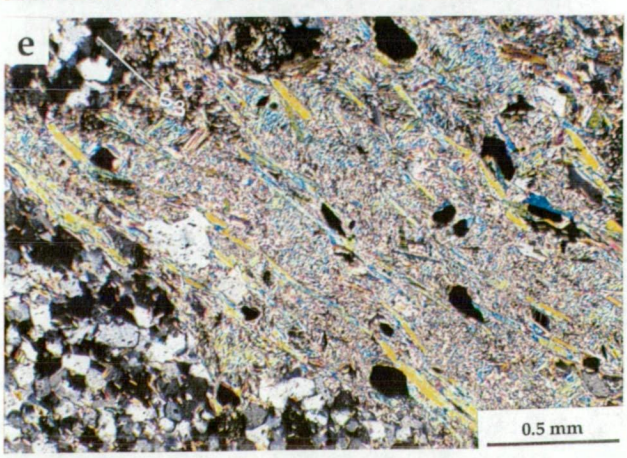
e
S_3
0.5 mm

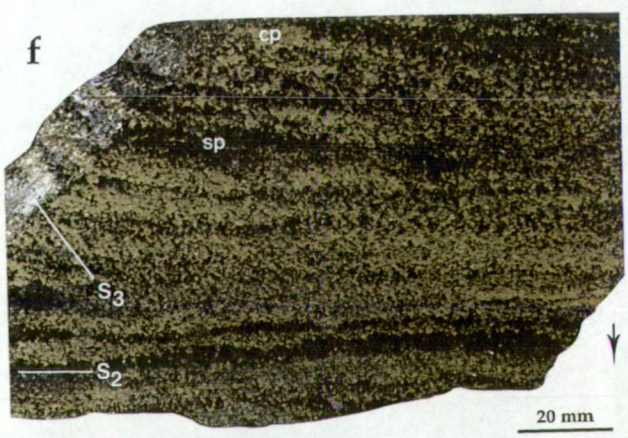
f
cp
sp
S_3
S_2
20 mm

chalcopyrite and sphalerite also fill dilation sites within these structures. In some cases the chlorite-phlogopite bands are less competent and are sheared between sulphide bands. The chlorite-phlogopite bands are interpreted as alteration assemblages formed prior to sulphide deposition (Chapter 11).

3.5 Pre-D_3 Structures

3.5.1 Open Folds

A long wavelength (λ < 10 km) kink is superposed on Thalanga, with bedding varying from steeply WNW-striking in West Thalanga, to steeply WSW-trends in East Thalanga (Fig. 3.7a,c). The fold axis is interpreted as subvertical and N-S trending. There is no axial planar cleavage associated with this kink, but this is reasonable with such an open fold (interlimb angle ~ 140°). S_2 cleavage is folded with bedding and sulphide banding (cf. Fig. 3.6, 3.7, 3.10), indicating that the open fold formed after D_2. Because E-W to ENE striking normal faults (interpreted to have formed during D_3; section 3.6) are subparallel to the ore horizon in East Thalanga, but cross-cut the ore horizon at larger angle in West and Central Thalanga, this open kink is interpreted to pre-date D_3.

Previous workers observed a spatial association between similar gentle folds and mineralisation elsewhere in the Mount Windsor subprovince (Laing, 1984; Wills, 1985). Berry (1991) suggested that alteration associated with mineralisation produces zones of weakness, and that the hinges of the open folds were focussed in these regions.

3.5.2 Brittle NNE-striking Normal Faults

There are two types of steep NNE-striking brittle structures at the Thalanga deposit (Fig. 3.13a,b). The earliest structures are normal faults that cause major offsets of the ore horizon, with west side down displacement. Whereas later (post-D_3; section 3.8.4) similarly oriented fractures have minor displacements and record strike-slip movement (Fig. 3.13b).

Subvertical, NNE-striking brittle faults are common along the Thalanga Range, where they form prominent lineations on aerial photographs. Laing (1984), Wills (1985), and Gregory *et al.* (1990) considered the NNE-striking faults to have caused major stratigraphic displacement at Thalanga, including the change in bedding orientation from West to East Thalanga. Laing (1984) identified dip-slip kinematic indicators on these faults at Thalanga and correlated then with similar trending normal faults throughout the Mount Windsor Province. He interpreted the NNE-striking faults as extensional normal faults involving

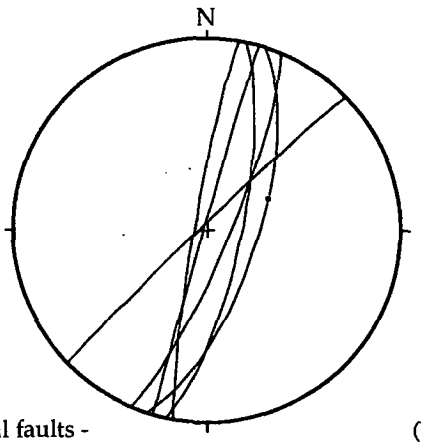

(a) Pre-D_3 normal faults - Central and West Thalanga.

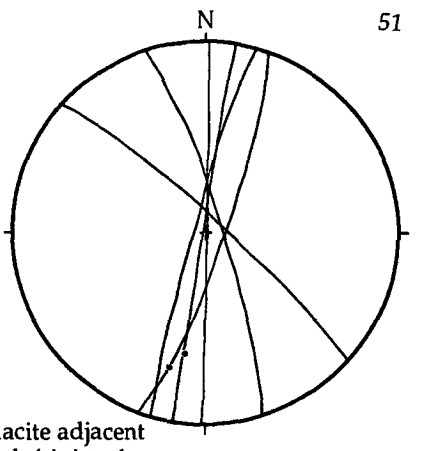

(b) Fractures in dacite adjacent to the Central Fault (sinistral movement).

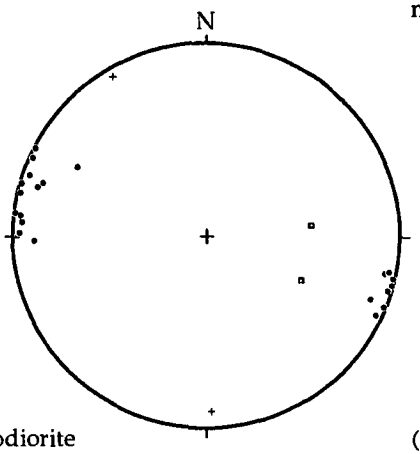

(c) Poles to microdiorite dykes from ▫ East, • Central, and + West Thalanga.

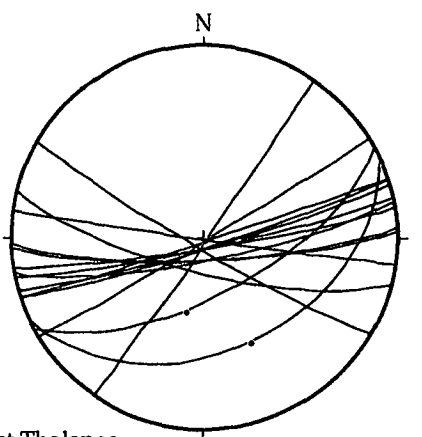

(d) D_3 faults - East Thalanga.

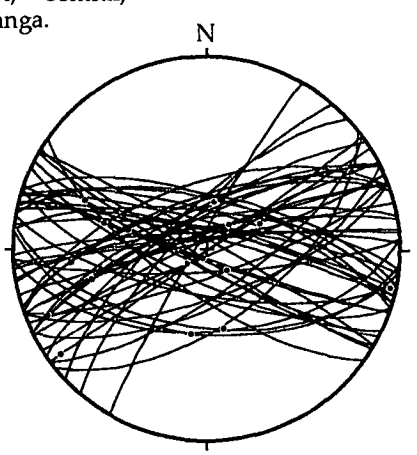

(e) D_3 faults - Central Thalanga.

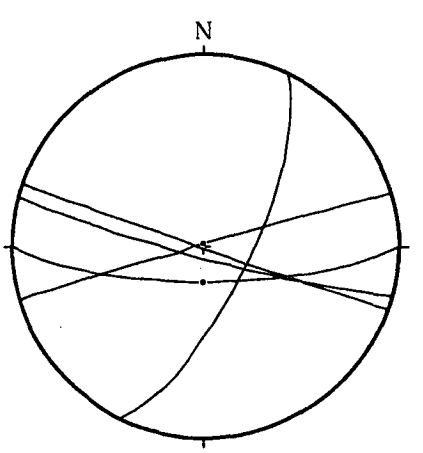

(f) D_3 faults - West Thalanga.

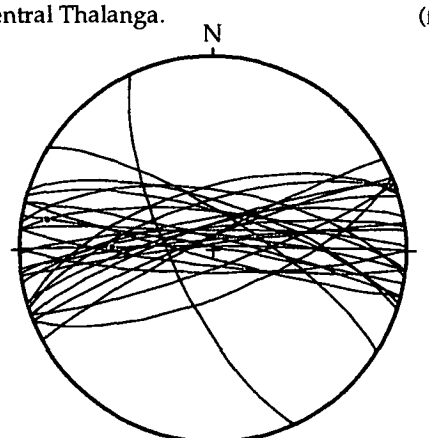

(g) Chlorite shears - Central Thalanga.

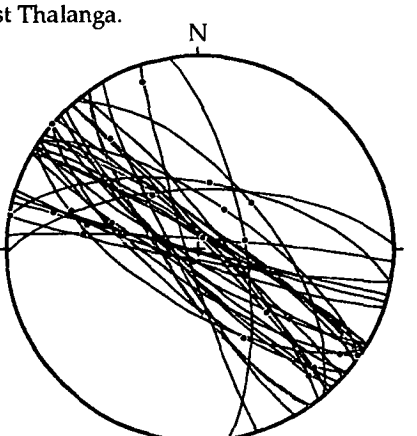

(h) Chlorite shears - West Thalanga. Quartz veins associated with shears in red.

Figure 3.13. Equal area stereonets of the main fault orientations and microdiorite dykes within the Thalanga deposit. Dyke measurements from West and East Thalanga are from the ore lenses, rather than the host volcanics, and reflect the rotation of the dyke fragments within the massive sulphides. Mineral fibres and striations on fault surfaces are depicted as dots.

mainly westerly down throw, although he recognised both strike-slip and normal displacement on faults in Central Thalanga.

The Central Fault is a sharply defined, chloritic, NNE-striking contact between dacite and massive sulphides at the western end of Central Thalanga (map M2-3). Dacite adjacent to the Central Fault in the open-pit is cross-cut by vertical, N- to NNE-striking brittle faults and close-spaced joints (Fig. 3.13b). Pyrite fibres on a surface within the fracture zone indicate sinistral movement, using criteria of Petit (1987), which is contrary to the dextral stratigraphic offset in plan view, and normal displacement in long section. The change in S_0 orientation, from WNW-striking on the west side of this fault, to E-W striking, and locally NNW-striking, on the east side of the Central Fault (map M2-3) is here interpreted to be due to younger, E-W to ENE-striking faults.

A NNE-striking fault with dip-slip kinematic indicators terminates the ore horizon at the western end of W780W Stope at 19 980 mE in West Thalanga (map M5). Calcite fibres and shear bands along the contact between dacite and massive sulphides indicate west side down movement along the fault. A similarly oriented brittle fault has truncated the massive sulphide lens, but has been later cross-cut by a bedding-parallel fault in the W690 Stope at 20 150 mE in West Thalanga (map M9). Gregory *et al.* (1990) considered that a NNE-striking normal fault (the East Fault) at the eastern limit of the Central Thalanga caused the main change in stratigraphic orientation, but such a fault is difficult to locate despite the number of drill holes in the area. ENE-striking faults are exposed in the open pit in this location (map M2 and M4a).

NNE-striking normal faults are interpreted here to be responsible for the separation of West and Central Thalanga. However, the timing of NNE-striking normal faults with respect to the open, N-S trending fold is uncertain. If the NNE-striking faults and microdiorite dykes (see below) are similar in age, then the consistent orientation of microdiorite dykes in East and West Thalanga indicates that dyke intrusion, and therefore normal faulting, post-dates the open fold.

3.5.3 Microdiorite Dykes

Vertical, N- to NE-striking microdiorite dykes (Fig. 3.13c), typically 0.5 -1 m wide, have transgressed all stratigraphic contacts at Thalanga. Exposures in the Central Thalanga open pit show that the microdiorite dykes have irregular to wavy margins, rather than pinch and swell structures documented by Wills (1985).

The microdiorite dykes are generally unfoliated and therefore must post-date D_2. Laing (1984) suggested that such a post-tectonic age for the dykes would correlate with intrusion of

the Ravenswood Granodiorite. Indeed, Wills (1985) regarded the microdiorite dykes as apophyses of the Ravenswood Granodiorite. However, Berry *et al.* (1992) suggested that Middle Ordovician granitoid intrusion pre-dated D_2 in the Mount Windsor subprovince, and this indicates that microdiorite intrusion is unrelated to the Middle Ordovician granitoids.

The consistent orientation of the microdiorite dykes from West to East Thalanga (Fig. 3.13c), is evidence that microdiorite intrusion must post-date formation of the gentle fold in stratigraphy from West to East Thalanga. The similarity of the microdiorite dyke orientation to NNE-striking brittle normal faults suggests both structures are closely related. The NNE-striking brittle faults probably pre-date the dykes, with these zones of weakness exploited during microdiorite intrusion. Local S_3 cleavage in the microdiorite is developed adjacent to normal faults, which offset the dykes, supporting the interpretation that the age of the microdiorite intrusions is pre-D_3.

3.6 D_3 Structures

3.6.1 S_3 Cleavage

A second spaced cleavage (S_3), present in rocks close to similarly oriented normal faults, is steeply dipping and strikes E-W to ENE (cf. Fig. 3.7b,d,f,h). S_3 is consistently oriented in the vicinity of the Thalanga deposit, and is always 30-45° anticlockwise of S_2, but locally clockwise from S_2 in East Thalanga. S_3 is most prominent in the phyllosilicate-rich units, where it occurs as a weak bifurcating crenulation cleavage (Fig. 3.12d,e). However, in phyllosilicate-rich units adjacent to normal faults, S_3 has completely overprinted the S_2 cleavage. S_3 has overprinted the banded chalcopyrite-dark brown sphalerite at the contact between massive sulphide and dacite in Central Thalanga, where it is weakly defined by the preferred orientation of sphalerite (Fig. 3.12f). S_3 is strong in most parts of East Thalanga due to the normal faults subparallel to stratigraphy and concentrated in or near the ore horizon.

Pressure shadows parallel to S_3 around phenocrysts and porphyroblasts are present in places, and are filled with recrystallised quartz, biotite, and locally, sphalerite (Fig. 3.14a,b). In places, quartz-filled pressure shadows have formed by two stages of growth parallel to both S_2 and S_3. For example, quartz fibre pressure shadows around pyrite grains, that are elongated parallel to S_2, are curved and parallel S_3, suggesting that quartz filled the pressure shadows during D_2 and was partly crenulated by S_3 (Fig. 3.14c,d). Both the quartz and pyrite in Figure 3.14(c,d) have been strongly recrystallised after cleavage formation (see section 3.10.6). Chlorite-biotite spots, common in the siltstone facies of the HWF (Chapter 4), are flattened in S_3 in most parts of Thalanga (Fig. 3.14e).

Figure 3.14 Microtextures associated with S_3 and fault structures inferred to be associated with ENE-striking normal faults.

(a) Photomicrograph of moderatedly quartz-muscovite-pyrite-rich rhyolitic volcanics from the immediate footwall of massive sulphides. S_3 cleavage is deflected around an altered felspar crystal, and recrystallised quartz and sphalerite are present in the pressure shadows. S_2 is crenulated by S_3. Elsewhere on this thin section, euhedral pyrite overgrows S_2 and is rarely elongate on S_3. Sample TH291-121.9, East Thalanga. Plane light.

(b) Sample in (a) under crossed nicols.

(c) Photomicrograph of elongated pyrite euhedra, with quartz-filled pressure shadows, in a matrix of fine grained muscovite and phlogopite. Pyrite is elongate parallel to S_2 and the quartz fibres in pressure shadows are curved and parallel to S_3, and have been strongly recrystallised. Locally, coarse grained phlogopite occurs in the pressure shadows. Sample TH238-114.5, adjacent to inferred D_3 fault in Central Thalanga. Plane light.

(d) Sample in (c) under crossed nicols.

(e) Asymmetric folds in banding and possible pumiceous clasts, with axial planes parallel to S_3. Weakly elongate chlorite spots are also parallel to S_3. Sample TH321-162, Vomacka Zone.

(f) Albite-quartz vein at inferred location of E-W to ENE-trending normal fault in dacite. Veins of quartz>albite, with traces of pyrite, occur in dacite adjacent to the vein. Sample C2037NH00-24.7, Central Thalanga.

(g) *Durchbewegung* textures in chalcopyrite-rich fault zone within the ore horizon. Irregularly folded clasts of chlorite-phlogopite occur in massive chalcopyrite, with minor dark, red-brown sphalerite and pyrite. Sample C2039NI25-28, Central Thalanga.

(h) Shallow-dipping quartz extension vein (see section 3.4.4) within rhyolitic volcanics truncated by E-W to ENE-trending normal fault. Location: E779 Stope access, East Thalanga, 30 455 mN, 32 065 mE, 779 mRL. Rule is 10 cm in length.

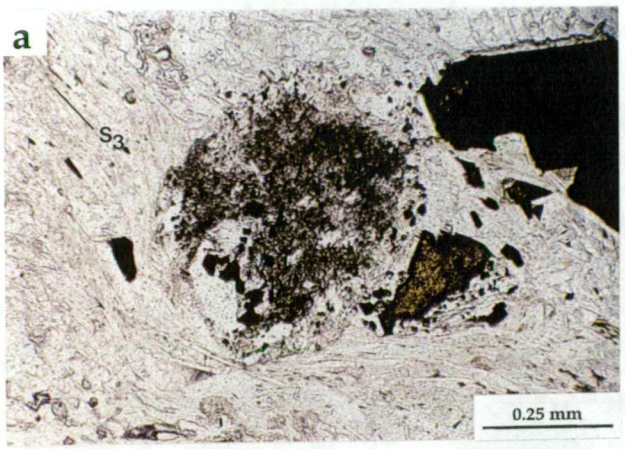
a
S_3
0.25 mm

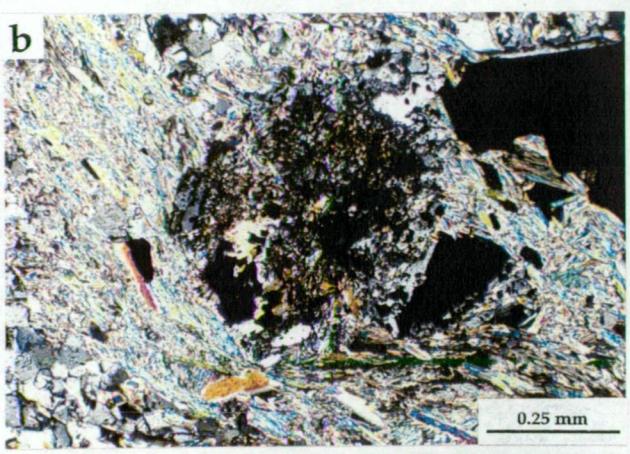
b
0.25 mm

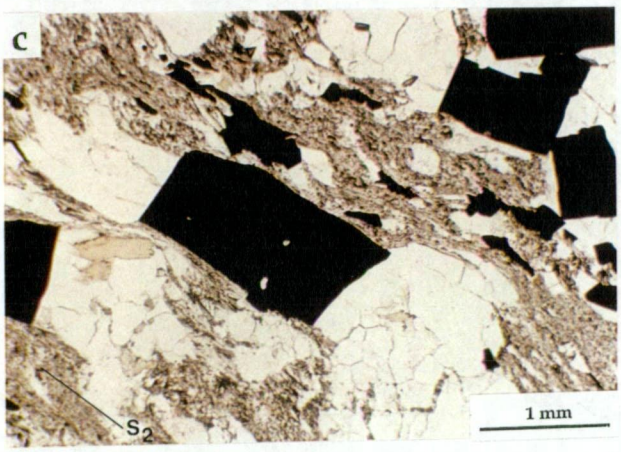
c
S_2
1 mm

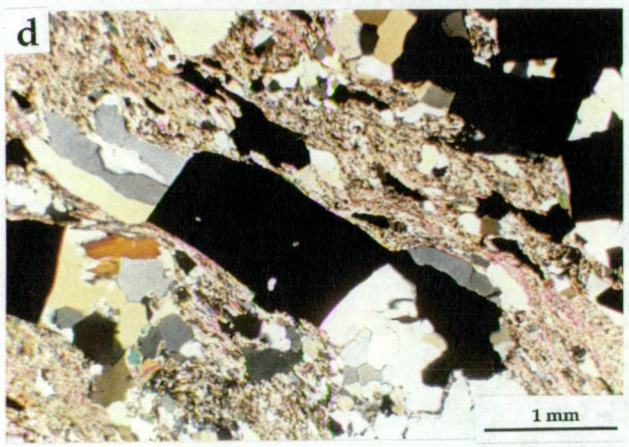
d
1 mm


e
S_3
10 mm


f
qz
alb-qz
20 mm


g
chl-phlog
cp-sp-py
20 mm


h
qz

3.6.2 Intersection Lineations

Laing (1984) and Gregory *et al.* (1990) noted a crenulation lineation subparallel to the mineral stretching lineation, and this is interpreted here to be a S_2/S_3 intersection lineation. Mineral intersection lineations are prominent at Waddys Mill (13 km northwest of Thalanga), where S_2/S_3 intersection lineations and elongated rhyolite clasts plunge steeply southeast (Berry, 1989; Berry *et al.*, 1992).

3.6.3 ENE-striking Normal Faults

Steeply dipping, E-W to NE-striking faults (named ENE-striking faults in this discussion) occur subparallel to the ore horizon in East Thalanga and offset the ore horizon in West and Central Thalanga (Fig. 3.13d-f, and maps M2-12). Despite the apparent dextral offset of the stratigraphy in plan view (maps M2-12), shear bands in volcaniclastic units adjacent to these faults indicate normal, south side up movement along the fault, as do rare early dip-slip striations on chloritic fault surfaces. South-dipping Riedel shears in a 1-2 m wide, ENE-striking, close-spaced fracture zone in the East Thalanga footwall (inferred to be a fault) also support south side up movement. Vertical displacement of up to 150 m is inferred for these ENE-striking faults. Subhorizontal striations in fault gouge and chloritic surfaces, and asymmetric quartz fibres, in the sense of Petit (1987), along some ENE-striking faults indicate late-stage sinistral strike-slip movement along these faults. The similarity between the orientation of these faults and the S_3 cleavage, together with the increase in intensity of S_3 close to the ENE-striking faults, suggests that S_3 was contemporaneous with ENE-striking normal faulting. The brittle characteristics of some ENE-striking faults (see below) may be the result of post-S_3 movement along the fault.

The ENE-striking normal faults strike NE in the hangingwall of the ore horizon, whereas in the footwall the same fault strikes more ENE to E-W (map M2), suggesting refraction due to differences in phyllosilicate abundance. In Central and West Thalanga, E-W to SE-striking chlorite shears within the ore horizon are parallel to the stratigraphy and 30-50° clockwise of the ENE-striking normal faults (Fig. 3.13g,h). These chlorite shears anastomose with the ENE-striking normal faults and are therefore interpreted to be the same age.

The ENE-striking normal faults are sinuous in plan view (maps M2-12) and are present as zones of intense fracturing, brecciation, fault gouge, chloritic shears, and/or quartz veins in the host rock. Both the ENE-striking normal fault boundaries and displacement of stratigraphy are typically sharp. Where present within the ore horizon and phyllosilicate-rich units, the ENE-striking faults appear ductile in style, whereas in silicified rhyolite and dacite, the same fault is brittle in style (Table 3.1).

Table 3.1 Description of D_3 faults in common lithologies at Thalanga.

Rock type	Manifestation of fault
Dacite	• fault breccia and fault gouge with intensely fractured dacite, • quartz vein(s) ± albite and silicification halo (**Fig.** 3.14f)
Andesite	• strong chlorite alteration, • close-spaced joints and fractures in <2 m wide zone
Hangingwall fragmental (HWF)	• strong foliation, with fault gouge in cleavage partings, close-spaced joints
Massive sulphides	• close-spaced joints and friable or porous massive sulphides or massive pyrite • vein quartz ± remobilised cp-sp • coarse chalcopyrite ± bands of sphalerite and minor magnetite, • *Durchbewegung* texture (**Fig.** 3.14g) • chlorite shears <1 m wide
Chlorite schist	• strongly foliated, overprinted by brittle fractures ± quartz veins
Rhyolitic volcanics (muscovite-chlorite ± pyrite-rich)	• strong cleavage with minor recrystallised cubic pyrite, fault gouge in cleavage partings
Rhyolitic volcanics (quartz-muscovite ± pyrite- or quartz-rich)	• ≤1 m wide zone of fault gouge and close-spaced fractures (**Fig.** 3.14h)

Zones of intense foliation and minor shearing mark the ENE-striking normal faults in the HWF, massive sulphides, chlorite schists, and strongly muscovite-chlorite-rich domains within the footwall rhyolitic volcanics (Table 3.1), and these are commonly overprinted by brittle fault gouge or brecciation. Where ENE-striking normal faults define lithological contacts, the contact is sharp, chloritic in some cases, and associated with close-spaced joints or strongly developed spaced cleavage adjacent to the fault. Areas enriched in muscovite and chlorite in the footwall rhyolitic volcanics are interpreted to have been preferentially deformed during formation of the ENE-striking normal faults, and display pervasive cleavage (S_3) parallel to faults (cf. Fig. 3.7f with 3.13e). Rocks adjacent to quartz veins along ENE-striking normal faults are moderately enriched in muscovite or quartz.

Shallowly-dipping quartz-filled extension veins, interpreted to have formed during D_2 (section 3.4.4), are truncated by the ENE-striking normal faults (Fig. 3.14h). Sharp changes in the orientation of S_2 and sulphide banding within the ore horizon occur close to the ENE-striking normal faults, and are evidence that the ENE-striking normal faults must post-date D_2. S_2 is also cross-cut by chalcopyrite-filled normal faults in places. The ENE-striking normal faults are subparallel to the ore horizon in East Thalanga (cf. Fig. 3.6c with **Fig.** 3.13d), but cross-cut stratigraphy in West and Central Thalanga (maps M2-10). Therefore, the ENE-striking normal faults are interpreted to post-date the change in stratigraphic orientation from West to East Thalanga. Comparison with S_3 cleavages and other NE to ENE-striking faults measured by Berry (1989, 1990) and Berry *et al.* (1992) elsewhere in the Mount Windsor volcanic belt, suggests that these ENE-striking normal faults at Thalanga are D_3 in age.

Normal Faults in Central and West Thalanga

D_3 faults are most prominent in Central Thalanga, where at least fifteen E-W to NE-striking normal faults are interpreted to cross-cut the ore horizon at 950 mRL (map M2-4). These faults have an important control on the location of massive sulphides in Central Thalanga, with the thickest massive sulphides formed by local structural stacking of the ore horizon (Fig. 3.15). Adjacent to some D_3 faults the massive sulphides may also be thickened by folding (e.g. fault 7, map M4a) and remobilised chalcopyrite, sphalerite and galena occupying sites of dilation. The ore horizon in West and Central Thalanga is truncated at depth and to the east by D_3 faults (Fig. 3.1, Fig. 3.15). The ore lens (and non-mineralised ore position) is repeated into the hangingwall along these faults (Fig. 3.1, Fig. 3.15). Barite-rich sulphides adjacent to a D_3 normal fault in the hangingwall of the Central Thalanga ore lens are interpreted to have been a distal part of the ore lens (as barite typically forms at the margins of massive sulphide deposits; Chapter 6; see also Large, 1992), that was faulted into its current position. Banding in these barite-rich sulphides (defined by sphalerite and pyrite bands) is subparallel to the D_3 fault (cf. Fig. 3.10f and Fig. 3.13e; map M4c).

Slices of HWF within the dacite in the open pit of Central Thalanga are parallel to D_3 faults (map M2). HWF <20 m thick adjacent to fault 12 in Central Thalanga is enigmatic as all other intersections of HWF are typically <10 m in thickness (map M2 and M4a). The large thickness of HWF adjacent to fault 12 may reflect depositional thickness and indicate a topographic basin in this location. Alternatively the thickness of HWF may be accentuated if fault 12 dips more shallowly in this location.

In West Thalanga there are fewer D_3 faults than in Central Thalanga, but a major normal fault (fault B) marks the eastern limit of the West Thalanga ore lens (Fig. 3.1 and Fig. 3.2a-f). This normal fault (fault B) intersects the pre-D_3 Central Fault between 20 310 mE and 20 330 mE, and at about 780 mRL (Fig. 3.2a,b), and is interpreted to accentuate the offset of the ore horizon between West and Central Thalanga.

The normal fault A (Fig. 3.1 and Fig. 3.2) offsets and repeats the ore horizon at approximately 20 170 mE in West Thalanga (see also maps M6-10). On some levels this D_3 fault does not extend into the dacite, occupying the contact between the ore horizon and dacite instead. Commonly, in these locations an earlier NNE-striking normal fault marks the contact between the ore horizon and the dacite (map M9). Repetition of the ore horizon to the south of the main ore lens in West Thalanga occurs along D_3 normal faults (Fig. 3.1). Stratigraphy is shallowly dipping between the main faults (Fig. 3.1), suggesting that this may be a large-scale parasitic fold on F_2, accentuated and faulted during D_3.

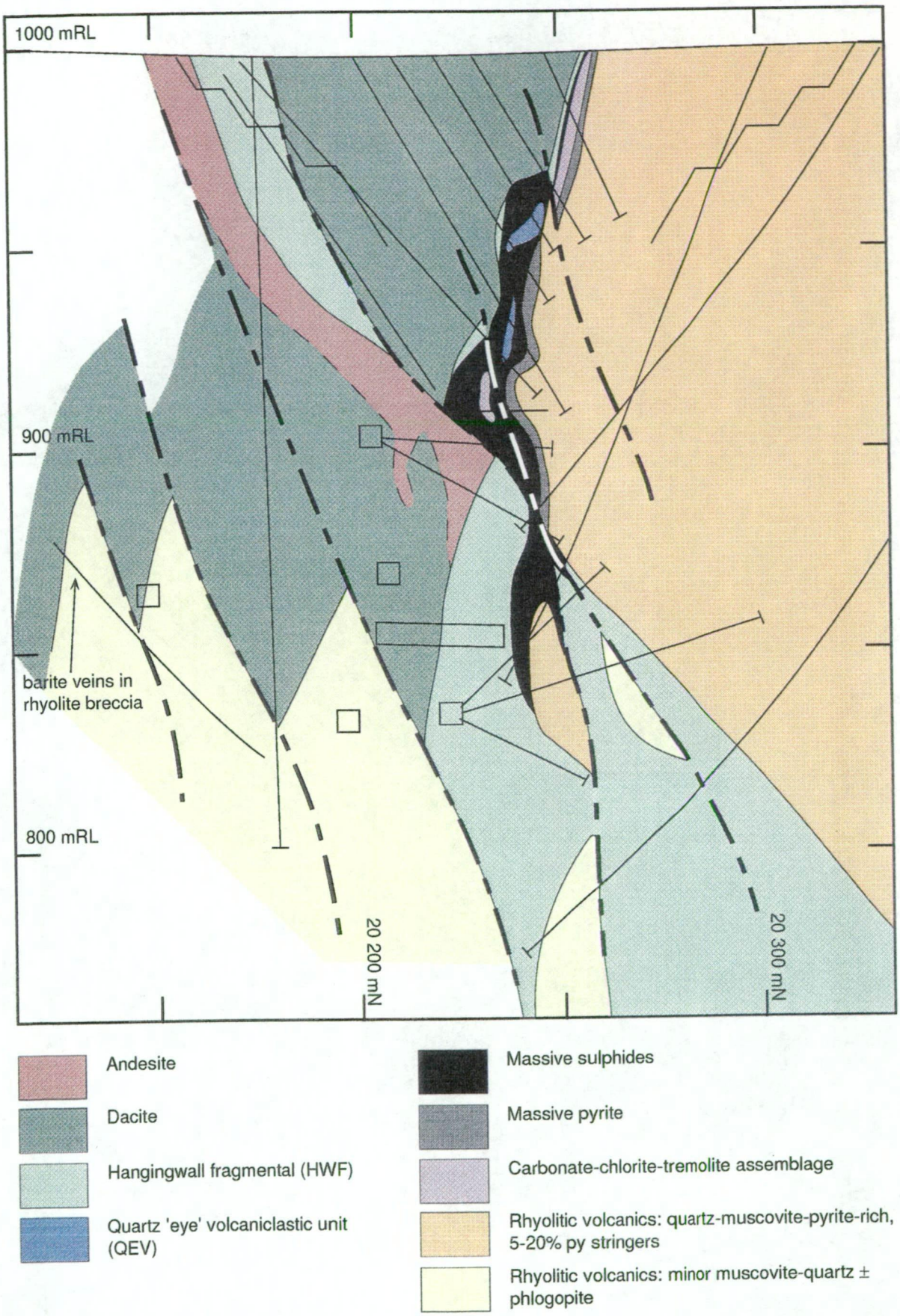

Figure 3.15 Cross section along 20 450 mE in Central Thalanga showing the truncation and repetition of the ore horizon along steeply-dipping normal faults.

Normal Faults in East Thalanga and the Vomacka Zone

At East Thalanga, the E-W to NE-striking D_3 normal faults are parallel with the stratigraphy in places (cf. Fig. 3.6c with Fig. 3.13d) and are typically located at lithological or alteration contacts. For example, in the E779 Stope (map M11) a D_3 fault defines the contact between the footwall ore lens and the overlying QEV between 31 950 mE and 32 000 mE, but also terminates the QEV and massive sulphides at 31 950 mE. In other parts of East Thalanga, D_3 faults may thicken the massive sulphides by repetition of the ore horizon.

The footwall ore lens and footwall rhyolitic volcanics in East Thalanga may have been offset along a D_3 normal fault (fault X; Fig. 3.16), which is interpreted to extend into the footwall along the chlorite ± tremolite-rich, fractured contact between the intensely silicified rhyolite and the quartz-muscovite ± pyrite-rich rhyolitic volcanics (Fig. 3.16). However, analysis of the volcanic facies suggests that the present geometry may be similar to the primary depositional geometry, with the thickness of QEV units increasing up-dip (Chapter 4). Furthermore, the footwall lens may have originally been discontinuous where it overlies intensely silicified rhyolitic volcanics (Chapter 4, 6, and 10). Fault X may therefore have only accentuated the primary lateral and vertical differences in composition of the ore horizon. The presence of QEV between the intensely silicified rhyolite and quartz-muscovite ± pyrite-rich rhyolitic volcanics on some cross-sections is best explained by a normal D_3 fault. The lack of QEV and massive sulphide lenses down-dip in East Thalanga may also be due to truncation of the ore horizon by a normal fault.

In the Vomacka Zone, 1-2 m wide zones of strongly sheared chlorite or close-spaced fractures and fault gouge that offset the ore horizon are interpreted to be D_3 normal faults. Locally, similar brittle fault zones may have overprinted faults associated with F_2 folds (Fig. 3.8, and 3.9). The lack of massive sulphide lenses between Central Thalanga and the Vomacka Zone may be partly due to the ENE-striking normal faults intersecting similarly oriented ore lenses in this location.

Shearing within the Ore Horizon

Wills (1985) noted that shearing is common along lithological contacts within the ore horizon at Thalanga. South side up movement is recorded at most contacts. HWF adjacent to D_3 faults is strongly foliated, with cleavage (S_3) parallel to the fault. Slight asymmetry to the cleavage wrapping around elongate volcanic clasts supports normal, south side up shearing within the HWF adjacent to the D_3 faults. Pressure shadows around quartz and feldspar crystals in QFP and QEV units at Thalanga are also slightly asymmetric and indicate south side up shearing. Fine grained sulphide veins and bands within carbonate-chlorite alteration, in the West and Central Thalanga ore lenses, display geometries indicative of

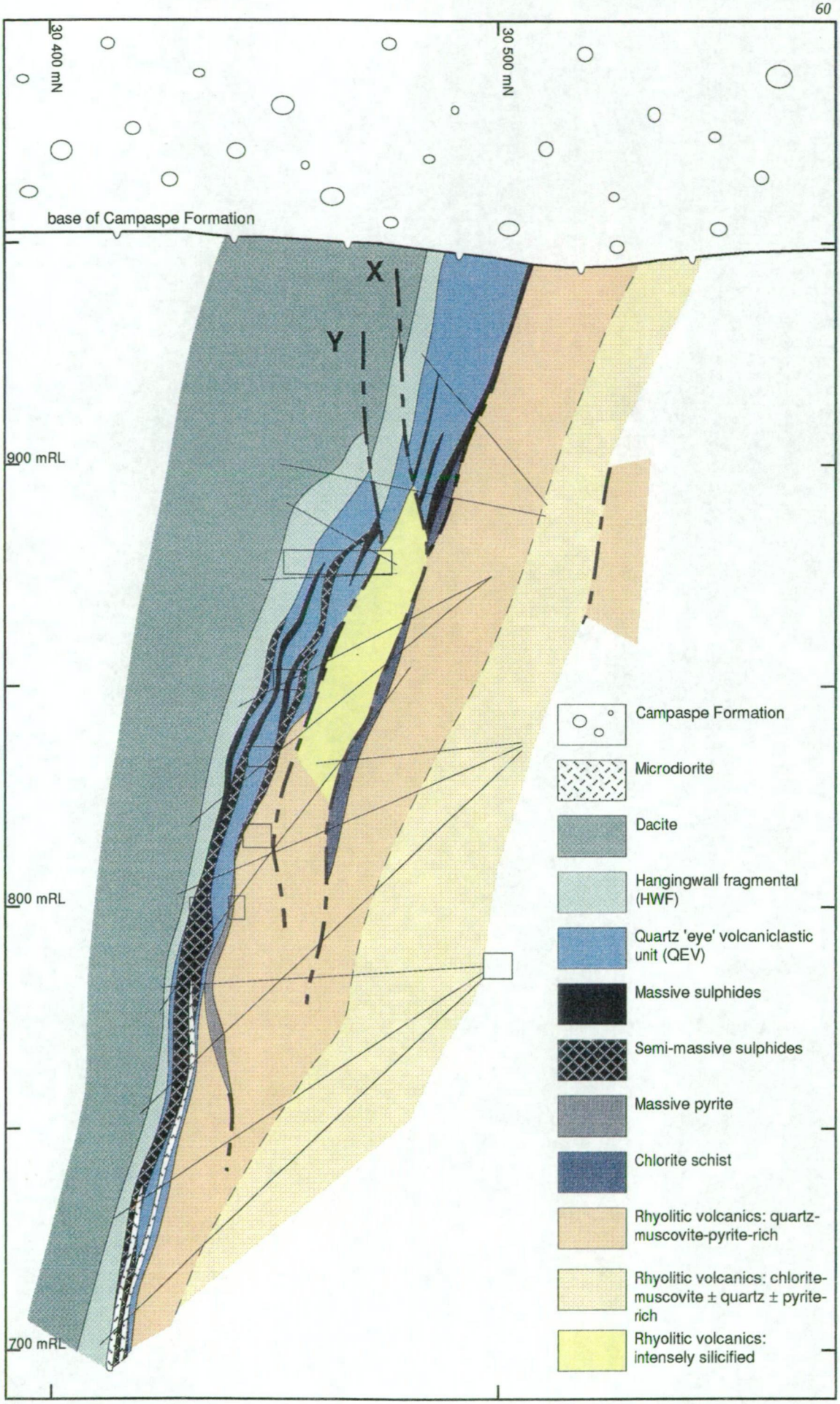

Figure 3.16 Cross section along 31 980 mE in East Thalanga.

ductile shearing within the ore horizon, with hangingwall lithologies displaced vertically with respect to the footwall lithologies (Fig. 3.17a-d). This south side up displacement is consistent with having formed contemporaneously with D_3 normal faults.

Typically, cross-cutting microdiorites are disrupted within the ore horizon (Fig. 3.17e), and coarse chalcopyrite-rich sulphides vein or envelope dyke fragments within the ore lenses. Banding within the sulphides adjoining rotated blocks of microdiorite is generally disrupted and overprinted by chalcopyrite. Shearing concentrated along the relatively ductile sulphide horizon at Thalanga is interpreted to have caused the dislocation of microdiorite dykes. Similar shearing along the sulphide horizon at the Sullivan deposit in Canada deformed cross-cutting gabbro dykes, resulting in blocks of gabbro isolated within massive sulphides (McClay, 1983).

3.7 Remobilised Sulphides

3.7.1 Description and Distribution

Coarse-grained (up to 5 mm) massive chalcopyrite, banded chalcopyrite and minor sphalerite ± traces of pyrite ± quartz and rare chlorite, or rarely massive dark red-brown sphalerite with minor to traces of galena have overprinted the ore lenses and their hangingwall contact in places (Fig. 3.17f and Fig. 3.18a,b). Given the spatial association between the ore lenses and the overprinting chalcopyrite-rich sulphides, and the association of massive chalcopyrite with extensional structures (Table 3.2), the chalcopyrite-rich sulphides are interpreted to have been remobilised from the pre-existing sulphide lenses.

Table 3.2 Location of remobilised sulphides within the ore horizon at Thalanga.

Sulphide	Location of sulphide	Interpretation
chalcopyrite	along shear bands in chlorite-rich alteration, especially at lithological contacts (e.g. map M5)	shearing within chlorite-rich alteration
chalcopyrite & minor sphalerite	along joints and in piercement veins and cusps at contact between massive sulphides and dacite or HWF, cross-cut by S_3(Fig. 3.18a,b)	extension of dacite or HWF at contact with massive sulphides (see below)
chalcopyrite & trace sphalerite	within massive sulphide lenses (*Durchbewegung* texture; cf. Marshall and Gilligan, 1989)	location of ENE-striking normal fault (see Table 3.1 and Fig. 3.14g)
chalcopyrite or sphalerite & galena	in veins parallel to and cross-cutting S_3 in the QEV (map M11)	replacement of QEV along S_3
galena	in pressure shadows around clasts in the footwall lens and QEV in East Thalanga	vertical extension of ore horizon
chalcopyrite or chalcopyrite-sphalerite-galena	shallowly-dipping, discontinuous veins at footwall contact of sulphide lenses (Fig. 3.18c,d and Fig. 3.19a)	tension gashes, formed by the vertical extension of the stratigraphic top of the footwall

Figure 3.17 Evidence of shearing within the ore horizon, and sites of chalcopyrite-rich remobilised sulphides.

(a) Lenses of chlorite, with minor tremolite, within the massive to banded sulphides preserve evidence of hangingwall side up shearing. Location: West Thalanga, W780 Stope, 20 305 mN, 20 237 mE. Hammer is 30 cm in length. Facing to right.

(b) Sketch of (a).

(c) Inclusion of chlorite, with minor tremolite and sulphide bands, within massive to banded sulphides. The sulphide bands within the chlorite inclusion are interpreted to indicate hangingwall side up shearing. Location: West Thalanga, W722 Stope. Magnet is 12 cm in length. Facing to right.

(d) Sketch of (c).

(e) Massive sulphide lens containing blocky, partly rotated clasts of microdiorite. Abundant chalcopyrite envelopes the microdiorite dyke fragments. Location: W747 Stope, West Thalanga. Facing to right.

(f) Piercement vein (filled with chalcopyrite) at the contact between dacite and the massive sulphides. Veins is about 2 m in length and the dacite has been overprinted by quartz-epidote veins. Chalcopyrite-rich sulphides, with bands of dark red-brown sphalerite, occur between the piercement vein and the stratigraphically underlying banded to massive polymetallic sulphides. C860 Stope, 882 mRL, Central Thalanga. Facing is into the photograph.


a

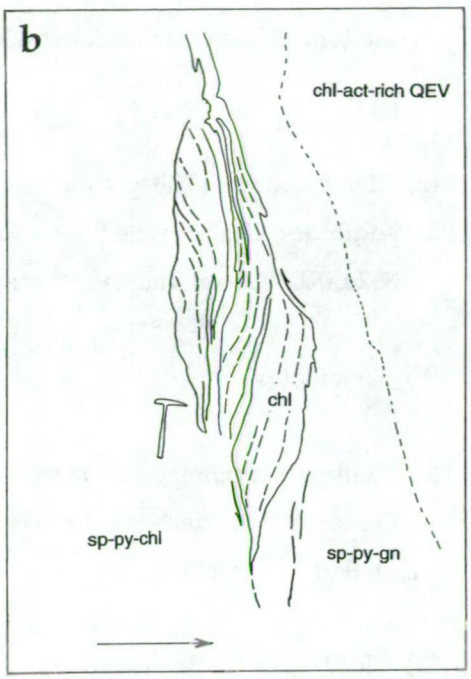
b
chl-act-rich QEV
chl
sp-py-chl
sp-py-gn


c

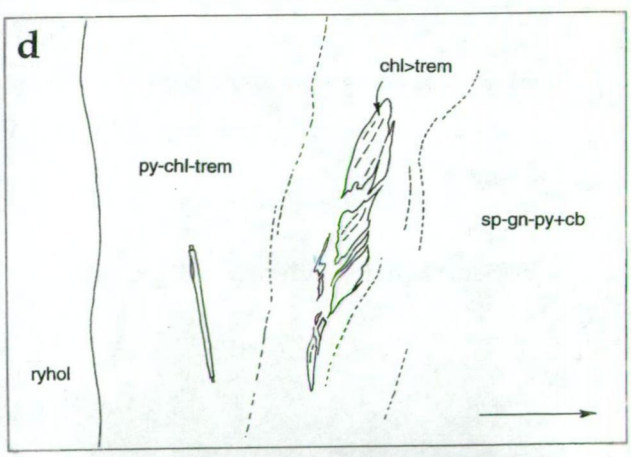
d
chl>trem
py-chl-trem
sp-gn-py+cb
ryhol

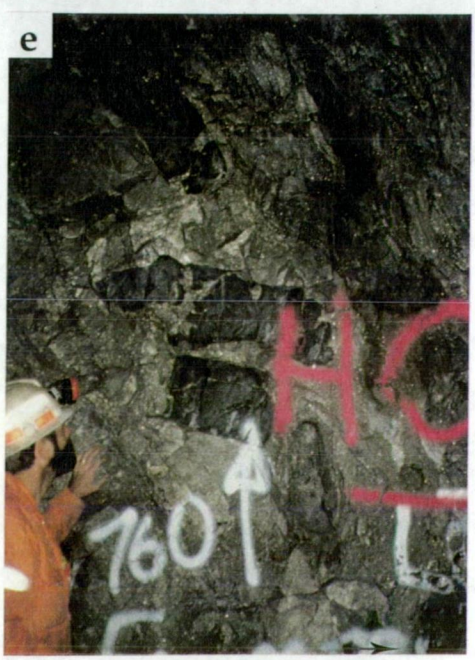
e
760


f
cp - sp
da
da

Figure 3.18 Structures associated with remobilised sulphides at Thalanga.

(a) Piercement vein (filled with chalcopyrite) at the contact between dacite and the massive sulphides. Chalcopyrite has locally replaced along fractures in dacite (arrow). C860 Stope, 882 mRL, Central Thalanga. Facing is into the photograph.

(b) Sketch of (a).

(c) Shallowly-dipping chalcopyrite-filled tension gashes in the footwall rhyolitic volcanics immediately underlying the massive sulphide lens. Location: C860 Stope (right), Central Thalanga. Facing to right.

(d) Close-up of (c). Pen is about 14 cm in length.

(e) Photomicrograph of chalcopyrite in pressure shadow (parallel to S_3) around euhedral pyrite in the graded sandstone facies of the QEV. Sample E3198SI30-10.9, East Thalanga. Reflected light.

(f) Sample in (e) under plane light.


a

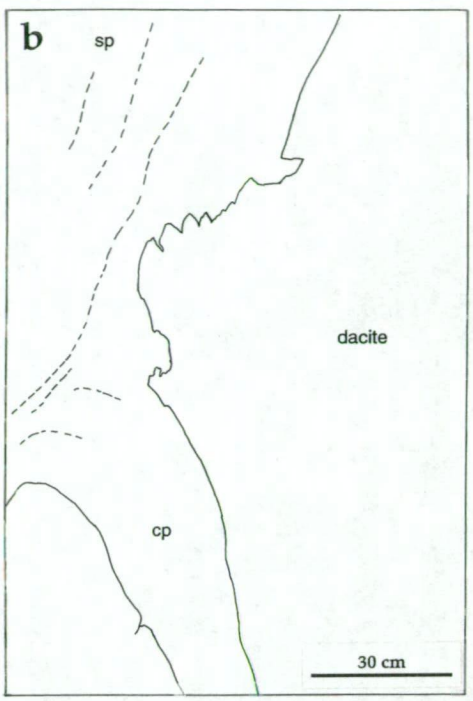
b
sp
dacite
cp
30 cm


c


d

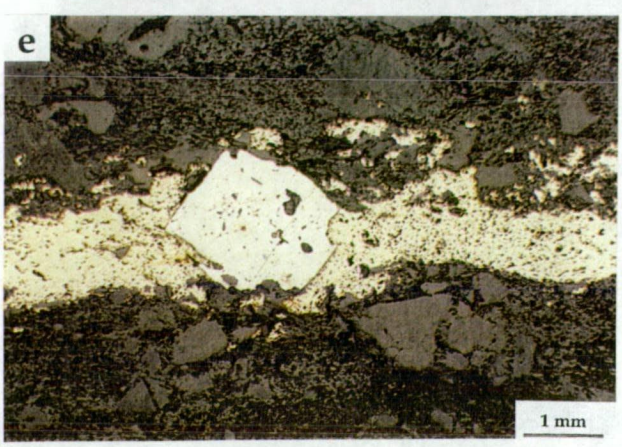
e
1 mm

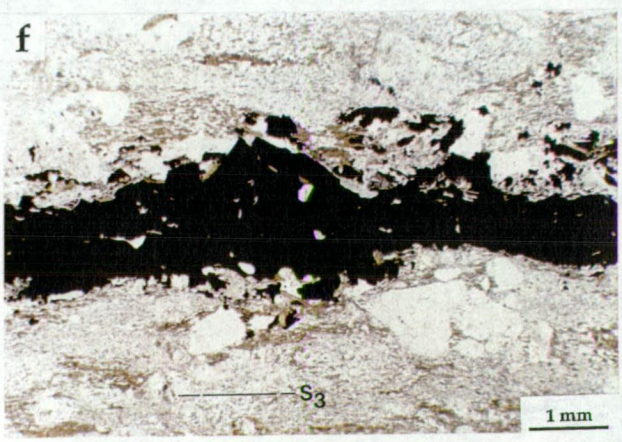
f
S3
1 mm

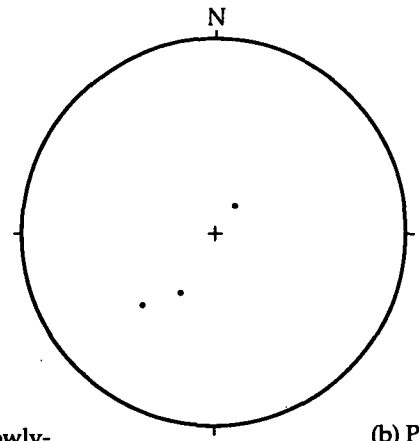

(a) Poles to shallowly-dipping chalcopyrite veins.

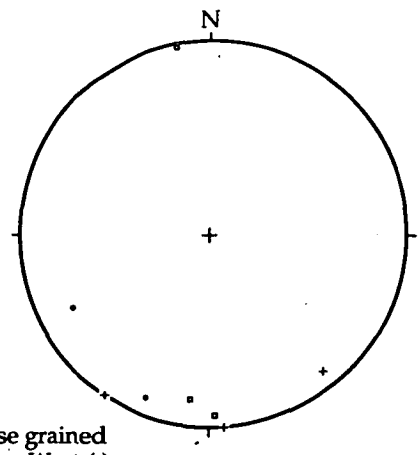

(b) Poles to coarse grained cp ± sp veins from West (+), Central (•), and East Thalanga (▫).

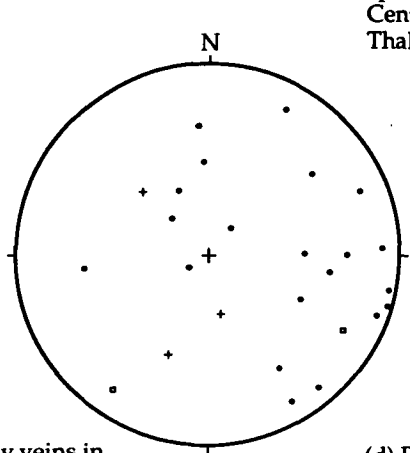

(c) Poles to qz>>py veins in West (+), Central (•), and East (▫) Thalanga.

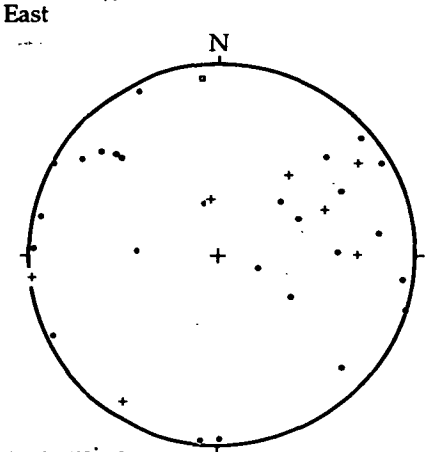

(d) Poles to barren qz veins in West (+), Central (•), and East (▫) Thalanga.

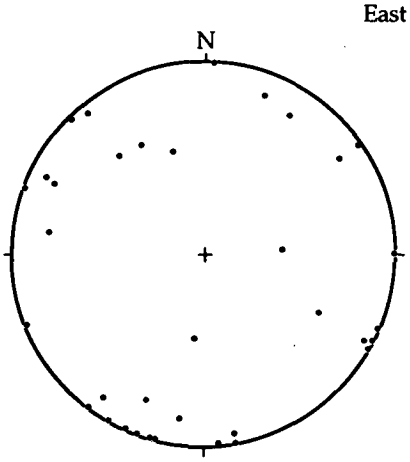

(e) Poles to barren qz veins from the Thalanga Range.

Figure 3.19 Equal area stereonets of (a-b) coarse grained chalcopyrite (cp) ± sphalerite (sp) veins, and (c-e) quartz (qz) ± pyrite (py) veins from Thalanga and the Thalanga Range.

The chalcopyrite-rich sulphides are typically present adjacent to or along normal faults and the S_3 cleavage in the footwall, ore lenses and hangingwall. Coarse grained chalcopyrite- or sphalerite-rich veins vary from steeply, NE-striking, to steeply E and SE striking (Fig. 3.19b). Pyrite and chalcopyrite veins in the footwall rhyolitic volcanics are parallel to S_3 only immediately adjacent to ENE-striking normal faults. Examples of remobilised sulphides are listed in Table 3.2.

Coarse milky quartz veins are commonly associated with the remobilised sulphides, particularly where sulphides form piercement veins into the dacite. In places, this quartz is intergrown with coarse albite (<1 cm grain size) and fine grained green chlorite (<0.03 mm grain size). In thin section, the quartz contains abundant two-phase fluid inclusions and has undulose extinction, and the chlorite has no preferred orientation and anomalous blue interference colours under crossed nicols. There is a distinct mineralogical zonation of the quartz-sulphide veins, with coarse quartz ± albite at the vein margins, then intergrown quartz and chlorite, a thin band of <2 mm sized sphalerite with minor chalcopyrite inclusions and rare interstitial galena, and then massive chalcopyrite with minor sphalerite bands. The sphalerite banding is parallel to the vein margins. Traces of arsenopyrite are disseminated in the massive chalcopyrite, together with rare quartz and chlorite gangue.

Sulphide remobilisation has occurred at all scales at Thalanga. At the microscopic scale, chalcopyrite or galena has infilled brittle fractures in euhedral pyrite (Chapter 7), chalcopyrite has filled pressure shadows around cubic pyrite disseminated in QEV (Fig. 3.18e,f), and sphalerite and quartz occur in pressure shadows parallel to S_3 around quartz or feldspar crystals (Fig. 3.14a,b). Chalcopyrite, sphalerite and galena infill cleavage partings in metamorphic tremolite and rare fine grained, elongate pyrite has overgrown S_2 and S_3. Further descriptions of deformed and metamorphic sulphide textures are presented in Chapter 7.

3.7.2 Piercement Structures

Piercement veins composed of chalcopyrite-rich massive sulphides occur at the hangingwall contact of the massive sulphides in places at Thalanga (Fig. 3.17f and Fig. 3.18a,b). Piercement structures typically occur in dacite, HWF or QEV on the hangingwall contact of the massive sulphides. Pre-existing joints in the dacite control the orientation of the piercement veins in a few places (Fig. 3.18a,b; map M5). Piercement structures are more common where massive sulphides directly contact the more competent dacite, compared to the few sulphide piercement veins at the massive sulphide to HWF contact. In most places at Thalanga, the piercement veins extend less than 5 m away from the massive sulphides.

There is a gradation in composition of the sulphides within piercement structures and typically coarse-grained chalcopyrite fills the piercement vein, with a gradual increase in dark red-brown sphalerite towards the non-remobilised massive sulphide contact. Coarse-grained chalcopyrite and sphalerite are present at the stratigraphic top of the massive sulphides, where bands of sphalerite in chalcopyrite are subparallel to the dacite contact and have been folded towards the piercement structure. In places (Central Thalanga), coarse grained massive sphalerite is up to 2 m thick at the stratigraphic top of the massive polymetallic sulphides and fills piercement veins which cross-cut S_2 in the overlying HWF. Where present, quartz typically occurs along the margin of the piercement vein.

These textures are comparable with the remobilised sulphide textures in metamorphosed stratiform massive sulphide deposits described by Gilligan and Marshall (1987), Maiden *et al.* (1986), Marshall and Gilligan (1989) and Osterman and Hutchinson (1994). Maiden *et al.* (1986) distinguished cusp structures from piercement structures at the hangingwall contact of the massive sulphides in the Matchless Cu deposit, Namibia, and explained that the difference in style of sulphide remobilisation is due to competency contrasts between the sulphides and silicate wall rocks. Maiden *et al.* (1986) concluded that cusps form where wall rocks are relatively ductile and that piercement structures form where that wall rocks are brittle. However, this interpretation was not supported by Marshall and Gilligan (1989) who argued that cusp structures form in response to low angle or layer-parallel compression along the contact between rocks of different competency and that piercement structures form due to low angle or layer-parallel extension along such contacts.

Further clarification of this controversy is possible using the examples from Thalanga, where both piercement veins and cusps are present at the HWF/massive sulphide contact (Fig. 3.20). Because there is no significant lateral variation in the competency of the HWF, the presence of both piercement veins and cusps indicates localised extension and compression along the contact between the HWF and massive sulphide lens, which supports the model of Marshall and Gilligan (1989). Immediately adjacent to the major D_3 normal fault in Central Thalanga is a large volume (up to 5 m in thickness) of remobilised chalcopyrite and quartz veins in the dacite at the stratigraphic top of the ore lens. Perhaps this concentration of chalcopyrite is due to hinge thickening of an incipient fold adjacent to the normal fault (Fig. 3.20).

3.7.3 Chalcopyrite Veins

Shallowly NE-dipping, discontinuous chalcopyrite veins (tension gashes) are locally present within the ore lenses and immediate footwall (Fig. 3.18c,d), and rarely occur along kink bands in the HWF. Rare subhorizontal chalcopyrite veins intersect the pyritic, coarse-grained base of a QEV sandstone near the stratigraphic top of the ore horizon in East Thalanga. Chalcopyrite veins also cross-cut the mesh-vein texture of metamorphic calcite in CTC units

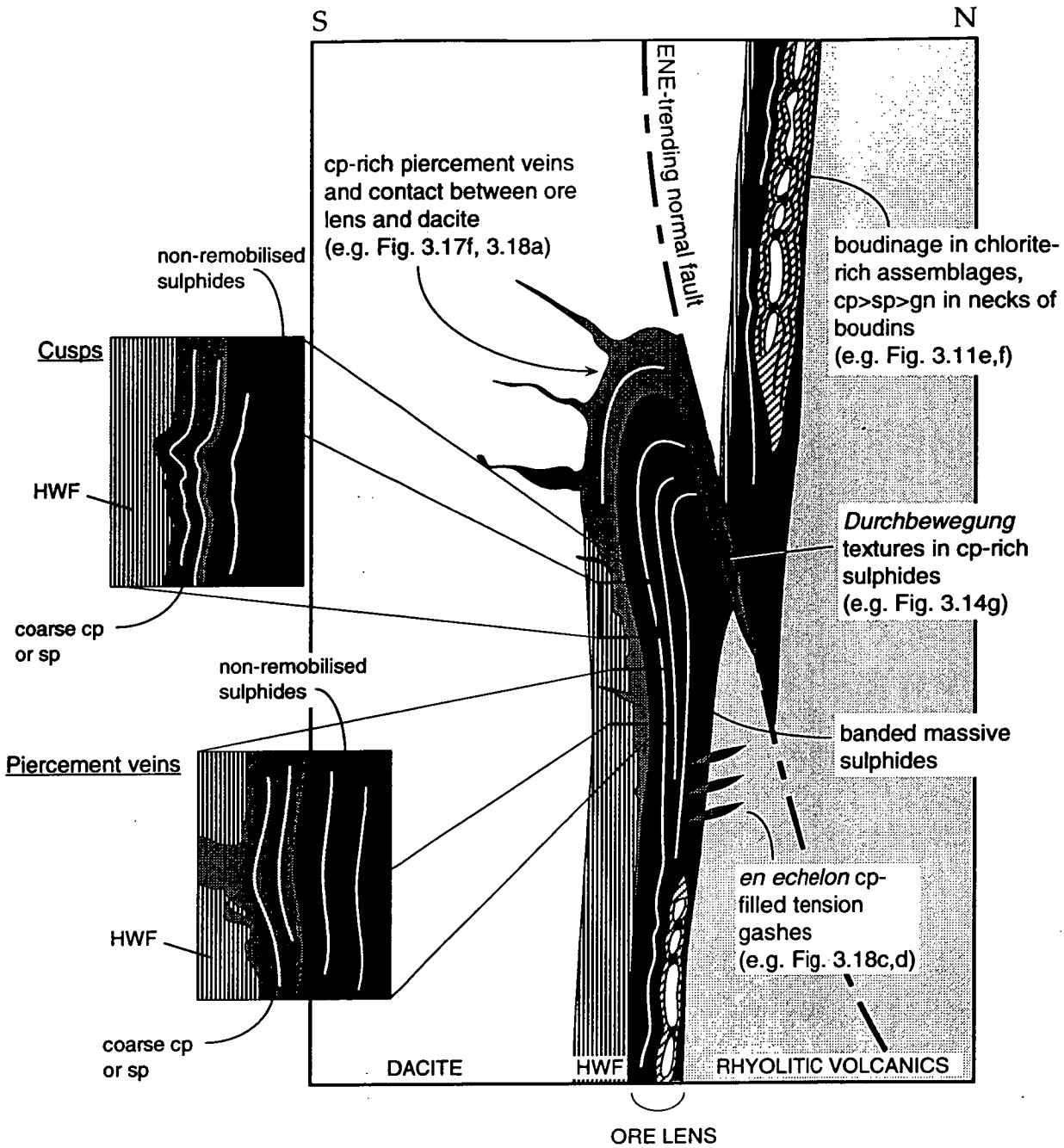

Figure 3.20 Schematic cross section illustrating the location of extensional structures and remobilised sulphides within the ore horizon at Thalanga. White lines represent sulphide bands within massive sulphides, and black lines in the chlorite-rich assemblages also represent sulphide bands. Sketches in the insets are based on mining faces in the C860 Stope, Central Thalanga. Abbreviations: cp = chalcopyrite, gn = galena, sp = sphalerite, HWF = hangingwall fragmental.

(see Chapter 11) and S_2 in chlorite schists, where the chalcopyrite veins are enveloped by phlogopite oriented parallel to vein margins.

Necks of foliation boudins (in chlorite) and pressure shadows around QFP clasts in the overlying massive sulphide lens are filled with remobilised sulphides, suggesting that the shallowly-dipping veins are the same age as other remobilised sulphides. The chalcopyrite tension gashes in the footwall rhyolitic volcanics are typically <1 cm thick and <1 m in length, with sharp but irregular margins and no alteration halo. In West Thalanga, chalcopyrite tension gashes (and rare intersecting subvertical chalcopyrite veins) in the QEV are enveloped by chlorite-tremolite-epidote-rich assemblages (Chapter 10).

3.7.4 Timing of Remobilisation

The location of remobilised sulphides in sites of dilation at Thalanga is interpreted to indicate remobilisation occurred during vertical extension of the ore horizon. Sulphide remobilisation probably occurred late in D_2, after cleavage formation, because remobilised sulphide veins cross-cut S_2, but have been locally overprinted by S_3. *Durchbewegung* textures in the massive sulphide lenses have not been overprinted by S_3, and are therefore interpreted to have formed along normal faults during D_3. Furthermore, some remobilised sulphides are intergrown with silicate minerals produced during metamorphism (post S3; section 3.10). This suggests that multiple episodes of sulphide remobilisation may have occurred during the history of the Thalanga deposit. Chalcopyrite-rich sulphides enveloping and cross-cutting fractured and disrupted microdiorite dykes within the ore horizon (Fig. 3.17e) could indicate that the dykes were dislocated during D_3. However, the intrusion of the microdiorite may have induced local remobilisation prior to D_3. Indeed, remobilised sulphides are commonly associated with post-ore dykes in some North American and Indian VHMS deposits, where the local elevation in temperature is considered to be responsible for the sulphide remobilisation and recrystallisation (Mookherjee, 1976). Nevertheless, the timing of the most significant sulphide remobilisation at Thalanga is interpreted to be during the final stages of D_2.

3.7.5 Mechanisms of Sulphide Remobilisation

Gilligan and Marshall (1987), Maiden *et al.* (1986), and Osterman and Hutchinson (1994) have suggested that migration of sulphides into fractures during deformation and metamorphism involves ductile deformation and probably occurs above the brittle-ductile transition of chalcopyrite, experimentally determined as about 200°C and P <500 bars (Kelly and Clarke, 1975). This low temperature explains the predominance of chalcopyrite remobilisation at Thalanga. The general lack of galena (a ductile sulphide highly amenable

to remobilisation) in the remobilised sulphides at Thalanga is probably due to the overall low abundance of galena in the ore lenses (see Chapter 6 and 7).

Marshall and Gilligan (1987) and Marshall and Gilligan (1993) suggest that mechanical remobilisation of sulphides is probable during prograde metamorphism (350°C -500°C), but more likely during retrogressive cooling in the 500°C - 350°C interval. The scale of sulphide remobilisation varies from cm-scale (e.g. Bierlein *et al.*, 1995) to m-scale, and Marshall and Gilligan (1993) suggest that during prograde metamorphism sulphide remobilisation can occur on the scale of 10's to <100 m, whereas during retrograde metamorphism (in shear zones) sulphides can be remobilised up to 1000 m. Because sulphide remobilisation at Thalanga occurred during the final stages of D_2 and post-S_3 formation, sulphide remobilisation is interpreted to have occurred as a retrograde event.

Marshall and Gilligan (1993) considered that metamorphic solutions derived from silicate assemblages would have limited effect on a sulphide assemblage and therefore regarded mechanical remobilisation of sulphides as more likely than chemical remobilisation. They were uncertain of the effects of quartz (and therefore a fluid phase during sulphide remobilisation) on the development of piercement structures. Because fluids are required to remobilise quartz, which will not readily flow in a ductile fashion, the presence of quartz with remobilised sulphides in piercement structures at Thalanga implies the involvement of fluids. This also happened at the Bousquet 2 deposit, Quebec (Tourigny *et al.*, 1993).

3.8 Post-D_3 Structures

3.8.1 Dolerite Dykes

A vertical, WNW to E-W trending dolerite dyke intrudes both the ore horizon and rhyolitic volcanics in West Thalanga (Fig. 3.1). This dyke is offset along a ENE-striking normal fault at the contact with Central Thalanga, and occurs only in the footwall rhyolitic volcanics north of the ore horizon in Central Thalanga. Beeson (1994; writt. comm.) recorded similarly oriented dykes in East Thalanga, where they cross-cut the ore horizon at a higher angle. Dolerite dykes vary from basaltic to gabbroic textures, but are always highly irregularly fractured, with striated, chloritic surfaces along most fractures.

It is evident from the comparable dyke orientations in all parts of the deposit that dolerite intrusion post-dates the open fold in stratigraphy from West to East Thalanga. The occurrence of a dolerite dyke near or along the contact between the ore horizon and the footwall rhyolitic volcanics in West Thalanga, yet > 50 m stratigraphically below this contact in Central Thalanga, supports the timing of dolerite intrusion as post NNE-striking normal

faults. Despite the lack of direct evidence, the timing of the dolerite dykes with respect to the NNE-striking normal faults suggests that the dolerite dykes may also be younger than the microdiorite dykes. Radiometric dating of the dolerite gives a K-Ar age of 340 Ma (Wills, 1985), which is younger than the intrusion of the Siluro-Devonian Lolworth Igneous Complex (see Table 2.2 in Chapter 2).

3.8.2 Quartz>>Pyrite Veins

Vertical, NE-striking quartz veins (Fig. 3.19c), with minor to traces of pyrite, are common at Thalanga. The exact timing of this quartz veining is unknown, although cross-cutting relationships show that it must post-date the quartz-epidote veins. Cross-cutting relationships were poorly exposed, and so the timing of other barren quartz veins in the Thalanga deposit and along the Thalanga Range (Fig. 3.19d,e) is not understood.

3.8.3 Kink Bands

S-dipping kink bands with normal movement, and rare conjugate N-dipping kinks, are present in the HWF (Fig. 3.21a). Both S_2 and S_3 are kinked. Rare chalcopyrite veins along kinks planes suggests that sulphide remobilisation may have occurred at more than one time, although late kink bands may have been localised on pre-existing structures.

3.8.4 Fractures and Joints

A conjugate set of dip-slip fractures, typically with pyrite fibres in the fracture surface, is prominent within the dacite in the hangingwall at Thalanga. There are two main movement directions delineated by pyrite fibres on the surface of moderately E-dipping fractures (Fig. 3.21b). The first movement was dip-slip faulting, with mostly normal displacement indicated, although in places reverse movement occurred initially. A second population of pyrite fibres overgrow the dip-slip fibres and are interpreted to have formed during a later oblique-slip event. These fractures cross-cut the microdiorite dykes, but their exact timing is uncertain.

Other faults measured in West and Central Thalanga are brittle structures, with minor displacement. Most of these faults are recognised by striations or gouge on the fault surface. Many of these brittle faults are parallel to common joint surfaces (Fig. 3.21c-f). The age of these brittle fractures is poorly understood. NNE-striking fractures and joints commonly cross-cutting the ore horizon are similar in orientation to normal faults interpreted as pre-D_3 in age

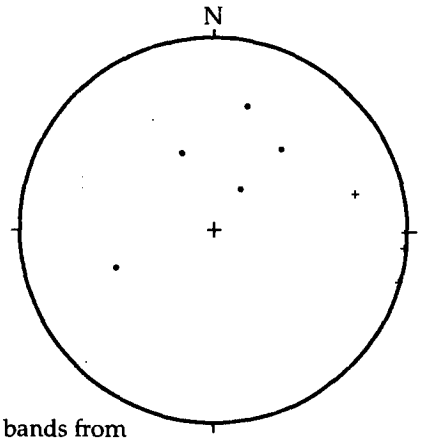

(a) Poles to kink bands from the Thalanga deposit (•) and the Thalanga Range (+).

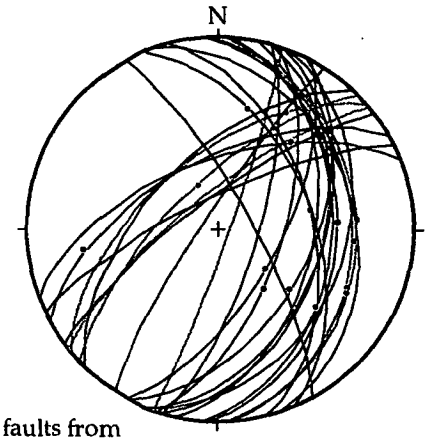

(b) All dip-slip faults from Central Thalanga; green = sinistral faults, blue = dextral faults.

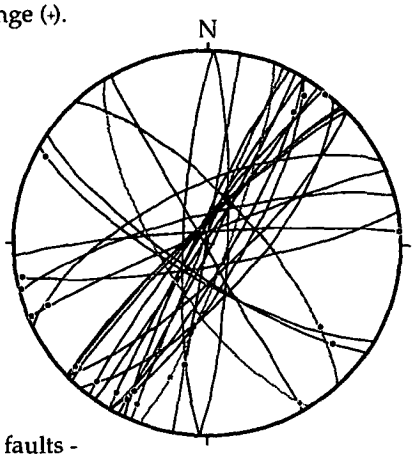

(c) All strike-slip faults - Central Thalanga; green = normal faults, blue = reverse faults.

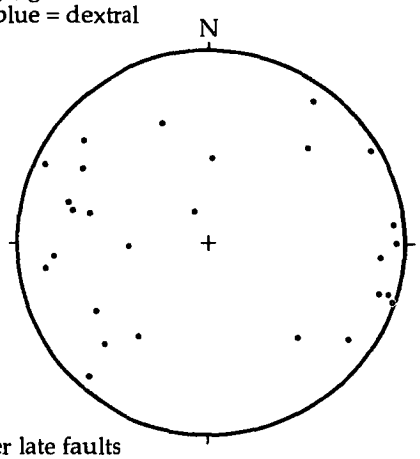

(d) Poles to other late faults in Central Thalanga.

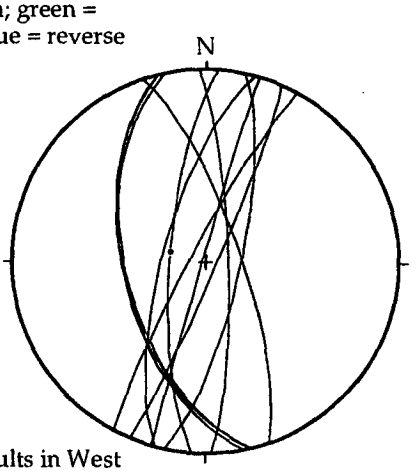

(e) Late brittle faults in West Thalanga, dot represents rare striations on fault surfaces.

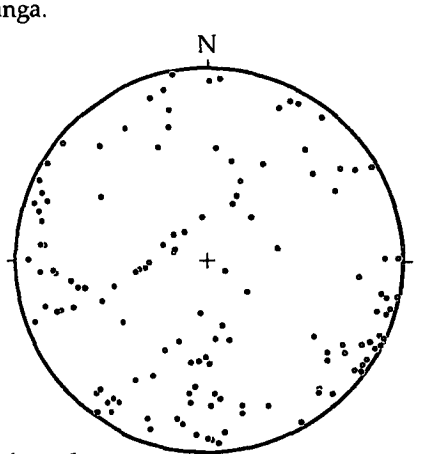

(f) Poles to joints from the Thalanga deposit.

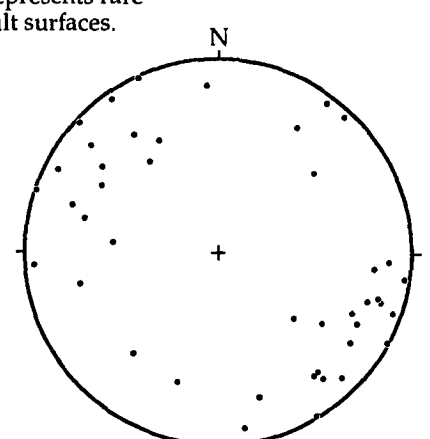

(g) Poles to calcite veins from the Thalanga deposit.

Figure 3.21 Equal area stereonets of late brittle faults, joint surfaces and calcite veins from Thalanga.

(section 3.4). However, these fractures record minor strike-slip movement and post-date the D_3 faults.

3.8.5 Calcite Veins

Steeply-dipping, 1 cm wide white calcite veins with very similar NNE trends to the late brittle fractures (Fig. 3.21g) also cross-cut the stratigraphy and have small amounts of both dextral and sinistral strike-slip movement recorded by striations in chloritic selvages. White calcite veins are common along the margins of the microdiorite dykes. Irregular, white calcite veins also cross-cut some dolerite dykes, commonly filling the abundant fractures in the dykes. All steep calcite veins cross-cut quartz-epidote veins. White to colourless, euhedral calcite fills voids created by fractures and joints within the ore horizon, and the remaining open-space in pink calcite-filled spheroids in the dacite.

3.9 Structural History of Thalanga

Table 3.3 and Figure 3.22 summarise the timing of the main structural features at Thalanga.

Table 3.3 Summary of the structural evolution of the Thalanga massive sulphide deposit.

	Footwall: rhyolitic volcanics	Ore horizon:	Hangingwall: HWF and dacite
Pre-deformation	• ?growth faults, • pyrite stringers	• normal grading in volcaniclastic units, • ?compositional banding in sulphide lenses	• normal grading in siltstone and sandstone, • local quartz-epidote veins
D_1	?	?	?
D_2 Mid to Late Ordovician age	• pervasive cleavage (S_2) anticlockwise from bedding • shallowly-dipping quartz veins	• S_2 cleavage, • shallowly-dipping quartz veins in QFP, • banding in massive sulphides, • sulphide remobilised into boudin necks, • chalcopyrite-filled piercement veins and tension gashes at hangingwall and footwall contacts of massive sulphides	• S_2 cleavage
Pre-D_3	• north-south open fold, cross-cut by NNE-striking normal faults (west side down) and NNE-striking microdiorite dykes.		
D_3 Silurian-Devonian? age	• S_3 crenulation cleavage, • brittle ENE-striking fault zones	• normal offset along steep ENE-striking faults, • *Durchbewegung* texture in massive sulphides adjacent to ENE-striking faults	• brittle ENE-striking normal faults, • S_3 cleavage adjacent to these faults, • chlorite-biotite spots elongate on S_3
Post-D_3	• quartz>>pyrite veins, • WNW-striking dolerite dyke cross-cuts ore horizon, • local brittle faults and calcite veins		

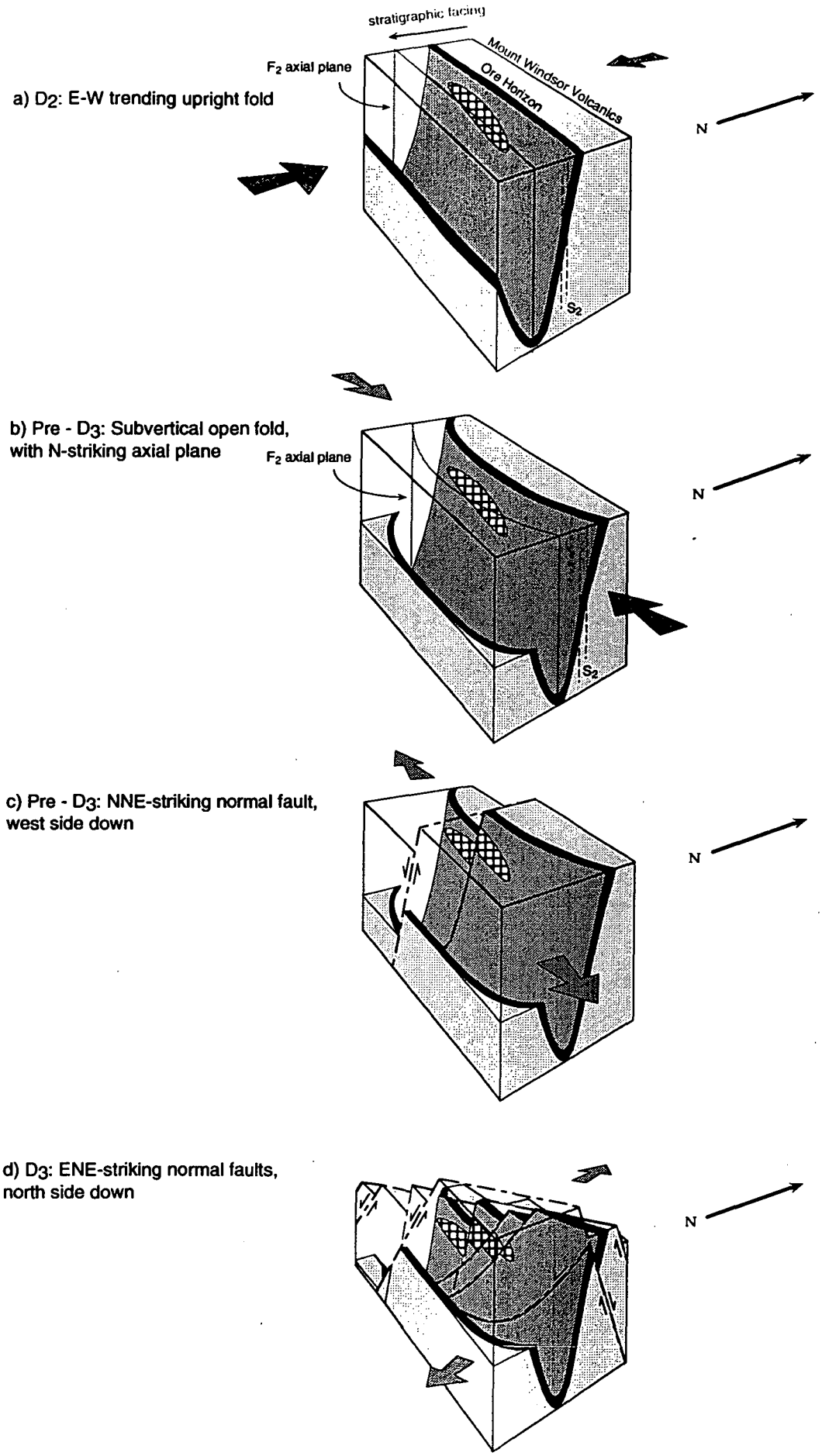

Figure 3.22 Schematic block models of the main deformation events at Thalanga, with the massive sulphide deposit represented by the hatch pattern. Depth to hinge of F_2 syncline is unknown.

D_2 at Thalanga is related to the regional east-west upright folding event that is interpreted to be Mid-Late Ordovician in age (Berry *et al.*, 1992). The similarity in orientation between the S_3 cleavage and ENE-striking normal faults at Thalanga, and regional structures interpreted to be Silurian-Devonian in age, suggests that D_3 at Thalanga may have occurred during the Silurian-Devonian.

3.10 Minerals Associated with Peak-Metamorphism

3.10.1 Biotite

Biotite (or phlogopite) parallel to S_2 is present in many of the host rocks at Thalanga, and in places it occurs in S_2 pressure shadows (Fig. 3.23a,b). Only rare examples of kinked biotite (kinks parallel to S_3) have been preserved (within the Puddler Creek Formation near Thalanga; Fig. 3.23c,d). These chlorite (after biotite) grains indicate that there was a metamorphic event prior to S_3. However, in most locations, biotite has decussate texture and has overprinted the S_3 crenulation cleavage, either mimetically (Fig. 3.23e,f), or as porphyroblasts (Fig. 3.23g,h). Biotite in pressure shadows (L_3 mineral lineation; section 3.6.2), also has decussate texture and is therefore interpreted to have formed mimetically along pre-existing S_3 cleavage (Fig. 3.24a,b). These textural relationships suggest that the peak of metamorphism at Thalanga post-dated the S_3 cleavage.

Biotite in the host volcanic units at Thalanga probably formed via the reaction:

sericite + chlorite = biotite + muscovite + quartz + H_2O, or

K-feldspar + chlorite = biotite + muscovite + quartz + H_2O (Yardley, 1989).

The reaction between sericite and chlorite is more likely to have proceeded in the hydrothermally altered footwall rhyolitic volcanics, whereas the reaction between K-feldspar and chlorite probably produced biotite in the hangingwall rocks and least altered footwall rhyolitic volcanics.

3.10.2 Muscovite

Fine grained muscovite in the matrix of the hydrothermally altered footwall rhyolitic volcanics is parallel to both S_2 and crenulated by S_3. Coarse grained muscovite (about 0.5 mm in length) is typically varies from decussate in texture to subparallel to S_3 (Fig. 3.12e), and is consistent with the peak of metamorphism post-dating S_3.

Figure 3.23 Photomicrographs illustrating the relationship between biotite texture, S_2 and S_3.

(a) Brown biotite is parallel to S_2 in pressure shadows and groundmass around feldspar (albite) crystals within weakly altered rhyolitic volcanics. Quartz within the pressure shadows has been recrystallised. Sample TH247-119, West Thalanga. Plane light.

(b) Sample in (a) under crossed nicols.

(c) Coarse chlorite grain (after biotite) that has been kinked (arrow) by S_3. Sample RT-13A, Puddler Creek Formation, located north of the Flinders Highway, near Thalanga. Plane light.

(d) Sample in (c) under crossed nicols.

(e) Coarse grained, decussate biotite has overgrown the S_3 crenulation cleavage in a muscovite and biotite-rich HWF unit. S_2 is crenulated at arrow. Sample TH382A 436.3, East Thalanga. Plane light.

(f) Sample in (e) under crossed nicols.

(g) Photomicrograph of phlogopite, chlorite and muscovite porphyroblasts that overgrow the S_3 crenulation cleavage, which is defined by the preferred alignment of fine-grained muscovite. Sample E3208SD36-12.8, East Thalanga. Plane light.

(h) Sample in (g) under crossed nicols.

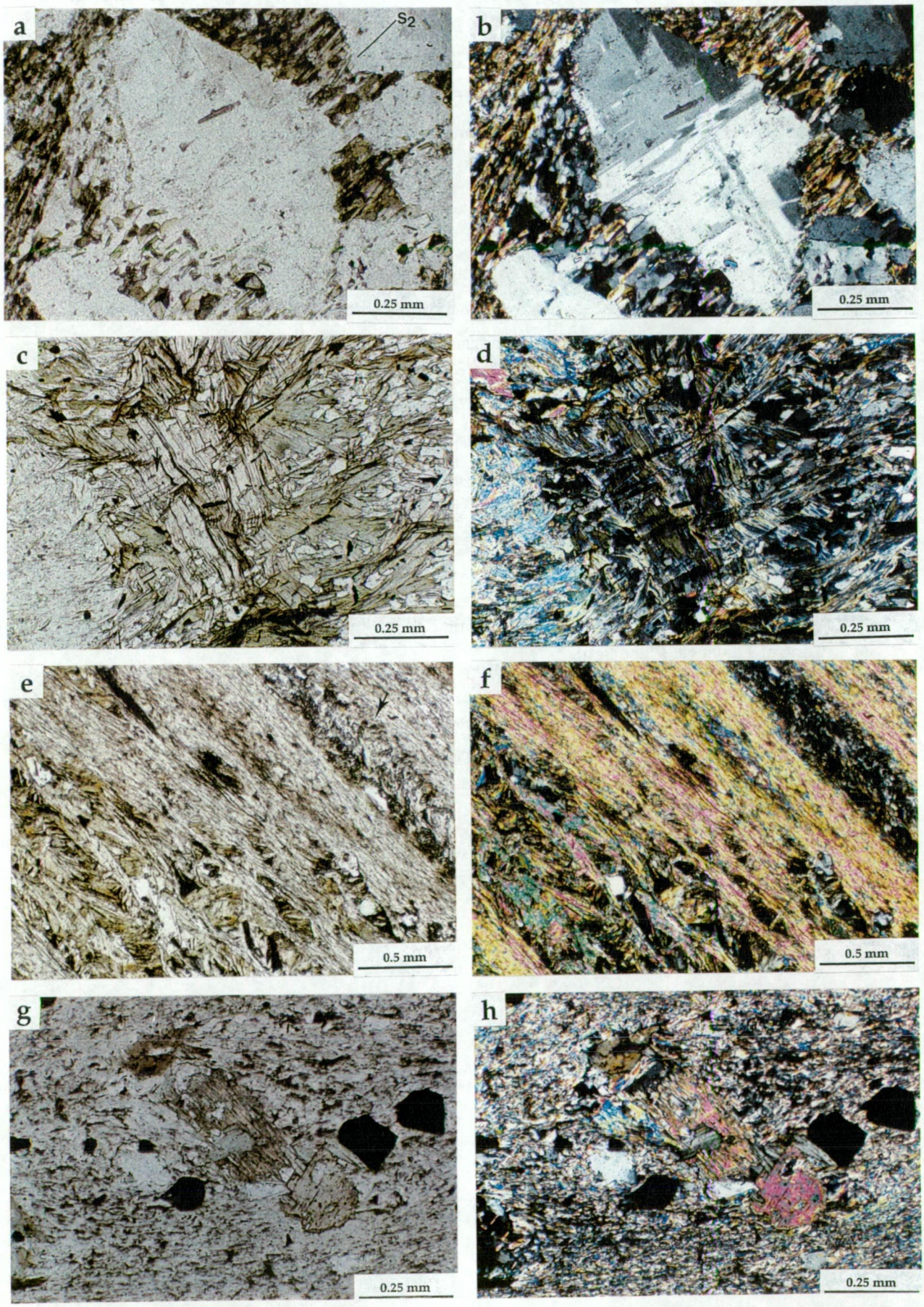
a
S2
0.25 mm
b
0.25 mm
c
0.25 mm
d
0.25 mm
e
0.5 mm
f
0.5 mm
g
0.25 mm
h
0.25 mm

Figure 3.24 Photomicrographs of garnets and minerals associated with garnets at Thalanga.

(a) Decussate biotite in pressure shadow (parallel to S_3) adjacent to partly altered feldspar crystal in sandy siltstone facies of the HWF. White mica in matrix has been crenulated by S_3. Sample TH382A-436.5, East Thalanga. Plane light.

(b) Sample in (a) under crossed nicols.

(c) Garnet porphyroblast, from within chlorite-phlogopite spot in the footwall rhyolitic volcanics, has overgrown S_3. Muscovite and phlogopite in the groundmass are decussate in texture and locally subparallel to S_3. Sample TH287-196, East Thalanga. Plane light.

(d) Sample in (c) under crossed nicols.

(e) Quartz and actinolite now occupy an actinolite-shaped inclusion in spessartine-rich almandine garnet. Biotite, chlorite, quartz and actinolite are intergrown around the anhedral garnet. Sample APH-127, Central Thalanga. Plane light.

(f) Quartz and green chlorite have filled fractures in spessartine-rich garnet. Sample APH-127, Central Thalanga. Plane light.

(g) Euhedral allanite inclusions in chlorite (after biotite). Chlorite has pleochroic halos around the inclusions. Sample APH-127, Central Thalanga. Plane light.

(h) Sample in (g) under crossed nicols.

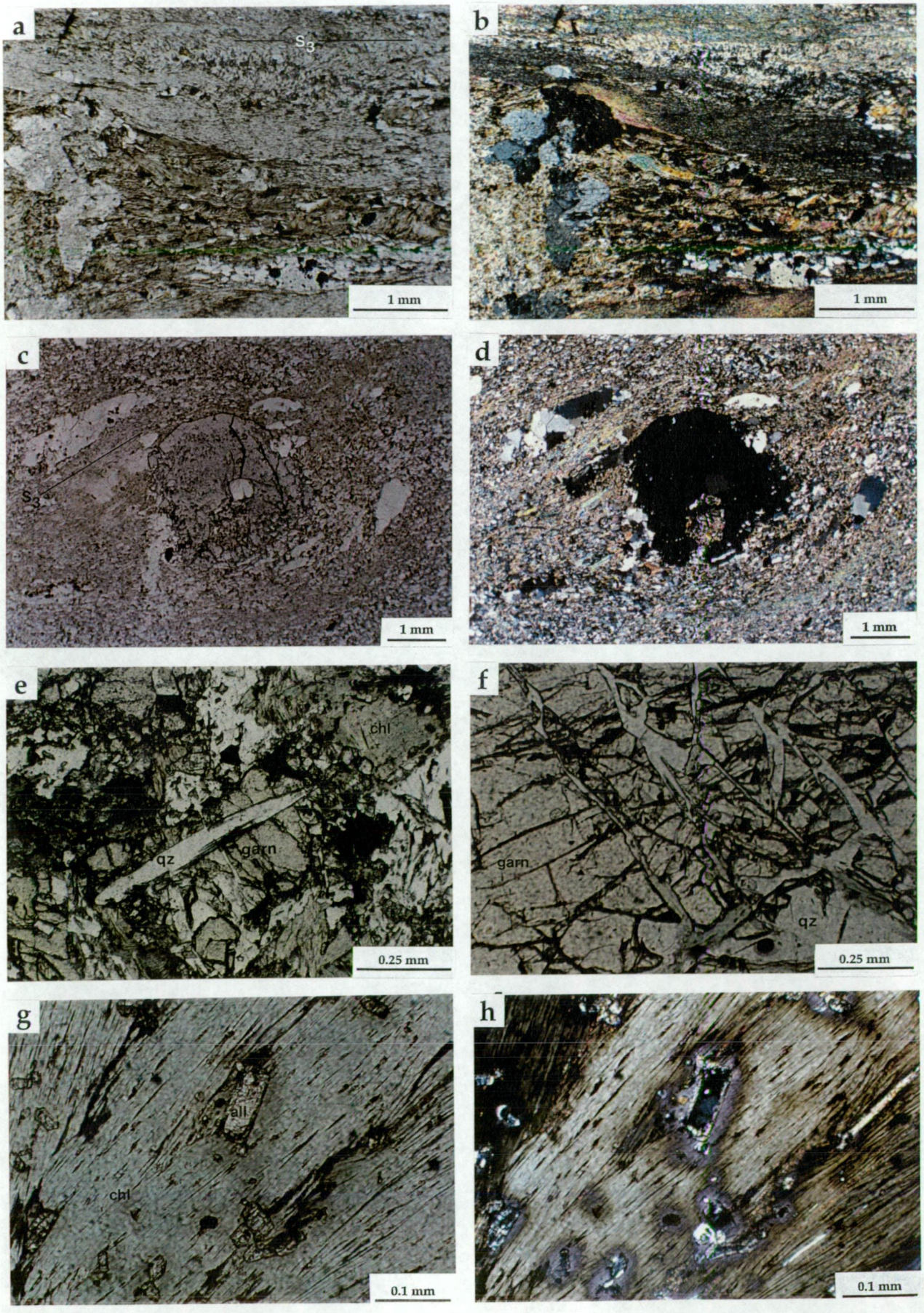
a
S3
1 mm
b
1 mm
c
S3
1 mm
d
1 mm
e
chl
qz
garn
0.25 mm
f
garn
qz
0.25 mm
g
all
chl
0.1 mm
h
0.1 mm

3.10.3 Garnet

Garnet Porphyroblasts in the Footwall Rhyolitic Volcanics

Rare pink spessartine-rich (section 3.11) almandine garnets occur in the cores of green chlorite-phlogopite spots in the footwall rhyolitic volcanics at Thalanga. The garnet porphyroblasts are subhedral. Minor quartz and muscovite-quartz inclusions (decussate muscovite) are present in some garnets (Fig. 3.24c,d). S_2 and S_3 is overgrown by the garnet porphyroblasts, which indicates that the thermal peak post-dates S_3 (Fig. 3.24c,d).

The garnets possibly formed via reaction between Mn-rich chlorite and muscovite according to the reaction:

Fe(Mn)-chlorite + muscovite = Mn-rich almandine + annite + quartz + H_2O.

The lack of Fe(Mn)-chlorite in the footwall (hydrothermal alteration is interpreted to have formed Mg-rich chlorite; Chapter 10) may explain the sparse number of garnet porphyroblasts in the rhyolitic volcanics at Thalanga.

Garnet-Biotite Assemblage within the Ore Horizon

A chlorite-garnet-biotite-quartz-actinolite assemblage at the margin of a large QFP boulder in Central Thalanga has no penetrative cleavage and is therefore interpreted to have post-dated S_3. This assemblage is composed predominantly of chlorite, with coarse grained biotite and actinolite. Pink spessartine-rich garnet porphyroblasts (see Appendix B for analyses) are intergrown with an acicular mineral (actinolite?) now defined by intergrown quartz, actinolite and rare biotite (Fig. 3.24e). The actinolite has sharp grain boundaries in contact with the quartz, but ragged contacts with chlorite. Quartz and green chlorite also fill fractures in the garnets (Fig. 3.24f). Decussate green to pale khaki brown biotite is typically altered to green chlorite, particularly along cleavage planes. Chlorite (after biotite) contains elongate clinozoisite inclusions, and has pleochroic halos around rare inclusions of allanite (Fig. 3.24g,h).

Other minor components of this assemblage include apatite, calcite, sphalerite, galena, chalcopyrite and barite. Subhedral apatite grains, up to 0.1 mm in length are concentrated in quartz grains (Fig. 3.25a). Biotite, garnet, actinolite (or quartz-actinolite precursor) and possible apatite are interpreted to be prograde minerals, whereas chlorite has replaced biotite during retrograde alteration. Sphalerite, galena and chalcopyrite have filled fractures in the garnet (Fig. 3.25b) and are therefore interpreted to have been mobile during metamorphism. Calcite is in textural equilibrium with quartz and the sulphides.

Figure 3.25 Photomicrographs of textures and mineralogical associations of garnet-bearing units in the ore horizon and in the HWF.

(a) Subhedral apatite grains in quartz-rich domain of chlorite-biotite-quartz-actinolite-garnet assemblage at margin of quartz-feldspar-porphyry clast within ore horizon. Sample APH-127, Central Thalanga. Plane light.

(b) Sphalerite is present within fractures in anhedral garnet porphyroblast. Quartz and chlorite are also present in the fractures. Sample APH-127, Central Thalanga. Plane light.

(c) Subhedral garnet porphyroblast has impinged on quartz grain within a quartz-feldspar sandstone. Green biotite and anhedral epidote is present within the biotite-rich matrix. Sample W2011NI05-22.4, West Thalanga. Plane light.

(d) Sample in (c) under crossed nicols.

(e) Garnet porphyroblast is partly intergrown with subhedral epidote grains. Decussate biotite is present within the quartz-rich matrix. Sample W2011NI05-22.4, West Thalanga. Plane light.

(f) Sample in (e) under crossed nicols.

(g) Euhedral epidote has overgrown anhedral, brown allanite within biotite-rich domain of biotitic quartz-feldspar sandstone. Sample W2011NI05-22.4, West Thalanga. Plane light.

(h) Sample in (g) under crossed nicols.

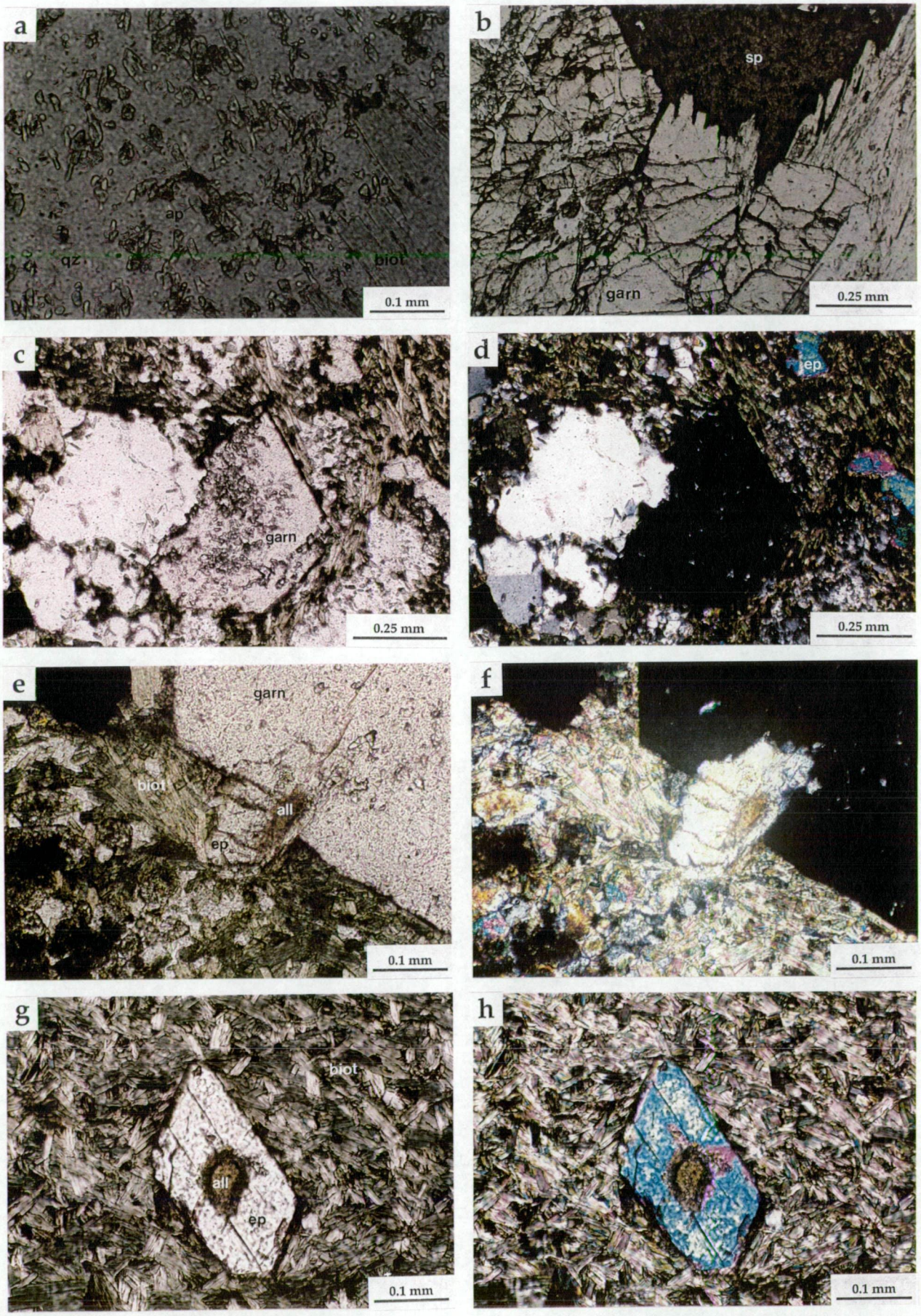
a
ap
qz
biot
0.1 mm
b
sp
garn
0.25 mm
c
garn
0.25 mm
d
ep
0.25 mm
e
garn
biot
all
ep
0.1 mm
f
0.1 mm
g
biot
all
ep
0.1 mm
h
0.1 mm

Garnet Porphyroblasts in the HWF

The few garnets in the HWF are associated with abundant green biotite, minor green chlorite, epidote, patchy actinolite, minor to traces of magnetite, rare calcite, sphalerite and chalcopyrite, and accessory apatite. Rare vesuvianite is present in some biotite-rich HWF units. This assemblage is present in a volcanic quartz and feldspar sandstone, and the garnets preferentially occur in biotite-rich bands. The biotite is undeformed and typically decussate, and is interpreted to have mimetically overgrown S_3 (Fig. 3.25c,d).

The garnet porphyroblasts are pink in plane light and irregular to euhedral in shape (Fig. 3.25c-f), with rare garnets elongate and parallel to the weak S_3. Most garnets are <0.5 mm in diameter, with rare porphyroblasts up to 1.5 mm in diameter. The garnets are typically composed of an irregularly-shaped, inclusion-rich core (mainly quartz inclusions, rarely magnetite and biotite inclusions), with a euhedral, inclusion-free rim (Fig. 3.25c,d). There is no consistent orientation of the inclusions in the garnet cores. The garnet rims are particularly euhedral where in contact with biotite-rich domains, whereas the rims are partly embayed where in contact with quartz in the sandstone matrix. In places the euhedral rims of the garnet porphyroblasts impinge on quartz grains and zoned epidote grains (Fig. 3.25e,f). Some irregular garnets are intergrown with magnetite or sphalerite. The absence of pressure shadows around the garnet porphyroblasts, and truncation of biotite in contact with garnet, is consistent with formation of garnet after S_3.

Epidote associated with the metamorphic garnet and biotite is subhedral, but varies to euhedral in shape where enclosed in biotite-rich domains (Fig. 3.25g,h). Many epidote grains are zoned, with a core of brown, anhedral allanite. Rare subhedral vesuvianite grains are present in this metamorphic assemblage in the HWF (in East Thalanga). The vesuvianite has no preferred orientation and directly contacts decussate biotite (and chlorite after biotite), appearing to have grown along the biotite grains (Fig. 3.26a,b). The vesuvianite grains are spatially associated with anhedral magnetite and sphalerite (Fig. 3.26a,b), and is interpreted to have formed from the metasomatic addition of magnetite and calcite to the quartz-feldspar sandstone facies of the HWF. Muscovite in the footwall rhyolitic volcanics contains elevated F, which is interpreted to have been hydrothermal in origin (Chapter 10). Therefore, the F required for vesuvianite formation may also have been originally hydrothermal and possibly associated with hangingwall-style alteration.

3.10.4 Chlorite Spots

Green chlorite spots are common in the volcaniclastic and sedimentary units both underlying and overlying the ore horizon at Thalanga, and are most common in the siltstone and sandy siltstone facies of the HWF (Fig. 3.26c,d). The chlorite spots are typically <1 cm in diameter

Figure 3.26 Textures of vesuvianite and chlorite spots.

(a) Subhedral vesuvianite grains associated with biotite, sphalerite, magnetite and epidote in a barite-rich quartz-feldspar sandstone (HWF). Sample E3208SD23-77.5. Plane light.

(b) Sample in (a) under crossed nicols.

(c) Hand specimen of siltstone (HWF) containing both rounded and elongate (parallel to S_3) chlorite spots. Biotite rims the spots. Sample TH263-173, East Thalanga.

(d) Hand specimen of quartz-muscovite-pyrite-rich rhyolitic volcanics with green chlorite spots that are elongate along S_3, but contain S_2 cleavage. Fine grained pyrite is parallel to S_3. Sample TH265-173, East Thalanga.

(e) Photomicrograph of chlorite spot in a quartz-feldspar sandstone facies of the HWF. Quartz, muscovite, chlorite and traces of biotite are present in the core of the spot, and biotite and chlorite occur at the margins. Sample E3207SD29-75.9, East Thalanga. Plane light.

(f) Photomicrograph of deformed chlorite spot from (c). Chlorite-quartz-muscovite and traces of biotite are present in the core of the spot and recrystallised quartz and chlorite are present in the weak pressure shadows. Sample TH263-173, East Thalanga. Crossed nicols.

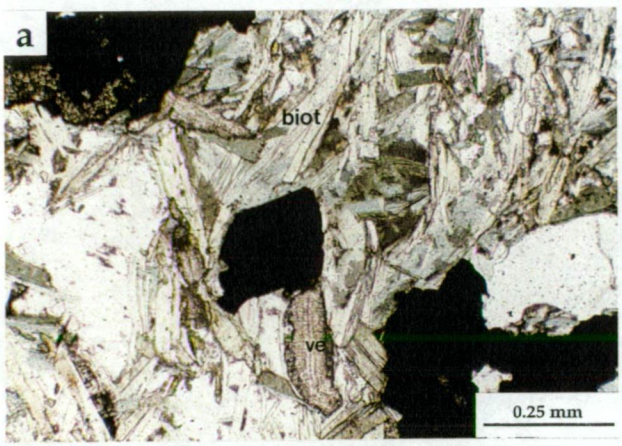
a
biot
ve
0.25 mm

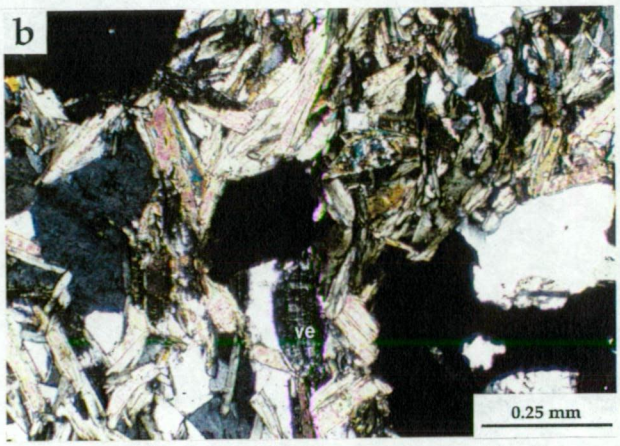
b
ve
0.25 mm


c
10 mm


d
S2
S3
20 mm

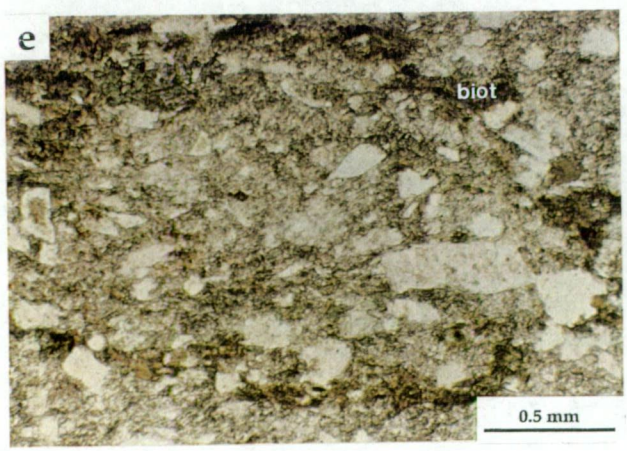
e
biot
0.5 mm

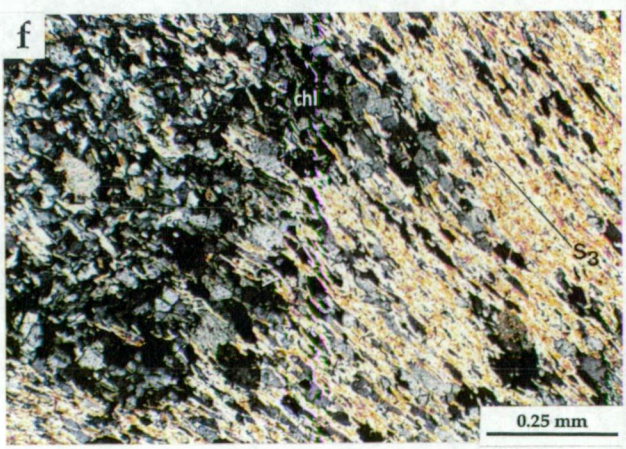
f
chl
S3
0.25 mm

and display either sharply defined or diffuse margins. In rhyolitic breccias in the footwall and in dacite breccias in the hangingwall, chlorite spots are up to 2cm in diameter and have diffuse margins. The spots vary from dominantly chlorite and biotite, to spheroidal chlorite-biotite-muscovite-quartz intergrowths, which are rimmed by green biotite or phlogopite (Fig. 3.26e,f). Rare chlorite spots are hexagonal in cross section, and garnet porphyroblasts are present within the chlorite spots in places. Chlorite spots are more abundant in East Thalanga, compared to Central and West Thalanga, which may be due to proximity to the granitoid inferred to have intruded ~1 km to the east of the East Thalanga ore lens (Gregory *et al.*, 1990).

In most parts of the HWF, the chlorite spots are elongate parallel to S_3, with round, undeformed chlorite spots present immediately adjacent to elongate spots in places. Where S_3 wraps the chlorite spots (indicating that locally, the chlorite spots were rigid during deformation) chlorite and quartz are present in the pressure shadows (Fig. 3.26f). Chlorite or quartz-filled fractures in some spots resemble pull-apart textures, also suggesting rigidity during deformation. In places, chlorite spots contain a foliation that is interpreted to be S_2, suggesting that chlorite spots overgrew S_2 prior to S_3 (Fig. 3.26d).

The chlorite-phlogopite-muscovite-quartz spots may be similar to chlorite spots common in hornfels zones (Winkler, 1979, Yardley, 1989), and may be after cordierite or biotite (e.g. McClay, 1983). The rare hexagonal shapes support the interpretation that the chlorite spots are after cordierite. Cordierite typically forms according to the reaction:

chlorite + muscovite = cordierite + biotite + quartz + H_2O (Yardley, 1989).

The production of biotite during this reaction explains the biotite rims of some of the chlorite spots. The retrogression of cordierite probably followed the above reaction in reverse. Alternatively, the chlorite spots may have formed by the retrogression of almandine garnets via:

almandine + biotite + H_2O = chlorite + muscovite + quartz.

3.10.5 Tremolite/Actinolite - Epidote Assemblages

Decussate tremolite is common in carbonate- and chlorite-rich units (Chapter 11) and the massive sulphide lenses where it overgrows S_2 and S_3. Mutual intergrowths of tremolite and recrystallised sulphides (chalcopyrite, sphalerite, galena, pyrite) are interpreted to indicate that tremolite formation coincides with sulphide remobilisation, which is interpreted to have occurred during the final stages of D_2 and also during D_3 (section 3.7).

Epidote-actinolite-rich assemblages have overprinted the QEV units at Thalanga, whereas clinozoisite-tremolite-rich assemblages occur in the uppermost parts of the footwall rhyolitic volcanics (Chapter 10). The tremolite/actinolite has decussate texture, with interstitial

clinozoisite/epidote, and minor quartz and chlorite. The presence of clinozoisite and tremolite, rather than epidote and actinolite, probably reflects bulk rock composition and therefore original hydrothermal alteration assemblages. Clinozoisite and tremolite may have formed by the reaction of Mg-rich chlorite with quartz and calcite according to:

$$3(Mg,Fe)_5Al_2\,Si_3O_{10}(OH)_8 + 10CaCO_3 + 21SiO_2$$

chlorite

$$= \underset{\text{clinozoisite}}{2Ca_2Al_3Si_3O_{12}(OH)} + \underset{\text{tremolite}}{3Ca_2(Mg,\,Fe)Si_8O_{22}(OH)_2}.$$

Actinolite occurs in rocks with a higher Fe-rich bulk composition, where it is usually present with epidote and green, Fe-rich chlorite.

3.10.6 Timing of Peak Metamorphism

Biotite, chlorite, muscovite, and tremolite are all coarse grained, decussate, and have overgrown (mimetically in places) the S_3 crenulation cleavage, as have the garnet porphyroblasts. These textures all indicate that the peak of metamorphism post-dates S_3 at Thalanga. The elongate chlorite spots (or their precursor) and local elongate garnet porphyroblasts probably formed during deformation (D_3). The timing of peak-metamorphic temperatures after S_3 explains the strongly recrystallised textures evident in both the massive sulphides and the host stratigraphy at Thalanga. Quartz phenocrysts, pre-S_2 quartz veins, and quartz in S_3 pressure shadows (Fig. 3.14c,d) has been strongly recrystallised after S_3.

There is little evidence of metamorphism prior to S_3, except the few kinked biotite grains, and muscovite pseudomorphs of andalusite that are elongate on S_3 within the Puddler Creek Formation northwest of Thalanga (Berry *et al.*, 1992). The presence of biotite associated with these textures indicates that the temperatures of metamorphism associated with S_2 were similar to the post-S_3 metamorphic event. It is possible that the earlier metamorphic event is associated with regional metamorphism. The post-S_3 metamorphism could have occurred during contact metamorphism associated with the intrusion of post-kinematic granitoids in the Silurian or Early Devonian (Berry *et al.*, 1992). However, except for abundance of chlorite spots, the textures and mineralogy of the peak metamorphic minerals is consistent from West to East Thalanga, and shows no variation with proximity to the granitoid (known from aeromagnetic interpretations to have truncated the easternmost part of East Thalanga; Gregory *et al.*, 1990).

3.11 Composition of Biotite, Chlorite, Muscovite and Garnet

3.11.1 Composition of Biotite

There is a systematic variation in the Fe and Mg content of biotite with respect to stratigraphy at Thalanga (Fig. 3.27a). Mg-rich, Fe-poor biotite (phlogopite) is present within the ore horizon and hydrothermally altered footwall rhyolitic volcanics, whereas Mg-poor, Fe-rich biotite is present in weakly hydrothermally altered volcanic units overlying the massive sulphides, and in weakly altered rhyolite in the footwall (Fig. 3.27a). A similar relationship between biotite composition and proximity to the orebody is reported from other greenschist facies metamorphosed massive sulphide deposits (e.g. Garpenberg, Vivallo, 1985). Biotite in the hangingwall rocks contains more Fe than biotite in the most distal (≥200 m from the ore horizon) and least hydrothermally altered rhyolite in the footwall (Fig. 3.27a). There is a range in the Fe content of biotite within the massive sulphides at Thalanga from ~0.5 to <2.5 Fe in unit formula (Fig. 3.27a).

In general, biotite in the hangingwall units (dacite and HWF) contains more Ti and less F than biotite from the footwall rhyolitic volcanics at Thalanga (Fig. 3.27b,c), and the positive correlation between Mg/(Mg+Fe) and the F content of biotite at Thalanga is consistent with the Fe-F avoidance rule recognised by Valley *et al.* (1982) and Munoz (1984). Biotite and phlogopite within the massive sulphide lenses have elevated F contents (generally 1-2 weight % F; Appendix B).

The relationship between biotite composition and stratigraphy is inferred to reflect pre-metamorphic, hydrothermally altered bulk rock compositions, and particularly the Mg-rich hydrothermal alteration assemblages in the footwall rocks. In many cases, the F content of biotite is inferred to have been inherited from the pre-metamorphic assemblage (Guidotti, 1984), which would suggest that the hydrothermally altered rhyolitic volcanics were elevated in F.

3.11.2 Composition of Chlorite

The composition of chlorite at Thalanga shows a similar variation across the stratigraphy as biotite. Chlorite (clinochlore) in the footwall is more Mg-rich than chlorite (chamosite) in the hangingwall units (Fig. 3.28). This variation in the Mg:Fe ratio of chlorite is similar to trends reported by Schmidt (1988), who attributed it to Mg-enrichment associated with hydrothermal alteration of the footwall to massive sulphides, and purely metamorphic chlorite in the hangingwall. Chlorite intergrown with the remobilised and non-remobilised massive sulphides has a wide range in composition (Fig. 3.28). In contrast, the Fe content of chlorite at Rosebery is reported to be related to the Fe content of the co-existing sulphides

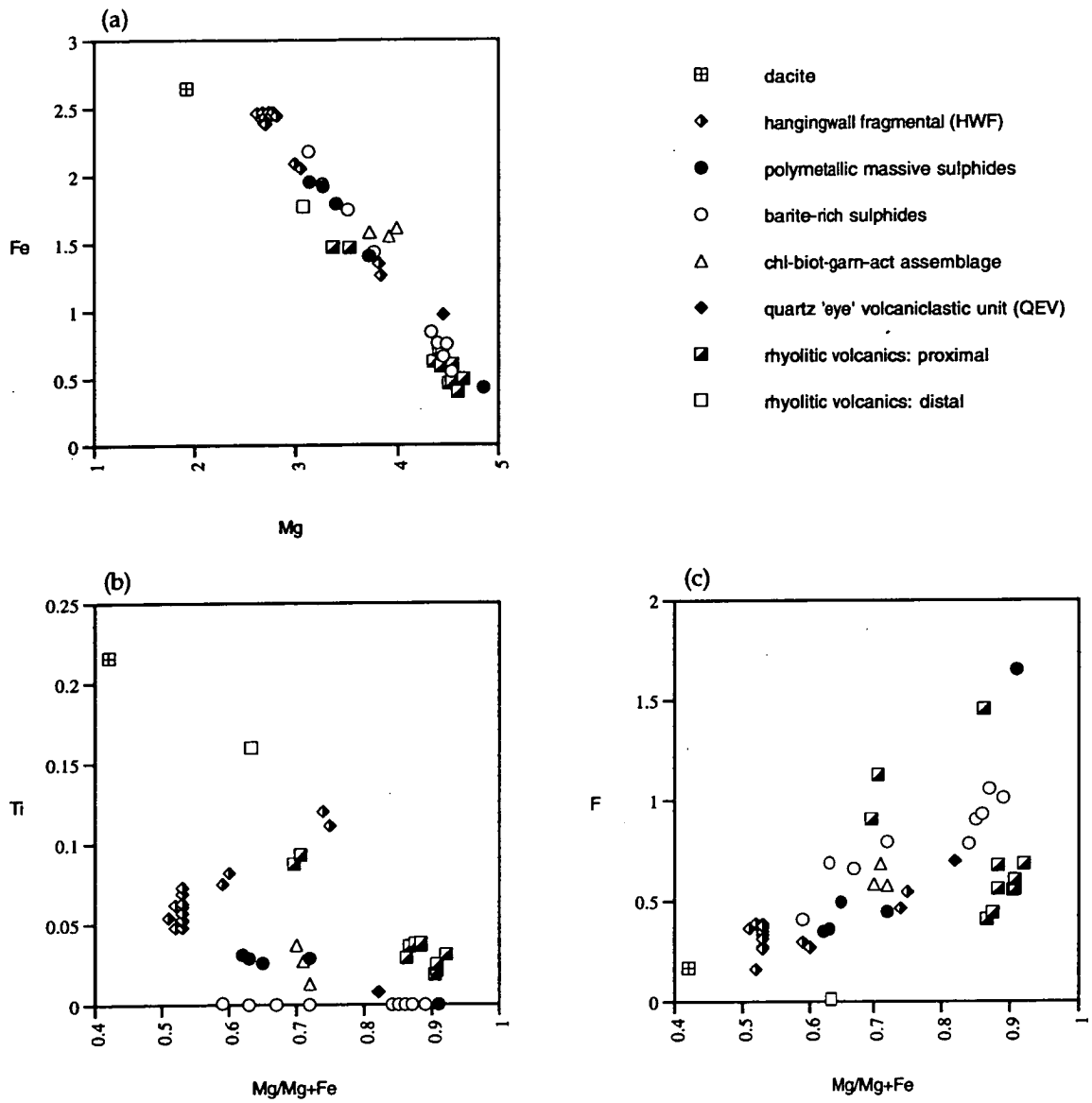

Figure 3.27 Variation in cation proportions of (a) Fe with Mg, (b) Ti with Mg/ (Mg+Fe), and (c) F with Mg/(Mg+Fe) of biotite at Thalanga.

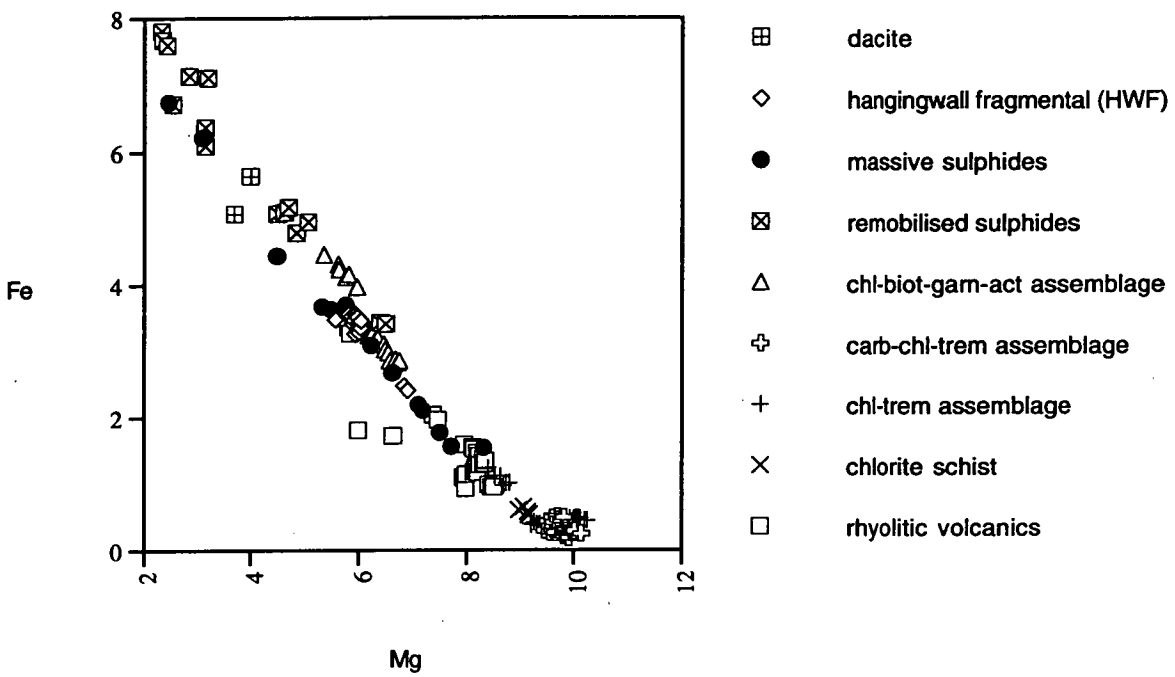

Figure 3.28 Variation in the content of Fe with Mg (cation proportions) of chlorite at Thalanga. Abbreviations: act = actinolite, biot = biotite, carb = carbonate, chl = chlorite, trem = tremolite.

1981). At Rosebery, Fe-rich chlorite is present in the pyrite-rich lenses and Fe-poor chlorite is intergrown with sphalerite-galena and barite-rich sulphide lenses (Green *et al.*, 1981). This type of association is not present at Thalanga.

3.11.3 Composition of Muscovite

Most of the muscovite disseminated through the footwall at Thalanga is too fine grained to be analysed by microprobe, and therefore only the coarse grained muscovite in pressure shadows around quartz crystals has been analysed (results in Appendix B). Muscovite from within the footwall rhyolitic volcanics can be distinguished from muscovite intergrown with massive sulphides by the higher K and Fe content of the former (Fig. 3.29a). Muscovite from less altered parts of the footwall (areas not overlain by massive sulphide lenses) contains slightly greater Fe, but less Al than muscovite from quartz-muscovite ± pyrite-rich rhyolitic volcanics (Fig. 3.29b). Muscovite within the footwall has variable Ti content, compared to muscovite within the massive sulphide lenses, which does not contain Ti, and muscovite from the HWF, which has a slightly greater Ti content (Fig. 3.29b). Some of the muscovite from the footwall rhyolitic volcanics contains significant amount if F, but generally, there is no consistent variation in the content of F with the Mg or Fe content of muscovite (Fig. 3.29c).

Because Ti is immobile during hydrothermal alteration (Winchester and Floyd, 1977; Barrett and MacLean, 1991), pre-metamorphic sericite gangue within the massive sulphide lenses possibly formed during hydrothermal exhalation from Ti-poor hydrothermal solutions, whereas sericite in the rhyolitic volcanics probably formed by hydrothermal alteration and therefore retained Ti. The F content of some muscovite at Thalanga is greater than most metamorphic muscovite (<0.25 weight % F; Guidotti, 1984), and may be the result of addition of magmatic solutions either during hydrothermal alteration or metamorphism. The presence of vesuvianite in biotite-rich parts of the HWF is consistent with an elevated F content of the pre-metamorphic assemblage.

3.11.4 Composition of Garnet

The high Mn content of the garnets (Appendix B) is probably due to original Mn-rich bulk composition, with Mn probably sourced from chlorite. The garnets in the footwall at Thalanga are compositionally zoned, with Mn-rich cores and rims containing less Mn and more Mg and Fe than their cores (Fig. 3.30a-c). There is no uniform variation in the abundance of CaO and Al_2O_3 in the garnet porphyroblasts. Mn is known to be taken up first into the cores of garnets (Winkler, 1979, Yardley, 1989), therefore the compositional zonation of the garnets is interpreted to have resulted from the scavenging of Mn from the precursor rocks during the early stages of garnet growth.

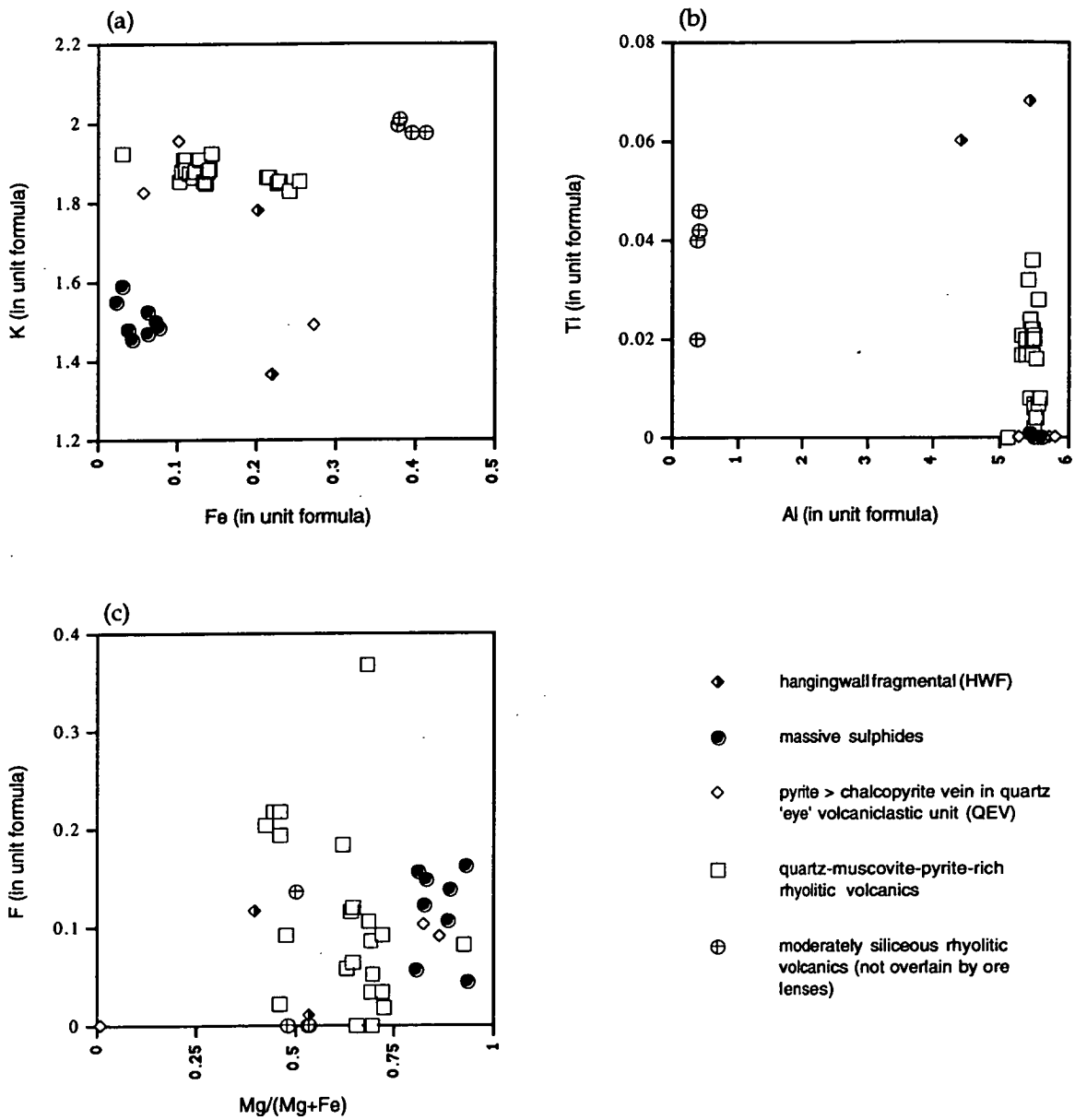

Figure 3.29 Variation in the (a) K and Fe^{2+} content, (b) Ti and Al content, and (c) F with Mg/(Mg+Fe) content of muscovite at Thalanga.

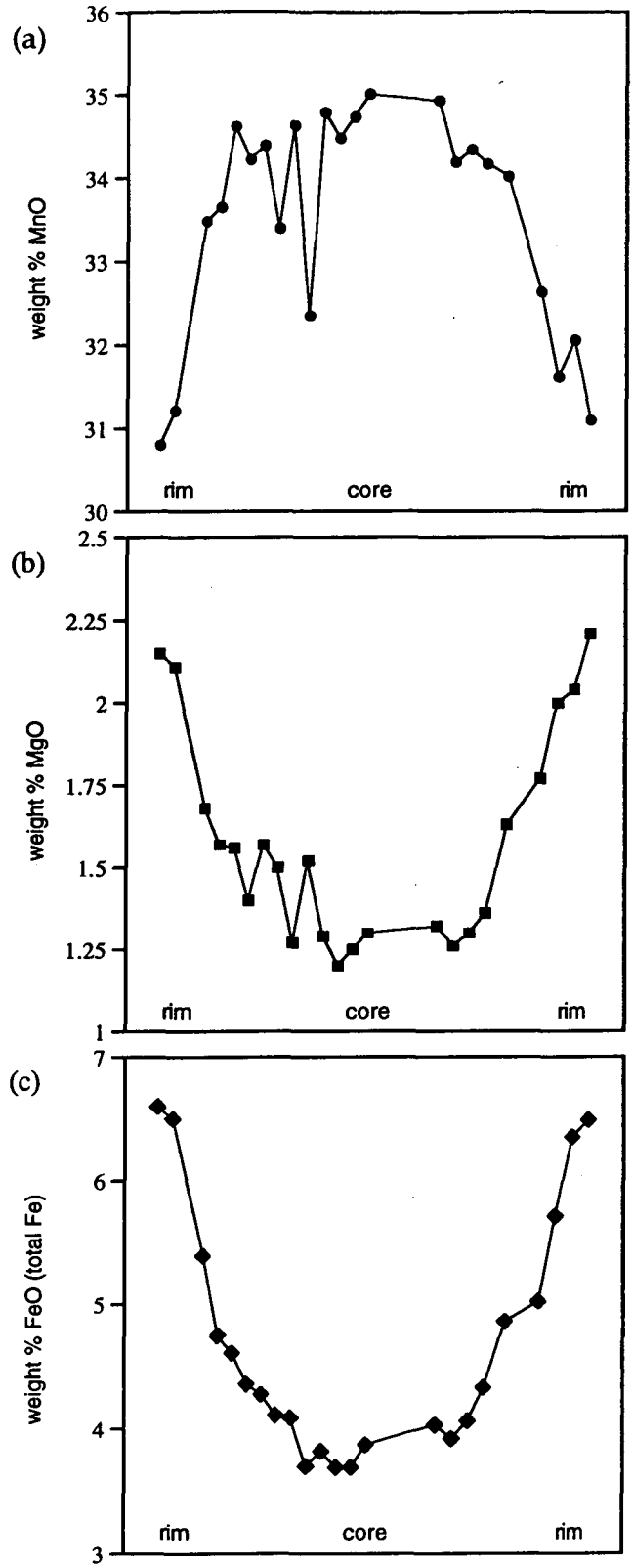

Figure 3.30 Variation in the (a) MnO, (b) MgO and (c) FeO content, from rim to rim, of a garnet porphyroblast located in the footwall rhyolitic volcanics at Thalanga. Sample TH287-196, ring 1.

Garnets from the biotitic HWF at Thalanga contain less Mn than those in the footwall, and this is interpreted to be due to original bulk rock composition (i.e. Mn enrichment due to hydrothermal alteration in the footwall). The cores of garnet porphyroblasts in the HWF contain greater Mn and lower Mg and Fe than the rim (Fig. 3.31a-c). This distribution of Mn, Mg and Fe is also interpreted to have resulted from the preferential concentration of Mn into the early-formed garnets, with later Mn-poor garnet formed due to the depletion of Mn in the bulk rock. However, even the Mn-poor garnets at Thalanga contain >17 weight % MnO (Appendix B).

3.12 Conditions of Peak Metamorphism

3.12.1 Temperature and Pressure Indicator Minerals

The presence of rare biotite kinked S_2 and post-S_3 biotite porphyroblasts indicates temperatures of >400° C for both pre-S_2 and post-S_3 metamorphism at Thalanga (Yardley, 1989). The presence of garnets in some parts of Thalanga does not indicate that metamorphism reached garnet-zone conditions, as such Mn-rich garnets can form at lower temperatures and pressures (Yardley, 1989). If the chlorite spots in the HWF were formed after cordierite, then this provides further constraints on the temperature and pressure of metamorphism. Formation of cordierite typically requires low pressures (<3 kbars, although see Yardley, 1989) and temperatures of >400° C (Ehlers and Blatt, 1982; Yardley, 1989). The above estimates are consistent with previous interpretations of about 450°C and 2-4 kbars pressure for regional metamorphism (Laing, 1984; Wills, 1985; Berry *et al.*, 1992).

3.12.2 Biotite-Garnet Geothermometry

Biotite-garnet assemblages are useful geothermometers because the exchange of Fe and Mg between biotite and garnet, according to the reaction annite + almandine = phlogopite + pyrope, is dependant on temperature (Ferry and Spear, 1978; Perchuk and Laverant'eva, 1983; Ehlers *et al.*, 1994). Goldman and Albee (1977) showed that increasing Ca and Mn in garnet, and Ti and Al^{vi} in biotite, results in lower temperature estimates. However, Ferry and Spear (1978) argued that the garnet-biotite geothermometer can be used without correction for non Mg-Fe components where (Ca+Mn) / (Ca+Mn+Fe+Mg) < 0.2 for garnet and (Al^{vi} +Ti) / (Al^{vi}+Ti+Fe+Mg) < 0.15 for biotite. Garnets at Thalanga are spessartine-rich (Appendix B) with (Ca+Mn) / (Ca+Mn+Fe+Mg) = 0.84, and associated biotite has (Al^{vi} +Ti) / (Al^{vi}+Ti+Fe+Mg) = 0.3, indicating that the geothermometer may not produce valid temperature estimates. The Fe/Fe+Mg ratio of the spessartine-rich garnets at Thalanga is about 0.7, which is less than the compositional range recommended by Ferry and Spear (1978).

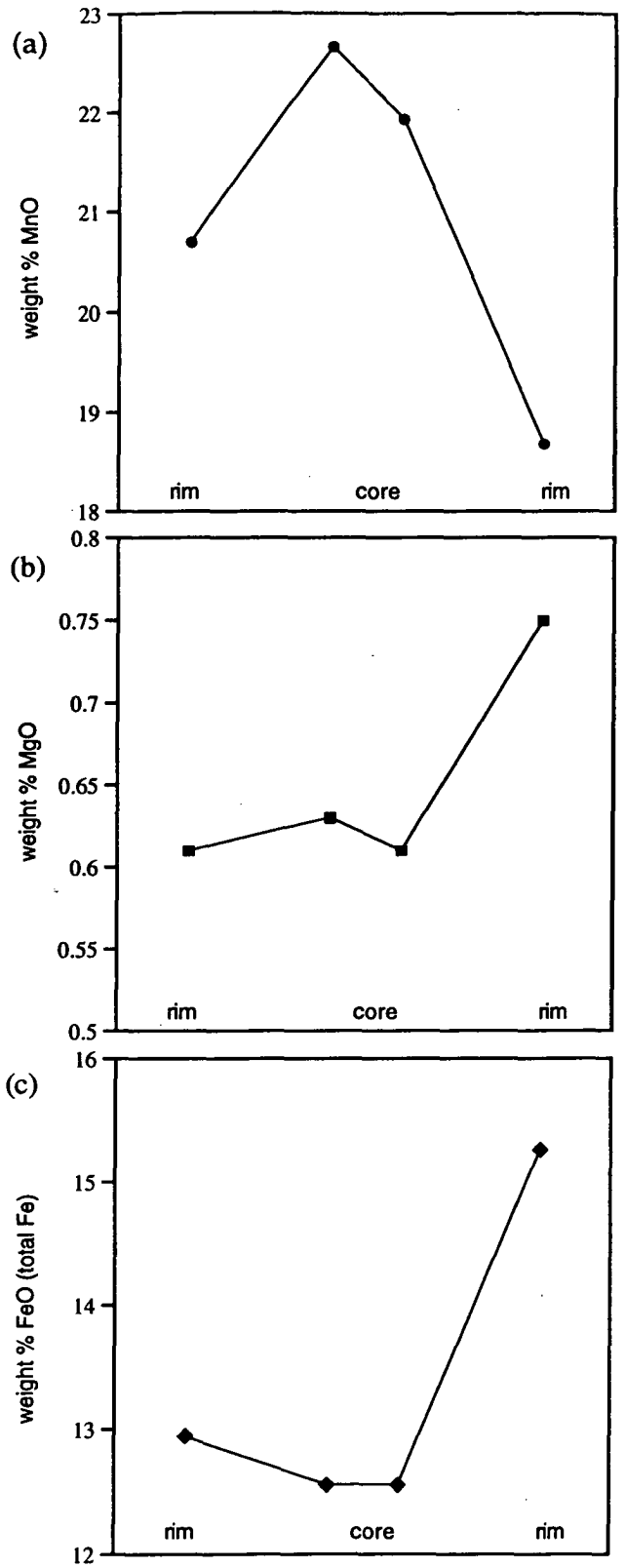

Figure 3.31 Variation in the (a) MnO, (b) MgO and (c) FeO content of a garnet porphyroblast from a biotite-rich zone of the hangingwall fragmental unit (HWF) that overlies the ore horizon at Thalanga. Sample W2011NI05-22.4, ring 1.

The garnet-biotite geothermometer has been reformulated by Bhattacharya *et al.* (1992) and Kleemann and Reinhardt (1994) using recent thermodynamic data and activity-composition relationships in Fe-Mg-Ca garnet solid solutions (Ganguly and Saxena, 1984; Hackler and Wood, 1989; Berman, 1990). The temperature and pressure of peak metamorphism at Thalanga was calculated for a garnet-phlogopite-muscovite-chlorite assemblage (TH287-196; Appendix B) using the THERMOCALC program (version 2.4) of Powell and Holland (1990), and using the garnet activity data model of Berman (1990). Using this technique, and assuming H_2O saturation, the peak metamorphic conditions at Thalanga are estimated to have been 485 ± 23°C and 2.5 ± 1.5 kbars (see Appendix B and C for mineral compositions, equations and activity data). This estimate is reasonable given the peak-metamorphic assemblages at Thalanga.

3.13 Summary of Deformation and Metamorphism at Thalanga

1. There is little evidence of syn-depositional faulting at Thalanga. Folded zones of actinolite-chlorite-epidote-carbonate ± diopside at the contact of quartz-muscovite-pyrite-rich rhyolitic volcanics, and weakly chloritic rhyolitic volcanics in the footwall of the Vomacka Zone are inferred to be the metamorphosed equivalents of hydrothermal alteration along a growth fault. Ascending hydrothermal solutions may have utilised this pathway, producing carbonate-chlorite assemblages along the fault, and quartz-sericite-pyrite alteration in the hangingwall above the fault.

2. Elsewhere at Thalanga quartz-muscovite-pyrite-rich assemblages are confined to semi-conformable zones within the footwall, suggesting that original porosity and permeability controlled the pattern of alteration, and that hydrothermal fluids moved through porous perlitic rhyolite or volcaniclastic units without any focus along faults. Irregular pyrite ± chalcopyrite veins within the footwall are folded, with axial planes subparallel to S_2, and pyrite disseminations and blebs have been recrystallised parallel to S_2.

3. The best preserved evidence of deformation prior to D_2 are subvertical quartz veins, that cross-cut S_0, but are boudinaged and locally tightly folded with axial planes parallel to S_2. It is unclear whether this veining occurred during D_1.

4. Stratigraphy at Thalanga was steeply tilted during regional N-S compression in the Ordovician (D_2). Bedding now faces south, and Thalanga is interpreted to lie on the northern limb of a NE-SW trending syncline. Pervasive axial planar S_2 is clockwise from S_0 at Thalanga. In places, metamorphic biotite is parallel to S_2. Banding in the massive sulphide lenses is also parallel to S_2 in most parts of Thalanga, and is interpreted to have formed during metamorphism associated with D_2.

5. Steeply NE to E-plunging mineral stretching lineations (L_2) indicate a subvertical extension direction during D_2. This lineation is defined by i) clusters of metamorphic biotite, ii) clusters of chlorite and Ti-oxide minerals after biotite, iii) elongated volcanic clasts, iv) minerals in pressure shadows, and v) elongate sulphide blebs. Shallowly-dipping quartz-filled tension gashes are perpendicular to L_2 and support the interpretation of subvertical extension during D_2.

6. An open fold ($\lambda < 10$ km), with subvertical fold axis centred at about Central Thalanga, changes the orientation of stratigraphy from WNW-striking in the West Thalanga ore lens to ENE-striking in the East Thalanga ore lens. S_2 cleavage is folded with the bedding, indicating that this kink in stratigraphy post-dates D_2. NNE-striking faults, with west side down dip-slip movement, post-date the deposit-scale kink and control the separation of West Thalanga from Central Thalanga. NNE-striking microdiorite dykes are inferred to have intruded along the NNE-striking normal faults.

7. A weak, bifurcating crenulation cleavage (S_3) has locally overprinted S_2. Minerals interpreted to have been stable during peak metamorphism are decussate and overgrow S_3, indicating that peak metamorphism at Thalanga post-dates S_3. Rare biotite kinked by S_3 indicates that metamorphism was present before S_3. Temperatures and pressures estimated from a garnet-phlogopite-muscovite-chlorite assemblage indicate that peak metamorphic conditions were 485 ± 23°C and 2.5 ± 1.5 kbars. Peak metamorphism at Thalanga may have occurred during the Silurian to Early Devonian as a result of contact metamorphism.

8. Kinematic indicators on the surfaces of ENE-striking faults have recorded an initial dip-slip movement, with south side up displacement, then later sinistral movement. The ore horizon has been repeated along the ENE-striking faults, resulting local thickened zones of massive sulphides. Adjacent to ENE-striking normal faults, sulphide bands are folded and become parallel to the fault. The similarity between the orientations of the ENE-striking normal faults and the S_3 cleavage, suggests that the normal faults may be syn- or post-S_3 in age.

8. Coarse grained chalcopyrite, sphalerite, and minor galena, have filled boudin necks, tension gashes and other sites of extension within the ore horizon, and are interpreted to have been remobilised from the massive sulphide lenses during D_2. Piercement structures at the contact between massive sulphide lenses and stratigraphically overlying dacite are filled with remobilised chalcopyrite and dark red-brown sphalerite. Chalcopyrite-rich *Durchbewegung* textures within the ore lenses are interpreted to have formed along ENE-striking normal faults during D_3.

CHAPTER 4.

VOLCANIC FACIES RELATIONSHIPS AND DEPOSITIONAL SETTING OF THE HOST VOLCANICS

4.1 Introduction

The host rocks at Thalanga are predominantly submarine volcanic units, with minor post-D_2 intrusions (the timing of which is discussed in Chapter 3). The Thalanga deposit occurs at the contact between rhyolitic volcanics of the Mount Windsor Volcanics and the overlying dacitic to andesitic volcanic units of the Trooper Creek Formation. Massive sulphide lenses and associated alteration are present within a 5 - 50 m thick interval composed of polymict breccia units, syn-volcanic sills, and graded sandstone and siltstone units. This section describes the composition and textures of the volcanic rocks and aims to interpret the processes and timing of formation and to reconstruct the environment of deposition for each volcanic facies. The effects of volcanism on the formation, deposition and preservation of the massive sulphide lenses is discussed in Chapter 6.

Primary volcanic textures have been preserved in most parts of the Thalanga massive sulphide deposit despite the upper greenschist facies regional metamorphism (Chapter 3). However, hydrothermal alteration associated with sulphide mineralisation (Chapters 6 and 10) was the most texturally destructive process at Thalanga. At Thalanga mine, the host rocks have been named and classified on the basis of their inferred pre-deformation and pre-metamorphic textures, and this convention has been adopted here.

In this section, the volcanic rocks at Thalanga are divided into four main units using terminology consistent with that used by the Thalanga mine geologists (Table 2.5, Chapter 2): (i) *rhyolitic volcanics* of the Mount Windsor Volcanics in the footwall, (ii) *quartz-feldspar porphyry* sills, the *quartz 'eye' volcaniclastic unit* and quartz-crystal-rich sandstone within the ore horizon, (iii) the *upper rhyolite breccia* within the ore horizon in East Thalanga, and (iv) volcanic units that overlie the mineralised horizon, consisting of the *hangingwall fragmental* (graded siltstone and sandstone), the *dacite* and associated breccia facies, and *andesite*. The volcanic units within and overlying the ore horizon are classified as the Trooper Creek Formation (section 4.3.1), although the upper rhyolite breccia within the ore horizon (unit iii; section 4.4) is considered by Herrmann (1994) to be part of the Mount Windsor Volcanics. The components and textures of these units are described in the following sections. The character of the Rollston Range Formation near Thalanga is also described in this chapter, together with the petrology of the post-tectonic dykes.

4.2 Rhyolitic Volcanics (unit i; Mount Windsor Volcanics)

At Thalanga, the footwall rhyolitic volcanics have been strongly quartz-sericite-pyrite ± chlorite altered, and subsequently metamorphosed to quartz-muscovite-pyrite ± phlogopite ± chlorite-rich assemblages (Chapter 10). This intense hydrothermal alteration and metamorphism has overprinted and destroyed most primary volcanic textures; typically, only quartz crystals have been preserved. Pseudoclastic textures are a common product of hydrothermal alteration of glassy lavas and intrusions (Allen, 1988) and in most cases pyroclastic textures described by early workers at Thalanga (e.g. Wills, 1985) were subsequently shown by Stolz (1989, 1991) and Berry *et al.* (1992) to have resulted from alteration. Stolz (1989) concluded that the units underlying the ore lenses at Thalanga are composed mainly of coherent rhyolite, as is much of the Mount Windsor Volcanics elsewhere in the Mount Windsor subprovince. This investigation shows that primary volcanic textures have been preserved in the less altered margins of the deposit, allowing some understanding of the variations in the volcanic facies within the footwall.

Pervasively silicified rocks have a massive, uniform appearance, whereas hydrothermal alteration has imparted an apparent clastic texture to the footwall rocks. In intensely altered parts of the footwall, textural domains comprising abundant, irregularly distributed, poorly sorted quartz crystals and crystal fragments are interpreted to have been originally volcaniclastic, whereas domains of evenly distributed, evenly-sized, euhedral to subhedral quartz crystals are interpreted to have been uniformly porphyritic rhyolite. Using this criterion, both coherent rhyolite facies (formed cooling and solidification of molten lava or magma; McPhie *et al.*, 1993), and rhyolitic volcaniclastic facies are present within the footwall rhyolitic volcanics at Thalanga. The dimensions and distribution of coherent versus volcaniclastic rhyolite facies at Thalanga are poorly constrained because the overprinting hydrothermal alteration has masked most primary volcanic textures. Furthermore, brittle faults typically occur at contacts between silicified coherent rhyolite and adjacent quartz-muscovite ± chlorite ± phlogopite ± pyrite-rich rhyolite.

4.2.1 Coherent Rhyolite Facies

Distribution of Coherent Rhyolite Facies

Coherent, flow-banded, perlitic quartz-feldspar-phyric rhyolite has been faulted into a hangingwall position in the eastern parts of Central Thalanga (Fig. 4.1). Locally, this rhyolite has gradational contacts with poorly sorted, clast-supported breccia of the same composition (Fig. 4.2a). Down-dip of the ore horizon in Central Thalanga, a similar quartz-feldspar phyric rhyolite has been faulted into a hangingwall position. This rhyolite is 50-60 m thick and extends for at least 60 m along strike and 150 m down-dip. Poorly sorted rhyolite

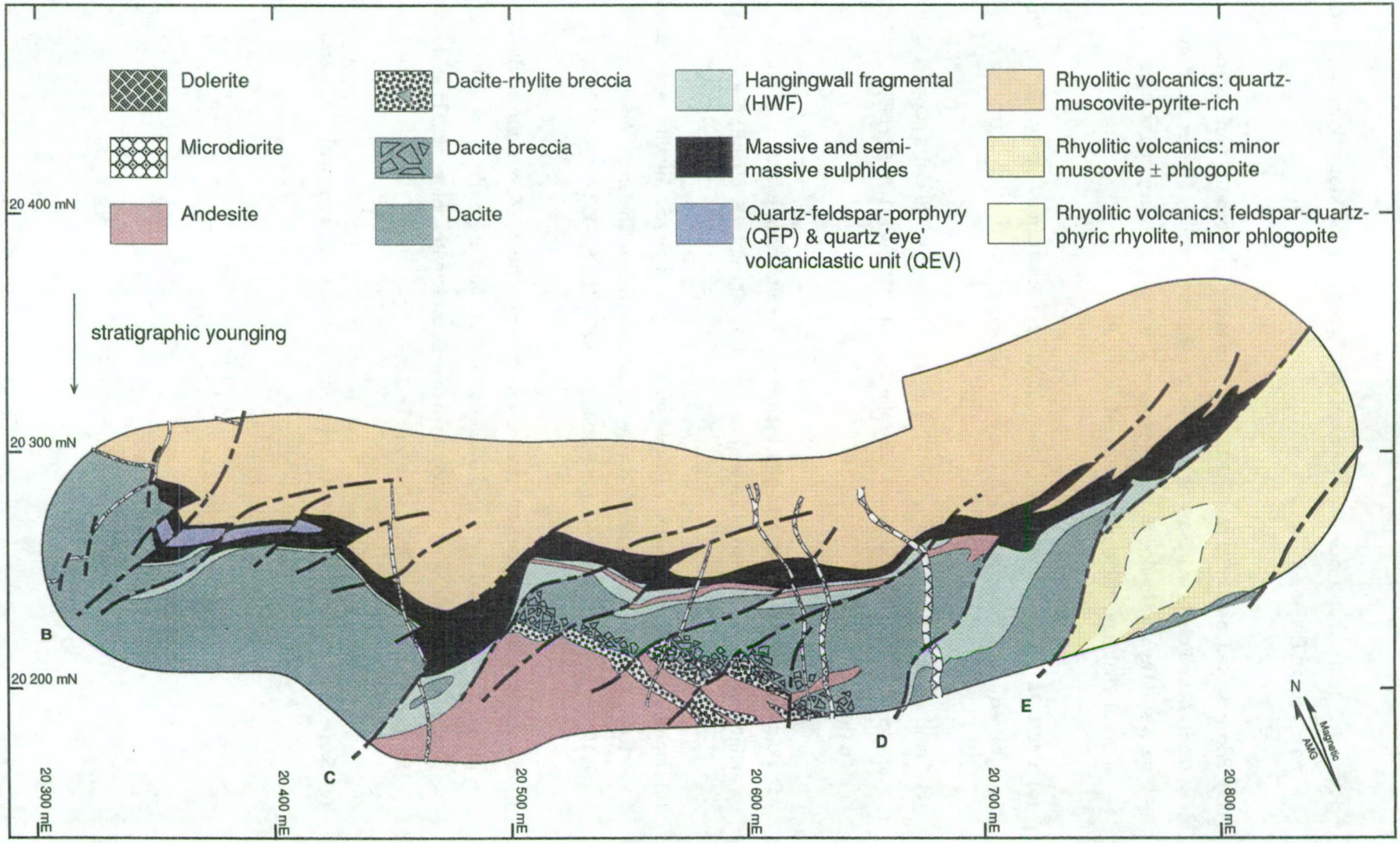

Figure 4.1 Simplified geology of the Central Thalanga open pit. Fact map is map M2.

Figure 4.2 Textural and facies variations in the rhyolites of the Mount Windsor Volcanics near and at Thalanga.

(a) Poorly sorted monomict rhyolite breccia. Clasts are flow-banded and perlitic, and grade from rotated clasts to jigsaw fit textures to coherent rhyolite. The breccia is interpreted to be *in situ* rhyolite hyaloclastite. Hammer is about 30 cm in length. Facing into page. Central Thalanga, 20250 mN, 20 780 mE, 955 mRL.

(b) Photomicrograph of partly embayed quartz phenocryst in intensely silicified rhyolite. Crossed nicols. Sample TH 265-216, East Thalanga.

(c) Hand specimens of intensely silicified quartz-phyric rhyolite clasts supported in a muscovite- and phlogopite-rich siltstone. Sample TH359-134 and TH359-135, East Thalanga.

(d) Folds in flow-banded quartz-phyric rhyolite. Located at intersection of Flinders Highway and the Thalanga Range [mine grid: 21 300 mN, 15 400 mE]. Facing towards left.

(e) Hand specimen of coherent silicified feldspar-quartz-phyric rhyolite from outside the intense hydrothermal alteration zone in the footwall at Thalanga. Abundant phlogopite is disseminated in the groundmass. Sample W2031ND46-132.4, West Thalanga.

(f) Photomicrograph of spherical structures in the groundmass of some muscovite-rich quartz-phyric rhyolites that have radial internal texture and are interpreted to be spherulites. Groundmass is composed of intergrown quartz, muscovite, phlogopite, Ti-oxides and apatite. Sample TH5-337.6, Central Thalanga.

(g) Same as (f) under crossed nicols. Spherulite is rimmed by recrystallised quartz.


a

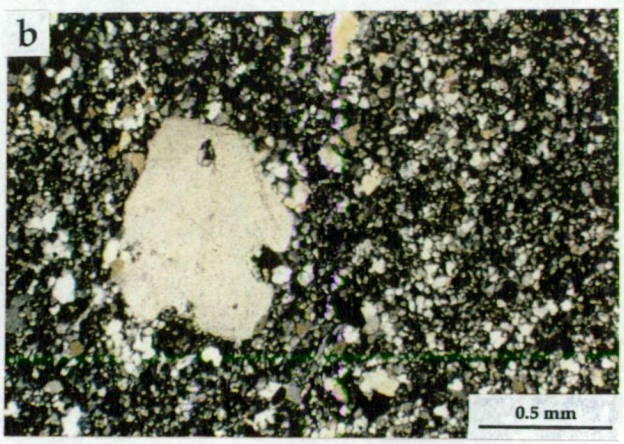
b
0.5 mm


c
20 mm


d
DNA
CM


e
10 mm

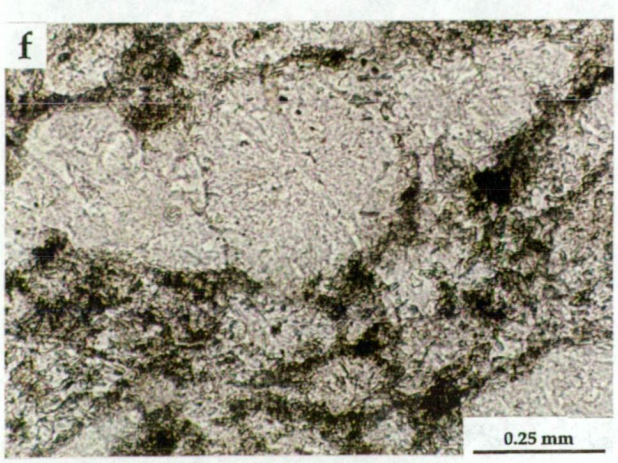
f
0.25 mm

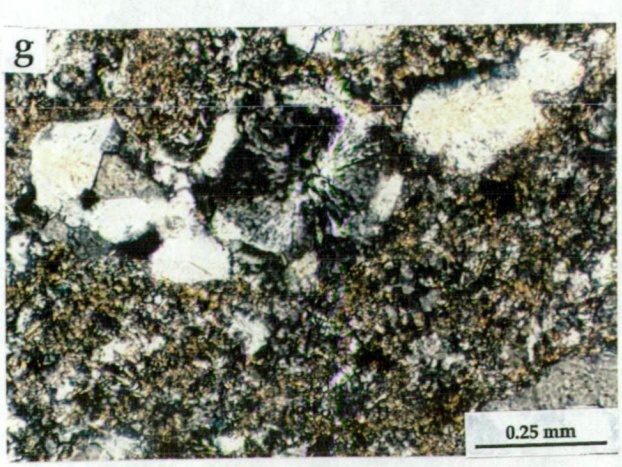
g
0.25 mm

breccia of the same composition occurs up-dip of the rhyolite and poorly sorted polymict breccia with both dacite and rhyolite clasts stratigraphically overlies the rhyolite. The relationship between the quartz-feldspar-phyric rhyolite and the overlying polymict breccia is unclear as it has only been intersected in one drill hole (diamond drill hole TH14).

The intensely silicified interval at the stratigraphic top of the rhyolitic volcanics in East Thalanga (Fig. 4.3a) contains sparse, evenly distributed euhedral and partly embayed quartz phenocrysts (Fig. 4.2b) and irregular albite grains that may be remnants of plagioclase phenocrysts or crystals. This rhyolitic domain is lozenge-shaped, extends about 200 m along strike and up-dip, is <30 m thick (Fig. 4.3a), and was considered to be coherent in previous interpretations (Hill, 1993). Angular, intensely silicified rhyolite clasts, supported in a sandy siltstone matrix occur up-dip from the silicified rhyolitic domain (Fig. 4.2c). Down-dip the silicified rhyolitic interval has a gradational contact with quartz-muscovite-pyrite-rich rhyolitic volcanics.

Less strongly silicified, coherent quartz-feldspar-phyric rhyolite is commonly present at a depth of at least 200 m stratigraphically below the massive sulphide lenses at Thalanga (e.g. Fig. 4.3a), but its dimensions are unknown because of the lack of drill holes into the footwall to the north of the massive sulphide deposit. Siliceous, flow-banded, quartz>feldspar-phyric rhyolite (Fig. 4.2d) makes up most of the topographic highs that define the Thalanga Range northwest of the Thalanga deposit.

Textures of the Coherent Rhyolite Facies

The best preserved coherent rhyolites (in hand specimen) at Thalanga are commonly moderately silicified quartz-phyric or quartz-feldspar-phyric (Fig. 4.2e). However, many strongly quartz-muscovite ± phlogopite ± chlorite ± pyrite-rich parts of the footwall with apparent clastic textures in fact have evenly distributed, hexagonal to bipyramidal quartz crystals, suggesting that they may also be coherent. Rare spherulites, composed of fine, radial quartz fibres and rims of recrystallised quartz, indicate that the groundmass was formerly glassy (Fig. 4.2f,g). Disseminated groundmass phlogopite is interpreted to be metamorphic in origin, and commonly defines a mineral extension lineation parallel to S_2 (Chapter 3).

Relic perlite is present in some of the least altered flow-banded, quartz-feldspar-phyric rhyolites at Thalanga, indicating that the rhyolite in this location was glassy and had been devitrified prior to hydrothermal alteration (Fig. 4.4a,b). Fine-grained muscovite and quartz commonly occupy the perlite kernels and the arcuate fractures have been overprinted by quartz, phlogopite or muscovite.

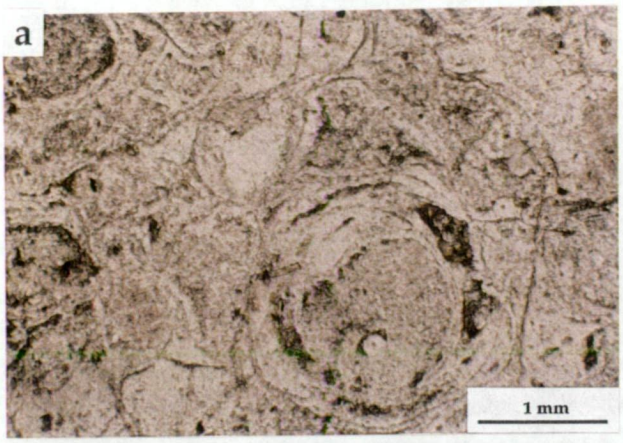
a
1 mm

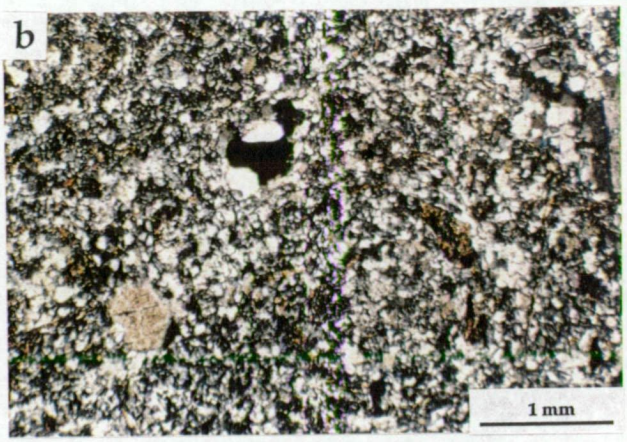
b
1 mm

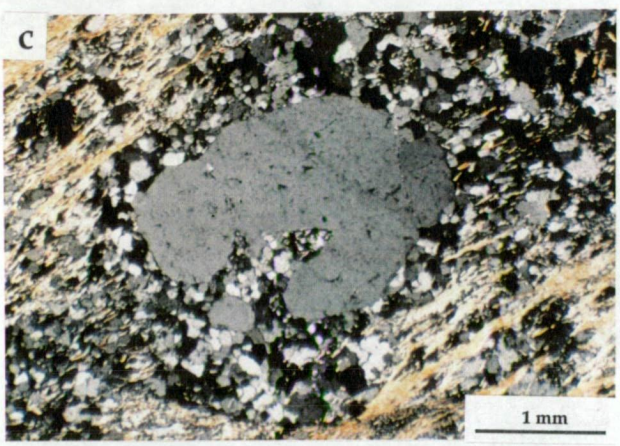
c
1 mm


d
10 mm


e


f
20 mm


g
10 mm


chl
rhyol
40 mm

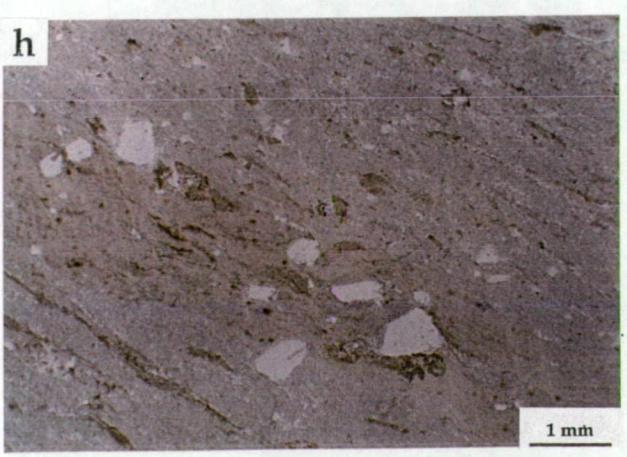
h
1 mm

The phenocryst content of coherent quartz-feldspar-phyric rhyolite at Thalanga is usually 2-5%, whereas the quartz-phyric rhyolites contain 2% phenocrysts. Quartz phenocrysts are either blue or colourless in hand specimen (Fig. 4.2e), typically 1-2 mm in size and in thin section, are subhedral to bipyramidal in habit, but are slightly round with embayed margins (Fig. 4.4c). Many quartz phenocrysts have undulose extinction or are composed of sub-grains, and have been enveloped by recrystallised quartz (Fig. 4.4c).

Where present in coherent rhyolites, the proportion of feldspar phenocrysts is generally equal to or greater than that of quartz phenocrysts. Feldspar phenocrysts are white in hand specimen and usually occur as glomerocrysts up to 3 mm in size (Fig. 4.4e). The feldspars are now about 98 % albite (microprobe analyses in Appendix B). Albitised feldspars in strongly silicified coherent rhyolite are also commonly partly replaced by quartz and with increasing alteration, the feldspars are replaced by muscovite, quartz and calcite (Chapter 10). Coarsely porphyritic rhyolite is present in some areas of the footwall. Although the quartz phenocrysts are larger, up to 4 mm in size, these coherent rhyolites have similar textures to the quartz-feldspar-phyric rhyolites described above.

4.2.2 Rhyolitic Volcaniclastic Facies

Distribution of Rhyolitic Volcaniclastic Facies

Volcaniclastic units are present at the stratigraphic base and near the top of the Mount Windsor Volcanics along the Thalanga Range and in this area, the abundance of rhyolitic breccia units increases towards the top of the Mount Windsor Volcanics (Fig. 4.5). At Thalanga, poorly sorted rhyolitic breccia and quartz sandstone are common near the stratigraphic top of the rhyolitic volcanics (Fig. 4.6a-c). However, single quartz-phyric rhyolite clasts that are isolated in a matrix of fine grained quartz-muscovite ± phlogopite ± chlorite ± pyrite (Fig. 4.4d) are widely dispersed through the footwall rhyolitic volcanics. Drill hole sections suggest that thin (<20 m) intervals of coherent facies separate volcaniclastic units which are 1-20 m in thickness.

Strongly silicified, well sorted feldspar- and quartz-bearing rhyolitic sandstone units have been faulted into a hangingwall position at the down-dip and eastern end of West Thalanga (Fig. 4.3b). Weakly altered rhyolitic sandstone units with fiamme-like textures are associated with the silicified sandstone.

Textures of the Rhyolitic Volcaniclastic Facies

Volcaniclastic Units in the Thalanga Range: A matrix-supported rhyolite breccia, 5-40 m thick, occurs at the stratigraphic top of the Mount Windsor Volcanics in places along the

(a)

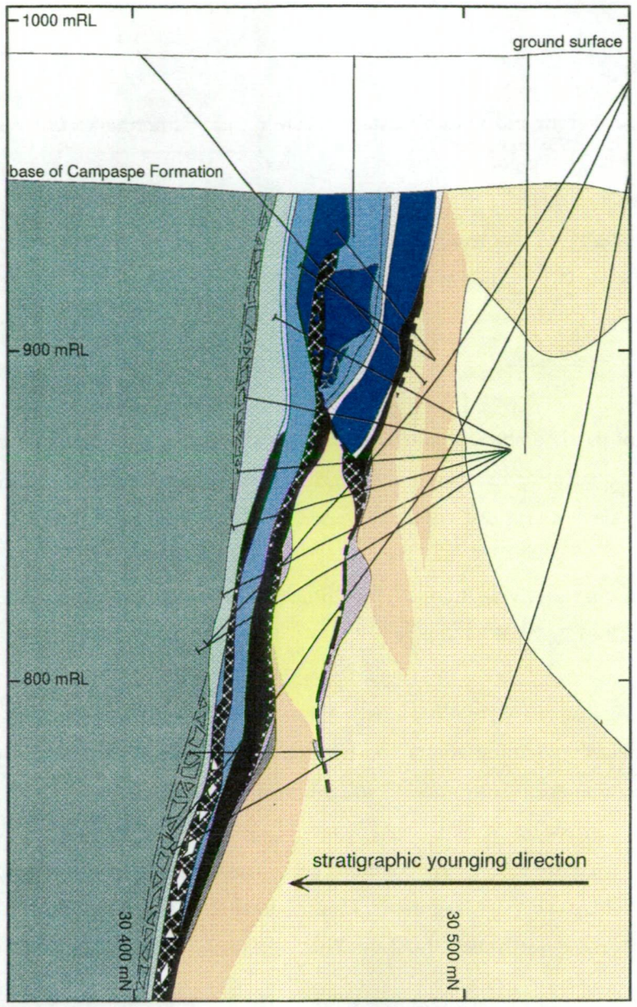

(b)

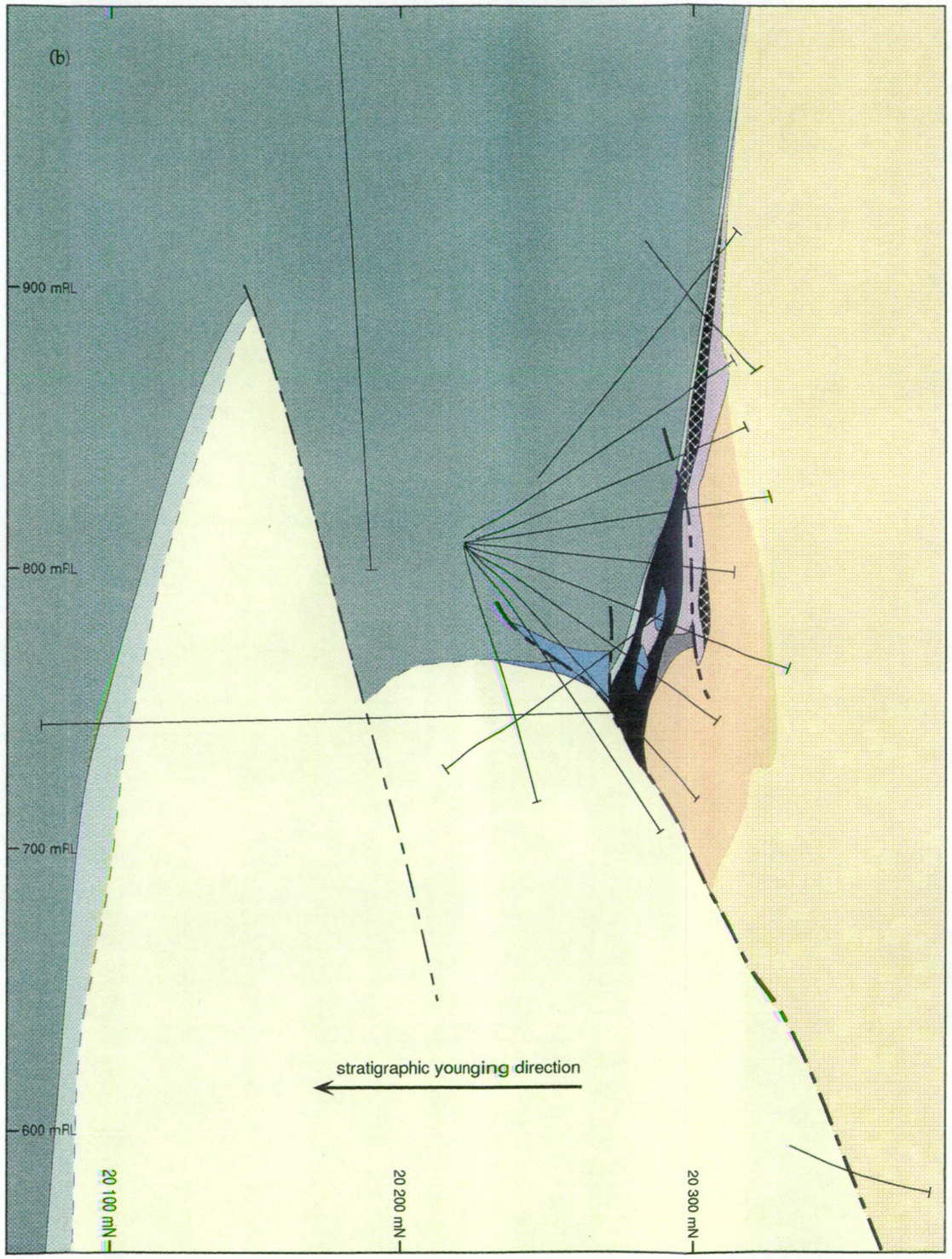

Dacite
Dacite breccia
Hangingwall fragmental (HWF)
Quartz & feldspar sandstone (QEV sandstone)
Quartz 'eye' volcaniclastic unit (QEV breccia)
Quartz-feldspar porphyry (QFP)
QFP clasts in QEV
Siltstone

Massive sulphides
Semi massive sulphides
Semi massive sulphides in upper rhyolite breccia
Massive pyrite
Carbonate-chlorite-tremolite in West Thalanga; massive chlorite in East Thalanga
Rhyolitic volcanics: pyrite stringer zone
Rhyolitic volcanics: quartz-muscovite-pyrite ± chlorite-rich
Rhyolitic volcanics: intense silicification
Rhyolitic volcanics: moderate to minor muscovite ± quartz ± phlogopite

Figure 4.3 Cross sections of the Thalanga deposit from West and East Thalanga. (a) Cross section of East Thalanga along the 32 040 mE section. (b) Cross section of West Thalanga along the 20 290 mE section. Top of diagram is approximately equal to ground surface.

Figure 4.4 Textures of coherent and volcaniclastic rhyolite facies within the Mount Windsor Volcanics near and at Thalanga.

(a) Photomicrograph of altered and metamorphosed perlite fractures in feldspar-quartz-phyric rhyolite. Sample 955-4, Central Thalanga, 20250 mN, 20 780 mE, 955 mRL.

(b) Same as (a) under crossed nicols.

(c) Photomicrograph of partly embayed quartz phenocryst enveloped by recrystallised quartz. Fine grained quartz and muscovite are common in the groundmass. Crossed nicols. Sample TH71-64.9, eastern end of Central Thalanga.

(d) Irregular, rounded quartz-phyric rhyolite clast in matrix of muscovite-quartz-phlogopite. Sample W2009ND10–61.2, West Thalanga.

(e) Rhyolite breccia: angular to subrounded clasts of quartz-feldspar-phyric rhyolite. Clasts are supported in matrix containing quartz and feldspar crystals. Located on southwest side of Thalanga Range, mine grid: 20 065 mN, 15 400 mE. Facing towards bottom.

(f) Quartz and feldspar sandstone. The dark coloured clasts are composed of siltstone to sandy siltstone with rare feldspar crystal fragments. Located near the base of the Mount Windsor Volcanics, on the northeast side of the Thalanga Range. Mine grid: 21 700 mN, 14 000 mE.

(g) Top: quartz-phlogopite-chlorite-rich rhyolite breccia, with trace pyrite. Flow-banded rhyolite clasts are blocky to irregular in shape. Sample E3208SD05-12.8, East Thalanga. Bottom: polychromatic rhyolite breccia, composed of blocky to cuspate chlorite-phlogopite-rich clasts (formerly glassy rhyolite?) and irregular to rounded siliceous rhyolite clasts. Sample TH278-94, East Thalanga. Facing towards left.

(h) Photomicrograph of wispy quartz-phyric phlogopite domains that may be altered pumice or dense glass. Quartz crystals are subhedral and slightly more abundant in the phlogopite domains than the matrix. Irregular clasts of siliceous quartz-feldspar-phyric rhyolite also present in this sample. Sample TH33-277, West Thalanga.

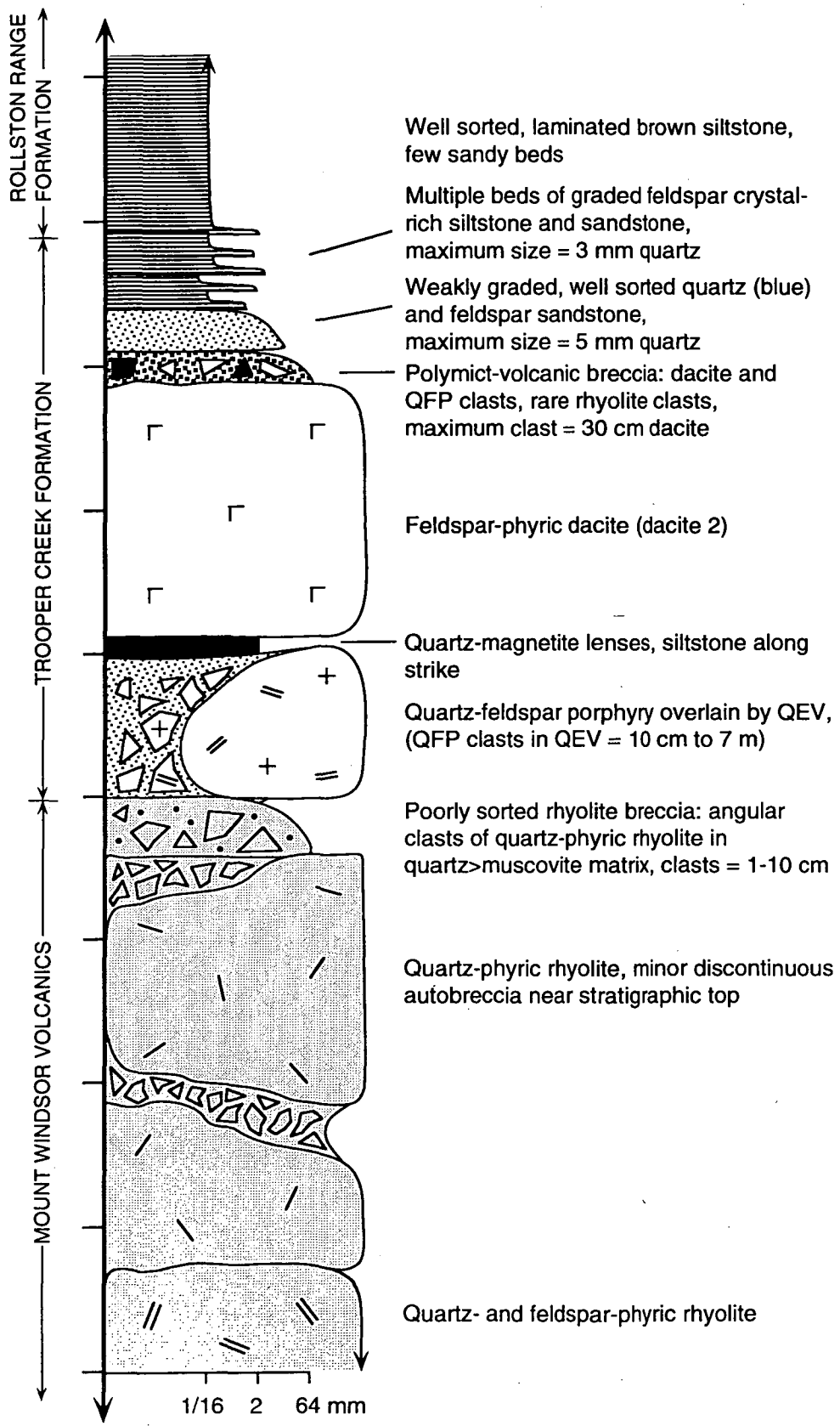

Figure 4.5 Simplified graphic log through the Thalanga Range near Flinders Highway (mine grid, 15 600 mE). Tick marks along the vertical axis are 100 m apart. QFP = quartz-feldspar porphyry, QEV = quartz eye volcaniclastic unit

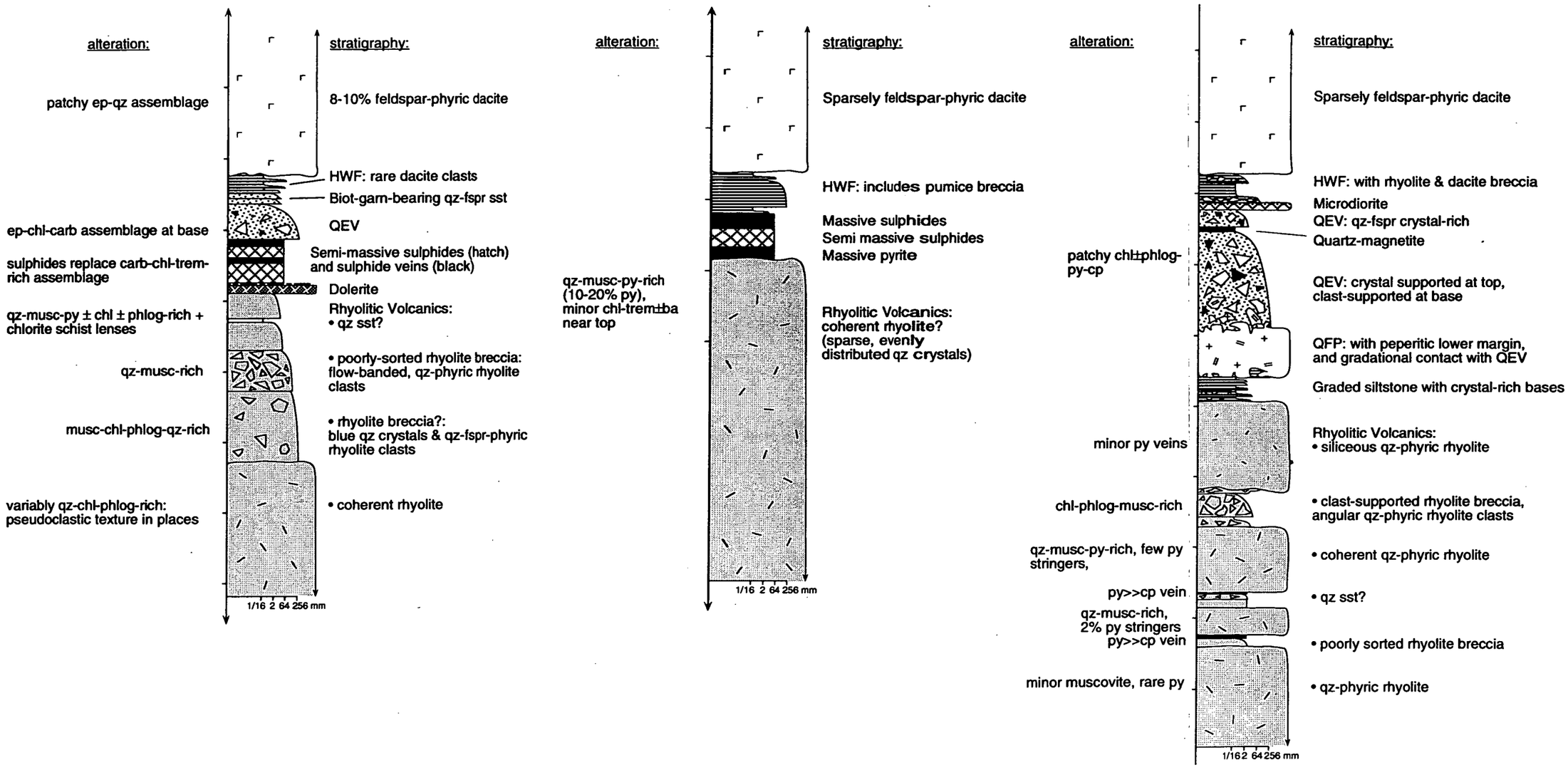

Figure 4.6 Typical stratigraphic columns of West, Central and East Thalanga. (a) Simplified graphic log of West Thalanga based on 20 110 mE section and drill holes TH247 and W2011ND10 and W2011ND39, (b) Simplified graphic log of Central Thalanga based on 20 430 mE section and drill holes TH230 and 2043NI30, (c) Simplified graphic log of East Thalanga based on 32 120 mE section and drill hole 3212SD18. Marks along vertical axis are 10 m apart, and for all logs, approximate true thickness is shown. Abbreviations: ba = barite, biot = biotite, carb = carbonate, chl = chlorite, cp = chalcopyrite, ep = epidote, fspr = feldspar, garn = garnet, HWF = hangingwall fragmental, musc = muscovite, phlog = phlogopite, py = pyrite, QEV = quartz eye volcaniclastic unit, QFP = quartz-feldspar porphyry, qz = quartz, sst = sandstone, trem = tremolite.

Thalanga Range. The breccia comprises rounded to angular quartz-feldspar-phyric rhyolite clasts supported by a matrix of fine-sand sized quartz crystals (Fig. 4.4e). The clasts are generally <50 cm, with an average size of <10 cm. Clast size increases along strike to the northwest, and reaches a maximum size of ≤2 m between 12 000 mE and 12 400 mE (mine grid).

A quartz and feldspar sandstone, about 30 m thick and 50 m in strike length, containing <5-10 % quartz-feldspar-phyric rhyolite and grey siltstone clasts is present close to the stratigraphic base of the Mount Windsor Volcanics on the northern side of the Flinders Highway (Hill, 1992). The breccia is composed of about 40 % crystals (1-5 mm in size) supported by a fine grained siliceous matrix and there is a higher proportion of feldspar crystals than quartz crystals (Fig. 4.4f). The siltstone clasts are typically flattened parallel to cleavage, some with feathery margins, and are poorly sorted (1 - 20 cm in size). Angular to sub-rounded quartz-feldspar-phyric rhyolite clasts are similar in size and also flattened parallel to cleavage.

Volcaniclastic Units at Thalanga: Monomict rhyolitic breccia units composed of clasts of flow-banded rhyolite or quartz-phyric rhyolite clasts (± flow-banding) are poorly sorted and non-graded (Fig. 4.4g top; Table 4.1). Units are generally <2 m in thickness, vary from matrix- to clast-supported, and contain angular quartz-phyric rhyolite clasts (≤40 cm), quartz crystals (maximum size about 4 mm) and rare feldspar crystals (Table 4.1). Polychrommatic breccia units are also present within the footwall rhyolitic volcanics at Thalanga (Fig. 4.4g bottom; Table 4.1).

Table 4.1 Breccias within the footwall rhyolitic volcanics at Thalanga.

Components	Matrix	Lithofacies	Preferred Interpretation
• Siliceous, flow-banded, quartz-phyric rhyolite clasts, maximum ~ 40 cm, blocky shapes, angular to rounded (Fig. 4.4g; upper sample)	• Fine-grained quartz-muscovite ± pyrite-chlorite • Quartz crystals, blue to colourless, <2 mm size	Matrix- to clast-supported, poorly sorted, massive	Autobreccia or resedimented hyaloclastite
• Quartz-phyric rhyolite clasts, irregular, ragged or cuspate shapes (Fig. 4.4g lower sample) • Massive, fine grained phlogopite clasts, blocky or cuspate shapes (formerly glassy?) (Fig. 4.4g lower sample)	• Fine-grained quartz-muscovite-chlorite • Colourless quartz crystals, *in situ* fractured to intact	Matrix- to clast-supported, poorly sorted, massive	Resedimented hyaloclastite, formed by gravitational collapse of quench-fragmented rhyolite dome, resulting in both glassy and crystalline clasts
• Fine grained muscovite- or phlogopite-rich clasts, with quartz phenocrysts, wispy irregular shapes with feathered ends, maximum >6 cm size (Fig. 4.7c,d) • Rare, siliceous quartz-feldspar-phyric rhyolite, maximum ~ 2 cm size (Fig. 4.7c,d)	• Fine-grained quartz-muscovite, trace pyrite • Quartz crystals, blue to colourless, ~ 1 mm size, broken, jigsaw-fit-texture • Feldspar crystals, ~ 1 mm size, broken, jigsaw-fit-texture	Matrix supported, moderately to poorly sorted, massive	Pumice-bearing, rhyolite breccia

Locally, lenticular muscovite- or phlogopite-rich patches (≤5 cm in size) with feathered ends that are enclosed by domains of fine grained quartz with minor phlogopite-muscovite and resemble fiamme (cf. McPhie *et al.*, 1993) are present in many parts of the footwall rhyolitic volcanics. In some cases, quartz crystals are larger and weakly concentrated within the phyllosilicate-rich domains (Fig. 4.4h). The quartz crystals within the phlogopite-muscovite domains are also subhedral, whereas anhedral crystals occur in the matrix. This uneven distribution of quartz crystals, together with the feathered ends of the clasts is interpreted to indicate that the fiamme in Figure 4.4(h) are altered porphyritic glass or pumice clasts. Uncollapsed pumice clasts, now composed of recrystallised quartz, with tube walls defined by muscovite (Fig. 4.7a,b), are rarely preserved within strongly altered parts of the footwall. Non-vesicular quartz-phyric rhyolite clasts are locally present within these pumice-bearing breccia units (Fig. 4.7c, d; Table 4.1).

The clastic texture of the strongly silicified feldspar and quartz sandstone unit (faulted into hangingwall at the eastern end of West Thalanga; Fig. 4.3b) is only recognisable in thin section, where subrounded quartz and feldspar crystals are supported in a matrix of irregular quartz grains (Fig. 4.7e,f). Rare small (5 mm), rounded clasts of myrmekitically intergrown quartz and albite, interpreted to be granitoid fragments, are present within this sandstone (Fig. 4.7g).

4.2.3 Contact Between the Rhyolitic Volcanics and the Overlying Ore Lenses

The contact between the footwall rhyolitic volcanics and the overlying ore horizon is generally sharp and irregular, or planar and sheared. In places, sulphide veins have overprinted the rhyolitic volcanics and gradually amalgamated to form massive sulphide lenses (Chapter 6). Inclusions of rhyolite within massive sulphide lenses directly overlying the footwall are interpreted to be relicts of rhyolite between coalesced sulphide veins, rather than genuine clasts deposited during sulphide accumulation. Where the footwall rhyolitic volcanics are directly overlain by chlorite schist or carbonate-chlorite-tremolite assemblages (Chapter 11), the contact is sharp and planar, or else rarely gradational.

4.2.4 Deposition of the Rhyolitic Volcanics

Emplacement of Coherent Rhyolite

Most parts of the rhyolitic volcanics at Thalanga are composed of evenly distributed quartz phenocrysts within a matrix of fine grained quartz, muscovite and minor phlogopite, chlorite and locally pyrite. These domains are interpreted to be strongly altered rhyolite lavas or intrusions. However, the dimensions and contact relationships of these units are unclear because of the intense hydrothermal alteration. In the less altered eastern parts of Central

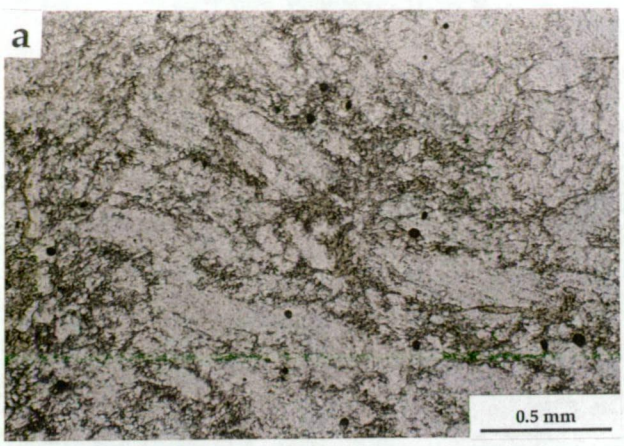
a
0.5 mm

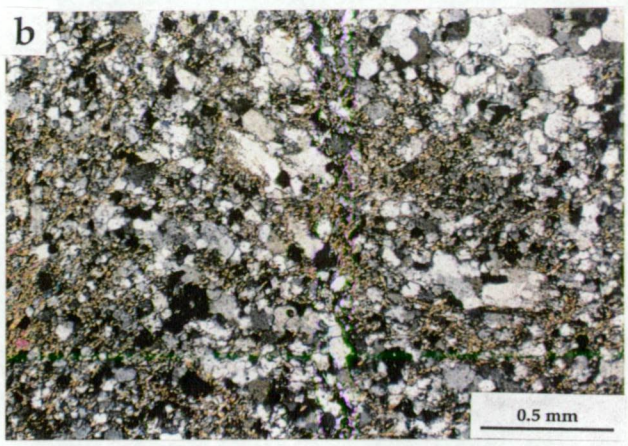
b
0.5 mm

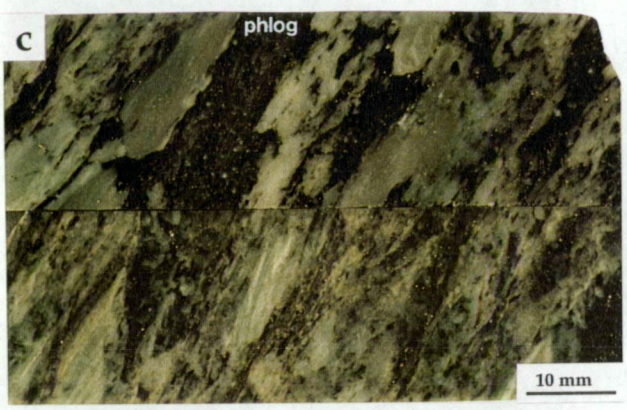
c
phlog
10 mm


d
10 mm

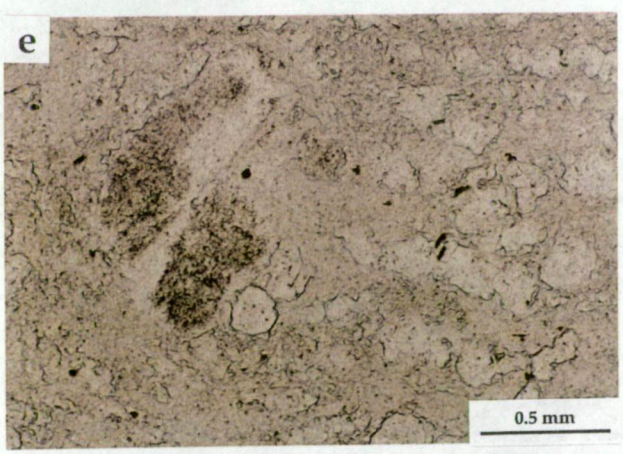
e
0.5 mm

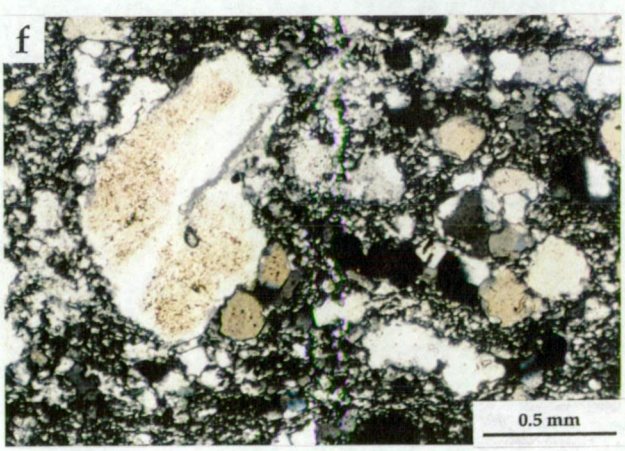
f
0.5 mm

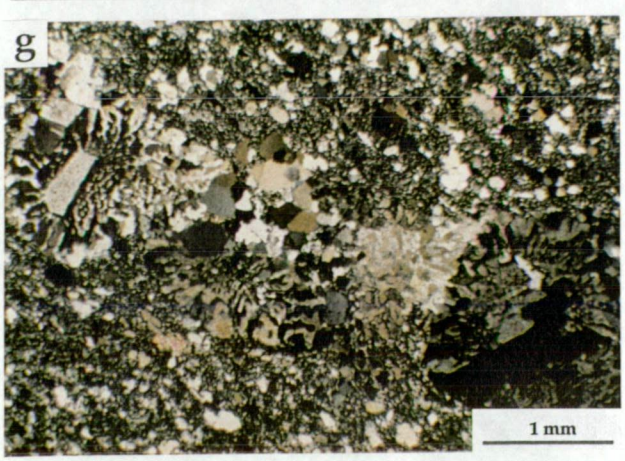
g
1 mm

Thalanga, the gradation from monomict rhyolite breccia with rotated clasts, to jigsaw-fit texture, to coherent rhyolite is consistent with subaqueous emplacement of the rhyolite as a lava or dome composed of a coherent core surrounded by *in situ* hyaloclastite.

It is not clear whether the coherent rhyolite located about 200 m stratigraphically below the top of the footwall rhyolitic volcanics (section 4.2.1) is less altered because it was located at the margin of the main zone of hydrothermal alteration, or whether it was emplaced after the hydrothermal activity was initiated. The second interpretation would imply that this coherent rhyolite was an intrusion.

The angular, strongly silicified rhyolite clasts that occur up-dip of the intensely silicified rhyolite interval in East Thalanga were previously interpreted to have spalled from a submarine dome by quench fragmentation (Hill, 1993). Yet there is no evidence of a hyaloclastite apron around the silicified rhyolitic domain and the angular siliceous rhyolite clasts are identical to rhyolite clasts in other volcaniclastic units within the ore horizon and could have been sourced from elsewhere. Furthermore, the low aspect ratio of this silicified rhyolitic domain is unusual for a felsic extrusion. Felsic lavas are typically highly viscous and therefore more likely to form domes with high aspect ratios (e.g. the Pual Ridge in the Manus Basin; Binns and Scott, 1993). The preferred interpretation is that intense silicification (Chapter 10) has resulted in an apparently coherent rhyolite and that the primary volcanic textures were completely destroyed during this alteration.

Deposition of Rhyolitic Volcaniclastic Facies

The presence of numerous quartz-phyric rhyolite clasts suggests that many part of the footwall underlying the ore lenses at Thalanga were originally volcaniclastic. In less altered rhyolitic volcanics, gradational contacts between rhyolite breccia, with jigsaw fit textures, and coherent rhyolite is consistent with *in situ* quench fragmentation, and such quenching may have been an important process in the production of volcaniclastic intervals in most parts of the footwall. Monomict rhyolitic breccia units composed of clasts of flow-banded rhyolite or quartz-phyric rhyolite clasts (± flow-banding) in quartz-muscovite-pyrite-rich assemblages are interpreted to be altered proximal resedimented hyaloclastite or autobreccia (Table 4.1). This interpretation is similar to that of Gregory *et al.* (1990) who considered that the footwall rhyolitic volcaniclastic units were hyaloclastites formed during the subaqueous eruptions of rhyolite lavas.

Intervals within the rhyolitic volcanics that contain pumice clasts also contain non-vesicular quartz-phyric rhyolite clasts, both of which could have formed via flow- or quench-fragmentation of variably vesicular coherent rhyolite. The poorly sorted, non-graded characteristics of the pumice-bearing breccia is consistent with transportation by mass flow,

and the pumice could have been transported larges distances from the site of original emplacement of a partly vesicular lava.

The origin of rounded granitoid clasts present within some rhyolitic volcanic sandstone units (section 4.2.2) is unknown, although it is clear that such particles were not locally derived. Either they were xenoliths erupted during rhyolite emplacement, or they were originally eroded from an older continental terrain, then transported by mass flows and redeposited at Thalanga.

Depositional Environment

At Thalanga, most contacts between coherent and volcaniclastic rhyolite facies have been overprinted by hydrothermal alteration and identification of the three-dimensional facies geometry is difficult. Facies analyses of ancient submarine volcanic successions demonstrate the importance of lavas, syn-volcanic sills and cryptodomes (Allen, 1992; Cas, 1992; McPhie and Allen, 1992). It is possible that one or all of these facies may occur in the rhyolitic volcanics at Thalanga. The presence of hyaloclastite breccia at the margins of the perlitic rhyolite in Central Thalanga suggests that the rhyolite may have broken through the seafloor either as a lava, dome or partly emergent cryptodome. Volcaniclastic facies elsewhere at Thalanga are probably *in situ* or resedimented autoclastic or hyaloclastic breccia. The dominance of rhyolite lavas/domes and *in situ* hyaloclastite, together with the paucity of other non-rhyolitic units is consistent with proximity to source. It is interpreted here that the footwall rhyolitic volcanics at Thalanga were emplaced as a submarine dome complex.

4.3 Coarse Quartz-bearing Rocks (unit ii)

4.3.1 Introduction

Coarse quartz crystal-rich rocks are intimately associated with the massive sulphide lenses within the ore horizon at Thalanga. The quartz crystals, up to 12 mm in diameter, are distinctive grey to deep blue colour in hand specimen and locally named quartz 'eyes'. Submicroscopic inclusions of rutile, ilmenite, or tourmaline are interpreted to cause the blue colour (due to the Rayleigh scattering of light) in natural quartz crystals (Stalder, 1966; Coblieg *et al.* 1986; Zolensky *et al.*, 1988; see Appendix D). Previous workers interpreted all rocks with large blue quartz crystals as massive crystal tuff, crystal lithic tuff, and quartz 'eye' tuff (Wills, 1985; Gregory *et al.*, 1990). However, this investigation distinguishes three quartz 'eye' facies at Thalanga: coherent quartz-feldspar porphyry (QFP); poorly sorted polymict breccia (quartz eye volcaniclastic unit: QEV breccia); and graded quartz and

described below as volcaniclastic facies I. Massive to graded siltstone and sandstone (volcaniclastic facies II) is also spatially associated with these facies. The similarity in components and spatial arrangement suggests that this facies association may have been produced during a single eruption. In this section, the quartz 'eye' facies variations are described first, and then their contact relationships documented in order to constrain their origin.

Although the QFP is classified as a rhyolite on the basis of it phenocryst and groundmass composition, the QFP within the ore horizon consistently has immobile element ratios indistinguishable from some of the dacite in the overlying Trooper Creek Formation, but different from the immobile element ratios of the underlying rhyolite of the Mount Windsor Volcanics (Chapter 5). This geochemical difference supports the classification of the QFP and QEV as part of the Trooper Creek Formation.

4.3.2 Coherent Facies: Quartz-Feldspar Porphyry

Distribution

QFP units are present within the ore horizon in East and Central Thalanga, and form prominent ridges along the Thalanga Range at the contact between the Mount Windsor Volcanics and the overlying dacite of the Trooper Creek Formation. The largest outcrop of QFP occurs between 16 200 mE and 18 600 mE (mine grid) along the Thalanga Range, where it is 120-150 m true thickness (map M1). Both the stratigraphic base and top of this QFP are sharp and planar. A quartz-phyric rhyolite inclusion (20 m diameter) of Mount Windsor Volcanics near the base of the QFP, suggests that this contact may be partly intrusive. QFP dykes within the Mount Windsor Volcanics at the eastern end of the Thalanga Range are at a low angle to bedding, and are interpreted to be feeder dykes to the QFP (map M1; Sainty and Hill; 1996).

The QFP at the western end of Central Thalanga is up to 10 m thick and 60 m in strike length (Fig. 4.1; map M3). It is surrounded by massive sulphides and truncated by normal faults down-dip. QFP units are not present in West Thalanga. At East Thalanga, units of QFP are 10-30 m thick and up to 500 m in strike-length (Fig. 4.8a), and have irregular contacts with QEV, graded siltstone, and massive sulphide lenses (section 4.3.5). At least two QFP units are present within the ore horizon, and in most parts of East Thalanga a weakly chloritic QFP unit stratigraphically overlies the footwall massive sulphide lens in up-dip parts of the ore horizon (Fig. 4.3a). A second siliceous QFP, is enveloped by QEV units near the stratigraphic top of the ore horizon, and locally repeated by faults (Fig. 4.3a).

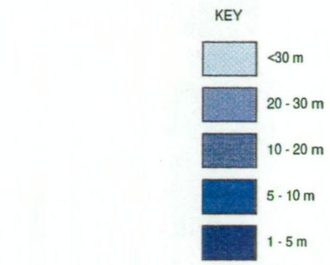

(a) QFP

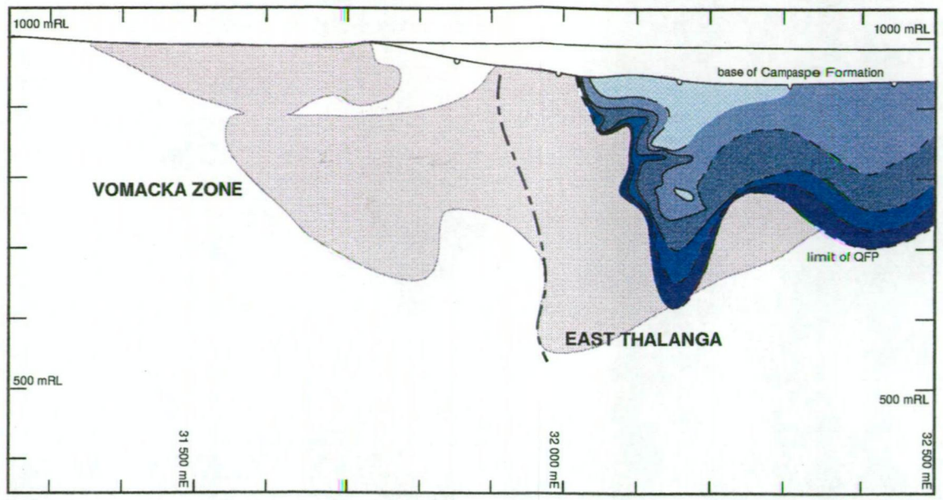

(b) QEV

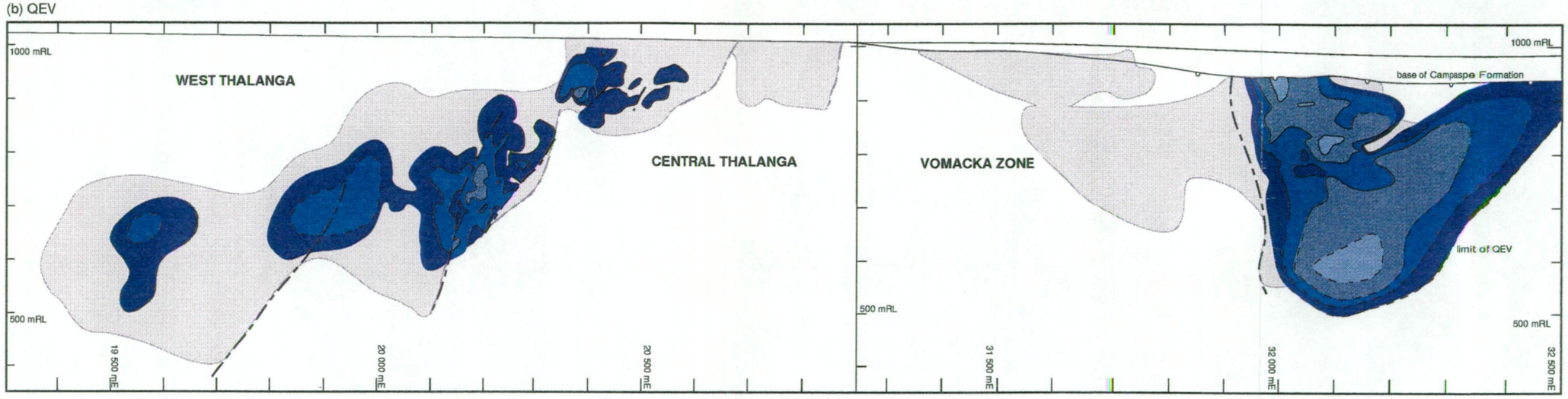

(c) orebody outline

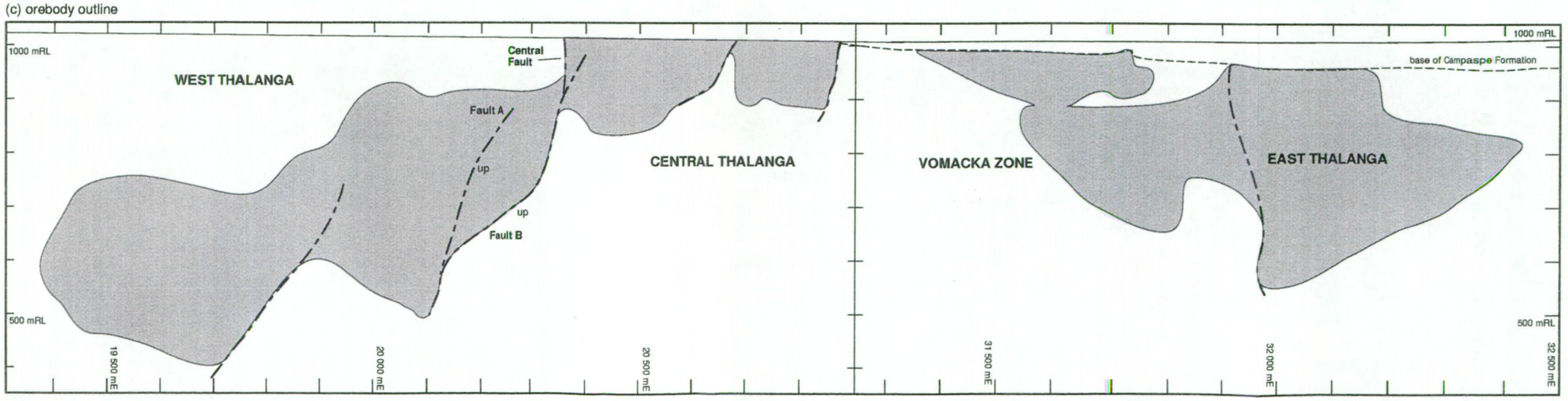

Figure 4.8 Isopach map showing contours of (a) QFP and (b) QEV thickness (metres) at Thalanga. QEV thickness comprises the total thickness of multiple QEV beds and QEV hosting massive sulphides within the ore horizon. Similarly, the thickness of multiple QFP sills are summed to determine the total thickness of QFP. The QFP in Central Thalanga is included in the QEV isopach contours . The distribution of QEV west of about 20 000 mE in West Thalanga is based on limited drill hole intersections. The western margin of the QEV in East Thalanga is interpreted, from underground mapping, to be defined by a brittle, ENE-trending normal fault. QEV is not present west of the fault. Information for these diagrams comes from drill hole interpretations and underground mapping. Information for areas east of about 32 200 mE and deeper than about 700 mRL was interpreted from a diagram by Herrmann (writt. comm., 1995), and dashed lines represent less reliable data.

Composition

Coherent QFP is typically silicified with 50-60 modal %, evenly distributed quartz and feldspar phenocrysts (Fig. 4.9a,b; Appendix E). At East Thalanga, the QFP contains about 30-40 % feldspar crystals and about 20-30 % quartz phenocrysts (5-8 mm diameter), whereas the QFP in Central Thalanga contains 20-25 % feldspar and about 30 % quartz phenocrysts (5-12 mm diameter), suggesting that there were two separate magmas. In thin section, apparently quartz-only porphyries contain subhedral feldspar pseudomorphs composed of intergrowths of fine grained muscovite or phlogopite-muscovite-calcite (Fig. 4.9b,c,d). These pseudomorphs are typically intensely deformed and transposed along the cleavage.

Quartz phenocrysts are hexagonal to bipyramidal in habit with rounded and embayed margins (Fig. 4.9e). Such resorption textures indicate that the quartz phenocrysts were in disequilibrium with the host magma after they had crystallised. Most quartz phenocrysts have undulose extinction and are typically now composed of subgrains. Some quartz phenocrysts have jigsaw-fit fracture patterns (Fig. 4.9f) indicating *in situ* fragmentation. Fractured quartz phenocrysts are elongate along S_2 and this is interpreted to indicate that brittle fragmentation was related to deformation.

Plagioclase (An_{35-40}; Fig. 4.10) phenocrysts are generally subhedral and commonly occur as glomerocrysts up to about 4 mm in diameter, whereas K-feldspar phenocrysts are 1-2 mm in size and constitute about 5 % of the total phenocryst population. Muscovite, calcite, quartz, epidote, and various sulphides have partly or wholly replaced some feldspars (Fig. 4.9c,d; particularly in Central Thalanga, Chapter 10). In some QFP samples the feldspar phenocrysts are broken with jigsaw-fit textures.

In most parts of East Thalanga, the QFP has a siliceous, blue-grey groundmass that is composed of microcrystalline (0.01-0.05 mm), irregularly shaped quartz and feldspar that has been partly overprinted by mosaics of equant fine-grained quartz (Fig. 4.9e). In Central Thalanga, the groundmass contains abundant fine-grained muscovite and uniformly sized (0.05-0.08 mm) spherical regions composed of recrystallised quartz (Fig. 4.9c,d). Crude radial quartz grains are present within the spheroids, with opposite sub-grains going to extinction simultaneously (Fig. 4.8g,h). These textures are interpreted to be altered, recrystallised spherulites and therefore indicate that the QFP groundmass in Central Thalanga was originally partly glassy.

Metamorphic, green-brown biotite is disseminated throughout the QFP groundmass, and is typically coarse-grained where intergrown with quartz and feldspar phenocrysts. Irregular wisps of fine grained biotite (<0.5 cm in length) with diffuse margins are dispersed in most QFP units. The disseminated muscovite and minor euhedral pyrite are interpreted to be

Figure 4.9 Textures of the quartz-feldspar porphyry (QFP) at Thalanga.

(a) Typical siliceous QFP composed of blue quartz and white feldspar phenocrysts, with fine grained biotite and quartz in the groundmass. Sample E3212SI18-45, East Thalanga.

(b) Groundmass of QFP in Central Thalanga is composed of fine grained muscovite and quartz. Quartz phenocrysts vary from colourless to blue and feldspar phenocrysts have been replaced by fine grained phlogopite. Sample C2039NI25-34.2.

(c) Photomicrograph of phlogopite pseudomorphs of feldspar phenocrysts in QFP. Circular structures in muscovite-rich groundmass are composed of recrystallised quartz. Sample TH4-92, Central Thalanga.

(d) Same sample as (c) under crossed nicols.

(e) Photomicrograph part of an embayed quartz phenocryst and groundmass composed of fine grained muscovite and quartz. Quartz phenocryst is now composed of subgrains, with undulose extinction in each subgrain. Sample TH205-71, Central Thalanga.

(f) Photomicrograph of *in situ* fragmented quartz phenocryst in QFP. Sample C2036NI30-33, Central Thalanga.

(g) Photomicrograph of circular domains of quartz in muscovite-rich groundmass of QFP. Same sample as in (c): TH4-92, Central Thalanga.

(h) Same sample as (g) under crossed nicols. The recrystallised quartz within the circles is crudely radial and the circular structures may be recrystallised spherulites.

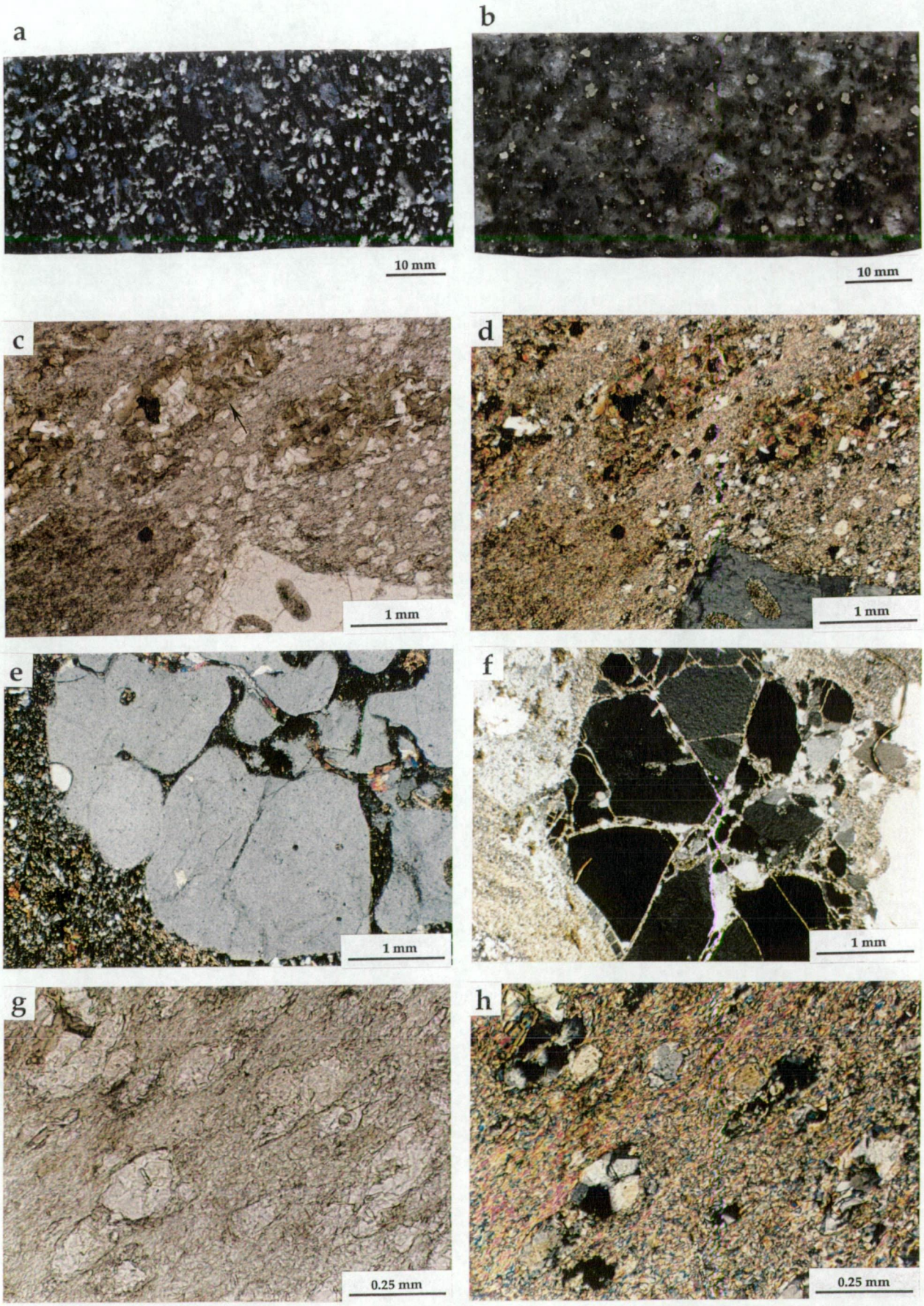
a
10 mm
b
10 mm
c
1 mm
d
1 mm
e
1 mm
f
1 mm
g
0.25 mm
h
0.25 mm

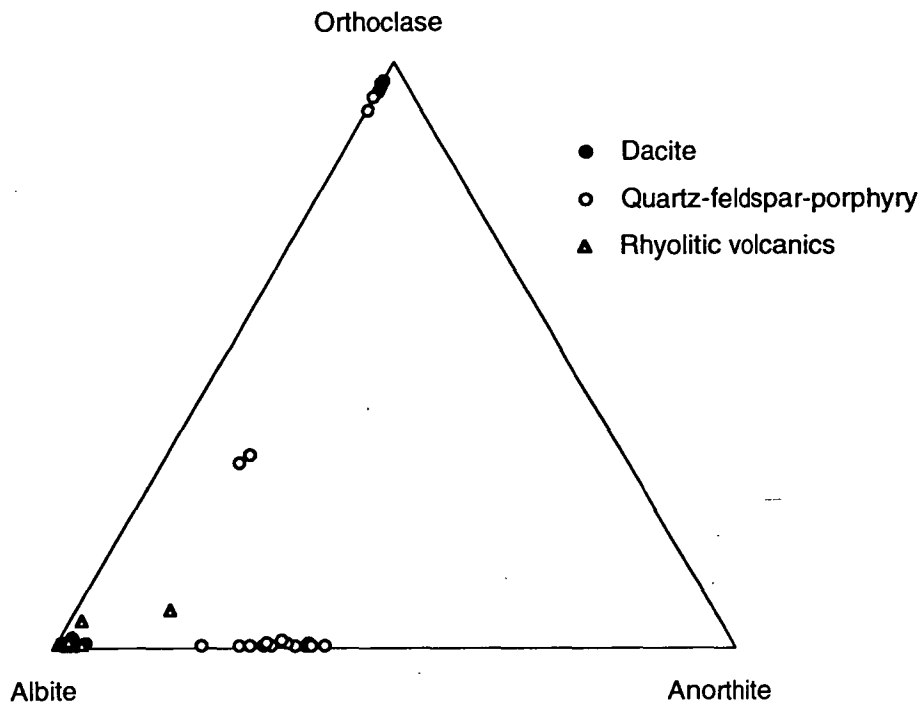

Figure 4.10 Composition of feldspar phenocrysts in volcanics that host the Thalanga massive sulphide deposit. Microprobe analyses of the feldspars are presented in Appendix 4B.

hydrothermal in origin, and were recrystallised during metamorphism. Accessory euhedral apatite crystals are also present within the groundmass of QFP units.

4.3.3 Volcaniclastic Facies I: Quartz 'Eye' Volcaniclastic Unit

Distribution

QEV units are present in most parts of East Thalanga and typically overlie both the footwall and the hangingwall ore lenses (Fig. 4.3a). In East Thalanga, the western margin of the QEV is sharply truncated by a ENE-trending normal fault (map M11 and Fig. 4.8a) and QEV units have not been repeated west of the fault. The thickness of the QEV and its relationship to the QFP, vary rapidly along strike and up and down dip (Fig. 4.11a-c), but overall, the QEV units decrease in thickness towards the western, eastern and down-dip limits of the East Thalanga ore lens (Fig. 4.8a). In general, thick QEV occurs adjacent to the thickest parts of the QFP units (cf. Fig. 4.8a, with Fig. 4.8b).

The QEV overlies the massive sulphide lens in West Thalanga (Fig. 4.3b) and occurs as a few, possibly interconnected domains that thin towards the margins of the West Thalanga ore lens (Fig. 4.8b). The distribution of the QEV in the westernmost parts of West Thalanga is poorly understood and it is uncertain whether the QEV in West Thalanga is continuous with the QEV overlying the Mount Windsor Volcanics in the Thalanga Range. The eastern and down-dip boundaries of the QEV have been overprinted by major ENE-trending normal faults that separate West and Central Thalanga (Fig. 4.8b). Only minor lenses of QEV are associated with QFP units east of the faults (in Central Thalanga), and prior to deformation, the QEV in Central Thalanga was probably located adjacent to the eastern part of West Thalanga (Chapter 3, section 3.2.2).

Components

Abundant coarse blue quartz crystals, broken quartz and feldspar crystals, and poorly sorted QFP clasts (with similar texture and geochemical compositions to the QFP units) are characteristic components of the QEV (Table 4.2; Fig. 4.12a,b). The distinctive quartz crystals and quartz crystal fragments in the QEV matrix are usually blue in hand specimen and highly fractured or composed of subgrains with undulose extinction in thin section (Fig. 4.12c,d). Many fractured crystals have jigsaw-fit textures that are interpreted as the results of *in situ* fragmentation during deformation. The coarse quartz crystals and quartz crystal fragments in the QEV have a similar degree of resorption to the quartz phenocrysts in the QFP. Although in general, the crystals within the QEV units are smaller on average (<3 mm) than those in the QFP, the maximum size of quartz crystals in the QEV (12 mm) is greater than the maximum size of quartz phenocrysts in the QFP units in East Thalanga (8 mm). The abundance

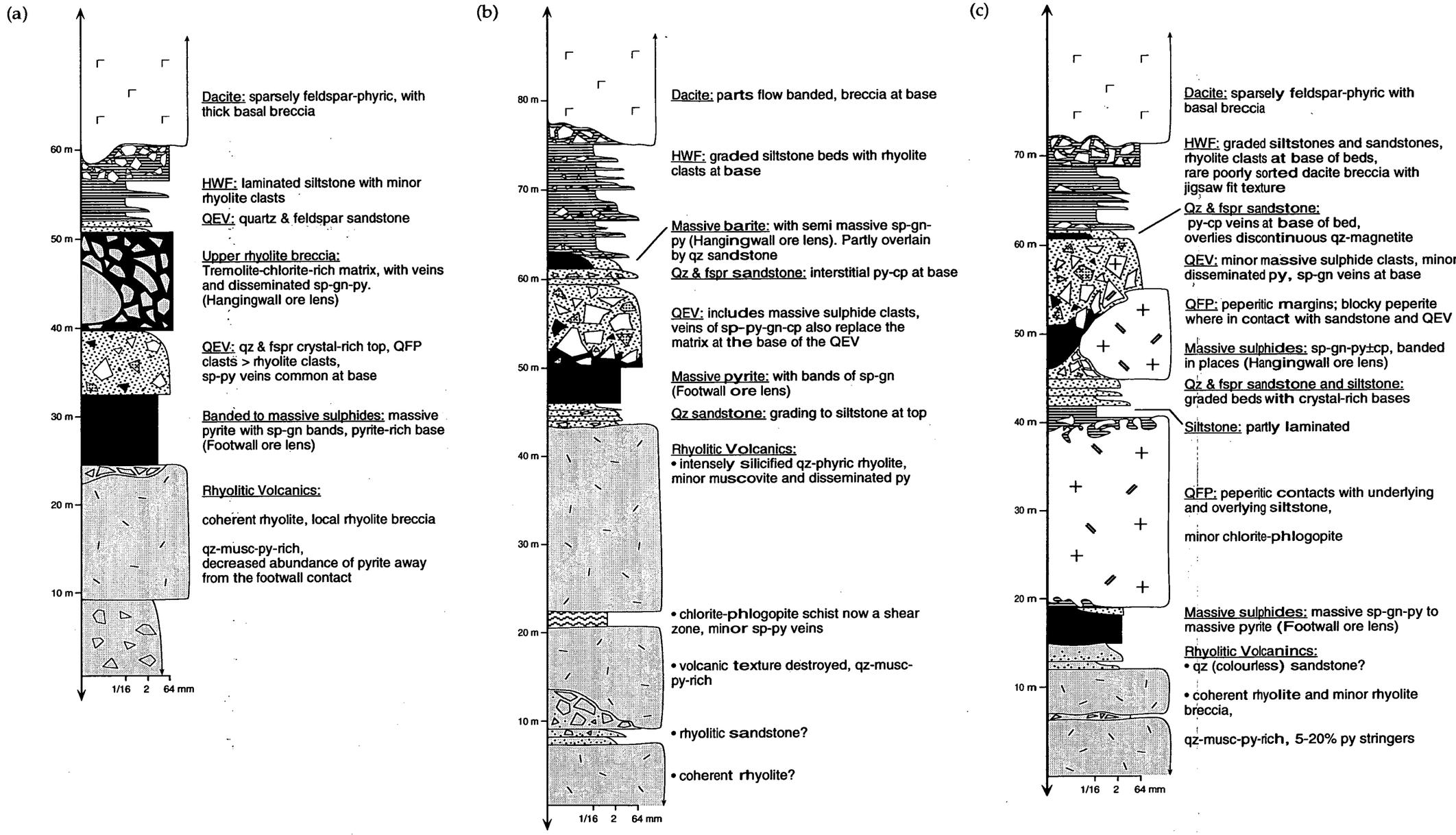

Figure 4.11 Simplified graphic logs of the geology of the ore horizon in East Thalanga on the 32080 mE section. (a) Interpreted geology of about 720 mRL, (b) interpreted geology of about 820 mRL, and (c) interpreted geology of about 920 mRL.

Figure 4.12 Components of the quartz 'eye' volcaniclastic unit (QEV) at Thalanga.

(a) Hand specimens of typical crystal-supported QEV. Top: QFP clasts and angular silicified rhyolite clasts (arrow) in matrix of quartz and feldspar crystals and crystal fragments. Sample E3204SI31-57, East Thalanga. Bottom: quartz-magnetite clast in a matrix of feldspar and quartz crystals. Muscovite-rich domain at left end of sample may be altered pumice or dense glass. Sample W2031ND24-9.5, West Thalanga.

(b) Graded QEV: quartz and feldspar sandstone, with rare quartz-phyric rhyolite clasts (quartz is blue) and wispy clasts of fine grained muscovite that may be after glass, grades upwards to sandy siltstone. Sample TH263-198, East Thalanga. Facing towards right.

(c) Photomicrograph of quartz and feldspar crystals in QEV. Matrix between crystals is composed of quartz, biotite and muscovite. Sample E3204 SI31-57, East Thalanga.

(d) Same sample as (c) under crossed nicols.

(e) Phlogopite-rich QEV breccia. Irregular QFP clasts are larger than the silicified rhyolite clasts. Quartz crystals and crystal fragments are common in the chlorite-phlogopite-pyrite-rich matrix. The few feldspar crystals within the matrix have been pseudomorphed by muscovite and clinozoisite. Sample TH236A-134, Central Thalanga.

(f) Phlogopite-rich QEV. Coarse, fractured quartz crystals and feldspar pseudomorphs within muscovite-phlogopite-rich domain may be altered and metamorphosed dense porphyritic glass. Elsewhere the quartz and feldspar crystals have been fractured and are transposed along the cleavage in phlogopite-rich domains, and therefore appear finer grained. Sample TH255-149.3, West Thalanga.

(g) Photomicrograph of muscovite-rich QFP clast within the QEV (orange line marks the clast margin). Quartz and feldspar crystals are much larger and more closely packed within the muscovite-rich domain, than within the matrix, and therefore may be an altered and metamorphosed pumiceous QFP clast. Sample E3207SI49-74.8, East Thalanga.

(h) Photomicrograph of irregular biotite wisp in QEV. Matrix is composed of fine grained quartz and biotite and also contains quartz and feldspar crystals. Sample E3198SI30-10.9, East Thalanga.

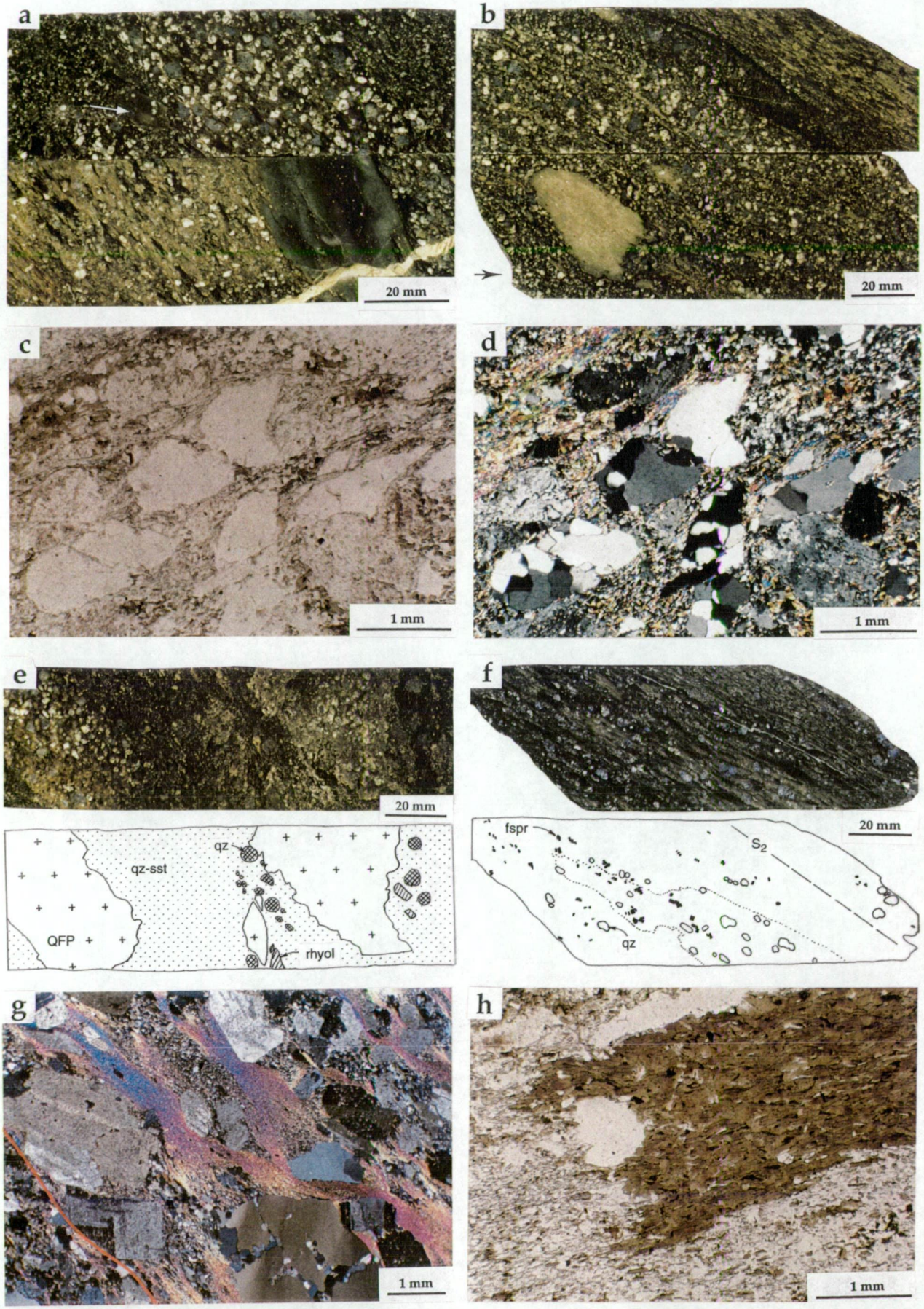
a
20 mm
b
20 mm
c
1 mm
d
1 mm
e
20 mm
qz
qz-sst
QFP
rhyol
f
20 mm
fspr
S2
qz
g
1 mm
h
1 mm

of crystals within the QEV varies from 12 % quartz crystals to 77 % quartz and feldspar crystals (Appendix E).

Table 4.2 Components of the quartz 'eye' volcaniclastic unit

Components	Size Range	Shape	Abundance
Quartz: blue to grey (Fig. 4.12a-d)	<1 mm to 12mm, average=6 mm	Rounded crystals to angular fragments	Variable, up to 60 %, common towards top of QEV
Feldspar: partly albitised plag, minor K-fspr crystals (Fig. 4.12a-d)	<1 mm to 4 mm	Subhedral crystals to angular fragments	Variable, absent in places, common towards top of QEV; Qz = fspr in West Thalanga, qz > fspr in East Thalanga
Non-vesicular QFP clasts (Fig. 4.12a,b,e)	1 cm to 5 m, commonly 10-40 cm	Angular to rounded, blocky to highly irregular	Common, up to 80 % of QEV in places
Qz-fspr-phyric rhyolite clasts: siliceous, phenocrysts ≤2 mm in size (Fig. 4.13a,b)	<1 cm to 60 cm, commonly 5-10 cm	Rounded to blocky and cuspate in places	Minor component, overall <10 % of QEV, smaller (average = 2-5 cm) and more abundant in West Thalanga, jigsaw fit textures in East Thalanga
Biotite wisps: patches of fine-grained biotite or chlorite after biotite (metamorphic phase) (Fig. 4.12h)	<1 cm	Angular to wispy, elongate parallel to cleavage	Patchy distribution, about 5-10 % of QEV
Muscovite-phlogopite-rich qz ± fspr phyric QFP clasts (Fig. 4.12f,g)	<5cm	Wispy, irregular clasts	Patchy distribution about 5-10 % of QEV? More common in West and Central Thalanga
Massive sulphide clasts: massive py to sp-gn ± cp (Fig. 4.13c-e)	<10 cm up to 1.5 m	Rounded to elongate parallel to cleavage	Patchy distribution, up 50 % of QEV
Siltstone clasts	≤10 cm, but possibly up to 30 cm	Irregular to rounded	Rare, more common in West Thalanga
Quartz-magnetite clasts (Fig. 4.12a)	up to 30 cm	Blocky to rounded and irregular	Rare

Abbreviations: cp = chalcopyrite, fspr = feldspar, gn = galena, plag = plagioclase, py = pyrite, qz = quartz, sp = sphalerite

Non-vesicular QFP clasts in the QEV are commonly siliceous with a groundmass composed of recrystallised quartz and muscovite (Fig. 4.12e). This quartz-muscovite assemblage is interpreted to post-date clast formation as there is a similar quartz-muscovite assemblage in the crystal-rich matrix of the QEV. Irregular domains composed of intergrown fine grained muscovite ± phlogopite that include coarse, subhedral to rounded quartz phenocrysts and muscovite-phlogopite pseudomorphs of feldspar, are interpreted to be strongly altered QFP clasts which had a glassy groundmass prior to alteration (Fig. 4.12f). Some of these clasts have feathery ends and contain subhedral crystals that are coarser and more abundant than in the matrix (Fig. 4.12g). These textures are similar to altered, compacted pumice clasts recognised in other ancient volcanic sequences (e.g. Allen, 1988). However, the strongly phyllosilicate-altered QFP clasts are difficult to identify because the matrix between clasts is similar to the groundmass within the clasts. In other samples that have no relative

Figure 4.13 Components and lithofacies variations of the quartz 'eye' volcaniclastic unit (QEV) at Thalanga.

(a) Blocky rhyolite (rhyol) clast in QEV with curviplanar to cuspate margins. QFP clasts (≥30 cm, and massive pyrite clasts also occur in the chlorite-rich sandstone (quartz and feldspar crystals) matrix. Lens cap is about 55 mm in diameter. Located in E676 Stope access, East Thalanga.

(b) Blocky to splintery rhyolite clasts, with some jigsaw-fit textures. Matrix is composed of quartz and feldspar crystals. Located in E893 Stope, East Thalanga.

(c) Clast-supported, polymict QEV breccia containing clasts of massive sulphide, QFP and quartz-phyric rhyolite with a chlorite-rich groundmass. Sample W2011NED103.7, West Thalanga.

(d) Banded sphalerite-galena-pyrite rich sulphide clast abutting QFP clast in QEV. Pen is about 14 cm in length. Located in E830 Stope, East Thalanga.

(e) Massive sphalerite-pyrite-galena rich sulphide clast in QEV. Minor chlorite and epidote is present at the contact between the QEV and sulphides. Split-set plate is about 30 cm along longest side. Located in W690 Stope, West Thalanga.

(f) Medium grained, well sorted, chlorite-rich quartz (with minor feldspars) sandstone. Sample W2009NDD05-27, West Thalanga.


a


b

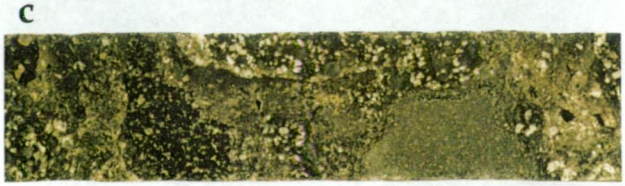
c
20 mm

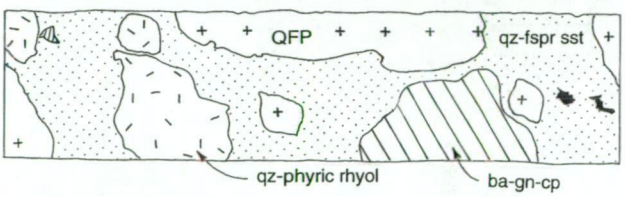
QFP
qz-fspr sst
qz-phyric rhyol
ba-gn-cp


d


e


f
10 mm

concentration of quartz and feldspar crystals, the groundmass may have been dense glass. These altered QFP clasts may be comagmatic with the siliceous, non-vesicular QFP clasts. Other small (<5 cm) irregular wisps composed of intergrown quartz and muscovite may also be altered pumice clasts or formerly glassy clasts. Irregular wisps of fine-grained metamorphic biotite are also present within the QEV units (Fig. 4.12h).

Non-vesicular QFP clasts are generally larger and more abundant than QFP pumice clasts and quartz-feldspar-phyric rhyolite (typically white to pink in colour, with ≤5 % quartz phenocrysts) clasts in all parts of the QEV (Table 4.2). However, the volume of QFP pumice clasts within the QEV is unknown because the intense alteration has made many formerly glassy QFP clasts difficult to distinguish from altered sandstone. Some rhyolite clasts are flow-banded and in places in East Thalanga, have curviplanar margins or a jigsaw-fit texture (Fig. 4.13a,b). The jigsaw-fit textures indicate *in situ* fragmentation. The groundmass of the rhyolite clasts is composed of irregular, evenly-sized (0.02 mm) quartz grains and scattered blebs of coarsely recrystallised quartz (0.2 mm). Some quartz-phyric rhyolite clasts have a chlorite-phlogopite-rich groundmass that may be altered and metamorphosed glass (Fig. 4.13c).

Quartz-magnetite lenses are present in many parts of the Mount Windsor subprovince and are interpreted to have formed on the seafloor from low-temperature hydrothermal solutions (Duhig *et al.*, 1992; Davidson *et al.*, 1993). Quartz-magnetite clasts within the QEV are more common in the western parts of West Thalanga and in the stratigraphically highest QEV units in East Thalanga, but are absent in Central Thalanga. In general the quartz-magnetite clasts are located at the base of the QEV units, and in places in East Thalanga, a bed of quartz-magnetite is interpreted to separate the QEV units (Fig. 4.6c).

Lithofacies

Single beds within the QEV are poorly sorted, although weakly graded with a crystal-rich sandy siltstone top and a clast-rich base. Clast size generally increases towards the base and massive sulphide clasts are commonly located near the base of the QEV. The QEV varies from matrix- or crystal-supported to clast-supported (cf. Fig. 4.12a,b and 4.13c) and typically consists of a thick interval of weakly graded, but poorly sorted, polymict breccia (QEV breccia) overlain by thinner, sandstone-rich QEV beds (QEV sandstone; Fig. 4.6a-c, Fig. 4.12b, and Fig. 4.14). In West Thalanga the main QEV breccia is 5-10 m thick, whereas in East Thalanga the main QEV breccia is 5-20 m thick. The overlying QEV sandstone units are <5 m in total thickness and are laterally discontinuous, with bed thickness and numbers of beds varying between adjacent drill holes.

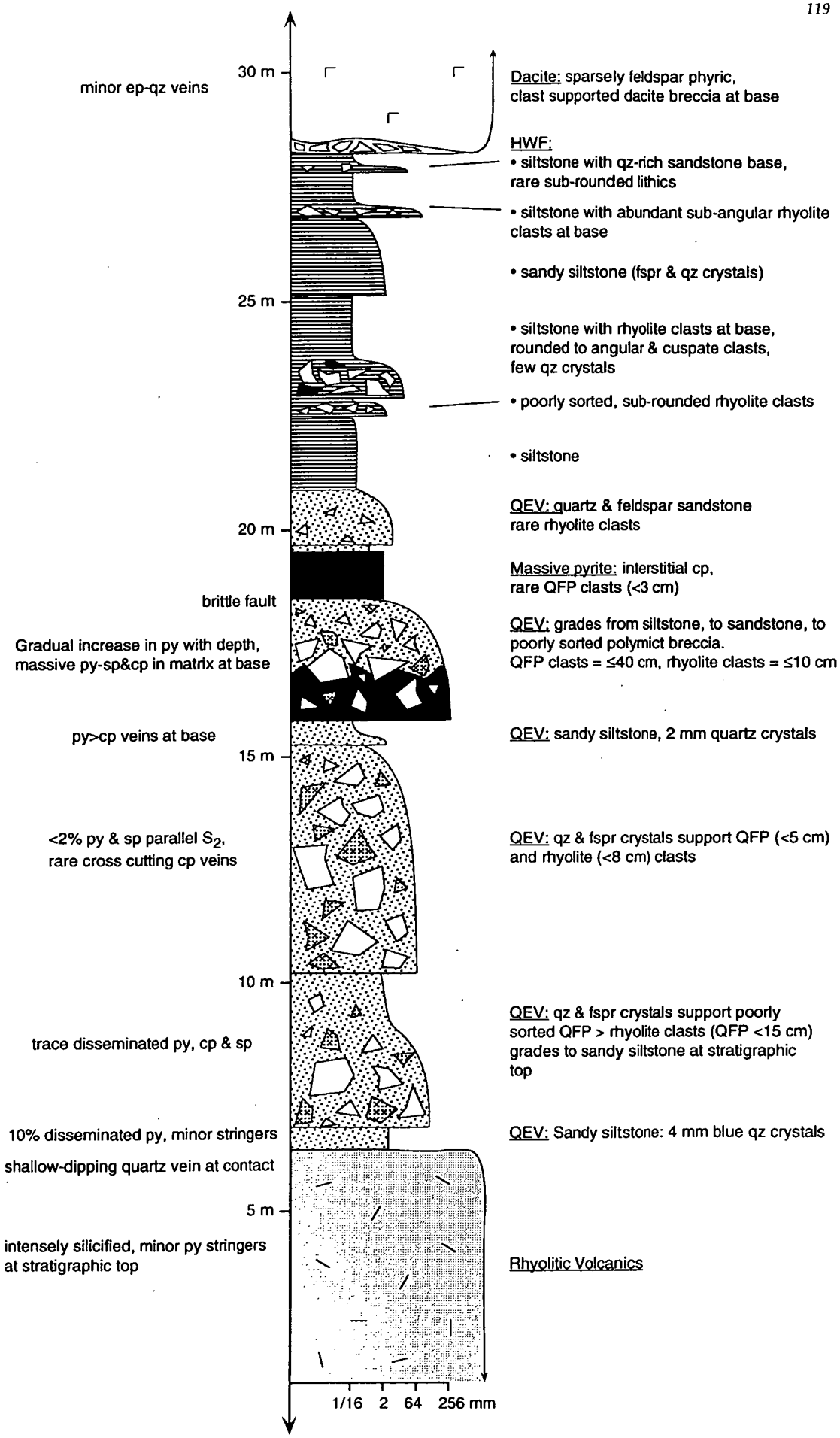

Figure 4.14 Simplified graphic log of the 3198SD05 drill hole in East Thalanga. Bedding thicknesses (marked on vertical scale) approximate true thickness as the hole is shallowly-plunging.

QEV sandstone beds are better sorted and have pronounced normal grading, higher crystal content and overall smaller grainsize than the QEV breccia (cf. Fig. 4.12b, Fig. 4.13f with Fig. 4.13c). Where the QEV breccia is absent at Thalanga (e.g. in the Vomacka Zone and most of Central Thalanga), the QEV sandstone is also absent. In West Thalanga, the QEV sandstone locally contains metamorphic biotite and garnet (Fig. 4.6a).

4.3.4 Volcaniclastic Facies II: Graded Siltstone

Beds of siltstone, graded siltstone and rare sandstone that grades to siltstone are present between the QEV and underlying footwall rhyolitic volcanics in parts of East Thalanga (Fig. 4.6c). Single beds are <50 cm in thickness, and the total thickness of this unit ranges from 1 to 4 m. The QFP units in the up-dip parts of the ore horizon in East Thalanga are enveloped by siltstone and graded sandstone units (Fig 4.3a). The siltstones are rarely laminated and are composed of fine grained quartz and muscovite, and some have thin (cm-scale) crystal-rich bases containing blue quartz and white feldspar grains (<4 mm in size), and rare siliceous quartz ± feldspar phyric rhyolite clasts (<1.5 cm in size). These siltstone and sandy siltstone units may have been deposited during a period of quiescence following the emplacement of the rhyolitic volcanics. Multiple graded beds suggest pulses of sediment influx.

4.3.5 Contact Relationships Between Facies

QEV, graded sandstone and massive siltstone units overlie and underlie the QFP units in East and Central Thalanga. Contacts between the QFP and volcaniclastic rocks vary from sharp and planar, to disrupted or gradational. In most cases, the QFP is not in direct contact with the massive sulphide lenses, the hangingwall fragmental or the dacite (unit iv), and where such a contact does occur it is typically faulted. The QEV in West and East Thalanga is directly overlain by the hangingwall fragmental units.

QFP—Siltstone Contact

The QFP overlying the footwall ore lens in the up-dip parts of East Thalanga is enveloped by massive to graded beds of siltstone and sandstone of volcaniclastic facies II (Fig. 4.3a and Fig. 4.12c). Commonly both the upper and lower contacts between QFP and siltstone grade from massive QFP, through QFP with small (<5 cm) irregular inclusions of siltstone, to siltstone with irregular bands, stringers and ragged clasts of QFP, to undisrupted siltstone (Fig. 4.15a,b). This zone of mixed siltstone and QFP extends <2 m into the siltstone from the QFP.

Quartz and feldspar phenocrysts are closely packed within the QFP clasts compared to their average density within the coherent QFP unit (cf. Fig. 4.9a and Fig. 4.15b). Point counting demonstrates that there is an increase in crystal abundance from about 50-60 modal % total

Figure 4.15 Peperite textures in QFP at Thalanga.

(a) Ragged clasts of QFP in siltstone are subparallel to S_2. Sample TH275-102, East Thalanga.

(b) Siltstone inclusion in QFP is bleached (due to baking and induration) at contact with QFP. Small joints extend through the siltstone, perpendicular to the contact between QFP and siltstone. Whitish muscovite patches in siltstone are interpreted to be due to alteration. Sample E3208NI28-14.6, East Thalanga.

(c) Siltstone inclusion in QFP has disrupted laminations and contains small QFP clasts. Broken quartz phenocrysts are present at the margins of QFP (arrows), and "clouds" of quartz crystals occur in the siltstone. Sample C2036NI30-36, Central Thalanga.

(d) Clast-supported, jigsaw fit texture in QFP breccia located at base of QEV. Matrix is phlogopite-rich and contains veins and disseminated sphalerite-pyrite. Sample TH269-144.5, East Thalanga.

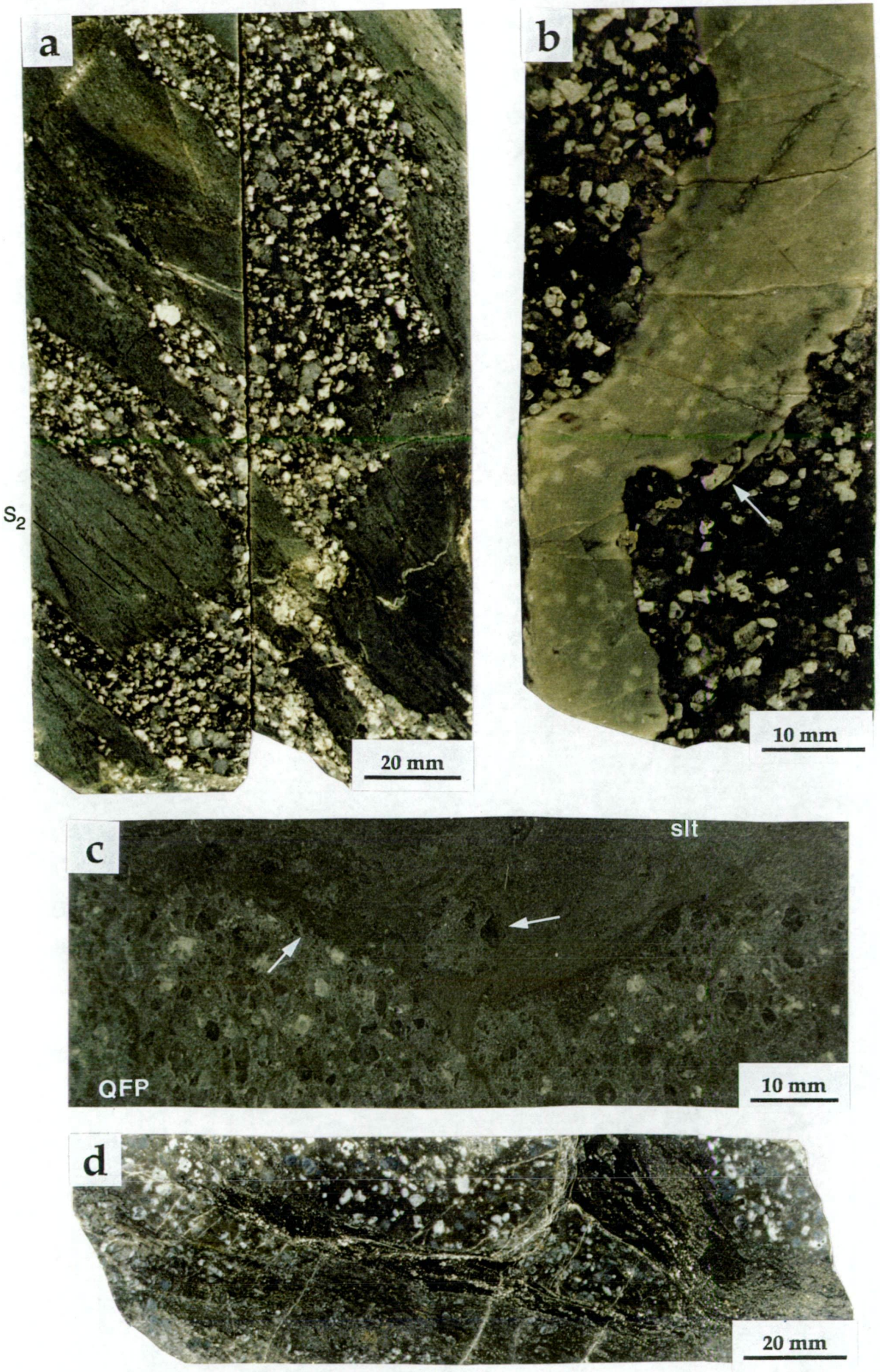
a
S_2
20 mm
b
10 mm
c
slt
QFP
10 mm
d
20 mm

phenocrysts within the QFP interior, to about 70 modal % total phenocrysts in the QFP clasts in the siltstone (Appendix E). The irregularly shaped QFP clasts hosted in siltstone are elongate parallel to S_2 (Fig. 4.15a), and in most places, the siltstone clasts in the QFP are similarly deformed. However, pre-tectonic joints normal to the siltstone margins have been preserved within some siltstone inclusions (Fig. 4.15b). These inclusions have paler margins where in contact with the QFP and siltstone also infills hairline fractures within the QFP (Fig. 4.15b).

These disrupted contacts between the QFP and siltstone are interpreted as peperitic, implying intrusion of QFP sills into wet, unconsolidated sediments. The restricted extent of the peperitic contact is consistent with the fine grain size of the siltstone, since dispersed peperites are more common in poorly-sorted host sediments (Busby-Spera and White, 1987). Rare inclusions of siltstone in coherent QFP in Central Thalanga are also interpreted as peperite (Fig. 4.15c). Prior to deformation, the elongate, ragged clasts of QFP within the peperite were probably fluidal in texture. The decrease in groundmass volume of the QFP clasts in the siltstone may indicate that the QFP was vesicular at its margins. The paler margins and internal joints of some siltstone inclusions in the QFP (Fig. 4.15b) are interpreted to have formed via baking and induration of the sediments during QFP sill emplacement.

QFP—QEV Contact

The weakly graded, polymict QEV breccia, with a poorly sorted, clast-supported base containing rhyolite and QFP clasts, partly overlies QFP at of East Thalanga. A typical contact grades stratigraphically upwards from QFP to monomict, clast-supported QFP breccia with jigsaw-fit texture, through to polymict QEV (Fig. 4.15d and Fig. 4.16a). The interval of jigsaw-fit QFP breccia extends for 0-1 m away from the QFP contact, where it sharply becomes typical QEV with both QFP and rhyolite clasts. The matrix between the jigsaw-fit QFP clasts is composed of siltstone, quartz and feldspar crystals, and few small (<3 cm) rhyolite clasts. In places, this jigsaw fit texture is absent, and there is a sharp change from coherent QFP to QEV breccia or sandstone facies (Fig. 4.16b,c). In these locations, the QFP could either pre-date (QEV deposited onto QFP lava), or post-date (passive intrusion of QFP into QEV) deposition of the QEV. Generally there is no evidence of baking of the QEV, although in several places the QEV is enriched in chlorite where in contact with QFP.

The possible relationships between the QFP and QEV are:
(i) some of the QFP clasts within the QEV breccia facies are part of an intrusive margin of the QFP. If the QEV was water-saturated and unconsolidated during QFP intrusion, then blocky peperite comprising clasts of QFP within the QEV may have formed at the contact between the QFP and QEV. This interpretation may explain the presence of rhyolite clasts between jigsaw-fit QFP clasts;

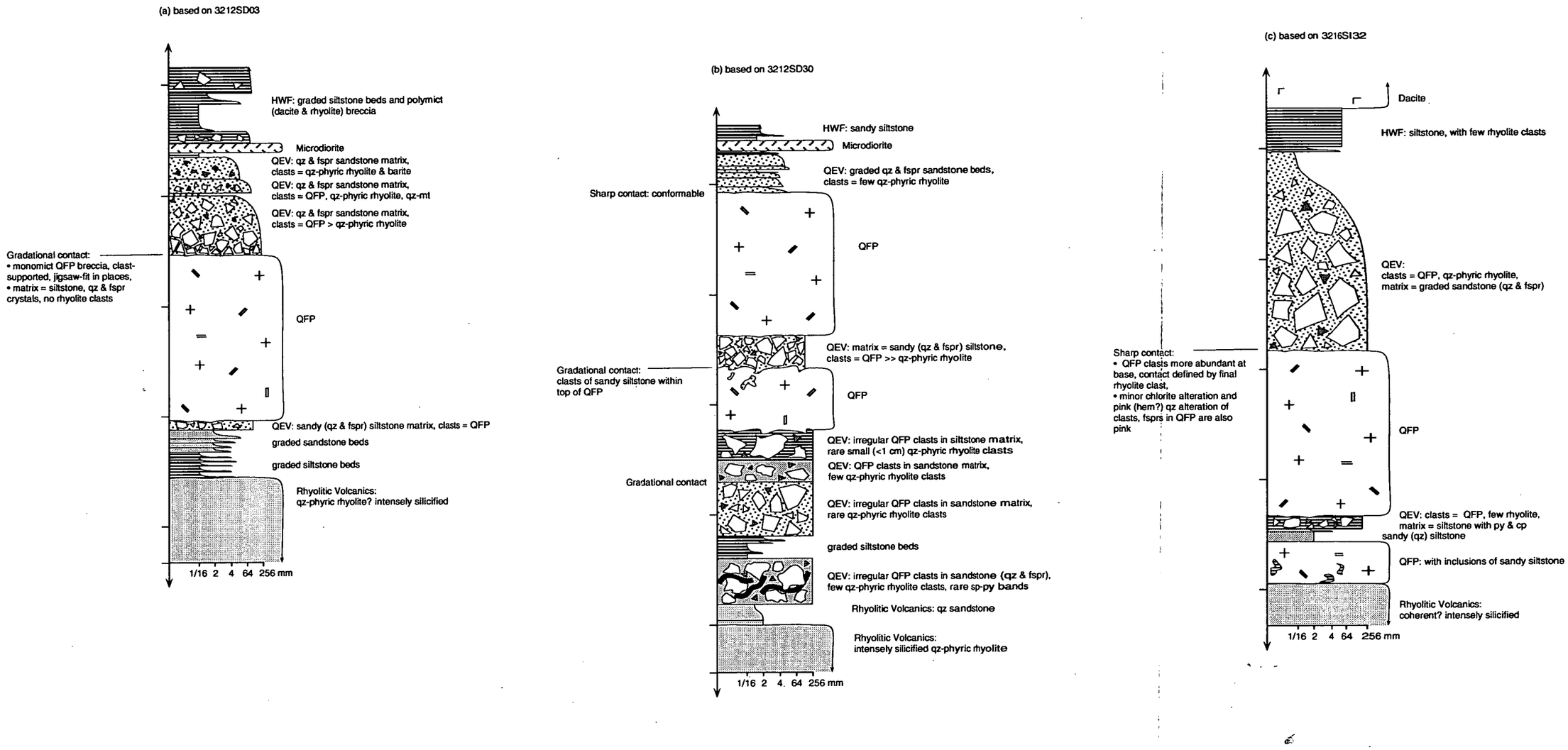

Figure 4.16 Details of the top and bottom contacts of the QFP in contact with the QEV. Thickness of units is approximately equal to true thickness. Marks on left side of graphic logs are 10 m apart.

(ii) the QFP clasts within the QEV breccia facies are resedimented QFP hyaloclastite. This interpretation better explains the presence of QFP clasts in the QEV breccia facies in West Thalanga where QFP units are not present.

The coarse-grained, poorly sorted, clast-supported QEV breccia facies would probably have been highly porous, possibly with high permeability prior to lithification. Busby-Spera and White (1987) have suggested that such properties of the host sediment will inhibit vapour-film development at the margins of an intruding magma, and instead favour rapid quench fragmentation of the magma and production of blocky clasts (blocky peperite). If in fact the QEV in East Thalanga was unconsolidated and intruded by the QFP, then blocky peperite would be the most likely texture to form.

The sharp, planar contact between the QFP and overlying QEV along the southeastern part of the Thalanga Range is more consistent with intrusion of the QFP rather than extrusion (e.g. Allen, 1992). Strongly foliated QEV sandstone along the top of the QFP may be resedimented hyaloclastite, and therefore indicate that the QFP in this area, or nearby, breached the seafloor.

4.3.6 Formation of the QEV

Mode of Fragmentation of QEV Components

Because the QFP sills at Thalanga contain crystals with smaller maximum size than the QEV units, the QFP sills in East Thalanga are interpreted to have originated from a different magma than the source of quartz and feldspar crystals in the QEV. The similarity in maximum size of quartz crystals within the QFP units in Central Thalanga, to those of the QEV units, may indicate a common parent magma.

(i) Crystals. The abundant quartz and feldspar crystals in the QEV are interpreted to have been liberated either from a highly porphyritic QFP magma by either explosive eruption (i.e. the crystals and crystal fragments are juvenile pyroclasts), or by intense quench fragmentation of a QFP dome or lava. If the QEV crystal components were erupted explosively from a volatile- and crystal-rich magma chamber, then the vent was probably subaerial or in shallow water possibly near the basin margin (Fig. 4.17; McBirney, 1963). The small volume of clasts that could be altered pumice clasts or glass shards within the QEV could indicate that most of the pumiceous fraction expected to be produced by an explosive eruption was separated from the crystals during eruption and/or transportation of the pyroclasts into the basin at Thalanga. Alternatively, and highly likely at Thalanga, strong hydrothermal alteration has made recognition of pumice clasts difficult and in fact there may be a much greater volume of pumiceous QFP clasts within the QEV units.

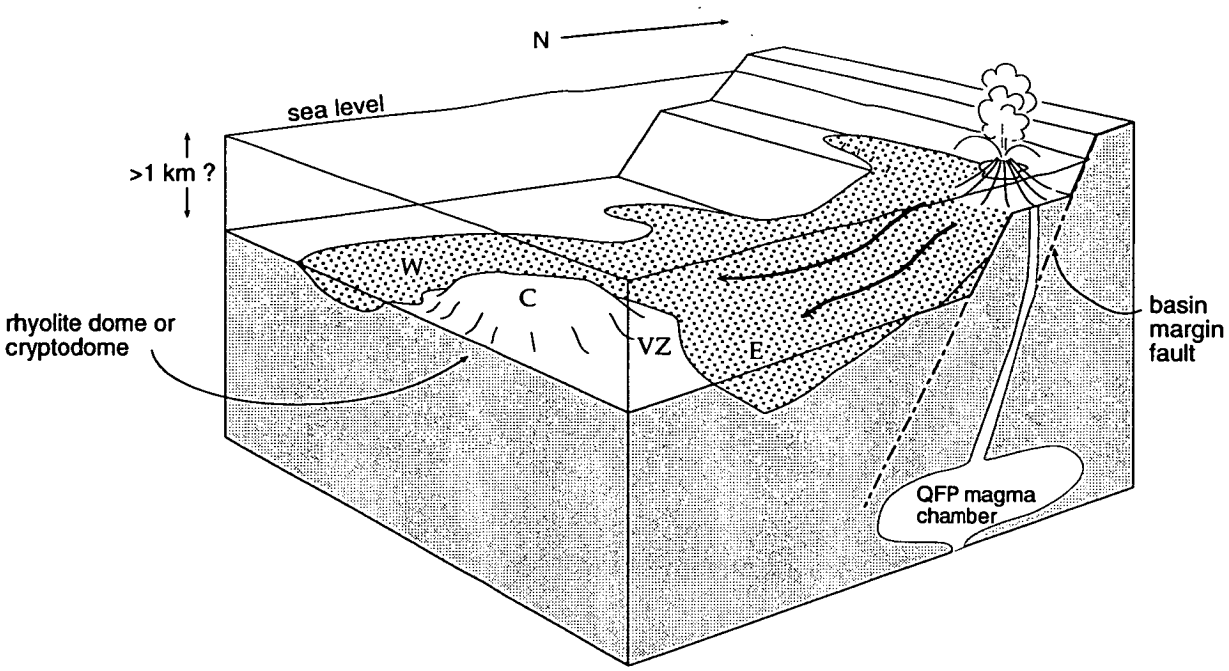

1) initial explosive eruption of volatile-rich QFP magma from a vent located in shallow water, probably at the basin margin (the location of which is poorly constrained).

2) transportation of the crystal-rich eruption products by subaqueous mass-flows, and deposition in basins at West and East Thalanga. Pumice clasts and the fine grained ash fraction separated from the subaqueous mass-flows by elutriation and flotation during transportation

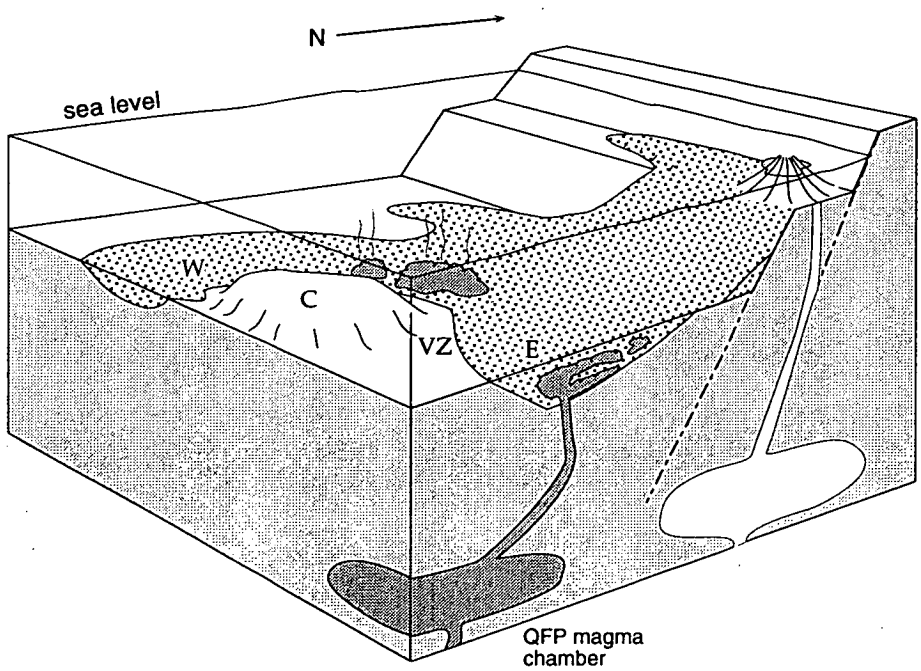

3) subsequent eruption from a second QFP magma chamber: QFP sills and possible cryptodomes are emplaced in East Thalanga, and partly emergent cryptodomes break through the QEV in the vicinity of Central Thalanga.

Figure 4.17 Block diagrams depicting a possible mechanism of eruption and deposition of QEV and QFP at Thalanga. Eruption of the QEV is interpreted to have occurred in shallow water, and emplacement of the QFP is interpreted to have occurred in water depths of at least belowstorm wave base. Abbreviations: C = Central Thalanga, E = East Thalanga, VZ = Vomacka Zone, W = West Thalanga.

Intense quench fragmentation of a QFP magma could also liberate crystals, and if formed by this process, there should be abundant QFP clasts, a gradational contact with *in situ* QFP hyaloclastite and coherent QFP, and a range in clast sizes from boulder size, down to less than crystal size (e.g. Yamagishi, 1987; Kurokawa, 1991; Cas, 1992). Such geometry is inconsistent with the presence of QEV in West Thalanga, where QFP domes are not present. However, Gimeno (1994) argued that proximal quartz-rich volcaniclastic deposits can be generated during growth and erosion of subaqueous rhyolite domes. He concluded that quartz grains with curviplanar margins were 'thermally shocked' quartz phenocrysts that had formed due to interaction between hot magma and water. Therefore, gravitational collapse and mass wasting of an intensely quench fragmented QFP dome or number of domes may have resulted in the resedimentation of crystals, crystal fragments and clasts into local basins at West and East Thalanga (Fig. 4.18). This process could have occurred at any water depth.

(ii) QFP clasts. The angular to rounded, blocky and irregular clast shapes of the siliceous, non-vesicular QFP (Table 4.2) suggest that quench fragmentation of a QFP dome or intrusion is a possible mechanism of clast production. Poorly-sorted QFP clasts with jigsaw-fit texture are consistent with quenching of the QFP magma on contact with wet QEV. However, such clasts are only present in the immediate vicinity of QFP sills, and the widespread distribution of QFP clasts within the QEV units in East and West Thalanga (where QFP units are not present) suggests that most of the QFP clasts are probably not quench-fragmented peperitic margins of QFP sills. Instead, quench fragmentation of a QFP dome or partly emergent cryptodome was probably an important clast-forming process. The resultant hyaloclastite may have been incorporated in subsequent crystal-rich QEV mass-flows (cf. Cas *et al.*, 1990; Boulter, 1993), or redeposited during gravitational collapse and mass wasting of a QFP dome (Fig. 4.18). If there are pumiceous QFP clasts (with groundmass now composed of muscovite and phlogopite) within the QEV units, then quench fragmentation and gravitational collapse of a locally pumiceous QFP dome may explain the incorporation of pumiceous QFP clasts in the QEV units. The wide distribution and poorly sorted nature of the QEV, with clasts of pumiceous and crystalline QFP and variable percentages of quartz and feldspar crystals, is consistent with the gravitational collaspe of a number of QFP domes (now eroded) at Thalanga.

(iii) Rhyolite clasts. Cuspate and curviplanar margins of some siliceous rhyolite clasts may indicate quench fragmentation of a rhyolite magma. Local *in situ* fragmentation textures suggest that some rhyolite clasts could have formed as intrusive hyaloclastite associated with emplacement of a rhyolite sill or cryptodome following deposition of the QEV. Quench-fragmented rhyolite clasts are larger and more abundant in the up-dip parts of East Thalanga, and may indicate that the rhyolite source is further up-dip, and now eroded. However, the origin of the majority of the rhyolite clasts in the QEV units is not clear.

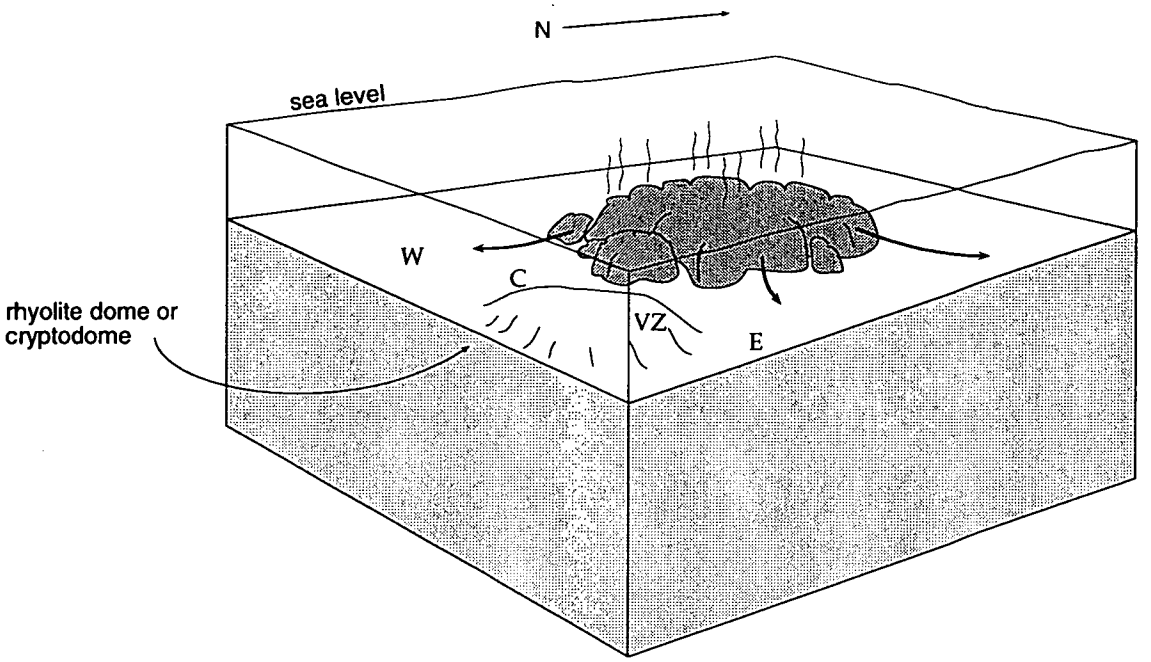

1) initial extrusion of QFP dome onto the seafloor (the location of the site of emplacement may be up-dip from Central Thalanga), followed by rapid quench fragmentation and granulation.

2) wholesale dome collapse and transportation of the crystal-rich hyaloclastite, by subaqueous mass-flows, and deposition in basins at West and East Thalanga.

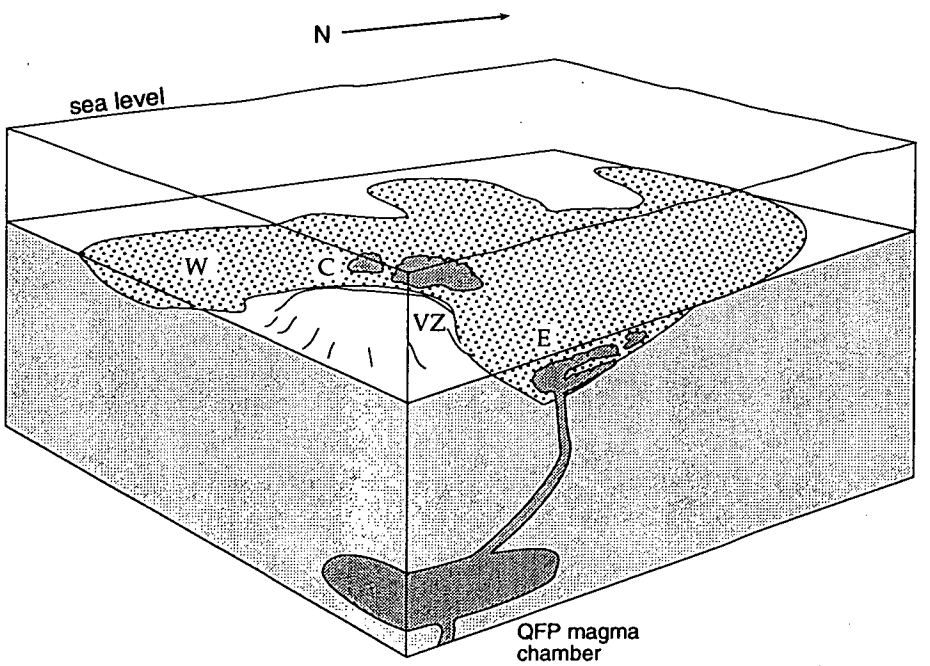

3) subsequent eruption from a second QFP magma chamber: QFP sills, with peperitic margins, are emplaced into the QEV units in East Thalanga. Remnants of the pre-existing QFP dome are preserved at Central Thalanga.

Figure 4.18 Block diagrams depicting the generation of the QEV by intese quench fragmentation of a QFP dome. Emplacement of the QFP dome and deposition of the QEV units are interpreted to have occurred in water depths of at least belowstorm wave base. Abbreviations: C = Central Thalanga, E = East Thalanga, VZ = Vomacka Zone, W = West Thalanga.

(iv) Quartz-magnetite and massive sulphide clasts. The presence of clasts of massive sulphide and quartz-magnetite within QEV units at Thalanga imply that massive sulphide lenses and quartz magnetite lenses were exposed on the seafloor, and eroded during transport of the QEV. It is not certain whether the massive sulphide clasts were eroded from the ore lenses at Thalanga, or from ore lenses along strike from Thalanga.

Transport and Deposition of the QEV and Emplacement of the QFP

Menzies (1979) and Wills (1985) suggested that the QEV is a submarine pyroclastic flow deposit. However, there is no positive textural evidence (e.g. welded textures, columnar jointing, or gas segregation pipes) indicating that the QEV was emplaced hot or from a gas-supported transport system. Gregory *et al.* (1990) recognised normal grading in the QEV and suggested that it was deposited from subaqueous mass flows. Such a depositional process is consistent with the poorly sorted characteristics of the QEV, with grading towards the stratigraphic top indicating some hydraulic sorting (cf. Cas, 1983).

Because at least some of the QFP clasts in the QEV units at East Thalanga may be dispersed peperitic margins of non-vesicular QFP sills, the emplacement of the QFP sills may have occurred while the crystal-rich QEV was wet and unconsolidated. However, the association of thick QFP and thin QEV units in East Thalanga (Fig. 4.8a,b) suggests that a QFP unit had been emplaced prior to QEV deposition and acted as topographic high, creating basins at its margins which filled with QEV. Therefore at East Thalanga, either there were two separate QFP units, with the first extruded onto the seafloor and partly overlain by subsequent QEV units, and the second emplaced as sills with peperitic margins (Fig. 4.19a), or else a single QFP magma may have been emplaced as a partly emergent cryptodome that breached the seafloor after QEV deposition, and also partly burrowed into the unconsolidated QEV and siltstone (Fig. 4.19b). The absence of *in situ* hyaloclastite at the stratigraphic top of the thickest parts of the QFP may be due to gravitational collapse and resedimentation of the hyaloclastite. Alternatively, intrusion and inflation of a shallow QFP sill beneath the QEV may have triggered the slumping of the overlying QEV.

Hyaloclastite associated with a QFP dome or lava in Central Thalanga may have been incorporated into crystal-rich mass flows during gravitational collapse of the QFP dome, and redeposited as the QEV. The spherulitic QFP units in Central Thalanga are interpreted to be outsized mega-clasts possibly derived from a now concealed or eroded QFP dome. This may have been the source of the QFP clasts, and possibly the abundant quartz and feldspar crystals, within the QEV units in West and Central Thalanga (Fig. 4.17c). These components may have been transported by mass flows to depositional sites in West and East Thalanga (Fig. 4.18).

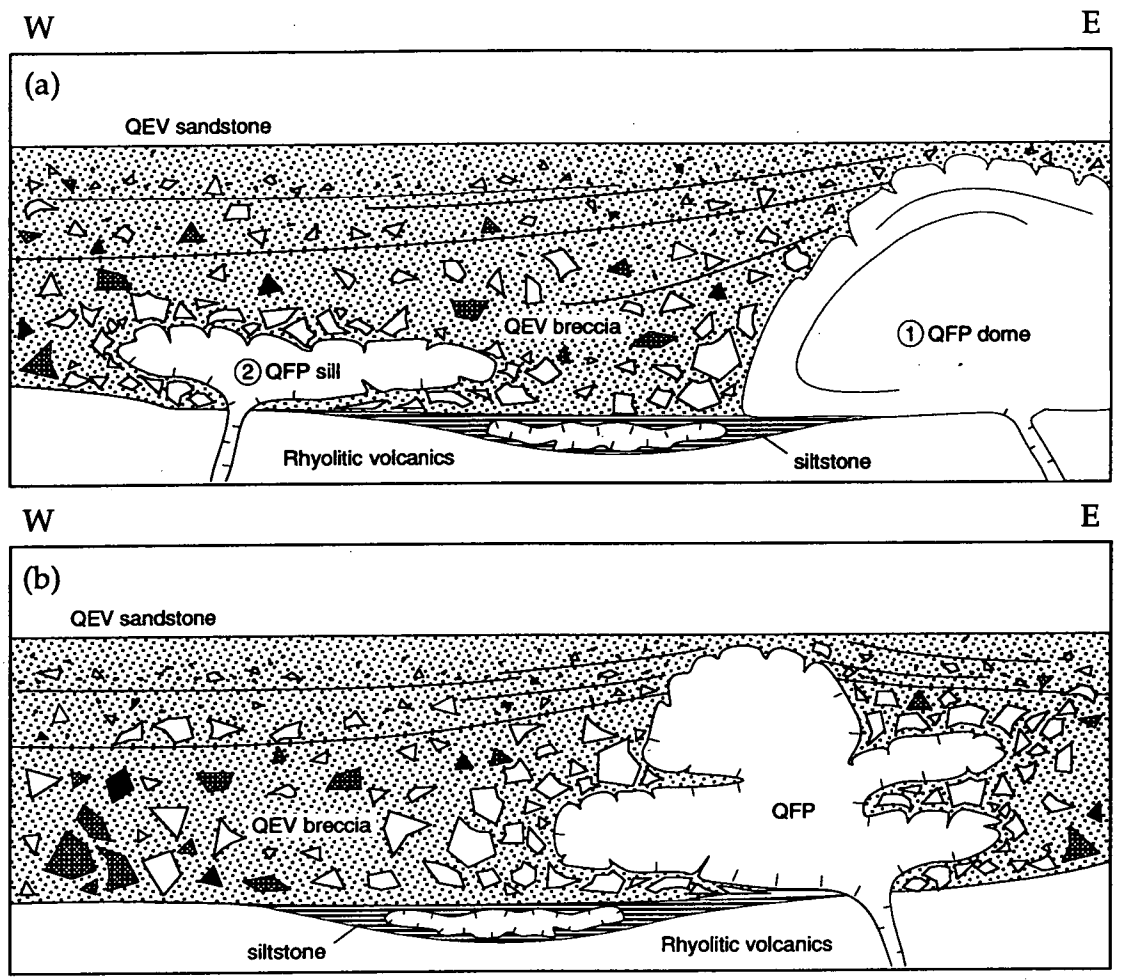

Figure 4.19 Schematic diagram depicting possible timing relationships between the QFP and QEV units in East Thalanga. (a) Extrusion of a QFP dome onto the seafloor, with QEV breccia formed during and following dome emplacement. Subsequent intrusion of a second QFP magma into wet, unconsolidated QEV breccia facies and siltstone units, resulted in formation of a blocky peperite at the contact between the sill and the QEV, and fluidal peperite at the contact between the sill and siltstone unit. (b) Alternatively, a single QFP unit may have been emplaced as a partly emergent cryptodome. In this model, at least some of the QEV must pre-date QFP emplacement as blocky peperite formed at contacts between QFP and the QEV.

The conformable nature of the overlying graded quartz ± feldspar crystal-rich sandstone facies of the QEV suggests rapid deposition of successive and gradually fining mass-flows. These units also contain QFP and rhyolite clasts, evidently collected from QFP hyaloclastite or underlying QEV units. The prevalence of the QEV sandstone facies in East and West Thalanga, compared with Central Thalanga, suggests either proximity to source, or that East and West Thalanga were local sediment traps. The absence of QEV units in the eastern half of Central Thalanga and in the Vomacka Zone supports the interpretation of separate basins in East and West Thalanga during QEV deposition.

4.4 The Upper Rhyolite Breccia (unit iii)

4.4.1 Distribution and Contact Relationships

A poorly sorted rhyolite breccia (named the upper rhyolite breccia; Table 2.5) hosts the hangingwall ore lens in parts of East Thalanga below about 800 mRL (Fig. 4.3a). Coherent rhyolite is present below about 650 mRL, where it stratigraphically overlies QEV units and the footwall ore lens. Mineralised parts of the upper rhyolite breccia have a sharp, sub-planar, partly sheared contact with underlying QFP, although in many places this contact is masked by recrystallised chalcopyrite or chlorite alteration. Commonly, coarse-grained quartz-feldspar sandstone (QEV sandstone facies) overlies the upper rhyolite breccia with sharp conformable contacts locally overprinted by irregular chalcopyrite-pyrite veins.

The lateral extent of the upper rhyolite breccia is poorly understood, and it may correlate with a polymict, but rhyolite-dominated, breccia in the ore horizon of the Vomacka Zone. Monomict rhyolitic breccia units are not recognised within the ore horizon in Central or West Thalanga.

4.4.2 Composition

Clasts are subangular, to irregular in shape with curviplanar margins (Fig. 4.20a,b) and mainly composed of quartz-phyric rhyolite, with subordinate quartz-feldspar-phyric and aphyric rhyolite clasts, minor angular chloritic rhyolite clasts and rare QFP clasts. Rare quartz-magnetite and barite clasts, with angular to irregular margins, are also present. The largest rhyolite clast is 5 m in diameter, and the accessory clasts are generally <20 cm in size. The breccia is variably matrix- to clast-supported, with local rhyolite clasts that have internal jigsaw-fit texture. The matrix is composed of semi-massive sulphides (Chapter 6) with tremolite-chlorite ± carbonate gangue and sparse feldspar and quartz crystals. Locally, diffuse contacts between the matrix (tremolite, chlorite, carbonate and sulphides) and the

Figure 4.20 Components and textures of the upper rhyolite breccia.

(a) Mineralised upper rhyolite breccia (hangingwall ore lens), composed of poorly sorted siliceous quartz-phyric rhyolite clasts with irregular, rounded margins. Matrix is composed of sphalerite-galena-pyrite bands in chlorite-tremolite gangue. Split-set plate is about 30 cm along longest side. Located at E765 Stope, East Thalanga.

(b) Close-up of (a). Irregular to blocky massive chlorite-biotite clasts may have been originally glassy, or are a non-mineralised part of the matrix. Located at E765 Stope, East Thalanga.

(c) Photomicrograph of the texture of the fine grained quartzo-feldspathic groundmass of the rhyolite clasts. Sample APH-128, East Thalanga.

(d) Variably mineralised polymict breccia in the ore horizon of the Vomacka Zone. Clasts are mainly rounded rhyolite and quartz-barite. Matrix is sandy siltstone. TH293 - 45-49, Vomacka Zone.

(e) Line drawing of (d).


a


b
rhyol

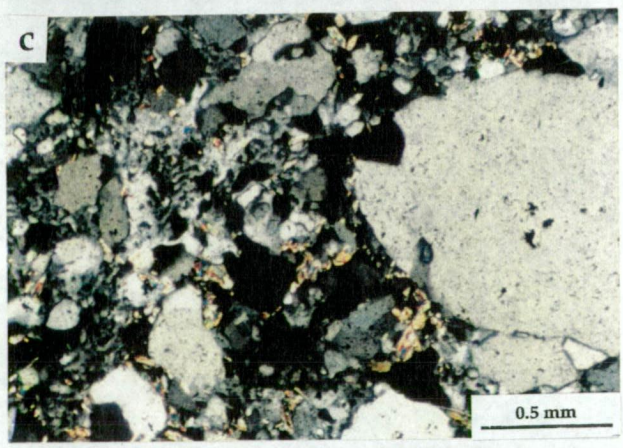
c
0.5 mm


d
6 cm

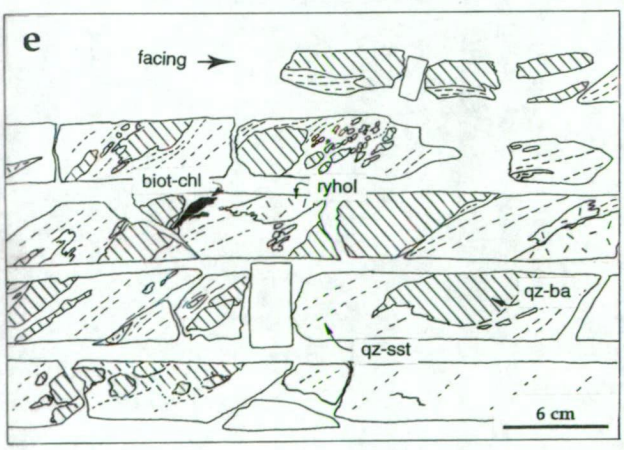
e
facing
biot-chl
ryhol
qz-ba
qz-sst
6 cm

rhyolite clasts are consistent with the replacement of the clast margins, which has accentuated the partly rounded clast shapes.

The groundmass of the rhyolite clasts is microcrystalline and composed of equant quartz grains that overprint fine, intergrown quartz and feldspar (Fig. 4.20c). The microcrystalline quartz-feldspar has a vague graphic texture, and in places is arranged in optically continuous patches. The chlorite-rich rhyolite clasts may have been formerly glassy.

Further down-dip in East Thalanga, the rhyolite breccia becomes monomict and has a gradational contact with a quartz-muscovite-rich coherent quartz ± feldspar phyric rhyolite. Monomict rhyolite breccia up-dip and underlying the coherent rhyolite is clast-supported and grades via jigsaw-fit breccia to coherent rhyolite.

In the Vomacka Zone a poorly sorted, polymict breccia within the ore horizon consists of quartz-phyric rhyolite clasts, with few quartz-magnetite ± barite clasts, and rare dacite clasts (Fig. 4.20d,e and drill hole TH321 in Appendix A). The clasts vary from 30 cm to mm-scale in size, and are supported in a sandy (quartz crystals) siltstone. Barite and sphalerite-galena ± barite veins cross-cut the breccia and have partly replaced the quartz-magnetite clasts. In places the matrix has been replaced by sphalerite-galena ± barite.

4.4.3 Interpretation

Mode of Clast Fragmentation

The rhyolite clasts are interpreted to be variably altered fragments derived from the coherent rhyolite located down-dip of the rhyolite breccia. The curviplanar to irregular clast margins are consistent with clast formation by quench fragmentation, mass-wasting and gravitational collapse of parts of a rhyolite dome. This style of fragmentation could yield clasts from the crystalline interior and also from the glassy margins, and may explain the presence of chlorite-rich (possibly formerly glassy) rhyolite clasts and quartz-feldspar-phyric rhyolite clasts in the breccia.

The QFP, barite, and quartz-magnetite ± barite fragments are non-juvenile lithic clasts and must have been incorporated into the rhyolite breccia during transport. It is unclear whether those components were clasts at the time of incorporation, or whether they were eroded from the mineralised horizon which may have been exposed during transportation of the rhyolite breccia.

Transport and Deposition

Monomict breccia with jigsaw fit textures immediately adjacent to the coherent rhyolite is interpreted as *in situ* hyaloclastite. Up-dip and along strike from the coherent facies the rhyolite clasts are close-packed, with variation from jigsaw-fit texture to dispersed and rotated clasts. Lithic clasts may have been incorporated during transport. These textures and the rhyolite clast shapes suggest that this facies of the upper rhyolite breccia may be partly resedimented hyaloclastite.

The facies geometry indicates that the coherent rhyolite may have been a lava or dome that extruded onto the seafloor in the vicinity of East Thalanga. *In situ* rhyolite hyaloclastite is preserved immediately adjacent to the coherent rhyolite, and the rhyolite breccia along strike and up-dip of the coherent facies is interpreted to be an apron of resedimented hyaloclastite that slumped off the rhyolite dome or lava as it inflated. The resedimented facies is not laterally extensive, occurring <200 m up-dip, but possibly continuous to the Vomacka Zone, suggesting that rhyolite dome growth, hyaloclastite formation and resedimentation was a restricted event.

Herrmann (1994) demonstrated that the coherent rhyolite in the upper rhyolite breccia is geochemically similar to the footwall rhyolitic volcanics, and it is interpreted that this rhyolitic facies association represents the final eruption of the magmas that had previously been the source of the Mount Windsor Volcanics. The sharp conformable contact with the underlying units, together with QFP clasts in the breccia, suggests that this rhyolitic eruption must post-date or be contemporaneous with QFP and some QEV deposition. The upper rhyolite breccia could be a source of rhyolite clasts within the overlying, or laterally equivalent polymict QEV.

The poorly-sorted, rhyolite-dominated polymict breccia in the Vomacka Zone could be a distal equivalent of the upper rhyolite breccia in East Thalanga. Alternatively, the polymict breccia in the Vomacka Zone may pre-date the QEV and QFP, and could be resedimented rhyolitic breccia that formed during emplacement of a rhyolite dome or cryptodome in Central Thalanga.

4.5 Hangingwall Volcanic Units at the Thalanga Deposit (unit iv)

4.5.1 Hangingwall Fragmental

Distribution

Massive to graded siltstone, sandy siltstone and breccia units of the hangingwall fragmental (HWF) are commonly present between the ore horizon and the overlying dacite in all parts of the Thalanga deposit (Fig. 4.1, Fig. 4.3a,b). Because these facies contain fresh to weakly altered feldspars and lacks pyrite stringers, they are interpreted to have been deposited after sulphide mineralisation, and are therefore regarded here as part of the Trooper Creek Formation. Contacts between the HWF and massive sulphides are sharp and mainly planar, and are interpreted to be conformable and depositional. Coarse-grained, remobilised sphalerite or chalcopyrite has locally overprinted the contacts.

Siltstone overlying the QFP along the Thalanga Range is interpreted to be equivalent to the HWF at Thalanga. Typically, the HWF in West Thalanga is ≤2 m in thickness and composed of siltstone, sandy siltstone, or graded siltstone with sandy bases. The HWF in West Thalanga is locally chlorite and biotite-rich and contains sparse blue quartz (<4 mm) and less common feldspar crystals.

In East Thalanga and the eastern parts of Central Thalanga, the HWF is considerably thicker (5 to 18 m) and contains abundant white, siliceous dacite and rhyolite clasts . Pumice breccia units within the HWF are mainly located in Central Thalanga, and increase in thickness down-dip. Where ore lenses are not present at the stratigraphic top of the rhyolitic volcanics, it is difficult to distinguish between weakly altered pumice breccia units in the footwall rhyolitic volcanics and weakly altered pumice breccia units in the HWF due to their similar compositions (quartz ± feldspar-phyric rhyolite pumice clasts).

Components and Lithofacies Variations

The multiple siltstone and sandy siltstone beds of the HWF contain variable proportions of white, non-vesicular quartz-phyric and quartz-feldspar-phyric rhyolite clasts (± flow-banding), feldspar-phyric dacite clasts and altered rhyolitic pumice (Table 4.3). Green, spherical chlorite-rich patches, commonly <1 cm in size, are widespread in the siltstone and sandy siltstone, and are interpreted to have formed during metamorphism (Chapter 3). Beds are typically normally graded and thicknesses vary from centimetre to metre scale, with the maximum total thickness being about 18 m. Single beds within the HWF are generally not continuous between drill holes. The largest dacite clast is about 10 m in diameter, and is

perlitic, contains quartz-filled amygdales, and is present in the HWF adjacent to the major normal fault in Central Thalanga (Fig. 4.1).

Irregular to wispy and lenticular phlogopite-muscovite-rich domains with cuspate margins that resemble fiamme (Fig. 4.21a,b) are common within the HWF, particularly in Central Thalanga. The pale green to white (in hand specimen) quartz-muscovite-rich matrix between the green phlogopite-muscovite-rich patches has an open-framework texture (Fig. 4.21a). These phyllosilicate-rich domains contain larger and more abundant quartz and feldspar crystals than the matrix (Fig. 4.21c), and locally have partly recrystallised spherulites. The concentration of crystals and spherulites in the green phyllosilicate domains is interpreted to indicate that these are altered clasts of formerly dense porphyritic glass. The fiamme texture is caused by the flattening of altered glass parallel to S_2. In more highly deformed zones, the fiamme are strongly flattened (cf. Fig. 4.21b middle with top). Subrounded, non-vesicular silicified quartz-feldspar-phyric rhyolite clasts (1-10 cm in size) are also present in this fiamme-bearing breccia (Table 4.3).

Table 4.3 Facies variations within the hangingwall fragmental.

Facies	Composition	Clast size	Lithofacies
Siltstone-sandstone	matrix = quartz, muscovite, minor chlorite and phlogopite grains = quartz & feldspar crystals and crystal fragments	0.02-0.05 mm <2mm	• sandstone grades upwards to siltstone • laminated siltstone in places
Rhyolite breccia	• silicified quartz-phyric and quartz-feldspar-phyric rhyolite clasts, rarely perlitic • blocky, angular, sub-angular or irregular in shape, with curviplanar margins (Fig. 21d,e)	<1-15 cm, rarely <60 cm	• poorly sorted, clast supported breccia grades upwards to siltstone (Fig. 4.21f), • some clasts (<5 cm in size) are matrix supported
Dacite breccia	perlitic dacite clasts with curviplanar to irregular margins (Fig. 4.21d,e,g)	<1-10 cm, but up to 10 m (Fig. 4.1)	• poorly sorted, non-graded, irregular top and bottom contacts • dacite clasts irregularly dispersed through HWF in places
Fiamme-bearing breccia	• phlogopite-muscovite-rich, quartz & feldspar phyric fiamme (Fig. 4,21a,b) • non-vesicular quartz-feldspar-phyric rhyolite clasts	1-10 cm	poorly sorted, normal grading to siltstone at top with few fiamme

Quartz-magnetite clasts (<50 cm in diameter) are present at the stratigraphic base of parts of the HWF in West Thalanga. Rare massive sulphide clasts (<5 cm in diameter) and barite clasts (<20 cm in diameter) also occur in the HWF (Fig. 4.21e,h)

Deposition of the Hangingwall Fragmental

Repeated graded bedding, with laminated silty tops, in the HWF suggest transport and deposition by turbidity currents. The lack of cross bedding and other tractional features

Figure 4.21 Components and textures of the hangingwall fragmental (HWF).

(a) Quartz and feldspar phenocrysts are concentrated in irregular chlorite-phlogopite-rich domains and few crystals are present in the quartz-muscovite-rich matrix. These textures suggest that it is a poorly sorted, matrix supported fiamme-bearing breccia. Located in C820 Stope, Central Thalanga, 20 230 mN, 20 415 mE, 820 mRL. Steel plate is 30 cm in length.

(b) Fiamme-bearing breccia in drill core. Wispy to cuspate fiamme are quartz- and feldspar-phyric and are flattened parallel to S_2 (middle sample is most strongly deformed). Samples (from top) C2047NI09-18, C2055NI21, and C2047NI09-10. All Central Thalanga.

(c) Photomicrograph of quartz and feldspar phenocrysts preferentially concentrated in chlorite-phlogopite domain of HWF. Sample C2037NI15-50.6, Central Thalanga.

(d) Hand specimens of HWF containing irregular, dark grey dacite clasts and blocky, white, perlitic quartz-feldspar-phyric rhyolite clasts. The rhyolite clasts have chloritic margins in places. Matrix is siltstone with few quartz and feldspar crystals. Samples (from top) E3198SD30-93 and C2055NI21-17.5, East and Central Thalanga respectively.

(e) Top: poorly sorted, clast supported dacite breccia, with and irregular massive pyrite-sphalerite clast. Dacite clasts are irregular and have jigsaw fit textures in places (arrow). Bottom: irregular flow-banded quartz-feldspar-phyric rhyolite clasts in sandy (feldspar crystals) siltstone. Chlorite domains are irregular with diffuse margins and are therefore inferred to have formed during alteration.

(f) Perlitic, sparsely feldspar-phyric dacite clast, with irregular contact to underlying chlorite-rich siltstone. Sample TH209-90.5, Central Thalanga.

(g) Massive barite clast in sandy siltstone. Located in E779 Stope, East Thalanga.


a


b
20 mm

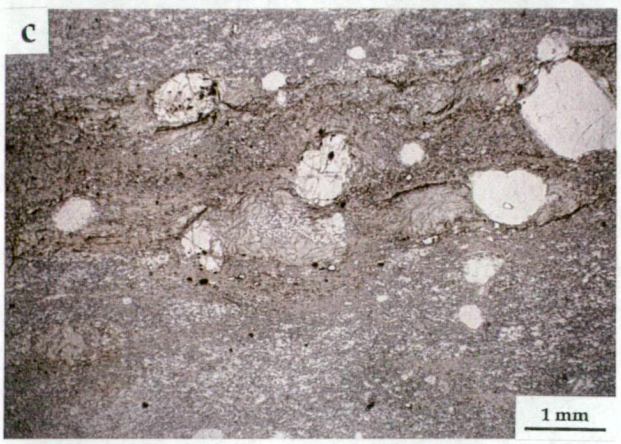
c
1 mm

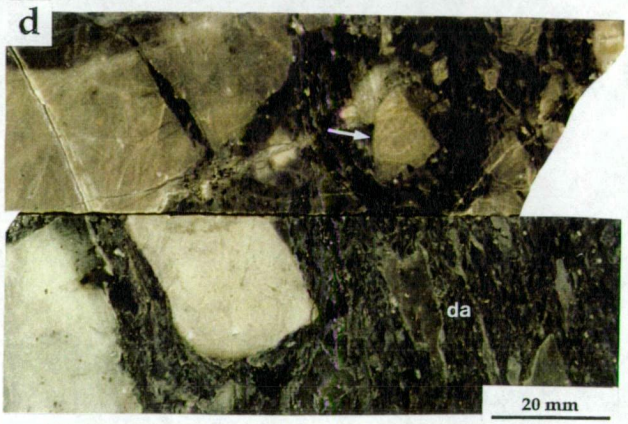
d
da
20 mm

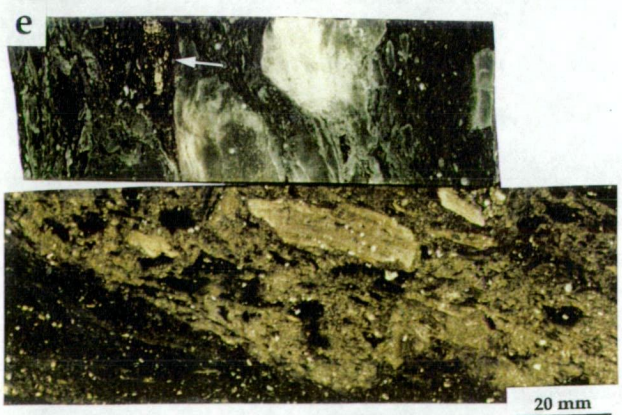
e
20 mm

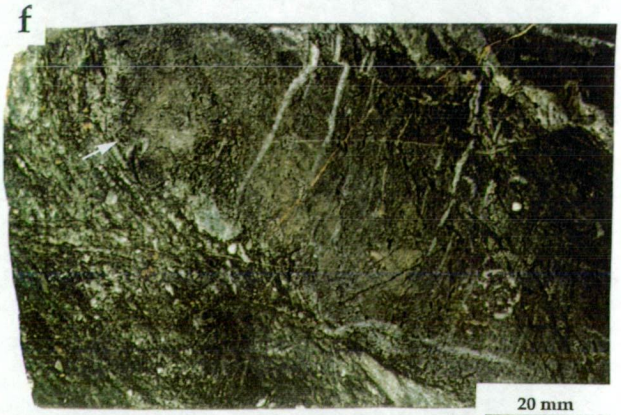
f
20 mm

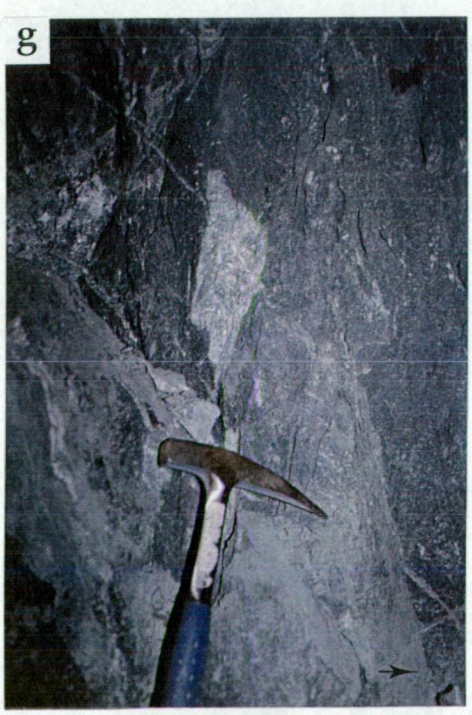
g

suggests that the HWF was deposited in a subaqueous basin below storm wave-base (which is 100-300 m in depth according to estimates by Busby-Spera, 1984). The quartz and feldspar crystals are interpreted to have been derived from older volcanic units, but the provenance of these components is poorly constrained, but may have been intra-basinal.

The presence of massive sulphide and quartz magnetite clasts is interpreted to indicate that massive sulphide and quartz magnetite lenses were exposed on the seafloor during transport of the HWF. The provenance of massive sulphide clasts could either be the Thalanga massive sulphide deposit or other massive sulphide deposits in the Trooper Creek Formation.

4.5.2 Dacite

Coherent, massive to flow-banded, feldspar-phyric dacite immediately overlies the HWF in the vicinity of the Thalanga massive sulphide deposit (Fig. 4.1, Fig. 4.3a,b). Coherent dacite is not exposed at surface west of the western margin of West Thalanga. Instead, a polymict breccia and sandstone units are exposed, and coherent dacite is not present for about 2.5 km along strike (Hill, 1992).

Petrology of the Coherent Facies

Two types of dacite can be distinguished petrographically: dacite with about 5-10 % feldspar phenocrysts (termed here dacite 1; Fig. 4.22a), and a sparsely feldspar-phyric (< 5 %) dacite (termed here dacite 2; Fig. 4.22b). Both types of dacite contain albitised plagioclase phenocrysts and glomerocrysts (1-2 mm in size) and K-feldspar phenocrysts (0.2-1 mm in size) (Fig. 4.10). Sheafs of bladed actinolite are common in dacite 2, and are inferred to be metamorphic in origin (Chapter 3). Elsewhere, the groundmass contains 5-10 % metamorphic biotite and in places this has been retrogressed to chlorite.

The groundmass in both dacites comprises intergrown microcrystalline quartz and feldspar, with microcrystalline feldspars parallel to flow-banding in places (Fig. 4.22c,d). Both dacite 1 and 2 are commonly perlitic, particularly at their top and bottom contacts, and the perlite fractures have been overprinted by brown biotite, or green chlorite after biotite (Fig. 4.22e). The presence of altered perlite indicates that these parts of the dacite were formerly glassy. Banded perlite has accentuated the flow-banding in places.

Both dacite 1 and dacite 2 are present in all parts of the Thalanga massive sulphide deposit. In general, dacite 2 immediately overlies the HWF in East Thalanga, the Vomacka Zone, and the eastern end of Central Thalanga, whereas dacite 1 overlies the HWF in West Thalanga and the western end of Central Thalanga. The contact between the two dacites in Central Thalanga may be the major normal fault (fault C, Fig. 4.1) that coincides with the

Figure 4.22 Textural variations in the dacite at Thalanga.

(a) Hand specimen of a 5-10 % feldspar-phyric dacite (dacite 1). Sample 955-7, Central Thalanga.

(b) Hand specimen of fine grained, aphyric dacite (dacite 2). Sample TH243-399.2, West Thalanga.

(c) Photomicrograph of the fine grained feldspar-rich groundmass of dacite 1. Biotite is disseminated through the groundmass, whereas Ti-oxides and oxide minerals form clusters. Sample 955-29, Central Thalanga. Plane light.

(d) Same sample as (c) under crossed nicols.

(e) Photomicrograph of biotite and chlorite along relic perlite fractures in dacite (top of dacite flow). Sample TH14-441.9, Central Thalanga.

(f) Poorly sorted, monomict dacite breccia with local jigsaw-fit texture. Sample E3207SI28-67.3, East Thalanga.

(g) Poorly sorted, clast supported, monomict, flow banded dacite breccia. Location: 20 200 mN, 20 590 mE, 955 mRL, Central Thalanga. Pencil is about 14 cm in length.

(h) Photomicrograph of perlitic dacite clast in poorly sorted, monomict dacite breccia. Matrix is composed of fine grained quartz, muscovite and minor chlorite. Sample TH71-284, east of Central Thalanga.

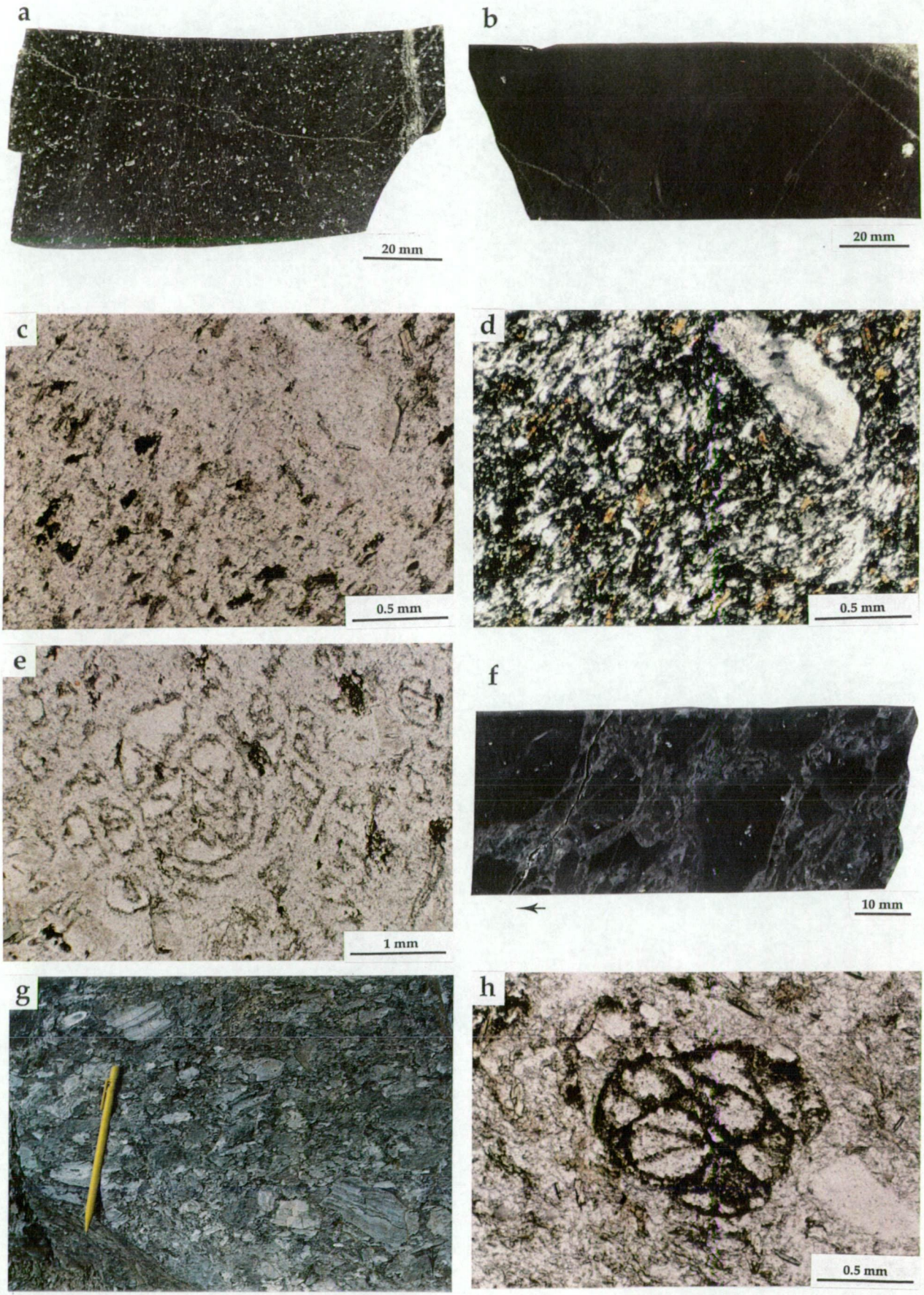
a
20 mm
b
20 mm
c
0.5 mm
d
0.5 mm
e
1 mm
f
10 mm
g
h
0.5 mm

change in bedding orientation. Elsewhere at Thalanga, units of dacite 1 overlie dacite 2 and vice versa.

Thickness of Coherent Dacite

The true thickness of the dacite is difficult to determine due to the numerous ENE-trending faults that offset and repeat the stratigraphy (Chapter 3). However, between Central Thalanga and the Vomacka Zone, about 60 m of dacite 2 overlies a similar thickness of dacite 1, which directly overlies HWF (e.g. diamond drill hole TH71). In West Thalanga, dacite 1 possibly has a maximum thickness of about 130 m. The thickness of dacite 2 in East Thalanga is not known from available drill holes. Coherent dacite is not exposed in the southeastern limits of the Thalanga Range, but is present further northwest along the range. On the north side of the Flinders Highway, dacite 2 is up to 270 m in true thickness.

Lower Contact

The contact between dacite 1 and the underlying HWF is sharp and typically planar. In contrast, the contact between dacite 2 and the HWF varies from sub-planar to irregular and disrupted. In several places, the basal part of dacite 2, and adjacent dacite clasts in the HWF, contain quartz-filled amygdales.

Poorly-sorted, monomict dacite breccia is present in places at the stratigraphic base of both dacites (although more common in dacite 2). The breccia is commonly clast-supported, with angular to blocky dacite clasts (the largest is ≤3 m in size, but most clasts are ≤30 cm in size), some with curviplanar margins and jigsaw-fit texture (Fig. 4.22f). Some clasts have chloritic margins. Close to the HWF, the matrix of the dacite breccia is composed of siltstone with few feldspar and quartz crystals. Intervals of dacite breccia vary in thickness and lateral extent (up to >6 m thick and about 100 m in strike length), and are interpreted to have formed by quench-fragmentation of the base of the dacite.

Upper Contact

Monomict dacite breccia. In the central and eastern parts of Central Thalanga, dacite breccia overlies dacite 2 with gradational contacts (Fig. 4.22f and Fig. 4.23). The breccia comprises monomict dacite 2 clasts and is poorly sorted, clast supported and has a jigsaw fit texture. The degree of clast-rotation in the dacite breccia increases with increasing distance from the coherent dacite (Fig. 4.23). The dacite clasts (<20 cm in size) have curviplanar margins and are angular, cuspate to partly rounded in shape (Fig. 4.22g,h). Irregular wispy clasts composed of biotite and fine grained muscovite may be altered pumice (Fig. 4.24a). However, such clasts are similar in texture to dacite clasts with banded perlite (Fig. 4.24b), and

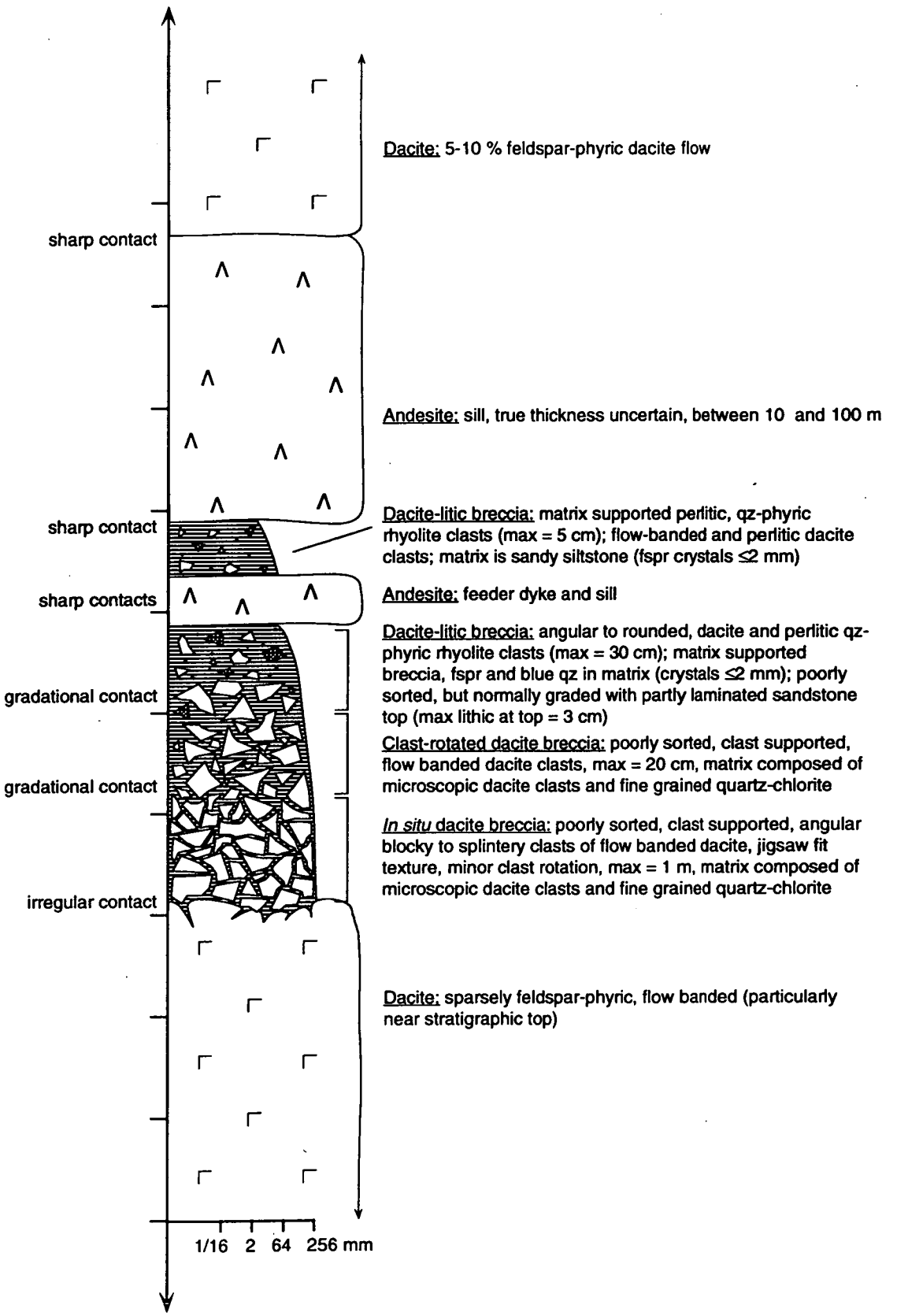

Figure 4.23 Simplified graphic log of the contact between the sparsely feldspar-phyric dacite and the andesite in Central Thalanga. Tick marks along vertical axis of log are 10 m apart. Abbreviations: max = maximum

Figure 4.24 Textures of the monomict dacite breccia and the dacite-rhyolite breccia.

(a) Photomicrograph of banded (due to biotite) dacite clast. Biotite could define tube walls of a dacitic pumice clasts or could mark banded perlite fractures. Sample TH71-284, east of Central Thalanga.

(b) Photomicrograph of perlitic dacite clast (biotite along fractures) with banded perlite grading to classical perlite (arrow). Sample TH71-284, east of Central Thalanga.

(c) Photomicrograph of biotite-rich dacite clast containing quartz spherulites. Sample TH71-284, east of Central Thalanga.

(d) Same sample as (c) under cross nicols. Spherulites have recrystallised quartz rim.

(e) Poorly sorted monomict dacite breccia. Dacite is partly flow-banded and clasts vary from jigsaw-fit to clast-rotated textures. Matrix is siltstone. Pencil is about 14 cm in length. Thalanga Range (mine grid: 20 760 mN, 14 110 mE).

(f) Poorly sorted monomict dacite breccia as above, with prominent jigsaw-fit textures. Thalanga Range (mine grid: 20 760 mN, 14 110 mE).

(g) Angular quartz-feldspar phyric rhyolite clast from the dacite-rhyolite breccia. Cuspate, curviplanar margins are accentuated by shearing (south side up) of the clast. Sample 955-2, Central Thalanga.

(h) Matrix supported dacite-rhyolite breccia. Matrix is composed of siltstone with feldspar crystals, small dacite clasts (<2 mm in size), and few quartz crystals. Sample 980-12, Central Thalanga.

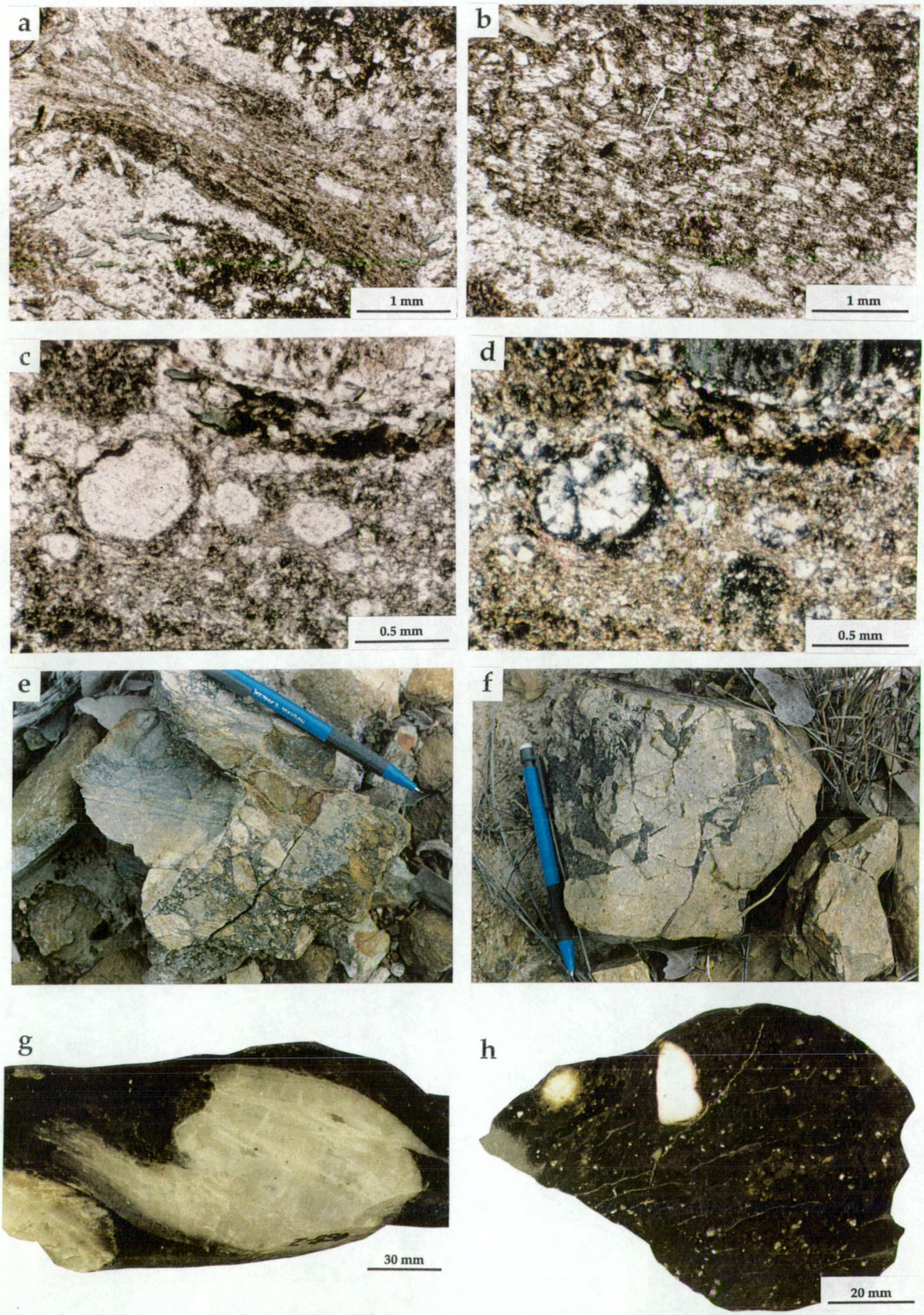
a
1 mm
b
1 mm
c
0.5 mm
d
0.5 mm
e
f
g
30 mm
h
20 mm

therefore are probably not pumice. Rare angular to blocky clasts composed of fine grained muscovite and containing partly recrystallised spherulites are also present in the dacite breccia (Fig. 4.24c,d). A gradational contact occurs between this monomict dacite breccia and the overlying poorly sorted dacite-rhyolite breccia.

A poorly sorted, clast supported dacite breccia marks the upper contact of the dacite 2 located immediately north of the Flinders Highway in the Thalanga Range. The breccia is composed of 5-100 mm sized, angular to blocky dacite 2 clasts and extends <1 m from the coherent dacite. The dacite clasts have jigsaw fit textures and a matrix of siltstone is present between the clasts (Fig. 4.24e,f). There is a sharp, but irregular contact with the overlying siltstone and graded sandstone units in this location.

Dacite-rhyolite breccia. White siliceous quartz-feldspar-phyric rhyolite clasts and perlitic dacite 2 clasts are the most abundant clast-types in the dacite-lithic breccia. The dacite-lithic breccia comprises three normally graded (but internally poorly sorted) and weakly stratified beds, with laminated sandy siltstone marking the stratigraphic top of each bed. Individual beds vary from 1 to 5 m in thickness in Central Thalanga (Fig. 4.1). The perlitic dacite clasts are strongly silicified, angular to irregular in shape, and are white to medium grey in hand specimen. Dacite clasts with few perlitic fractures are typically medium grey in hand specimen. Generally the dacite clasts are <10 cm in size.

The rhyolite clasts are strongly silicified, white in hand specimen and are highly angular to cuspate in shape (Fig. 4.24g). The rhyolite clasts are <20 cm in diameter and grade to <3 cm in diameter near the stratigraphic top of the dacite-rhyolite breccia (Fig. 4.24h). The groundmass of the rhyolite clasts is composed of recrystallised quartz and feldspar, and has been overprinted by coarsely recrystallised quartz. Both dacite and rhyolite clasts are supported by a silt-sized matrix containing small dacite fragments (<1 mm, identified in thin section), and blue quartz and fresh feldspar crystals (<1 mm).

Interpretation of Dacite Emplacement

The dacite breccia at the base of dacite 2, in East Thalanga and the eastern part of Central Thalanga, is interpreted to include both *in situ* hyaloclastite and intrusive hyaloclastite or blocky peperite involving siltstone of the underlying HWF. The dacite breccia overlying dacite 2 in Central Thalanga includes facies thought to range from *in situ* hyaloclastite immediately adjacent to the coherent dacite, through dispersed hyaloclastite to resedimented hyaloclastite, as indicated by the stratified nature of the dacite-rhyolite breccia. These relationships are consistent with subaqueous dacite extrusion, and the shedding and redeposition of hyaloclastite from the top of the dacite dome or lava (cf. Yamagishi, 1987; Kurokawa, 1991; Allen, 1992). Therefore dacite 2 in Central and East

Thalanga is interpreted to have flowed over and foundered into partly consolidated HWF. Because spherulites are typically located near the core of lavas or domes, rather than quenched-fragmented margins (Fink and Manley, 1987; Duffield and Dalrymple, 1990; McPhie *et al.*, 1993) the presence of spherulitic dacite clasts in the monomict dacite breccia, is consistent with gravitational collapse and mass-wasting of the dacite. The provenance of the angular and cuspate rhyolite clasts in the overlying resedimented hyaloclastite (the dacite-rhyolite breccia) is unknown.

Emplacement of the dacite 1 in West Thalanga and the western part of Central Thalanga is poorly understood, although the lack of peperite at dacite contacts with the HWF in West Thalanga may indicate that the HWF in West Thalanga was consolidated at the time of dacite emplacement. Thus the dacite 1 in West Thalanga may post-date emplacement of dacite 2 in East Thalanga. However, in other volcanic sequences, passive contacts do occur between the bases of lavas or domes and unlithified sediments (e.g. Allen, 1992). The nature of the original top of the dacite 1 unit in West Thalanga is poorly understood because an andesite sill is present between the dacite and overlying dacite-pumice breccia (section 4.5.3).

There is a gradational contact between the dacite breccia and underlying coherent dacite 2 that is located in the Thalanga Range (north of the Flinders Highway). There is no evidence that sediment infilled the brecciated top of the dacite. Rather, the lack of bedding in the siltstone matrix, and jigsaw-fit textures and blocky shapes of the dacite clasts in the breccia are interpreted to indicate that the breccia is an intrusive hyaloclastite.

4.5.3 Polymict Breccia and Sandstone Facies

Dacite-Pumice Breccia

A poorly sorted polymict breccia, containing abundant irregular dacite 2 clasts and feldspar-phyric chlorite-biotite-rich clasts, is present between dacite domes or lavas in West Thalanga (Fig. 4.3b). Minor muscovite-rich quartz-feldspar-phyric tube pumice and silicified rhyolite clasts are also present in this dacite-pumice breccia (Fig. 4.25a; Table 4.4). Few of both the dacite 2 and silicified rhyolite clasts are perlitic. The feldspar-phyric chlorite-biotite-rich clasts are flattened parallel to S_2, and have feathered ends similar to altered, compacted pumice clasts or fiamme from other ancient volcanic sequences (e.g. Allen, 1992). This breccia is clast supported, with a matrix composed of sandy siltstone with quartz (blue) and feldspar crystals (2-4 mm in size).

The dacite-pumice breccia is normally graded from coarse breccia (largest clast = 10 cm dacite 2), to granular breccia (largest clast = 3 mm dacite 2), to fine sandstone (<1 mm sized grains). Layers of siltstone are interbedded in fine sandstone at the top of the breccia. In diamond drill

Figure 4.25 The dacite-pumice breccia, andesite and post-tectonic intrusions at Thalanga.

(a) Poorly sorted, polymict dacite pumice breccia. Top: feldspar-phyric, biotite-chlorite-rich clasts, that may be altered and metamorphosed clasts of dacite pumice or dense glass, and possible rhyolite pumice clasts are supported in a poorly sorted matrix of smaller pumice clasts, blocky dacite clasts and feldspar crystals. Sample TH33-144.5, West Thalanga. Bottom: irregular sparsely feldspar-phyric dacite clasts are more abundant, and are more variable in size) that intensely silicified rhyolite clasts. Sample TH33-152, West Thalanga.

(b) Photomicrograph of hornblende phenocrysts within the andesite at Thalanga. Fine grained hornblende, feldspar and biotite are present in the groundmass. Sample 980-9, Central Thalanga.

(c) Same sample as (b) under crossed nicols.

(d) Photomicrograph of microdiorite. The presence of quartz intergrown with feldspar in the groundmass, and absence of hornblende phenocrysts are the main textural and compositional differences between microdiorite and andesite. Sample C2067ND58-41.5, Central Thalanga.

(e) Same sample as (d) under crossed nicols.

(f) Photomicrograph of dolerite. Rounded intergrowths of fine grained chlorite may be after olivine. Plagioclase is intergrown with augite and magnetite in the groundmass. Sample W2013ND27-76.5, West Thalanga.

(g) Same sample as (f) under crossed nicols.

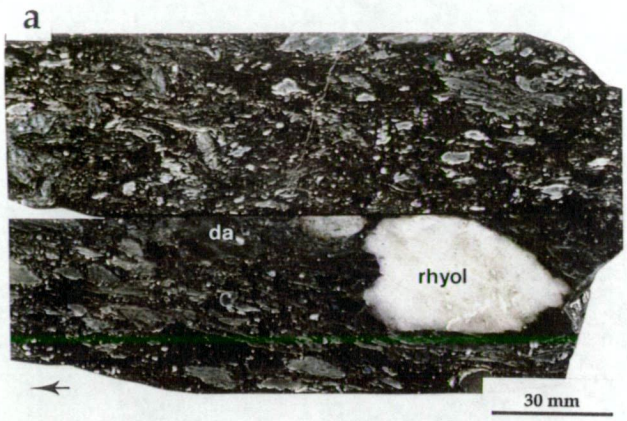
a
da
rhyol
30 mm

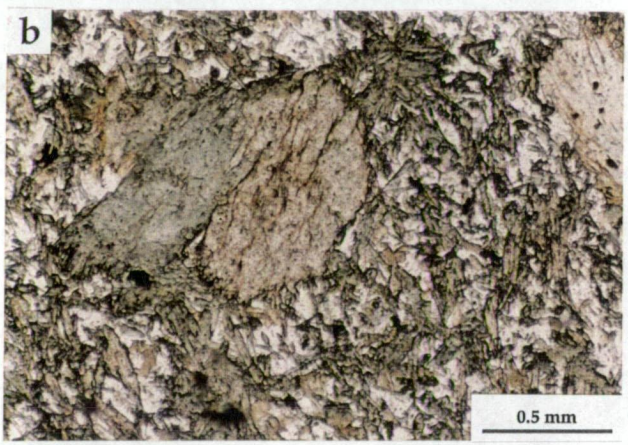
b
0.5 mm

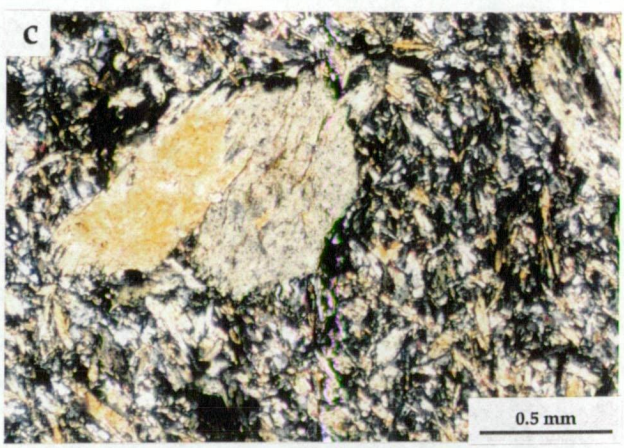
c
0.5 mm

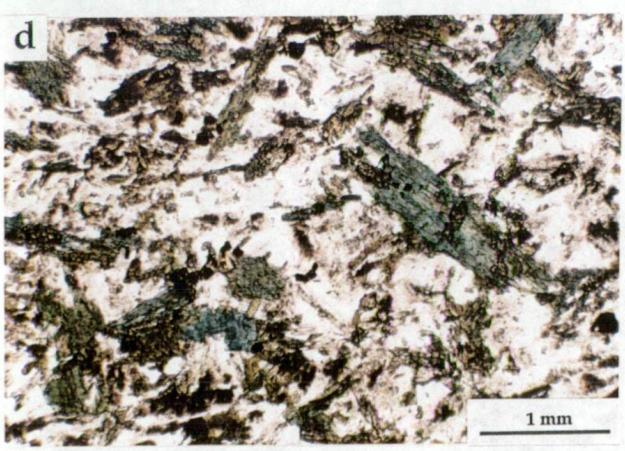
d
1 mm

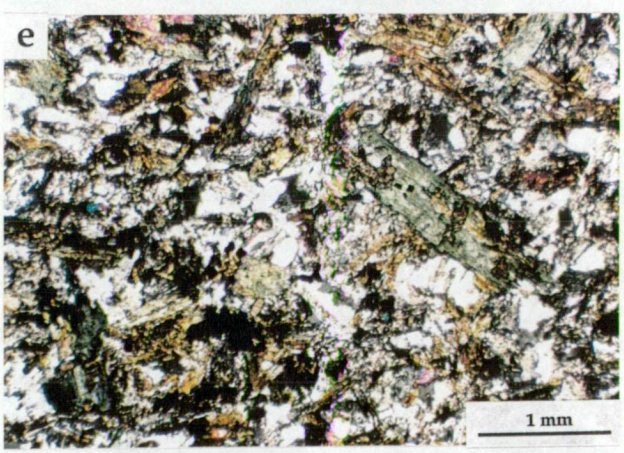
e
1 mm

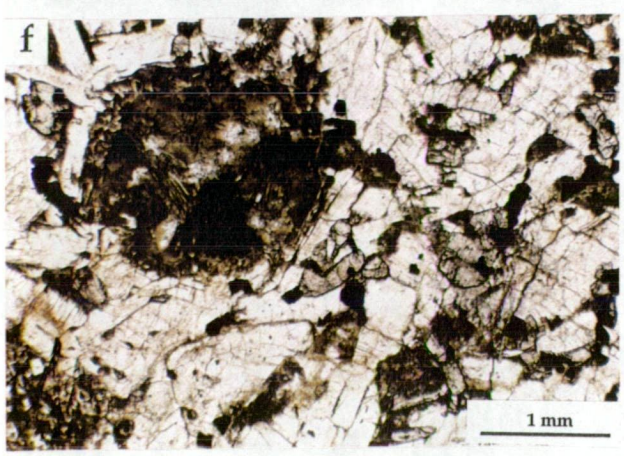
f
1 mm

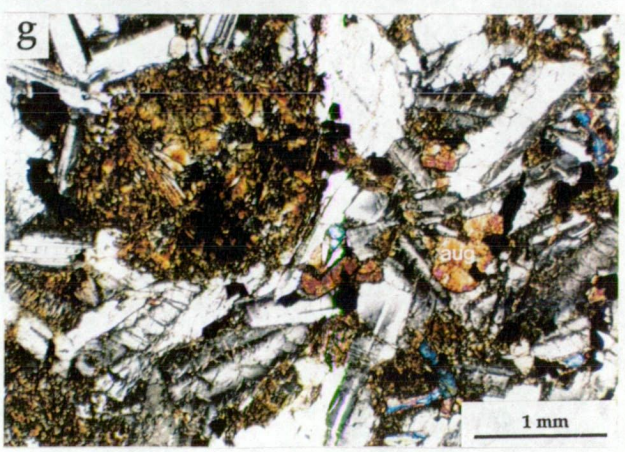
g
aug
1 mm

hole TH33 in West Thalanga, the dacite-pumice breccia comprises three normally graded units (10 m, 3 m, and 5 m in true thickness). The lowermost dacite-pumice breccia has a sharp planar contact with andesite interpreted to be a sill (section 4.5.4), and the top of the dacite-pumice breccia has a sharp, irregular contact with overlying amygdaloidal dacite 2 dome or lava (Fig. 4.3b). The internal characteristics of the dacite-pumice breccia units are consistent with subaqueous mass-flow transport and deposition.

Table 4.4 Types of clasts in the dacite-pumice breccia.

Clasts	Clast shape	Size range	Abundance & distribution
Dacite 2	irregular to angular	5 mm to 10 cm, but mostly <3cm	abundant evenly distributed
Altered, feldspar-phyric pumice or dense glass	irregular, wispy, lenticular, with feathered ends	<0.5cm to 3.5 cm	abundant, more abundant, but smaller near top of breccia
Altered, quartz-feldspar phyric pumice	irregular to wispy with feathered ends	largest = 10cm, generally < 2cm	minor, dispersed throughout
Silicified quartz-feldspar-phyric rhyolite	angular to blocky with curviplanar margins	3 cm - 6 cm	few concentrated near base of breccia

Polymict Volcanic Breccia

A poorly sorted, normally graded, polymict breccia (20 to 50 m in true thickness) overlies the dacite or QFP in most parts of the southeastern extent of the Thalanga Range (Fig. 4.5). The polymict volcanic breccia is composed of angular to sub-rounded dacite clasts, sub-rounded siliceous QFP clasts and rounded aphyric siliceous rhyolite clasts in a quartz and feldspar crystal-rich matrix (clasts 2 to 50 cm in size, with largest clast = 5 m). Crystal-rich sandstone is common at the uppermost parts of this breccia.

The poorly sorted texture and normal grading of the polymict volcanic breccia are consistent with the transport and deposition of the clasts and crystals as a subaqueous mass flow. The partly rounded, polymict clasts suggest that the clasts have been reworked prior to mass-flow resedimentation, possibly in a river or beach environment. The relationship between the polymict volcanic breccia and the dacite-pumice breccia in West Thalanga is unclear from available drill hole data.

Graded Quartz-Feldspar Sandstone

Multiple beds of quartz-feldspar crystal-rich sandstone to feldspar crystal-rich sandstone, composed of well rounded, moderately sorted and closely packed crystals ≤5 mm in size, locally overlie the polymict volcanic breccia or the dacite along the Thalanga Range. Sub-angular to rounded dacite clasts (≤5 cm in size) are common in the base of the sandstone beds, which grade upwards to siltstone. Single beds vary from <30 cm to ~1 m in true thickness, and

intervals of the multiple beds vary from 5 to 25 m in thickness. The crystals in the graded sandstone are interpreted to have been reworked and derived from older, crystal-rich volcaniclastic deposits.

4.5.4 Andesite

Distribution and Contacts with Enclosing Rocks

Andesite units are present in the hangingwall at Thalanga. The andesite is weakly foliated (S_2), is offset along D_3 faults (Fig. 4.1) and is therefore inferred to be similar in age to the underlying volcanic units. In Central Thalanga, andesite units within the HWF are interpreted to be coeval with andesite that overlies and partly intrudes the dacite hyaloclastite and dacite-rhyolite breccia (Fig. 4.1 and Fig. 4.23). Both the stratigraphic top and base of the andesite in Central and West Thalanga are sharp and subplanar. Although there is no evidence of baking of the adjacent dacite, dacite-rhyolite breccia or dacite-pumice breccia, the passive contacts and the genetic link between the volcaniclastic facies and underlying dacite lava/dome suggest that the andesite units at Thalanga are a series of sills.

Petrography

The sparsely (~2 %) green hornblende-phyric andesite is medium to dark green in hand specimen and contains rare calcite-filled amygdales. In thin section, the hornblende, and chlorite after hornblende, phenocrysts are subhedral, <1.5 mm in size, and have irregular margins that appear to be intergrown with the groundmass (Fig. 4.25c,d). Acicular green hornblende (<0.4 mm in length) and interstitial feldspar are the main components of the groundmass (both 30-40 % of groundmass). Olive brown biotite (weakly aligned and inferred to be metamorphic, 10-20 % of groundmass) and accessory apatite are also present. The biotite has been partly chloritised, and the minor Fe-oxides, sphene, epidote and calcite within the groundmass are interpreted to be alteration minerals.

4.5.5 Location of Quartz-Magnetite Lenses

Quartz-magnetite lenses are present stratigraphically above and below the Thalanga massive sulphide horizon in places along the Thalanga Range (Duhig, 1991; Duhig *et al.*, 1992). Quartz-magnetite lenses occur at the contact between the rhyolites of the Mount Windsor Volcanics and the QFP, between the QFP and the overlying dacite, and between the dacite and the overlying quartz-feldspar crystal-rich sandstone (Fig. 4.26). The quartz-magnetite lenses are considered to be the metamorphosed equivalents of exhalative silica-hematite lenses present in the eastern and central parts of the Mount Windsor subprovince (Duhig, 1991; Duhig *et al.*, 1992; Davidson *et al.*, 1993). Along the Thalanga Range the quartz

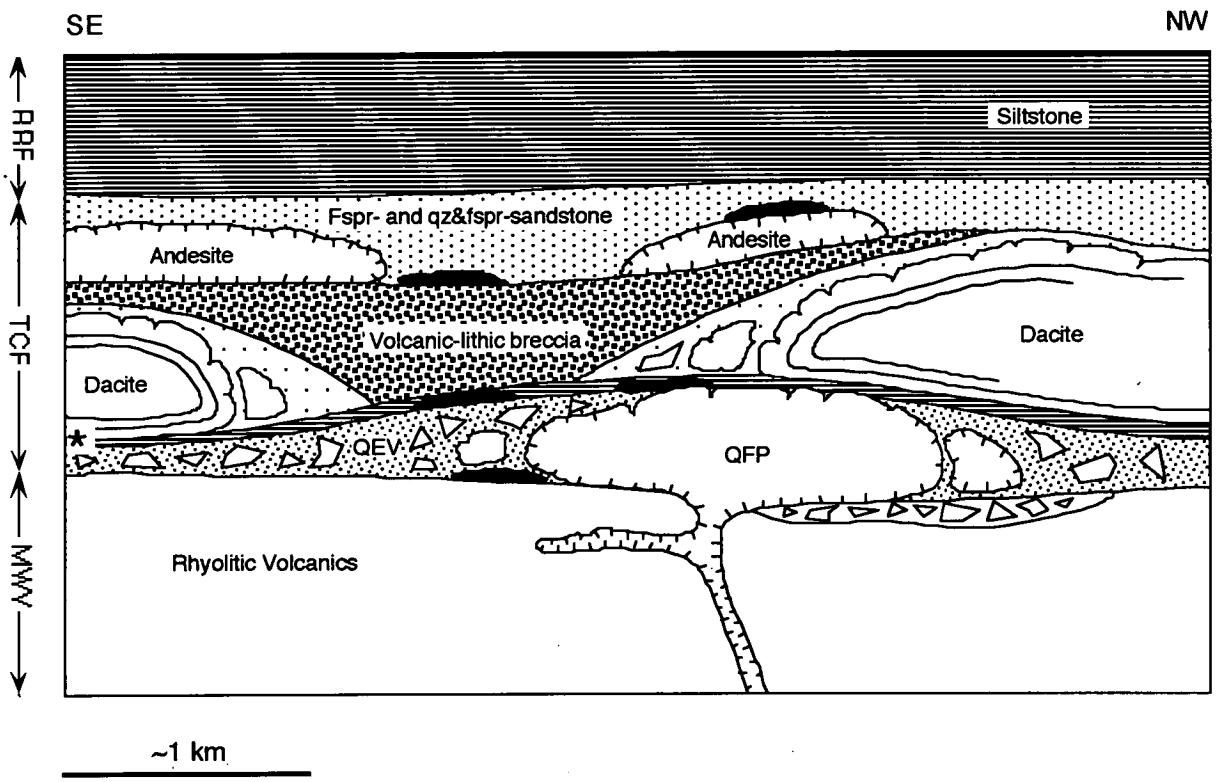

Figure 4.26 Schematic facies architecture of the volcanic succession, from the Mount Windsor Volcanics (MWV), through the Trooper Creek Formation (TCF), to the Rollston Range Formation (RRF), along the Thalanga Range northwest of the Thalanga massive sulphide deposit. The Thalanga deposit occurs at the left hand margin of this diagram, at the asterisk. Black pods represent quartz magnetite lenses. Trooper Creek Formation varies from 200 m to 350 m in true thickness.

magnetite forms discontinuous pods (1-65 m in strike length) parallel to bedding. Only one example of a quartz-magnetite vein cross-cutting coherent dacite was observed stratigraphically below a quartz-magnetite pod. Siltstone is commonly present along strike from the quartz-magnetite units. These packages are interpreted to represent ambient basin sedimentation and local hydrothermal exhalations, intercalated between units generated primarily by volcanic eruptions.

4.6 Rollston Range Formation

Multiple beds of brown, partly micaceous laminated siltstone, and minor sandstone (2 mm size grains) grading to siltstone beds, overlie the quartz and feldspar crystal-rich sandstone in the vicinity of the Thalanga Range (Hill, 1992). The siltstone is silicified in places. There is a gradational contact between these siltstone and graded sandstone beds and the underlying (coarser) quartz and feldspar crystal-rich sandstone, with siltstone interbedded with the sandstone in places.

The siltstone and graded sandstone beds are interpreted to have a partly non-volcanic provenance, with no indication of contemporaneous intrabasinal volcanism. They reflect the cessation of volcanism and record the return to ambient basin sedimentation dominated by reworked terrigenous sediments. The micaceous siltstone and graded sandstone beds are therefore interpreted to be part of the Rollston Range Formation.

4.7 Summary of Volcanism at Thalanga

The sequence of volcanic events that resulted in the deposition of rhyolitic through the dacitic and andesitic rocks at the Thalanga deposit are summarised in Figure 4.27. The footwall rhyolitic volcanics (Mount Windsor Volcanics) are possibly composed of rhyolite domes or cryptodomes, syn-eruptive breccias, syn-volcanic sills, and breccia units deposited from mass-flows (Fig. 4.27a). Construction of a rhyolite dome in Central Thalanga may have resulted in the formation of local basins in West and East Thalanga. The minor amount of siltstone overlying the rhyolitic volcanics in parts of East Thalanga is interpreted to be coeval with massive sulphide deposition and represents resumption of ambient sedimentation during a period of quiescence following rhyolite emplacement and prior to deposition of the QEV (Fig. 4.27a).

QEV deposition in West and East Thalanga is followed by emplacement of QFP sills or partly emergent cryptodomes in East Thalanga (Fig. 4.27b). Some QFP domes may have been extruded prior to QEV deposition. Mega-clasts of QFP in Central Thalanga may be remnants

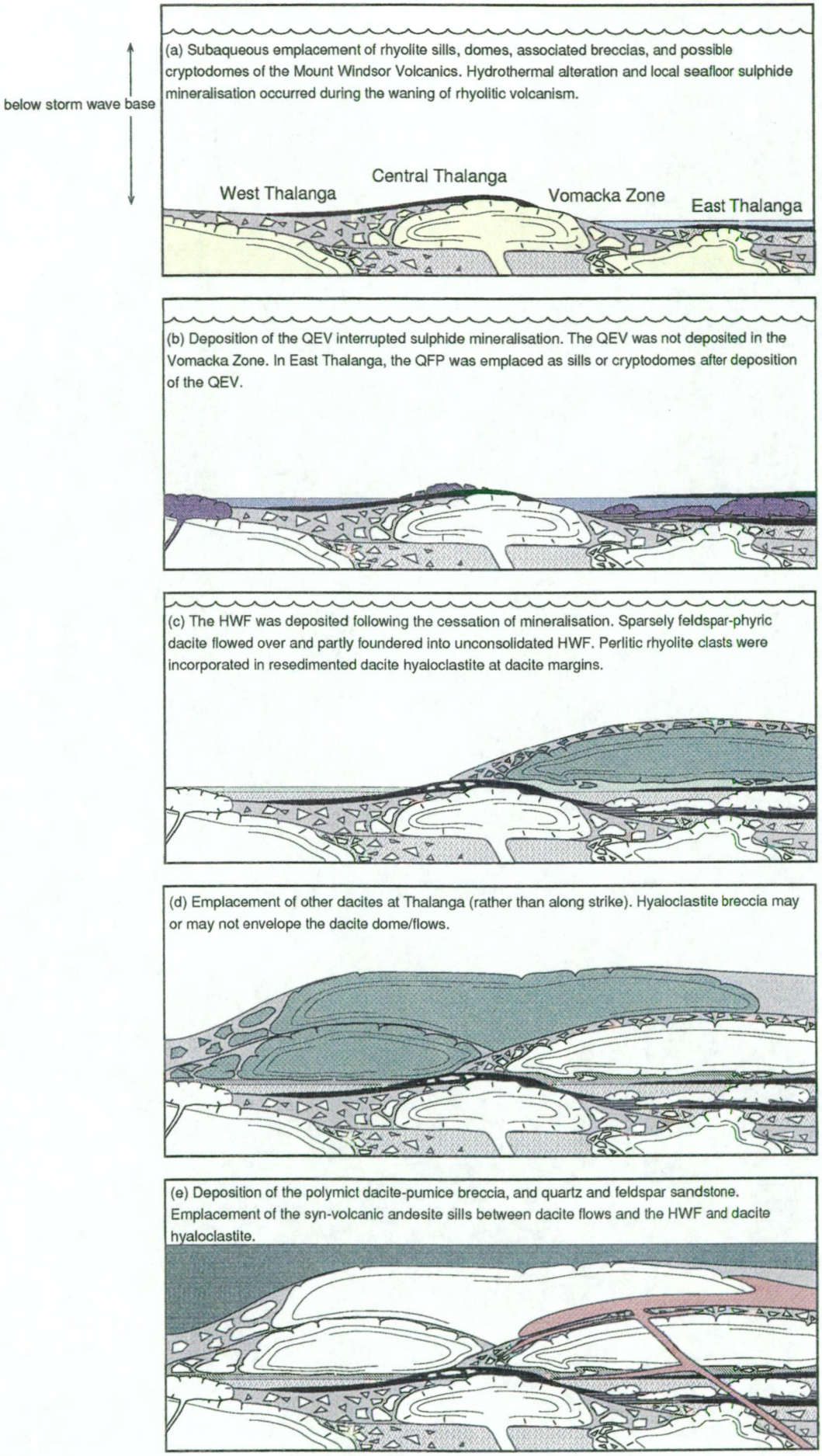

Figure 4.27 Schematic diagram depicting the order of deposition and emplacement of the volcanics at the Thalanga massive sulphide deposit.

of a collapsed QFP dome that was the source of QFP clasts in the QEV units. The interpretation of the upper rhyolite breccia (in East Thalanga) as hyaloclastite (*in situ* and partly resedimented) implies continued rhyolitic volcanism after QEV deposition in East Thalanga. There is no evidence of rhyolitic volcanism after the deposition of the QEV in Central or West Thalanga. In Central and East Thalanga, sulphide mineralisation continued after deposition of the QEV and upper rhyolite breccia (Chapter 6).

Multiple beds of graded siltstone and sandy siltstone (HWF) overlying the massive sulphide lenses, QEV and QFP sills indicate temporary cessation of effusive volcanism at Thalanga (Fig. 4.27c). Dacite is interpreted to have flowed into the deepest part of the basin at Thalanga and partly foundered into the underlying unconsolidated HWF (Fig. 4.27c). Hyaloclastite from the top of the dacite lava was resedimented (by gravitational collapse) at the margins of the flow prior to emplacement of subsequent dacite lavas. Polymict mass-flow deposits (dacite-pumice breccia) indicate redeposition of dacitic pyroclasts (unknown provenance) into local basins during dacite extrusion (Fig. 4.27d). Continued volcanic activity at Thalanga is marked by the emplacement of syn-volcanic andesite sills (Fig. 4.27e). The andesite typically occurs in the volcaniclastic facies between dacite lavas, or along the contact between volcaniclastic units and dacite lava. The top of the volcanic pile at the Thalanga deposit has not been drilled, but along strike in the southeastern part of the Thalanga Range, well sorted micaceous siltstone of the Rollston Range Formation indicates the cessation of volcanism.

4.8 Post-tectonic Intrusions

4.8.1 Microdiorite

Microdiorite dykes trend NNE and cross cut the stratigraphy in all parts of the Thalanga massive sulphide deposit. Many dykes are intersected in drill core in the eastern parts of East Thalanga, four dykes are present in Central Thalanga, and one or two microdiorite dykes occur in West Thalanga. Some of the dykes in East Thalanga are coarser grained (about 1 mm) than those in Central Thalanga (0.1-0.5 mm), and this is probably due to differences in dyke width and extent of chilled margins.

The microdiorite dykes are superficially similar to the andesite sills in hand specimen, but contain ophitic hornblende and altered feldspar crystals, and quartz in the groundmass (Fig. 4.25e,f). The main components are 30-50 % muscovite pseudomorphs of feldspar (0.4 mm in length), 20-30 % euhedral, acicular green hornblende (0.5 mm in length), 5-20 % olive brown biotite (now mostly chloritised), 2-10 % interstitial quartz, and accessory apatite and sphene.

Some hornblende grain boundaries are irregular and have rims with different pleochroism from the core of the crystal. In places the hornblende has been variably replaced by chlorite. Biotite is also commonly altered to chlorite and Ti-oxides. Epidote is disseminated in several microdiorite dykes and there is a spatial association between epidote and hornblende. Traces of euhedral pyrite are disseminated through the dykes.

4.8.2 Dolerite

A fine-grained dolerite dyke, dark grey to black in hand specimen, cross cuts the mineralised horizon and the S_2 cleavage in the footwall of West Thalanga. The dolerite is typically highly fractured, with white calcite common along irregular joints. In thin section, the dolerite is ophitic in texture, and is composed of 60 % plagioclase (≤2 mm in length), 10-20 % chlorite after olivine, 5-10 % augite, minor magnetite and accessory apatite. The plagioclase is unaltered, except for chlorite-filled fractures (Fig. 4.25g,h). Chlorite is also interstitial to the plagioclase laths.

4.9 Synthesis: Depositional Environment and Basin Architecture

4.9.1 Water Depth

The abundance of clastic units with lithofacies characteristics typical of subaqueous sediment gravity flow deposits, hyaloclastite at the margins of domes and lavas, peperitic margins of sills, and graded to massive siltstone within the ore horizon all support a subaqueous environment of deposition. Water depth is difficult to estimate, but it is evident from well laminated siltstone at the stratigraphic top of the massive sulphides, and the absence of reworking of the fine grained tops of sediment gravity flow deposits, that the massive sulphide deposit was at least below storm-wave base. Rounded clasts in the polymict volcanic breccia along strike from Thalanga indicate some reworking, and may have been sourced from shallow beach or river environments. However, the rounded clasts do not constrain water depth because they have been resedimented.

4.9.2 Importance of Proximal Volcanism at Thalanga

At Thalanga, the footwall rhyolitic volcanics (Mount Windsor Volcanics) are approximately 1200 m thick, compared to 500 m in thickness at the rail cutting through the Thalanga Range (Hill, 1992). This thickness of rhyolite may be due to concentration of constructional rhyolitic volcanism (domes and cryptodomes) at Thalanga. Structural repetition may also have increased the apparent thickness of the rhyolitic volcanics. Within the vicinity of the Thalanga massive sulphide deposit, the main site of constructional rhyolitic volcanism may

have been located down-dip and east of the ore lenses at Central Thalanga. This area now partly overlies the ore horizon due to normal faulting. Hyaloclastite or autoclastic breccia and mass-flow deposits may have formed preferentially in local basins elsewhere at Thalanga (Fig. 4.27a, Table 4.5).

The volume of QEV and QFP, and the relationship of the sulphides to these facies, vary across the massive sulphide deposit, and the most prominent differences are between West and East Thalanga (Fig. 4.6; Table 4.5). The high proportion of QFP sills and cryptodomes in East Thalanga and along the southeastern end of the Thalanga Range suggests that these areas were volcanic centres during the time of QFP emplacement. Numerous thick QEV units in West and East Thalanga and the southeastern end of the Thalanga Range, indicate that these areas were also important depocentres. The absence of QEV in the eastern part of Central Thalanga and the Vomacka Zone is interpreted to indicate that West and East Thalanga were separate basins during the time of QEV deposition (Fig. 4.27b), which supports the suggestion that parts of Central Thalanga may have been a topographic high, created by emplacement of rhyolite domes or cryptodomes. The presence of QFP sills and the upper rhyolitic breccia (interpreted to be hyaloclastite from a collapsed rhyolite dome) in East Thalanga (Table 4.5) indicate that volcanic activity was concentrated in East Thalanga during sulphide mineralisation.

There is a greater thickness of HWF in the eastern part of Central Thalanga, the Vomacka Zone, and East Thalanga, which indicates these areas were locally deeper than West Thalanga during deposition of the HWF. Intrusive dacite hyaloclastite within the HWF and at the contact between dacite lavas and the underlying HWF are restricted to these areas containing thick HWF. Therefore the first dacite is interpreted to have flowed into the deepest part of the basin at Thalanga and partly foundered into the underlying unconsolidated HWF. It is not clear from the available drill holes whether more than one dacite lava is present between Central and East Thalanga, but given that the dimensions of younger, subaqueous siliceous domes and lavas vary from 50-1000 m (Pichler, 1965; Lonsdale and Hawkins, 1985) to 10 km in lateral extent (Cas, 1992), it is likely that one dacite lava extends from Central to East Thalanga (about 150 m).

Subsequent dacite units are located in the immediate vicinity of the massive sulphide deposit. Dacite is not present immediately west of Thalanga. Instead polymict volcanic breccia, quartz-feldspar crystal-rich sandstone and siltstone occur in the equivalent stratigraphic position (map M1), supporting the interpretation that the Thalanga massive sulphide deposit is located at a volcanic centre which was a topographic high.

The concentration of coherent and proximal volcaniclastic facies at Thalanga (Table 4.6) is consistent with a regime of high heat flow, which has significant implications for driving

Table 4.5 Comparison of the volcanic facies of the Vomacka Zone, East, Central and West Thalanga.

Stratigraphic Location	West Thalanga	Central Thalanga	Vomacka Zone	East Thalanga
Hangingwall	Dacite-pumice breccia: distribution poorly understood; Dacite: generally 5-10 % feldspar-phyric (dacite 1); HWF: sandy siltstone, <2 m in thickness	Dacite: 5-10 % feldspar-phyric dacite (dacite 1) mainly confined to west of fault C, and sparsely feldspar-phyric dacite (dacite 2) generally present east of fault C; HWF: sharp increase in thickness east of fault C. Perlitic dacite clasts also present in HWF east of fault C	Dacite: mainly sparsely feldspar-phyric dacite (dacite 2); HWF: 1-10 m in thickness, multiple graded siltstones and sandy siltstone, abundant siliceous rhyolite clasts in places	Dacite: sparsely feldspar-phyric dacite (dacite 2); HWF: 5-18 m in thickness, multiple graded silstones and sandy siltstones, with peperitic dacite clasts and siliceous rhyolite clasts
Ore horizon	QEV: generally one graded mass flow unit, with rare overlying sandstone or thinner QEV units. QEV overlies sulphide lenses; QFP: not present.	QEV: minor discontinuous lenses; QFP: spherulitic mega-clasts west of fault C; QEV and QFP clasts enveloped by sulphides.	QEV & QFP: not present; Poorly sorted, polymict rhyolitic breccia, partly overprinted by sulphide veins.	Siltstone and graded sandy siltstone overly footwall; QEV: extensive, multiple beds, overly and are overlain by sulphide lenses; QFP: syn-volcanic sills, partly intrude QEV, and are not mineralised; Poorly sorted rhyolitic breccia, overlies and interfingers with QEV. Is overprinted by sulphide veins.
Footwall	Rhyolitic Volcanics: coherent rhyolite, possibly with volcaniclastic units at stratigraphic top	Rhyolitic Volcanics: coherent quartz-feldspar-phyric rhyolite, local rhyolite hyaloclastite, rare pumice-bearing rhyolite breccia	Rhyolitic Volcanics: coherent rhyolite, with zones of poorly sorted, clast-supported rhyolite breccia	Rhyolitic Volcanics: coherent rhyolite, possibly with volcaniclastic units at stratigraphic top

the circulation of the hydrothermal fluids in the footwall. This would suggest that areas within the Mount Windsor volcanic belt that contain abundant proximal facies associations should be important targets in the exploration for massive sulphides. The presence of graded mass flow deposits indicates that Thalanga was a depocentre between episodes of constructional volcanism and importantly, the period of quiescence prior to and after QEV deposition at Thalanga is approximately coeval with massive sulphide formation.

The poor sorting and normal grading of the fiamme- and pumice-bearing breccia units are consistent with transport into the Thalanga area by particle-rich, sediment gravity currents, or mass-flows (cf. Cas, 1983), and therefore these units are inferred to represent relatively distal volcanic facies (Table 4.6). Conversely, most of the proximal volcaniclastic facies associations at Thalanga (Table 4.6) are inferred to have been generated by quench-fragmentation and gravitational collapse of coherent lavas or domes. The lithofacies characteristics of the dacite-pumice breccia, QEV and pumice-bearing rhyolite breccia units at Thalanga suggest that these units are syn-eruptive volcaniclastic deposits (e.g. McPhie and Allen, 1992), whereas the siltstone and graded sandstone units at Thalanga are inferred to have been derived from older volcanic units.

Table 4.6 Proximal versus relatively distal volcanic facies at Thalanga

	Proximal facies	Distal Facies
Hangingwall (unit iv)	Andesite, Dacite lavas, Dacite hyaloclastite, Dacite-lithic breccia (resedimented dacite hyaloclastite) HWF: graded rhyolite breccia, dacite intrusive hyaloclastite, fiamme-bearing breccia	Quartz-feldspar crystal-rich sandstone, Pumice in dacite-pumice breccia, HWF: siltstone, graded sandstone
Ore horizon (unit ii & iii)	Upper rhyolite breccia (resedimented rhyolite hyaloclastite), QFP sills and mega-clasts, Components of the QEV	Crystals in QEV? Siltstone and graded sandstone
Footwall (unit i)	Rhyolite domes, cryptodomes, and sills, Rhyolite hyaloclastite, autobreccia and resedimented hyaloclastite, Pumice-bearing rhyolite breccia?	Feldspar- and quartz-bearing sandstone

4.9.3 Importance of the QEV and QFP

Significance of Large Quartz Crystals

The fluidal peperite at the contact between the QFP and siltstone (section 4.3.5) suggests that the QFP was less viscous than expected given its high crystal content and siliceous composition. The viscosity could have decreased due to high confining pressure, high magma temperature, or elevated volatile contents (McBirney and Murase, 1970; Cas, 1978). The large size of the quartz crystals in the QFP at Thalanga may reflect elevated volatile (especially

water) contents in the QFP magma because in general, crystallisation of water-rich magmas produces large euhedral crystals (Carmichael *et al.*, 1974; Ehlers and Blatt, 1982).

The highly resorbed nature of the quartz phenocrysts in the QFP is indicative of disequilibrium conditions in the magma chamber or during eruption. McBirney (1980) suggested that disequilibrium between crystals and the melt could be evidence of fractionation within the upper part of the magma chamber. Other mechanisms that will move a melt into disequilibrium with its crystal components are changes in volatile content, pressure reduction as the magma ascends or as volatiles are episodically released, or by mixing with a new batch of magma (change in chemistry and/or temperature).

Implications of QFP Peperite

The shape of igneous clasts in peperite may be partly influenced by the porosity and permeability of the host sediments. Where magma intrudes wet, fine-grained and well sorted sediments, a steam carapace may be maintained and insulate the magma, producing fluidal-shaped igneous clasts (Busby-Spera and White, 1987). The siltstone enveloping the QFP at East Thalanga is well sorted and is interpreted to have favoured the production of fluidal peperite. Acting in opposition to this is the felsic composition and abundant coarse quartz and feldspar phenocrysts in the QFP, which suggest that the QFP would have been highly viscous. Such high viscosity would probably affect the texture and extent of peperite development, with blocky peperite more likely to have formed.

Textural evidence suggests that the irregular QFP clasts in siltstone at the margin of QFP sills in East Thalanga are deformed fluidal peperite, which is unusual for siliceous intrusions (cf. Hanson and Wilson, 1991, 1993). However, viscosity of felsic magma is reduced under high confining pressure, high magma temperature, or by retention of volatile components (Kushiro, 1976, 1978, 1980; Kushiro *et al.*, 1976; McBirney and Murase, 1970; Cas, 1978; Williams and McBirney, 1979). The intrusion of a felsic sill into sediments under deep water or into a thick sedimentary pile, and therefore under high hydrostatic or lithostatic pressure, may have decreased the viscosity of the intrusion (Hanson and Wilson, 1991; Kano *et al.*, 1991). Thus, fluidal peperite, rather than blocky peperite, may preferentially form at the contact between felsic magma (e.g. the QFP) and wet, fine-grained sediments in deep water.

Peperitic QFP margins indicate that siltstone overlying the footwall rhyolitic volcanics was unconsolidated at the time of QFP intrusion. These siltstone units are <5 m in total thickness, yet completely envelope the QFP sills (Fig. 4.3b). Most studies of peperite formation concentrate on the mechanisms of peperite formation (e.g, Kokelaar, 1982, 1986), or on the effect of variation in physical properties of the magma or host sediment on peperite textures (e.g. Busby-Spera and White, 1987). Few workers have discussed the minimum thickness of

sediment required for peperite rather than hyaloclastite formation. However, in some case blocky peperite is equivalent to intrusive hyaloclastite because the magma is broken up by quench-fragmentation processes (e.g. Kokelaar, 1982; Busby-Spera and White, 1987; Hanson, 1991; McPhie, 1993).

Minimum Sediment Thickness and Peperite Formation

The depth of sediment affects the degree of compaction, and therefore permeability of the host sediment. Deeply buried sediments are more likely to have reduced permeability and thus hinder fluidisation and peperite formation (Bryant *et al.*, 1981; Einsele, 1986). The combined effect of hydrostatic and lithostatic pressure in subaqueous environments will partly control the level at which a rising magma will spread laterally and form sills (Einsele, 1986), and also control the point at which sediment fluidisation and peperite formation can occur. Therefore, in deep water, magmas may be intruded to shallow depths below the sediment-water interface (e.g. Einsele, 1986; McPhie, 1993).

In shallower water, and/or with thin overlying sediments, the sediment-seawater interface may be breached, resulting in resedimented peperite or hyaloclastite formation (Table 4.7; White and Busby-Spera, 1987; Hanson and Wilson, 1993). At the Highway-Reward massive pyrite deposit east of Thalanga, mass-flow emplaced breccia units contain both resedimented hyaloclastite and peperite clasts. These are interpreted to have formed as syn-volcanic sills intruded into thin (<10 m) wet sediments, and inflation of the sill and emergence at the seafloor caused slumping of the peperitic sill-margin. Hyaloclastite formed as the magma encountered cold seawater and was resedimented with the peperitic clasts (Doyle and McPhie, 1994).

There is evidence that in some subaqueous settings, intrusions in <30 m of sediments may breach the seafloor and either erupt explosively or fragment by quenching (Table 4.7). However, breaching may also depend on local geometry, magma supply rate, and magma composition and viscosity. Therefore, in order to prevent the breaching of the 2-5 m thick silt cover at East Thalanga, the QEV is interpreted to have been deposited prior to the intrusion of QFP sills. Alternatively, the water depth may have been great enough to provide a high hydrostatic pressure and thus prevent breaching of the sediment-seawater interface.

Where QFP is conformably overlain by only thin, QEV sandstone (e.g. Fig. 4.16b), the QFP is inferred to have broken through the overlying QEV breccia. Quench-fragmented clasts of QFP likely to have produced by the partial extrusion of the QFP may have been redeposited, by gravitational collapse, in areas adjacent to the QFP cryptodome.

Table 4.7 Comparisons between water depth, sediment thickness and sills with peperitic margins vs emergent peperite or hyaloclastite.

Sill composition and location	Sediment type	Thickness of overlying sediment	Water depth	Volcanic products	Reference
Basalt; 1989 seafloor eruption, Japan	unconsolidated felsic tuff	30 m	100 m	inflation of sedimentary cover, followed by phreatomagmatic eruption of magma and host sediment	Yamamoto *et al.* (1991)
Basalt, Guaymas Basin, Gulf of California	mud turbidites	≤30 m (above youngest sill)	2000 - 3000 m	hyaloclastite or emergent peperite not reported	Fig. 2 in Einsele *et al.* (1982)
Quartz-feldspar phyric porphyry; Rio Tinto, Spain	mudstone, turbidites	<20 m	?	• peperitic margins of sills and abundant resedimented hyaloclastite breccia	Boulter (1993)
		50-75 m	?	• peperitic margins of sill, no breaching of sediment-water interface	
Rhyolite, southern Chile	volcaniclastic turbidites, mudstone, chert	-	below storm wave base	peperite around sill, with local resedimented peperite where rhyolite breached sediment-water interface	Hanson and Wilson (1993)

4.9 Summary

1. The thick sequence of rhyolitic volcanics in the footwall at Thalanga is inferred to record construction of rhyolite domes and cryptodomes, and possibly emplacement syn-volcanic sills. Quench-fragmentation controlled the formation of most of the volcaniclastic facies within the footwall. Rare non-welded, rhyolite pumice clasts within some rhyolite breccia units may have been formed by quench fragmentation of a variably pumiceous rhyolite lava or dome.

2. The unit previously described as quartz 'eye' tuff comprises (i) coherent quartz-feldspar porphyry sills and cryptodomes (QFP); (ii) polymict, quartz and feldspar crystal-rich breccia (QEV breccia); and graded quartz and feldspar crystal-rich sandstone (QEV sandstone). Grades sandy siltstone and siltstone beds are locally present within the ore horizon. The QEV is interpreted to be a syn-eruptive volcaniclastic deposit that was rapidly transported by mass flows and deposited within the Thalanga basin before intrusion of peperitic QFP sills. Rare massive sulphide clasts in the QEV indicate that either the Thalanga massive sulphide deposit, or another massive sulphide deposit in the Trooper Creek Formation, was exposed on the seafloor at the time of QEV transportation.

3. The abundant quartz and feldspar crystals and angular crystal fragments in the QEV may have formed by the explosive eruption of a coarsely porphyritic magma, implying water depths of ≤1 km (McBirney, 1963) at the source vent. Transport to sites of deposition was by mass flows. However, the preferred interpretation is that the crystal and clast components of the QEV units were generated during intense quench fragmentation, gravitational collapse, and mass wasting of a QFP dome or number of domes. This could have occurred at any water depth. Graded units of quartz and feldspar crystal-rich sandstone which conformably overlie the QEV in most parts of West and East Thalanga are interpreted to have been deposited from successive, gradually fining mass flows.

4. Dacite domes or lavas have *in situ* hyaloclastite breccia at their stratigraphic tops that in places grade into resedimented hyaloclastite and dacite-lithic breccia. The concentration of dacite domes or lavas in the hangingwall at Thalanga, rather than along the adjacent Thalanga Range, together with the abundance of proximal volcanic facies associations, is interpreted to indicate that the Thalanga massive sulphide deposit occurs close to a volcanic centre.

5. Graded siltstone and sandstone units within and overlying the ore horizon are interpreted to have been deposited during periods of quiescence between episodes of intrabasinal constructional volcanism. Deposition of the siltstone immediately overlying the footwall rhyolitic volcanics in parts of Thalanga may be coeval with massive sulphide formation. The absence of reworking in these siltstone and sandstone units and the fine grained tops of the QEV units indicate that the Thalanga deposit formed in water depths at least below storm-wave base.

6. The location of a proximal volcanic centre at Thalanga implies positive relief, whereas negative relief is required for the deposition of mass flow deposits (e.g. the QEV). It is suggested that small basins were present at the top of the volcanic pile prior to deposition of the mass flows and that these basins were formed either between adjacent domes or flows, or by syn-volcanic faulting.

CHAPTER 5.

GEOCHEMISTRY OF THE VOLCANIC UNITS

5.1 Introduction

5.1.1 Volcanic Geochemistry

Whole-rock geochemistry provides information about the magmatic affinities of a volcanic suite and can be used to interpret source rock compositions and the tectonic setting in which the volcanic rocks were generated (e.g. Pearce and Cann, 1971, 1973; Winchester and Floyd, 1977; Crawford *et al.*, 1992). Bivariant, total alkalis versus silica diagrams are commonly used to classify volcanic rocks (Rollinson, 1993). A K_2O - SiO_2 variation diagram shows that the least altered rocks from the Mount Windsor volcanic belt have a continuous range from basaltic to rhyolitic in composition (Stolz, 1989; Berry *et al.*, 1992). However, these rocks have a wide range in K_2O concentrations that are most likely due to the effects of post-eruptive alteration and metamorphism (Stolz , 1989; Berry *et al.*, 1992).

Most major elements are mobile during alteration or metamorphism, consequently immobile elements such as Ti, Zr, Al, Nb, Y and other high field-strength elements (HFSE) are commonly used to distinguish magmatic groups in altered and metamorphosed rocks (Cann, 1970; Pearce and Cann, 1973; Winchester and Floyd, 1977; MacLean and Kranidiotis 1987; Barrett and MacLean, 1991; MacLean and Barrett, 1993). Herrmann (1994) showed that the overlap of SiO_2, MgO, Na_2O, and K_2O concentrations between the dacites and rhyolites at Thalanga is due to the mobility of Si, Mg, Na, and K during hydrothermal alteration or metamorphism, and that Ti, Al and Zr were immobile. Locally, Y and Nb were also immobile. This section aims to characterise the volcanic units according to their immobile element ratios and to use this to determine magmatic affinities of the volcanic rocks at Thalanga.

Rare Earth Elements (REE) are considered to be immobile during weak hydrothermal alteration and low grade metamorphism, and are commonly interpreted to reflect parent compositions, and therefore tectonic settings (Humphries, 1984; Rollinson, 1993). Typical calc-alkaline lavas from island arc settings are relatively enriched in light rare earth elements (LREE) compared to heavy rare earth elements (HREE) in chondrite-normalised diagrams (Ewart, 1979). However, REE, particularly the LREE, are demonstrably mobile during strong hydrothermal alteration associated with massive sulphide deposition, high grade metamorphism, and weathering (e.g., Baker and De Groot, 1983; Campbell *et al.*, 1984; MacLean, 1988; Whitford *et al.*, 1988; Schade *et al.*, 1989; Scheepers and Rozendaal, 1993;

Daux *et al.*, 1994; Poitrasson *et al.*, 1995). Therefore, the REE of a selection of the least altered coherent volcanic rocks at Thalanga were determined in order to geochemically fingerprint the host volcanic units, and to resolve any magmatic relationships.

5.1.2 Samples and Analytical Methods

Whole-rock analyses of representative samples of the volcanic host rocks from Thalanga and the Thalanga Range were determined by ALS in Brisbane, Queensland. A selection was also analysed by XRF at the University of Tasmania for comparison. The complete data set, together with a comparison between laboratories and description of techniques is presented in Appendix F.

The samples consisted of half-core specimens 0.3-1.0 m in length and a few hand specimens from the Thalanga deposit and the Thalanga Range. Most rhyolite samples are quartz-muscovite ± phlogopite ± chlorite-pyrite-rich and the pre-metamorphic hydrothermal alteration assemblage is interpreted to have been variable quartz-sericite ± chlorite ±pyrite (Chapter 10). The least altered rhyolites are inferred to be the quartz-feldspar-phyric rhyolites faulted into a hangingwall position in Central Thalanga. The quartz-feldspar porphyry (QFP) samples can be divided into least altered, silicified QFP with dark blue-grey groundmass, and more altered muscovite-rich QFP with variable degrees of feldspar preservation. Dacite is less altered and several samples contain traces of epidote.

Volcaniclastic rocks were included in the whole-rock analyses for comparison and to test whether source material could be determined. Uniform, crystal-rich samples of the quartz 'eye' volcaniclastic unit (QEV) were collected, with few samples containing QFP or rhyolite clasts larger than 2 cm. The hangingwall fragmental (HWF) samples are massive siltstone, sandy siltstone and fiamme-bearing breccia. Andesite feeder dykes in the hangingwall units were sampled and samples of the post-tectonic microdiorite and dolerite dykes were also collected.

5.2 Results

5.2.1 Immobile Elements

The volcanic units of the Mount Windsor subprovince have calc-alkaline affinities (Stolz, 1989; Berry *et al.*, 1992). There is a negative correlation between Ti/Zr and SiO_2 contents of the least altered volcanic rocks in the Mount Windsor sub-province, providing a useful classification scheme, and approximate Ti/Zr boundaries between major rock types are rhyolite < 20, dacite = 20-40, andesite = 40-100, and basalt > 100 (Stolz, 1989; Berry *et al.*,

1992). Stolz (1989) noted that dacite at Thalanga has relatively high silica (>70 %) and plots in the rhyolite field using this classification, with Ti/Zr > 10.

Herrmann (1994) showed that the Ti/Zr values of dacite at Thalanga range from 10 to 21. The dacites with the large data set of Herrmann (1994) can be divided into two distinct geochemical groups, both of which have Ti/ Zr < 20 and fall in the rhyolite field defined by Stolz (1989) and Berry *et al.* (1992). Including the dacites analysed for this study, one group has Ti/Zr ~ 15-19 and the other has Ti/Zr ~ 9-12 (Fig. 5.1a). The geochemical differences between the two dacite groups correspond to differences in phenocryst content, with sparsely feldspar-phyric dacite (dacite 2; see Chapter 4) having Ti/Zr values similar to the QFP (Fig. 5.1a), whereas the feldspar-phyric dacites with 5-10 % phenocrysts (dacite 1; see Chapter 4) have the higher Ti/Zr values. The rhyolites at Thalanga have Ti/Zr <4 (Fig. 5.1a), although using all geochemical data from Thalanga, the rhyolite has Ti/Zr <5 (Herrmann, 1994).

The similarity of Ti/Zr values for dacite 2 and the QFP is apparent in a TiO_2 - Zr diagram (Fig. 5.1b,c), where the least altered dacite, QFP, and rhyolites fall on lines of constant Ti/Zr radiating from the origin, supporting Herrmann's (1994) interpretation of the immobility of these elements. Lines depicting the Ti/Zr values of rhyolite (<5), dacite 2 (~9), and dacite 1 (~15) are also shown on Figure 5.1(c). QEV analyses (Ti/Zr ~ 3-10) plot along the line of QFP and spread towards the rhyolite line (Fig. 5.1b,c). Most HWF samples plot slightly under the line of rhyolites, with one sample along the line of QFP and dacite 2 (Fig. 5.1b,c).

The andesite samples analysed in this study fall in the basalt field in the Ti/Zr - SiO_2 classification diagram (Fig. 5.1a). The location of andesite analyses on the TiO_2 - Zr diagram (Fig. 5.1b) is comparable with the low-Ti andesites identified by Stolz (1989) in the lower part of the Trooper Creek Formation at Thalanga and Waterloo.

Despite using the least altered rocks, the spread of data on diagrams with Nb and Y shows that these elements are somewhat mobile at Thalanga (Fig. 5.2a,b), a point made by Herrmann (1994). The scatter of points on the Y - Zr diagram used by MacLean and Barrett (1993) demonstrates that it is not particularly useful for classifying the volcanic units at Thalanga (Fig. 5.2a), with rhyolite and the muscovite-rich QFP having variable Y content. However, it is important to note that Y values measured using ICP (Appendix F) are inaccurate at low values. The distinction between the volcanic units at Thalanga is better illustrated on a Nb - Zr diagram, where rhyolite, QFP and dacite plot along separate lines, with the QFP falling between dacite and rhyolite, and partly falling within the cluster of dacite analyses (Fig. 5.2b).

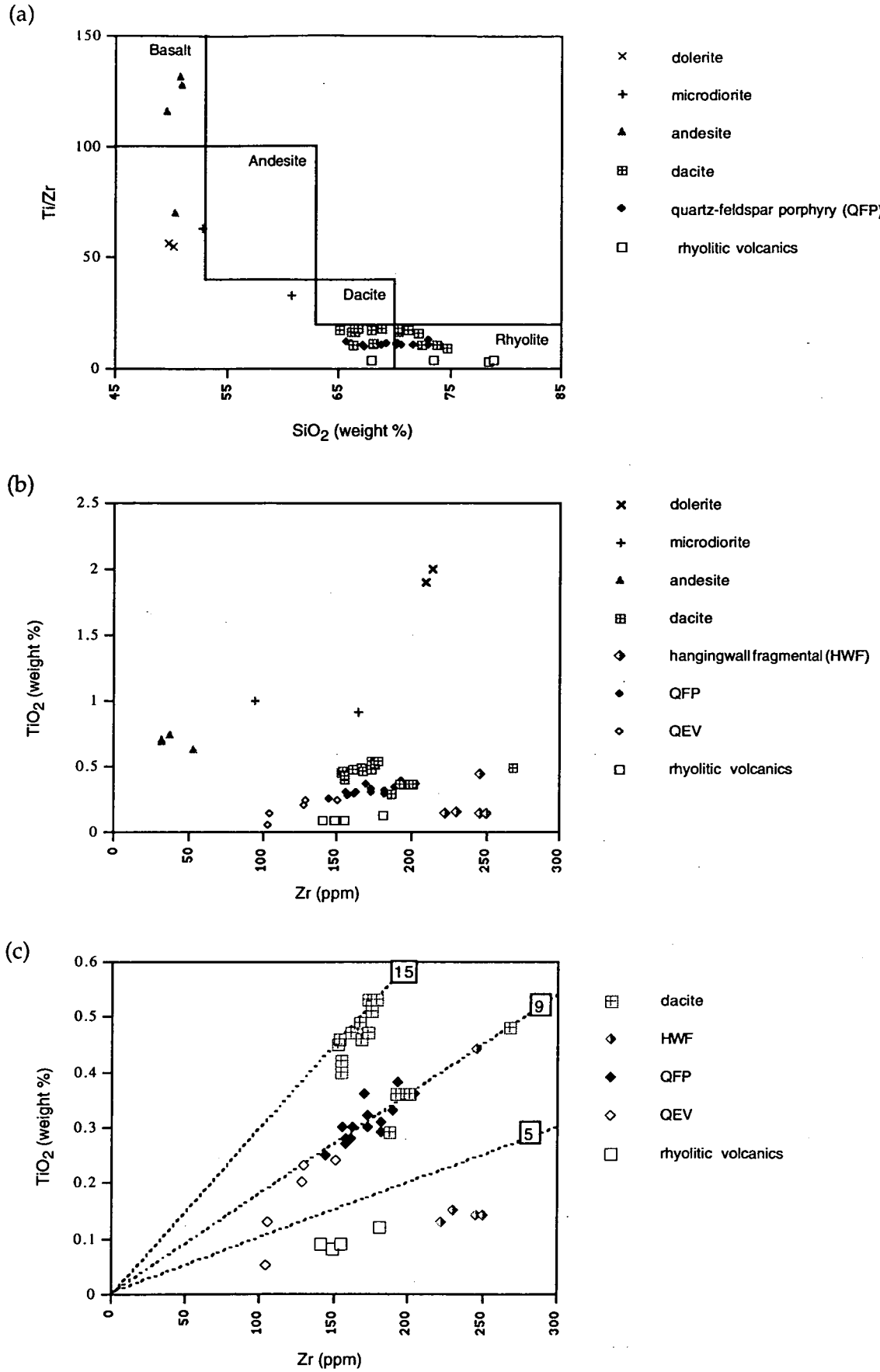

Figure 5.1 Plots of selected volcanic rocks that host the Thalanga massive sulphide deposit. (a) Plot of Ti/Zr against SiO_2 of the least altered volcanic units, showing the lithological divisions of the Mount Windsor subprovince of Stolz (1989) and Berry *et al.* (1992). (b) Plot of TiO_2 against Zr for the main rock types at Thalanga. (c) Magnification of part of (b) showing only dacite, HWF, QFP, QEV and the rhyolitic volcanics from Thalanga. The dashed lines represent Ti/Zr values.

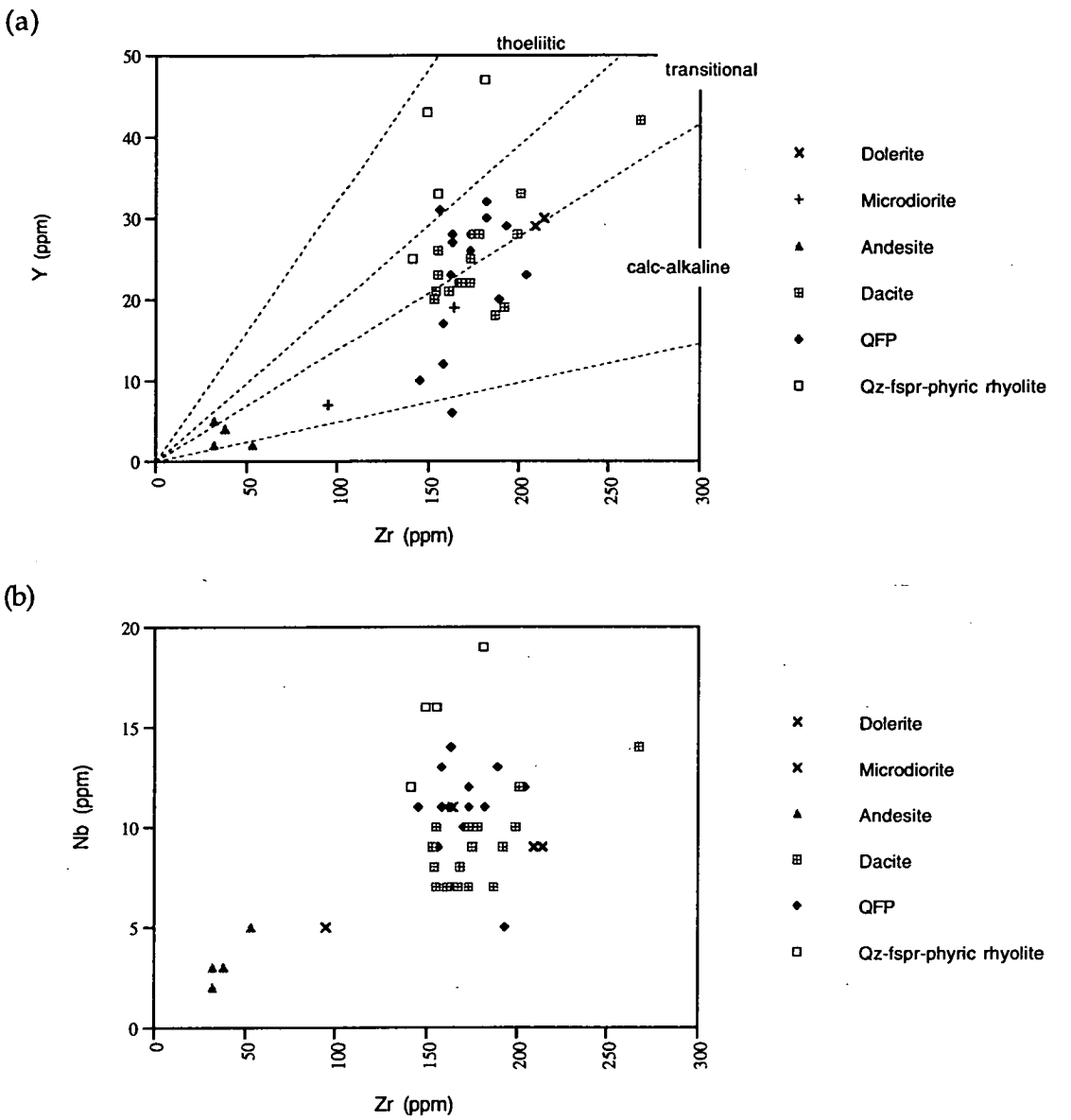

Figure 5.2 Discrimination diagrams showing the variation of Y and Nb against Zr of the least altered volcanic units and intrusions from the Thalanga massive sulphide deposit. (a) Plot of Y versus Zr, calc-alkaline, transitional and thoeliitic divisions are from MacLean and Barrett (1993); (b) Plot of Nb versus Zr.

5.2.2 *Rare Earth Elements*

Using the least altered rocks from the entire Mount Windsor volcanic belt, Stolz (1995) reported that rhyolites and dacites from the Trooper Creek Formation have lower total REE and flatter REE patterns than rhyolites from the Mount Windsor Volcanics. He also noted that rhyolites from the Mount Windsor Volcanics have a significant negative Eu anomaly compared with the rhyolites and dacites from the Trooper Creek Formation. The likelihood of REE mobility due to both hydrothermal alteration and metamorphism at Thalanga means that the least altered samples may not reflect original igneous compositions. However, the samples analysed in this study have similar absolute values, and display similar LREE enrichment as the unaltered samples of Stolz (1995), and are therefore interpreted to represent original igneous values.

Dacite 1 contains significantly less total REE than dacite 2, but both display small negative Eu anomalies (Fig. 5.3). Despite plotting within the envelope of REE of felsic volcanic units from the Trooper Creek Formation defined by Stolz (1995), it is likely the flat REE pattern of dacite 1 reflects alteration (and LREE mobility) as well as magmatic differences to dacite 2. Both dacites are weakly altered (chlorite pseudomorphs of biotite) and therefore could have variable shifts in REE contents. Dacite 2 has similar total REE and chondrite-normalised REE pattern to both the QFP samples, although it has slightly less relative LREE enrichment. One QFP sample exhibits a small negative Eu anomaly. The total REE of the least altered rhyolite at Thalanga is higher than both the dacite and QFP samples, and it has a more pronounced negative Eu anomaly (Fig. 5.3).

5.3 Interpretation

Trace elements were used to investigate whether the change from rhyolitic to dacitic then andesitic volcanism with time, which is opposite to normal fractionation trends, is related to changes in composition of the underlying magma chamber. The trace element composition of the QFP and QEV may also indicate if these intervening units relate to magmatic evolution.

The separation of the main volcanic units at Thalanga along different lines that converge towards the origin on immobile element diagrams (Fig. 5.1b,c; and to some extent on Fig. 5.2b), suggests that the volcanic units had different parent magmas. The distinctive low Ti/Zr values (<5), and the larger negative Eu anomaly of the rhyolite from the Mount Windsor Volcanics compared with the QFP and dacite from the Trooper Creek Formation is also consistent with separate parent magmas. Herrmann (1994) also reported a lack of magmatic affinity between the dacite, QFP, and rhyolite at Thalanga, as the rhyolites have higher Y/Zr and Nb/Zr ratios than dacite, but concluded that the rhyolites (Mount Windsor

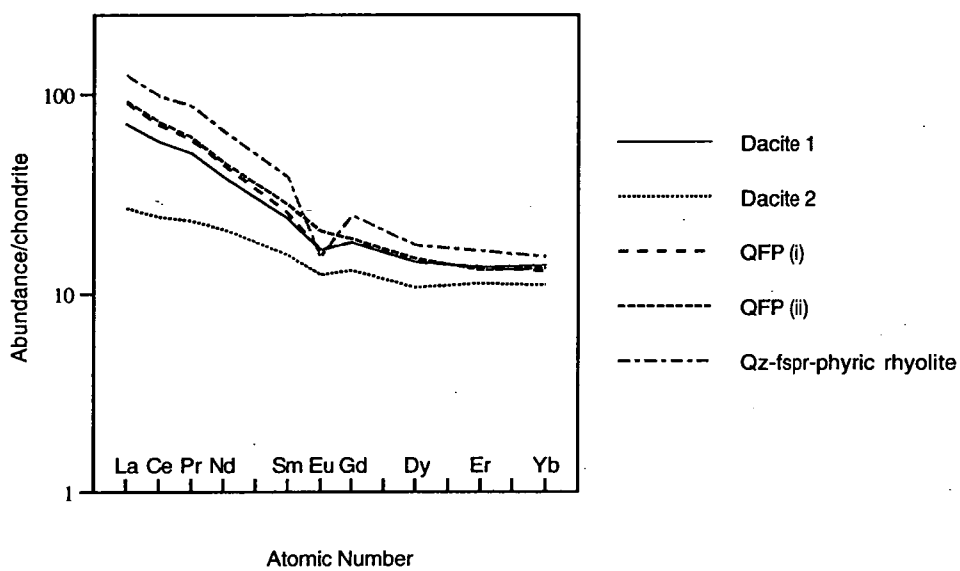

Figure 5.3 Chondrite-normalised rare earth element abundances of least altered felsic volcanic units at Thalanga deposit. Chondrite values used for normalisation are: La = 0.315, Ce = 0.813, Pr = 0.116, Nd = 0.597, Sm = 0.192, Eu = 0.0722, Gd = 0.259, Dy = 0.325, Er = 0.213, Yb = 0.208 (Taylor and Gorton, 1977).

Volcanics) from the Thalanga deposit and the Thalanga Range have a single magma source (Herrmann, 1994).

The differing trace element composition of volcanic units in the Mount Windsor Volcanics compared to volcanic units in the Trooper Creek Formation supports the interpretation of Stolz (1995), that the parent magma of the Mount Windsor Volcanics was different from that of the Trooper Creek Formation. Stolz (1995) used minor and trace elements, and Nd isotopes to propose that the Mount Windsor Volcanics were derived from the partial melting of Precambrian continental crust, whereas the mafic progenitors of the volcanic units in the Trooper Creek Formation were derived from depleted asthenosphere that had been "variably modified by subduction processes". Assimilation or mixing of different batches of magma within a persistent magma chamber may account for the variation in immobile and trace element composition of volcanic units at Thalanga. Following emplacement of the Mount Windsor Volcanics, mafic magma injected into the rhyolite magma chamber may have assimilated or mixed with the rhyolite parent, producing the parent magma of the volcanic units in the Trooper Creek Formation.

The similarity between Ti/Zr values of the QEV and QFP (Fig. 5.1b,c) suggests that many of the QEV components are derived from the QFP. The QEV samples containing abundant rhyolite clasts have Ti/Zr values similar to rhyolite from the Mount Windsor Volcanics, confirming the textural interpretation (Chapter 4) that both the QFP and footwall rhyolitic volcanics are the source of QEV clasts. The Ti/Zr values and location on the TiO_2-Zr diagram (Fig. 5.1b,c) of the HWF samples are consistent with some rhyolitic and dacitic component to the HWF (as indicated in Chapter 4).

Identification of at least two types of dacite (dacite 1 and 2) at Thalanga based on phenocryst abundance (Chapter 4) is supported using immobile element ratios and REE compositions. Both the Ti/Zr and REE patterns of dacite 1 and dacite 2 are different and indicate different parent magmas, possibly formed following mixing or assimilation of a new magma within the magma chamber. The similarity in immobile element ratios of the QFP and dacite 2 at Thalanga suggests that they may have similar origins. For example, the overlap of dacite 2 and all QFP samples on a TiO_2 versus Zr diagram (Fig. 5.1b,c) is consistent with a common parent magma. The similar total REE and parallel patterns of the QFP and dacite 2 are also interpreted to indicate a similar magmatic source, and would therefore place the QFP within the Trooper Creek Formation rather than the Mount Windsor Volcanics.

5.4 Summary

1. REE patterns and immobile element compositions of the least altered rhyolite (Mount Windsor Volcanics) at Thalanga are different from those of the dacite in the overlying Trooper Creek Formation, and are interpreted to indicate their derivation from different parent magmas that may have formed as a result of mixing or assimilation of the rhyolite parent and batches of mafic magma. The REE data and Ti/Zr values of the dacites shows that there is at least two types of dacite in the Trooper Creek Formation at Thalanga. These geochemical differences correspond to dacites with differing feldspar phenocryst abundances, and may reflect further injection and mixing of magma in the magma chamber.

2. Both Ti/Zr values and REE patterns of the QFP and sparsely feldspar-phyric dacite are similar and suggest that these units are derived from the same parent magma. On the basis of this geochemical similarity, the QFP is classified as part of the Trooper Creek Formation.

CHAPTER 6.

ORE DEPOSIT GEOLOGY

6.1 Introduction

Detailed textural and facies analyses have shown that the stratiform massive sulphides at the Thalanga deposit are confined to a single horizon at the stratigraphic top of the Mount Windsor Volcanics, and that the massive sulphide lenses are overlain by siltstone and breccia units (HWF), and coherent dacite of the Trooper Creek Formation (Chapter 4). The massive sulphide lenses at Thalanga have an intimate spatial association with the QFP and QEV units, and therefore these volcanic units are included as part of the mineralised horizon. The location of intense hydrothermal alteration (with similar deformation and metamorphic overprints to the mineralised horizon) in the rhyolitic volcanics underlying the deposit, together with the lack of significant alteration in the overlying dacite (Chapter 10), supports the interpretation that the sulphides at Thalanga are syn-volcanic. Wills (1985) and Gregory *et al.* (1990) both considered the Thalanga deposit to be syn-volcanic, and to have formed on the seafloor.

Evidence for the relative timing of volcanism at Thalanga suggests that sulphide mineralisation was interrupted by deposition of the quartz 'eye' volcaniclastic units (QEV) in East Thalanga (Chapter 4). Detailed examination of the textural and stratigraphic relationships between the massive sulphides and the QEV may reveal whether sulphide formation was by sub-seafloor replacement of the volcanic units, or via exhalation on to the seafloor. The geology and contact relationships of each ore lens is therefore documented in this chapter, with the aim of defining the timing and style of mineralisation at Thalanga.

Recent studies of Rosebery have generated controversy over the timing of sulphide mineralisation with respect to volcanism and deformation, and consequently the mechanisms of sulphide deposition (cf. Aerden, 1991, 1993, 1994a,b; Allen and Cas, 1990; Allen, 1994; Brathwaite, 1974; Green *et al.*, 1981). Green *et al.* (1981) proposed that Rosebery was formed on the seafloor via deposition of sulphides from reversely buoyant plumes of hydrothermal fluids, with overprinting deformation and greenschist facies metamorphism responsible for folding the ore lens and locally recrystallising the sulphides. Aerden (1991, 1994b) argued that both mesoscopic and microscopic textures of the Rosebery massive sulphide lenses suggest that the sulphides replaced the host volcanic units along cleavage planes and sites of dilation during regional deformation and greenschist facies metamorphism. Allen (1994) argued that detailed analysis of the relationships between the sulphides, host volcanic units

and local faults supports a syn-volcanic, sub-seafloor replacement mechanism of sulphide deposition. Each of these models are examined in the context of Thalanga, and therefore it is critical to understand the relationship between the sulphide lenses and the host volcanic units. Because the metamorphic grade at Thalanga is higher than that at Rosebery (upper greenschist facies at Thalanga, compared to greenschist facies at Rosebery; Green *et al.*, 1981), distinguishing between primary sulphide textures and contact relationships, and metamorphic sulphide textures and structural contacts is important in determining the genesis of the Thalanga Zn-Pb-Cu deposit. Sulphide textures are examined in Chapter 7.

6.2 Composition and Geometry of the Massive Sulphide Lenses

Massive sulphide mineralisation is restricted to the same stratigraphic interval at West, Central and East Thalanga, and in the Vomacka Zone. This 'favourable' horizon (terminology from Herrmann, 1994) is continuous (although structurally offset) between the ore lenses, but is only mineralised intermittently along its strike length. Pyrite, sphalerite, galena and chalcopyrite are the main sulphide minerals, and tetrahedrite-tennantite, magnetite and arsenopyrite are minor components (Table 6.1). Ore lenses composed mostly of sphalerite-galena-pyrite-chalcopyrite (>50 % sulphides) are hereafter referred to as massive sulphides. The main gangue minerals in the massive sulphide lenses are quartz, barite, chlorite, calcite, dolomite, tremolite and muscovite. The mineralogy and textures of the ore lenses are discussed in detail in Chapter 7.

Table 6.1 Minerals in the hypogene ore at Thalanga (data from Wills, 1985; Gregory *et al.*, 1990; Huston, 1989, 1991; and this study).

Major	Minor	Trace	Supergene	Gangue
Pyrite, sphalerite, galena, chalcopyrite	Tetrahedrite-tennantite, magnetite, arsenopyrite	Argentite, cubanite, bismuth, bornite, boulangerite, electrum, freibergite, native silver, stibnite, pyrrhotite	Chalcocite, covellite, digenite, marcasite	Actinolite, barite, biotite, calcite, celsian, chlorite, dolomite, epidote, hyalophane, muscovite, phlogopite, siderite, sphene, talc, tremolite, quartz

In most parts of Thalanga, pyrite ± chalcopyrite-rich lenses are present at the stratigraphic base of the ore horizon and are overlain by massive to banded sphalerite-galena-pyrite ±

chalcopyrite-rich sulphides. Sulphide banding is defined by centimetre-scale alternating pyrite-rich and sphalerite-rich domains, and is mainly subvertical and subparallel to the dominant cleavage (S_2; Chapter 3), although locally it follows the irregular margins of the sulphides. There is considerable variation in the location and volume of volcanic units, and composition of associated alteration, within the ore horizon (Chapter 4, 10 and 11).

The composition, geometries and distribution of remobilised sulphides at Thalanga are described in Chapter 3, and are briefly summarised here. Remobilised sulphides are typically chalcopyrite-rich, with bands of dark red-brown sphalerite and rare galena, and are interpreted to have originated by remobilisation from the massive sulphide ore lenses at Thalanga. The location of chalcopyrite-rich sulphides along normal faults, in piercement structures at the hangingwall contact, in tension gashes at the footwall contact, in boudin necks, and in pressure shadows is evidence that sulphides were remobilised and concentrated in sites of extension during D_2 (Chapter 3). However, multiple episodes of sulphide remobilisation are interpreted to have occurred. Chalcopyrite- and sphalerite-rich sulphide veins and piercement structures parallel to and cross-cutting S_3 are interpreted to indicate that sulphide remobilisation also occurred during the final stages of D_3, and coarse grained chalcopyrite-rich sulphides that envelope microdiorite dykes in the mineralised horizon at Thalanga indicate that microdiorite intrusion may have induced local remobilisation of sulphides prior to D_3.

6.2.1 West Thalanga

Geometry

The cross section along 20 250 mE represents a typical section through the West Thalanga ore lens (Fig. 6.1). In West Thalanga, single to multiple lenses (<5 m in thickness) and irregular patches of polymetallic massive sulphides are hosted within a carbonate-chlorite-tremolite-rich (CTC) assemblage (Fig. 6.2a,b). A single lens of massive pyrite is typically present at the stratigraphic base, and down-dip parts of the ore horizon (Fig. 6.1, maps M6,M7, and M9), and is more common at the eastern parts of West Thalanga. A pyritic chlorite schist stratigraphically overlies the footwall rhyolitic volcanics where massive pyrite is not present (Fig. 6.3a-d). The ore lenses and CTC assemblages are stratigraphically overlain by the QEV, which is locally present as lenses within the massive sulphides.

The up-dip and western parts of the West Thalanga lens contain abundant chlorite-rich CTC assemblages. The thickness of the massive sulphide lenses decreases, but the amount of barite gangue within the ore lenses increases towards the up-dip and western parts of West Thalanga. Barite gangue is also more common at the stratigraphic top of the massive sulphide lenses. The ore lenses in the up-dip and western parts of West Thalanga are locally

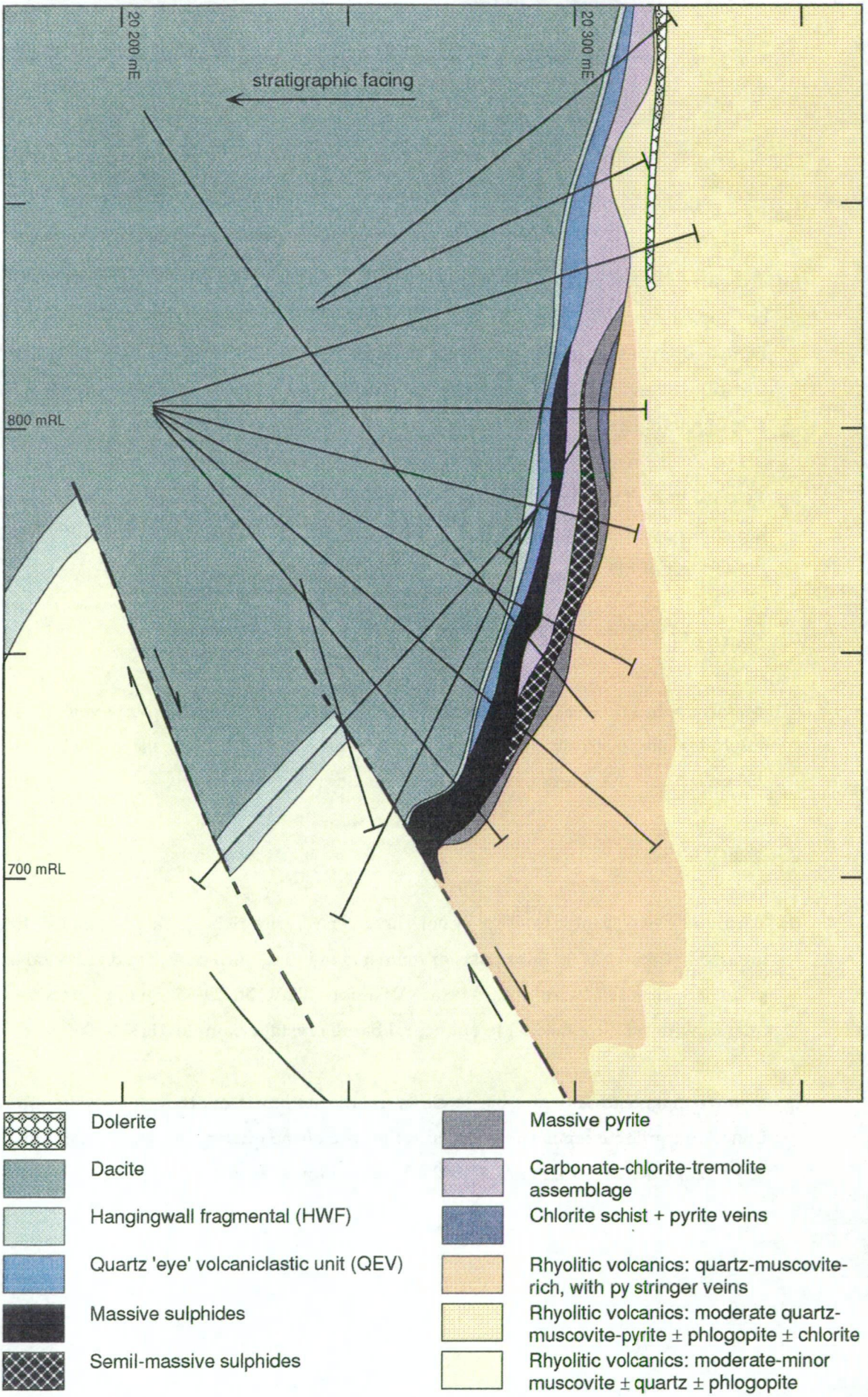

Figure 6.1 Cross section through West Thalanga along the 20 250 mE (mine grid) section.

Figure 6.2 Mesoscopic textures of the ore lens in West Thalanga.

(a) Irregular patches of coarsely recrystallised sphalerite- (dark red-brown) and chalcopyrite-rich sulphides hosted in a carbonate-chlorite-tremolite assemblage. Diffuse domains of honey sphalerite (whihch have overprinted the carbonate-chlorite-tremolite alteration) have a gradational contact with massive sulphides on the right side of photograph. West 780 Stope, view looking west, 20 297 mN, 20 225 mE.

(b) Possible vein of banded sulphides in chlorite ± tremolite assemblage. The sulphide vein has chalcopyrite-rich margins and a sphalerite-rich core, and separates into two veins at the top-left of the face. West 722 Stope (Right). Facing towards right.

(c) Sketch of (b).

(d) Massive sphalerite-rich sulphides cross-cut by numerous irregular pyrite veins. All sulphides have been strongly recrystallised. West 675 Stope (Left), view looking east, 20 280 mN, 20 225 mE. Facing towards right.

(e) Sketch of (d).

(f) Baritic massive sulphides. Top: sphalerite-galena-pyrite-rich sulphide bands in fine grained (<1 mm) barite. Rare clasts or remnants of intergrown quartz and euhedral barite grains are enclosed by sulphides (arrow). Sample W2011ND29-35. Bottom: massive quartz, with minor euhedral to subhedral barite crystals. Sample TH384-106.

(g) Quartz-magnetite and rare barite clasts in chlorite-barite-quartz-chalcopyrite matrix. Euhedral pyrite disseminations occur in the core of the quartz-magnetite clast. West 780W Stope access. 20 319 mN, 20 080 mE. Facing towards left.

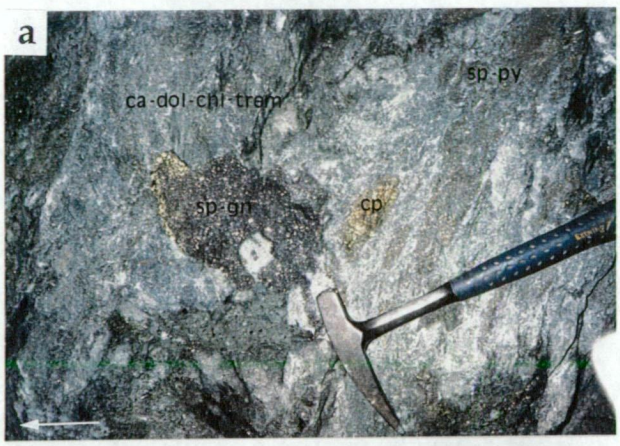
a
ca-dol-chl-trem
sp-py
sp-gn
cp

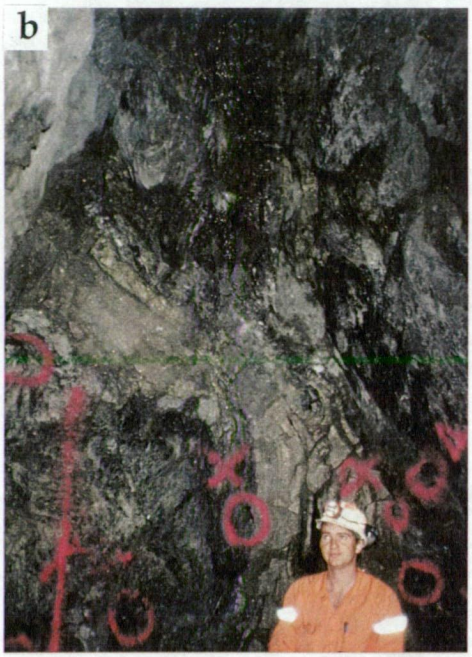
b


d

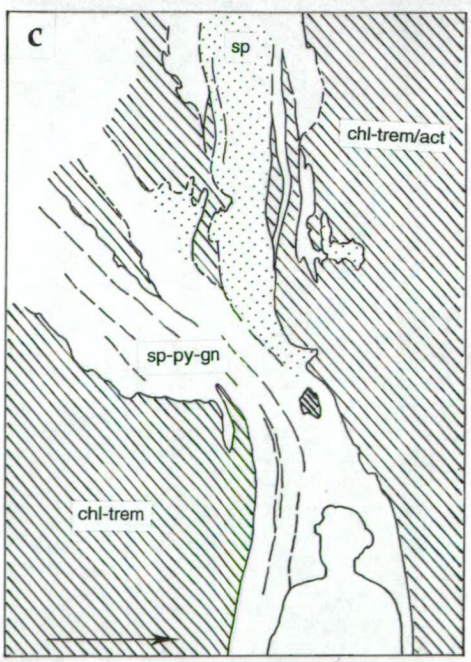
c
sp
chl-trem/act
sp-py-gn
chl-trem

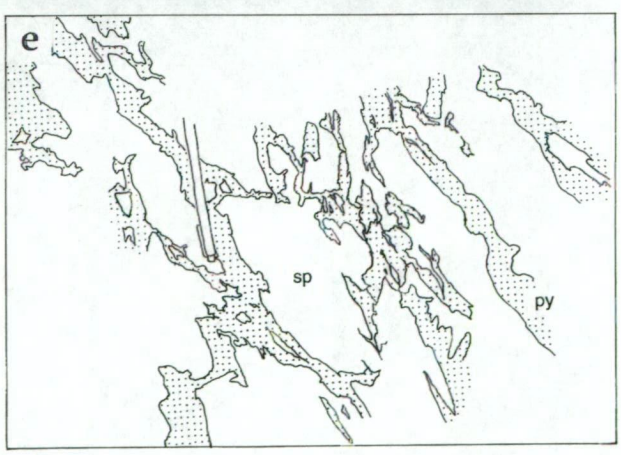
e
sp
py

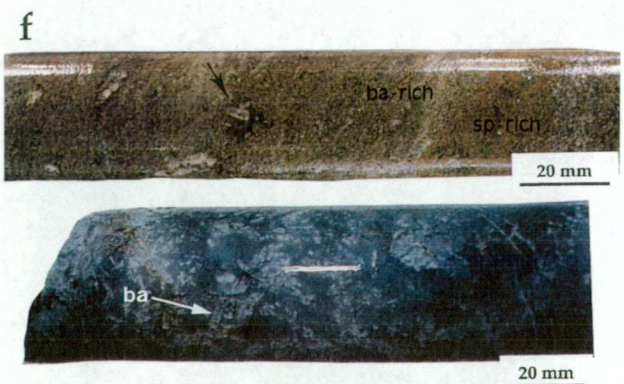
f
ba-rich
sp-rich
20 mm
ba
20 mm

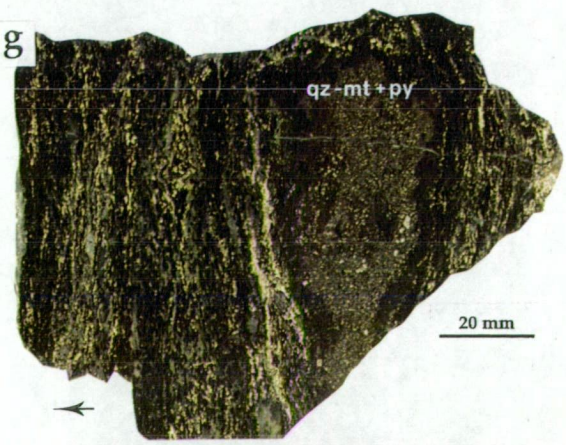
g
qz-mt+py
20 mm

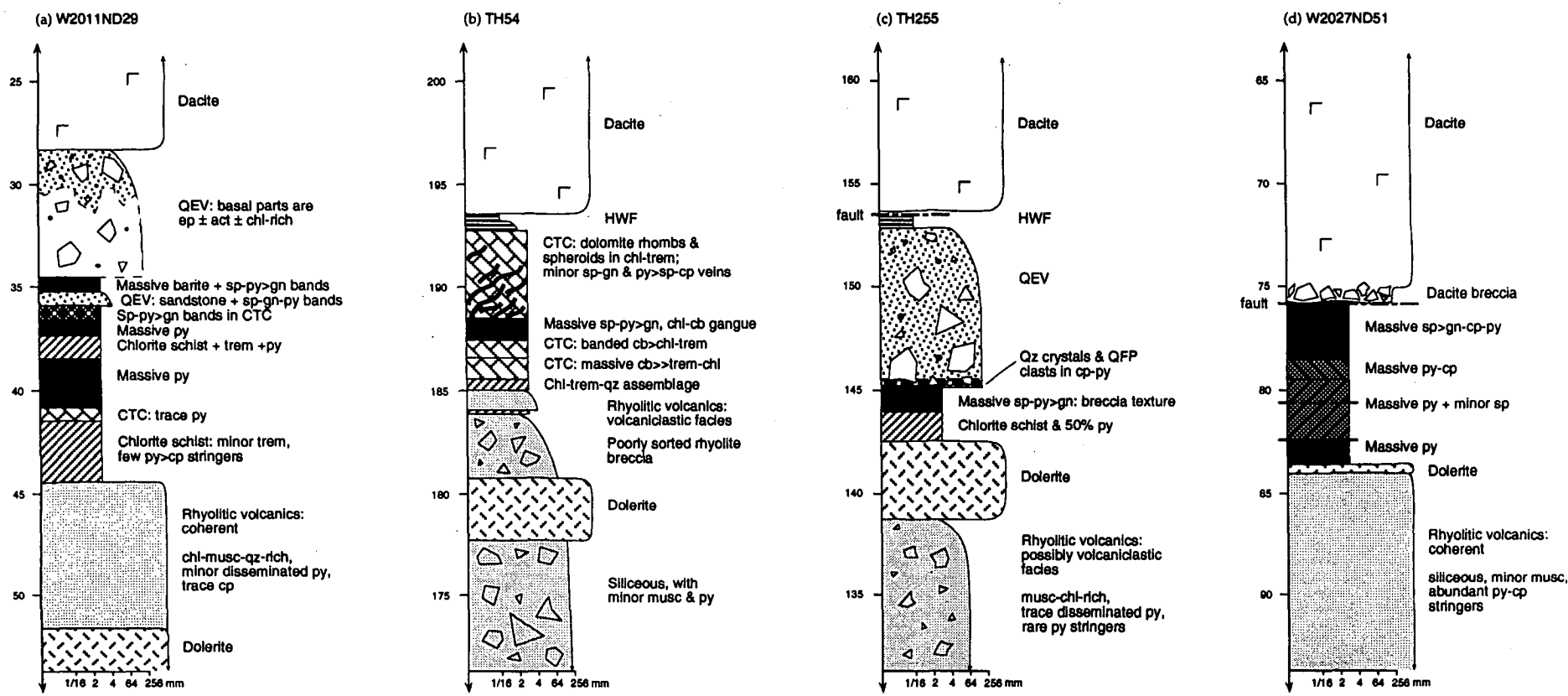

Figure 6.3 Simplified graphic logs of drill holes from West Thalanga; (a) W2011ND29, (b)TH54, (c) TH255 and (d) W2027ND51. The holes are from sections 20 110 mE (W2011ND29 and TH54), 20 230 mE (TH255) and 20 270 mE (W2027ND51). Measurements along vertical scale are distance down the hole (metres). Horizontal scale measures maximum clast size of volcanic units, but not grain size of sulphide or CTC assemblages. Abbreviations: act = actinolite, cb = carbonate, chl = chlorite, cp = chalcopyrite, ep = epidote, gn = galena, musc = muscovite, py = pyrite, qz = quartz, sp = sphalerite, trem = tremolite.

composed of semi-massive sulphides or sphalerite-galena-pyrite ± chalcopyrite veins subparallel to S_2. The ore horizon in West Thalanga is truncated at depth and to the east by a ENE-striking normal fault (Fig. 6.1).

Massive sulphides are not present within the repeated ore position south of the mineralised horizon in West Thalanga (Fig. 6.1). The increased thickness of massive sulphides and the pyrite stringer zone in the underlying rhyolitic volcanics, to reach a maximum thickness adjacent to the normal fault (Fig. 6.1), suggests that this fault may have controlled the ascent and discharge of hydrothermal solutions. However, restoration of the ore horizon to inferred pre-deformation geometry indicates that mineralised parts of the ore horizon were present south of the fault (and are now part of Central Thalanga), and that any structure in this position was not a growth fault (Chapter 3).

Composition of the Ore Horizon at West Thalanga

Polymetallic sulphides: The massive sulphide lenses at West Thalanga are composed of sphalerite-galena-pyrite ± chalcopyrite, with minor tremolite-, chlorite-, or barite-rich gangue. Irregular patches and disseminations of massive to semi-massive sulphides are present within the CTC assemblages at the margins of massive sulphide lenses in West Thalanga (Fig. 6.2a). The separation of a single 5 m wide zone of massive sulphides into two discrete bands of massive sulphides within massive tremolite-chlorite in West Thalanga is consistent with the massive sulphides occurring as veins (Fig. 6.2b,c) and similarly, the many bands of massive sulphides within the CTC assemblages (recognised in drill core; Fig. 6.3b) may also be veins. Locally, irregular to blocky clasts of massive carbonate and massive chlorite are present within the massive sulphides.

Massive pyrite: The massive pyrite lenses contain minor chalcopyrite, and locally minor tremolite and sphalerite (e.g. Fig. 6.3d). The pyritic chlorite schist contains pyrite veins to disseminated pyrite, with minor chalcopyrite and tremolite, and typically underlies or has enveloped massive pyrite lenses (Fig. 6.3a,c). In the easternmost parts of West Thalanga, massive sphalerite-rich sulphides, that locally stratigraphically overlie the footwall rhyolitic volcanics (map M10), are cross-cut by irregular, to subvertical, pyrite veins (Fig. 6.2d,e).

Barite-rich sulphides: In parts of West Thalanga, apparent clasts of intergrown quartz and barite have been enveloped by sulphides (Fig. 6.2f, top). In the ore lens position further west, barite crystals are similarly intergrown with massive quartz (Fig. 6.2f, bottom). Rare, irregular bands of massive barite have overprinted massive pyrite towards the base of the massive sulphides in parts of West Thalanga (e.g. diamond drill hole 2027ND51-81.5 m; Appendix A), and occur at the contact between QEV and underlying pervasively actinolite-

chlorite altered QEV (e.g. diamond drill hole 2031NI26-86 m; Appendix A). Bands of barite within coarse grained chalcopyrite-pyrite adjacent to faults (e.g. diamond drill hole 2031ND24-56.2 m; Appendix A) may have been remobilised during deformation and metamorphism.

Quartz-magnetite: Quartz-magnetite clasts are present in graded quartz-rich sandstone and QEV units that directly overlie the mineralised horizon in West Thalanga. Chalcopyrite veins have locally overprinted the chlorite-barite-rich matrix to the quartz-magnetite clasts (Fig. 6.2f). Elsewhere, a quartz-magnetite breccia has gradational contacts with underlying massive barite, which contains minor sphalerite-pyrite-galena (e.g. drill hole 2011NI35; Appendix A).

Contact Relationships

The massive sulphide lenses vary from having gradational and irregular, to sharp and planar subvertical contacts with the CTC assemblages. The irregular contacts are due to sulphide veins and blebs within the CTC units (e.g. Fig. 6.3b). The contacts between massive sulphides and underlying massive pyrite are typically sharp and subvertical. The massive sulphide lenses have a faulted contact where directly overlain by dacite (Fig. 6.3d).

Adjacent to the major normal fault that defines the eastern margin of West Thalanga, massive pyrite ± sphalerite is interfingered with the altered rhyolitic volcanics (map M9). The geometry of this pyrite-rich region is consistent with feeder veins. Elsewhere, the contact between the mineralised horizon and the underlying rhyolitic volcanics is sharp, planar and subvertical. In contrast, the contact between the massive sulphides and the overlying QEV is sharp, but irregular (maps M7 and M9), with patchy epidote-actinolite-chlorite-rich assemblages present within the QEV (Fig. 6.3a). The petrology and origin of these metamorphosed alteration assemblages in the QEV is discussed in Chapter 10.

6.2.2 Central Thalanga

Geometry of Central Thalanga

The geology of the 20 430 mE section is typical of the western parts of Central Thalanga, with down-dip termination and repetition of the ore horizon controlled by ENE-striking normal faults (Fig. 6.4). The lateral limits of Central Thalanga are also defined by ENE-trending normal faults (map M2). In addition to the major normal offsets of the mineralised horizon, repetition along normal faults within the mineralised horizon is interpreted to have caused the irregular thickening of the massive sulphides (Chapter 3).

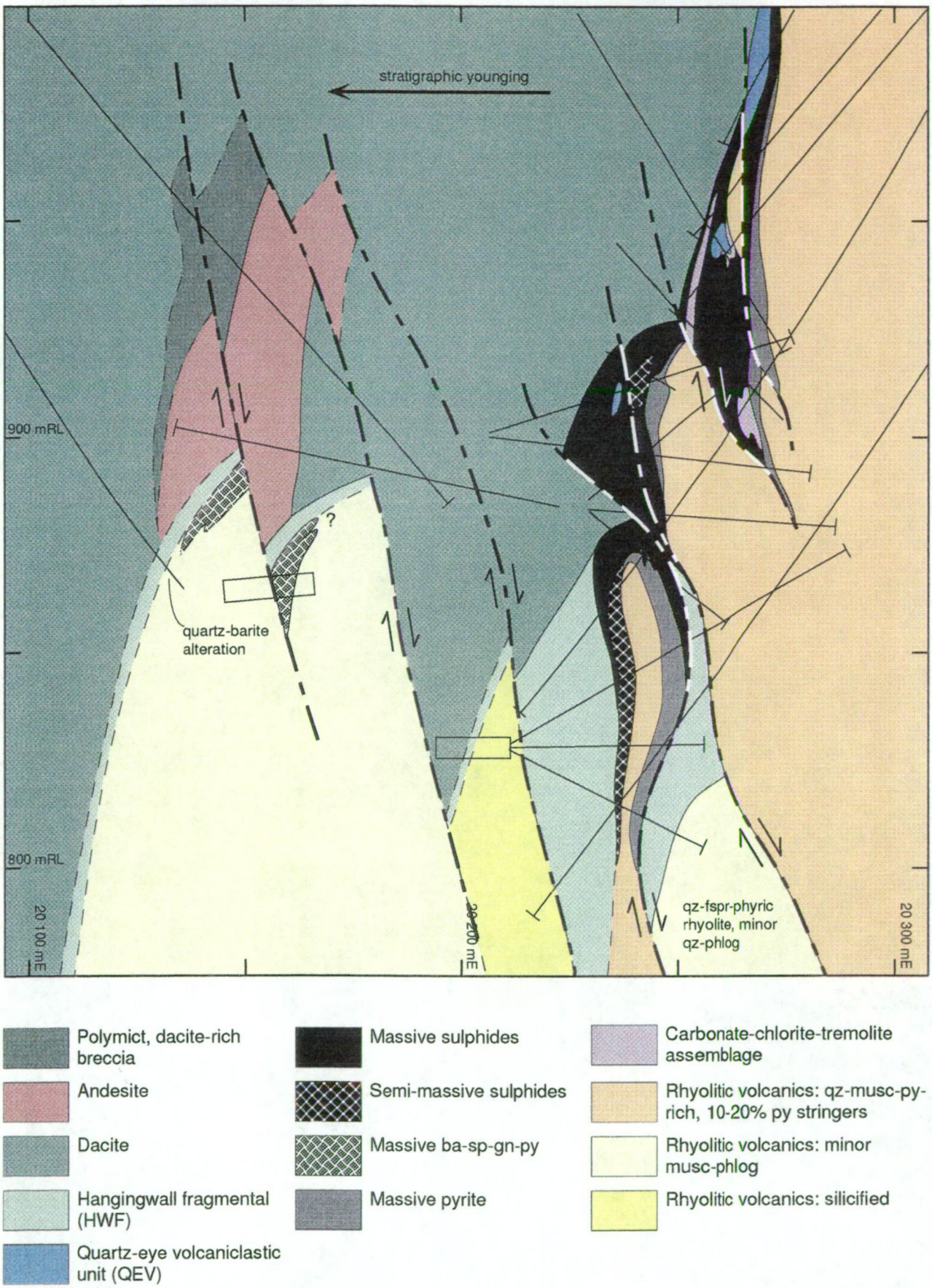

Figure 6.4 Cross section through Central Thalanga along the 20 430 mE (mine grid) section.

Massive to banded sphalerite-galena-pyrite ± chalcopyrite-rich sulphides are present at the stratigraphic top of the ore lens (Fig. 6.5a,b), and massive pyrite ± chalcopyrite typically underlies the polymetallic sulphides (Fig. 6.6a). The lenses of massive pyrite overlie or are intergrown with lenses of chlorite schist (Fig. 6.5a,b). The up-dip and western parts of the ore horizon in Central Thalanga contain abundant sphalerite-galena-pyrite-rich sulphides, patchy CTC assemblages, QFP mega-clasts, and minor lenses of QEV (Fig. 6.4; Fig. 6.5a,b; map M3). The QFP mega-clasts are typically located along strike from carbonate-rich CTC assemblages (map M3). The down-dip and eastern parts of the ore horizon in Central Thalanga are dominated by pyrite-rich sulphide lenses, and local semi-massive sphalerite-galena-pyrite lenses (Fig. 6.4; Fig. 6.5c; maps M2-4).

The gradational change to pyrite-rich sulphides in the eastern and down-dip parts of the ore lens in Central Thalanga coincides with the truncation of the mineralised horizon by ENE-striking normal faults (Fig. 6.4; maps M2-4). In the eastern and down-dip parts of the ore lens, weakly altered rhyolitic volcanics of the Mount Windsor Volcanics are faulted into a hangingwall position (Fig. 6.4). Barite-sphalerite-galena-pyrite-rich sulphides in the decline in Central Thalanga (Fig. 6.4) are interpreted to be a structural repetition of the mineralised horizon. However, in adjacent drill holes, the repeated ore horizon is not mineralised.

Composition of the Ore Horizon in Central Thalanga

Polymetallic sulphides: The polymetallic sulphides are typically banded, with both compositional banding (Fig. 6.6b,c) and banding defined by grainsize variations (Fig. 6.6d). Bands of pyrite-rich sulphides, subparallel to bedding, have locally overprinted the sphalerite-rich sulphides, resulting in discontinuous sphalerite bands in massive pyrite (Fig. 6.6c). Small boulders of QFP (<0.5 m in size), rimmed by intergrown chlorite-tremolite, are common within the banded to massive sulphides in Central Thalanga (Fig. 6.6e,f).

Semi-massive sulphide lenses within Central Thalanga are hosted by either CTC assemblages (typically carbonate-rich) or siliceous rhyolitic volcanics. Irregular patches and wisps of massive carbonate (0.1 to 1.0 m in size) within massive sulphides are interpreted to be remnants of carbonate-rich CTC assemblages (Fig. 6.7a,b).

Massive pyrite: Variable amounts of chalcopyrite and rare magnetite are associated with the pyrite-rich lenses in Central Thalanga. The pyrite lenses vary from medium grained (1-2 mm) massive pyrite with quartz-muscovite gangue, to coarse grained (1-5 mm) massive pyrite with minor sphalerite and traces of quartz, to chlorite schist ± tremolite with disseminated porphyroblasts of pyrite and traces of chalcopyrite (Fig. 6.7c). Magnetite is common towards

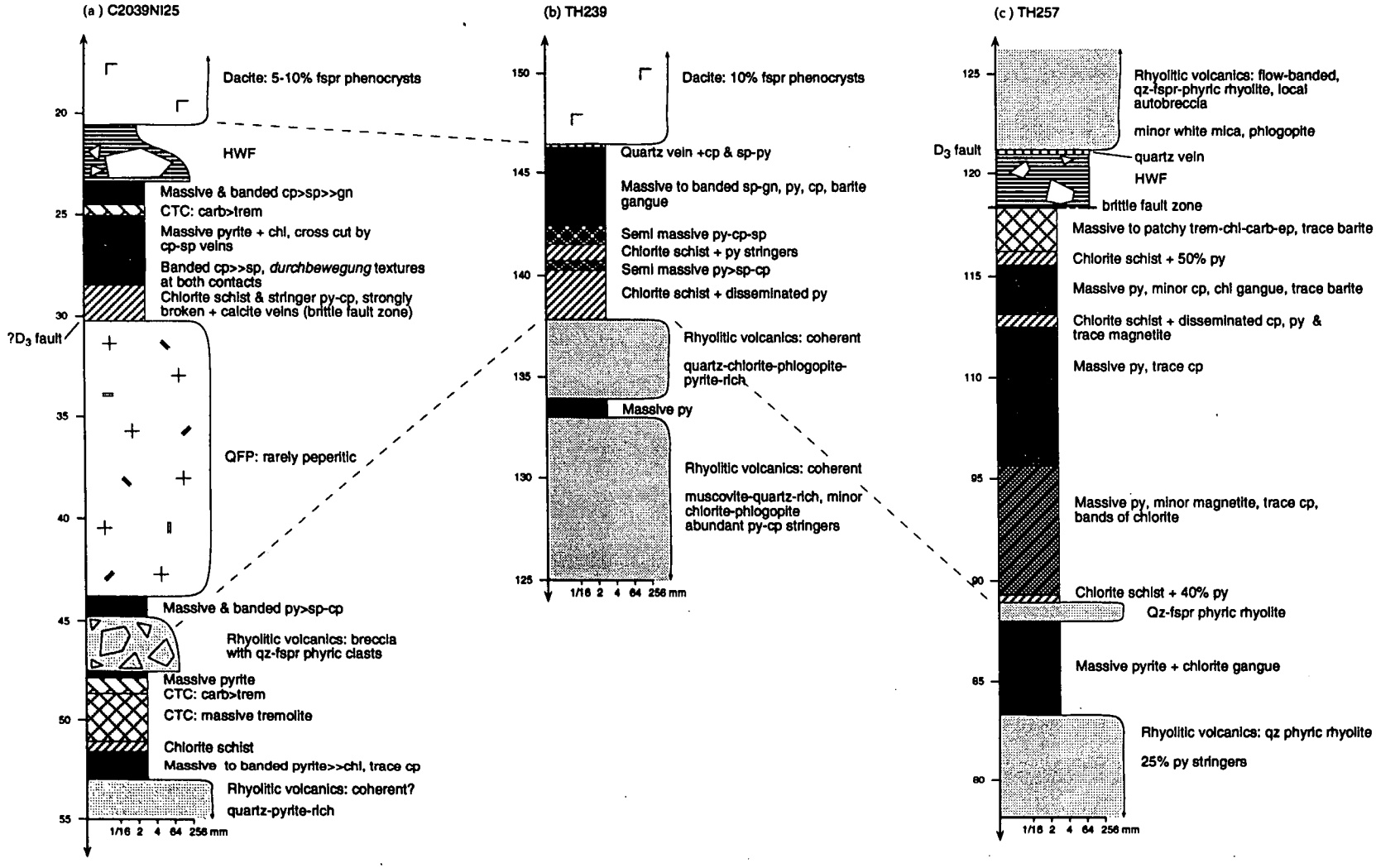

Figure 6.5 Simplified graphic logs of drill holes from Central Thalanga; (a) C2039NI25, (b) TH239, and (c) TH257. The holes are from sections 20 390 mE (C2039NI25), 20 450 mE (TH239) and 20 790 mE (TH257). Measurements along vertical scale are distance down hole (metres). Horizontal scale measures maximum clast size of volcanic units, but not grain size of sulphide or CTC assemblages. Abbreviations: carb = carbonate, chl = chlorite, cp = chalcopyrite, ep = epidote, fspr = feldspar, gn = galena, py = pyrite, qz = quartz, sp = sphalerite, trem = tremolite.

Figure 6.6 Massive to banded sulphides from the Central Thalanga ore lens.

(a) Sharp contacts, parallel to bedding, between the pyrite-chalcopyrite-rich part of the ore lens and the overlying sphalerite-galena-rich massive sulphides. Note the slightly irregular, chlorite-rich contact between the quartz-pyrite-rich footwall rhyolitic volcanics and the overlying pyrite-chalcopyrite-rich massive sulphides. Chalcopyrite-filled tension veins extend into the footwall from the pyrite-chalcopyrite-rich sulphides. Split-set plates are about 30 cm in length. Central 860 Stope (882 mRL). Facing towards left.

(b) Typical banded sulphides from Central Thalanga. Top: bands defined by alternating pyrite-rich, sphalerite-rich and galena-rich domains. Chalcopyrite is concentrated in pyrite- and galena-rich bands, and occurs in minor amount in the sphalerite-rich bands. Sample TH209-86.5. Bottom: bands defined by alternating pyrite-rich and sphalerite-rich domains. Minor chalcopyrite is most common in pyrite-rich bands. Irregular calcite veins overprint banding. Sample TH208-74.5.

(c) Hand specimen of distinct pyrite-rich and sphalerite-rich bands, with sharply defined boundaries between each band. Apparent fold (arrow at hinges) is interpreted to be the result of replacement of the sphalerite-rich sulphides by pyrite veins, which was further accentuated during deformation. Central 860 Stope. Black arrow off rock points to facing direction.

(d) Bands of pyrite in coarsely recrystallised dark red-brown sphalerite from near the stratigraphic top of the massive sulphide lens. Sample CT-91-45. Central 860 Stope. Arrow points to facing direction.

(e) Rounded clast of strongly silicified quartz-feldspar porphyry within banded sphalerite-galena-pyrite-tremolite. Sulphide bands wrap around the clast. Central 860 Stope. 20 250 mN, 20 427 mE. Facing towards right.

(f) Sketch of (e).

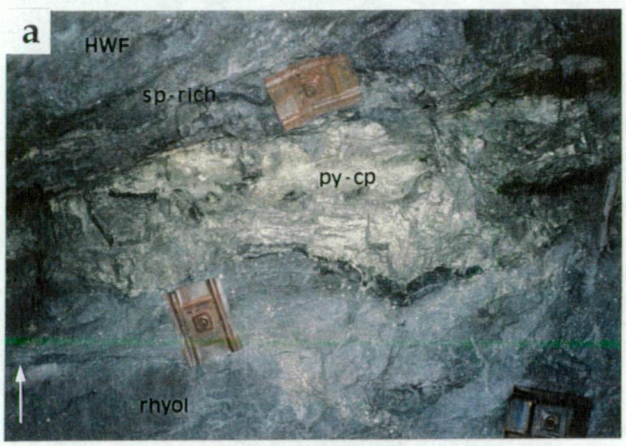
a
HWF
sp-rich
py-cp
rhyol

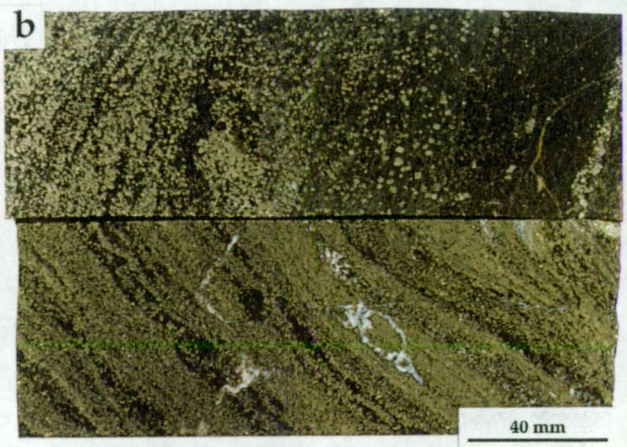
b
40 mm

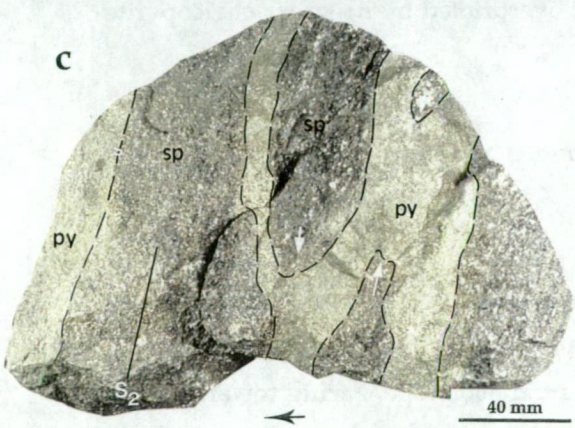
c
sp
sp
py
py
S_2
40 mm

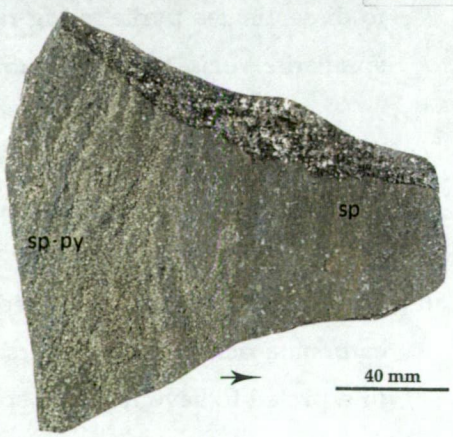
d
sp
sp-py
40 mm


e

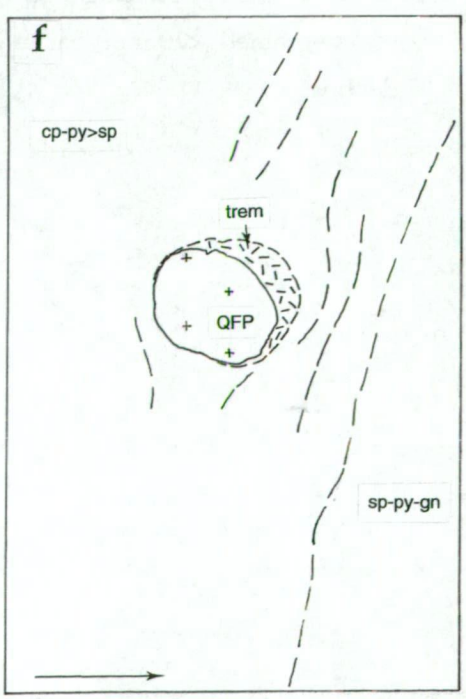
f
cp-py>sp
trem
QFP
sp-py-gn

Figure 6.7 Components of the massive sulphides in Central Thalanga.

(a) Irregular carbonate clasts (now mainly calcite) in both sphalerite- and chalcopyrite-rich sulphides. Central 860 Stope. Facing towards left.

(b) Sketch of (a).

(c) Drill core specimens of pyrite-rich massive sulphides from the eastern end of Central Thalanga. Top: massive pyrite (grainsize varies from <1-6 mm) with disseminated and stringer magnetite, and minor quartz gangue. Sample TH257-100.5. Bottom: semi-massive to disseminated pyrite in Mg-rich chlorite, overprinted by irregular chalcopyrite-sphalerite veins. Sample TH257-112.9.

(d) False fold at contact between sphalerite- and chalcopyrite-rich massive sulphides. Central 860 Stope. Facing towards left.

(e) Contact between coarse-grained chalcopyrite-rich sulphides (containing banded carbonate-rich clast) and coarse-grained sphalerite-rich sulphides. The chalcopyrite is interpreted to have replaced sphalerite. Central 860 Stope. Facing towards left.

(f) Barite-rich sulphides located within the repeated ore horizon position south of the ore lenses in Central Thalanga. Sphalerite, galena and pyrite are disseminated within coarse-grained (<10 mm) barite oriented parallel to S_2. Sample UG-2. Central Thalanga decline.

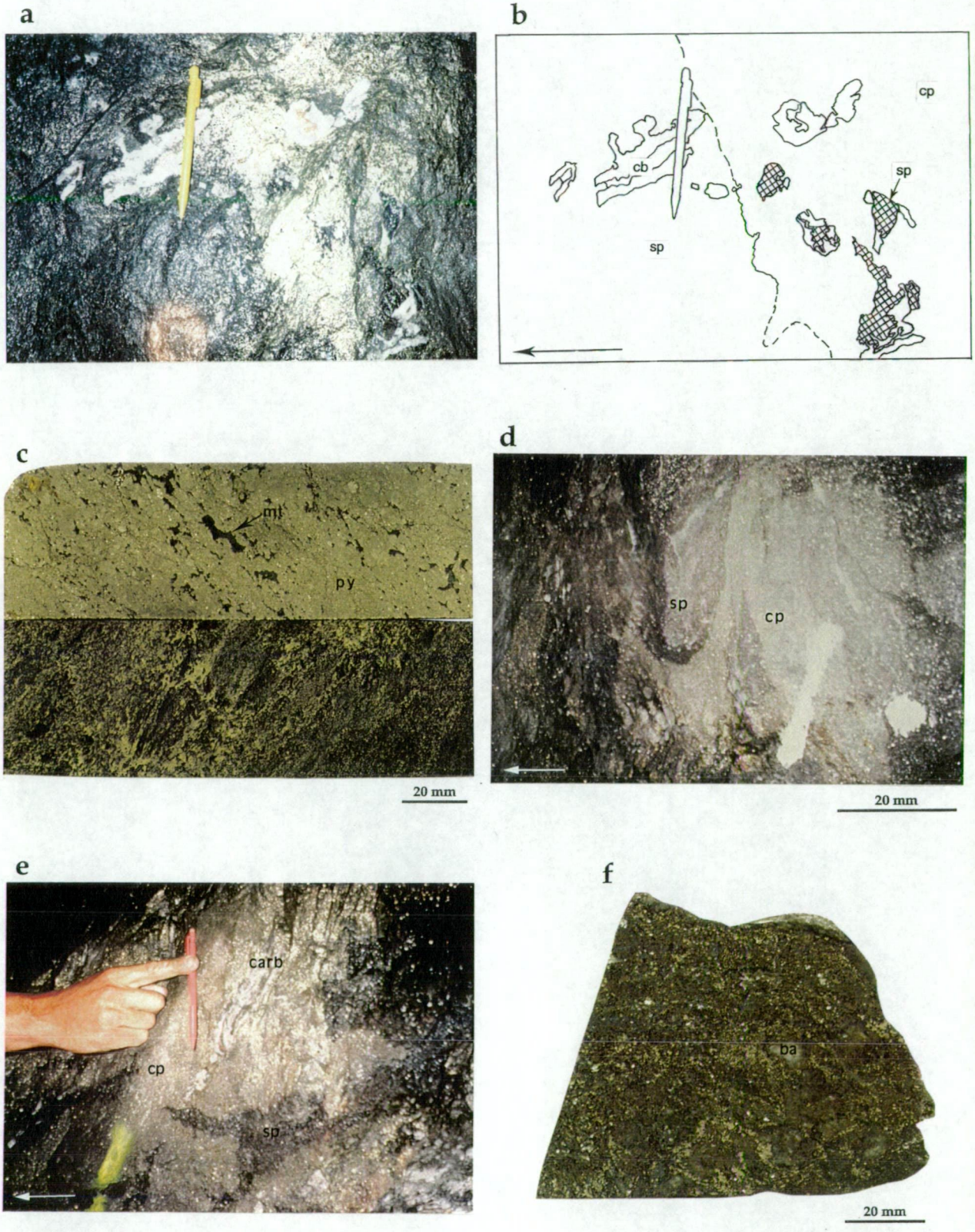
a
b
cp
cb
sp
sp
c
mf
py
20 mm
d
sp
cp
20 mm
e
carb
cp
sp
f
ba
20 mm

the base of pyrite lenses, where it is present as disseminations and fine bands (e.g. Fig. 6.5c; Fig. 6.7c).

Remobilised sulphides: Remobilised sulphides are abundant in Central Thalanga where there are numerous normal faults that have displaced the ore lens (Chapter 3). Regions of coarse-grained, massive chalcopyrite-rich sulphides are present at the stratigraphic top of the ore lens where the ore horizon is cross-cut by, and possibly folded against, normal faults (Chapter 3). Coarse-grained chalcopyrite-rich domains and coarse-grained, dark red-brown Fe-rich sphalerite-rich domains (Fig. 6.6d) within the massive to banded sulphides are interpreted to mark local 'internal' remobilisation (terminology from Gilligan and Marshall, 1987).

Contact Relationships

Most lithological contacts within the Central Thalanga ore horizon are sharp and subplanar, and locally have been overprinted by coarse-grained, remobilised chalcopyrite (i.e. piercement veins; Chapter 3). Locally, the contacts between massive polymetallic sulphides and the QFP mega-clasts are sheared. Pyrite-rich lenses have sharp, subvertical contacts with the underlying rhyolitic volcanics.

Contacts between the chalcopyrite- and sphalerite-rich remobilised sulphides vary from subplanar, with apparent folds present in places (Fig. 6.7d), to irregular, with evidence of mutual replacement fronts (Fig. 6.7e). Irregular patches of medium-grained sphalerite-galena-carbonate within massive chalcopyrite are probably remnants of the massive or semi-massive sulphide lens overprinted by remobilised chalcopyrite.

6.2.3 Vomacka Zone

Geometry of the Vomacka Zone

The ore horizon in the Vomacka Zone occurs in an upright fold and is offset by E-W to ENE trending brittle faults (Fig. 6.8). The maximum thickness of the ore lens (>10 m) occurs in the hinge region of the prominent anticline in up-dip parts of the ore lens. Elsewhere, the ore lens is commonly ≤5 m thick (Fig. 6.8). The ore lens is laterally zoned, with the northern limb of the anticline composed of massive sphalerite-galena-pyrite-rich sulphides with minor barite, variable chalcopyrite, and minor chlorite-actinolite gangue. The barite content of the ore lens, and occurrence of rhyolite and quartz-magnetite clasts, increases in the fold hinge and along the southern limb of the anticline. Below about 800 mRL (on the southern limb of the anticline) sphalerite-galena-pyrite-barite veins and stringers have overprinted a rhyolite breccia that contains rare barite clasts (e.g. diamond drill hole TH15; Appendix A).

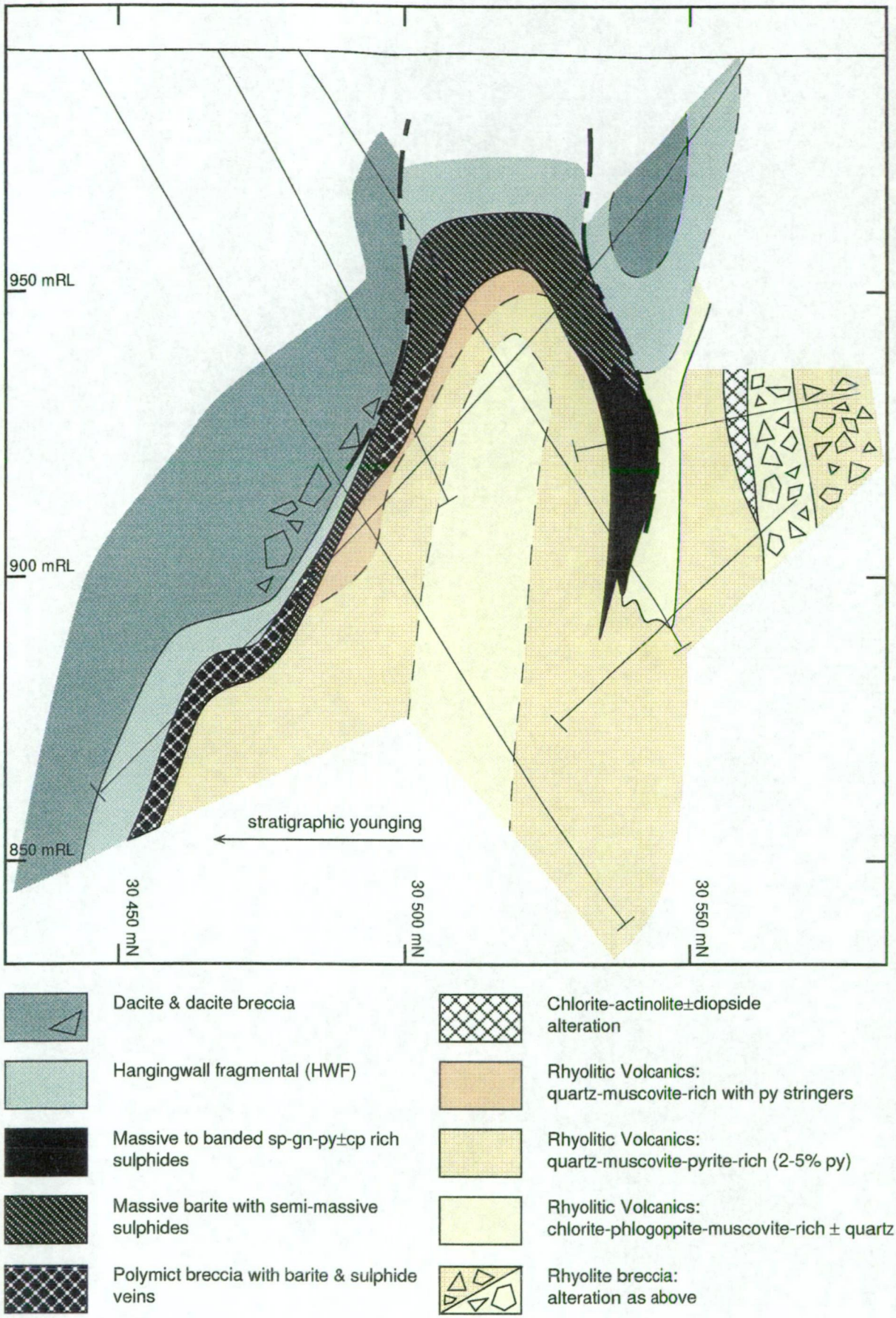

Figure 6.8 Cross section along the 31 580 mE section in the Vomacka Zone. Abbreviations: cp = chalcopyrite, gn = galena, py = pyrite, sp = sphalerite

The massive sulphides decrease in thickness in down-dip parts of the northern limb, until they are either truncated by a brittle fault, or grade to stringer veins in typical quartz-muscovite-pyrite-rich footwall rhyolite. The ore lens position may have extended around the syncline prior to brittle faulting, but the up-dip sections of the northern limb of the syncline are not mineralised.

Stratigraphic zonation within the Vomacka Zone ore lenses is poorly developed, but generally massive barite ± disseminated sulphides overlie the massive sphalerite-galena-pyrite ± barite-rich sulphides. In places, a mineralised, polymict breccia overlies the massive barite.

Composition of the Ore Horizon in the Vomacka Zone

Polymetallic massive sulphides: Massive sphalerite-galena-pyrite-rich sulphides constitute <40 % of the total mineralised ore lens in the Vomacka Zone. These massive sulphides contain abundant interstitial barite, barite bands, and local carbonate bands, and variable amounts of chalcopyrite.

Barite-rich sulphides: The mineralised horizon in the Vomacka Zone contains abundant barite, both as massive barite and intergrown with massive to semi-massive sulphides. Coarsely bladed barite veins (up to 10 cm in thickness), containing minor honey-coloured sphalerite, galena and pyrite, are present in all variants of the ore lens (Fig. 6.9a). The sulphides are typically interstitial to, or occur along grain boundaries of the coarse barite crystals. Massive barite is commonly composed of coarse grained (<3 cm) acicular to tabular crystals of barite. Barite veins have cross-cut the massive sulphides in the basal parts of the ore lens, and in places, coarse barite veins have been cross-cut by pyrite stringers, which have been cross-cut by coarse-grained barite veins (e.g. diamond drill hole TH326 42-51 m; Appendix A).

Mineralised breccia: Rare barite ± quartz clasts occur in a poorly sorted rhyolite breccia at the stratigraphic top of the footwall, and in places this breccia has been overprinted by sphalerite-galena-pyrite ± barite and barite ± pyrite veins (Fig.6.9b,c). Quartz-magnetite clasts are present in places, and the clasts are supported in a barite-chlorite or sandy siltstone matrix. This mineralised polymict breccia is locally similar in composition and texture to the overlying HWF, suggesting that the base of the HWF may have been mineralised (diamond drill hole TH293, Appendix A). Where not mineralised, this rhyolite breccia has a gradational contact with the underlying footwall rhyolitic volcanics (e.g. diamond drill hole TH15; Appendix A).

Figure 6.9 Composition of the ore lens in the Vomacka Zone and East Thalanga.

(a) Textures of the barite-rich ore in the Vomacka Zone. Top: coarse barite crystals appear to have overprinted fine grained barite. Honey brown sphalerite, galena and minor chalcopyrite are interstitial to the coarse barite crystals. Minor pyrite is disseminated through the fine barite. Sample TH326-49.5. Bottom: massive barite intergrown with, or overprinted by, stringers of pyrite and rare sphalerite-galena-pyrite. Traces of chalcopyrite. Sample TH326-43.8.

(b) Example of mineralised polymict breccia from the Vomacka Zone. Veins of barite>pyrite-chalcopyrite-chlorite, barite-sphalerite-galena, and sphalerite-galena>>pyrite-barite-chalcopyrite (with sphalerite-barite-rich margins) occur in the matrix of the breccia. Breccia contains quartz-feldspar phyric rhyolite, quartz-phyric rhyolite, feldspar-phyric dacite, and quartz-magnetite clasts, with quartz and feldspar crystals scattered in the matrix. Drill hole TH321-141.5 to 147.7.

(c) Typical banded sphalerite-pyrite-rich sulphides in the footwall lens of East Thalanga. Sample TH254-272..

(d) Inclusions of flow-banded rhyolite (strongly silicified) and clasts of QFP within the footwall lens (banded pyrite-sphalerite>galena) in East Thalanga. East 796 (Left) Stope.

(e) Pyrite-rich part of the hangingwall lens in East Thalanga. Silicified QFP and rhyolite clasts are present, as well as single blue quartz crystals. Chalcopyrite is interstitial to the pyrite. Sample TH275-122.5.

(f) Mineralised upper rhyolite breccia in the hangingwall lens. Top: semi-massive sphalerite (honey), pyrite, minor galena and trace of chalcopyrite in quartz-chlorite (matrix of rhyolite breccia). Calcite occurs between the semi-massive sulphides and the non-mineralised chlorite-rich patches (arrow). Sample E3208SD05-61. Bottom: clasts of rhyolite and possibly barite (arrow) in matrix of chlorite and semi-massive sphalerite-pyrite>galena>chalcopyrite. Sample E3208SD05-62.5.


a
40 mm
ba
py
20 mm

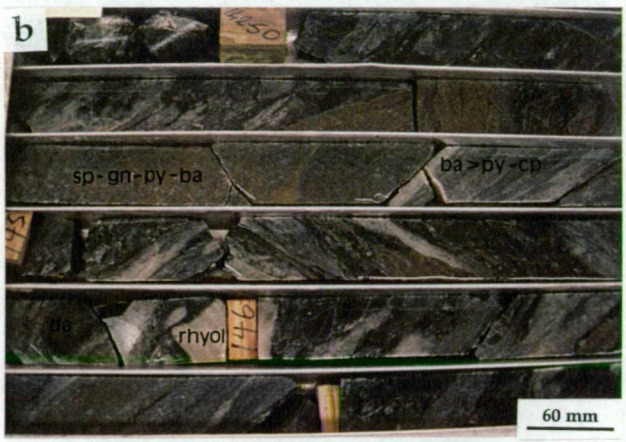
b
sp-gn-py-ba
ba>py-cp
ba
rhyol
60 mm

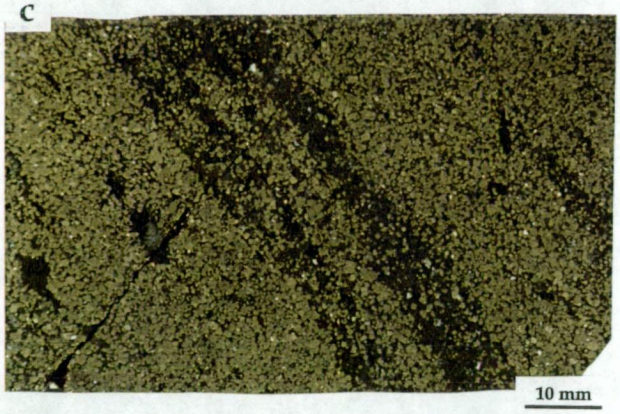
c
10 mm

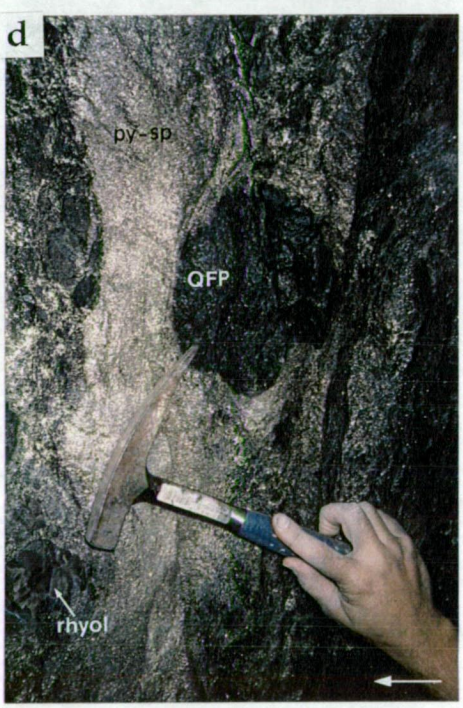
d
py-sp
QFP
rhyol

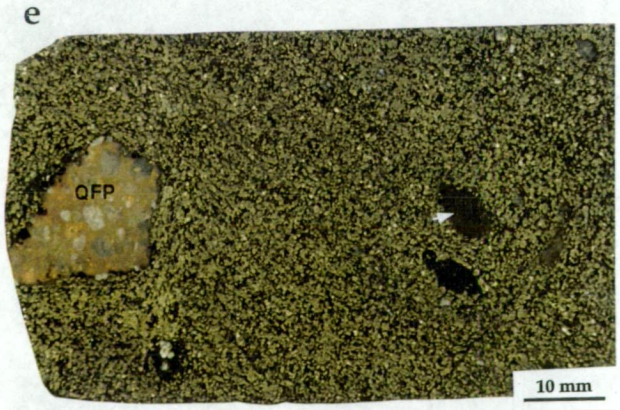
e
QFP
10 mm

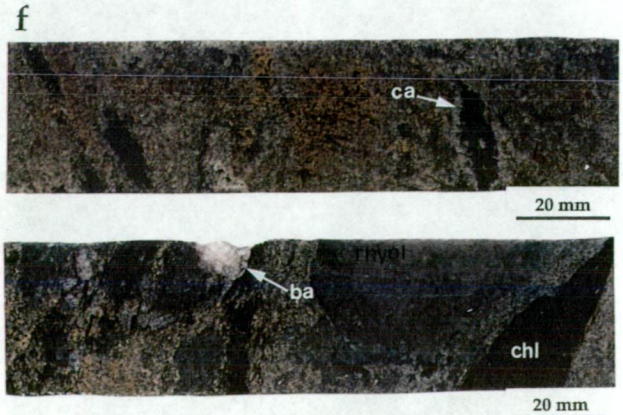
f
ca
20 mm
rhyol
ba
chl
20 mm

Contact Relationships

Contacts between ore types are parallel to bedding , and vary from sharp to gradational. The massive barite and polymetallic sulphides within the ore lens have sharp and planar contacts with the underlying footwall rhyolitic volcanics, and the overlying HWF. Gradational contacts are present between the mineralised polymict breccia and the underlying rhyolitic volcanics and overlying HWF.

6.2.4 East Thalanga

Geometry of the Ore Horizon

East Thalanga consists of two ore lenses; the footwall lens, which directly overlies altered rhyolitic volcanics, and the hangingwall lens, which overlies the QEV breccia facies (Fig. 6.10). Thinner QEV sandstone units stratigraphically overlie the hangingwall lens. QFP sills occur between the two ore lenses, although the hangingwall ore lens is typically poorly developed, or not present, where underlain by QFP.

The footwall lens, and overlying QFP sill, appear to have been repeated along a fault in the up-dip parts of East Thalanga (e.g. above ~850 mRL; Fig. 6.10). However, because the stratigraphically lowest sill has peperitic contacts with sandy siltstone, whereas the overlying QFP sill has blocky peperite at contacts with QEV breccia (Chapter 4), it is unlikely that a single QFP sill was structurally repeated. The preferred interpretation is that the present geometry is similar to the location of QFP sills, and therefore location of sulphide lenses, prior to deformation.

Only one ore lens position is present in the western parts of East Thalanga, and due to its barite-rich composition, this lens is interpreted to be continuous with the hangingwall lens, and possibly the Vomacka Zone ore lens (Fig. 6.10; Fig. 6.11a; map M11). In this location, semi-massive chalcopyrite-pyrite-chlorite-quartz and massive sphalerite-galena-barite-quartz are present at the stratigraphic top of the footwall rhyolitic volcanics, which are quartz-muscovite-phlogopite-chlorite-pyrite-rich and locally cross-cut by shallowly dipping chalcopyrite-pyrite-magnetite-barite veins (Fig. 6.11a).

There is a vertical and lateral zonation in the composition of both the footwall and hangingwall ore lenses at East Thalanga. In up-dip and western parts, the footwall lens is composed of massive to semi-massive sphalerite-galena-pyrite-rich sulphides. Down-dip and towards the eastern parts of East Thalanga, the footwall lens is composed of massive to banded sphalerite-pyrite, with gradually increasing amounts of pyrite-chalcopyrite. The hangingwall lens varies from pyrite-rich massive to semi-massive sulphides hosted in QEV

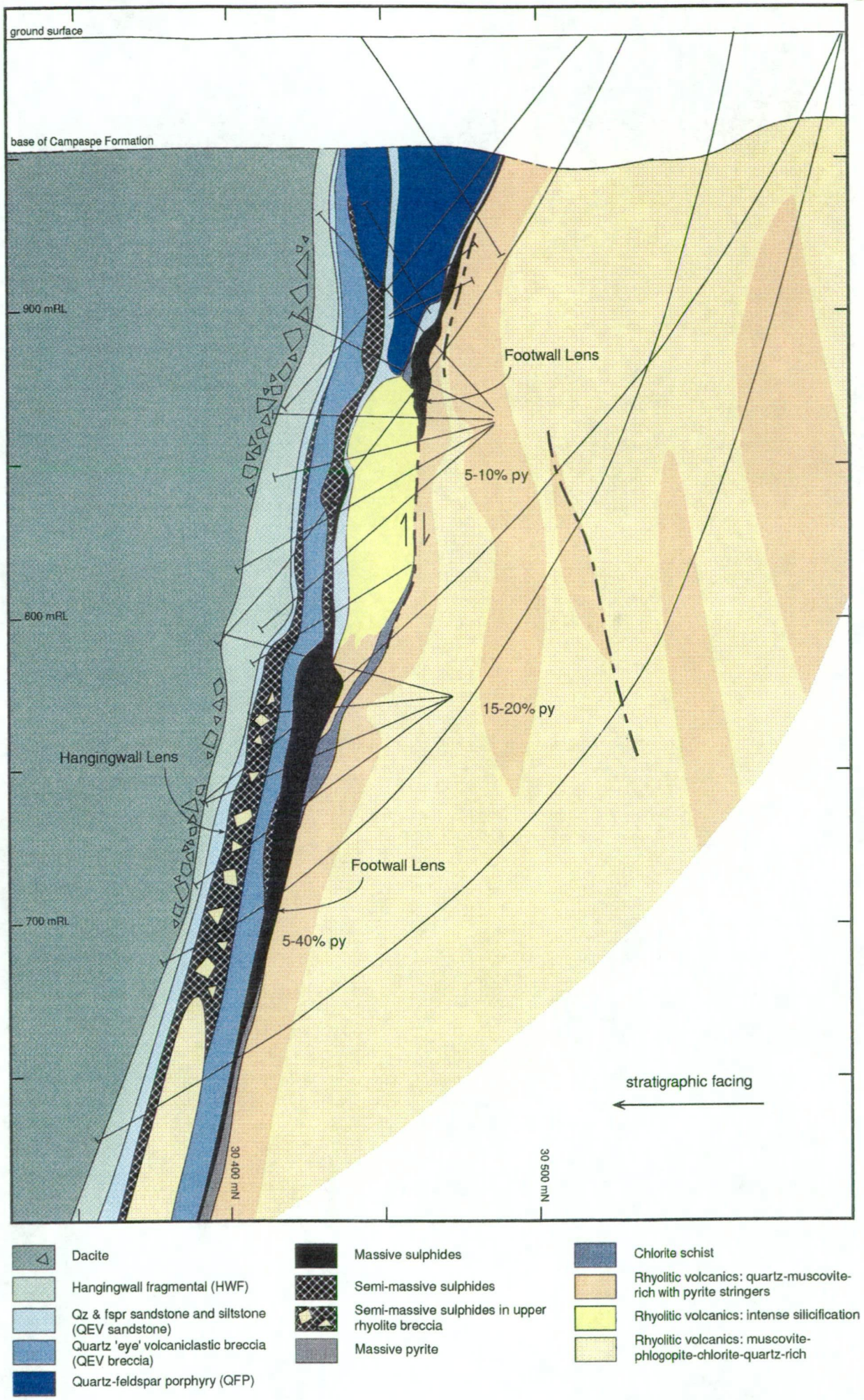

Figure 6.10 Cross section along 32 080 mE section in East Thalanga.

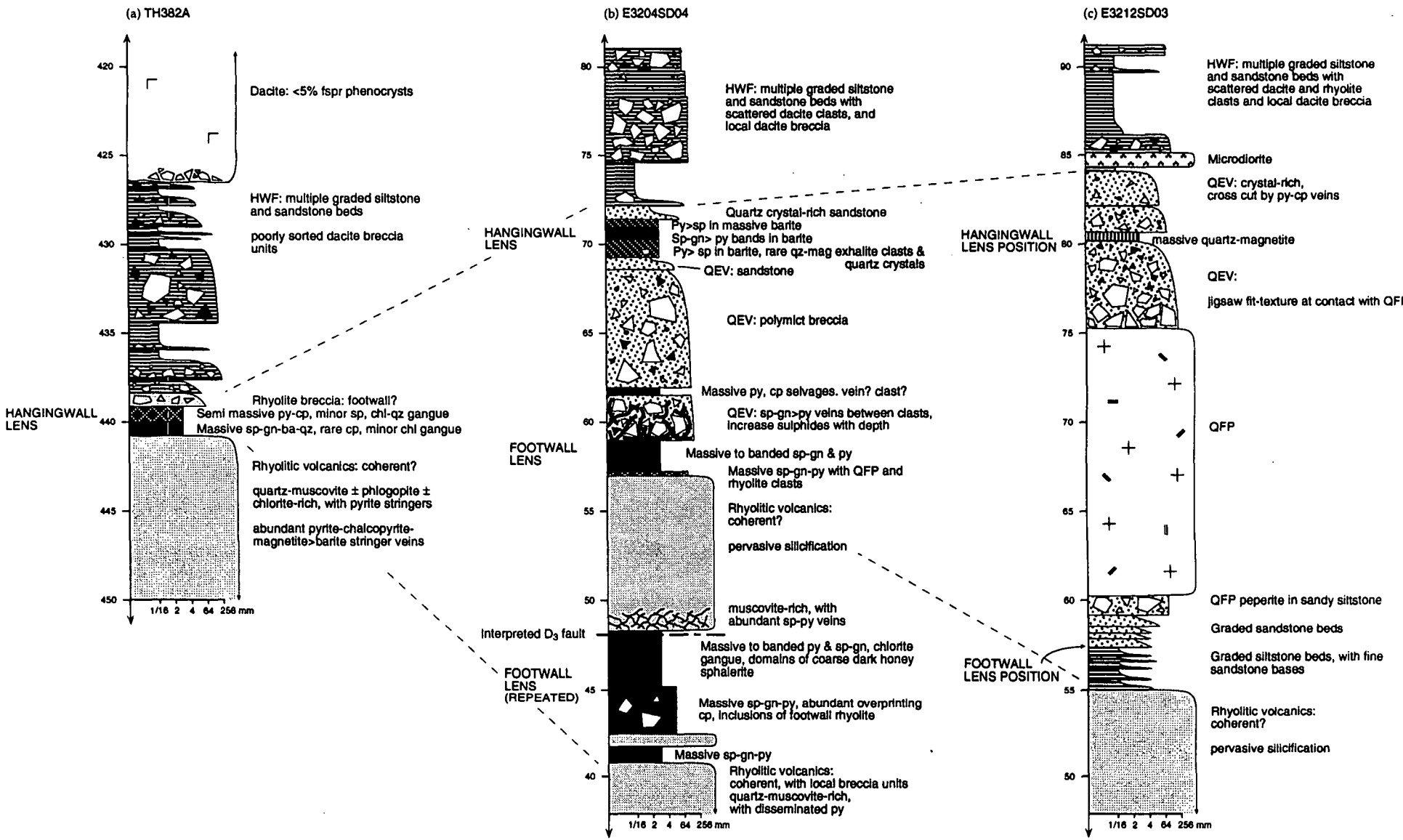

Figure 6.11 Simplified graphic logs of drill holes from East Thalanga; (a) TH382A, (b) E3204SD04, and (c) E3212SD03. The holes are from sections 31 940 mE (TH382A), 32 040 mE (E3204SD04) and 32120 mE (E3212SD03). Measurements along vertical scale are distance down the hole (metres). Horizontal scale measures maximum clast size of volcanic units, but not sulphides or CTC assemblages. See Fig. 6.3 and 6.5 for abbreviations.

sandstone units in up-dip parts, to barite-rich sulphides, then semi-massive to banded polymetallic sulphides hosted in the upper rhyolite breccia with depth. Locally, quartz-magnetite clasts are present instead of the hangingwall ore lens (Fig. 6.11c).

Composition of the Ore Lens

Footwall Lens: The footwall lens is 1-12 m in thickness, and composed of massive to banded sphalerite-pyrite-galena ± chalcopyrite ± barite, or massive pyrite with discontinuous bands of sphalerite-galena ± chalcopyrite (Fig. 6.9d). The basal part of the footwall lens is typically strongly banded, whereas the upper parts are coarsely recrystallised and non-banded (e.g. map M12, inset). Multiple, graded quartz-feldspar sandstone and siltstone and siltstone units directly overlie the intensely silicified rhyolitic footwall at localities where the footwall ore lens is absent, and are overlain and partly intruded by QFP sills (Fig. 6.11c).

Rounded to sub-rounded siliceous rhyolite and QFP clasts (<50 cm) and blue quartz crystal fragments in the massive to banded sulphides are common, and are locally cross-cut by coarse-grained chalcopyrite-galena ± sphalerite ± pyrite veins (Fig. 6.9e). QFP clasts are only present in the massive sulphides where the footwall lens is directly overlain by QEV. In these parts of the footwall ore lens, sulphide bands and sulphide clasts are common between the QFP clasts at the base of the QEV. Rare domains of rhyolite breccia occur within the massive pyrite-sphalerite-rich sulphide lens, and contain quartz-phyric rhyolite clasts (<15 cm diameter) and 3-10 mm quartz crystals. Irregular inclusions composed of finely intergrown chlorite-tremolite or calcite are present in a few places in the footwall lens, with coarse grained sphalerite-galena ± chalcopyrite commonly associated with calcite rather than tremolite.

Hangingwall Lens: The hangingwall lens is ≤5 m in thickness where composed of massive to semi-massive pyrite-rich sulphides in the coarse grained bases of QEV sandstone units. Single quartz crystals and altered feldspar crystals (now muscovite ± epidote ± quartz ± calcite), together with angular, siliceous QFP clasts (<5 cm), are present within the pyrite-rich sulphides (Fig. 6.9f). Minor chalcopyrite and traces of sphalerite are interstitial to the euhedral pyrite. In this part of the hangingwall lens, the base of the QEV sandstone units are commonly overprinted by pyrite ± chalcopyrite veins, and some of the overlying QEV sandstone units contain pyrite in their crystal-rich bases.

The barite-rich part of the hangingwall lens is generally 1-3 m thick and is composed of massive sphalerite-galena-pyrite ± barite to massive barite with bands and blebs of pyrite-sphalerite-galena-rich sulphides (e.g. Fig. 6.11b). This part of the hangingwall lens increases in thickness with depth and has gradational contacts with the mineralised upper rhyolite breccia, which is about 10 m in thickness.

Sulphide bands and disseminations occur within a tremolite-chlorite-quartz-muscovite-rich matrix between the rhyolite clasts within the upper rhyolite breccia (Fig. 6.9g). In general, chalcopyrite-sphalerite-pyrite are associated with chlorite ± tremolite gangue, whereas sphalerite-galena-pyrite are associated with irregular veins of calcite. Irregular, shallowly-dipping calcite veins are also present in the pressure shadows of some rhyolite clasts (especially those clasts >5 m in size). Locally, barite and quartz-magnetite clasts occur within the mineralised upper rhyolite breccia (e.g. diamond drill hole E3204SEH00; Appendix A).

Contacts with Host Volcanics

Footwall Lens: The contact between the footwall ore lens and the underlying rhyolitic volcanics is typically sharp, but irregular, regardless of the textures of the rhyolite (Fig. 6.12a-d), but has been overprinted by coarse grained chalcopyrite and galena. Rhyolite clasts within the massive sulphides are interpreted to be remnants of the footwall rhyolites, and to therefore indicate that the sulphide lens partly replaced the top of the footwall rhyolitic volcanics (Fig. 6.13a,b). In rare parts of the footwall lens, a monomict rhyolite breccia directly overlies the massive sulphides (Fig. 6.12c). There is a gradational decrease in sulphides from the massive sulphide lens to the overlying rhyolite breccia.

At some localities, a QFP sill directly overlies the footwall ore lens, and has been overprinted by sulphide veins. However, typically in the up-dip parts of the footwall ore lens, a poorly sorted silty sandstone to polymict sandstone breccia directly overlies (with sharp contacts) the massive sulphides and is overlain and partly intruded by the QFP (Fig. 6.12c,d). The sandstone breccia is usually matrix-supported and contains quartz-phyric rhyolite clasts, QFP peperite, and rare massive sulphide clasts (Fig. 6.13c). Disseminated pyrite, sphalerite and galena are common within the sandy siltstone matrix, and have overprinted the peperitic margins of the QFP in places (Fig. 6.13d). Most of the sulphides disseminated in the silty sandstone are coarsely recrystallised and have overprinted the dominant cleavage (Fig. 6.13c). Sulphide veins that are now subparallel to S_2 (Fig. 6.13c), are interpreted to have been present prior to deformation.

There is a sharp, but irregular contact between the footwall lens and the overlying QEV breccia units, with pyrite-sphalerite-galena ± chalcopyrite bands common between clasts in the base of the overlying QEV breccia (Fig. 6.13e). The presence of massive sulphide clasts within the QEV (Chapter 4) is consistent with massive sulphide bands recognised in drill core being massive sulphide clasts that were concentrated at the base of the QEV due to their high density during transportation and deposition by mass flow. However, some sphalerite-pyrite ± chalcopyrite disseminations and bands are interpreted to be veins (Fig. 6.13f,g). Coarse-grained bands of chalcopyrite>sphalerite-galena-pyrite between QFP clasts are

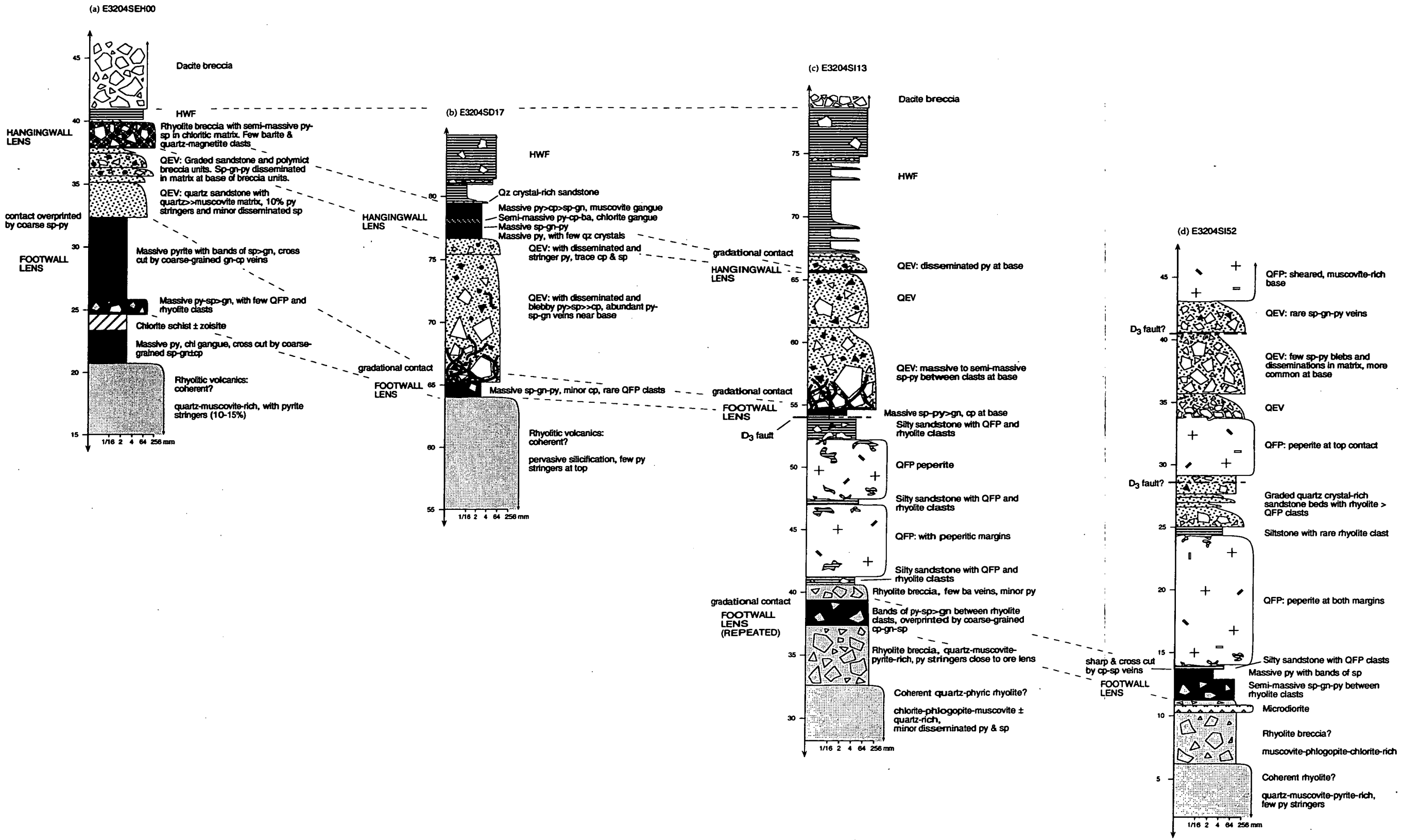

Figure 6.12 Simplified stratigraphic logs of the footwall lens and enclosing volcanics in East Thalanga (32 040 mE section). The logs are arranged such that the deepset hole is on the left and the shallowest hole is on the right of the diagram. Contacts are sharp unless otherwise indicated on left side of log. Scale down left side is metres down drill hole, and scale along the base is size of largest component within the volcanic units, but not within the sulphide lenses or CTC assemblages. See Figure 6.3 or 6.5 for abbreviations.

Figure 6.13 Geometry of the contacts between the sulphide lenses and the volcanic units in East Thalanga.

(a) Pyrite±chalcopyrite veins in strongly silicified rhyolite in the immediate footwall of the footwall lens. East 765 Stope. Facing towards top.

(b) Sharp contact between footwall ore lens and the overlying sandstone breccia (containing QFP peperite). Pyrite is disseminated through the sandstone and may also occur as clasts. Coarse chalcopyrite-sphalerite veins (shallowly dipping) cross cut the contact between massive pyrite and sandstone. Sample E3204SI52-13.6. Arrow points to facing direction.

(c) Sphalerite-pyrite-rich sulphides have overprinted QFP peperite at the stratigraphic base of a QFP sill. Late chalcopyrite-pyrite-sphalerite-galena veins have also cross-cut the QFP clasts. Sample E3212SI18-53. Arrow points to facing direction.

(d) Coarse-grained chalcopyrite-pyrite-chlorite vein between QFP clasts in the QEV overlying the footwall lens in East Thalanga. Chalcopyrite, tremolite and margarite have partly replaced feldspar phenocrysts at the margins of the QFP clast. Sample TH263-171.

(e) Contact between the banded sphalerite-pyrite-galena-rich footwall ore lens and the overlying QEV. Veins of pyrite-sphalerite (overprinted by S_2) extend from the ore lens and have cross cut the QEV. East 830 Stope (Left). Facing to right.

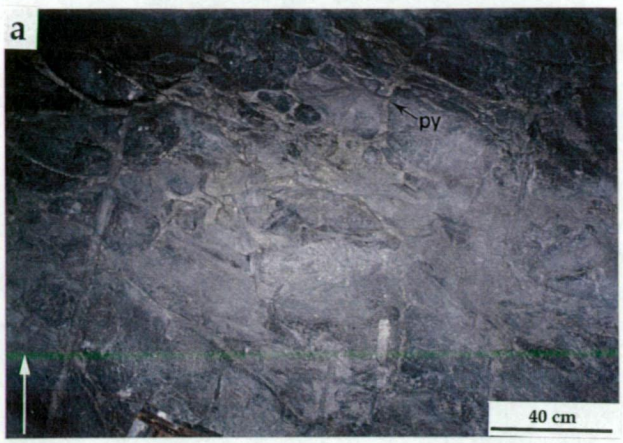
a
py
40 cm

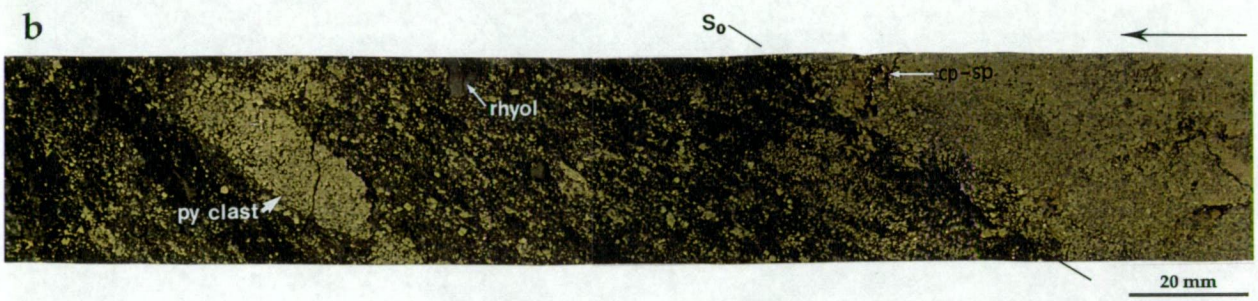
b
S_0
cp-sp
rhyol
py clast
20 mm


c
20 mm
QFP
cp

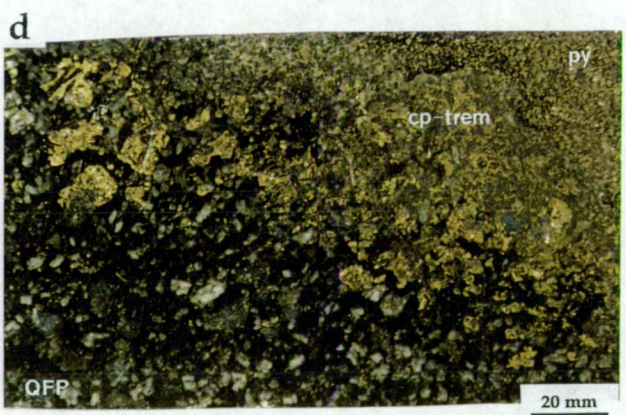
d
py
cp-trem
QFP
20 mm


e
QEV

interpreted to have been remobilised, and in places these have partly replaced the margins of QFP clasts (Fig. 13e).

Hangingwall lens. The stratigraphic base of the pyrite-rich hangingwall lens is typically sharp, parallel to bedding and has been locally cross-cut by coarse grained, shallowly-dipping chalcopyrite ± sphalerite ± pyrite veins. A gradational decrease in the pyrite content (co-incident with decreasing crystal size) marks the stratigraphic top of the pyrite-rich lens (Fig. 6.12c).

Both stratigraphic top and basal contacts of the barite-rich hangingwall lens are typically parallel to compositional banding within the ore lens (Fig, 6.11b). In some drill holes, the ore lens has a gradational contact with an overlying polymict breccia (e.g. E3198SD06; Appendix A). This breccia is poorly sorted, clast-supported and contains irregular-shaped clasts of massive barite ± quartz, quartz-magnetite and siliceous rhyolite in a matrix of barite-muscovite (similar to parts of the ore horizon in the Vomacka Zone). Semi-massive to disseminated sphalerite-galena-pyrite ± chalcopyrite has overprinted the polymict breccia, which is interpreted to indicate that the polymict breccia was deposited prior to, or during, sulphide mineralisation.

The basal contact of the mineralised upper rhyolite breccia is sharp, parallel to banding within the sulphides, and locally has been overprinted by coarse grained chalcopyrite. The QEV sandstone units overlie the mineralised upper rhyolite breccia, and in some locations, the crystal-rich base of the QEV sandstone contains pyrite ± chalcopyrite in the matrix. At other locations, a zone of pervasive chlorite alteration, with minor chalcopyrite-pyrite veins, has gradational contacts with the mineralised upper rhyolite breccia, and sharp contacts with the overlying QEV sandstone.

6.3 Discussion

6.3.1 Deposit Geometry

The interpreted pre-deformation geometry of the Thalanga ore horizon, including the massive sulphide lenses, is summarised in Figure 6.14(a). Massive sulphides occur at the same stratigraphic location (the top of the Mount Windsor Volcanics) in West, Central and East Thalanga and in the Vomacka Zone and are interpreted to have been continuous between West and Central Thalanga, and also between the Vomacka Zone and East Thalanga. However, there is no evidence that the ore lens was continuous between Central Thalanga and the Vomacka Zone. The sulphide lenses in West, East and western parts of Central Thalanga occur above and below QEV units and QFP sills. The QEV units were deposited in local basins

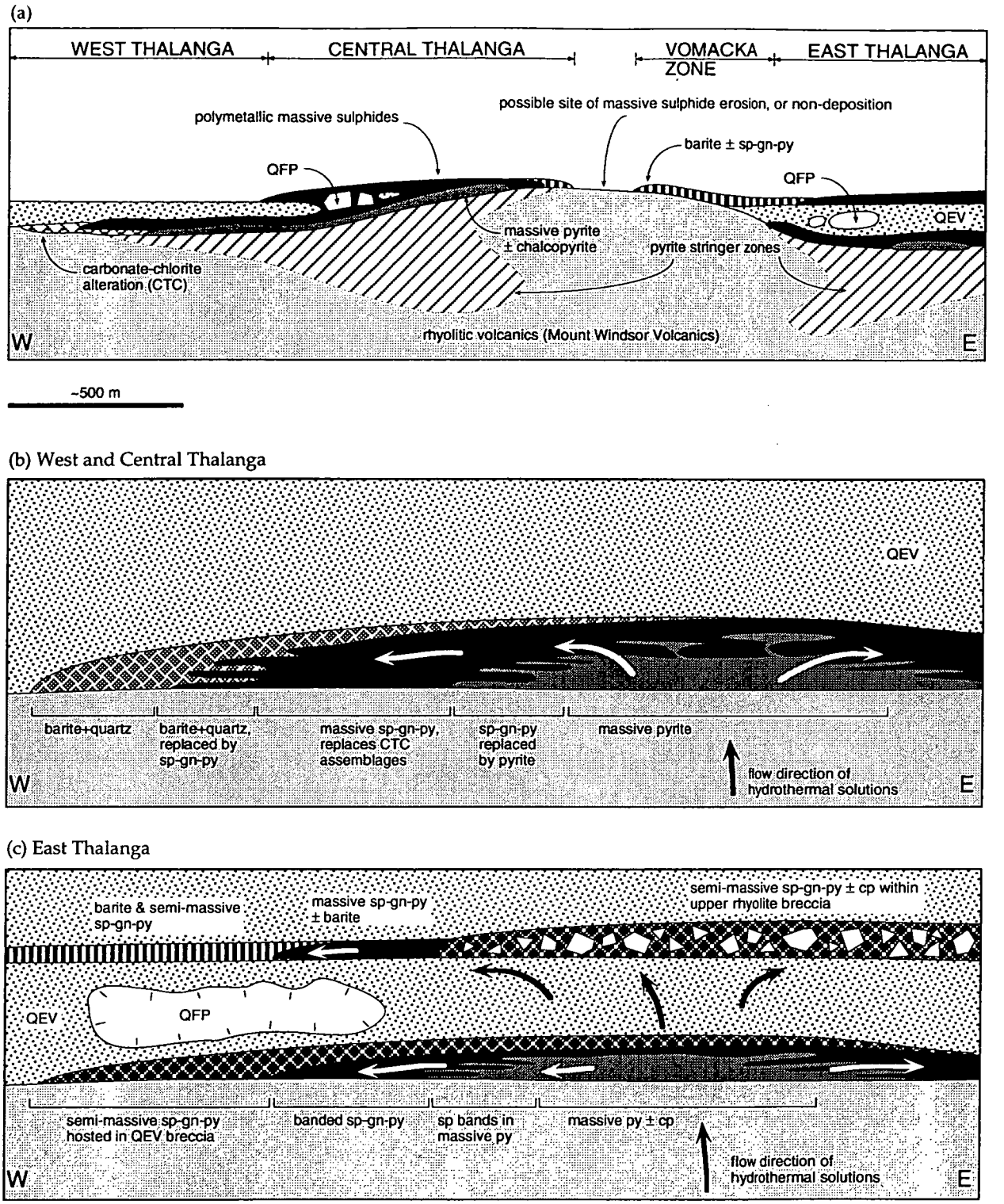

Figure 6.14 Schematic diagram of the (a) interpreted pre-deformation (and pre-dacite deposition) spatial relationship between West, Central and East Thalanga and the Vomacka Zone, (b) evolution and movement of the mineralising solutions during formation of the massive sulphide lens in West and Central Thalanga, and (c) evolution and direction of fluid flow during sulphide deposition in East Thalanga, with the hangingwall ore lens continuous to the Vomacka Zone.

at the stratigraphic top of the footwall rhyolite (Chapter 4), and the absence of these units in the Vomacka Zone and eastern parts of Central Thalanga is interpreted to indicate that these areas were topographic highs at the time of QEV deposition.

The hangingwall lens in East Thalanga is interpreted to extend to the Vomacka Zone, where it is barite-rich (Fig. 6.14a). Discontinuous lenses of QEV within Central Thalanga are enclosed by massive sulphides. However, the presence of massive sulphides above and below the QFP mega-clasts in Central Thalanga is partly a result of structural repetition (Chapter 3), but may also be depositional in origin, because the QFP contains altered feldspars and is muscovite-quartz-phlogopite-rich (Chapter 10). The QEV in West Thalanga is not overlain by massive sulphides.

The barite-rich sulphides in the Vomacka Zone, parts of the hangingwall lens of East Thalanga, parts of Central Thalanga, and the western parts of West Thalanga, are interpreted to have formed at sites where lower temperature fluids (200° to 250°C; Large, 1992) have discharged. In most of these localities, early-formed quartz-barite assemblages have been partly overprinted by sphalerite-pyrite-rich sulphides. Deposition of the barite-rich lenses is therefore interpreted to have occurred at the margins of the hydrothermal system, with those localities closer to the fluid source being partly replaced by sulphides in a process similar to the zone refining processes described by Eldridge *et al.* (1983) and Huston and Large (1988). Therefore, the Vomacka Zone and the western parts of West Thalanga are interpreted to be the margins of the East Thalanga and West/Central Thalanga hydrothermal systems respectively. Barite-rich sulphides that are repeated in the hangingwall of Central Thalanga may also have formed at the cooler temperature margin of the hydrothermal system; either at the eastern and down-dip margins of the Central Thalanga ore lens, or possibly the western limits of the Vomacka Zone, or alternatively a separate hydrothermal system. The absence of a mineralised ore position between Central Thalanga and the Vomacka Zone is interpreted to indicate either that West and Central Thalanga formed from a different hydrothermal system to the Vomacka Zone and East Thalanga, or that deformation and subsequent erosion have removed the connection between the Vomacka Zone and Central Thalanga.

Zones of massive pyrite ± chalcopyrite commonly occur at the stratigraphic base of VHMS deposits and are believed to precipitate from high temperature hydrothermal solutions (270° to >350°C; Large, 1992). Massive pyrite ± chalcopyrite lenses are present in West, Central and East Thalanga between the rhyolitic footwall and the overlying polymetallic massive sulphides (Fig. 6.14a). In West Thalanga, massive pyrite at the eastern and down-dip parts of the ore lens may have been continuous with massive pyrite in Central Thalanga. The massive pyrite lenses are interpreted to have formed over the zones of discharge of high temperature hydrothermal solutions.

6.3.2 Deposition of Sulphides

In parts of West and Central Thalanga, zones composed of pyrite bands and veins that have overprinted sphalerite-rich sulphides (e.g. Fig. 6.2d; Fig. 6.6c) overlie the massive pyrite lenses. These textures are interpreted to have been produced by the syn-mineralisation replacement of sphalerite-rich sulphides (formed earlier from mineralising solutions at 235°-270°C; Large, 1992) by pyrite (formed from higher temperature mineralising solutions; e.g. 270°-350°C; Large, 1992), possibly along pre-existing compositional bands (Fig. 6.14b). Syn-volcanic hydrothermal replacement of massive sulphides (zone-refining) is regarded as an important process in the growth of massive sulphide mounds (Eldridge *et al.*, 1983; Huston and Large, 1988; Large, 1992). The gradational contact from banded sphalerite-pyrite-rich sulphides, to massive pyrite with discontinuous sphalerite-rich bands, to massive pyrite down-dip within the footwall lens in East Thalanga is consistent with formation by a similar process. The massive pyrite-chalcopyrite in down-dip parts of the footwall lens is interpreted to have formed from high temperature hydrothermal solutions (e.g. 270°-350°C; Large, 1992) which replaced the pre-existing sphalerite-pyrite lens as the hydrothermal solutions ascended and moved laterally through the massive sulphides (Fig. 6.14c). The sphalerite-rich sulphides are interpreted to have been redeposited as the hangingwall lens (Fig. 6.14c).

Barite veins that locally cross-cut the massive sulphide lenses in West Thalanga, are interpreted to have formed during the latest stage of mineralisation. Because the formation of barite requires cool hydrothermal solutions and mixing with seawater to provide sulphate, the presence of barite implies that the rhyolitic footwall had remained porous after deposition of the massive sulphides.

Clasts of quartz-magnetite are present at the stratigraphic top of the ore lenses in parts of West and East Thalanga. Quartz magnetite lenses (interpreted to have formed from low temperature hydrothermal fluids on the seafloor; Duhig *et al.*, 1992) outcrop at the Thalanga ore horizon position in the south eastern parts of the Thalanga Range (Chapter 4), and perhaps clasts from these locations may have been transported by mass-flows to Thalanga. It is possible that some quartz-magnetite lenses were formed *in situ* at Thalanga, from low temperature hydrothermal solutions, during the early stages of sulphide deposition. In most places, the quartz-magnetite clasts have been overprinted by sulphides or barite, and this is interpreted to have occurred during formation of the massive sulphide lenses.

6.3.3 Seafloor Deposition vs Sub-seafloor Replacement

The sulphide lenses at Thalanga vary from having sharp contacts with the enclosing rocks, to gradational upper and lower contacts and are therefore interpreted to be at least partly

replacive in origin. The best-preserved evidence that the massive sulphide lenses were exposed on the seafloor are the clasts of massive sulphides in the overlying QEV and HWF (Table 6.2). Although the mineralogy of the massive sulphide clasts is identical to that of the Thalanga massive sulphide deposit, the source of the sulphide clasts may have been other massive sulphide deposits within the Trooper Creek Formation.

Table 6.2 Interpretation of mesoscopic features of the ore lenses relevant to the timing of volcanism and mechanism of sulphide formation

Mesoscopic texture	Interpretation
Massive sulphide clasts in overlying QEV	Erosion of massive sulphides exposed on seafloor and incorporation into QEV
QFP clasts and/or blue quartz and feldspar (altered) crystals in massive sulphide lenses	QEV partly replaced by sulphides, or QFP clasts accidentally deposited on growing massive sulphide lens on seafloor
Rhyolite clasts in massive sulphides	Top of rhyolitic volcanics partly replaced as coalescing feeder veins merged into massive sulphide lens
Gradational contacts between massive sulphides and overlying QEV (East Thalanga)	Base of QEV partly replaced by sulphides
Quartz-muscovite-pyrite-rich QEV between footwall and hangingwall lenses (East Thalanga)	Quartz-sericite-pyrite alteration when mineralising solutions moved through QEV to deposit sulphides in hangingwall lens position
Semi-massive to massive sulphides in matrix of upper rhyolite breccia (East Thalanga)	Matrix of rhyolite breccia was replaced by sulphides
Vein style sulphides in CTC units (West Thalanga)	Sulphides replaced CTC units
Massive barite (± sulphides) or quartz-magnetite between multiple QEV units (hangingwall lens, East Thalanga)	Exhalites at seafloor position
Barite ± sulphide veins in polymict breccia and gradational contact with overlying HWF (Vomacka Zone)	Base of HWF partly mineralised

The presence of sulphide veins and disseminations within the CTC assemblages in West and Central Thalanga are interpreted to indicate that the CTC units were replaced by sulphides in a sub-seafloor position (Table 6.2). The CTC assemblages are interpreted to have formed by alteration of the footwall rhyolitic volcanics prior to mineralisation (Chapter 11), and irregular to blocky clasts of massive carbonate and massive chlorite within the massive sulphides are interpreted to be remnants of the CTC assemblages. The seafloor in West Thalanga was probably either at the stratigraphic top of the CTC units, or at the top of the overlying QEV (which may have acted as an impermeable barrier; Chapter 10 & 11) during the formation of sulphides. Alternatively, the position of the seafloor may have migrated from the top of the CTC units to the top of the QEV during sulphide deposition.

The textural characteristics of the stratigraphic top of the footwall rhyolitic volcanics are interpreted to have controlled the nature of the contact with the overlying ore lens. Monomict rhyolite breccia is present at the stratigraphic top of the footwall rhyolitic volcanics in most parts of Thalanga (Chapter 4), and the irregular contact with the overlying ore lens is

consistent with the partial replacement of the top of a rhyolite breccia (Table 6.2). However, sharp, conformable contacts between the massive sulphide lenses and the underlying footwall rhyolitic volcanics may have resulted from the deposition of sulphides onto the seafloor. Where the footwall lens in East Thalanga is overlain by a rhyolite breccia, the massive sulphides are interpreted to have replaced a rhyolite breccia in a subsea-floor position. The gradational decrease in sulphides up stratigraphy from the sulphide lens to the overlying rhyolite breccia supports this interpretation.

The QEV that overlies the ore lens in West Thalanga generally has sharp contacts with the massive sulphides, but contains epidote-actinolite-rich assemblages, whereas in East Thalanga, QEV units overlie both the footwall and hangingwall lens with gradational contacts defined by decreasing sulphide content. The QEV breccia between the footwall and hangingwall lenses in East Thalanga, and the QEV units and QFP mega-clasts in Central Thalanga, are quartz-muscovite-pyrite-rich (inferred to be metamorphosed quartz-sericite-pyrite alteration; Chapter 10). This variation in alteration type is interpreted to be the result of formation of sulphides at Central and East Thalanga following deposition of the QEV (Table 6.2). The presence of sulphide veins that are folded or are subparallel to S_2 and cross cut peperitic QFP margins and the base of the QEV breccia in East Thalanga, supports the interpretation that the QFP peperite and QEV breccia were partly replaced by sulphides during mineralisation. Coarsely recrystallised sulphide veins that overprint S_2 are interpreted to have been remobilised during deformation and metamorphism.

The presence of two ore lens positions in East Thalanga is interpreted to indicate that QEV deposition interrupted the formation of sulphides in East Thalanga. Lack of abundant QFP and rhyolite clasts in all parts of the footwall lens suggests that locally massive sulphides formed on the seafloor, rather than by replacement of the QEV breccia. Given that the QEV units have normal grading (Chapter 4), and that the contact between the QEV breccia and overlying hangingwall lens is sharp and conformable, the top of the main QEV is interpreted to have been the seafloor during the deposition of the hangingwall lens. The hangingwall lens is interpreted to have been partially formed on the seafloor (quartz-magnetite lenses and the barite-rich sulphides) and partially formed by replacement of the upper rhyolite breccia and the coarse-grained base of overlying QEV sandstone units.

6.3.4 Comparison with Other Deposits in the Mount Windsor Subprovince

The mineralogies and stratigraphic locations of other massive sulphide deposits in the Mount Windsor subprovince are reviewed in Chapter 2. Most deposits are stratiform, with underlying sericite ± quartz ± chlorite ± sulphide alteration zones, except for the pipe-like Reward deposit, which is composed mainly of massive pyrite (Beams *et al.*, 1990; Berry *et al.*, 1992). Generally, other massive sulphide deposits in the Mount Windsor volcanic belt are

less coarsely recrystallised than Thalanga due to the lower metamorphic grade in most other parts of the volcanic belt (Berry *et al.*, 1992).

Sphalerite and pyrite are the dominant sulphide minerals in the other massive sulphide deposits and most contain abundant galena and chalcopyrite (Table 2 in Berry *et al.*, 1992). Barite, quartz, carbonate and sericite are common gangue minerals and both the Liontown and Handcuff stratiform massive sulphide deposits are associated with barite and quartz-carbonate assemblages (Berry *et al.*, 1992; Beams, 1993; Miller, 1996). The Agincort and Waterloo deposits contain abundant pyrite, chalcopyrite, sphalerite and galena, with minor tennantite/tetrahedrite, traces of arsenopyrite and electrum, and barite, sericite, quartz, carbonate gangue, although the Waterloo prospect contains tennantite and galena as minor phases (Huston *et al.*, 1995a).

Electrum has been reported from the Reward, Waterloo and Agincort deposits (Berry *et al.*, 1992) and Au is associated with Zn and the Agincort deposit, whereas it is associated with Cu at the Waterloo prospect (Huston *et al.*,1992a, 1995a). Au- and Ag-bearing tellurides (altaite, hessite, calaverite and petzite) are present within the massive sulphides at the Waterloo prospect (Huston *et al.*, 1995a), but have not been reported from other deposits within the Mount Windsor subprovince (Berry *et al.*, 1992). The more gold-rich Agincort and Waterloo deposits are interpreted to have formed from more oxidised hydrothermal fluids than those that produced Thalanga (Huston *et al.*, 1995a).

6.4 Summary

1. Although the massive sulphide lenses at Thalanga are present at the same stratigraphic position in West, Central and East Thalanga and the Vomacka Zone, the nature and geometry of the massive sulphides varies in each lens. Polymetallic massive sulphides in most parts of the Thalanga deposit are composed of sphalerite-galena-pyrite-rich sulphides with variable amounts of chalcopyrite. In general, the polymetallic massive sulphides occur at the stratigraphic top of the ore lens. Massive pyrite ± chalcopyrite ± chlorite lenses occur at the stratigraphic base of the West and Central Thalanga ore lenses, whereas massive pyrite-sphalerite-rich sulphides, with local massive pyrite ± chalcopyrite, constitute the footwall lens at East Thalanga. Lenses of massive pyrite are absent from the Vomacka Zone. Massive barite and barite-rich sulphides occur in the Vomacka Zone, the hangingwall lens in East Thalanga, down-dip parts of Central Thalanga, and rarely, in West Thalanga (up-dip), are interpreted to have formed from cooler, more oxidised hydrothermal solutions than the underlying sulphides.

2. QEV deposition at East Thalanga and parts of Central Thalanga interrupted the formation of sulphide lenses, resulting in two ore positions at East Thalanga. Sulphide deposition occurred via sub-seafloor replacement and minor seafloor exhalation at East Thalanga. The stratigraphic top of the footwall has been locally replaced, the stratigraphic base of the QEV breccia and QEV sandstone units are replaced, and the matrix of the upper rhyolite breccia has also been replaced by sulphides. The timing of sulphide formation and QEV deposition in West Thalanga is unclear, but the sulphides are inferred to have replaced carbonate-chlorite alteration stratigraphically underlying the QEV.

3. Zonation from pyrite ± chalcopyrite-rich sulphides to sphalerite-galena-pyrite ± barite-rich sulphides, to barite-quartz lenses is interpreted to have formed by the zone-refining process during sub-seafloor replacement.

CHAPTER 7.

ORE DEPOSIT MINERALOGY AND TEXTURES

7.1 Introduction

All lenses at Thalanga have the same ore and gangue mineralogy, and therefore the description of the mineralogy and textures of the ore horizon is not separated into a discussion on each lens. The objectives of this chapter are to describe the textures and compositional variations (as determined by electron microprobe) of each of the main sulphide and gangue minerals, and to distinguish between primary and metamorphic sulphide textures.

The massive to banded sulphides in the Thalanga deposit are typically strongly recrystallised and annealed (Fig. 7.1a). Finely intergrown sphalerite, galena and chalcopyrite (Fig. 7.1b) are rarely preserved, yet fine-grained intergrowths of fine grained chalcopyrite, galena, tetrahedrite-tennantite and arsenopyrite are common (Fig. 7.1c). In places, the morphology of the sulphides is controlled by the co-existing gangue minerals, with sphalerite, galena, and chalcopyrite common along chlorite or tremolite cleavages.

Sphalerite is less abundant than chalcopyrite in the dilational sites at Thalanga. This is consistent with the results of experimental studies by Clark and Kelly (1973, 1978), Kelly and Clark (1975), Salmon *et al.* (1974), Atkinson (1974) and Roscoe (1975), who examined the behaviour of sulphides during metamorphism and deformation. Similarly, textural studies indicate that galena, chalcopyrite and pyrrhotite were deformed in a more ductile manner than sphalerite at the Broken Hill sediment-hosted massive sulphide deposit (Plimer, 1980). The textures of remobilised and non-remobilised sphalerite and chalcopyrite are described in this chapter.

7.2 Sphalerite

7.2.1 Sphalerite Textures

Sphalerite occurs as rounded grains typically enclosed by, or intergrown with galena or chalcopyrite in the massive to banded sphalerite-galena-pyrite lenses at Thalanga. The margins of rounded sphalerite grains locally contain galena inclusions (Fig. 7.1d,e). Equant grains within domains of massive sphalerite have 120° grain boundaries, and minute inclusions of galena and/or chalcopyrite are aligned along the grain boundaries or trapped at

Figure 7.1 Photomicrographs of the sphalerite-rich parts of the massive sulphide ore lenses at Thalanga (under reflected light).

(a) Typical coarsely recrystallised sphalerite-galena and chalcopyrite. Galena typically occurs interstitial to large sphalerite grains and occurs with chalcopyrite along boundaries between sphalerite grains. Sample E3204SI13-47.1. East Thalanga.

(b) Fine grained sphalerite, chalcopyrite, galena and minor tetrahedrite at the contact between sphalerite grains and galena. Sample TH209-86.5a. Central Thalanga.

(c) Fine grained intergrowths of chalcopyrite, arsenopyrite, tetrahedrite, minor sphalerite and trace of galena in a chalcopyrite-rich domain of polymetallic massive sulphides. Hexagonal pyrite is rare at Thalanga. The large electrum grain occurs in galena. Sample TH209-86.5b. Central Thalanga.

(d) Rounded grains of sphalerite in galena. Small sphalerite>chalcopyrite grains are intergrown with galena at the contact between sphalerite and galena. Sample TH209-86.5a. Central Thalanga.

(e) Intergrown sphalerite, galena and minor tetrahedrite at margin of sphalerite grains. Sample E3204SI13-39.1. East Thalanga.

(f) Chalcopyrite "disease": chalcopyrite inclusions along grain boundaries and cleavage plains in sphalerite. Sample TH208-74.6. Central Thalanga.

(g) Chalcopyrite in brittle fracture through sphalerite grains. Irregular arsenopyrite is intergrown with chalcopyrite in places along the fracture. Sample TH29-294.8. Central Thalanga.

(h) Growth twins in recrystallised sphalerite (sample etched by H_2SO_4 and $KMnO_4$ solution). Sample TH239-146.2, Central Thalanga.

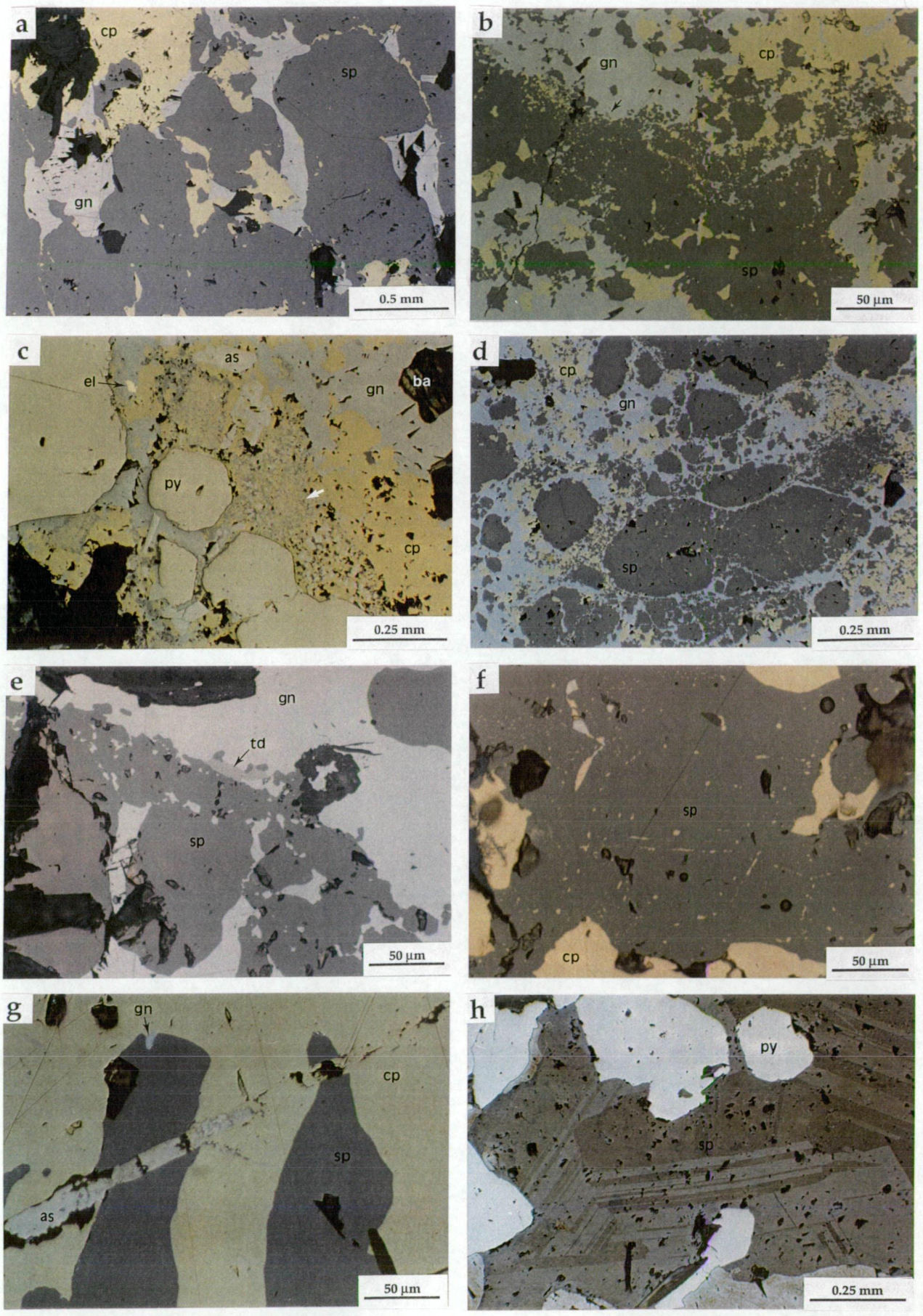
a
cp
sp
gn
0.5 mm
b
gn
cp
sp
50 µm
c
as
el
gn
ba
py
cp
0.25 mm
d
cp
gn
sp
0.25 mm
e
gn
td
sp
50 µm
f
sp
cp
50 µm
g
gn
cp
sp
as
50 µm
h
py
sp
0.25 mm

the triple points. It appears that the effect of metamorphic recrystallisation has been to increase the grainsize of sphalerite, and to cause less abundant co-existing minerals trapped between the coarsened sphalerite to have migrated towards the enclosing, less competent sulphides or triple point junctions.

Sphalerite at Thalanga typically contains abundant chalcopyrite inclusions (chalcopyrite disease of Barton and Bethke, 1987), particularly along cleavage planes and grain contacts (Fig. 7.1f). Chalcopyrite inclusions are generally more abundant in darker coloured (Fe-rich) sphalerite than in pale coloured (Fe-poor) sphalerite. Huston (1991) suggested that the incidence of chalcopyrite disease in sphalerite at Thalanga should decrease with greater degrees of metamorphic recrystallisation. However, even the most coarsely recrystallised and remobilised sphalerite at Thalanga contains chalcopyrite inclusions.

Experimental work and textural studies of Wiggins and Craig (1980), Barton and Bethke (1987), Eldridge *et al.* (1983), Scott (1983) and Bortnikov *et al.* (1991) have shown that fine-grained inclusions of chalcopyrite within sphalerite are not exsolution textures, but are indicative of the replacement of sphalerite during recrystallisation, following reaction between sphalerite and Cu and Fe-bearing solutions. However, Bortnikov *et al.* (1991) also suggested that chalcopyrite disease could also form by the co-precipitation of chalcopyrite and sphalerite. High temperature (400-750 °C) synthetic production of chalcopyrite disease by Bente and Doering (1993) only occurred in Fe-rich sphalerite and not Fe-poor sphalerite, in contrast to the observations of Bortnikov *et al.* (1991) who reported natural chalcopyrite inclusions in Fe-rich and Fe-poor sphalerite. Bente and Doering (1993) concluded that chalcopyrite disease will form only in Fe-rich sphalerite if the Cu-bearing fluid has a higher sulphur fugacity than the solution that sphalerite was deposited from. Therefore at Thalanga, where chalcopyrite is inferred to have been remobilised and recrystallised with sphalerite, chalcopyrite is inferred to have precipitated from Cu-bearing solutions, with high sulphur fugacity, and partly replaced sphalerite along cleavage planes.

Deformed sphalerite is rare at Thalanga, with recrystallised sphalerite typically concentrated in areas of extension within the mineralised horizon. Rare brittle fractures are filled with chalcopyrite (Fig. 7.1g). Etching of sphalerite with $KMnO_4$ and H_2SO_4 (using the methods outlined in Raymond, 1992) has revealed equant grains with undeformed growth twins (Fig. 7.1h). Such textures are present in both remobilised and non-remobilised sphalerite at Thalanga, supporting the interpretation that sphalerite recrystallisation post-dated deformation.

Sphalerite in the banded sulphide lenses at Thalanga varies in colour from dark red-brown to pale yellowish- or tan-brown in plane light (Fig. 7.2a). Golden-yellow to colourless sphalerite is associated with massive pyrite at the base of the ore lens in Central Thalanga,

Figure 7.2 Photomicrographs of deformed, metamorphosed and recrystallised sphalerite, galena and pyrite (under reflected light unless otherwise stated).

(a) Straw yellow to orange-red sphalerite in a quartz-chalcopyrite-sphalerite vein. Chlorite gangue. Sample UG-12. Central Thalanga. Transmitted light.

(b) Pale yellow to colourless sphalerite intergrown with pyrite, phlogopite and chlorite (after phlogopite). Sample T16-11.5. Central Thalanga. Transmitted light.

(c) Fractures in anhedral pyrite grains filled (replaced?) with galena. Finely intergrown chalcopyrite>galena-sphalerite-tetrahedrite also present along fractures in pyrite grains. Sample E3204SI13-54.5. East Thalanga, footwall lens.

(d) Folded cleavage pits in galena between pyrite grains. Sample TH258-132. Central Thalanga.

(e) Folded cleavage pits in galena between pyrite grains. Sample TH209-86.5b. Central Thalanga.

(f) Annealed (or foam) texture in massive to semi-massive pyrite, with quartz and chlorite gangue. Minor chalcopyrite and galena is present along grain boundaries. Sample E3207SI02-56. East Thalanga, hangingwall lens.

(g) Massive pyrite with irregular to bulging grain boundaries and some 120° grain boundaries. Sample TH257-100.5. Central Thalanga.

(h) Euhedral pyrite grains disseminated in intergrown chlorite and phlogopite. Sample TH21-292.5. Central Thalanga.

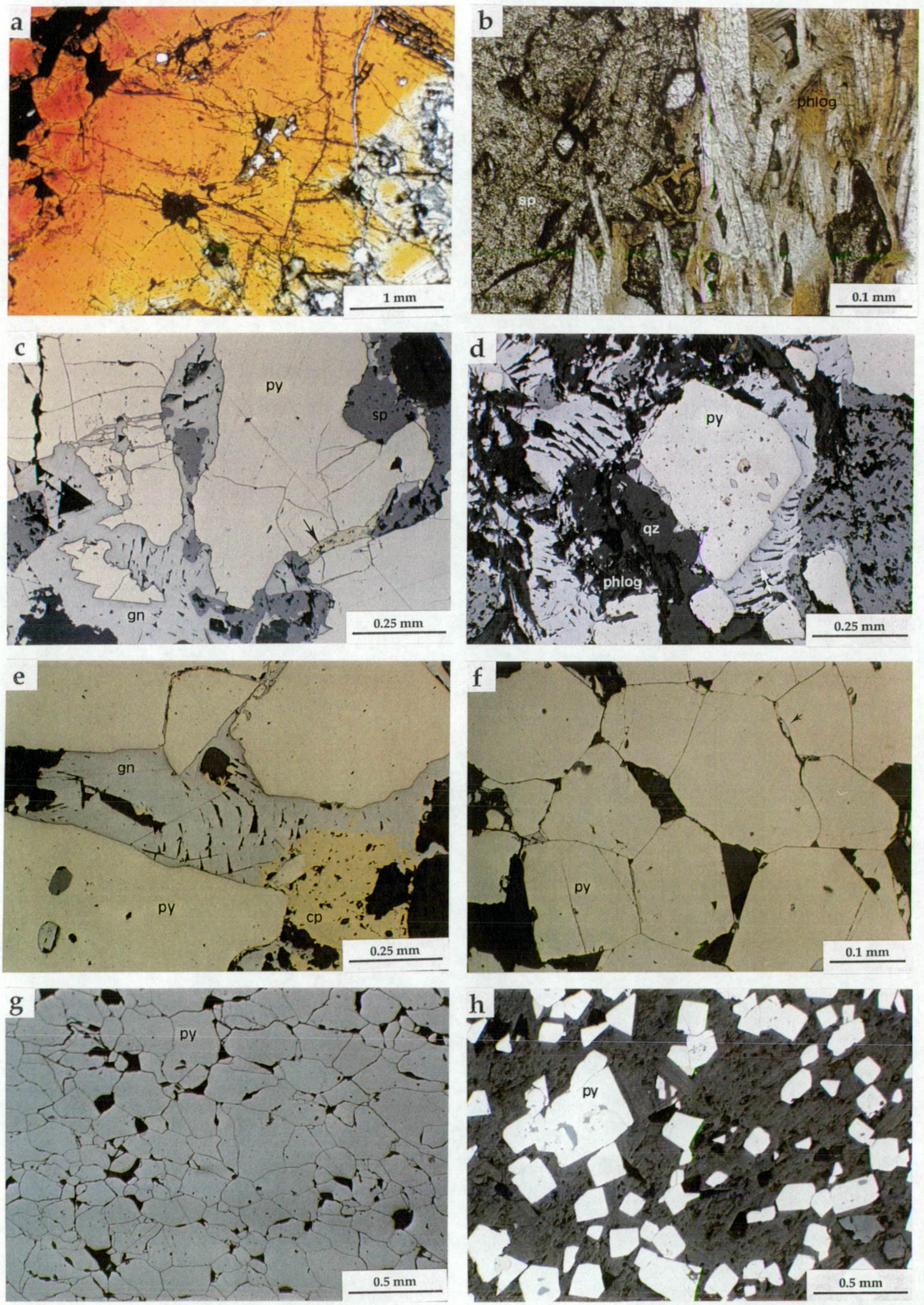
a
1 mm
b
phlog
sp
0.1 mm
c
py
sp
gn
0.25 mm
d
py
qz
phlog
0.25 mm
e
gn
py
cp
0.25 mm
f
py
0.1 mm
g
py
0.5 mm
h
py
0.5 mm

and with pyrite disseminated in the footwall (Fig. 7.2b). Sphalerite within the overlying massive to banded sulphides is typically honey brown coloured. Golden-tan sphalerite is associated with tremolite at the contact between calcite inclusions and massive sulphides that containing red to honey brown sphalerite. Remobilised sphalerite varies from orange to dark red-brown in colour (Fig. 7.2a), but is typically dark red-brown. Such variation in sphalerite colour has long been attributed to variation in Fe content, with the darker colours usually associated with Fe-rich sphalerite (Mookherjee, 1964; McDonald, 1967; Mookherjee, 1976; Brooker *et al.* 1987).

7.2.2 *Sphalerite Composition*

Fe Content of Sphalerite

A total of 97 sphalerite grains from the Thalanga deposit were analysed by microprobe in order to determine the Fe content of the sphalerite. The results are tabulated in Appendix G. Close-spaced chalcopyrite inclusions were avoided during probing, and at most analysis sites, the total Cu recorded was less than the detection limit of Cu (165 ppm Cu at the 95 % confidence level). Despite this, all Cu in each analysis was assumed to be due to the presence of finely disseminated chalcopyrite, and the equivalent moles of Fe were deducted from the total Fe in order to remove the effect of chalcopyrite.

The FeS content of all sphalerite grains analysed ranges from 1.3 to 16.1 mole % FeS (Fig. 7.3a; Table 7.1). Sphalerite grains within the massive sulphide lenses in East Thalanga have a broad spread of FeS contents, with median FeS = 7.1 mole % (Table 7.1). This contrasts with the distribution of FeS content of sphalerite in West and Central Thalanga, where the compositional range is similar , but a weak bimodal distribution of FeS content is present (Fig. 7.3b). The two populations (group I and group II; Table 7.1) have ranges of about 1-6 mole % and about 8-12 mole % FeS. Sphalerite with the highest FeS composition occurs as inclusions in pyrite, and therefore is interpreted to have re-equilibrated with pyrite during recrystallisation. Sphalerite with the lowest amount of Fe (<2 mol% FeS) is intergrown with chalcopyrite and barite that are interstitial to massive pyrite, but the analysis sites were not immediately adjacent to pyrite.

The FeS contents of sphalerite disseminated within the chlorite schist in West Thalanga and the chlorite-rich footwall alteration in East Thalanga fall into two similar populations (Fig. 7.3c; Table 7.1). The FeS contents of sphalerite grains within the remobilised quartz-chalcopyrite-sphalerite vein and the quartz-epidote-sulphide veins present in the hangingwall at the Thalanga deposit also have a bimodal distribution of compositions (Fig. 7.3d). Golden yellow sphalerite grains in the remobilised quartz-chalcopyrite-sphalerite vein (no pyrite) have FeS contents ranging from 4.9 to 7.7 mole %, whereas dark red brown

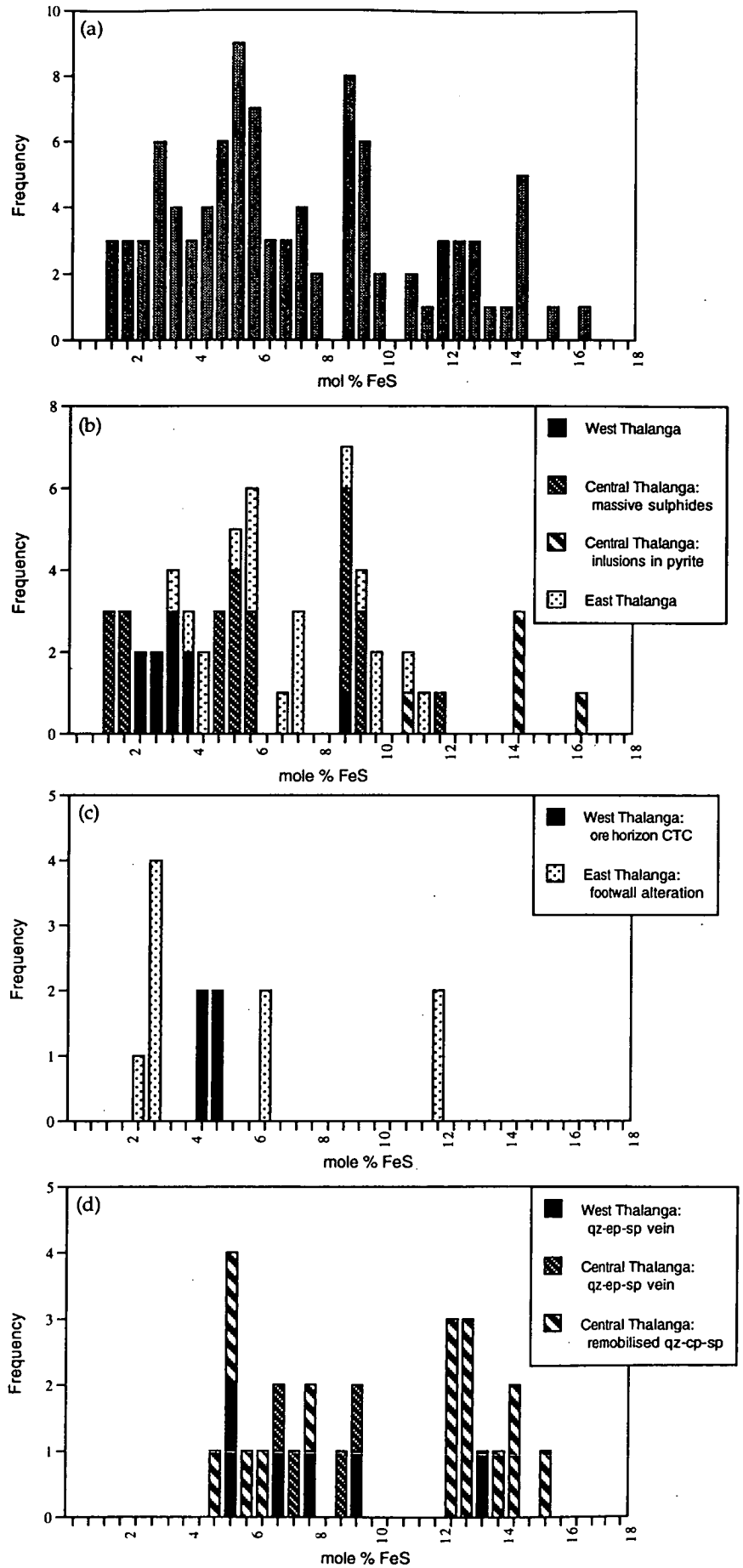

Figure 7.3 Frequency graphs of the FeS content of sphalerite at the Thalanga deposit, (a) all analyses, (b) sphalerite within the massive sulphide lenses, (c) sphalerite disseminated in chlorite-rich assemblages, and (d) sphalerite in qz-ep and remobilised sulphide veins in the overlying dacite.

sphalerite contains 12 to 15.3 mole % FeS (Table 7.1), thus supporting the association of higher Fe contents with darker coloured sphalerite. Pyrite is not intergrown with this remobilised Fe-rich sphalerite, but minor chalcopyrite, galena and Fe-rich chlorite are present.

Table 7.1 Summary of the Fe content of sphalerite from the Thalanga deposit (data in Appendix G).

Rock Type	No. of Analyses	Min.	Max.	Mean	Median
Massive sulphides:					
West Thalanga	10	2.4%	8.8%	3.6%	3.1%
group I	9	2.4%	3.9%	3.1%	3.0%
Central Thalanga	25	1.3%	11.7%	5.8%	5.5%
group I	16	1.3%	5.8%	3.9%	4.8%
group II	9	8.6%	11.7%	9.2%	9.0%
East Thalanga	18	3.4%	11.1%	7.0%	7.1%
Sphalerite inclusions in pyrite (remobilised ore)	5	10.7%	16.1%	13.9%	14.4%
Chlorite-rich alteration:					
West Thalanga (chlorite schist)	4	4.4%	4.9%	4.6%	4.6%
East Thalanga (footwall alteration)	9	2.3%	11.9%	5.4%	2.9%
group I	5	2.3%	2.9%	2.6%	2.6%
group II	4	6.0%	11.9%	8.9%	8.9%
Remobilised sulphides:					
West Thalanga (qz-ep-sp vein)	6	5.4%	13.3%	7.9%	7.3%
Central Thalanga					
qz-ep-sp vein	4	6.9%	9.0%	8.1%	8.2%
qz-cp-sp vein: group I	6	4.9%	7.7%	5.9%	5.7%
qz-cp-sp vein: group II	10	12.0%	15.3%	13.2%	12.6%

Abbreviations: cp = chalcopyrite, ep = epidote, min. = minimum, max. = maximum, qz = quartz, sp = sphalerite

These results demonstrate that the darkest coloured and most Fe-rich sphalerite (12 to 16 mole % FeS) at Thalanga occurs with massive chalcopyrite and in the quartz-chalcopyrite veins that are interpreted to have been remobilised during deformation (Chapter 3). The remaining two populations approximately correspond to the two main colour variations of sphalerite within the massive sulphides at Thalanga: pale yellow sphalerite has Fe contents of about 1 to 6 mole % FeS, and honey sphalerite has FeS = 8 to 12 mole %.

Bimodal distribution of FeS contents of sphalerite inclusions in pyrite has been reported from the Cherokee deposit, Tennessee, where sphalerite-only inclusions are composed of sphalerite with the highest FeS, whereas low FeS sphalerite is present with chalcopyrite or cross-cut by fractures (Brooker *et al.*, 1987). Sphalerite with high FeS contents is interpreted to have equilibrated at peak metamorphic temperatures and pressures, and the low FeS sphalerites are interpreted to have lost Fe during retrograde metamorphism due to re-equilibration at lower temperatures (Brooker *et al.*, 1987). At Thalanga, the *in situ* FeS-rich sphalerite is interpreted to have re-equilibrated with pyrite at the peak of metamorphism. The population with the lowest FeS values (the palest sphalerite grains) could have retained the original, unmetamorphosed sphalerite compositions, or may be due to the distance of the analysis site from pyrite. Sphalerite with FeS values between the two peak

values could be the product of incomplete re-equilibration of the sphalerite during retrogression, as suggested by Brooker *et al.* (1987) for the Cherokee deposit. Given the difference in Fe contents between the *in situ* and remobilised sphalerite, the remobilised Fe-rich sphalerite is likely to have gained Fe during remobilisation and re-equilibrated during peak metamorphism.

Relationship Between Fe Content of Sphalerite and Au content of the Ore Lens

Hannington and Scott (1987) suggested that the Au content of a massive sulphide deposit is related to the Fe content of co-existing sphalerite. At Thalanga, elevated Au contents are common in massive sulphide lenses that contain pale yellow, low Fe sphalerite, and Au-poor massive sulphides contain honey-coloured, Fe-rich sphalerite (Fig. 7.4). However, elevated Au is also present within ore lenses that contain Fe-poor sphalerite (cf. samples TH54 -189.6 and T16-11.5, Fig. 7.4), and high grades of Au are present in some remobilised chalcopyrite-rich sulphides that contain Fe-rich sphalerite (Fig. 7.4). Therefore there is no relationship between Fe content of sphalerite and the Au grade at Thalanga. Metamorphism may have destroyed any relationships, or perhaps the low total Au content of Thalanga (0.62g/t; Chapter 1) makes the relationship between Au and the Fe content of co-existing sphalerite difficult to predict.

7.2.3 Sphalerite Geobarometry

The FeS content of sphalerite varies with temperature, pressure and FeS activity, but at temperatures of 300-600 °C, and where buffered by pyrite and pyrrhotite, the FeS content of sphalerite decreases with increasing pressure (Barton and Toulmin, 1966; Scott and Barnes, 1971; Scott, 1973, 1976; Scott *et al.*, 1977; Hutchinson and Scott, 1981; Bryndzia *et al.*, 1988, 1990). This makes the FeS content of sphalerite a useful geobarometer where sphalerite co-exists with pyrite and pyrrhotite (e.g. Sundblad *et al.*, 1984; Brown, 1994; Cook *et al.*, 1994).

Using the recalculated sphalerite geobarometer of Toulmin *et al.* (1991) at Thalanga, for FeS compositions of sphalerite-only inclusions in pyrite (which also contains pyrrhotite-only inclusions), indicates that at metamorphic temperatures of 400-450°C, the pressures were in the range 3-6.5 kbars. At temperatures of 450-500°C, the pressure estimate is 4-7 kbars. This estimate is higher than the pressure determined from a garnet-phlogopite-muscovite-chlorite assemblage within the footwall rhyolitic volcanics (1-4 kbars; Chapter 3). Although Scott (1983) and Brooker *et al.* (1987) used the Fe content of sphalerite-only inclusions in pyrite to provide reasonable estimates of the pressure conditions of metamorphism at the Cherokee deposit, Tennessee, more recent work by Cook *et al.* (1994) has shown that only sphalerite that co-exists with both pyrite and pyrrhotite will provide geologically sensible pressure estimates. Therefore, the lack of co-existing sphalerite, pyrite,

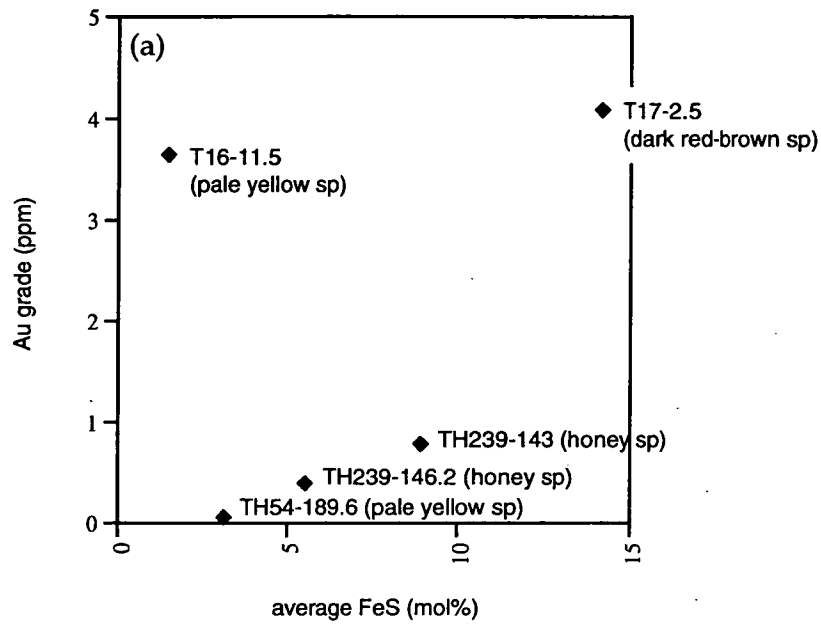

Figure 7.4 Comparison of the FeS content of sphalerite with the Au content of the massive sulphides. FeS values represent averaged probe analyses of individual sphalerite grains, and metal grades represent whole rock assays of drill core intervals of 0.5 to 1 m in length. Samples are from the ore lenses in West and Central Thalanga, and each represents the average of 4 to 9 sphalerite analyses:

T16-11.5: massive py with interstitial sp (pale yellow) and gn.
T17-2.5: massive cp (remobilised?) with sp inclusions in coarse py.
TH54-189.6: bands of massive sp-gn-py and minor cp overprinting dolomite.
TH239-143: typical massive sp-py>gn, minor cp, weakly banded.
TH239-146.2: typical massive sp-py>gn, trace cp.

and pyrrhotite in the ore lenses at Thalanga explains the over-estimated metamorphic pressure conditions calculated from the FeS composition of sphalerite.

7.3 Galena

7.3.1 Galena Textures

Galena has lobate contacts with sphalerite and chalcopyrite, and occurs interstitial to rounded sphalerite grains and euhedral pyrite (Fig. 7.1a-e). Galena is typically less abundant in the massive sulphide lenses than sphalerite and constitutes about 5–15 % of most thin sections examined from the polymetallic ore lenses at Thalanga. Individual galena grains are anhedral, have 120° dihedral grain boundaries, and are typically undeformed. The presence of galena along fractures in pyrite grains (Fig. 7.2c), in pressure shadows around rigid clasts and crystals, and in necks of boudins is interpreted to indicate that galena was remobilised during deformation, but prior to metamorphic recrystallisation. Evidence of deformation of galena grains has probably been mostly obliterated by the recrystallisation annealing. However, rare deformed galena is preserved between euhedral pyrite grains (Fig. 7.2d,e).

Tetrahedrite-tennantite inclusions are present in galena in many parts of the Thalanga deposit, and bismuth inclusions occur in coarsely recrystallised galena. This mineralogical association is responsible for the association between Pb and Ag (Chapter 8), and the strong correlation between Pb and Sb observed in whole-rock analyses (R.A. Sainty, writt. comm., 1991). Tetrahedrite-tennantite may have exsolved from the galena during cooling, probably from peak metamorphism.

7.3.2 Composition of Galena

Several galena grains from West, Central, and East Thalanga were analysed by microprobe in order to determine their Ag, Sb and Bi content (Appendix G). The Ag content of galena at Thalanga varies from about 0.03 to 0.29 weight %, but is relatively uniform within individual grains on the scale of a thin section. In contrast, Plimer (1980) reported that the Ag content of galena from the Broken Hill deposit varied from 0.05 to 0.12 % Ag within single grains. The Sb content of galena varies from negligible to <0.17 weight % Sb, and Bi content varies in proportion to Ag content from 0.2 to 0.9 weight % (Appendix G). The uniform composition of galena at Thalanga is probably due to homogenisation during metamorphism.

7.4 Pyrite

7.4.1 Pyrite Textures

Anhedral, euhedral, and porphyroblastic (metablastic) pyrite are the most common textures of pyrite at Thalanga (Table 7.2). These textures are similar to pyrite from other metamorphosed and deformed massive deposits (e.g. the Balcooma deposit, Queensland, Huston *et al.*, 1992b; the Vangorda deposit, Canada, Brown and McClay, 1993; the Matchless deposit, Namibia, Cook *et al.*, 1994; the Mobrun deposit, Canada, Larocque and Hodgson, 1995). Triple point grain boundaries that occur in regions of massive pyrite at Thalanga (Fig. 7.2f) are indicative of metamorphic recrystallisation, although in some places, grain boundaries are irregular rather than planar (Fig. 7.2g). Such annealed pyrite textures are comparable to the "foam" texture of Stanton (1964, 1972). The preferred metamorphic pyrite texture at Thalanga depends on the percentage of associated sulphides or gangue (Table 7.2). Craig and Vokes (1993), in a review of the effects of metamorphism on pyritic ores, also found that euhedral pyrite is associated with abundant co-existing sulphides, whereas anhedral pyrite formed with small amounts of co-existing sulphides.

Table 7.2 Typical textures of metamorphosed pyrite from the Thalanga deposit

Pyrite Texture	Associated minerals	Effect of Deformation
• Euhedral pyrite (Fig. 7.2h; but see Fig. 7.5a,b)	• abundant chlorite ± phlogopite, • abundant muscovite ± quartz, or • abundant chalcopyrite	• grains are elongated parallel to cleavage, • quartz, chlorite, or chalcopyrite-filled pressure shadows
• Porphyroblasts (metablasts) of pyrite (Fig. 7.5c)	• abundant sphalerite, galena, chalcopyrite-rich sulphides	• some cataclastic deformation: fractures filled with chalcopyrite or galena
• Annealed anhedral pyrite (Fig. 7.2f)	• few to no other minerals, • trace chalcopyrite, rare sphalerite or galena in interstices	• grains are elongated parallel to cleavage, • cataclastic deformation: fractures filled with chalcopyrite or galena

The morphology of rounded, subhedral to anhedral pyrite grains disseminated in regions of massive sphalerite may be partly due to the replacement of pyrite by sphalerite (Fig. 7.5a). Cuspate pyrite grains enveloped by sphalerite are also interpreted to be the result of replacement of pyrite by sphalerite (Fig. 7.5a). Rare examples of pre-existing pyrite with poikiloblastic margins (galena inclusions) that has been partly replaced by sphalerite are shown in Figure 7.5(a,b). In many parts of the polymetallic massive sulphides at Thalanga, pyrite has been enclosed by galena and chalcopyrite, and then by sphalerite (Fig. 7.5c,e), and in most places the pyrite is porphyroblastic to poikiloblastic (Fig. 7.5c,d). Rare examples of pyrite that has been partly replaced by chalcopyrite are preserved (Fig. 7.5e). Spheroidal

Figure 7.5 Photomicrographs of pyrite from Thalanga (under reflected light).

(a) Subhedral to anhedral pyrite disseminated in massive sphalerite. Note the angular to cuspate shape of the pyrite grain at left (arrow). Small inclusions of sphalerite are present in the core of the largest pyrite grain. Sample E3204SI13-37.4. East Thalanga, footwall lens.

(b) Close-up of pyrite grain in centre of (a) showing galena inclusions at margin of pyrite that have been overprinted by sphalerite. Sample E3204SI13-37.4. East Thalanga, footwall lens.

(c) Pyrite porphyroblast with large galena-filled inclusion and embayed margin. Sphalerite has partly replaced pyrite near the embayment. Sample TH239-146.2. Central Thalanga.

(d) Poikiloblastic pyrite grain with sphalerite and galena inclusions and embayments at its margin. These phases are contained within a galena-rich band in massive sulphides. Sample TH209-86.5a. Central Thalanga.

(e) Anhedral pyrite grain partly replaced by chalcopyrite and minor galena along fractures. Chalcopyrite and minor galena has engulfed the pyrite grain and are contained within coarse sphalerite grains and tremolite gangue. Sample W2011ND50-47.2. West Thalanga, massive sulphide clast in QEV.

(f) Recrystallised pyrite framboids and euhedral pyrite, contained within anhedral chalcopyrite, from the pyrite-chalcopyrite rich parts of the ore lens. Sample TH230-110. Central Thalanga.

(g) Close-up of recrystallised pyrite framboids in (f).

(h) Spheroidal pyrite (recrystallised framboid?), with chalcopyrite and tetrahedrite along fractures in radiating pyrite rim. Calcite is present in the core. Sample TH230-110, Central Thalanga.

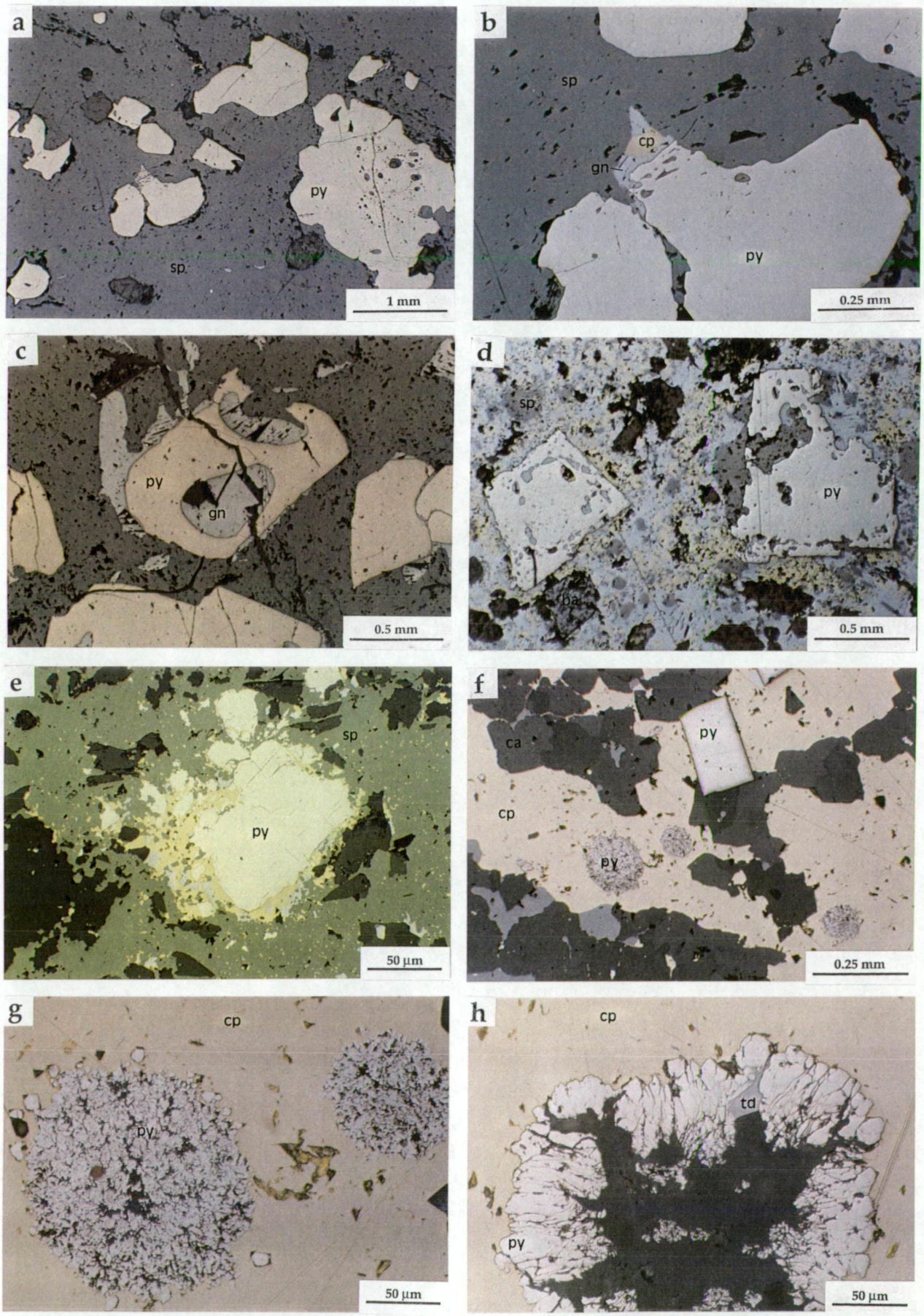
a
py
sp
1 mm
b
sp
cp
gn
py
0.25 mm
c
py
gn
0.5 mm
d
sp
py
ba
0.5 mm
e
sp
py
50 µm
f
ca
py
cp
py
0.25 mm
g
cp
py
50 µm
h
cp
td
py
50 µm

pyrite, interpreted to be recrystallised pyrite framboids (Fig. 7.5f-h), is uncommon, and occurs in pyrite-chalcopyrite-rich, basal parts of the ore lens.

Most pyrite grains contain fine grained (≤0.5 mm), wormy to spherical inclusions of sphalerite, galena, chalcopyrite ± cubanite and, rarely, pyrrhotite (Fig. 7.5a,b). The distribution of inclusions suggests that at least two stages of pyrite deposition may have occurred, because inclusion-rich cores have been encrusted by inclusion-free euhedral rims (Fig. 7.5a). Sphalerite, galena, chalcopyrite and cubanite occur together within single polymetallic inclusions in places. Rare bismuth inclusions are present within coarsely recrystallised pyrite associated with remobilised chalcopyrite. Pyrrhotite inclusions in the recrystallised pyrite are aligned, and are interpreted to have been deposited along annealed fractures. Euhedral magnetite inclusions are also present in coarse pyrite crystals. Some pyrite metablasts have sphalerite-, galena- or chalcopyrite-filled embayments where intergrown with sphalerite, galena, and chalcopyrite (Fig. 7.5c). Rare marcasite has replaced pyrite along fractures.

7.4.2 Textures of Deformed Pyrite

In general, pyrite grains are undeformed. However, local brittle deformation textures occur in euhedral pyrite within the pyrite-rich parts of Thalanga, and either galena or chalcopyrite are present along fractures within the pyrite (Fig. 7.6a,b). Chalcopyrite-filled pressure shadows around pyrite euhedra disseminated in the QEV at Thalanga are interpreted to indicate that pyrite behaved rigidly during deformation (Fig. 3.21e). Rare plastic deformation textures are present where pyrite is disseminated in the footwall rhyolitic volcanics or chlorite schists: pyrite is elongated parallel to S_2, and quartz or chlorite occupy the pressure shadows (Fig. 3.20d).

In other deformed massive sulphide deposits, pyrite is typically cataclastically deformed due to the high temperatures and pressures required to reach the brittle-ductile transformation boundary for pyrite (450°C and 300 MPa; Atkinson, 1975; Cox *et al.*, 1981; Marshall and Gilligan, 1987; Cook *et al.*, 1994). Based on a review of experimental studies, Marshall and Gilligan (1987) found that temperatures in excess of 550 °C are required to recrystallise pyrite. Typically sulphides such as galena, chalcopyrite, and in some cases sphalerite, that have ductile deformation textures, fill fractures and extension sites in highly fractured pyrite (Vokes and Craig, 1993).

McClay and Ellis (1984) concluded, by examination of natural pyritic ores, that pressure solution and cataclasis are the main mechanisms of pyrite deformation at temperatures <300°C. At higher temperatures, and under conditions of high fluid pressure, dislocation creep or solution-precipitation creep is considered to produce ductile deformation textures in

Figure 7.6 Photomicrographs of chalcopyrite textures at Thalanga (under reflected light).

(a) Chalcopyrite-filled fractures in anhedral pyrite form the base of a graded QEV sandstone. Sample E3208SI15-60. East Thalanga, hangingwall lens.

(b) Chalcopyrite and finely intergrown chalcopyrite-sphalerite-galena-tetrahedrite within fractured pyrite. Sample E3204SI13-54.5. East Thalanga, footwall lens.

(c) Euhedral pyrite intergrown with tremolite in massive to semi-massive sulphides. Stibnite is disseminated through the anhedral grains of chalcopyrite and sphalerite. Sample W2031ND07-66.9b. West Thalanga.

(d) Fine-grained chalcopyrite and bornite present at the contact between sphalerite and galena. Sample TH239-146.2. Central Thalanga.

(e) Contact between sphalerite and galena, with minor chalcopyrite and tetrahedrite. Sample E3204SI13-47.1. East Thalanga, footwall lens.

(f) Chalcopyrite and trace of magnetite that have partly replaced euhedral pyrite (hosted in massive chlorite). Sample CT-91-28. Central Thalanga.

(g) Growth twins in etched chalcopyrite grains from a quartz-chalcopyrite-sphalerite vein. Etching has revealed that arsenopyrite is present at the boundaries between chalcopyrite grains. Sample UG-12. Central Thalanga.

(h) Cubanite exsolution lamellae in chalcopyrite. Sample TH260-206.2. Central Thalanga.

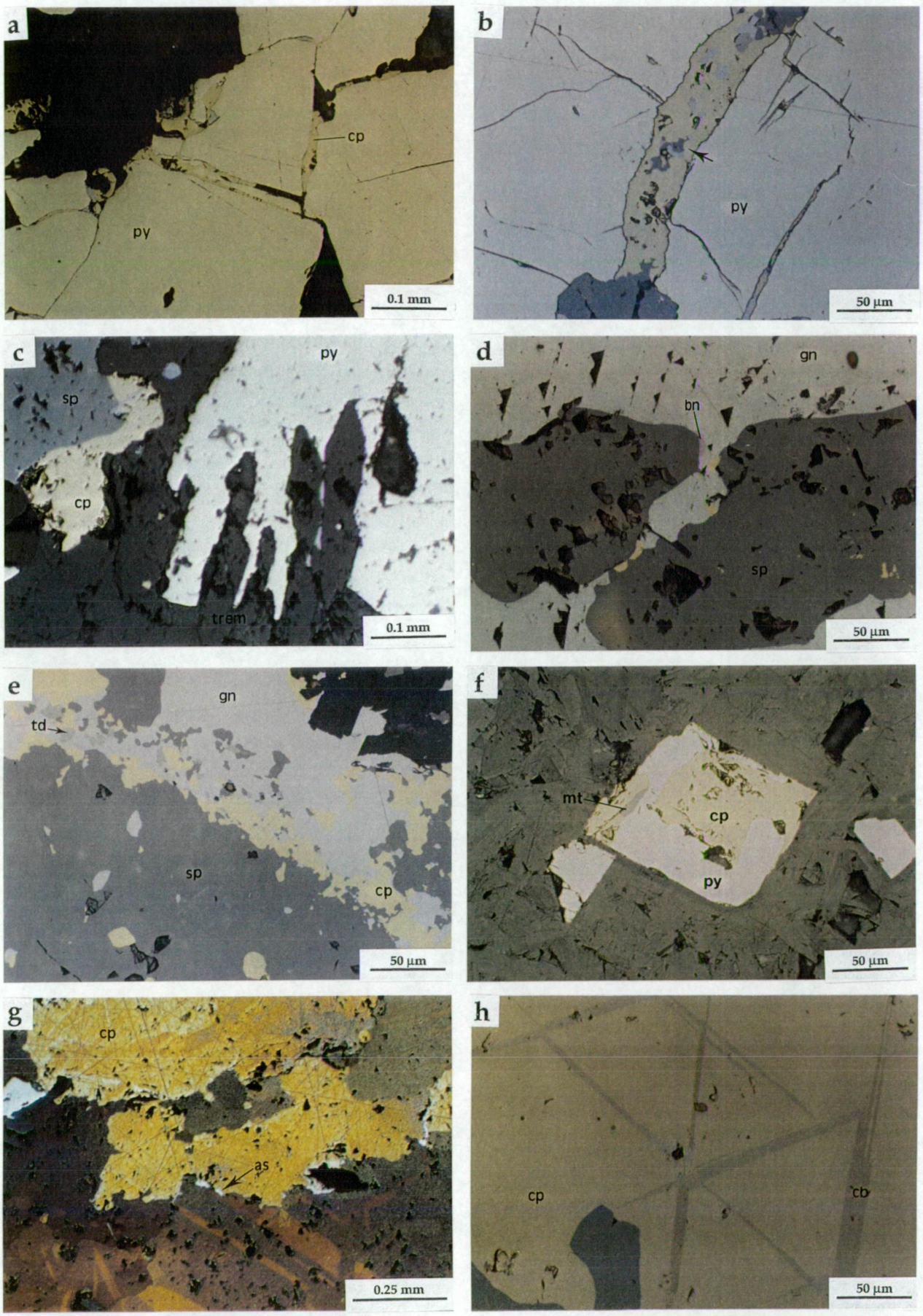
a
cp
py
0.1 mm
b
py
50 µm
c
py
sp
cp
trem
0.1 mm
d
gn
bn
sp
50 µm
e
gn
td
sp
cp
50 µm
f
mt
cp
py
50 µm
g
cp
as
0.25 mm
h
cp
cb
50 µm

pyrite (Cox *et al.*, 1981; Cox, 1987). In particular, pyrite disseminated through silicate host rocks is predicted to deform via solution-precipitation creep (Cox, 1987; Marshall and Gilligan, 1987), and therefore, pyrite elongated parallel to S_2 in the footwall at Thalanga is interpreted to have recrystallised during D_2 deformation by this mechanism (ie. syn-tectonic recrystallisation). Intergrowths of pyrite and tremolite porphyroblasts at Thalanga indicate contemporaneous (re)crystallisation during metamorphism (Fig. 7.6c).

7.5 Chalcopyrite

Chalcopyrite is present as irregular bands subparallel to sphalerite-pyrite bands within the massive sulphides, and in veins that overprint massive pyrite at the stratigraphic base of the ore lens in Central and West Thalanga. Massive chalcopyrite is associated with sphalerite and buck quartz at the contact between the massive sulphides and the overlying dacite in Central Thalanga and parts of West Thalanga. Chalcopyrite has typically infilled extension sites within the mineralised horizon, including tension gashes, boudins necks, and pressure shadows. The chalcopyrite is commonly annealed and brittle fractures are rare.

Chalcopyrite is interstitial to pyrite grains in regions of massive pyrite, and occurs as irregular grains intergrown with fined grained (<0.5 mm), myrmekitic galena, arsenopyrite and tetrahedrite-tennantite (Fig. 7.1c). Small grains of chalcopyrite are common at the boundaries between sphalerite and galena (Fig. 7.6d), locally in association with tetrahedrite-tennantite (Fig. 7.6e). In rare places, chalcopyrite ± magnetite ± calcite has replaced pyrite euhedra (Fig. 7.6f). Irregular grains of arsenopyrite occur at the margins of chalcopyrite grains within domains of remobilised chalcopyrite (Fig.7.6g).

Irregular blebs and exsolution lamellae of cubanite are common within remobilised chalcopyrite at Thalanga (Fig. 7.6h). Cubanite is thought to exsolve from chalcopyrite during cooling due to of high Fe contents in the chalcopyrite structure (Deer *et al.*, 1966). At Thalanga, excess Fe may have been incorporated into chalcopyrite during sulphide remobilisation, and cubanite is interpreted to have exsolved during post-peak metamorphic cooling.

The low temperatures required to remobilise chalcopyrite (200°C; Kelly and Clark, 1975) mean that the distribution of chalcopyrite in metamorphosed and deformed massive sulphide deposits is typically structurally controlled. For example, chalcopyrite is present in fold hinges and piercement structures at the hangingwall-ore lens boundary in the Matchless Cu deposit, Namibia, whereas the pyrite lens is stratiform (Adamson and Teichmann, 1986; Maiden *et al.*, 1986). Chalcopyrite that has infilled pressure shadows around pyrite grains at Mount Lyell, Tasmania, is interpreted to have been mobilised (from a distance of several

grain diameters) into extension sites via solution-precipitation creep (Cox, 1987). These textures are similar to the location of chalcopyrite at Thalanga.

7.6 Magnetite

Euhedral magnetite grains are present at the margins of chalcopyrite, sphalerite and rarely galena grains, particularly where the sulphides are in contact with calcite or other gangue minerals (Fig. 7.7a). This texture could have formed via the partial replacement of chalcopyrite and sphalerite by magnetite. Locally, magnetite has also replaced pyrite (Fig. 7.6f). Magnetite also occurs as disseminations, and as bands, in massive (remobilised) chalcopyrite, where it is associated with calcite and chlorite gangue. Coarse pyrite grains within remobilised chalcopyrite contain euhedral magnetite inclusions. Gregory *et al.* (1990) suggested that the euhedral magnetite at Thalanga was originally colloform. However, there is no textural evidence preserved to support this interpretation. The euhedral shape of the magnetite grains at Thalanga is interpreted here to indicate that magnetite post-dated deformation.

Primary magnetite and deformed/metamorphic magnetite textures have been documented from other VHMS deposits in Australia. Magnetite pseudomorphs of colloform hematite-goethite within the massive sulphides at the Golden Grove deposit (lower to middle greenschist facies) are interpreted to pre-date deformation and metamorphism (Frater, 1985a). In contrast, elongate magnetite crystals that are parallel to phyllosilicate minerals are interpreted to have recrystallised during deformation and metamorphism (Frater, 1985b). Both primary (deformed magnetite stringers, with magnetite recrystallised parallel to S_2) and retrograde magnetite (magnetite after pyrite porphyroblasts and hematite laths) are reported to occur in the Balcooma deposit (Huston *et al.*, 1992b).

7.7 Arsenopyrite

7.7.1 Arsenopyrite Textures

Diamond-shaped euhedral to poikiloblastic arsenopyrite is typically intergrown with chalcopyrite, tetrahedrite-tennantite, minor sphalerite and traces of galena (Fig. 7.7b). The fine-grained intergrowths are confined to rectangular domains, suggesting that the sulphides have replaced a pre-existing mineral. Wills (1985) suggested that the chalcopyrite-arsenopyrite-tetrahedrite/tennantite assemblage had replaced tetrahedrite.

Figure 7.7 Photomicrographs of less common ore minerals in the massive sulphide lenses at Thalanga (under reflected light).

(a) Euhedral magnetite at the contact between calcite and sphalerite, chalcopyrite and galena. Sample TH230-110. Central Thalanga.

(b) Euhedral to poikiloblastic arsenopyrite intergrown with chalcopyrite, tetrahedrite, minor sphalerite and traces of galena. Sample APH-106, West 690 Stope. West Thalanga.

(c) Arsenopyrite and marcasite at the contact between calcite and chalcopyrite. Sample TH239-141.4. Central Thalanga.

(d) Spherical arsenopyrite inclusions in chalcopyrite. The core of the arsenopyrite spheroid has been plucked from the spheroid during sample preparation. Sample TH230-110. Central Thalanga.

(e) Spherical pyrrhotite inclusions in chalcopyrite. Arsenopyrite inclusions are aligned radially within the pyrrhotite. Sample TH239-141.4. Central Thalanga.

(f) Chalcopyrite occurs in fractures (or along grain boundaries) in tetrahedrite at the margins of anhedral chalcopyrite grains. Sample TH230-110. Central Thalanga.

(g) Rectangular-shaped, finely intergrown chalcopyrite-arsenopyrite-tetrahedrite, with tennantite rim. Larger grains of arsenopyrite are arranged radially at the contact between tennantite and the intergrowth of chalcopyrite-arsenopyrite-tetrahedrite. Sample TH209-86.5b. Central Thalanga.

(h) Finely intergrown chalcopyrite, arsenopyrite, tetrahedrite, galena and minor sphalerite. Electrum is present in coarse arsenopyrite grains. Sample TH209-86.5b, Central Thalanga.

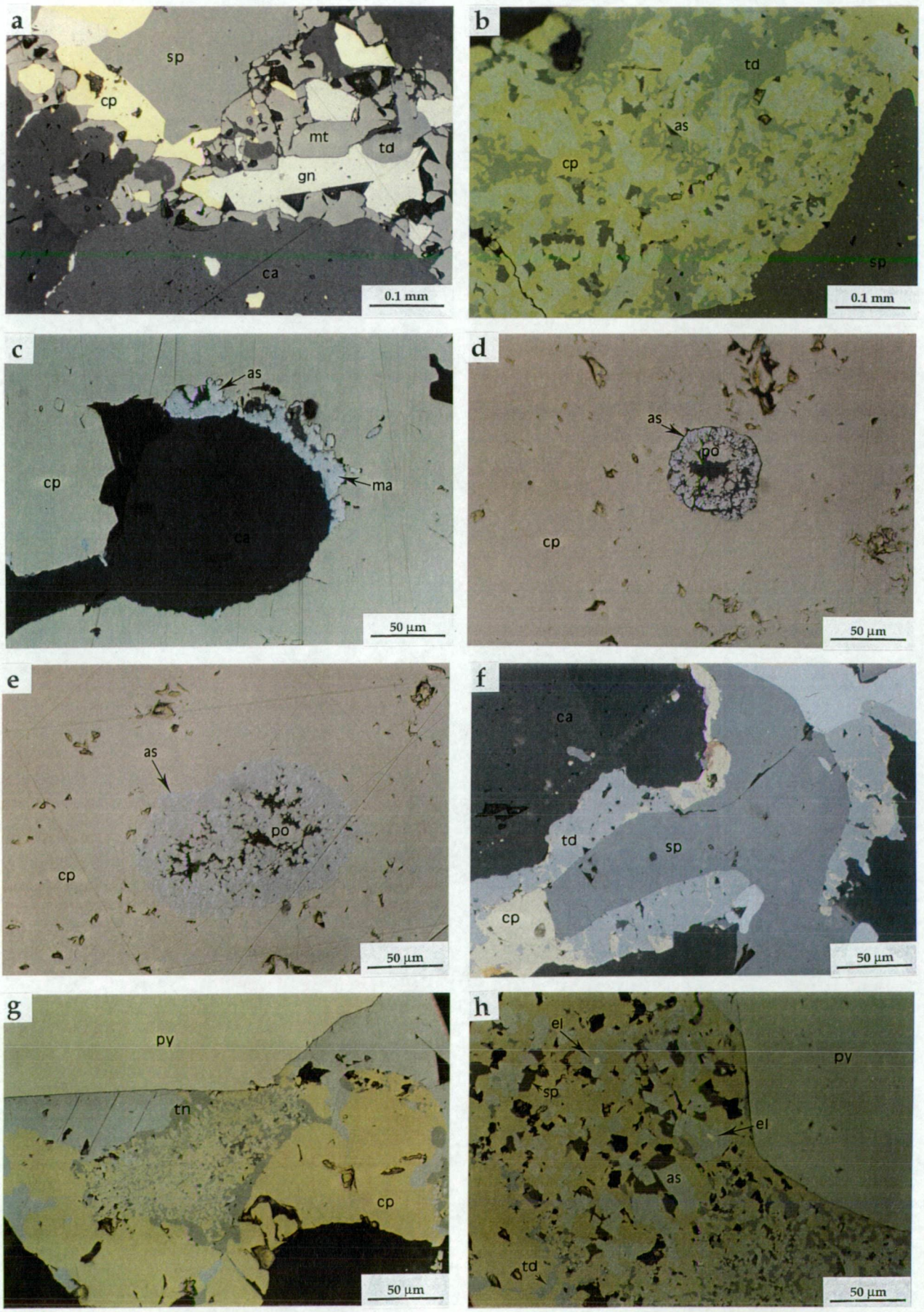
a
sp
cp
mt
td
gn
ca
0.1 mm
b
td
as
cp
sp
0.1 mm
c
as
cp
ma
ca
50 µm
d
as
po
cp
50 µm
e
as
po
cp
50 µm
f
ca
td
sp
cp
50 µm
g
py
tn
cp
50 µm
h
el
py
sp
el
as
td
50 µm

Arsenopyrite porphyroblasts occur at the contact between massive chalcopyrite and gangue minerals (Fig. 7.7c), where the are interpreted to have recrystallised earlier than chalcopyrite. Spheroidal aggregates of arsenopyrite are common in coarse-grained anhedral chalcopyrite within the pyrite-chalcopyrite-rich parts of the ore lenses. The arsenopyrite spheroids have weakly defined radial fractures (Fig. 7.7d), and have been locally replaced by pyrrhotite, with remnant arsenopyrite defining the radial structure of the spheroids (Fig. 7.7e). The spheroidal textures could be the result of point-source nucleation of arsenopyrite.

7.7.2 *Arsenopyrite Geothermometry*

The proportion of As in arsenopyrite that co-exists with sphalerite, pyrite and/or pyrrhotite can be used to calculate temperatures of metamorphism using the graphical techniques of Kretschmar and Scott (1976) and Scott (1983). However, the sulphides must be in equilibrium, and sphalerite that occurs in association with arsenopyrite and pyrite must contain >10 % FeS (Scott, 1983). At Thalanga, arsenopyrite is commonly associated with pyrite, but is in contact with sphalerite at only a few locations. The arsenopyrite at Thalanga contains about 30 atomic % As (determined by microprobe and presented in Appendix G), and this indicates metamorphic temperatures of about 350°C. However, the co-existing sphalerite contains 2.4 -3.9 mole % FeS and therefore this temperature estimate should be treated with caution. Furthermore, this estimate is significantly less than that determined from the metamorphic assemblages in the host stratigraphy (485 ± 23°C; Chapter 3).

7.8 Tetrahedrite-Tennantite

Irregular grains of tetrahedrite-tennantite (or fahlore) are commonly associated with galena in the massive sulphides at Thalanga. Tetrahedrite grains are typically enclosed by galena at contacts between sphalerite and galena grains in most parts of the massive sulphide lenses. Inclusions of galena or chalcopyrite at the margins of poikiloblastic tetrahedrite grains are rare, and in places tetrahedrite appears to have formed later than the associated chalcopyrite (Fig. 7.7f). The presence of tetrahedrite/tennantite inclusions in galena is similar to other massive sulphide deposits, and it has been documented as occurring either near galena-chalcopyrite contacts, as at Broken Hill (Plimer, 1980), or at sphalerite-galena boundaries (e.g. the Woodlawn deposit; McKay and Hazeldene, 1987). Tetrahedrite is an important sources of Ag in many massive sulphide deposits (e.g. Van Hook, 1960; Amcoff, 1976; Jeppsson, 1987; McKay and Hazeldene, 1987), and at Thalanga, tetrahedrite contains about 17 weight % Ag (Appendix G).

Tennantite (confirmed by microprobe) encloses the rectangular domains of fine grained intergrowths of chalcopyrite, arsenopyrite, tetrahedrite-tennantite, and sphalerite that

occur sporadically through the massive sulphide lenses (Fig. 7.7g). Coarse, subhedral grains of arsenopyrite occur between the interlocking chalcopyrite, arsenopyrite, tetrahedrite-tennantite and sphalerite grains and the surrounding tennantite. Similar fine-grained or eutectoid textures of intergrown tetrahedrite-tennantite, arsenopyrite, chalcopyrite and sphalerite surrounded by tetrahedrite-tennantite, have been documented at the Rajpura-Dariba massive sulphide, India (Mookherjee and Mishra, 1984) and at the Kedabek Cu deposit in Azerbaijan (Bortnikov *et al.*,1993). The fine-grained sulphides are interpreted to have formed by the decomposition of a precursor tetrahedrite-tennantite due to change in the activity of S and Sb or As in the residual mineralising fluids (Mookherjee and Mishra, 1984; Bortnikov *et al.*,1993). Earlier workers suggested that such intergrowths formed from tetrahedrite-tennantite in response to pressure changes (Ramdohr, 1980) or cooling (Tarantov and Garvilina, 1969). The enveloping tetrahedrite-tennantite is reported to be undecomposed parent fahlore (Mookherjee and Mishra, 1984). Bortnikov *et al.* (1993) suggested that the decomposition of tennantite was initiated along fractures in tennantite, and that the end-product comprised intergrown chalcopyrite, arsenopyrite, sphalerite and tetrahedrite, rimmed by tennantite.

The decomposition of tennantite at Thalanga could have proceeded during metamorphism according to the reaction:

$$[(Cu, Ag)(Fe, Zn)]_{12}As_4S_{13} = CuFeS_2 + FeAsS + ZnS + [(Cu,Ag)(Fe,Zn)]_{12}Sb_4S_{13}$$

tennantite = cp + asp + sp + tetrahedrite

in the presence of excess Fe, Zn, As, Ag, Sb and S (cf. Bortnikov *et al.*, 1993).

7.9 Electrum

Gold at Thalanga is present mainly as electrum, and most electrum grains have a fineness between 690 and 850 (Huston *et al.*, 1992a). Five occurrences of electrum in the massive sulphides of the Thalanga deposit were recognised by Huston *et al.* (1992a):

i) within fine-grained chalcopyrite-arsenopyrite-tetrahedrite-tennantite intergrowths, where the coarsest electrum grains are typically present within galena, euhedral to poikiloblastic arsenopyrite, or in chalcopyrite-filled veins in tetrahedrite-tennantite (Fig. 7.8a,b).
ii) with chalcopyrite,
iii) within chalcopyrite-sphalerite ± galena intergrowths,
iv) in cracks or as inclusions in pyrite, and
v) intergrown with remobilised tetrahedrite-tennantite.

No further mineralogical associations of electrum have been identified during this study.

Figure 7.8 Photomicrographs of electrum and trace minerals in the massive sulphides at Thalanga (under reflected light, unless otherwise indicated).

(a) Coarse electrum grain in chalcopyrite, is associated with intergrown chalcopyrite-arsenopyrite-tetrahedrite-sphalerite-galena and adjacent to poikiloblastic pyrite. Sample TH209-86.5b. Central Thalanga.

(b) Stibnite grains at contact between chalcopyrite and sphalerite. Tremolite and calcite gangue. Sample W2031ND07-66.9, West Thalanga.

(c) Galena-boulangerite-argentite-tetrahedrite inclusion in pyrite. Sample TH239-144. Central Thalanga.

(d) Irregular to lamellar bismuth inclusions in galena. Sample TH21-292.5. Central Thalanga.

(e) Bismuth-galena-chalcopyrite-sphalerite inclusion in coarsely recrystallised pyrite (associated with remobilised chalcopyrite). Pyrite is strongly fractured and also contains abundant chalcopyrite- and magnetite-only inclusions. Sample T17-2.5. Central Thalanga.

(f) Boulangerite needles (intergrown with pyrite and barite) that have been partly replaced by secondary covellite and digenite. Sample UG-13. Central Thalanga.

(g) Coarse, euhedral barite crystals intergrown with sphalerite, galena and pyrite. Sample UG-2. Central Thalanga. Transmitted light.

(h) Barite, quartz, phlogopite and chlorite gangue to pyrite disseminated in quartz sandstone. Sample E3207SI02-56. East Thalanga, hangingwall lens. Transmitted light.

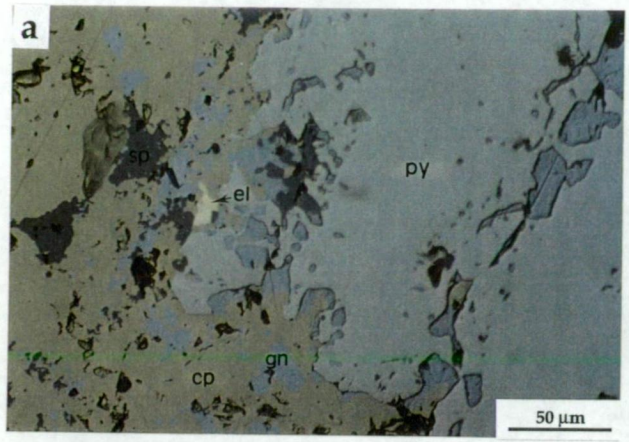
a
sp
el
py
gn
cp
50 µm

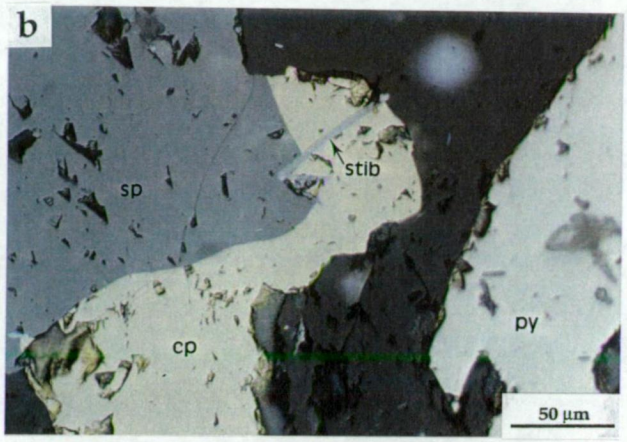
b
sp
stib
py
cp
50 µm

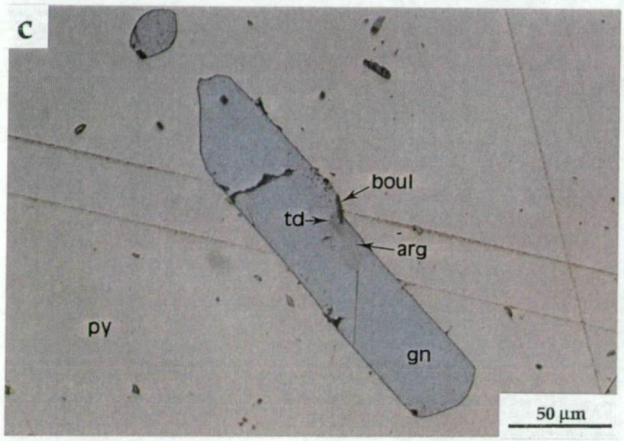
c
boul
td
arg
py
gn
50 µm

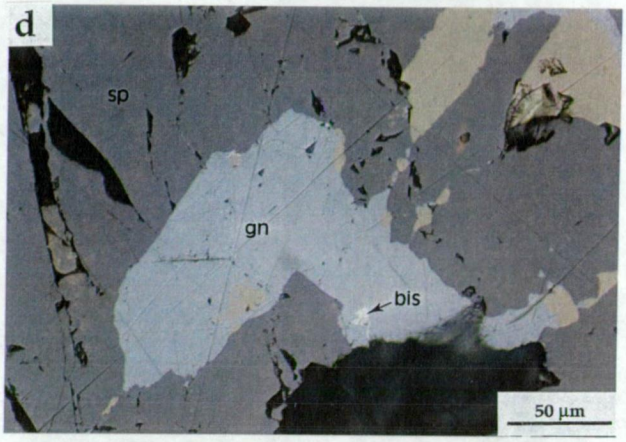
d
sp
gn
bis
50 µm

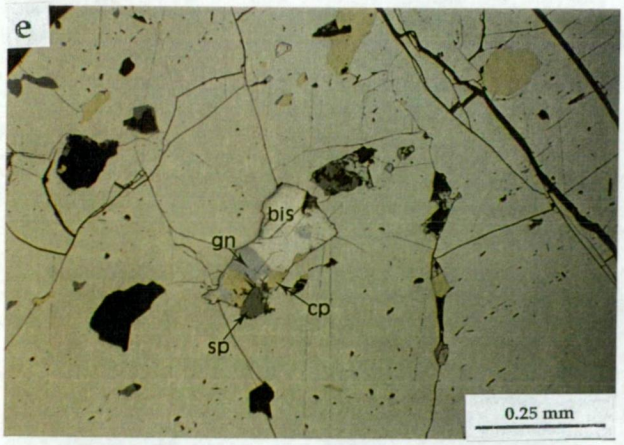
e
bis
gn
cp
sp
0.25 mm

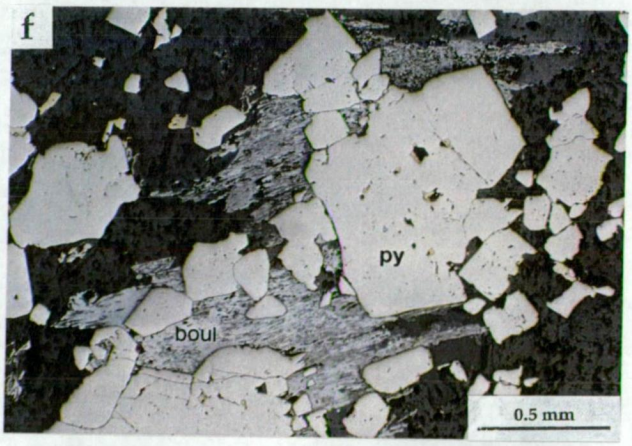
f
py
boul
0.5 mm

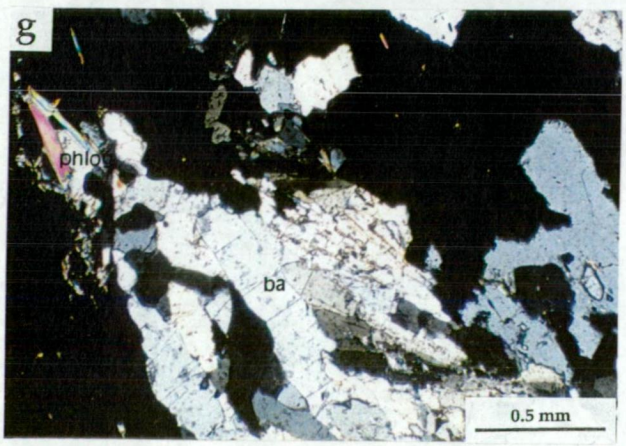
g
phlog
ba
0.5 mm

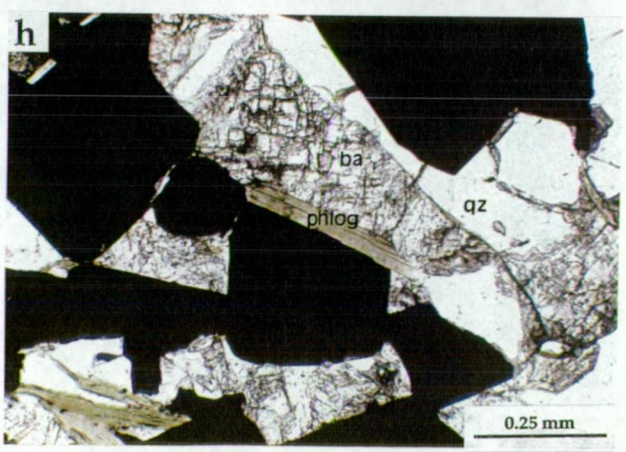
h
ba
qz
phlog
0.25 mm

7.10 Other Ore Minerals

Other sulphide and sulphosalts within the ore lenses at Thalanga include traces of stibnite, boulangerite, argentite, pyrrhotite, cubanite, bornite and bismuth (Table 6.1). Elongate stibnite grains are present in intergrown sphalerite and chalcopyrite that are disseminated in chlorite-altered wall rocks (Fig. 7.6c). Traces of boulangerite, argentite and tetrahedrite are present in galena inclusions in subhedral pyrite grains (Fig. 7.8c), and pyrite grains typically contain chalcopyrite and intergrown bornite inclusions. Bornite is present in some myrmekitic chalcopyrite-arsenopyrite-tetrahedrite-tennantite-sphalerite intergrowths, and is intergrown with covellite around arsenopyrite grains. Inclusions of bismuth are also present in coarsely recrystallised galena and pyrite (Fig. 7.8d,e). No tellurides minerals have been identified within the ore lenses at Thalanga.

Secondary (supergene) minerals include chalcocite, covellite and digenite. These typically occur along grain boundaries and fractures in chalcopyrite, sphalerite, boulangerite (Fig. 7.8f) and magnetite. The occurrence of the supergene minerals is restricted to within 50 m of the present-day erosion surface at Thalanga.

7.11 Gangue Mineralogy and Textures

Gangue minerals within the ore lenses at Thalanga are listed in Table 6.1 (Chapter 6). Many of these minerals are also common in skarn deposits (e.g. epidote, tremolite, diopside, spessartine-rich garnet), and are interpreted to have formed during metamorphism of the carbonate-rich parts of the ore horizon. The most common gangue minerals within the massive or semi-massive sulphides at Thalanga are quartz, barite, biotite, calcite, chlorite, dolomite, phlogopite, muscovite and tremolite. Gregory *et al.* (1990) and Huston (1991) reported traces of anthophyllite, siderite and wagerite; however, these minerals were not identified in this study. Quartz is ubiquitous, and is typically present as rounded, anhedral grains intergrown with barite, biotite, phlogopite, chlorite and/or sulphides. The textural variations of barite, biotite, phlogopite, chlorite and muscovite gangue are discussed below. The textures and compositional variations of the dolomite, calcite, chlorite and chlorite in the CTC assemblages are discussed in Chapter 11.

7.11.1 Barite

Barite is a common component of the sphalerite-galena-pyrite-rich parts of ore lenses in all parts of the Thalanga deposit, where it is present as coarse (0.1 to >6 mm), anhedral rounded, to subhedral elongate grains that have sharp, triple point grain boundaries with co-existing quartz (Fig. 7.8g,h). Euhedral barite crystals up to 3 cm in length are present in the barite-

rich parts of the hangingwall lens in East Thalanga and in veins in the Vomacka Zone ore horizon. The pyrite-chalcopyrite-rich lenses in the ore horizon generally do not contain barite. However, barite is present with quartz and biotite in the pyrite ± chalcopyrite-rich bases of QEV sandstone units that form the hangingwall lens in parts of East Thalanga (Fig. 7.8h). Minor barite is also present in mineralised parts of the carbonate-chlorite-tremolite lenses in West Thalanga.

7.11.2 Phlogopite and Biotite

Phlogopite and minor biotite are sporadically disseminated through the barite-sphalerite-galena- and pyrite-rich parts of the massive sulphides at Thalanga. Phlogopite and biotite are both present in some thin sections, but they generally do not occur in contact with each other. Biotite (or chlorite after biotite) typically occurs at the margins of rhyolite or QFP clasts within the massive sulphides, where it defines the S_2 cleavage and is overgrown by phlogopite and chlorite porphyroblasts. Irregularly scattered phlogopite and chlorite are intergrown with remobilised chalcopyrite and non-remobilised sphalerite-pyrite (Fig. 7.2b).

The colourless to pale green or brown phlogopite grains are parallel to S_2 in places, but generally have random orientations, which is interpreted to indicate recrystallisation of phlogopite and the enclosing sulphides after deformation. Weakly coloured phlogopite can be distinguished optically from muscovite by its weak pleochroism and lack of birds-eye extinction.

7.11.3 Chlorite

Chlorite is present within the ore lenses at Thalanga as bands of chlorite ± phlogopite (≤5 cm in thickness) parallel to bedding, as discontinuous lenses (<1 cm in thickness) within the massive sulphides, and as grains of chlorite disseminated within massive sulphides. Colourless chlorite is a common gangue mineral in the pyrite ± chalcopyrite-rich parts of West and Central Thalanga, where it typically occurs parallel to S_2. Colourless chlorite is also intergrown with carbonate and tremolite in West and Central Thalanga. In contrast, green, Fe-rich chlorite is intergrown with massive pyrite-chalcopyrite in the footwall lens at East Thalanga. Chlorites within the sphalerite-galena-pyrite-rich massive sulphides at Thalanga vary from brown to green in colour, generally have good crystal shapes, and are interpreted to have replaced biotite, based on the presence of remnant brown cores and pleochroic haloes around sub-microscopic inclusions. Chlorite is not present in barite-rich sulphides in Central Thalanga.

7.11.4 Muscovite

Coarse grained muscovite is irregularly disseminated in the massive sulphides at Thalanga, where it is commonly associated with quartz and barite gangue in sphalerite-galena-pyrite-rich parts of the ore lenses (Fig. 6.23c). Muscovite is less common than phlogopite within the massive sulphides, and the two minerals generally do not co-exist. Thin, discontinuous bands of muscovite within massive to semi-massive sulphides define the S_2 cleavage in parts of the ore lenses (e.g. TH1-183.1m). Locally, however, coarse muscovite crystals within the massive sulphides have no preferred orientation. Fine grained muscovite has partly replaced feldspar gangue.

7.11.5 Tremolite

Irregular, poikiloblastic tremolite crystals are intergrown with massive and semi-massive sulphides at many localities within the Thalanga deposit. Tremolite is intergrown with chlorite in the mineralised matrix of the upper rhyolite breccia in the East Thalanga hangingwall lens. The tremolite has no preferred orientation and typically has a radiating or sheaf-like habit. Calcite is commonly associated with tremolite and it partly replaces tremolite crystals along cleavage planes. Sulphides are intergrown with the tremolite, as inclusions and filling cleavage planes, and are interpreted to have recrystallised after tremolite formation.

7.12 Discussion

7.12.1 Origin of Sulphide Banding

There are four main explanations for the origin of the fine mineralogical banding reported from many massive sulphide deposits:
i) Sedimentary banding: The conformable nature of massive sulphide deposits, and the similar orientation of sulphide bands and bedding, together with the interpretation that the sulphides precipitated as chemical sediments, has lead to the proposal that the banding formed by primary sedimentation (e.g. Brathwaite, 1974; McKay and Hazeldene, 1987). Alternating bands of fine grained sphalerite and granular to nodular pyrite are interpreted to be a primary sulphide facies at the Mobrun deposit in Quebec (Larocque *et al.*, 1993; Larocque and Hodgson, 1995). Graded sulphide beds, with possible cross-bedding in the Woodlawn deposit have been reported by McKay and Hazeldene (1987), and a graded sulphide breccia overlying the Mount Chalmers deposit has been reported by Large and Both (1980). The pulsatory venting of negatively buoyant plumes has been proposed to explain the alternation of pyrite-rich and sphalerite-rich bands (Solomon, 1981; Solomon *et al.*, 1990). Yui (1983) and

Yui and Ishitoya (1983) interpreted bands of alternating sulphides to be caused by changes in physio-chemical conditions in the hydrothermal fluids and bands of graded sulphides to have been deposited by intermittent venting of hydrothermal fluids at the seafloor.

ii) Spontaneous compositional layering of sulphides from a gel: Bubela and McDonald (1969) demonstrated experimentally that fine sulphide bands can form from a gel containing sulphide ions when interacted with solutions containing metal ions, and postulated that the small-scale sulphide banding at the McArthur River deposit may have formed by similar mechanisms.

iii) Tectonic banding: Fine galena bands overprint the massive sulphides and folded pyrite bands at Que River, Tasmania. Their orientation parallel to the axial planar cleavage is evidence that the galena bands formed tectonically (Large *et al.*, 1988). Laminated galena and sphalerite bands parallel to the cleavage at Que River are interpreted to be mylonite zones, whereas the folded pyrite bands could be deformed primary banding (Large *et al.*, 1988). Alternating bands of pyrite and pyrrhotite, and rare sphalerite and galena, in the Bousquet 2 deposit, Quebec, are parallel to the cleavage, are well-developed in zones of high strain, and are therefore interpreted to be metamorphic banding formed during prograde metamorphism and regional deformation (Tourigny *et al.*, 1993).

iv) Replacement and preservation of pre-existing rock structures: Aerden (1991, 1994a,b) has argued that the banding in the massive sulphides at Rosebery could have formed by the successive replacement of adjacent cleavage bands by ore minerals. Bodon and Valenta (1995) have suggested that graded and banded sulphides at the Currawong massive sulphide deposit formed by the replacement of host turbidites and epiclastic rocks while they were unconsolidated and permeable.

Comparison with bedding and cleavage orientations at Thalanga shows that the compositional banding in the massive sulphides is parallel to S_2, but also locally to S_0 and S_3 (Chapter 3). Banding in several locations is folded into D_3 shear zones along the base of the ore lens (map M7), which indicates that sulphide banding must predate D_3. Where sulphide bands are parallel to footwall contacts, adjacent subparallel shear zones may have controlled the orientation of the sulphide bands. The similarity between the orientation of sulphide banding and S_2 is interpreted to indicate that the sulphide bands at Thalanga are tectonic (D_2) in origin. Furthermore, banding in sulphides in vein-style lenses in West Thalanga and partly replacive lenses in East Thalanga cannot have formed by sedimentary deposition of sulphides.

It is unclear whether the compositional banding at Thalanga is a recrystallised mylonite, or formed by diffusive mass transfer as suggested by Tourigny *et al.* (1993), or if primary

sulphide bands were isoclinally folded. The lack of abundant galena- or chalcopyrite-rich bands within the alternating sphalerite-and pyrite-rich bands, where mylonites would readily develop (Large *et al.*, 1988; Large, 1992), does not preclude shearing as a possible origin of banding in the sulphide lenses at Thalanga. For example, chemical etching of pyrite grains from the Renström deposit in Sweden revealed pressure solution textures and C and S fabrics that are interpreted to have formed via shearing within the sulphide deposit during retrograde greenschist facies metamorphism (Duckworth and Rickard, 1993). Since layer-parallel shearing within the Thalanga ore horizon is likely to have occurred during D_2 (Chapter 3), then it is reasonable to assume that the massive sulphide lenses (which would probably have been less competent than the enveloping siliceous volcanic units) would also have been sheared, and that the banding in the sulphide lenses could have initially formed as mylonites. Subsequent recrystallisation during contact metamorphism could have then destroyed the mylonitic fabric.

Tight to isoclinal folding of primary sulphide layers during D_2 may also have produced banding parallel to S_2 . However, there is no evidence of isoclinal folds within the sulphide lenses at Thalanga, although apparent folds are interpreted to have formed by partial replacement of sphalerite-rich sulphides by pyrite (section 6.2.2). The distribution of the pyrite-rich layers and sphalerite-rich layers in these locations may have been controlled by pre-existing banding in the sphalerite-rich sulphides. Alternatively, irregular pyrite veins may have replaced sphalerite-rich sulphides.

Metamorphic segregation of the sulphides by diffusive mass transfer (remobilisation) is another process that could explain the compositional banding in the massive sulphides. Segregation probably occurred during prograde metamorphism associated with regional deformation, resulting in banding parallel to S_2. There is no conclusive evidence that any of the above three mechanisms produced the alternating pyrite-rich and sphalerite-rich bands in the ore lenses at Thalanga, and similar difficulties in determining the origin of sulphide banding are reported from other deformed and metamorphosed massive sulphide deposits (e.g. banding is tectonic in origin at Grevet, Quebec, but may also have been primary; Lacroix *et al.*,1993).

The preferred interpretation at Thalanga is that compositional banding is tectonic in origin. Compositional banding may have formed during primary sulphide deposition and was partly replaced by successive pulses of syn-volcanic hotter mineralising fluids that were undersaturated in Zn and Pb. This resulted in the local dissolution of sphalerite and galena, replacement by pyrite, and re-precipitation of sphalerite and galena at the top of the massive sulphide lens (cf. Knuckey *et al.*, 1982; Eldridge *et al.*, 1983; Huston and Large, 1988). Redistribution of the sulphides during prograde metamorphism and shearing of the ore lenses during D_2 may have produced compositional banding, but the recrystallisation of sulphides

during subsequent contact metamorphism overprinted and obscured any mylonite textures in the sulphide lenses.

7.12.2 Primary vs Metamorphic Sulphide Microtextures

In most parts of the Thalanga deposit, the polymetallic sulphides are coarsely recrystallised and equant, with sharp grain boundaries and triple point grain contacts. Recrystallised pyrite framboids are the best evidence of sulphide textures prior to metamorphism. The poikiloblastic and granuloblastic sulphide textures at Thalanga are typical of many other metamorphosed massive sulphide deposits (e.g. Pesquera and Velasco, 1993; Vokes and Craig, 1993). The metamorphic texture of pyrite at Thalanga appears to have depended on the co-existing mineral assemblage, with granuloblastic pyrite common in regions of massive pyrite, poikiloblastic or metablastic pyrite intergrown with abundant sphalerite-galena and/or chalcopyrite, and euhedral pyrite disseminated through massive chalcopyrite or chlorite schists (Table 7.2). Primary sphalerite textures are absent from the Thalanga ore horizon, and the texture of recrystallised sphalerite and galena depends on the amount of galena associated with the sphalerite. Rounded grains of sphalerite (± poikiloblastic grain boundaries) occur in galena-rich zones. Where the galena content is low, sphalerite has 120° dihedral grain boundaries, and small grains of galena are trapped in the triple point junctions.

Sphalerite, galena and chalcopyrite in the ore lenses at Thalanga have preserved rare textural evidence of deformation, and only some pyrite crystals intergrown with these sulphides have cataclastic deformation textures. In contrast, coarsely recrystallised pyrite grains in lenses of massive pyrite have brittle deformation fractures, and replacement by chalcopyrite and galena has occurred along the fractures. This different response of individual sulphide minerals to deformation has been reported from other massive sulphide deposits, and is a result of the difference in strength and ductility of the sulphides. Galena the weakest and most ductile sulphide, followed by chalcopyrite, sphalerite, then pyrrhotite. Those sulphides reach their brittle-ductile transition boundaries at lower temperatures and pressures (and in that order) than pyrite (Clark and Kelly, 1973, 1978; Kelly and Clark, 1975; Atkinson, 1974, 1975; Salmon *et al.*, 1974; Cox *et al.*, 1981; Marshall and Gilligan, 1987). The galena, chalcopyrite and sphalerite in the ore lenses at Thalanga could therefore have taken up increasing strain during prograde metamorphism, but pyrite intergrown with the sulphides would have remained undeformed. Recrystallisation during contact metamorphism would have then obliterated any ductile deformation textures in the 'softer' sulphides.

7.12.3 Sulphide Paragenesis and Metamorphic Reactions

Thermal annealing of the sulphides at Thalanga is interpreted to have overprinted and destroyed primary textures. Therefore, it is impossible to determine the primary sulphide paragenesis. Furthermore, the recrystallisation of sulphides during metamorphism has overprinted earlier deformation (D_2) textures within the sulphides, making the metamorphic paragenesis of the massive sulphides difficult to resolve. The possible evolution of the Thalanga deposit, as interpreted from textural evidence, is illustrated in Table 7.3.

Table 7.3 Textures of sulphide formation, deformation and metamorphism at Thalanga.

Event	Response	Resulting texture
Sulphide deposition	• Polymetallic massive sulphides overlying massive pyrite, ± synvolcanic replacement of sphalerite-rich sulphides	• Banding parallel bedding? • Local overprinting of sphalerite-rich sulphides by pyrite-rich sulphides, along primary banding? • Pyrite framboids
D2 deformation and associated metamorphism (biotite grade)	• Ductile sulphide minerals deformed, intergrown pyrite is undeformed • Remobilisation of sulphides into zones of extension	• Banded polymetallic sulphides ...mylonite? ...metamorphic banding • Coarsening of sulphides • Recrystallisation of framboids
D3 deformation and post S3 metamorphism (biotite grade)	• Thermal annealing of sulphides • Local sulphide remobilisation • Local brittle deformation of pyrite	• Coarsening of sulphides • *Durchbewegung* texture along faults • Sulphides intergrown with metamorphic silicates

It is evident from the intergrowth of tremolite and sphalerite, galena, chalcopyrite and pyrite, that sulphide recrystallisation post-dates the initiation of metamorphism and tremolite formation at Thalanga. The presence of electrum and the more ductile sulphides such as galena and chalcopyrite along fractures in pyrite are interpreted to indicate that brittle deformation and remobilisation occurred after the recrystallisation of pyrite. Chalcopyrite remobilisation at all scales has been an important process in the generation of the sulphide textures now preserved at Thalanga, and there is no evidence of primary chalcopyrite textures. Chalcopyrite is the most abundant sulphide in dilational sites associated with vertical extension of the ore horizon, including cusps and piercement veins at the hangingwall contacts, tension gashes and boudin necks (Chapter 3). Dark red-brown, Fe-rich sphalerite is associated with chalcopyrite at such sites. On the microscopic scale, remobilised chalcopyrite and galena have filled pressure shadows around euhedral pyrite and quartz grains. Chalcopyrite that occurs along fractures in sphalerite grains indicates that at Thalanga, chalcopyrite remained ductile after sphalerite entered the brittle field during post-peak metamorphic cooling.

There is sparse evidence for replacement reactions between sulphide minerals at Thalanga, which is interpreted to be due to the re-equilibration of sulphide textures during metamorphic recrystallisation. Replacement of sulphides by chalcopyrite and/or magnetite is interpreted to have occurred during contact metamorphism. Chalcopyrite has replaced pyrite along fractures, and replaced sphalerite along cleavage planes. In places, chalcopyrite, sphalerite and pyrite have been replaced by magnetite along grain margins and along contacts with calcite. This indicates that magnetite formed towards the final stages of contact metamorphism. However, it is uncertain whether magnetite originated from within the ore lenses, or whether magnetite formed via metasomatism.

The microtextural evidence that sphalerite has replaced pyrite is not reflected within the massive sulphide lenses at Thalanga. Instead, pyrite is interpreted to have replaced the sphalerite-rich lenses during formation of the massive sulphides by zone refining processes (Chapter 6). The partial replacement of pyrite by sphalerite is therefore interpreted to have occurred during metamorphism and sulphide remobilisation. The elevated Fe content of remobilised sphalerite may have been due to this pyrite dissolution.

The breakdown of tennantite to myrmekitic intergrowths of chalcopyrite, arsenopyrite, tetrahedrite-tennantite and sphalerite is interpreted to have also occurred during contact metamorphism. Tetrahedrite is interpreted to have exsolved from galena during cooling from peak metamorphic temperatures. This contrasts with tetrahedrite and other Ag sulphosalt inclusions in galena from less metamorphosed deposits, where exsolution is considered to have occurred during cooling after sulphide deposition (e.g. Amcoff, 1984).

7.13 Summary

1. Primary textures in the massive sulphides are rarely preserved at Thalanga. Most of the sulphides have been recrystallised and annealed. Only rare evidence of deformed sulphides is preserved due to sulphide recrystallisation during contact metamorphism. Banding within the ore lenses is defined by alternating pyrite-rich and sphalerite-rich bands. These bands are parallel to the S_2 cleavage and are therefore interpreted to have formed during prograde metamorphism associated with D_2 deformation.

2. Pyrite has annealed and has triple point grain boundaries in lenses of massive pyrite, but is typically euhedral or porphyroblastic where intergrown with galena, chalcopyrite, sphalerite or gangue minerals. Both elongate pyrite grains and cataclastic textures occur in pyrite at Thalanga. Sphalerite, galena and chalcopyrite were ductile during deformation.

3. Remobilised sphalerite is more Fe-rich than non-remobilised sphalerite at Thalanga. Pressure estimates based on the Fe content of sphalerite inclusions in pyrite, yielded pressures of deformation and metamorphism in the range 3-7 kbars, which is higher than the estimate based on metamorphic silicate assemblages (Chapter 3). Temperature estimates based on the composition of arsenopyrite yielded unreasonable results.

CHAPTER 8.

METAL ZONATION

8.1 Introduction

Vertical and lateral zonation in base metal contents of VHMS deposits have been well documented by Stanton (1965), Sangster (1972), Large (1977), Franklin *et al.* (1981), Eldridge *et al.* (1983) and Ohmoto *et al.* (1983). These workers have shown that typical massive sulphide deposits exhibit a zonation in metal content from Fe and Fe-Cu-rich bases, through to Cu-Zn-Pb-rich ore, then to Pb-Zn-Ba-rich sulphides at the top and distal regions. Commonly, the zonation in mineralogy and metal contents of sulphide chimneys on the modern seafloor is comparable to that of ancient massive sulphide deposits (e.g. Graham *et al.*, 1988; Paradis *et al.*, 1988; Peter and Scott, 1988). The mineralogical and metal zonation of Australian Archaean to Palaeozoic VHMS deposits has been reviewed by Large (1992) and studies of the metal zonation within individual deposits include Golden Grove (Frater, 1983), Mount Chalmers (Large and Both, 1980; Huston and Large, 1989), Que River (Large *et al.*, 1988), Rosebery (Brathwaite, 1974; Green *et al.*, 1981; Huston and Large, 1988; Huston and Large, 1989) and Scuddles (Ashley *et al.*, 1988).

The zonation of metals within VHMS deposits has been used to understand the mechanisms of sulphide deposition (e.g. Large, 1977; Knuckey *et al.*, 1982) and in unravelling the structural history of deposits (e.g. at Rosebery, Green *et al.*, 1981; and Que River, Large *et al.*, 1988). Variation in the Zn ratio [100 Zn/(Zn+Pb)] and Cu ratio [100 Cu/(Cu+Zn)] is similarly useful in studies of the genesis of VHMS deposits (Huston and Large, 1987). For example, the coincidence of the lowest Zn ratios, highest Cu ratios and most abundant pyrite within the massive sulphides at the Hellyer deposit has been interpreted to define the locations of high temperature feeder zones (Gemmell and Large, 1990).

The distribution of base metals and metal ratios in the Thalanga deposit are contoured here on both long section and several cross sections in order to: (1) determine whether the distribution of metals corresponds to the gross mineralogical zonation of the deposit; (2) to locate possible feeder zones; and (3) to determine whether deformation and metamorphism have influenced the metal zonation.

8.2 Zinc Ratio

Huston and Large (1987) demonstrated that the Zn ratio of all VHMS deposits is between 60 and 90. They interpreted differences in the average Zn ratio between deposits, and lenses within a single deposit, to reflect variations in depositional temperatures and salinity. For example, the barite lens in the Rosebery deposit has an average Zn ratio = 68.9, compared to the sphalerite-galena-rich massive sulphides with Zn ratio = 74.5 (Huston and Large, 1987). Zn ratios were calculated for the main ore types and altered rocks in West, Central and East Thalanga in order to compare Thalanga with other massive sulphide deposits and to identify any variation in the Zn ratio, and therefore possible variation in the physicochemical conditions of deposition, between each lens and each ore type.

8.2.1 Source of Samples

The analyses represent assays of split drill core, 0.3 to 1.0 m in length, sampled during exploration and production drilling. Samples were selected from drill holes widely spaced across the deposit; the drill holes used are listed in Appendix H. The drill holes used from West Thalanga are located from 19 550 mE to 20 310 mE. In order to eliminate spurious results from supergene mineralisation, most samples from Central Thalanga are from production drill holes located in the western part of this lens below about 900 mRL. Only two drill holes from the eastern part of Central Thalanga were used. Selected drill holes from between 32 000 mE and 32 450 mE in East Thalanga were used and samples from the Vomacka Zone were excluded due to the large number of ore intersections at depths above 900 mRL.

8.2.2 Results

The Zn ratios of the Thalanga deposit (Fig. 8.1a-c) are consistent with those of other Phanerozoic VHMS deposits reported by Huston and Large (1987). Central Thalanga has the highest mean and median Zn ratio (79.1 and 81.1 respectively), followed by West Thalanga, then East Thalanga, which exhibits the most variable Zn ratio (standard deviation = 15.9). This pattern could indicate that on average, mineralising solutions in East Thalanga were of a lower temperature than those in West and Central Thalanga. The samples with Zn ratio <40 are located mainly in the altered QEV breccia between the ore lenses in East Thalanga, and are interpreted to be due to the abundance of non-remobilised sphalerite-pyrite veins, sulphide clasts in the QEV, and remobilised chalcopyrite-sphalerite veins in this location (Chapter 6). The zinc ratios of the remobilised chalcopyrite-rich sulphides are comparable to those of the non-remobilised ore lenses at Thalanga (Fig. 8.1d).

The results from each lens were also separated on the basis of rock type and stratigraphic location (Appendix H) and this shows that the altered rhyolitic volcanics in the footwall

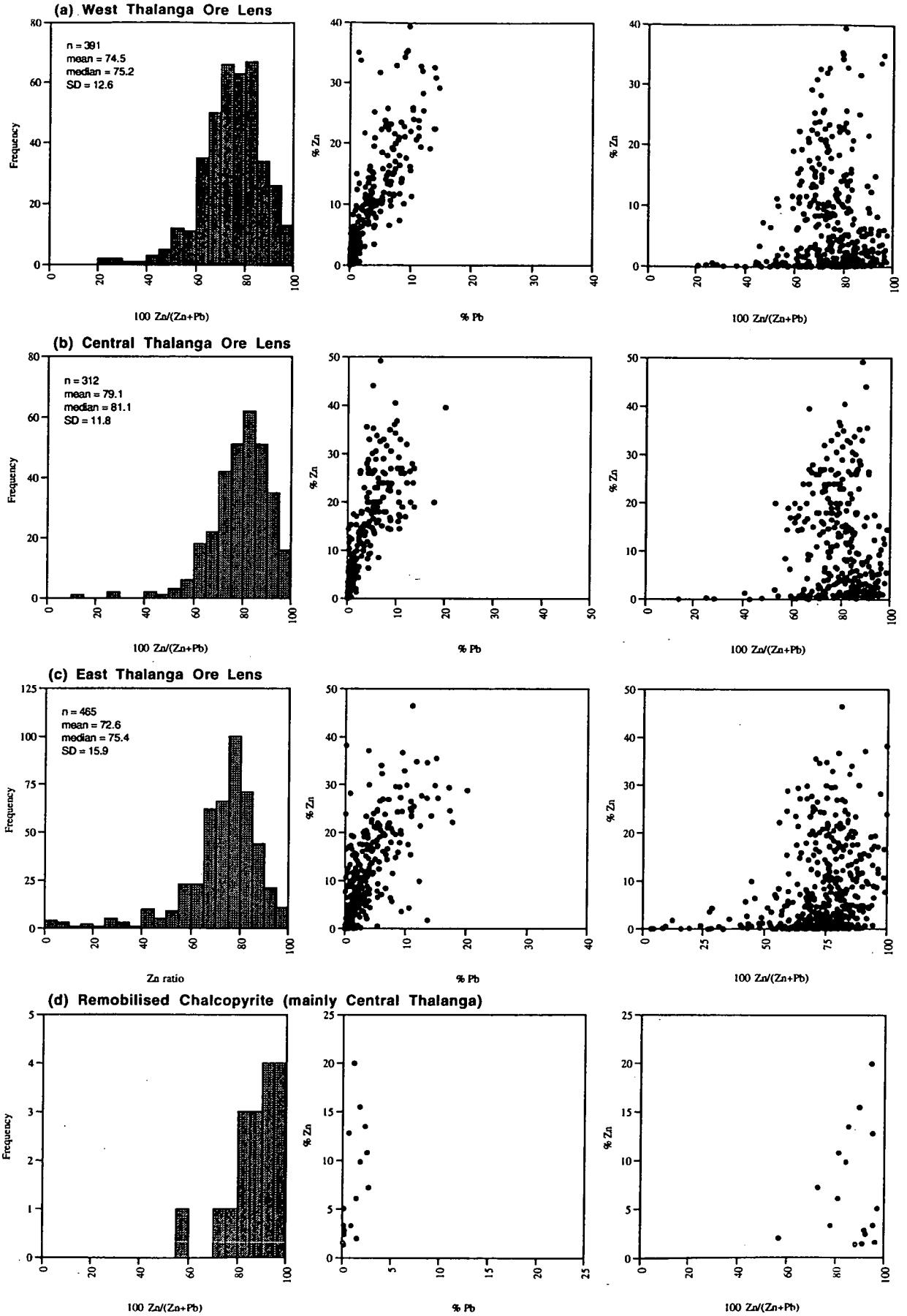

Figure 8.1 Zn ratio diagrams and Zn-Pb content of the rocks within the ore horizon in (a) West Thalanga, (b) Central Thalanga, (c) East Thalanga, and (d) remobilised chalcopyrite-rich sulphides. See Appendix H for separation into various ore types and comparison with the footwall and hangingwall rocks.

have a mean Zn ratio less than their associated sulphide lenses, and standard deviations greater than the sphalerite-galena-pyrite-rich sulphides. This relationship is compatible with the expected increase in mean Zn ratio of the sulphides with stratigraphic height (Huston and Large, 1987). However, there is no consistent trends in variation of the mean Zn ratio of the ore types with stratigraphy. In East Thalanga, the Zn ratio of the massive sulphides in the footwall lens is greater than that of both hangingwall lenses. Similarly, the mean Zn ratio of the massive pyrite in Central Thalanga is higher than the mean Zn ratio of the sphalerite-galena-pyrite-rich massive sulphides, whereas in West Thalanga massive pyrite has a lower mean Zn ratio than massive sphalerite-galena-pyrite, which conforms to similar trends reported by Huston and Large (1987).

8.3 Metal Contours

8.3.1 Methods

Contour diagrams depicting the metal distribution at Thalanga were generated using Minex software from the block model of the Thalanga deposit. The block model is based on 1.0 m drill hole composites and individual blocks, 5*2*2 m in dimension, were calculated using the inverse distance squared method (C.J. Kendall, pers. comm., 1995). The long section contour diagrams were generated by bulking together the samples from within the mineralised horizon (between the top of the rhyolitic volcanics and the base of the HWF). At Thalanga mine, the block model of the West and Central ore lenses is separate from that of East Thalanga and the Vomacka Zone. Due to circumstances beyond my control, the long sections of metal distribution at West and Central Thalanga were calculated separately and with slightly different contour intervals to those for East Thalanga and the Vomacka Zone. This means that the distribution of metals on long section in West and Central Thalanga are not directly comparable to that of East Thalanga and the Vomacka Zone.

Until recently, samples from underground production drill holes were not consistently analysed for Au, therefore pulps from drill holes on the 20 250 mE, 20290 mE and 20430 mE sections were re-assayed for Au and Ba by Australian Laboratory Services Pty Ltd in Charters Towers and Brisbane (see Appendix F for the methods of analysis). Only these samples, together with those from the older exploration drill holes on the same cross section, were used in the scattergrams depicting metal associations (304 samples; section 8.4).

8.3.2 Long Sections

Deposit-scale variations in metal distribution at Thalanga, together with lateral variations in metal content, are best illustrated on long sections (Fig. 8.2a-g). In general, the distribution

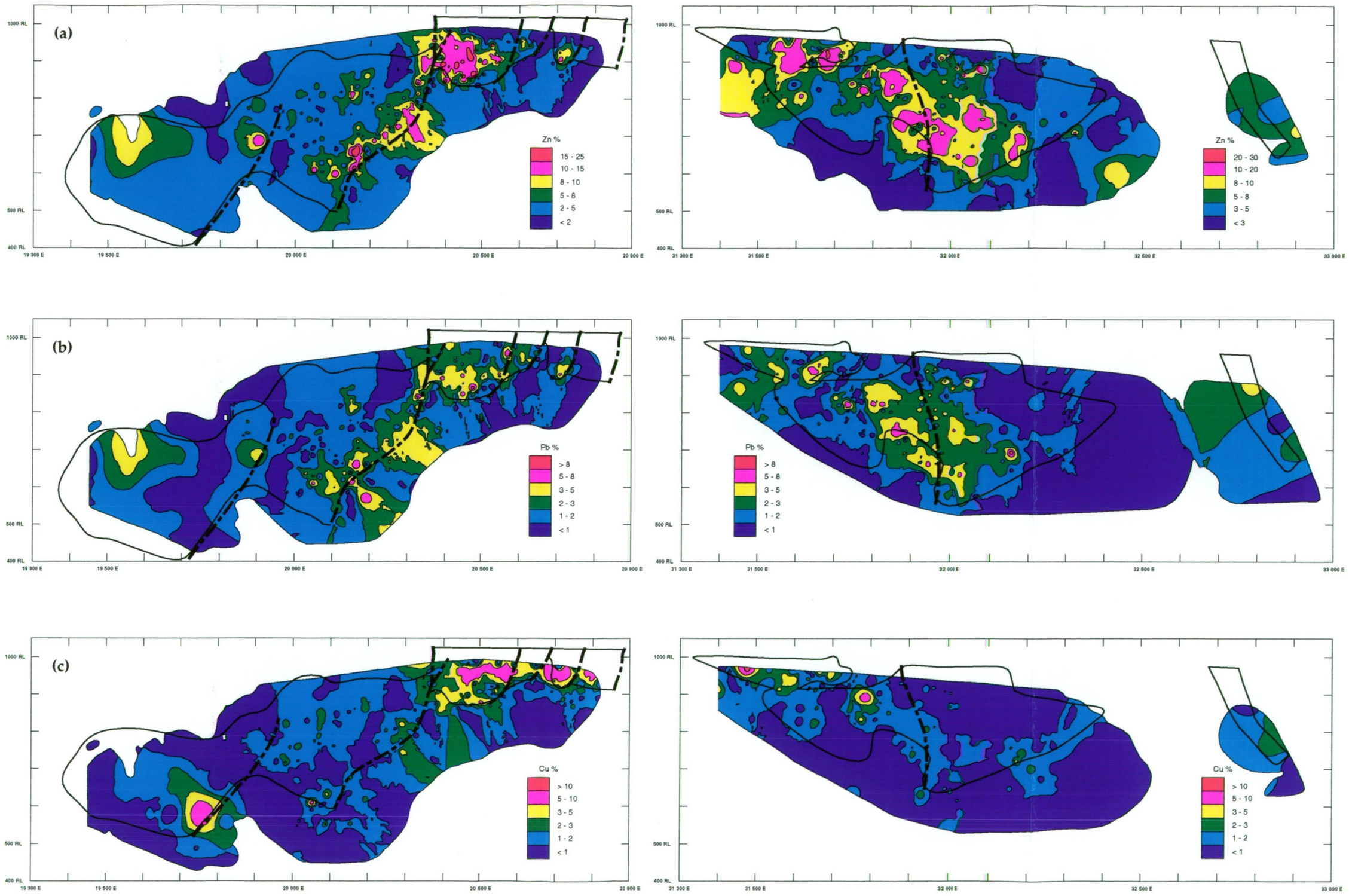

Figure 8.2 Distribution of (a) Zn, (b) Pb and (c) Cu at Thalanga on long section

1:10,000

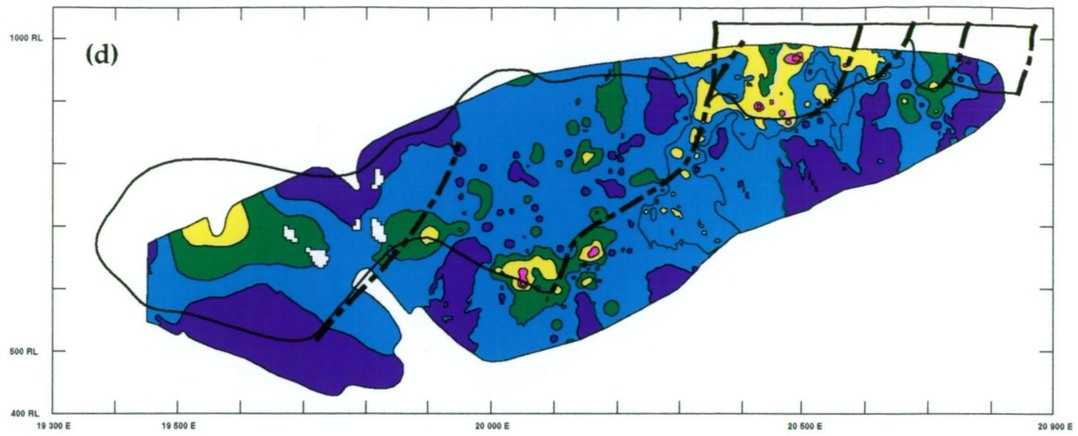

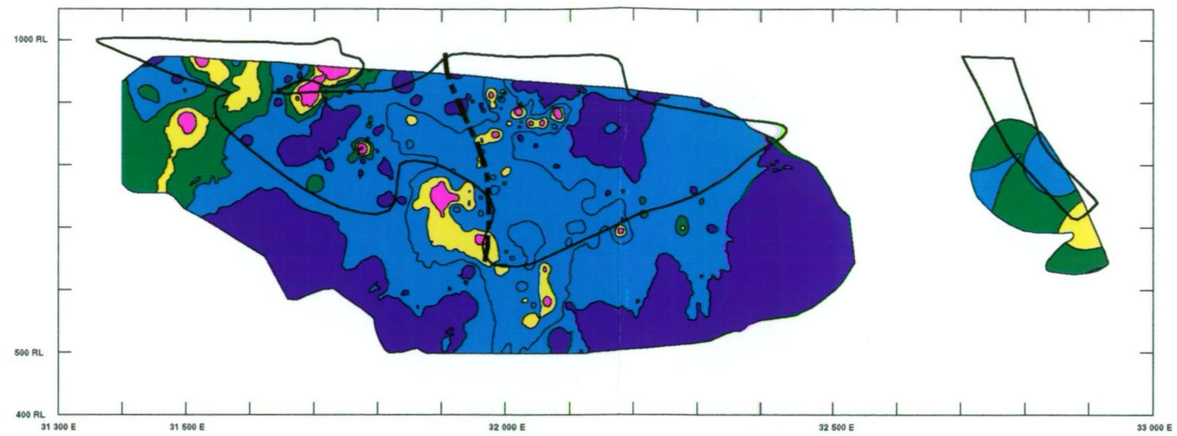

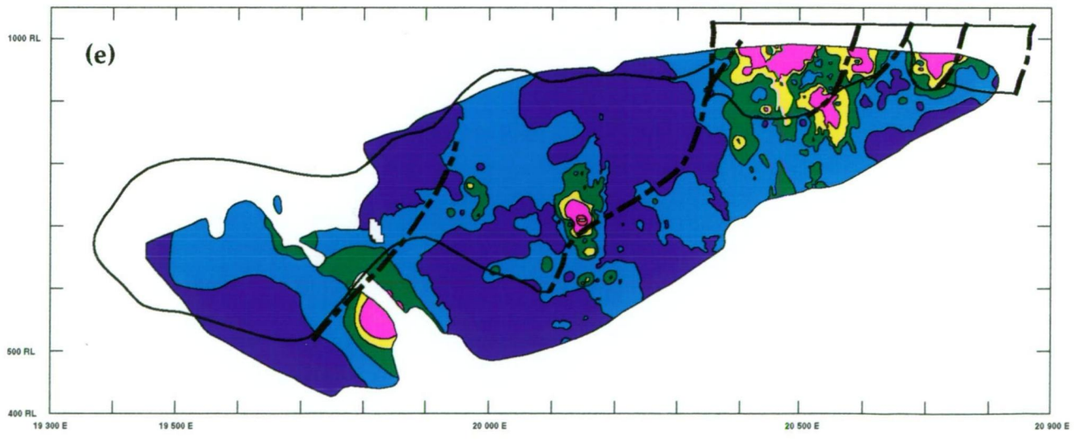

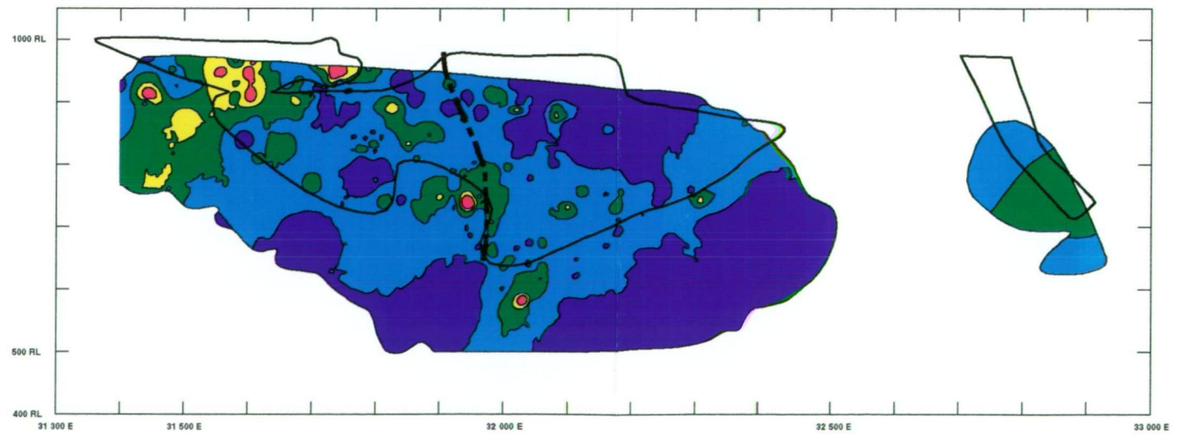

Figure 8.2 Distribution of (d) Ag and (e) Au at Thalanga on long section

1:10,000

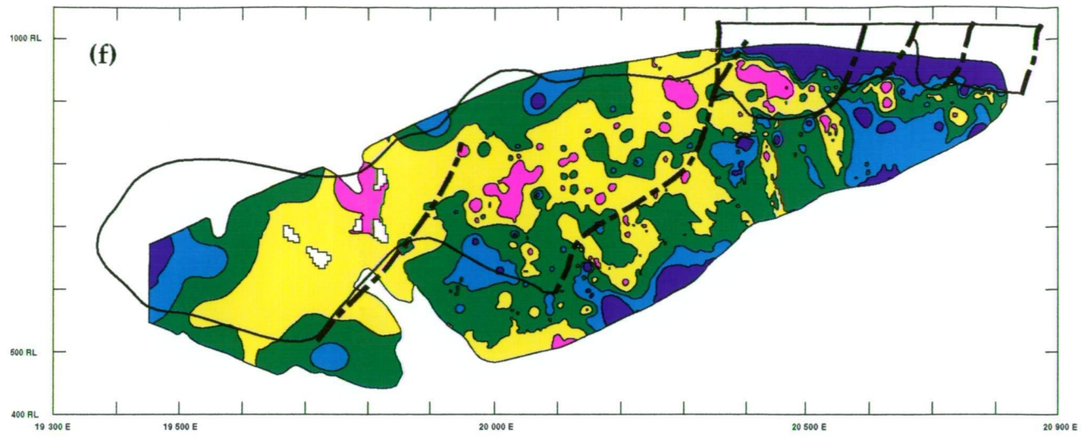

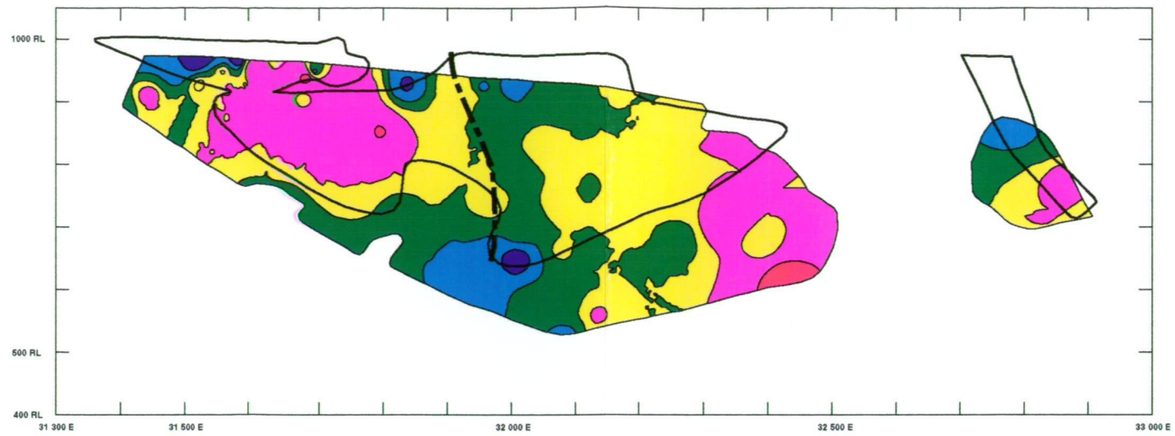

100 Cu / Cu + Zn

- > 90
- 80 - 90
- 75 - 80
- 70 - 75
- 65 - 70
- < 65

100 Cu / Cu + Zn

- > 90
- 80 - 90
- 75 - 80
- 70 - 75
- 60 - 70
- < 60

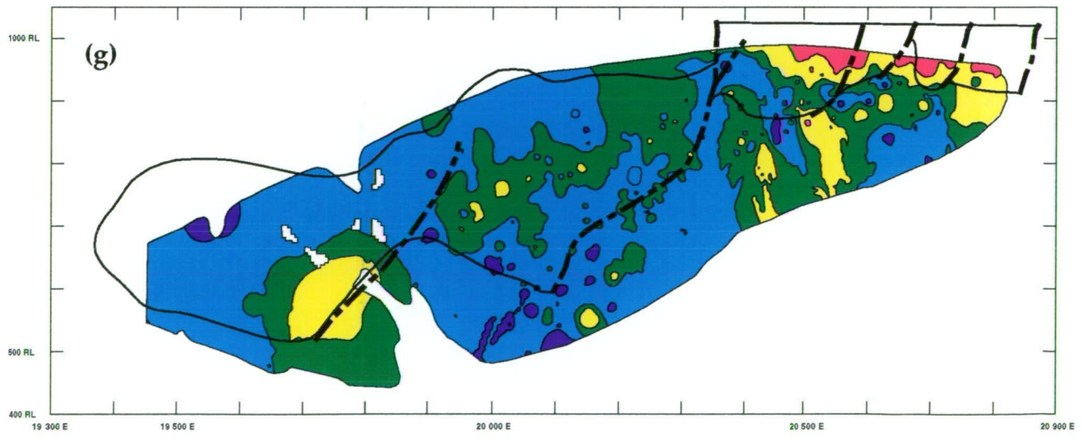

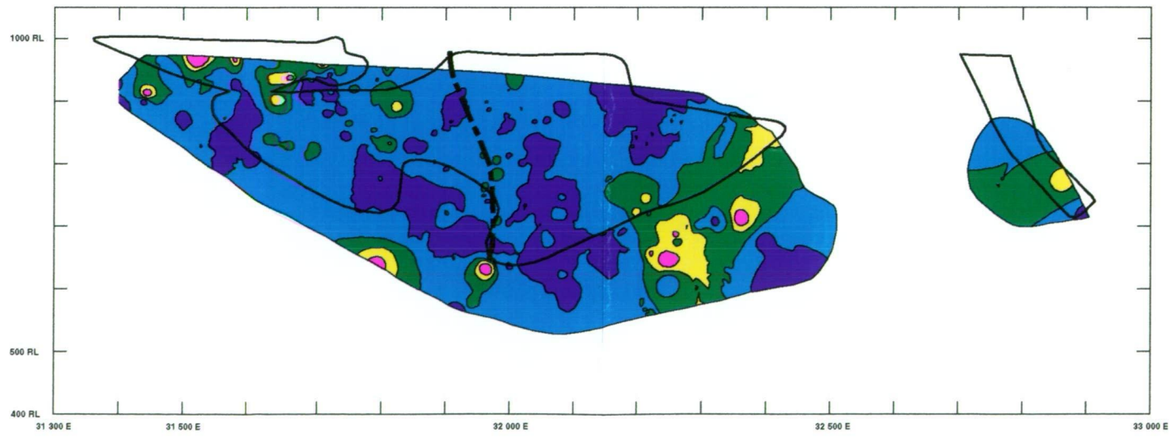

100 Cu / Cu + Zn

- > 75
- 45 - 75
- 30 - 45
- 15 - 30
- < 15

100 Cu / Cu + Zn

- > 80
- 60 - 80
- 45 - 60
- 30 - 45
- 15 - 30
- < 15

Figure 8.2 Distribution of (f) Zn ratio and (g) Cu ratio at Thalanga on long section

1:10,000

of Zn, Pb and Ag in long section are closely correlated (Fig. 8.2a,b,d). Regions of highest Zn, Pb and Ag values correspond to the thickest regions of sulphide mineralisation and are present at:

i) the eastern end of West Thalanga between 20 000 mE and 20 350 mE, and about 550 mRL to 800 mRL,

ii) the western end of Central Thalanga between 20 300 mE and 20 550 mE and generally above 750 mRL,

iii) the Vomacka Zone, and

iv) East Thalanga between about 31 800 mE and 32 200 mE.

Minor outlying areas with elevated Zn, Pb and Ag may represent satellite hydrothermal systems (e.g. the disseminated sphalerite intersected by diamond drill hole TH45 west of the West Thalanga ore lens, and the Orient ore lens to the east of East Thalanga).

The long section contours demonstrate that Cu and Au are present at higher concentrations (up to 20 % Cu and 6 ppm Au) and in larger areas, in West and Central Thalanga compared to East Thalanga. The latter contains a maximum of 13 % Cu and 3 ppm Au (Fig. 8.2c,e). Areas in Central Thalanga and the Vomacka Zone above about 930 mRL that contain elevated Cu and Au and low Zn, probably represent concentration of Cu and Au and depletion of Zn, by leaching during supergene alteration. This zonation supports Huston (1991) who reported that Cu is depleted and Au enriched in the gossan at Thalanga and Cu has been concentrated and Au slightly enriched in the supergene zone of Central Thalanga.

West and Central Thalanga

The main patterns of metal distribution at West and Central Thalanga are:

i) elevated Zn (>5 %), Pb (>3 %) and Ag (>75 ppm) occur in an elongate zone extending from about 20 000 mE, 600 mRL to about 20 350 mE, 800 mRL, where this zone overlaps with Central Thalanga (but has been offset along a normal fault; Chapter 3). This region of high Zn, Pb and Ag represents the thickest and most economic part of the West Thalanga ore lens, and is subparallel to the eastern limits of West Thalanga (Fig. 8.2a,b,d).

ii) high Zn, Pb and Ag occur together in most parts of Central Thalanga. A subvertical zone of low base and precious metal grades separates the large western part of Central Thalanga from the smaller zone of elevated Zn, Pb, Ag and Au at about 20 700 mE, 900 mRL (Fig. 8.2a-e).

iii) there is a subvertical pattern to Zn and Pb distribution within the zone of high Zn, Pb and Ag, and a similar grain to the distribution of Cu and Au in Central Thalanga and the western parts of West Thalanga (Fig. 8.2a-e). This steeply-plunging pattern of high metal grades occurs within the thickest and most economic parts of the ore lenses, and is subparallel to the mineral stretching lineation which is steep- to moderately NE-plunging (Chapter 3).

iv) in general, the location of Cu >1 % in West and Central Thalanga is coincident with the regions of Zn >5 %. There is a bulls-eye area of elevated Cu and Au at about 600 mRL between 19 700 mE and 19 800 mE (Fig. 8.2c,e), and up-dip is a zone of elevated Zn, Pb and Ag (19 500-19600 mE, 700 mRL; Fig. 8.2a,b,d).

v) the steeply-plunging zones of Zn ratio >75 within the main part of the West Thalanga (Fig. 7.2f) are similar in orientation to the zones of elevated Zn, Pb and Cu in the same region (Fig. 7.2a-c), but are not evident on the long section of Cu ratios (Fig. 7.2g). There is a large area with Zn ratio >75 trending parallel to, but at shallower depths than, the main part of the ore lens in West Thalanga (Fig. 7.2f,g).

vi) steeply-plunging zones of Zn ratio >75 are coincident with zones of Cu ratio >45 in the western half of Central Thalanga.

The pattern of metal distribution at West and Central Thalanga is interpreted to suggest that:
i) there is a prominent structural control on location of elevated metal grades in the thickest part of the ore lenses. The steeply-plunging pattern of Zn, Pb, Cu and Au grades within the main part of the ore lenses is interpreted to be subparallel to the L_2 mineral stretching lineation (steep- to moderate NE-plunge; Chapter 3).

ii) the bulls-eye area of elevated Cu and Au in western parts of West Thalanga is coincident with high Cu ratios and low Zn ratios and therefore may have formed over a local feeder zone. Elevated Zn, Pb and Ag is present up-dip from the Cu-rich bulls-eye, and is likely to be distal mineralisation related to the adjacent Cu- and Au-rich feeder zone.

iii) the area with Zn ratio >75 trending parallel to, but at shallower depths than, the main part of the ore lens in West Thalanga (Fig. 7.2f,g) is coincident with semi-massive sphalerite-galena-rich sulphides (Chapter 6), and may indicate lower temperatures of sulphide deposition.

Vomacka Zone and East Thalanga

The main patterns of metal distribution at the Vomacka Zone and East Thalanga are:
i) areas of elevated Zn, Pb and Ag in the Vomacka Zone have similar locations and all, except for some Zn, occur within the zone of >1 % Cu.

ii) the Vomacka Zone contains larger areas of high Au (1-3 ppm) than present in East Thalanga and generally these Au-rich areas are coincident with elevated Zn, Pb, Ag and rarely Cu.

iii) Zn, Pb and Ag in East Thalanga have similar distribution patterns and the largest regions of abundant Zn, Pb and Ag are concentrated adjacent to the sharp western and deepest margins of the ore lens (Fig. 8.2a,b,d). Smaller and more discontinuous areas containing elevated Zn, Pb and Ag are present to the east and at shallower depths above the main high grade zone in East Thalanga. There is one area of elevated Zn (>8 %) at about 32 400 mE and 600 mRL, but this is not associated with high Pb, Ag, Cu or Au.

iv) in general, the location of >1 % Cu in East Thalanga has a reasonable match with the location of Zn >8 %. There is a weak association between >1 % Cu and the rare, small areas of elevated Au (<3 ppm) in East Thalanga, although the deepest area of high Au is coincident with elevated Zn rather than Cu (cf. Fig. 8.2a,c,e).

v) areas with Zn >8 %, Pb >3 %, Cu >1 %, Ag >75 ppm and Au >0.5 % at the western part of East Thalanga are aligned (Fig. 8.2a-e). This line has a similar pitch to the steep- to moderately-plunging mineral elongation lineation (L_2; Chapter 3). Zones of elevated Cu and Au are aligned along the trace of the ENE-trending normal fault (subvertical dashed line).

vi) at shallow depths and between 32 100 and 32 300 there is only low values of Zn, Pb, Cu and Ag and Au (Fig. 8.2a-e). This zone is coincident with the location of thick QFP (Fig. 4.8a; Chapter 4). The region of 1 % Cu and 1 ppm Au in East Thalanga defines an arc around the thickest region of QFP.

vii) there is only one area with Zn ratio <60 in East Thalanga, and this occurs below about 700 mRL and centred on 32 000 mE (Fig. 8.2f). This area is coincident with corresponds to small areas of elevated Cu, Ag, Au and Cu ratios (Fig. 8.2c-g). The Zn ratios increase to >80 on both the eastern and western sides of this low Zn ratio zone.

The main interpretations of the pattern of metal distribution at the Vomacka Zone and East Thalanga are:

i) the moderate plunge of the line of high grade zones in East Thalanga is interpreted to indicate a strong structural control (parallel to L_2) on the distribution of metals. The ENE-trending normal faults are interpreted to have post-dated L_2 (Chapter 3), and therefore the presence of elevated Cu and Au, but not Zn, Pb or Ag, along the trace of the ENE-trending normal fault may be due to later remobilisation of chalcopyrite-rich sulphides.

ii) the lack of elevated metal grades at the location of thick QFP at shallow depths in East Thalanga is interpreted to indicate that the location of QFP sills or domes may partly control the distribution of massive sulphide lenses.

iii) the area of Zn ratio <60 and elevated Cu, Ag, Au and Cu ratios at depth in East Thalanga may represent sulphide lenses proximal to a high temperature feeder zone. The Zn ratios increase to >80 on both the eastern and western sides of this low Zn ratio zone, and this is interpreted to represent mineralisation further from the feeder zone.

8.3.3 Cross Sections

Metal grades on cross sections from West, Central and East Thalanga were contoured in order to investigate the distribution of metals within the mineralised horizon, in particular to document variation in metal distribution with stratigraphy. Only one section from each part of the Thalanga deposit is presented in this section; metal zonation contours from a second cross section in both West (20 290 mE) and Central (20 390 mE) Thalanga are submitted in Appendix I.

West Thalanga

The main patterns of metal distribution on the 20 250 mE section (Fig. 8.3a-f) in West Thalanga are:

i) elevated metals occur in two zones parallel to bedding. These zones correspond to lenses of massive polymetallic sulphides and massive pyrite (Fig. 6.1). Semi-massive to vein-style sphalerite-galena-pyrite-rich sulphides hosted in carbonate-chlorite-rich assemblages overlie the massive pyrite (Fig. 6.1). The locations of the highest grades of Zn on the 20 250 mE section have a similar distribution to that of elevated Pb, Ag, Au and some Cu (Fig. 8.3a-e). The margins of the polymetallic massive sulphide lens is coincident with >5 % Zn (Fig. 8.3a). Similar grades of Zn occur in the zone of semi-massive sulphides overlying the massive pyrite (Fig. 8.3a). The highest Zn and Pb grades are present within the down-dip parts of the massive sulphide lens (Fig. 8.3a,b). There is little Pb in the massive pyrite. The highest Ag values are not associated with the highest Zn and Pb in the massive sulphides, but are located in the underlying semi-massive sulphides (Fig. 8.3c).

ii) the distribution of Cu >1 % is coincident with the massive and semi-massive sulphides and the massive pyrite (Fig. 8.3d). The Cu content of the massive pyrite decreases up-dip. High levels of Cu (5 to >10 %) at the stratigraphic top of the mineralised horizon are associated with remobilised chalcopyrite-rich sulphides. High Au (>1 ppm) also occurs with these remobilised sulphides (Fig. 8.3e).

iii) there is a prominent enrichment in Ba (>5 %) in the up-dip parts of the mineralised horizon on this section (particularly in association with the QEV), and the Ba content of the massive sulphide lens gradually decreases in the down-dip direction (Fig. 8.3f). There are traces of Ba >1 % in the massive pyrite. The apparent down-dip increase in Ba within the

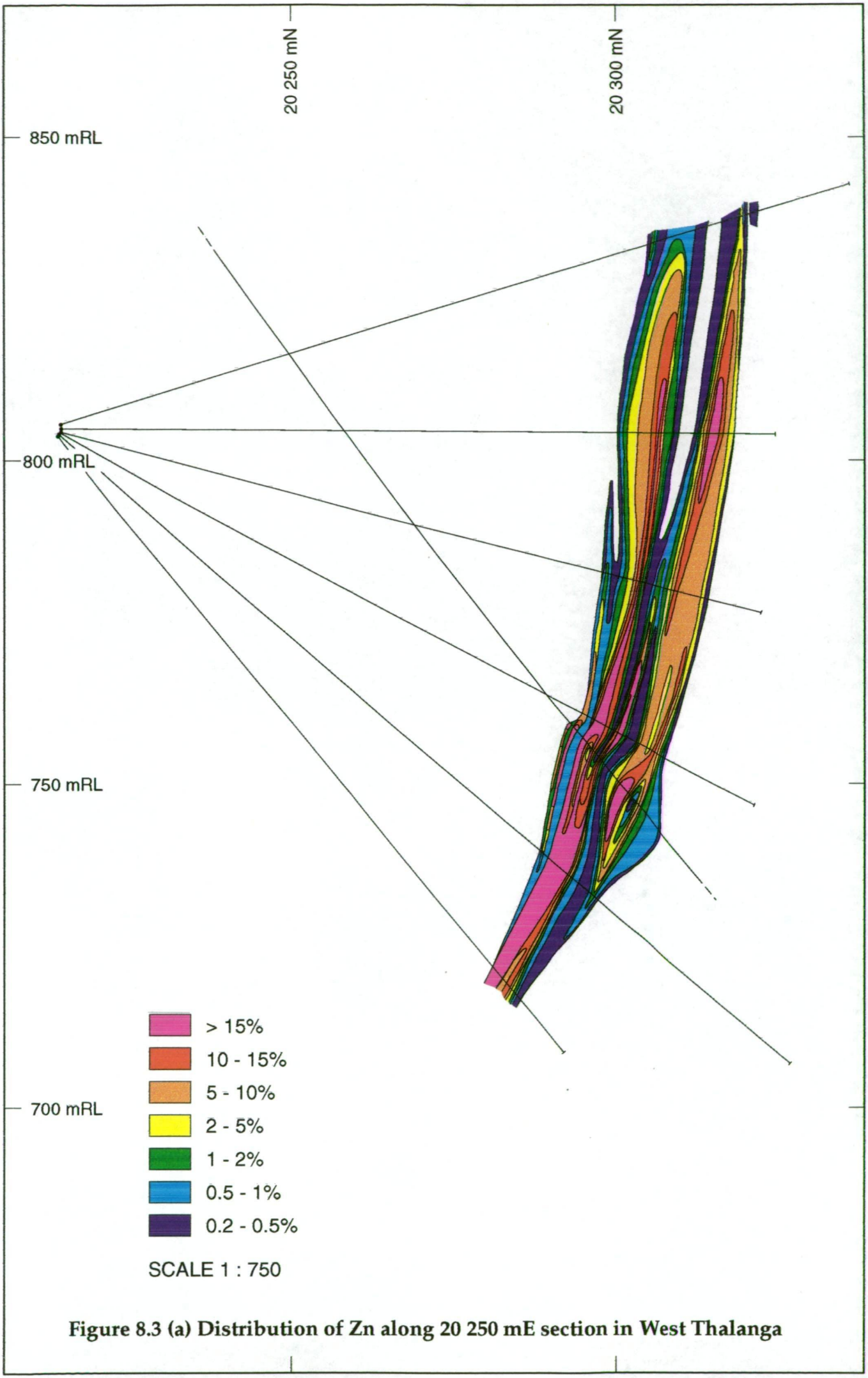

Figure 8.3 (a) Distribution of Zn along 20 250 mE section in West Thalanga

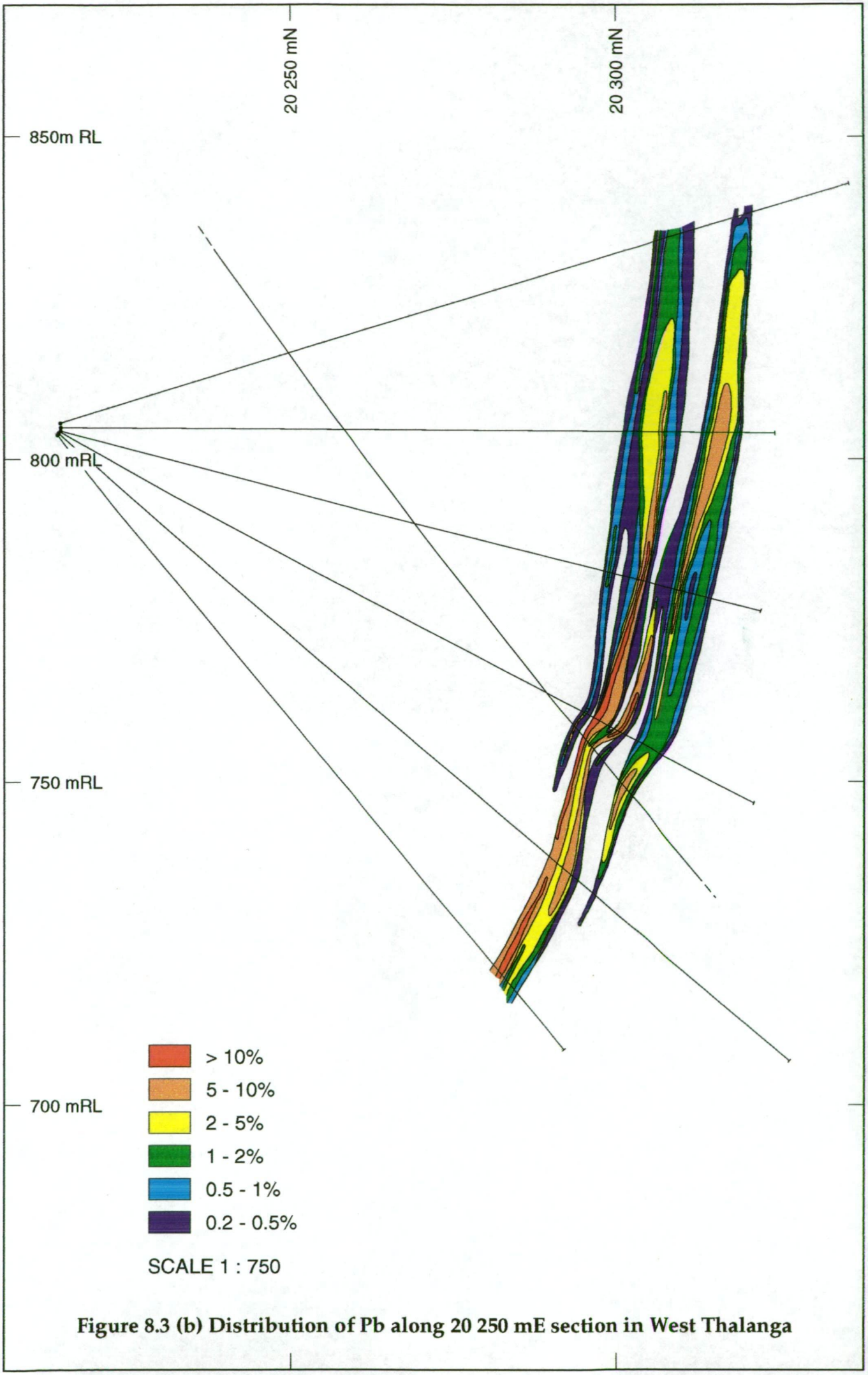

Figure 8.3 (b) Distribution of Pb along 20 250 mE section in West Thalanga

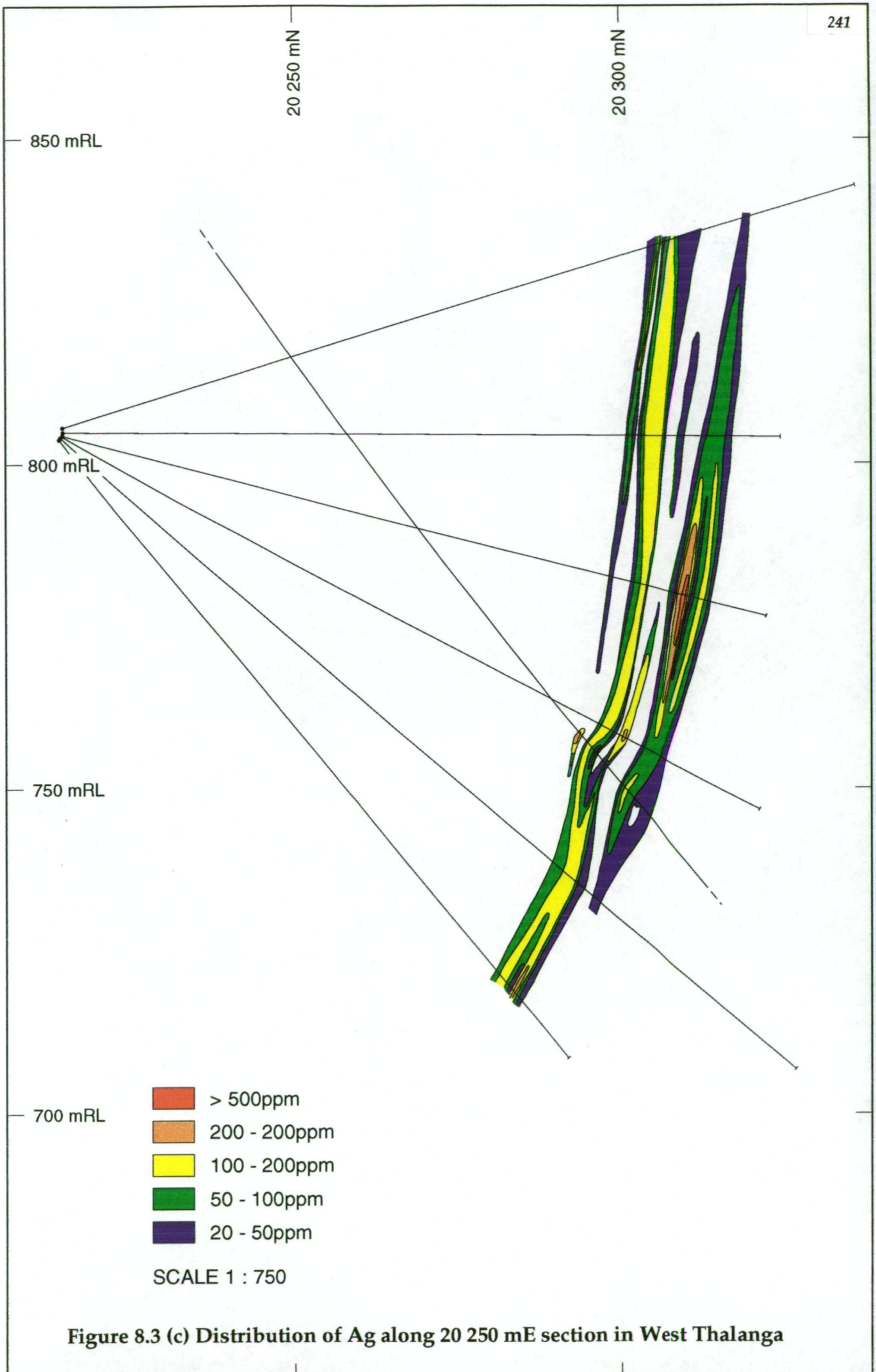

Figure 8.3 (c) Distribution of Ag along 20 250 mE section in West Thalanga

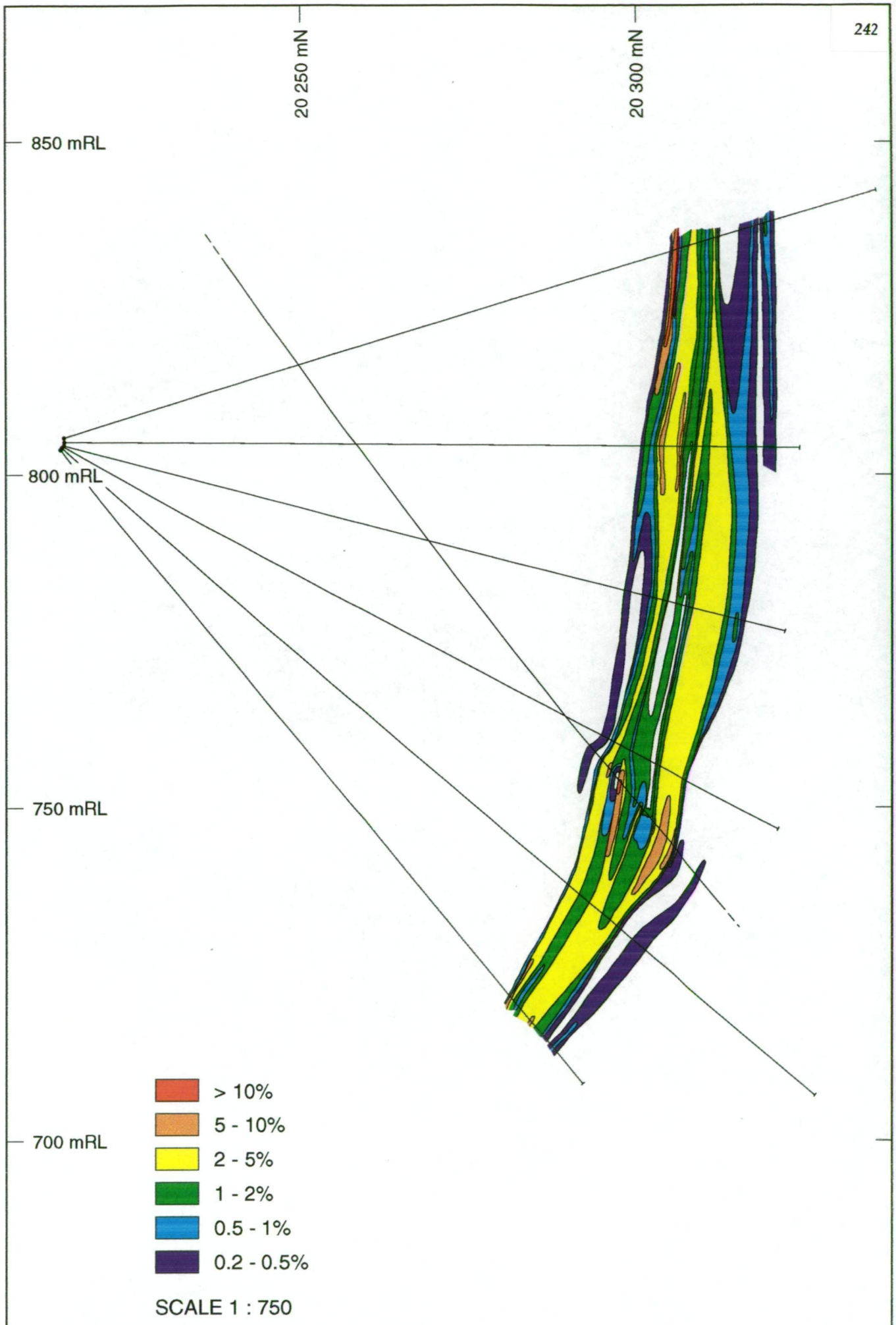

Figure 8.3 (d) Distribution of Cu along 20 250 mE section in West Thalanga

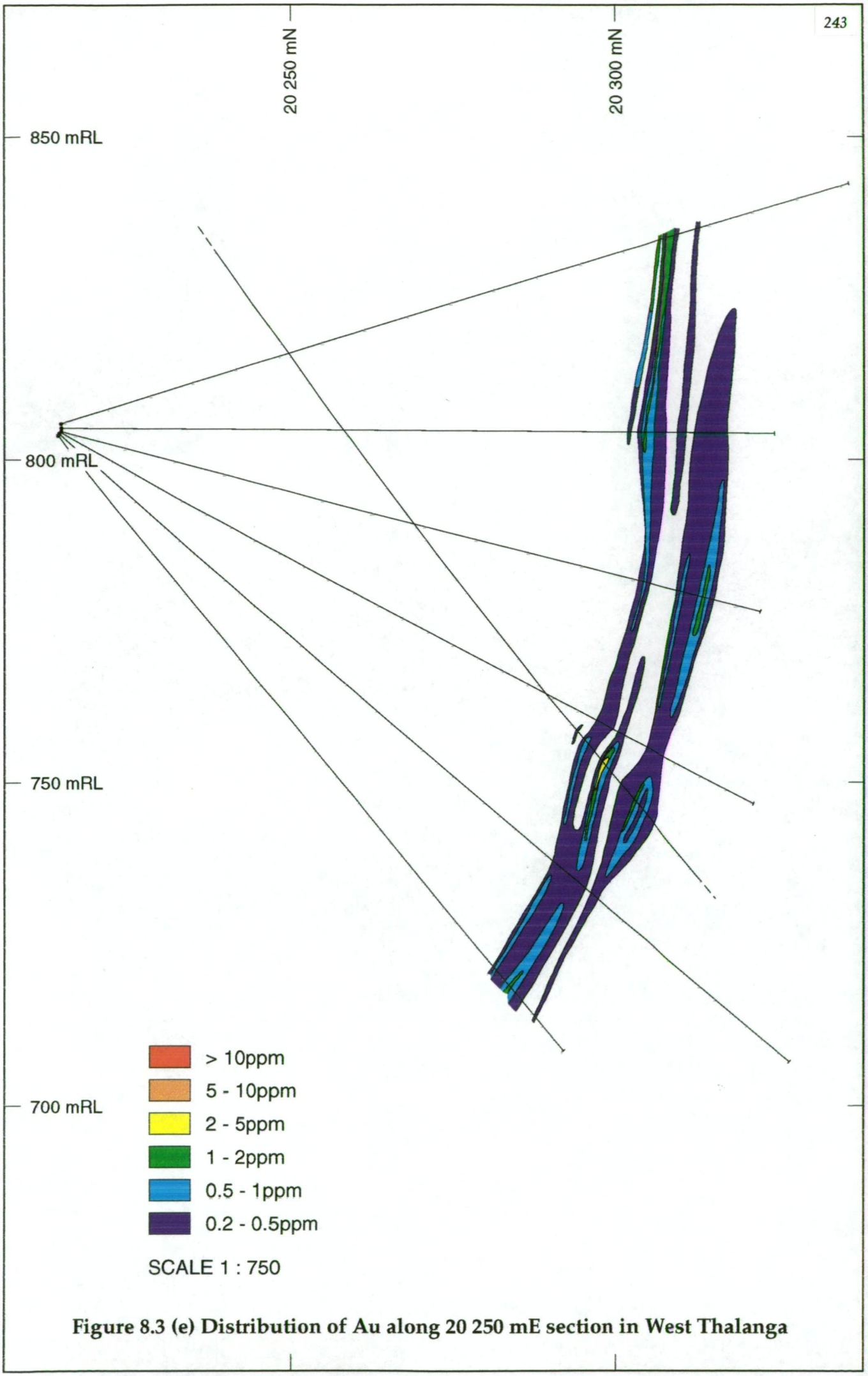

Figure 8.3 (e) Distribution of Au along 20 250 mE section in West Thalanga

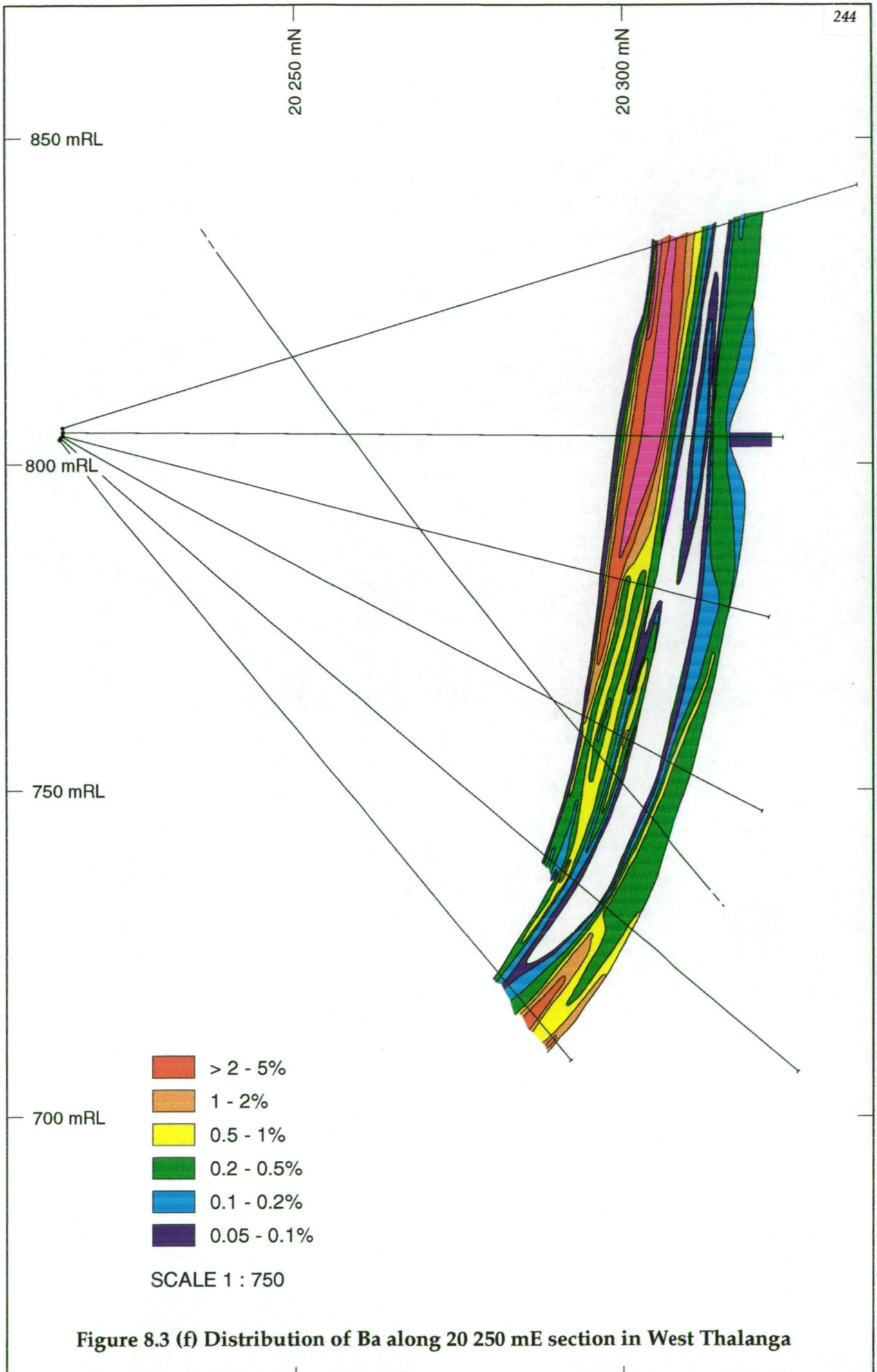

Figure 8.3 (f) Distribution of Ba along 20 250 mE section in West Thalanga

massive pyrite lens reflects the amalgamation of the massive pyrite with polymetallic sulphides in this location (Fig. 6.1).

The main interpretations of the metal zonation on the 20 250 mE section in West Thalanga are:
i) the location of elevated Zn and Pb grades in the areas overlying massive pyrite is similar to the metal zonation described from less metamorphosed massive sulphide deposits (e.g. Eldridge *et al.*, 1983), which is interpreted to indicate a decrease in temperature of sulphide deposition from a hotter pyrite-rich core, to lower temperature sphalerite-galena-barite-rich outer zone.

ii) the pattern of Ba zonation, combined with the zonation in Zn distribution, is consistent with the up-dip parts of the polymetallic sulphides representing distal sulphides that formed from cooler, more oxidised mineralising solutions. The decreasing intensity of hydrothermal alteration in the footwall in the up-dip direction (Chapter 10) supports this interpretation.

Central Thalanga

Due to the modification of primary metal distribution by supergene leaching processes in most parts of Central Thalanga (Huston, 1991), the distribution of base metals on the 20430 mE section were contoured because on this section the zone of structurally thickened sulphides (Chapter 3) is below the supergene boundary. Figure 8.4 (a-f) shows that patterns of metal distribution in Central Thalanga are:
i) there are two main subvertical zones of elevated Zn values within the mineralised horizon and in most places elevated Pb and Ag are associated with the high Zn (Fig. 8.4a-c). In general, the highest grades of these metals occur in the thickest parts of the ore lens.

ii) multiple zones of elevated Zn, Pb and Ag occur within the zone of thick sulphides. The amount of Zn, Pb and Ag gradually decreases in the down-dip direction, corresponding to the decrease in thickness of the massive sulphides and presence of semi massive sulphides hosted in the footwall rhyolitic volcanics.

iii) elevated Cu (>5 %) is present as multiple elongate zones parallel to the ore lens, with four zones of elevated Cu in the thickest region of massive sulphides (Fig. 8.4d). The region of >15 % Cu at the stratigraphic top of the ore lens (at about 900 mRL) corresponds to remobilised chalcopyrite-rich sulphides at the contact between massive sphalerite-galena-pyrite and coherent dacite. Lenses of high grade Cu (2 -10 %) at the stratigraphic base of the ore lens occur in massive pyrite and are partly associated with high Zn, Pb and Ag.

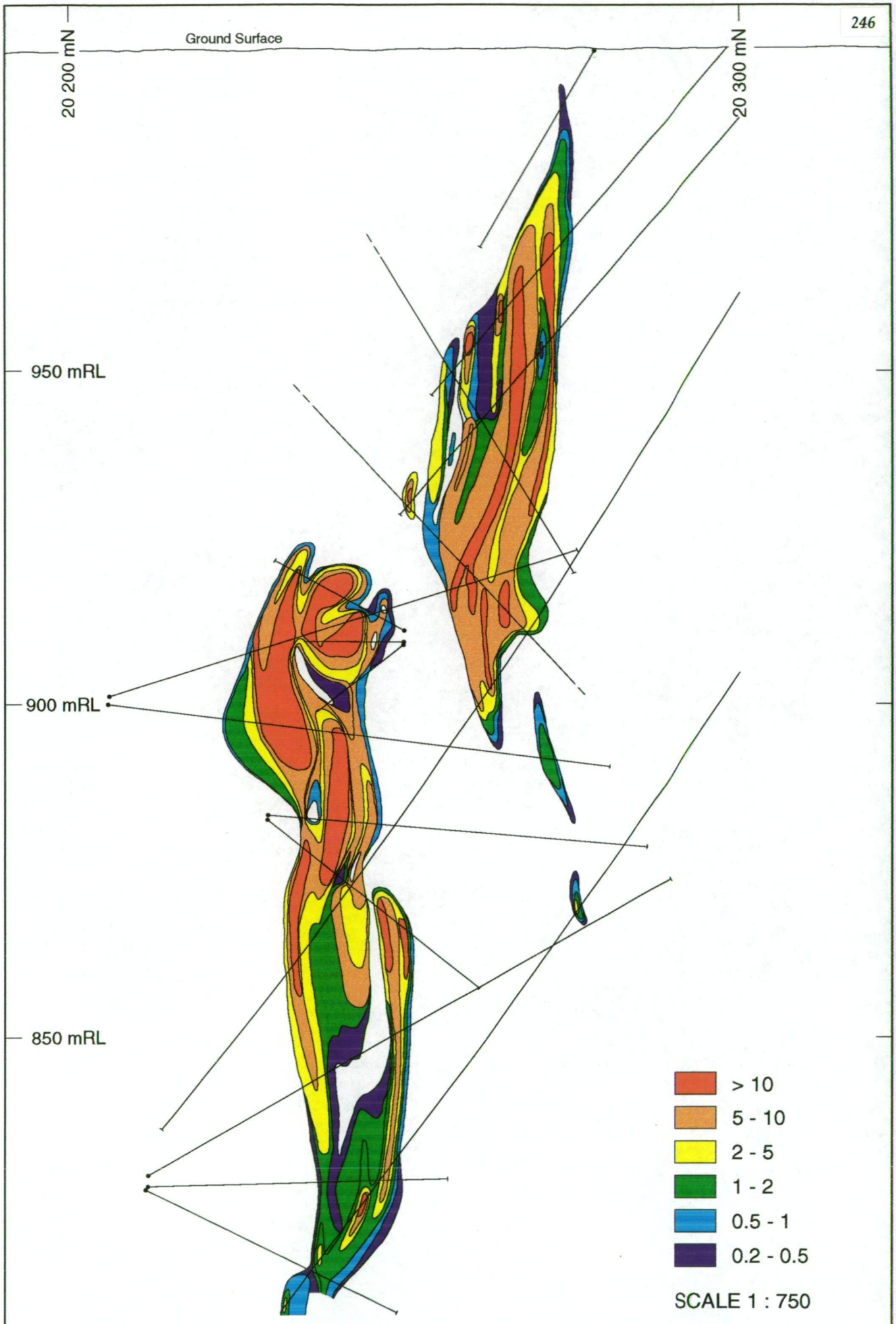

Figure 8.4 (a) Distribution of Zn along 20 430 mE section in Central Thalanga

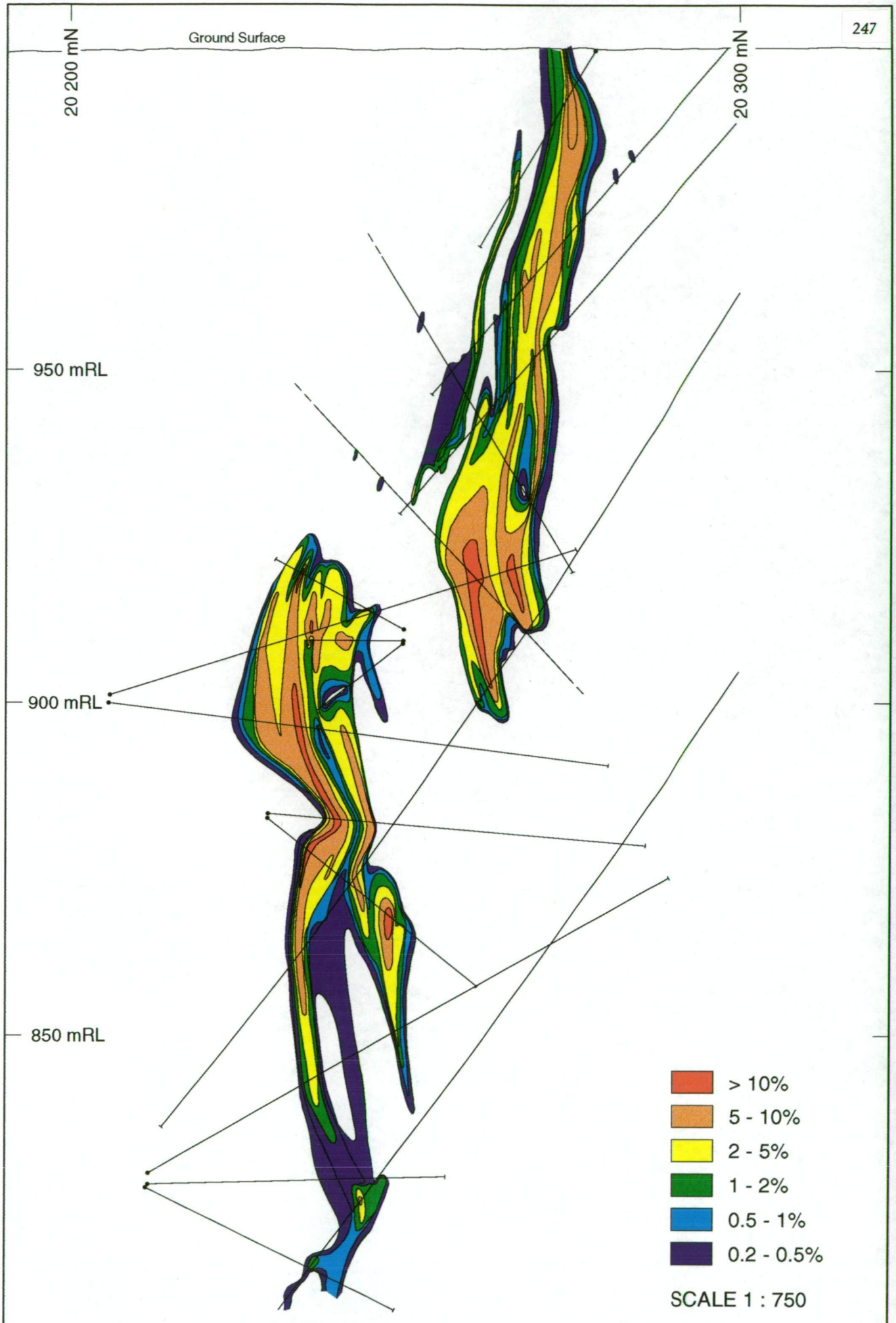

Figure 8.4 (b) Distribution of Pb along 20 430 mE section in Central Thalanga

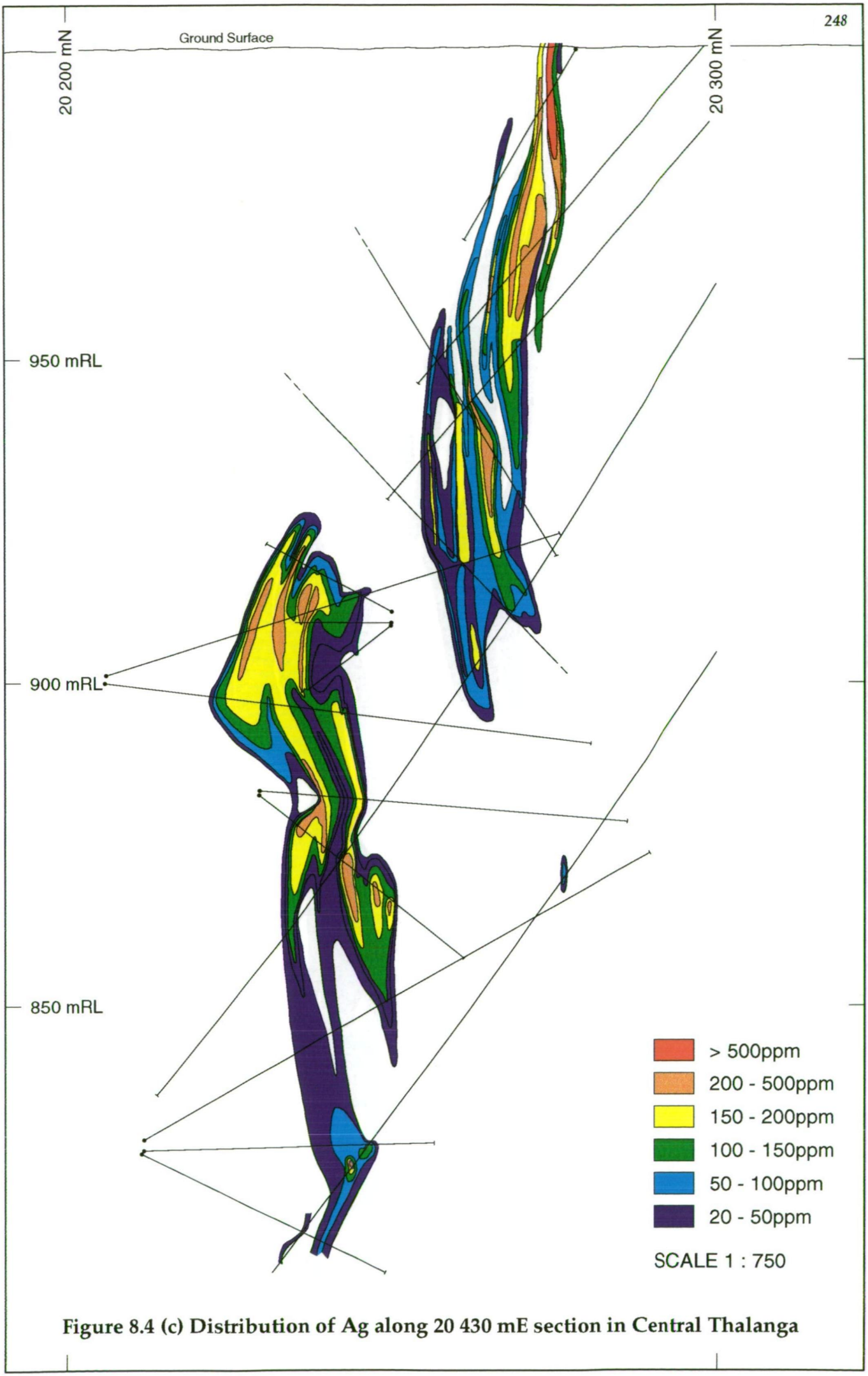

Figure 8.4 (c) Distribution of Ag along 20 430 mE section in Central Thalanga

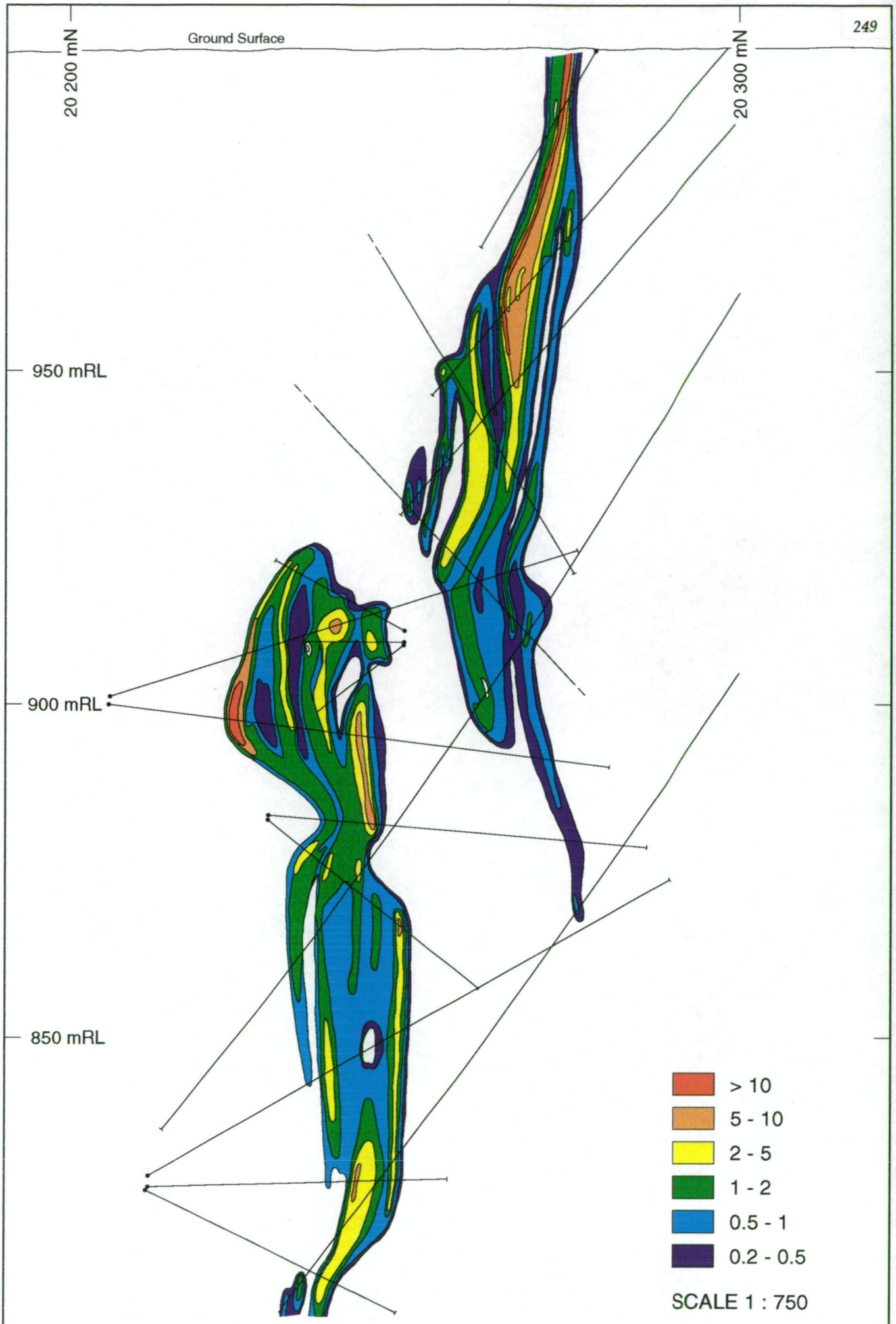

Figure 8.4 (d) Distribution of Cu along 20 430 mE section in Central Thalanga

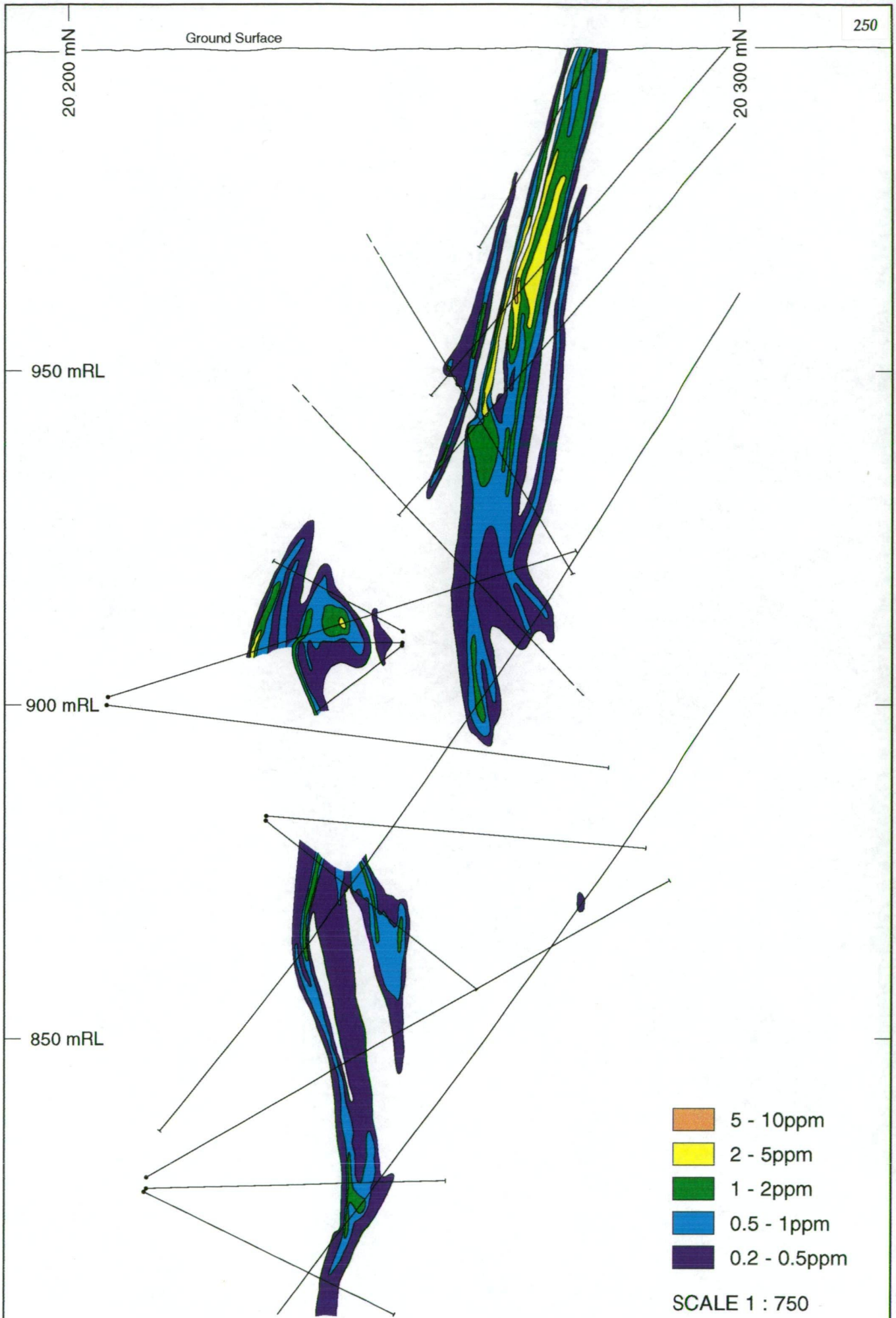

Figure 8.4 (e) Distribution of Au along 20 430 mE section in Central Thalanga

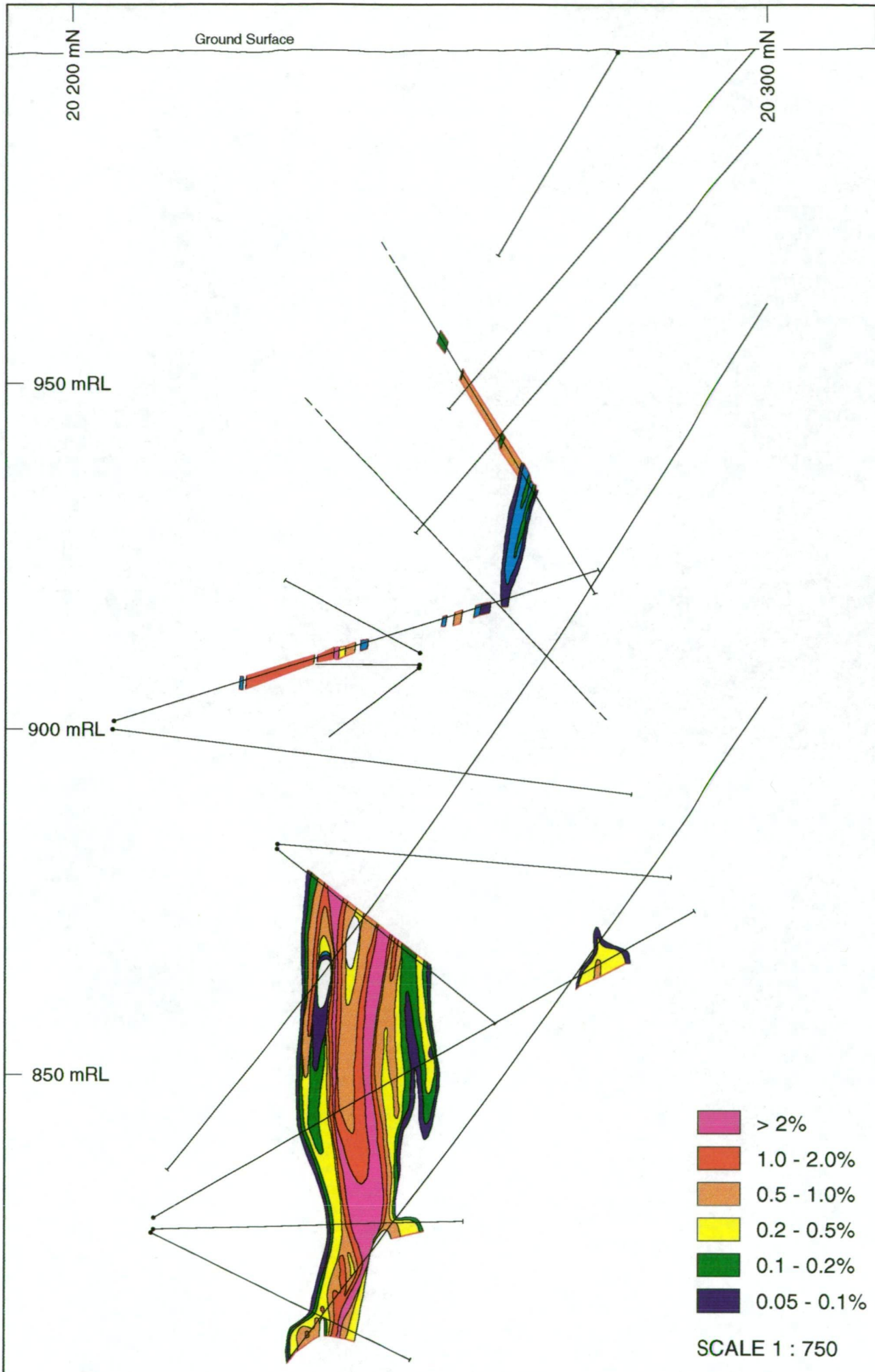

Figure 8.4 (f) Distribution of Ba along 20 430 mE section in Central Thalanga

iv) the 20 2430 mE section is incompletely sampled for Au, but clearly shows the low grades of Au at Thalanga (Fig. 8.4e). The only sites of Au >2 ppm are within the zone of supergene weathering and as small areas associated with high Cu within the region of thickest massive sulphides. There is a consistent pattern of Ba zonation on this section, despite the limited Ba analyses, with high grades of Ba present towards the stratigraphic top of the massive sulphides (Fig. 8.4f). Elevated Ba within the mineralised horizon is also present at depth.

Important interpretations of the metal distribution at Central Thalanga are that:
i) the apparent cyclicity of the distribution of elevated Zn, Pb, Cu and Ag within the zone of thick sulphides are consistent with the structural interpretation of repetition of the ore lenses along steeply dipping, ENE-striking normal faults (Chapter 3). Prior to deformation the ore lens is interpreted to have comprised a Cu-rich base overlain by Zn- and Pb-rich sulphides. Remobilisation of chalcopyrite-rich sulphides along the normal faults and other sites of extension (Chapter 3) may also explain parts of the multiple zones of elevated Cu.

ii) despite attempting to avoid the influence of supergene processes and weathering, the low Zn grades, together with high Pb and Ag, all at shallow depths (>980 m) on this section are consistent with the leaching of Zn and concentration of Pb and Ag during weathering.

East Thalanga

The main patterns of metal distribution on the 32 080 mE section (Fig. 8.5a-e) in East Thalanga are:
i) the massive to semi massive sulphide lenses are best defined by the Zn >5 % and Pb >2 % contour lines (Fig. 8.5a,b; see Fig. 6.10 for geology). The distribution of elevated Ag correlates well with the distribution of Zn and Pb, although the highest Ag does not always occur with the highest Zn grades (Fig. 8.5a-c).

ii) the abundance of Zn, Pb and Ag within the footwall lens gradually decreases down-dip, whereas the number of areas with elevated Zn, Pb and Ag in the hangingwall lens increase but become more patchy in the down-dip direction.

iii) Zn, Pb and Ag are elevated with the footwall ore lens at both up-dip and down-dip margins of the lozenge-shaped zone of intensely silicified rhyolitic volcanics (cf. Fig. 8.5a-c with Fig. 6.10).

iv) the sulphide lenses in East Thalanga are poorly defined by Cu and Au contour diagrams, due the low amounts of these metals in this part of Thalanga (Fig. 8.5d,e). There are patchy areas of >2 % Cu within the footwall lens and generally the hangingwall lens contains <0.5

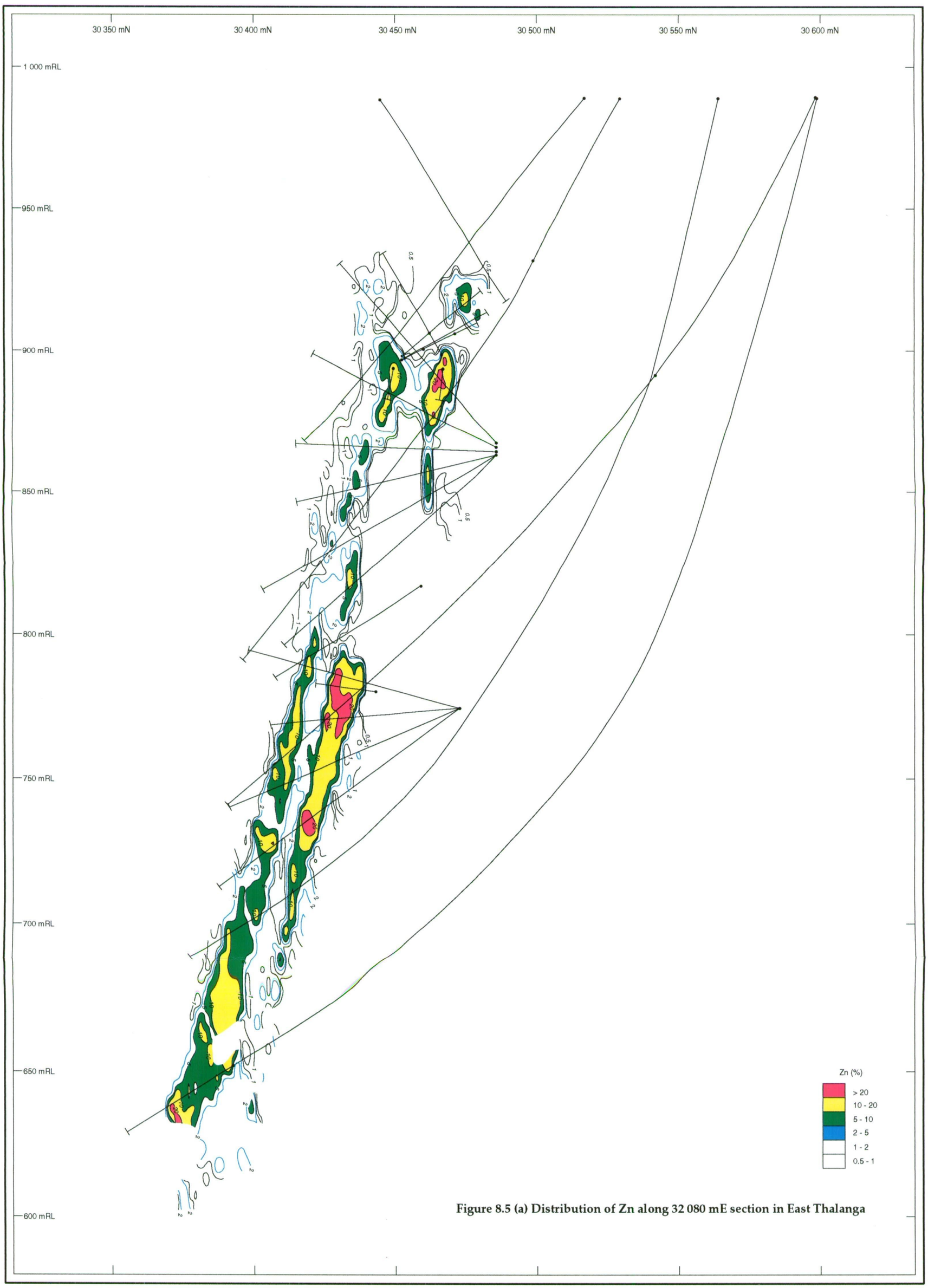

Figure 8.5 (a) Distribution of Zn along 32 080 mE section in East Thalanga

30 350 mN
30 400 mN
30 450 mN
30 500 mN
30 550 mN
30 600 mN

1 000 mRL
950 mRL
900 mRL
850 mRL
800 mRL
750 mRL
700 mRL
650 mRL
600 mRL

Pb (%)
> 10
5 - 10
2 - 5
1 - 2
0.5 - 1

Figure 8.5 (b) Distribution of Pb along 32 080 mE section in East Thalanga

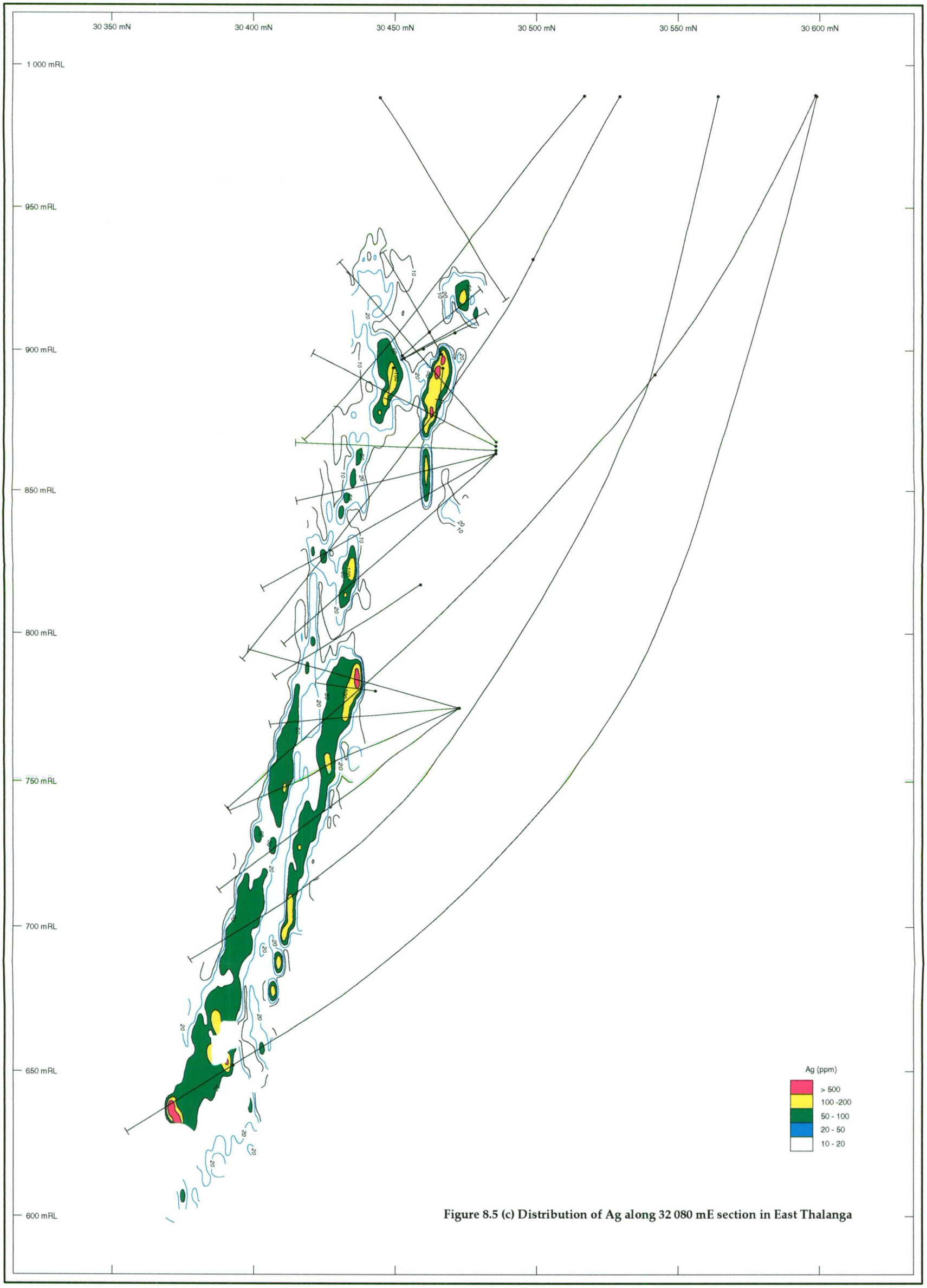

Figure 8.5 (c) Distribution of Ag along 32 080 mE section in East Thalanga

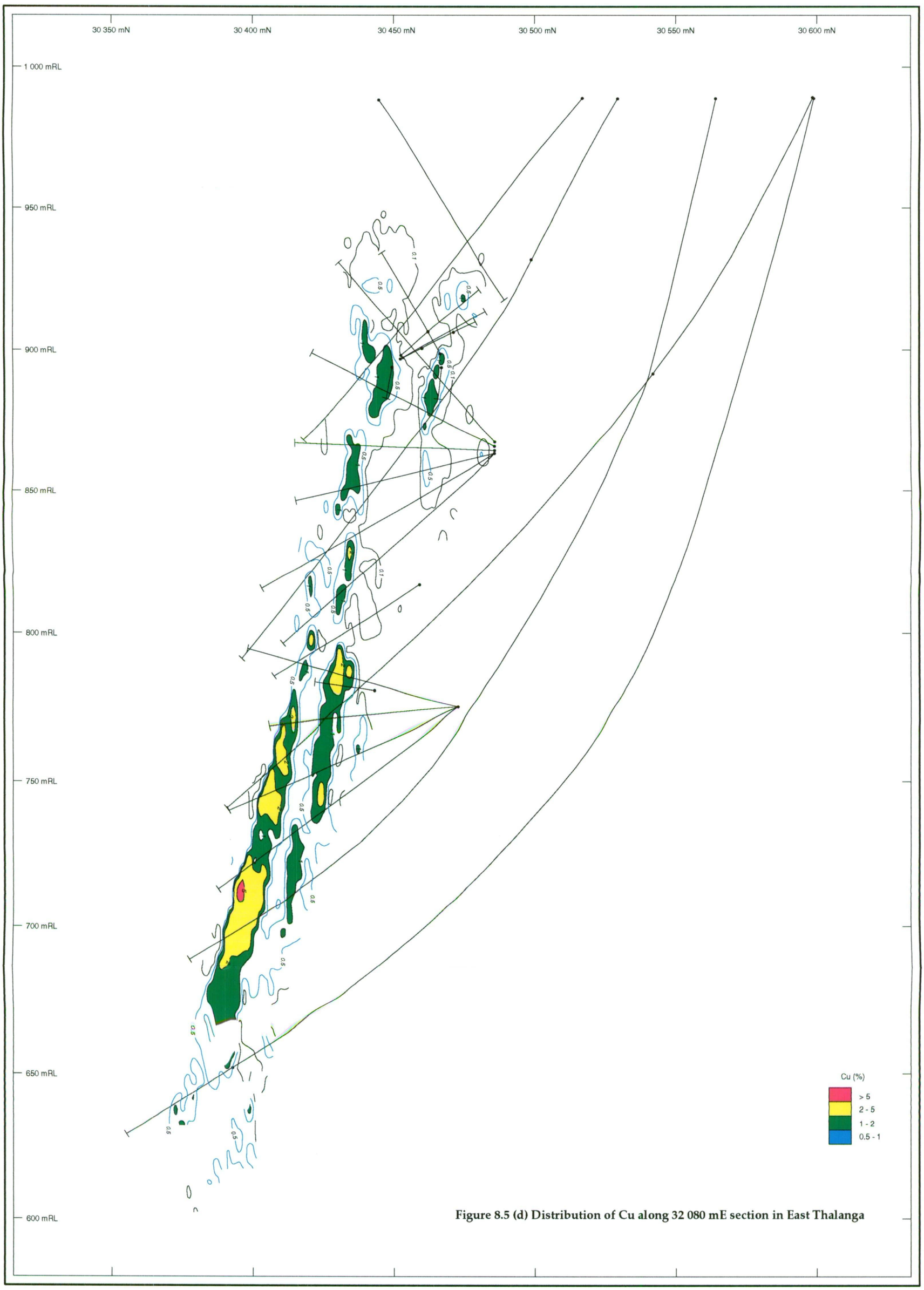

Figure 8.5 (d) Distribution of Cu along 32 080 mE section in East Thalanga

30 350 mN
30 400 mN
30 450 mN
30 500 mN
30 550 mN
30 600 mN

1 000 mRL
950 mRL
900 mRL
850 mRL
800 mRL
750 mRL
700 mRL
650 mRL
600 mRL

Au %
> 2
1 - 2
0.5 - 1
0.1 - 0.5

Figure 8.5 (e) Distribution of Au along 32 080 mE section in East Thalanga

% Cu. Conversely, the highest Au grades are present in the hangingwall lens rather than the footwall lens.

The main conclusions based on the metal distribution contours in Figure 8.5(a-e) are:
i) the location of elevated Zn, Pb, Cu and Ag within the down-dip parts of the footwall lens matches the distribution of thick lenses of massive sphalerite-pyrite-rich sulphides. The patchy distribution of elevated Zn, Pb, Cu and Ag at East Thalanga is consistent with the semi-massive characteristics of the hangingwall and locally the footwall lens. There is no clear zonation from a Cu-rich base to Zn- and Pb-rich top within East Thalanga.

ii) the concentration of elevated Zn, Pb and Ag in the footwall lens is consistent with remobilisation of sulphides into pressure shadows at the up- and down-dip extent of the intensely silicified rhyolite during deformation. The presence of remobilised galena-chalcopyrite ± sphalerite in pressure shadows ore lenses at Thalanga supports this mechanism of base metal concentration (Chapter 3). Alternatively, the increase in grade in these areas could be due to high primary fluid flow at the margins of the intensely silicified rhyolite. This second explanation is consistent with the lack of continuous massive sulphide directly overlying the intensely silicified rhyolite in East Thalanga. It is highly likely that a combination of both mechanisms resulted in the concentration of metals in this location.

8.4 Metal Associations

Metal contour diagrams display the spatial variation in metal concentrations within the ore lenses and can show gross metal correlations, but scattergrams are useful in illustrating the degree of correlation between the various metals. Huston and Large (1988) recognised a distinction between the massive barite lenses, the sphalerite-galena-pyrite-rich ore and the pyrite-chalcopyrite-rich ore at the Rosebery deposit based on Cu, Pb, Zn, Ag and Au contents, and used log-normal scattergrams to demonstrate the metal associations. Similar comparisons of the metal associations between ore lenses were conducted by Huston *et al.* (1992a) for the Balcooma and Dry River South prospects in northern Queensland. Scattergrams were generated from selected drill holes in East, Central and West Thalanga, and are combined on the basis of rock type in Figure 8.6(a-g) and 8.7(a-g). There is no correlation between Ba and Cu, Pb, Zn, Ag or Au in any of the West, Central or East Thalanga ore lenses.

There are two main occurrences of Au in VHMS deposits, a Pb-Zn-Ag-Au association in sphalerite-galena-rich sulphides and a Cu-Au association in pyrite-chalcopyrite-rich sulphides and stringer zones (e.g. Hannington *et al.*, 1986; Ashley *et al.*, 1988; Huston and Large, 1989; Larocque *et al.*, 1993). Generally, only one type of Au association is present within a deposit. For example, there is a prominent Zn-Au association at the Rosebery

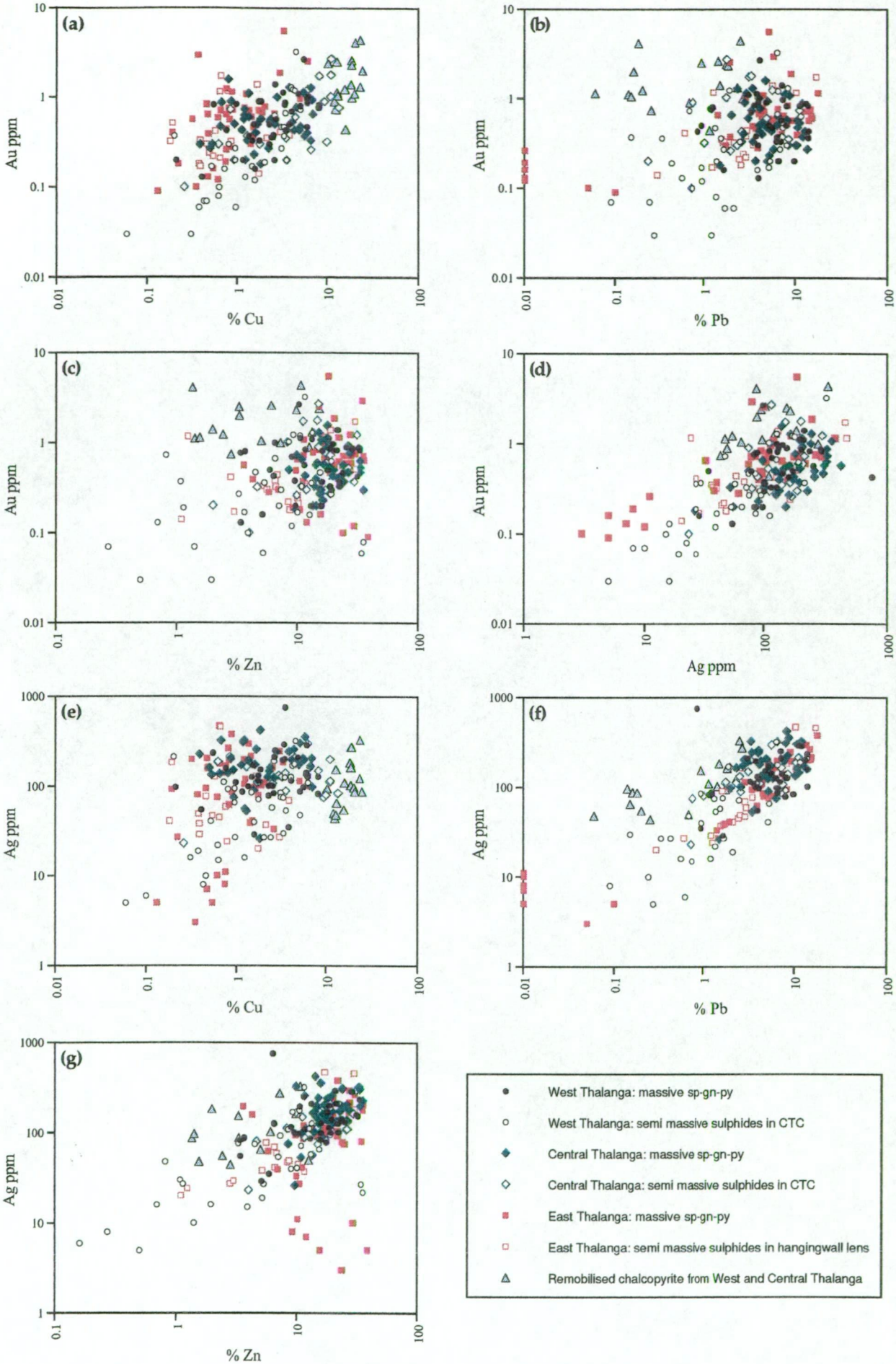

Figure 8.6 Scattergrams depicting the relationship between Au and Ag and the main ore metals within the polymetallic massive sulphide lenses at Thalanga. Sources of data listed in Appendix H.

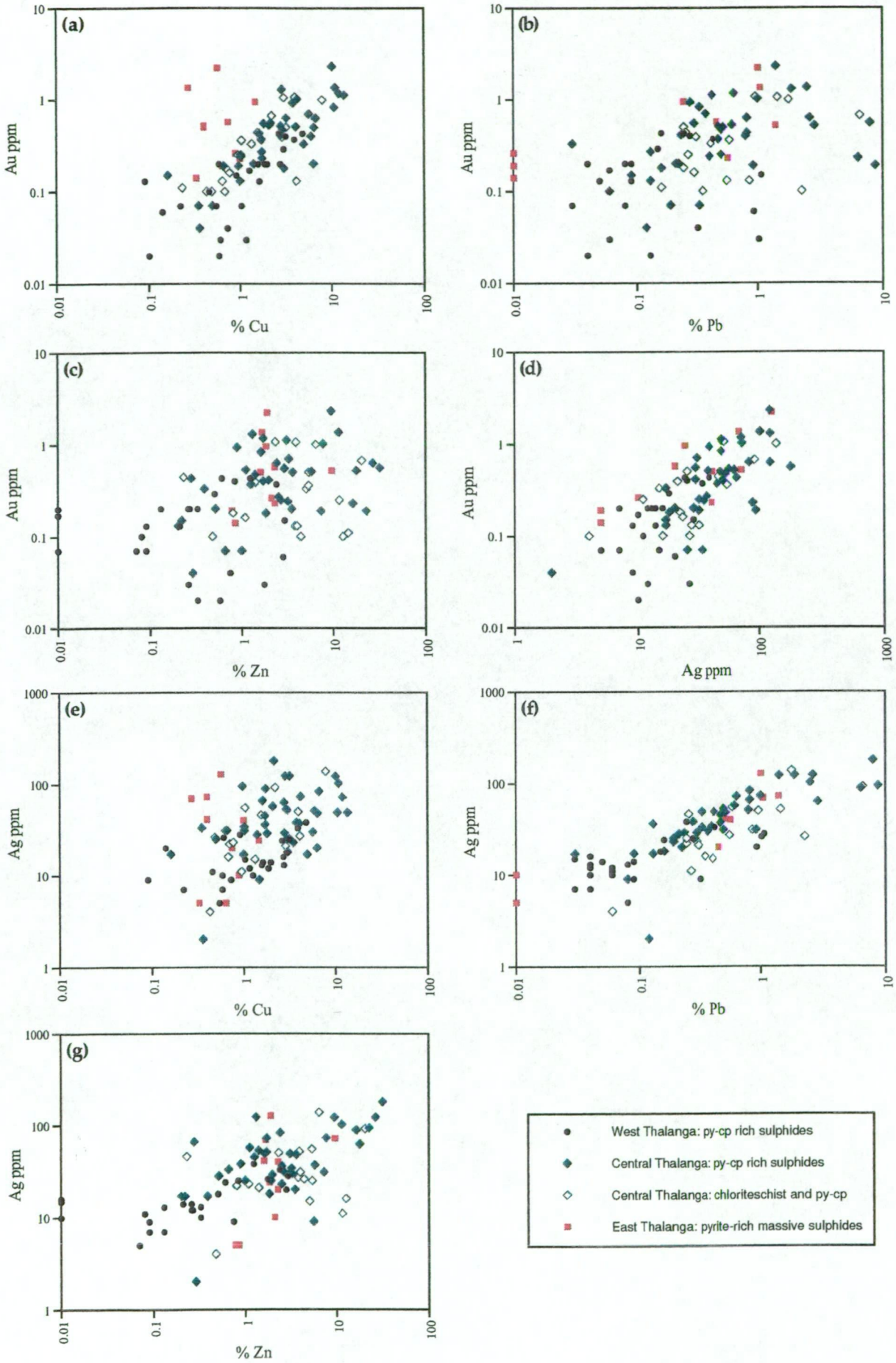

Figure 8.7 Scattergrams depicting the relationship between Au and Ag and the main ore metals within the pyrite-rich ore lenses at Thalanga. Sources of data are listed in Appendix H.

deposit, yet in both the sphalerite-galena-pyrite-rich sulphides and the pyrite-chalcopyrite-rich sulphides there is a good correlation between Au, Ag and Zn (Huston and Large, 1989). Au also has a good correlation to both Zn and Cu in the massive barite lens at Rosebery (Huston and Large, 1988).

8.4.1 Gold

Au has a moderate correlation with Cu in both the pyrite-rich sulphides and the sphalerite-galena-pyrite-rich sulphides at Thalanga (cf. Fig. 8.6a and 8.7a). Elevated Au is also associated with elevated Cu values in the remobilised sulphides (Fig. 8.6a). The Au-Cu association is most pronounced in the pyrite-chalcopyrite-rich sulphides in West and Central Thalanga (Fig. 8.7a), where lenses of massive pyrite ± chalcopyrite underlying sphalerite-galena-pyrite-rich sulphides are more common than in East Thalanga (Chapter 6). In the sphalerite-galena-pyrite-rich sulphides, the most prominent Au-Cu association is present in West Thalanga (Fig. 8.6a).

Au is weakly correlated with Zn and Pb in semi-massive sulphides hosted by carbonate-chlorite-rich assemblages in West Thalanga (Fig. 8.6b,c), but there is no correlation between Au and either Zn or Pb in the massive pyrite lenses in all of Thalanga. Similarly, there are no clear associations between Au and Zn or Pb in the remobilised sulphides. Therefore, the Thalanga deposit can be classified as having a Cu-Au association, as proposed by Huston *et al.* (1992b).

8.4.2 Silver

The contours of Ag distribution in long section and cross sections (Figs 8.2-8.5) show that elevated Ag is coincident with elevated Zn and Pb and also high Au in places at Thalanga. This metal association is supported by the scattergrams in Figure 8.6(d-g) and 8.7(d-g) that show a positive linear relationship between Ag and Zn, Pb and Au in both the sphalerite-galena-pyrite-rich sulphides, the pyrite-chalcopyrite-rich sulphides, and the remobilised chalcopyrite-rich sulphides. The correlation between Ag and Au is particularly prominent in the semi-massive sulphides from West Thalanga (Fig. 8.6d) and the massive pyrite lenses (Fig. 8.7d), but in other lenses this association is moderate. Ag and Pb have the strongest association in all ore-types and in all lenses at Thalanga (Fig. 8.6f and Fig. 8.7f). There is a moderate correlation between Zn and Ag grades in Central and West Thalanga, but the sphalerite-galena-pyrite lenses in East Thalanga exhibit variable Ag content with consistent Zn contents (Fig. 8.6g).

There is a weak correlation between Ag and Cu in the sphalerite-galena-pyrite ore in West Thalanga and the remobilised chalcopyrite-rich sulphides, but there is no relationship

between Ag and Cu in the other ore lenses (cf. Fig. 8.6e and 8.7e). The association of Ag with Cu in the remobilised chalcopyrite-rich lenses probably reflects the residence of Ag in chalcopyrite when galena is unavailable.

The distribution of Ag in the Thalanga ore lenses is similar to other massive sulphide deposits where Ag displays a strong correlation with Pb and rarely with Cu (Amcoff, 1984). However, Ag is associated with Cu in the pyrite-chalcopyrite-rich sulphides and also has a good correlation with Pb in the sphalerite-galena-pyrite-rich sulphides at Balcooma (Huston *et al.*, 1992a).

8.5 Discussion

8.5.1 Location of Feeder Zones

The mineralogical and metal zonation at Thalanga provides the best guide to the formation and growth of the massive sulphide deposit. The gross mineralogical zonation at Thalanga, from footwall to hangingwall, is 1) massive to semi massive pyrite ± chalcopyrite, with Mg-rich chlorite gangue, overlain by 2) massive sphalerite-galena-pyrite ± chalcopyrite-rich sulphides, containing quartz, barite, chlorite, phlogopite and muscovite gangue (Chapter 6). Barite-rich sulphides are present in the uppermost and more distal parts of the ore lenses (e.g. the Vomacka Zone) and quartz magnetite lenses along the Thalanga Range are the distal equivalent of the massive sulphides (Duhig *et al.*, 1992). Such a mineralogical zonation is comparable to the mineralogical zonation reported from other ancient less metamorphosed VHMS deposits (e.g. Franklin *et al.*, 1981; Large, 1992) and from the Kuroko deposits of Japan (e.g. Eldridge *et al.*, 1983), where Fe-rich sulphides overlie the hydrothermal vent or feeder zone and are overlain by Fe-Cu ± Au-rich sulphides, followed by Zn-Pb-Ag-rich sulphides, and then a Ba or quartz-enriched cap (e.g. the Hellyer deposit, McArthur and Dronseika, 1990).

This distribution of sulphides at Thalanga is broadly reflected in the metal zonation, whereby Zn, Pb, Ag and Ba are enriched at the stratigraphic top of the ore lenses, particularly in West and part of Central Thalanga. The distribution of elevated Cu is partly controlled by stratigraphy (regions of high Cu are associated with massive pyrite at the base of the ore lenses) and partly structurally controlled. High grades of Cu typically coincide with late faults or zones of extension (especially at the hangingwall contact). This makes the distribution of elevated Cu within the ore lenses (particularly in the intensely faulted Central Thalanga ore lens) a poor indicator of possible feeder zones. Zn and Cu ratios are more useful at Thalanga and the location of regions of Zn ratio <60 and Cu ratio >30 is interpreted to indicate hydrothermal feeder zones. In West and Central Thalanga, areas of Zn ratio <60

associated with massive pyrite lenses is inferred to indicate zones of high temperature fluid discharge.

The coincidence of high Cu grades, massive pyrite and low Zn ratios in several locations suggests that the thickest parts of the massive sulphides (particularly in West and Central Thalanga) may overlie multiple hydrothermal vents (Fig. 8.8a). A crude restoration to possible depositional geometries (Fig. 8.8b) shows that the inferred feeder zones are aligned parallel to the margin of the massive sulphides. This orientation, together with the possible elongate shape of the massive sulphide lenses, may have been the result of focussed venting of hydrothermal solutions along a pre-existing structure. However, no evidence of such a pre-deformational structure was identified in this study.

Barite-rich sulphide zones typically occur at the margins and tops of massive sulphide deposits, and are interpreted to form during the waning of the hydrothermal system (cf. Eldridge *et al.*, 1983; McArthur and Dronseika, 1990; Large, 1992). Massive barite and barite-rich sulphides in the ore lenses at Thalanga are therefore interpreted to have formed from lower temperature (and oxidised) hydrothermal solutions either at the top or side margins of the deposit. Thus the barite-rich Vomacka Zone may be the western margin of the East Thalanga ore lens (Fig. 8.8b). The lack of continuity of ore lenses from the Vomacka Zone to Central Thalanga (as determined from available drill holes) supports the interpretation that the East Thalanga ore lens was fed from a separate hydrothermal vent to West and Central Thalanga.

The inferred asymmetry of the undeformed West and Central orebody may be similar to the pre-deformational morphology of East Thalanga. The main focus of hydrothermal discharge is interpreted to have been the eastern end of each orebody, where syn-volcanic structures may have controlled the location of the main feeder zone. However, the fault that now truncates the eastern end of Central Thalanga is D_3 in age (Chapter 3).

8.5.2 Effect of Deformation on Metal Distribution

The apparent cyclicity of the distribution of base metals within the ore lenses, particularly at Central Thalanga, is interpreted to be due to repetition of the ore lens along ENE-striking normal faults during D_3 (Chapter 3). The alternating Cu- to Zn-Pb-rich zones subparallel to bedding are interpreted to be repeated, normally zoned massive sulphide lenses. Cu-rich zones probably also mark the location of the normal faults.

The steeply- to moderately-plunging zones of elevated metals recognised in long section are interpreted to have been caused by the internal remobilisation of sulphides during deformation. The pitch of the high grade zones is similar to that of the L_2 mineral elongation

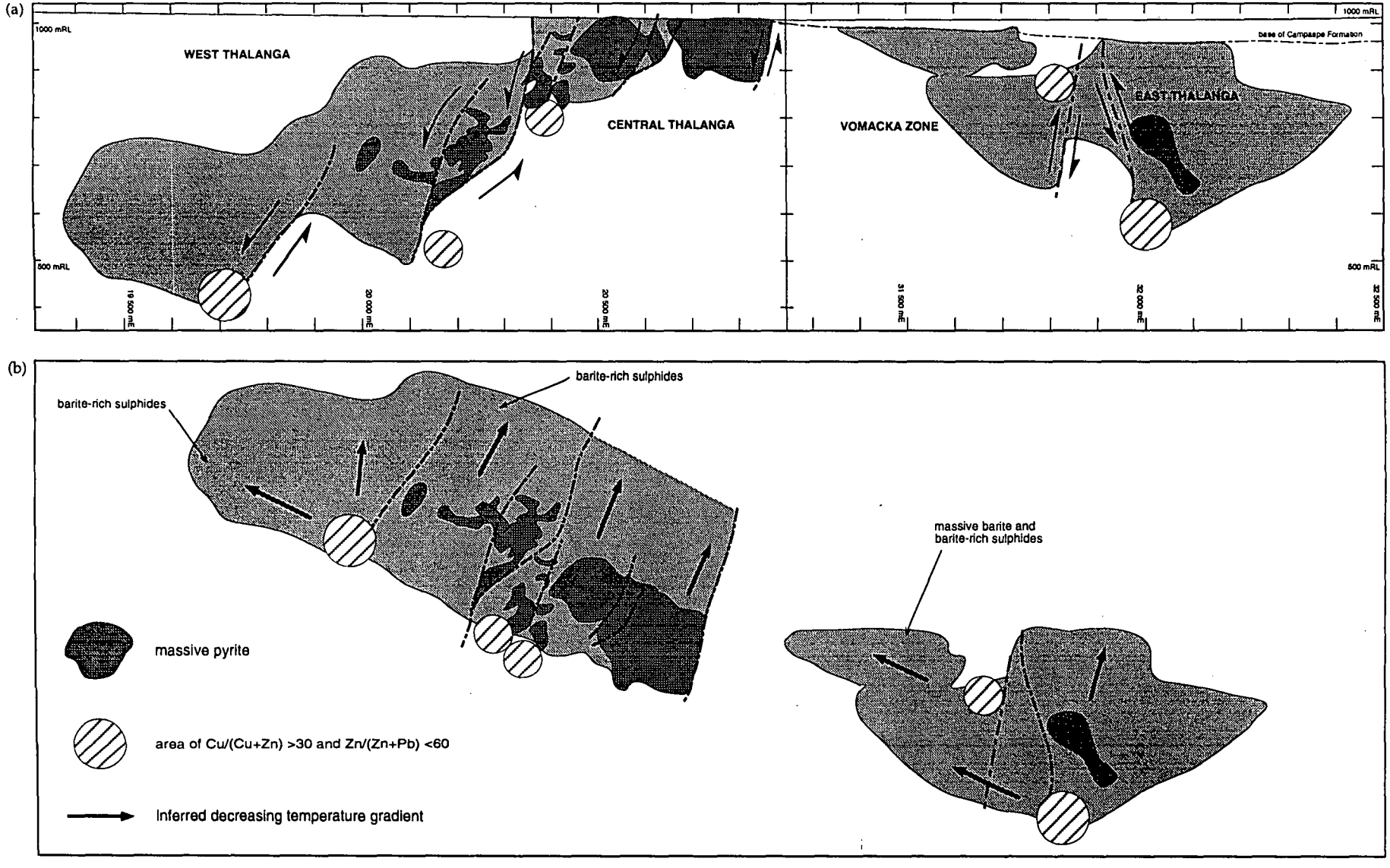

Figure 8.8 Long section of the location of massive pyrite ± chalcopyrite lenses and regions with both high Cu ratio and low Zn ratio with respect to the (a) current orebody outline and (b) possible pre-deformation orebody outline. The areas of high Cu ratio and low Zn ratio were estimated from Figure 8.2 (f,g). The distribution of massive pyrite is based on underground mapping and drilling information. The location of massive pyrite ± chalcopyrite-only lenses in East Thalanga is not well constrained, and may extend down-dip to the region of high Cu ratio and low Zn ratio.

lineation (Chapter 3), and therefore remobilisation is interpreted to have occurred (on a grain scale) during D_2. Remobilisation during D_2 may also explain the Zn, Pb and Ag enrichment in macro-pressure shadows at the up- and down-dip margins of the intensely silicified rhyolitic volcanics at East Thalanga. However, high primary fluid flow at the margin of the intensely silicified rhyolitic volcanics may have increased the metal content (section 8.3.3).

8.5.3 Location of Au

There is a good association between Au and Cu in the massive pyrite lenses of West and Central Thalanga, where the electrum is present as inclusions and in fractures with chalcopyrite (Chapter 7). Au may also be present in pyrite as colloid-size Au or as structurally bound Au (e.g. Larocque *et al.*, 1995). The location of electrum with chalcopyrite in fractures in pyrite at Thalanga is consistent with brittle deformation of pyrite in lenses of massive pyrite and the coincident remobilisation of Au and chalcopyrite (cf. Larocque *et al.*, 1993; Tourigny *et al.*, 1993). Visible electrum was not observed in the remobilised chalcopyrite-filled piercement veins in the hangingwall, but elevated Au is consistently present within zones of remobilised sulphides (e.g. the zone of dilation at the possible fold hinge in Central Thalanga). The relationship may support the proposal, of Huston *et al.* (1993) and Larocque *et al.* (1993), that Au is released from pyrite during metamorphic recrystallisation and redeposited as electrum and in solid solution within chalcopyrite. Larocque *et al.* (1993) further suggested that greater degrees of metamorphic recrystallisation and deformation of pyrite will result in greater degrees of Au enrichment.

Electrum also occurs with chalcopyrite in fractures in tetrahedrite-tennantite, with arsenopyrite in myrmekitic chalcopyrite-arsenopyrite-tetrahedrite-tennantite intergrowths and sporadically intergrown with chalcopyrite-sphalerite ± galena (Chapter 7). These mineralogical associations are reflected in the Cu-Au and the Ag-Au association in the polymetallic massive sulphide lenses at Thalanga.

8.6 Summary

1. Coincidence of low Zn/(Zn+Pb) values, Cu/(Cu+Zn) values and massive pyrite lenses suggests that feeder zones are located down dip in the central part of East Thalanga, and along the eastern and down-dip margin of West and Central Thalanga. The overall higher Cu-grades in West and Central Thalanga are interpreted to indicate higher temperatures of mineralisation these lenses, compared to the Vomacka Zone and East Thalanga.

2. Multiple, alternating Cu- to Zn-Pb-rich zones subparallel to bedding within the Central Thalanga ore lens are interpreted to have resulted from the repetition of the ore horizon

along steep normal faults. The Cu-rich zones probably mark the location of the faults as well as the base of repeated normally zoned massive sulphide lenses.

3. The effect of deformation on the distribution of base and precious metals at Thalanga is also manifest as moderate- to steep-plunging elongate zones of elevated metal grades within each ore lens. The pitch of the high grade zones is similar to the mineral elongation lineation (L_2) and is therefore interpreted to have resulted from internal remobilisation during D_2.

4. Despite the overall low Au grades, the Thalanga deposit is classified as having a Cu - Au association, and this association is prominent in the massive pyrite ± chalcopyrite zones at the base of the ore lens in West and Central Thalanga. Elevated Au is also coincident with the remobilised chalcopyrite-rich sulphides located at the stratigraphic top of the ore horizon in Central Thalanga.

CHAPTER 9.

SULPHUR ISOTOPE GEOCHEMISTRY

9.1 Introduction

Sulphur isotopes are important to the study of massive sulphide deposits, particularly in constraining the source of sulphur and estimating temperatures and other physico-chemical conditions of sulphide deposition (Ohmoto and Rye, 1979). Seawater, magmatic and biogenic sulphur are the main potential sources of sulphur in hydrothermal fluids responsible for VHMS deposition, with magmatic sulphur either directly contributed to the fluids or leached from the host rocks (Shanks *et al.*, 1981; Ohmoto, 1986, Solomon *et al.*, 1988).

Sulphur isotope ratios were determined for pyrite, sphalerite, chalcopyrite, galena and barite from the Thalanga deposit in order to determine the source of sulphur, and to evaluate any spatial variation in sulphur isotopic composition. The spatial distribution of $\delta^{34}S$ values has yielded valuable information about the source of sulphur and the evolution of hydrothermal solutions (Ohmoto *et al.*, 1983; Ohmoto, 1986; Gemmell and Large, 1992 & 1993). Sulphur isotope ratios were also determined for two pyritic quartz magnetite samples from Central Thalanga and a sample of massive barite from the Thalanga Range.

Methods

Sulphur and sulphate isotopes were determined on a VG Micromass 602D mass spectrometer in the Central Science Laboratory at the University of Tasmania. Sulphide and barite mineral separates were drilled from hand specimens, sulphides were combusted with excess Cu_2O and sulphates were combusted twice with excess Cu_2O and SiO_2 in order to produce SO_2 (Coleman and Moore, 1978; Fritz *et al.*, 1974 ; Robinson and Kusakabe, 1975). Minor contamination from fine grained intergrowths of other sulphides or gangue (muscovite, chlorite or barite) was present in most sulphide separates. The barite specimens were uniformly coarse grained and the mineral separates consequently pure.

The results are presented as standard notation relative the Cañon Diablo Troilite (CDT). Replicate analyses of internal standards showed that reproducibility of results was ±0.2 ‰, and that precision was to the 1σ level. These results are combined with unpublished data from D.L. Huston (pers. comm., 1990) and N.C. Duhig (pers. comm., 1990), and analyses determined for Penarroya Australia Pty Ltd by the Department of Scientific and Industrial

Research (DSIR), New Zealand (B.W. Robinson, writt. comm. to Penarroya Australia Pty Ltd, 1981). The data from the DSIR also have reproducibility of ±0.2 ‰.

9.2 Results

The $\delta^{34}S$ values of pyrite from the Thalanga deposit (Appendix J) range from +5.6 to +17.3 ‰, with a median of +14.0 ‰ (Fig. 9.1a). Chalcopyrite, sphalerite and galena display more restricted ranges and slightly lower median values, with the mean $\delta^{34}S$ value of chalcopyrite > the mean $\delta^{34}S$ value of sphalerite > the mean $\delta^{34}S$ value of galena (see Appendix J). However, the $\delta^{34}S$ values of co-existing sulphide mineral pairs at Thalanga generally follow the pattern of $\delta^{34}S_{pyrite} > \delta^{34}S_{sphalerite} > \delta^{34}S_{chalcopyrite} > \delta^{34}S_{galena}$ as documented by Ohmoto (1972) and Rye and Ohmoto (1974). Local isotopic disequilibrium conditions is indicated as some sulphide samples do not exhibit this fractionation in $\delta^{34}S$ values. The $\delta^{34}S$ values of barite from the Thalanga deposit and the Thalanga Range vary between 27.7 and 32.4 ‰ (Fig. 9.1a), with median $\delta^{34}S$ = 30.5 ‰.

Figure 9.2 illustrates the variation of $\delta^{34}S$ values of sulphides with respect to stratigraphic location and mineralogical associations. There is little variation between the average $\delta^{34}S$ values of sulphides (disseminated and stringer pyrite) within the altered footwall rhyolitic volcanics, sulphides within the mineralised horizon, and pyrite disseminated in the hangingwall rocks, except for one $\delta^{34}S$ value of 5.6 ‰ from pyrite disseminated in the HWF. Remobilised sulphides, and sulphides associated with quartz veins, have similar or lower $\delta^{34}S$ values compared to the non-remobilised sulphides within the ore lenses. Pyrite disseminated in a dolerite dyke has the same $\delta^{34}S$ as the pyrite in the enclosing altered rhyolitic volcanics.

The $\delta^{34}S$ values of pyrite associated with quartz magnetite clasts from within the ore horizon vary from 2.8 to 15.6 ‰ (Fig. 9.2), and this variation reflects the stratigraphic location of each sample. Sample UG-1 overlies the barite-rich sulphides at the stratigraphic top of fault-repeated rhyolitic volcanics in Central Thalanga, and sample 955-27 is a lithic clast within the quartz 'eye' volcaniclastic unit (QEV) in Central Thalanga and is overprinted by a sphalerite-rich vein. These samples have $\delta^{34}S$ values of 15.0 and 15.6 ‰ respectively. Pyrite with the lowest $\delta^{34}S$ is disseminated in a quartz magnetite clast within the hangingwall fragmental (HWF).

9.3 Spatial Distribution of $\delta^{34}S$ values

The $\delta^{34}S$ values of sulphides from West, Central, and East Thalanga, and the Vomacka Zone have similar $\delta^{34}S$ values of 12 to 16 ‰ (Fig. 9.1b-e). However, there is significant variation

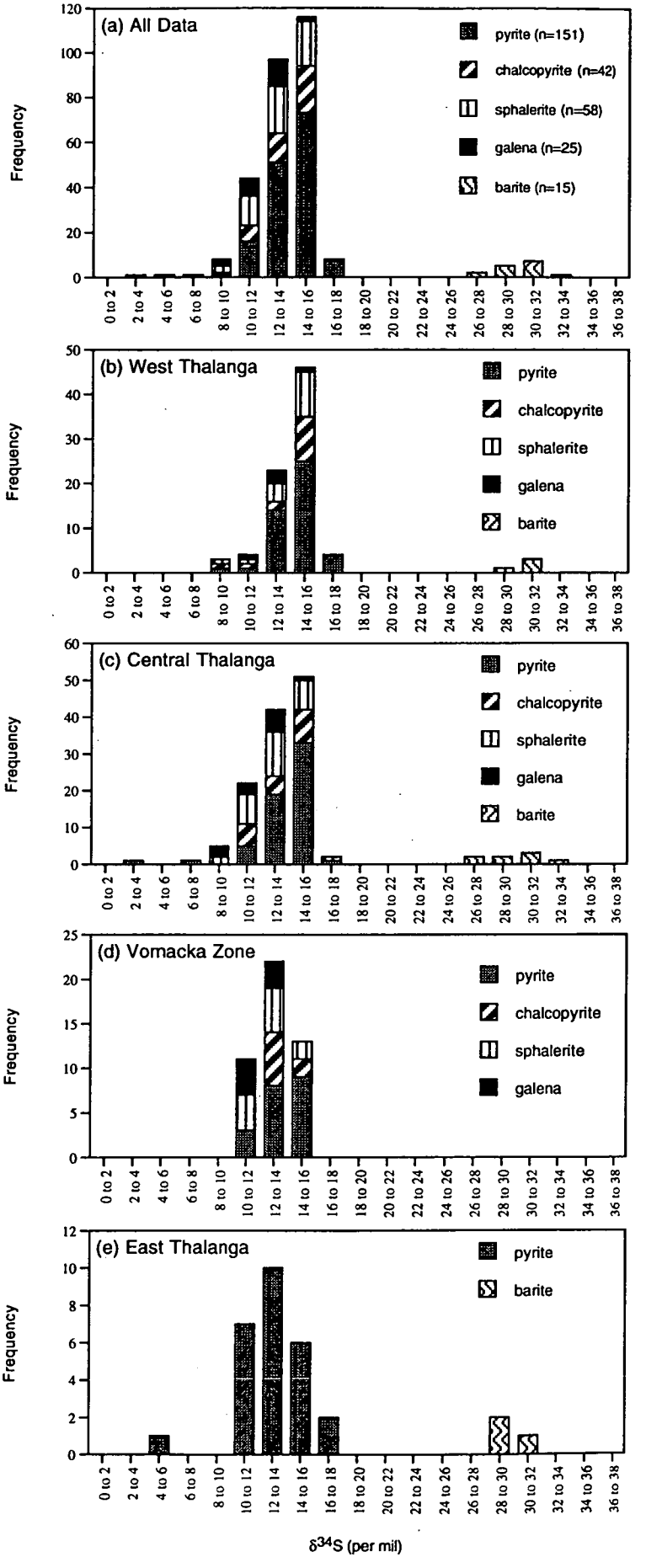

Figure 9.1 $\delta^{34}S$ values of sulphides and barite from (a) the Thalanga massive sulphide deposit, (b) West Thalanga, (c) Central Thalanga, (d) Vomacka Zone, and (e) East Thalanga.

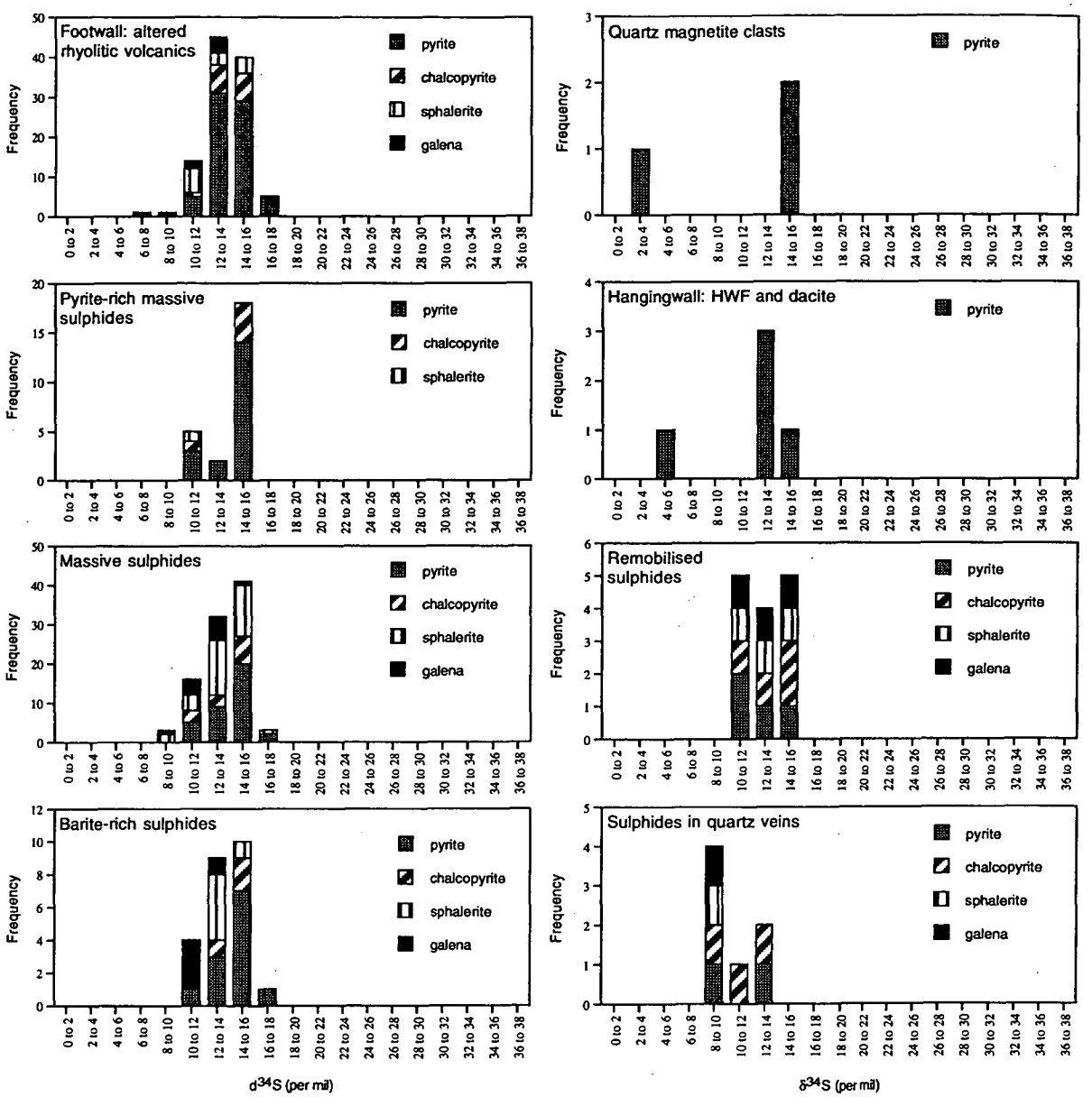

Figure 9.2 Sulphur isotope data from various rock types and stratigraphic locations at Thalanga.

in the $\delta^{34}S$ values of pyrite within the rhyolitic volcanics underlying the massive sulphide lenses. The following trends in $\delta^{34}S$ values at Thalanga are apparent:

i) Typically, there is a gradual increase in the $\delta^{34}S$ values of pyrite within the rhyolitic volcanics towards the ore horizon, particularly in the longer drill holes (e.g. TH2, TH54, TH85A, and TH245; Fig. 9.3 a-c). In shorter drill holes, with fewer samples, there is no systematic variation in $\delta^{34}S$ values of pyrite (e.g. TH4, TH11; Fig. 9.3b). This suggests that the decrease in $\delta^{34}S$ values of pyrite within the footwall rhyolitic volcanics is over 50-100's of metres, whereas local fluctuations occur over distances of less than 10 m. Where massive sulphide lenses are not present at the stratigraphic top of the footwall, there is no systematic increase in $\delta^{34}S$ values of pyrite in the rhyolitic volcanics (e.g. TH15; Fig. 9.3d).

ii) Pyrite associated with lenses of chlorite schist or massive pyrite, either in the footwall rhyolitic volcanics or near the base of the ore lenses, commonly has lower $\delta^{34}S$ values than adjacent pyrite associated with quartz-muscovite-rich assemblages. For example, a massive to semi massive pyrite vein in TH2 has $\delta^{34}S$ = 12.2 ‰, compared to the enveloping quartz-muscovite-rich rhyolitic volcanics that have $\delta^{34}S$ = 13.5 and 14.4 ‰ (Fig. 9.3b). Pyrite disseminated in chlorite-rich footwall rhyolitic volcanics in TH270 has $\delta^{34}S$ = 11.5 ‰, compared to the underlying quartz-muscovite-rich assemblages which have $\delta^{34}S$ = 17.3 ‰ (Fig. 9.3c). This relationship indicates that the distribution of the $\delta^{34}S$ values of pyrite at Thalanga may be better elucidated with a more detailed comparison between alteration types and $\delta^{34}S$ values of pyrite.

iii) The $\delta^{34}S$ values of pyrite within the ore horizon varies from higher than the footwall pyrite, particularly near the base of the ore lens (e.g. TH269; Fig. 9.3c), to lower than pyrite in the footwall (e.g. TH270; Fig. 9.3c). Close-spaced samples within the ore horizon of TH24 (Fig. 9.3a) exhibit small variation (<1 ‰) in $\delta^{34}S$ regardless of stratigraphic position within the massive sulphide lens, but $\delta^{34}S$ decreases at the stratigraphic top of the overlying QEV. Pyrite intergrown with barite at the stratigraphic top of the ore lenses typically has lower $\delta^{34}S$ than the underlying massive sulphides, and in East Thalanga, $\delta^{34}S$ value of pyrite within the hangingwall lens is lower than pyrite in the footwall lens (e.g. TH269: $\delta^{34}S_{\text{footwall lens}}$ = 14.3 ‰, and $\delta^{34}S_{\text{hangingwall lens}}$ = 11.4 ‰; Fig. 9.3C). In Central Thalanga, the $\delta^{34}S$ values of pyrite within the massive sulphides gradually decrease towards the stratigraphic top of the ore lens (e.g. TH4; Fig. 9.3b).

iv) The $\delta^{34}S$ value of pyrite disseminated in the HWF or dacite is commonly less than the $\delta^{34}S$ values of pyrite within the underlying ore lenses (e.g. TH4, TH 54, TH85A, TH245; Fig. 9.3a-c). In TH85A (Fig. 9.3c), the $\delta^{34}S$ values of pyrite within the footwall rhyolitic volcanics gradually increase towards the ore horizon, and reach a maximum of 17.2 ‰ at the

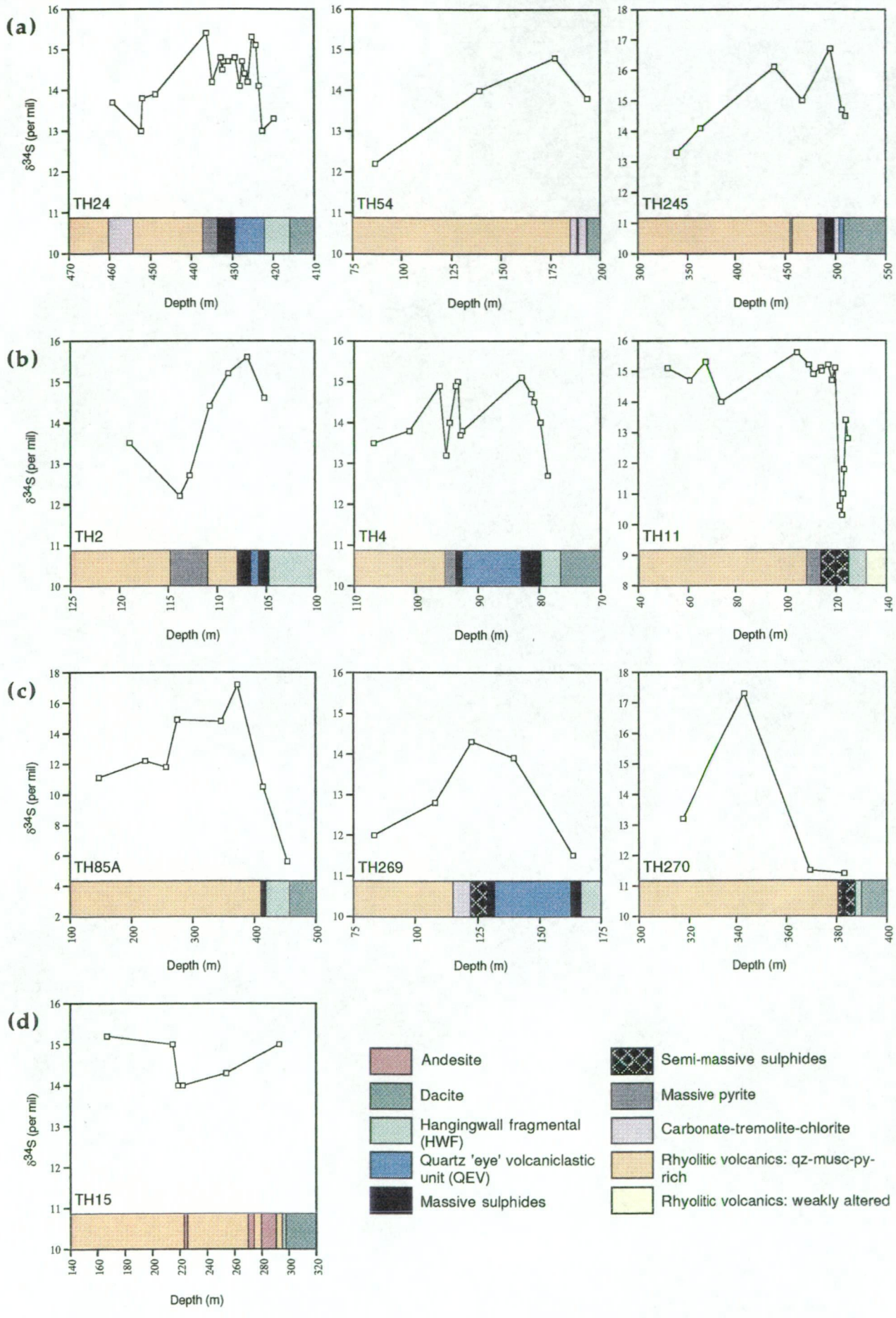

Figure 9.3 Sulphur isotope variations with respect to depth down drill holes in (a) West Thalanga, (b) Central Thalanga, (c) East Thalanga, and (d) the Vomacka Zone. Stratigraphic younging is to the right in each diagram. Abbreviations: musc = muscovite, py = pyrite, qz = quartz.

stratigraphic top of the footwall. The $\delta^{34}S$ values of pyrite within the QEV and overlying HWF are lower at 10.5 ‰ and 5.6 ‰ respectively.

9.4 Discussion

9.4.1 Source of Sulphur

The $\delta^{34}S$ values of the Thalanga massive sulphide deposit support the observations of Sangster (1968), Stanton (1972), and Franklin *et al.* (1981) that the $\delta^{34}S$ values of sulphides in Phanerozoic VHMS deposits fall between 0 ‰ and the $\delta^{34}S$ value of the coeval seawater sulphate (about 30 ‰ in Cambrian to Ordovician times; Claypool *et al.*, 1980), and that the $\delta^{34}S$ value of barite is similar to that of the contemporaneous seawater sulphate (Ohmoto, 1986). The favoured interpretation of such results is that the sulphur was sourced from a mixture of Cambro-Ordovician seawater sulphate, inorganically reduced during convection, and dissolved igneous (or rock) sulphur (e.g. Ohmoto *et al.*, 1983; Green *et al.*, 1981; Solomon *et al.*, 1988). The amount contributed from these sources of sulphur to the hydrothermal fluids, and subsequent $\delta^{34}S$ value of the sulphide mineralisation, depends on the thermal history of the hydrothermal system and the chemistry of the host rocks (Ohmoto, 1986).

Sulphides

The variation in $\delta^{34}S$ values of sulphides around massive sulphide deposits can provide evidence of the evolution of hydrothermal system in terms of variation of the source of sulphur with time (e.g. Green *et al.*, 1981; Solomon *et al.*, 1988; Gemmell and Large, 1992 & 1993). Gemmell and Large (1992, 1993) reported that the $\delta^{34}S$ values of sulphides within the stringer zone underlying the Hellyer deposit are lower than the $\delta^{34}S$ values of sulphides within the stringer envelope zone and in the host volcanic units outside the stringer zone. Gemmell and Large (1993) also showed that in general $\delta^{34}S$ values increase from footwall to hangingwall within the massive sulphide deposit, and pyrite in the baritic cap at the Hellyer deposit has higher $\delta^{34}S$ than pyrite in the underlying massive sulphides (Sharpe, 1991). The decrease in $\delta^{34}S$ values towards the centre of the feeder zone is interpreted to have been produced by the early circulation of hydrothermal solutions that contained high proportions of partly reduced seawater sulphate, which mixed with solutions, sourced from deeper in the convection cell and containing high proportions of dissolved igneous sulphur, in the feeder zone (Gemmell and Large, 1992 & 1993).

Rye and Ohmoto (1974) reported that the $\delta^{34}S$ values of pyrite at the kuroko deposits of Japan decrease upwards from the pyrite alteration in the footwall to the upper parts of the ore deposit. Similarly, Çagatay and Eastoe (1995) reported that the massive sulphides at

Madenköy in Turkey, have lower $\delta^{34}S$ than the sulphides in underlying stringer veins. This change in $\delta^{34}S$ values is interpreted to be due to a change in pH and fO_2 conditions in the hydrothermal solutions (due to increased seawater in the hydrothermal solutions which would change the proportion of oxidised to reduced sulphur in solution), rather than a change in the source of sulphur, towards the later stages of alteration and sulphide deposition (Kajiwara, 1971; Rye and Ohmoto, 1974). Similarly, the low $\delta^{34}S$ values of barren lenses of pyrite-barite in the Mount Read Volcanics are thought to have resulted from highly oxidised hydrothermal solutions (Solomon *et al.*, 1988).

Conversely, at Rosebery in Tasmania the $\delta^{34}S$ values of the sulphides increases upwards through the footwall to the ore deposit (Green *et al.*, 1981). This trend is considered to indicate progressive mixing of the hydrothermal solutions with reduced seawater sulphate (Green *et al.*, 1981), and a decrease in the igneous sulphur content of the hydrothermal fluid with time (Solomon *et al.*, 1988). Similarly, sulphur isotopes were interpreted to suggest that cold seawater circulated through the footwall rhyolite autobreccias and mixed with hot hydrothermal fluids at depths of up to 100 m at the Uwamuki deposits in Japan (Bryndzia *et al.*, 1983).

Increasing $\delta^{34}S$ values of sulphides upwards through stratigraphy is a common pattern of biogenic pyrite in sedimentary rocks (Ohmoto, 1986). However, a biogenic origin for sulphur at Thalanga is ruled out for the same reasons as Green *et al.* (1981) discounted this model for the Rosebery deposit:
i) there is a similar range of $\delta^{34}S$ values of pyrite in the footwall and the ore lenses, and therefore sulphides were probably transported in the same hydrothermal solutions, and
ii) the range of $\delta^{34}S$ is much smaller than that reported from ancient and modern sedimentary rocks (Schwarcz and Burnie, 1973).

The average $\delta^{34}S$ value of the sulphides at Thalanga (average = 14 ‰) is higher than the Cambrian deposits in Tasmania (average = 10 ‰; Large, 1992), although the Tasmanian deposits have variable $\delta^{34}S$, with the massive sulphides at Hellyer having $\delta^{34}S$ 5.3 to 9.4 ‰ (Gemmell and Large, 1993), Mt Lyell having $\delta^{34}S$ = 5 to 10 ‰ (Solomon *et al.*, 1988), but Rosebery having $\delta^{34}S$ = 7.8 to 19.8 ‰ (Green *et al.*, 1981). The difference between Thalanga and the Tasmanian deposits could be caused by a slightly greater contribution of reduced sulphate from contemporaneous seawater to the hydrothermal solutions, via mixing within the footwall (composed of altered perlitic rhyolite lavas and rhyolite breccia units; Chapter 4) at Thalanga. The increase in $\delta^{34}S$ values of pyrite towards the stratigraphic top of the footwall at Thalanga is interpreted to have been produced by an increased degree of mixing between ascending hydrothermal solutions (containing evolved seawater sulphur and dissolved igneous sulphur) and cold Cambro-Ordovician seawater within the porous footwall rhyolitic volcanics. The lower $\delta^{34}S$ values of massive pyrite veins (>1 m in thickness)

relative to surrounding quartz-muscovite-pyrite-rich rhyolitic volcanics is interpreted to reflect the reduced ability of cold seawater to mix with hydrothermal solutions ascending along major fluid conduits.

Decreased mixing between cold Cambro-Ordovician seawater and ascending hydrothermal solutions may also explain the sharp decrease in $\delta^{34}S$ values of pyrite in some massive sulphide lenses at the stratigraphic top of the ore horizon, and pyrite disseminated in the hangingwall rocks at Thalanga. Perhaps deposition of the overlying HWF units, near the end of the hydrothermal system's life, may have reduced the infiltration of seawater into the footwall units. This may have increased the contribution of sulphur from the hydrothermal solutions (containing evolved seawater sulphur and leached igneous sulphur) and thus decreased the $\delta^{34}S$ values of depositing sulphides.

Alternatively, if the solutions from which the sulphides were deposited became progressively more oxidised towards the end of the life of the hydrothermal system, then the $\delta^{34}S$ values of the sulphides at the stratigraphic top of the ore horizon and disseminated in the overlying volcanic units would decrease (as argued by Rye and Ohmoto, 1974). Incorporation of incompletely reduced cold seawater into the hydrothermal solutions could increase the fO_2 of the mineralising solutions and thus form sulphides with $\delta^{34}S$ values lower than sulphides deposited from earlier solutions. This interpretation is preferred because it is consistent with the presence of barite in the massive sulphides at the stratigraphic top of the ore lenses at Thalanga (Chapter 6). The mixing of reduced S (in the hydrothermal solutions) and seawater sulphate must have occured at temperatures above 200°C in order for equilibrium to have been attained (cf. Ohmoto and Lasaga, 1982; Ohmoto *et al.*, 1983).

The $\delta^{34}S$ values of sulphides at Thalanga are significantly higher than those reported from the Waterloo (-6 to 7 ‰) and Agincort (4 to 9 ‰) deposits located within the Mount Windsor volcanic belt to the east of Thalanga (Huston *et al.*, 1995a). The low isotopic signature of sulphides at the Waterloo and Agincort deposits is interpreted to be the result of highly oxidised mineralising solutions (bornite and barite are present; Huston *et al.*, 1995a). Both Waterloo and Agincort have patterns, similar to Thalanga, of increasing $\delta^{34}S$ of pyrite upwards through the footwall to the ore position (Huston *et al.*, 1995a).

Barite

The heavy $\delta^{34}S$ values of barite (27.6 to 32.4 ‰) from the Thalanga deposit and the Thalanga Range are probably due to the source of sulphur being Cambro-Ordovician seawater ($\delta^{34}S$ ~30 ‰). The similar $\delta^{34}S$ values of barite in barite-pyrite and barite-sphalerite veins within the footwall at Thalanga is also probably due to a seawater source of sulphur, which

therefore requires circulation of the overlying seawater through the rhyolitic volcanics during sulphide mineralisation.

Barite from the Thalanga deposit has significantly lower $\delta^{34}S$ values than the barite lens in the Rosebery deposit (34.6 to 41.2 ‰, Green *et al.*, 1981) and the barite cap in the Hellyer deposit (40.4 to 42.9 ‰, Jack, 1989; and 26.0 to 44.9 ‰, Sharpe, 1991). Solomon *et al.* (1988) and Gemmell and Large (1992) argued that incomplete reduction of Cambrian seawater sulphate would explain the heavy isotopic ratios of the barite cap at Rosebery and Hellyer.

9.4.2 $\delta^{34}S$ of Pyrite in Quartz-Magnetite Clasts

Pyrite associated with quartz-magnetite lenses in the Thalanga Range area, along strike from the Thalanga deposit, has negative $\delta^{34}S$ values that are interpreted to indicate a biogenic reduction of seawater sulphate (Duhig *et al.*, 1992). $\delta^{34}S$ values of pyrite in quartz-magnetite decrease with distance from the massive sulphide lenses at Thalanga, and this is interpreted to have been caused by an increase in biogenic activity away from sulphide mineralisation (Duhig *et al.*, 1992). The quartz-magnetite clasts within the HWF (with $\delta^{34}S$ = 2.8 ‰) could have been eroded from quartz-magnetite lenses along strike from the Thalanga deposit.

The similarity between the sulphur isotopic ratios of pyrite disseminated in quartz-magnetite clasts present within the ore horizon ($\delta^{34}S$ = 15.0 ‰ and 15.6 ‰; clasts typically contain remobilised sulphides, Chapter 6) and those of the majority of sulphides from the ore lenses at Thalanga suggests a similar source of sulphur. If the quartz-magnetite clasts at Thalanga were eroded from distal quartz-magnetite lenses prior to sulphide mineralisation at Thalanga, then perhaps the original biogenic signature was modified or overprinted by the hydrothermal pyrite. Quartz-magnetite clasts present within the HWF have not overprinted by polymetallic sulphides, and consequently have $\delta^{34}S$ values that differ from the massive sulphide lenses.

9.4.3 Geothermometry

The difference between the $\delta^{34}S$ values of sulphide-sulphide pairs (commonly sphalerite-galena and pyrite-galena) can be used to estimate temperatures of sulphide formation, if the co-existing sulphides were deposited in equilibrium and that no isotopic exchange between the sulphides occurred after deposition (Ohmoto and Rye, 1979). It is recommended that the results from such calculations are compared to temperatures determined from fluid inclusions within the sulphides so that the degree of isotopic exchange can be evaluated (Ohmoto and Rye, 1979). Large-scale pre-metamorphic $\delta^{34}S$ variations are considered to be preserved during metamorphism, and re-equilibration of sulphur isotopes is thought to go to completion

only at metamorphic grades above upper amphibolite facies (Ohmoto and Rye, 1979). However, Lusk and Crockett (1969) argued that re-equilibration of the sulphur isotopes of co-existing sulphides occurred during metamorphism of the Heath-Steele massive sulphide deposit, and that the temperatures calculated from sulphide pairs were consistent with metamorphic temperatures (350-450 °C).

The effect of metamorphic recrystallisation of the sulphides at the Thalanga deposit is to produce textural equilibrium that disguises original paragenetic relationships (Chapter 7). Some isotopic exchange between co-existing sulphides may have occurred during metamorphism at Thalanga. Comparison of the $\delta^{34}S$ values of co-existing sulphides shows that there is evidence of isotopic disequilibrium amongst both remobilised and non-remobilised sulphides at Thalanga, with $\delta^{34}S$ of sphalerite and chalcopyrite higher than the $\delta^{34}S$ of co-existing pyrite in some samples (Appendix J). Therefore temperatures were not estimated for these samples. Sphalerite-galena pairs are regarded as the most useful in sulphur isotope geothermometry (Ohmoto, 1986), and equations from Ohmoto and Rye (1979) were used to estimate temperatures from sphalerite-galena and also pyrite-galena pairs. Green *et al.* (1981) used barite-sulphide mineral pairs to estimate temperatures of mineralisation at the Rosebery deposit. Temperatures were calculated from barite-pyrite, barite-sphalerite and barite-galena pairs from Thalanga for comparison, although Ohmoto (1986) considered that sulphide-sulphate pairs yield unreliable estimates of the temperature of mineralisation.

Figure 9.4(a,b) depicts the wide variation in temperatures determined using these calculations. The most frequent results are between 350 °C and 550 °C, and these are probably more realistic metamorphic temperatures than temperatures of sulphide formation. Results above 550 °C are probably due to disequilibrium conditions between the co-existing sulphides. Calculated temperatures greater than 900 °C correspond to small differences in the $\delta^{34}S$ values of the sulphides and these differences are within the error range in most cases (Appendix J). Temperatures calculated from pyrite-chalcopyrite pairs vary from 100 °C to 1800 °C and thus are unrealistic temperatures of either mineralisation or metamorphism, and reflect the isotopic disequilibrium of remobilised chalcopyrite and the sulphides that co-exist with it. Barite-sulphide pairs yield temperatures between 340 °C and 480°C (Fig. 9.4b), which are interpreted to be consistent with the metamorphic grade at Thalanga.

9.5 Conclusions and Sulphur Isotope Model

1. The massive sulphides and pyrite in the footwall at the Thalanga deposit have $\delta^{34}S$ between 6 and 18 ‰, which is consistent with formation from hydrothermal fluids containing dissolved igneous (or rock) sulphur and Cambro-Ordovician seawater sulphate that had been

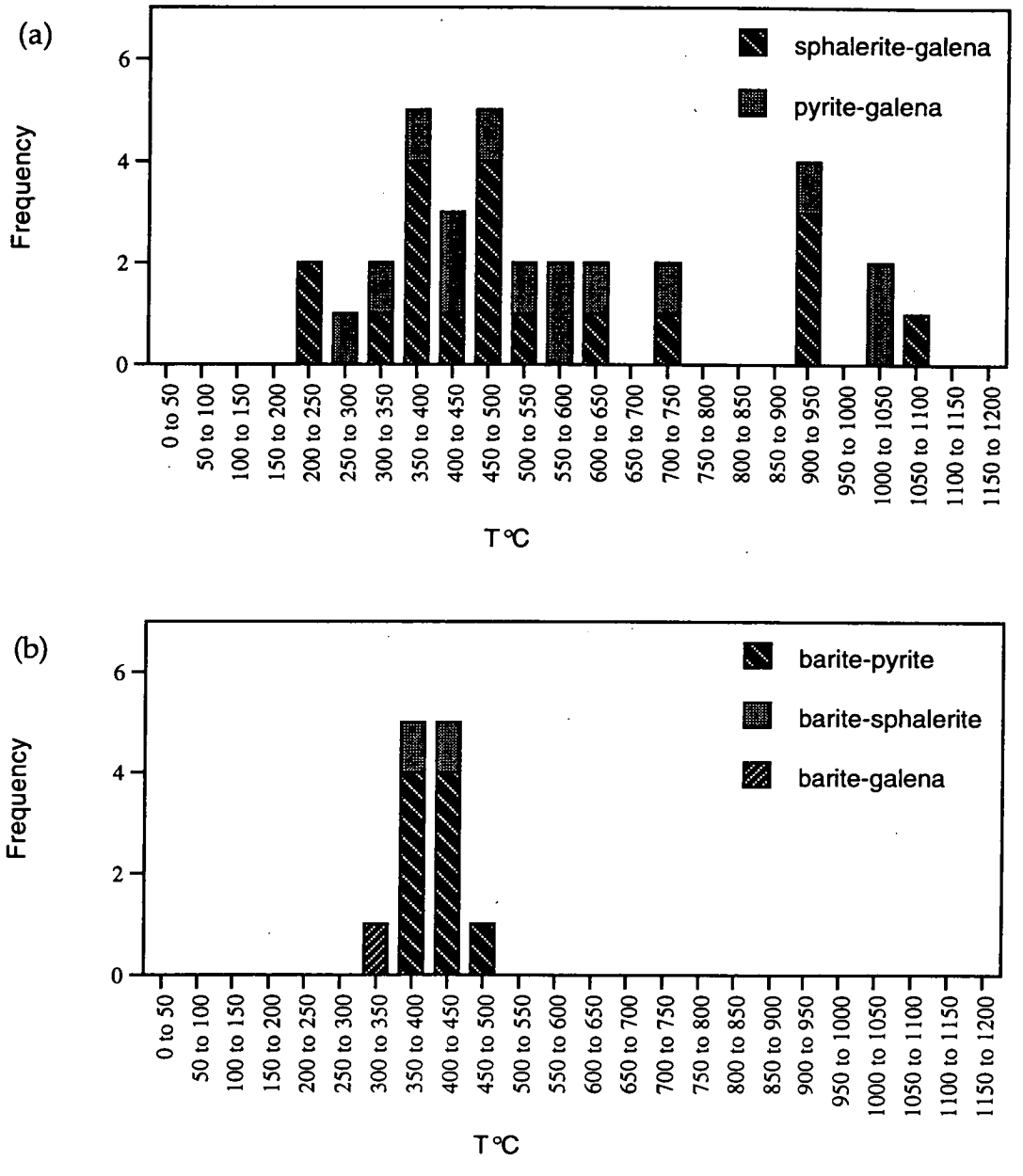

Figure 9.4 Frequency histograms depicting temperatures calculated from (a) sulphide-sulphide and (b) barite-sulphide pairs from the Thalanga deposit. Mineral pairs used in temperature calculations are indicated in Appendix J.

inorganically reduced during hydrothermal convection. The increase in $\delta^{34}S$ values of disseminated and stringer pyrite in the footwall rhyolitic volcanics towards the massive sulphide deposit is a consequence of hot hydrothermal fluids containing reduced seawater sulphate and abundant igneous sulphur (possibly leached from the underlying rhyolite), mixing with cold seawater near the top of the footwall, and depositing massive sulphides on the seafloor or in a sub-seafloor position (Fig. 9.5a). As the hydrothermal system waned, the volume of partly reduced seawater increased, resulting in more oxidised hydrothermal solutions and therefore lower $\delta^{34}S$ values of sulphides towards the stratigraphic top of the ore lens (Fig. 9.5b). Barite is deposited (overprinting the sulphides) during the final stages of mineralisation when the hot hydrothermal solutions mix with cold seawater after venting at the seafloor, with the overlying seawater providing sulphate for barite formation.

2. Temperatures of sulphide mineralisation at Thalanga are not able to be constrained using the sulphur isotope data, because most of the sulphide mineral pairs are in isotopic disequilibrium. Temperatures calculated from sphalerite-galena and pyrite-galena pairs that do exhibit equilibrium isotope patterns vary from 200 °C to 1000 °C, confirming that disequilibrium amongst co-existing sulphides is widespread at Thalanga. The most frequent calculated temperatures (350 °C to 550 °C) partly correspond to temperatures predicted for chalcopyrite mineralisation (200-350 °C; Large, 1992), but are more comparable to the temperature of metamorphism estimated from host rock mineralogies (Chapter 3).

3. The $\delta^{34}S$ values of pyrite disseminated in quartz-magnetite clasts located within the massive sulphide ore lenses are identical to that of the enveloping massive sulphides. This contrasts with the $\delta^{34}S$ values of pyrite in quartz-magnetite lenses along strike from the deposit, and higher in the stratigraphy at Thalanga, where the $\delta^{34}S$ is significantly lower. Duhig *et al.* (1992) interpreted this pyrite with low $\delta^{34}S$ to have formed via biological reduction of seawater sulphate. The quartz-magnetite lenses may have been eroded and redeposited at Thalanga prior to sulphide mineralisation. Overprinting sulphide mineralisation may have modified the $\delta^{34}S$ values of pyrite disseminated in the quartz magnetite clasts, resulting in similar $\delta^{34}S$ values to the enveloping massive sulphides.

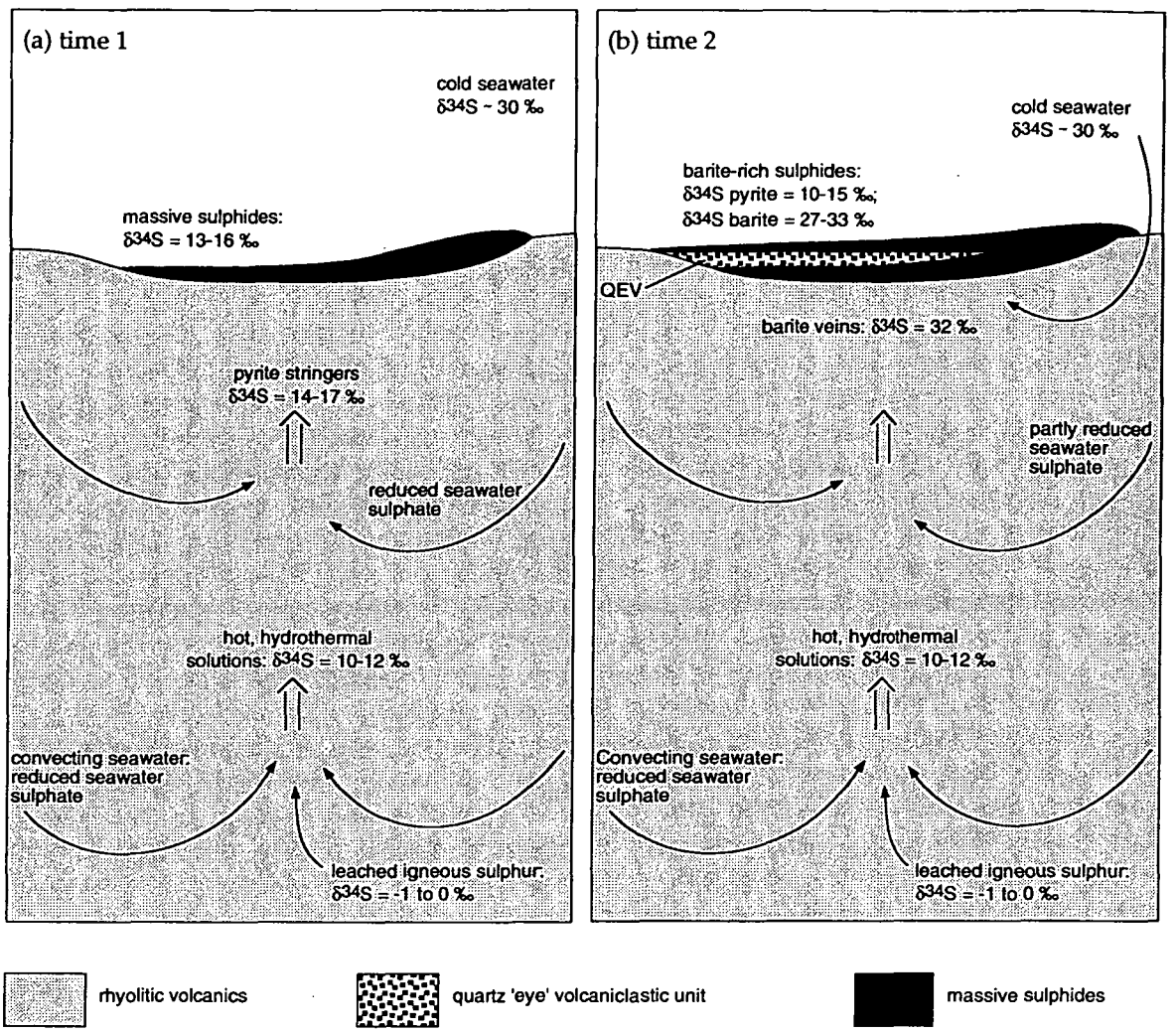

Figure 9.5 Schematic depiction of the evolution of mineralising solutions and sulphur sources at the Thalanga deposit. The $\delta^{34}S$ values are for pyrite, except where noted for barite. (a) Igneous sulphur was leached from volcanics beneath the deposit by convecting hydrothermal solutions that contain reduced seawater sulphate. Ascending hydrothermal solutions mixed with reduced Cambro-Ordovician seawater near the top of the footwall. Sulphides were deposited at the seafloor or partly replace suitable volcanics or alteration in a sub-seafloor position. (b) As the hydrothermal system waned, increased amount of incompletely reduced seawater mixed with the hydrothermal solutions, and deposited sulphides with lower $\delta^{34}S$ values. Barite was deposited at seafloor, with sulphate sourced directly from overlying seawater.

CHAPTER 10.

TEXTURAL AND MINERALOGICAL CHARACTERISTICS OF HYDROTHERMAL ALTERATION

10.1 Introduction

In modern and ancient seafloor hydrothermal systems, the ascent of mineralising fluids to the seafloor, and possible mixing with seawater en route, results in distinctive alteration in the rocks comprising the seafloor. The most common mass changes to the footwall rocks involve the addition of significant Fe, Mg, K and S, and the loss of Na, Ca and Si (Barrett and MacLean, 1994; Lianghat and MacLean, 1995). These mass changes are reflected in the mineralogy of the altered seafloor rocks, with many VHMS deposits in felsic volcanic units associated with intense footwall quartz-sericite-chlorite-pyrite alteration (e.g. Green *et al.*, 1981; Date *et al.*, 1983; MacLean and Hoy, 1991; Large, 1992).

The distribution of minerals interpreted to have formed as the result of hydrothermal alteration of the volcanic units that host massive sulphide deposits may reflect the composition and permeability of the footwall at the time of mineralisation (e.g Morton and Franklin, 1987; Large, 1992). Significant volumes of hydrothermal fluids can only flow through impermeable volcanic units, such as lavas, domes and sills, if suitable structures or zones of weakness are available to focus the fluids. Distinct alteration pipes may form in these circumstances, with sulphide deposition immediately above the structure or fluid pathway (e.g. Millenbach, Riverin and Hodgson, 1980; Knuckey *et al.*, 1982; Hellyer; Gemmell and Large, 1992). Fluid flow is less focussed in permeable volcanic breccia or sandstone units, resulting in extensive, stratabound alteration of the footwall with little evidence of mineralogical zonation (e.g. Rosebery, Green *et al.*, 1981; Que River, Offler and Whitford, 1992; the Lau basin, Fouquet *et al.*, 1991). Large (1992) noted that the resulting sulphide deposit is thinner and more extensive in this situation than those developed over a more focussed discharge zone. Permeability of the volcanic units associated with VHMS deposits is directly related to the compositions of the volcanic units, with siliceous and more viscous magmas commonly producing volcaniclastic deposits, whereas more impermeable lavas or sills are commonly produced from less siliceous parent material, the exceptions including highly vesicular lavas or glassy products with perlitic fractures that may form in either mafic or felsic magmas.

Similarly, the patterns and compositions of alteration in rocks overlying massive sulphide deposits may provide evidence of the timing of sulphide deposition and the evolution in the

composition of hydrothermal fluids. Hangingwall alteration is typically more subtle than footwall alteration and can vary from diffuse, blanket-style alteration (e.g. at Mt Chalmers, Large and Both, 1980; and Scuddles, Ashley *et al.*, 1988), to more pipe-like (e.g. Hellyer, Jack, 1989).

Despite textural and mineral modification due to metamorphism, the whole-rock compositions of alteration zones associated with VHMS deposits are generally inferred to have been inherited from the protolith (e.g. McLeod and Stanton, 1984; Ashley *et al.*, 1988). Although Huston (1993) has suggested that parts of the footwall alteration zones at Balcooma are metasomatic in origin. However, sharp compositional changes in metamorphosed alteration zones underlying other metamorphosed massive sulphide deposits are interpreted to have been present prior to metamorphism (Riverin and Hodgson, 1980; Schmidt, 1988).

The objectives of this chapter are to document the mineralogy and textures of footwall hydrothermal alteration at Thalanga and also to describe the distribution of the hydrothermal minerals in the footwall. The composition, textural variations and distribution of alteration within the ore horizon and the hangingwall volcanics are also described in this chapter and compared with the style and relative timing of footwall alteration. Herrmann (1994) calculated mass changes in the composition of variously altered rhyolitic volcanics in the footwall at Thalanga and therefore similar calculations are not presented here.

10.2 Footwall Alteration

10.2.1 Types and Distribution of Footwall Alteration

Quartz-muscovite ± chlorite ± pyrite-rich assemblages are confined to the rhyolitic volcanics and parts of the quartz 'eye' volcaniclastic unit (QEV) within the ore horizon at Thalanga. Variation in the relative proportions of these minerals has resulted in five main styles of metamorphosed footwall alteration at Thalanga, and these are:
(i) quartz-muscovite ± chlorite ± phlogopite ± <5 % pyrite,
(ii) quartz-muscovite ± phlogopite alteration with >5 % pyrite veins,
(iii) intense silicification,
(iv) chlorite schist ± pyrite, and
(v) clinozoisite-chlorite-tremolite assemblages.

Quartz-muscovite ± chlorite ± phlogopite ± pyrite-rich assemblages are widespread and have overprinted the footwall rhyolitic volcanics for the entire strike length, and up- and

down-dip extent, of the massive sulphide lenses at Thalanga. Generally, the intensity of alteration decreases with distance from the massive sulphide lenses, and the quartz-muscovite ± chlorite ± phlogopite ± pyrite assemblage extends up to 200 m stratigraphically below the mineralised horizon. The presence of partly to weakly altered feldspar crystals in the rhyolitic volcanics corresponds with a decreasing intensity of metamorphosed footwall alteration.

Variations in the content of chlorite, phlogopite and pyrite are typically manifest as subvertical zones of quartz-muscovite ± phlogopite-rich assemblages (with pyrite veins in places) or chlorite-phlogopite > quartz-muscovite-rich assemblages that intersect the ore horizon at a low angle (Fig. 10.1a-c). In places, zones of chlorite-quartz-muscovite grade into zones of chlorite schist. Typically, the zones of chlorite schist ± pyrite and clinozoisite-chlorite-tremolite-rich assemblages are more abundant towards the stratigraphic top of the footwall rhyolitic volcanics. Lenses of chlorite schist are present at the stratigraphic top of the rhyolitic volcanics in West and Central Thalanga (Chapter 11). Clinozoisite-chlorite-tremolite assemblages are also more common in West and Central Thalanga, particularly underlying areas of carbonate-chlorite-tremolite (CTC) alteration within the ore horizon (e.g. diamond drill hole TH243A; Appendix A).

An abrupt change in the abundance of pyrite marks the contact between quartz-muscovite ± chlorite ± phlogopite-rich assemblages and the subvertical zones of quartz-muscovite and pyrite veins (referred to as stringer zones) in the footwall rhyolitic volcanics. Stringer zones range from 5-70 m in thickness (Herrmann, 1994) and contain irregular to subvertical pyrite veins that are folded with axial planes parallel to S_2 (Chapter 3). In East Thalanga and the Vomacka Zone, multiple stringer zones are present in the footwall rhyolitic volcanics and the thickest lenses of massive sulphides are typically present where these stringers zones intersect the ore horizon (Fig. 6.10).

In the footwall rhyolitic volcanics at West and Central Thalanga, there is one main zone composed of abundant quartz-muscovite with numerous pyrite veins (Fig. 10.1a-c). The maximum thickness of this stringer zone directly underlies the thickest part of the ore horizon and extends down-dip, where it is truncated by a steep, N-dipping normal fault (Fig. 10.1a-c). This stringer zone decreases in thickness up dip (as do the massive sulphide lenses) and generally does not extend up-dip of the massive sulphides. A second subvertical quartz-muscovite-rich assemblage, with minor pyrite and traces of chlorite, is present approximately 50 m north of the main stringer zone in West Thalanga (Fig. 10.1a).

Zones of intense silicification are located at the stratigraphic top of the footwall rhyolitic volcanics and locally up to 200 m stratigraphically below the ore horizon. In East Thalanga, a lozenge-shape zone of intensely silicified rhyolite is present at the stratigraphic top of the

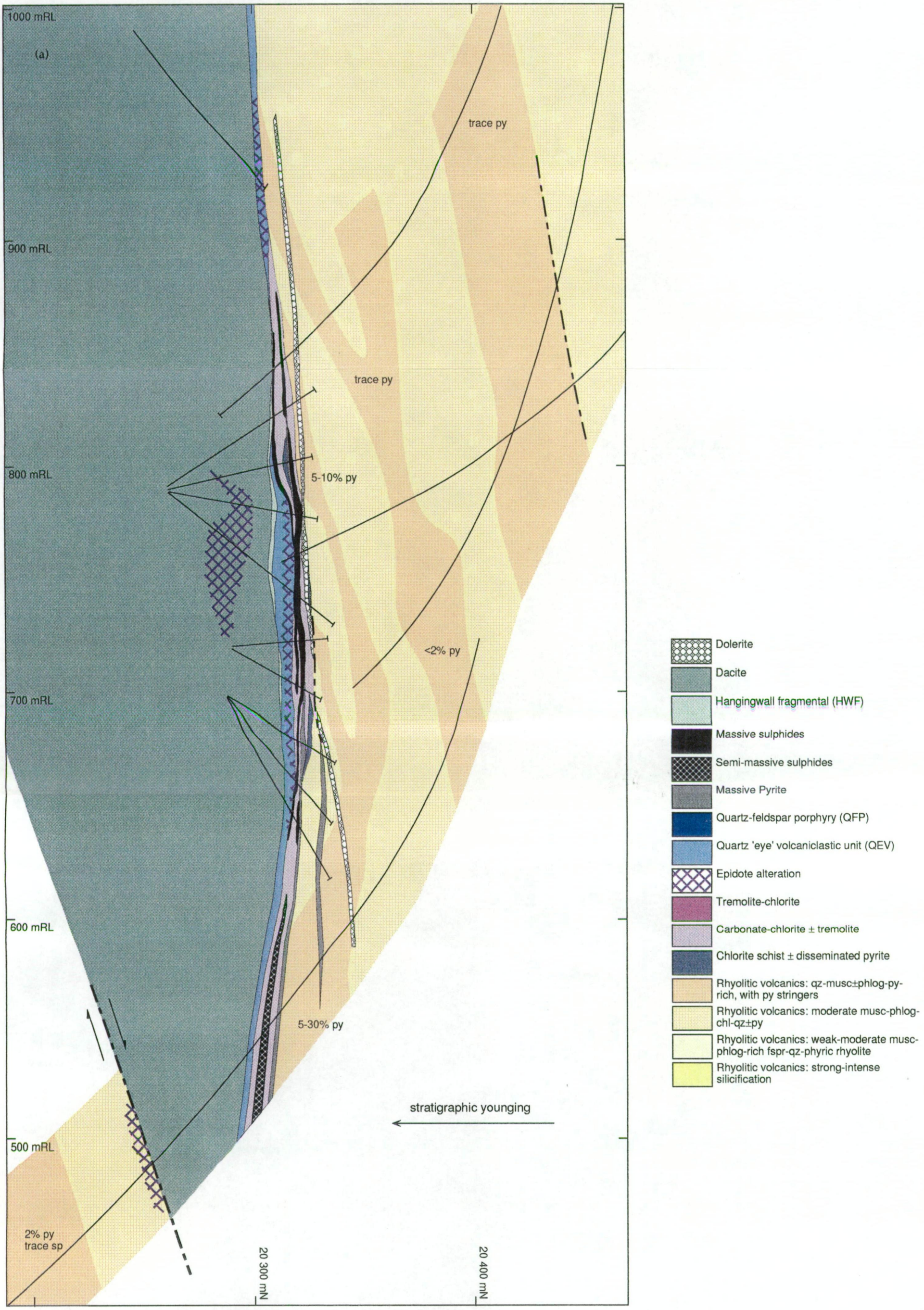

Figure 10.1 Cross sections along (a) 20 110 mE and (b) 20 310 mE in West Thalanga, and (c) 20 390 mE in Central Thalanga. The pyrite content of the stringer zones is a visual estimation. Heavy dashed lines are faults. Abbreviations: chl = chlorite, fspr = feldspar, musc = muscovite, phlog = phlogopite, py = pyrite, qz = quartz, sp = sphalerite.

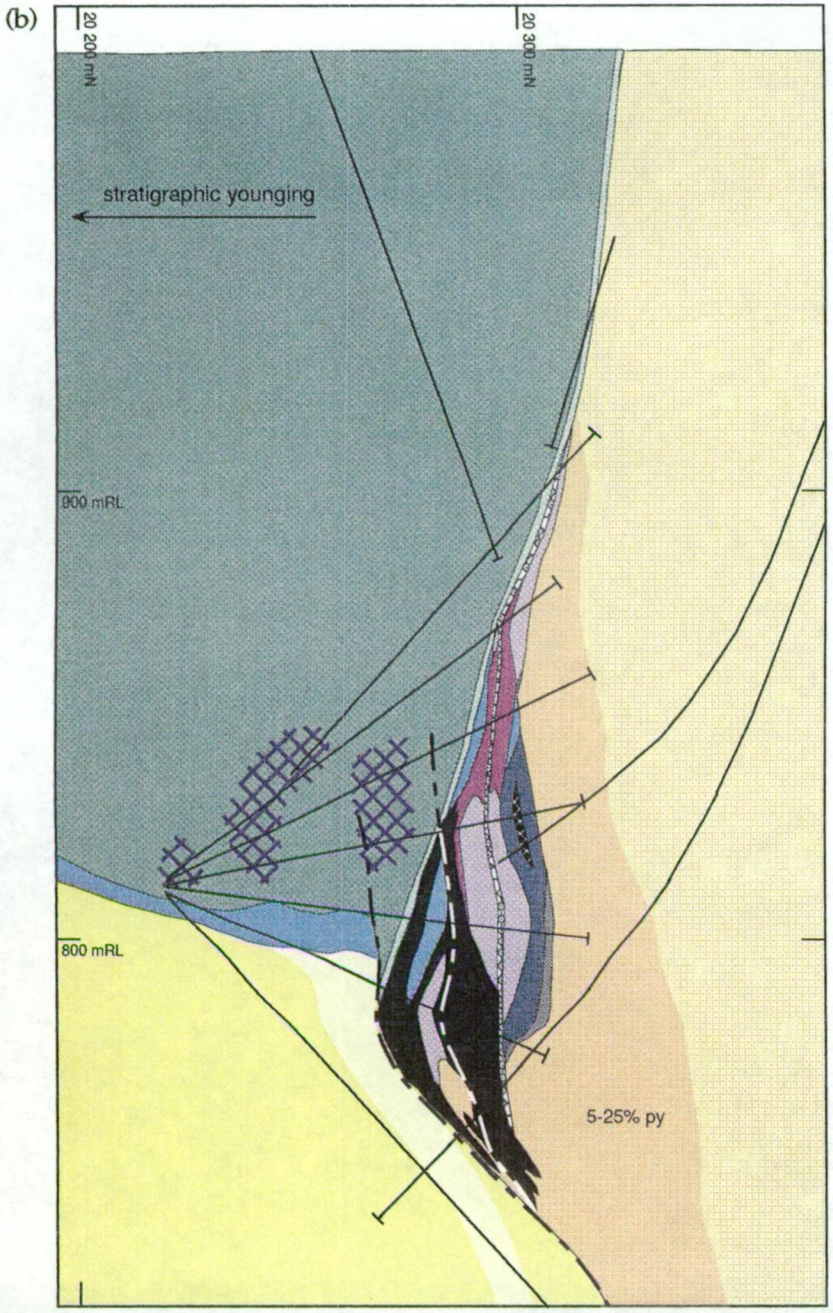

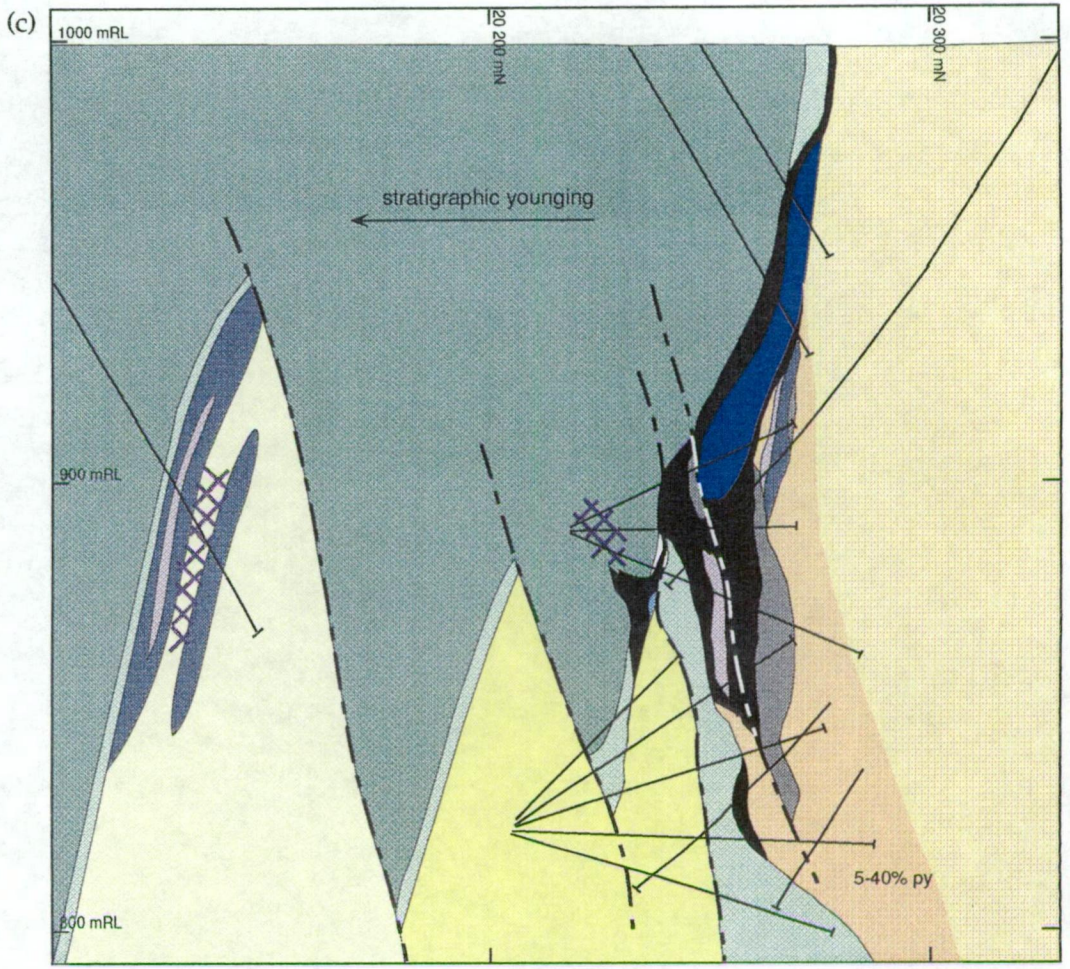

Figure 10.1 Cross sections along the (b) 20 310 mE at the eastern end of West Thalanga, and (c) 20 390 mE section in Central Thalanga. See Fig. 10.1a for legend.

footwall (Fig. 6.10). Quartz-muscovite-pyrite-rich assemblages (including pyrite veins) underlie and are present at up-and down-dip of this intensely silicified zone. In West Thalanga and western parts of Central Thalanga, the rhyolitic volcanics that have been moved upwards on the southern side of a normal fault (Fig. 10.1b,c) are locally strongly silicified (varying from light grey to pink in hand specimen) to weakly altered, with minor phlogopite and muscovite. The rhyolitic volcanics in this part of West and Central Thalanga are not overlain by massive sulphide lenses and are therefore interpreted to be located at the margins of the zone of hydrothermal alteration.

10.2.2 Petrology and Microtextures of Footwall Alteration

Quartz-Muscovite ± Chlorite ± Phlogopite ± Pyrite Assemblage

Most volcanic textures have not been preserved in zones of quartz-muscovite-rich assemblages (e.g. Fig. 10.2a) within the footwall at Thalanga. Typically only quartz crystals have been preserved and feldspars are not present. However, there are a few locations where pseudomorphed feldspar crystals (white in hand specimen) are present within the rhyolitic volcanics immediately underlying massive sulphides. In thin section, the feldspars have been replaced by fine grained muscovite, calcite, epidote, quartz and locally chlorite (Fig. 10.2b,c), and are associated with a matrix of abundant fine grained muscovite, with chlorite and quartz. In some of the least altered rhyolitic volcanics, feldspar crystals have been albitised and partly replaced by quartz.

The quartz-muscovite-rich assemblages are characterised by extensive mosaics of fine grained (<0.1 mm) equant quartz, with triple point grain boundaries, and variable amounts of fine grained (<0.05 mm) muscovite. These assemblages are interpreted to be the metamorphosed equivalent of a quartz-sericite hydrothermal alteration assemblage. The quartz and muscovite vary from evenly distributed and intergrown, to circular domains of intergrown quartz enveloped by muscovite (Fig. 10.2d-g). Variable proportions of phlogopite, chlorite, calcite and pyrite are typically disseminated through the intergrown quartz and muscovite. Coarse grained (0.5-1.0 mm) muscovite (confirmed by microprobe analysis), chlorite and phlogopite, are commonly present in pressure shadows around quartz or altered feldspar crystals and intergrown with euhedral pyrite.

Increased abundance of chlorite and phlogopite is commonly at the expense of quartz or muscovite. Chlorite and phlogopite are typically intergrown with muscovite, and pseudofiamme textures are common. In places, domains of fine grained phlogopite ± chlorite may be altered pumice (Fig. 10.3a,b). Phlogopite is interpreted to have been metamorphosed from a chlorite-sericite hydrothermal alteration assemblage. Locally, chlorite and phlogopite porphyroblasts have overgrown the cleavage defined by fine grained muscovite

Figure 10.2 Textures of quartz-muscovite ± phlogopite-rich footwall rhyolitic volcanics.

(a) Silicified rhyolite clasts in a quartz-muscovite-rich matrix that also contains minor pyrite and traces of phlogopite. Sample TH255-135.5, West Thalanga.

(b) Photomicrograph strongly altered feldspar crystal, now composed of fine grained muscovite, zoisite, quartz and phlogopite, within quartz-phlogopite-muscovite-rich rhyolitic volcanics in immediate footwall to massive sulphides. E765 Stope, 30 450 mN, 31 910 mE. Plane light.

(c) Same as (b) under crossed nicols.

(d) Photomicrograph of quartz-muscovite-rich rhyolitic volcanics (possibly a breccia) with vague circular texture. Quartz has been strongly recrystallised, including embayed quartz phenocrysts (arrow). Sample C2037NI15-67.8, Central Thalanga. Plane light.

(e) Same as (d) under crossed nicols.

(f) Photomicrograph of typical strongly recrystallised quartz-muscovite-phlogopite-rich rhyolitic volcanics. Sample E3208SD36-40.8, East Thalanga. Plane light.

(g) Same as (e) under crossed nicols.

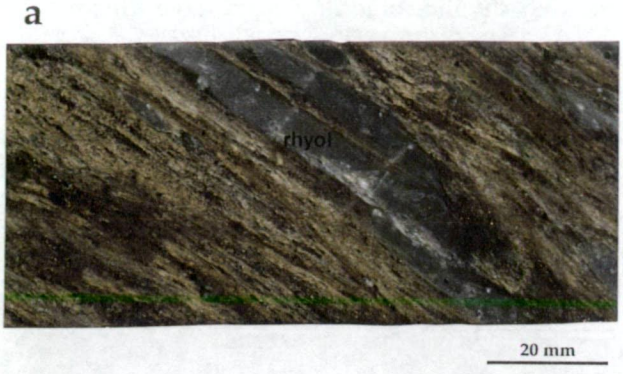
a
rhyol
20 mm

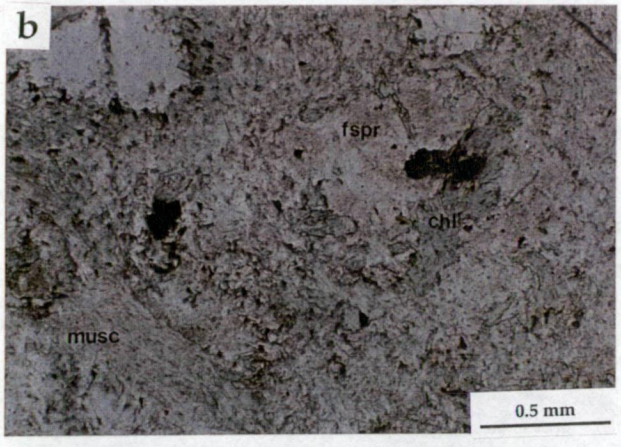
b
fspr
chl
musc
0.5 mm

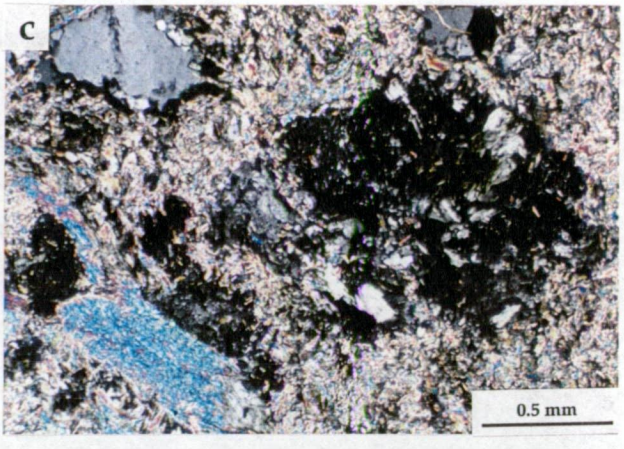
c
0.5 mm

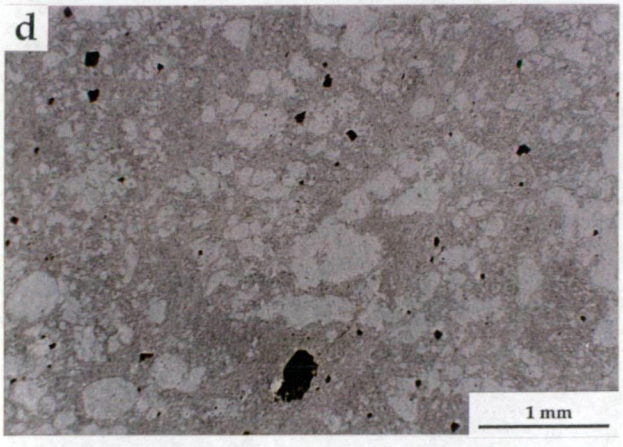
d
1 mm

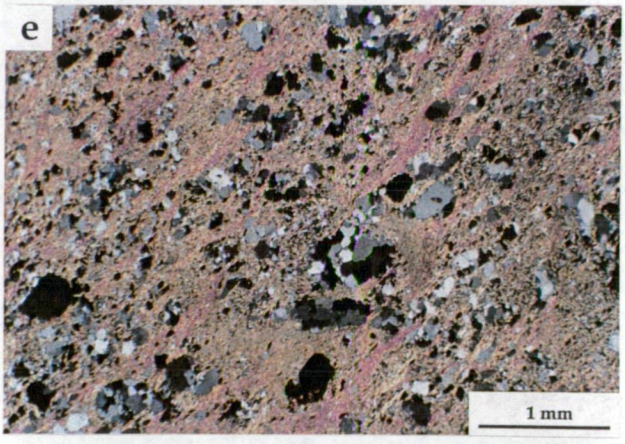
e
1 mm

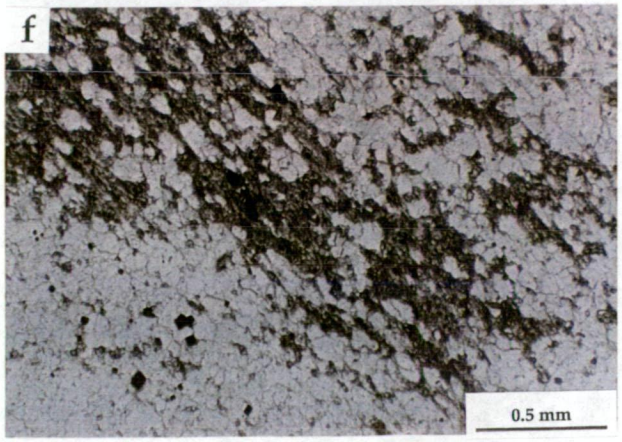
f
0.5 mm

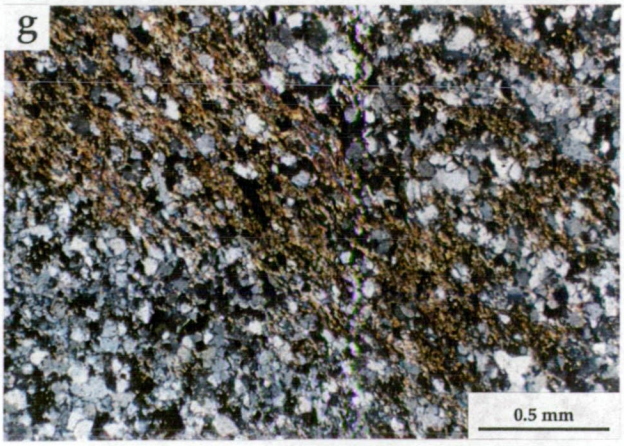
g
0.5 mm

Figure 10.3 Variations in the composition and textures of altered footwall rhyolitic volcanics.

(a) Typical quartz-phlogopite-muscovite-pyrite-rich rhyolite breccia. Clasts have diffuse margins (arrow) and are more siliceous that matrix, which is mostly composed of blue quartz crystals and fine grained phlogopite. Sample TH35-201, East Thalanga.

(b) Quartz-chlorite-phlogopite-rich rhyolitic volcanics. Rare blue quartz crystals are present in both the chlorite-phlogopite domains and quartz-rich domains. Vague arcuate textures may be the result of alteration of perlitic rhyolite or perlitic rhyolite breccia. Sample C2037NI15-81.4, Central Thalanga.

(c) Samples of the footwall pyrite stringer zone. Top: strongly pyritic quartz-muscovite-rich assemblage. Sample TH238-114.5, Central Thalanga. Bottom: quartz-muscovite-pyrite-rich assemblages with stringer pyrite. Sample E3208SD36-40.8, East Thalanga.

(d) Pyrite stringers, and traces of chalcopyrite, within quartz-muscovite-phlogopite-rich rhyolitic volcanics. Sample TH137A-185.2, West Thalanga.

(e) Massive pyrite vein from within stringer zone. S_2 cross cuts vein boundary. Sample TH230-138.6, Central Thalanga.

(f) Strongly siliceous stringer zone containing fine grained sphalerite disseminations and veins around altered pumice clasts. Sample E3198SI12-19.8, East Thalanga.

(g) Strongly silicified rhyolitic volcanics (type A) from East Thalanga. Top: intensely silicified quartz-phyric rhyolite, containing trace of muscovite (concentrated in veins subparallel to, but cross cut by cleavage). Sample TH359-160.5. Bottom: strong-intensely silicified rhyolitic volcanics, with muscovite parallel to cleavage. Sample E3204SI31-4.5.

(h) Strongly silicified rhyolitic volcanics (type B) from West and Central Thalanga. Top: strongly silicified quartz sandstone (blue quartz grains). Pink colour due to disseminated fine grained hematite. Sample C2037NI15-33.5. Bottom: strongly silicified quartz sandstone with rare pyrite veins cross cut by quartz veins. Sample W2031ND46-29.5.

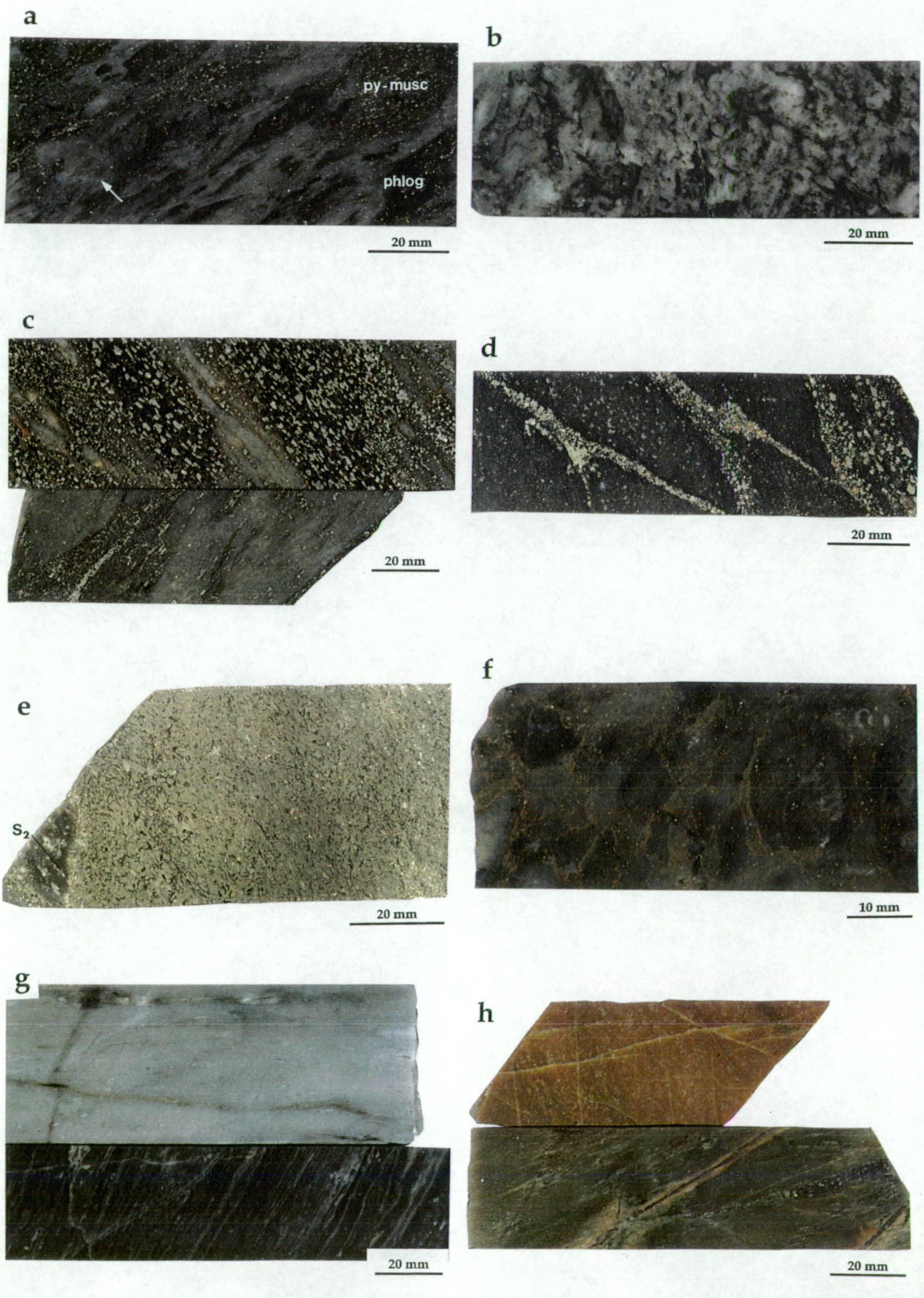
a
py - musc
phlog
20 mm
b
20 mm
c
20 mm
d
20 mm
e
S_2
20 mm
f
10 mm
g
20 mm
h
20 mm

and elongate microcrystalline quartz (Chapter 3). Chlorite blotches (up to 2 cm in diameter) appear to have overprinted quartz-muscovite assemblages in parts of the footwall. In thin section, these blotches are composed of fine grained muscovite, minor phlogopite and chlorite.

Quartz-Muscovite ± Phlogopite Assemblage with Pyrite Veins (Stringer Zones)

Stringers zones are typically composed of 5-50 % pyrite veins that are intergrown with quartz- or quartz-muscovite-rich assemblages (up to 35 % muscovite) (Fig. 10.3c,d). However, pyrite veins are also present within zones of quartz-muscovite-phlogopite assemblages and strong chlorite alteration. It is therefore interpreted that pyrite stringer veins were present in quartz ± sericite, quartz-sericite-chlorite and chlorite alteration zones prior to metamorphism. Stringer zones close to the massive sulphide lenses contain more pyrite and chalcopyrite (≤50 % pyrite veins, ≤2 % chalcopyrite) than stringer zones further from the ore horizon (e.g. Fig. 6.10)

Pyrite stringer zones have similar microtextures to quartz-muscovite-rich assemblages, with abundant equant, fine grained quartz, minor domains of fine grained muscovite and disseminated euhedral pyrite. Pyrite veins vary from <5 mm to 2 m in thickness (Fig. 10.3d,e) and comprise intergrown subhedral to anhedral pyrite grains, with rare interstitial chalcopyrite, or euhedral pyrite disseminated in either muscovite or colourless chlorite. In a few locations in Central and East Thalanga, sphalerite and sphalerite-pyrite veins are present within the footwall rhyolitic volcanics (Fig. 10.3f). Phlogopite and quartz gangue is present in some sphalerite-pyrite veins. Pyrite-barite veins cross cut the pyrite stringer veins in the immediate footwall to the massive sulphides in Central Thalanga and locally in East Thalanga (Chapter 3).

Intense Silicification

Intensely silicified rhyolitic volcanics at Thalanga appear coherent in hand specimen, but the presence of rare non-volcanic lithic clasts (evident in thin section) indicates that some intensely silicified rhyolitic volcanics were originally clastic (Chapter 4). Most intensely silicified rhyolitic volcanics at Thalanga are grey to white and rarely pinkish in hand specimen with small (<2 mm) colourless or rarely blue quartz crystals (Fig. 10.3g,h). Microtextures indicate that there are at least two types (here named types A and B) of intensely silicified rhyolitic volcanics at Thalanga.

Type A silicification: The intensely silicified (type A) rhyolitic volcanics are white to grey in hand specimen (e.g. Fig. 10.3g, top) and are composed of a mosaic of fine grained (0.01-0.2 mm) quartz and minor muscovite. Rare irregular albite grains are present and may have

formerly been feldspar phenocrysts (Fig. 10.4a). Evenly distributed, subhedral, partly embayed quartz crystals are also present in intensely silicified rhyolitic volcanics.

Type B silicification: Type B silicified rhyolitic volcanics are grey to pink in hand specimen (e.g. Fig. 10.3h). The matrix of type B is composed of two populations of quartz; (i) cryptocrystalline (<0.01 mm in size) quartz and possible feldspar, and (ii) irregular quartz grains that are 0.05-0.1 mm in size (Fig. 10.4b), and is therefore inferred to be a silicified rhyolitic sandstone. Subhedral quartz and feldspar crystals are 0.5-2 mm in diameter, and the feldspars have been albitised and partly replaced by quartz.

Traces of phlogopite and pyrite are disseminated through both styles of silicification, resulting in weakly developed cleavage. Pyrite stringers sub-parallel to S_2 are common at the margins of the intensely silicified rhyolitic volcanics (type A) at the stratigraphic top of the footwall in East Thalanga, but are generally absent from other intensely silicified rhyolitic volcanics elsewhere at Thalanga.

Chlorite Schist ± Pyrite

Massive, fine grained chlorite is present as discrete domains within the footwall and chlorite is also disseminated in parts of quartz-muscovite-pyrite-rich assemblages. Zones of massive, fine grained chlorite within footwall are typically strongly foliated (now chlorite schist) and have a mottled texture due to disseminated phlogopite (Fig. 10.4 c). The chlorite is Mg-rich (Chapter 3) and colourless in thin section. Pyrite is present as either disseminated, euhedral grains, or as irregular veins subparallel to cleavage. Volcanic textures are typically not preserved in the zones of chlorite schist, except for rare quartz crystals and clinozoisite grains that may be after feldspar crystals.

Clinozoisite-Chlorite-Tremolite Assemblage

Clinozoisite is pink to white in hand specimen and is present as both pervasive anhedral intergrowths with chlorite and tremolite (or actinolite in places) (Fig. 10.4d), and as irregular zones of clinozoisite blebs within chlorite ± phlogopite ± muscovite alteration, that may be pseudomorphs of feldspar crystals (Fig. 10.4e, top). In thin section, clinozoisite rims irregular grains of zoisite, both of which are intergrown with tremolite. The chlorite is Mg-rich (Chapter 3) and colourless in thin section, with grey green birefringence. Fine grained (<0.1 mm) muscovite and rare subhedral grains of sphene are present in some samples. Zones of clinozoisite-chlorite-tremolite have diffuse contacts with the quartz-muscovite ± phlogopite-rich assemblages (Fig. 10.4e, bottom).

Figure 10.4 Further examples of footwall alteration at Thalanga.

(a) Photomicrograph of type A silicified rhyolitic volcanics with irregular albite grain and minor fine grained muscovite in a mosaic of recrystallised, equigranular quartz. Sample E3216SD48-29.3, East Thalanga. Crossed nicols.

(b) Photomicrograph of type B strongly silicified rhyolitic volcanics (feldspar- and quartz-bearing sandstone) comprising quartz crystals, fine grained quartz matrix, and intermediate-sized quartz grains. Sample C2039ND20-40, Central Thalanga. Crossed nicols.

(c) Hand specimen of chlorite schist, with minor phlogopite and veins of pyrite and dark red-brown sphalerite. Located between intensely silicified (type A) rhyolite and quartz-muscovite-pyrite-rich rhyolitic volcanics. Sample TH265-181.3, East Thalanga.

(d) Pervasive clinozoisite-tremolite-chlorite alteration, with irregular patches of pink clinozoisite intergrown with tremolite and chlorite. Sample TH243A-334, West Thalanga.

(e) Examples of less pervasive clinozoisite-tremolite-chlorite alteration. Top: subhedral clinozoisite grains in chlorite (and minor phlogopite) -rich matrix cross cut by pyrite veins. Sample TH245-482.3, West Thalanga. Bottom: diffuse, irregular contact between pervasive clinozoisite-tremolite-chlorite alteration and quartz-phlogopite altered rhyolitic volcanics. Sample C2037NI15-62, Central Thalanga.

(f) Pervasively altered rhyolitic volcanics: beige domain is composed of diopside intergrown with clinozoisite, which has overprinted the green domain of tremolite. Sample E3160SD30-59.1, Vomacka Zone.

(g) Pseudoclastic texture produced by phyllosilicate-rich domains (fine grained phlogopite) between interconnected domains of quartz-rich alteration. Bipyramidal blue quartz phenocrysts (total = 5 %) are present in both areas. Minor disseminated pyrite is concentrated in phlogopite-rich domains. Sample TH252-51, East Thalanga.

(h) Phlogopite-rich quartz-feldspar-phyric rhyolite, with relic perlite and patchy, irregular quartz-rich domains. Sample 955-4, Central Thalanga.

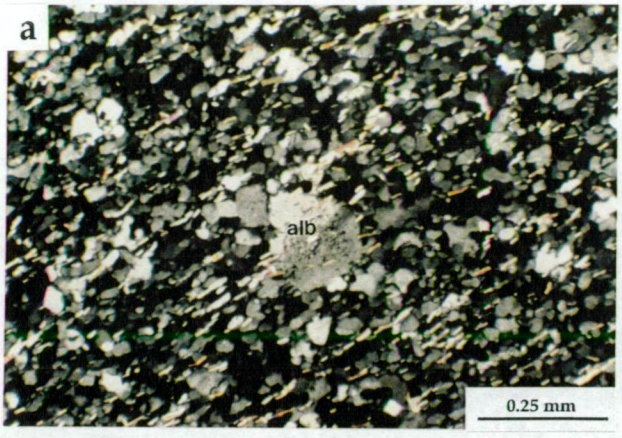
a
alb
0.25 mm

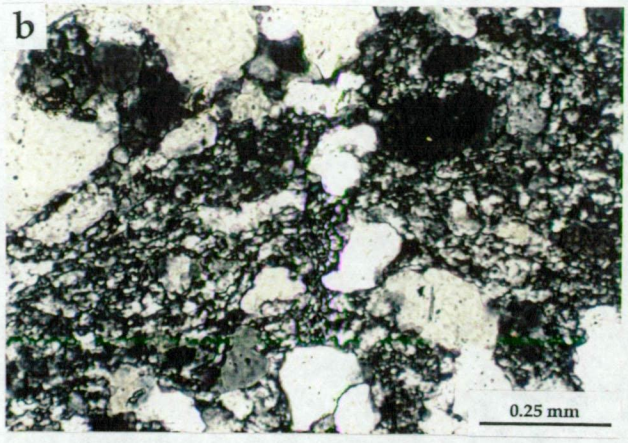
b
0.25 mm


c
20 mm

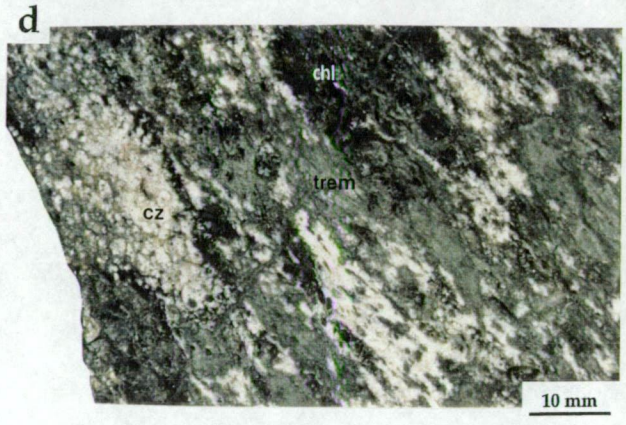
d
chl
trem
cz
10 mm

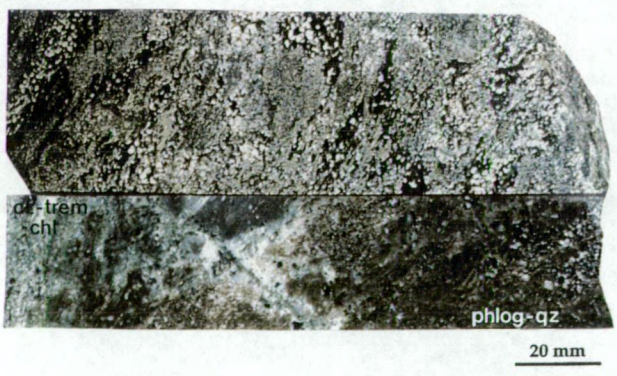
e
py
qz-trem
chl
phlog-qz
20 mm


f
trem
diop-cz
10 mm

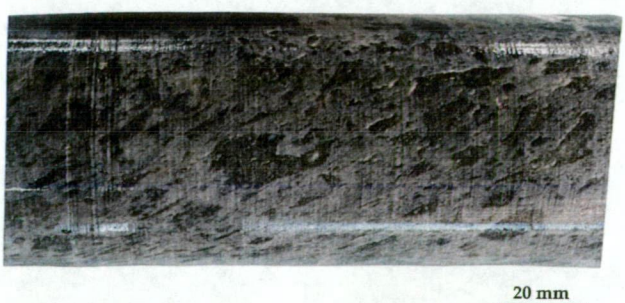
g
20 mm

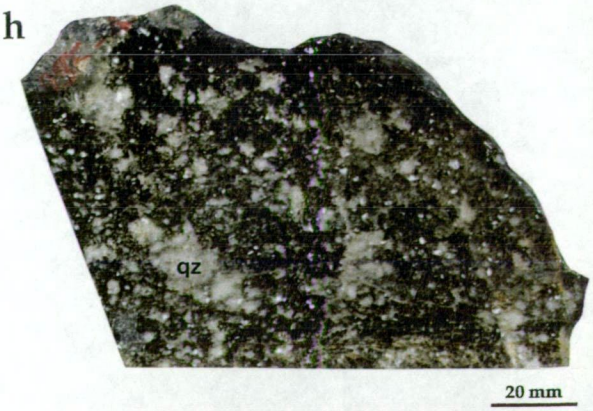
h
qz
20 mm

Subhedral quartz crystals are present in zones of weak clinozoisite-chlorite-tremolite alteration, but are typically absent in areas of intense clinozoisite-chlorite-tremolite alteration. This indicates that clinozoisite may have formed by reaction between chlorite, calcite and quartz during metamorphism (producing clinozoisite and tremolite; Chapter 3), and therefore chlorite and calcite are the likely precursor phase produced during the hydrothermal alteration. Quartz may have been both hydrothermal in origin and also present as volcanic crystals.

In some places, diopside is also present in this alteration assemblage (Fig. 10.4f). In these locations, diopside is intergrown with clinozoisite and calcite and appears to overprint domains of randomly oriented tremolite. This suggests that diopside is a metamorphic phase produced by the reaction between tremolite, calcite and excess quartz according to the reaction:

$$Ca_2Mg_5Si_8O_{22}(OH)_2 + 3CaCO_3 + 2SiO_2 = 5CaMgSi_2O_6 + 3CO_2 + H_2O$$

tremolite + calcite + quartz = diopside.

10.2.3 Mesotextures of Footwall Alteration

Pseudoclastic Textures

Pseudoclastic textures are common in the footwall rhyolitic volcanics and are present in both primary volcaniclastic and coherent rhyolite facies. As described in Chapter 4, distribution and abundance of quartz (and feldspar where present) crystals may indicate whether alteration has overprinted coherent or clastic facies. Evenly distributed crystals in both the apparent clasts and the 'matrix' are interpreted to indicate that the precursor was uniformly porphyritic. The most common pseudoclastic texture in the footwall at Thalanga comprises wispy phyllosilicate-rich patches that resemble flattened pumice clasts. These are referred to as pseudofiamme (Fig. 10.4g).

Most pseudofiamme are composed of chlorite-, phlogopite- or muscovite-rich domains enveloped by quartz-rich domains. Where present, fine grained euhedral pyrite is preferentially disseminated in the chlorite or phlogopite, rather than the quartz-rich, domains. Crystal composition and distribution does not vary between the phyllosilicate-rich patches and the matrix, and together with unbroken crystals overlapping the margins of phyllosilicate-rich areas, this indicates that two-stage hydrothermal alteration (involving initial phyllosilicate alteration, followed by quartz alteration) had overprinted a possibly coherent, glassy or partly devitrified precursor (cf. Allen, 1988).

Altered Perlite

Perlite is present in the least altered, formerly glassy, coherent feldspar-quartz-phyric rhyolites at Thalanga, where it is accentuated by phlogopite in the kernels and quartz along the arcuate fractures (Fig. 4.4). Figure 10.4h shows incipient pseudoclastic texture in a perlitic rhyolite, whereby irregular domains (pseudoclasts) of quartz are enclosed by phlogopite (metamorphosed from chlorite-sericite alteration). In thin section, the phlogopite and perlitic fractures have been overprinted by quartz and fine grained muscovite (Fig. 10.5a,b), resulting in phlogopite-rich pseudoclasts in a "matrix" of quartz-muscovite in more altered rhyolites (Fig. 10.5c). Elsewhere, fine grained muscovite occurs along the perlitic fractures, producing a network of muscovite enveloping circular quartz kernels (Fig. 10.5d). Convincing perlitic textures are destroyed with increased abundance of muscovite (increased sericite alteration), although isolated kernels of recrystallised quartz in abundant fine grained muscovite hints at a possible perlitic precursor (Fig. 10.5e,f). The presence of partly recrystallised spherulites in Figure 10.5 (e,f) supports the interpretation that this sample was formerly a glassy rhyolite. Comparison with perlitic dacite, where biotite has overprinted the perlitic fractures, shows that there are domains containing abundant fractures that now appear as a polygonal network of biotite (Fig. 10.5g,h), similar to some altered rhyolitic volcanics.

Altered Pumice Breccia

In some samples, domains of elongate quartz separated by fine grained muscovite and anhedral calcite are interpreted to be altered tube pumice clasts (Fig. 10.6a,b). The muscovite and calcite may define tube walls and the quartz is inferred to have filled tubes. The pumice clasts are inferred to have been uncollapsed prior to alteration because quartz was able to fill the tubes, thus indicating that the alteration must have predated burial compaction and deformation. Fine grained sphalerite stringer veins occur around the silicified pumice clasts (Fig. 10.3f), further indicating that silicification pre-dated mineralisation. Phyllosilicate alteration of pumice clasts in the footwall rhyolitic volcanics must also predate deformation, as they are flattened parallel to S_2 (Chapter 4). However, it is unclear whether phyllosilicate alteration predated or post-dated diagenetic compaction.

10.3 Alteration within the Ore Horizon

10.3.1 Alteration of the QEV

There are two main types of metamorphosed alteration assemblages within the QEV units at Thalanga; (i) quartz-muscovite-rich assemblages, and (ii) epidote-actinolite-rich

Figure 10.5 Textural evidence of the alteration of formerly glassy rhyolitic volcanics at Thalanga.

(a) Photomicrograph of recrystallised fine grained quartz that has overprinted the partly altered perlitic textures (defined by phlogopite-chlorite) within a quartz-feldspar-phyric rhyolite. Sample 955-4, Central Thalanga. Plane light.

(b) Same as (a) under crossed nicols.

(c) Quartz-muscovite-phlogopite-pyrite-rich rhyolite, with arcuate textures that are interpreted to be altered perlitic fractures. Irregular phlogopite-rich domains have diffuse contacts with interconnected domains of quartz-muscovite, and are therefore interpreted to be pseudoclasts. Sample CT-91-38, C860 Stope: 20250 mN, 20 429 mE, Central Thalanga.

(d) Photomicrograph of altered perlitic rhyolite breccia: arcuate textures defined by fine grained muscovite within domains of recrystallised quartz are interpreted to be altered perlitic fractures. Sample W2033ND34-82.8, West Thalanga. Plane light.

(e) Spheroidal zones of equant, recrystallised quartz and partly recrystallised spherulites are enveloped by a network of fine grained muscovite, which may be altered and metamorphosed perlitic fractures. Sample TH5-337.6, Central Thalanga. Plane light.

(f) Same as (e) under crossed nicols.

(g) Relic classical perlitic fractures in dacite, now overprinted by biotite. Local polygonal texture occurs where polygonal domains of fine grained quartz-feldspar groundmass are enclosed by a network of biotite. Sample TH5-143.7, Central Thalanga. Plane light.

(h) Same as (g) under crossed nicols.

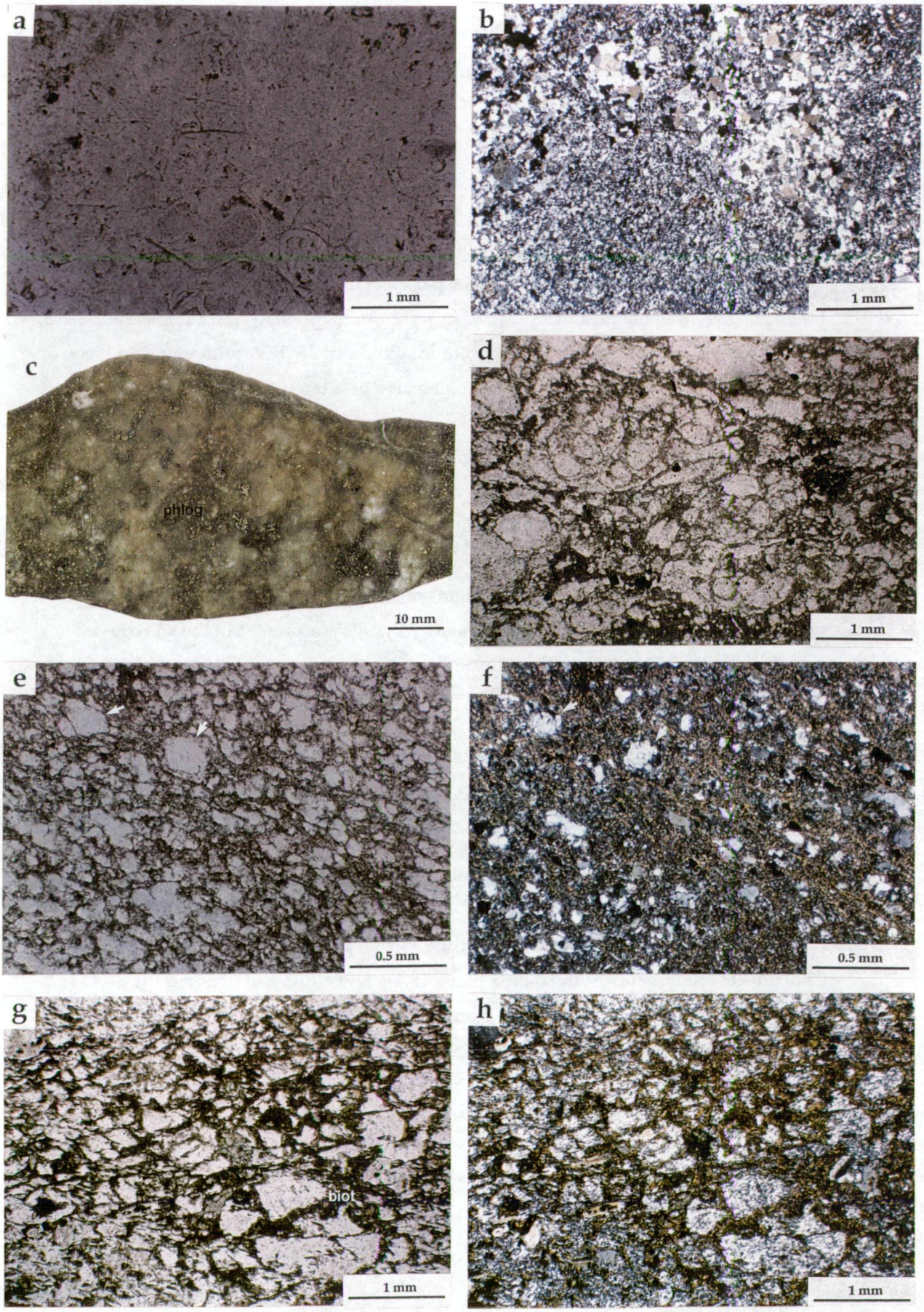
a
1 mm
b
1 mm
c
phlog
10 mm
d
1 mm
e
0.5 mm
f
0.5 mm
g
biot
1 mm
h
1 mm

Figure 10.6 Altered tube pumica breccia (footwall rhyolitic volcanics) and alteration variations within the quartz 'eye' volcaniclastic unit (QEV).

(a) Photomicrograph of altered tube pumice breccia. Tube wall are defined by fine grained muscovite and anhedral calcite, and recrystallised quartz has filled the tubes. Sample E3198SI12-14.8, East Thalanga (same as Fig. 10.3f). Plane light.

(b) Same as (a) under crossed nicols.

(c) Strongly altered QEV. Top: muscovite- and quartz-rich matrix between quartz crystals also contains altered (now muscovite) feldspar crystals. Dark grey streaks are phlogopite. Galena is present in the pressure shadows of some quartz phenocrysts. Sample TH262-225, East Thalanga. Bottom: chlorite-phlogopite-muscovite-rich QEV, with elongate blebs of pyrite. Some elongate muscovite-rich domains may be altered feldspar or, where attached to quartz crystals, altered groundmass of formerly glassy or pumiceous QFP clasts. Sample TH249-209, West Thalanga.

(d) Quartz-muscovite-rich QEV, with disseminated pyrite and minor sphalerite. Wispy, irregular domains of fine grained muscovite, with clinozoisite pseudomorphs of feldspar, may be altered pumice, although the margins of clasts are difficult to determine due to the overprinting alteration. Coarse blue quartz crystals are present in the siliceous matrix. Sample TH249-222.5, West Thalanga.

(e) Irregular, vertical chalcopyrite vein within the QEV is enclosed by epidote-rich assemblage. Shallowly-dipping, discontinuous chalcopyrite veins extend from the footwall side of the chalcopyrite. Location: W690 Stope, West Thalanga. Facing to right.

(f) Massive actinolite with interstitial epidote. Sample TH245-502, West Thalanga.

(g) Epidote-albite-tremolite/actinolite-rich zone within the QEV breccia facies. Clinozoisite pseudomorphs the quartz phenocrysts and albite has replaced the groundmass of QFP clasts. The matrix is now composed of tremolite-chlorite and minor epidote/clinozoisite. Sample W2011ND28-28.8, West Thalanga.

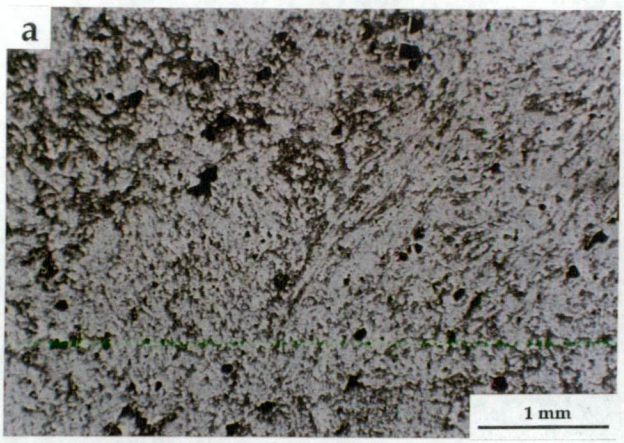
a
1 mm

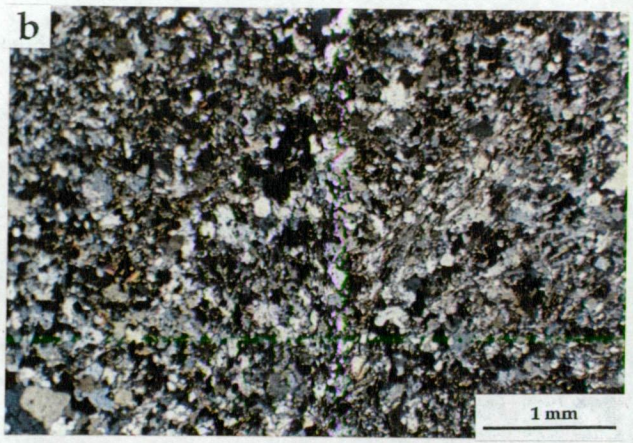
b
1 mm

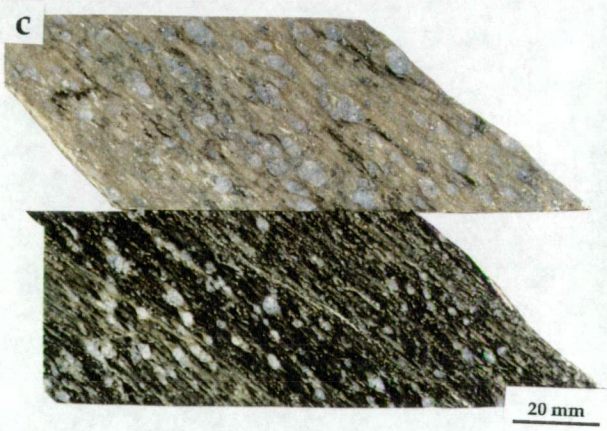
c
20 mm

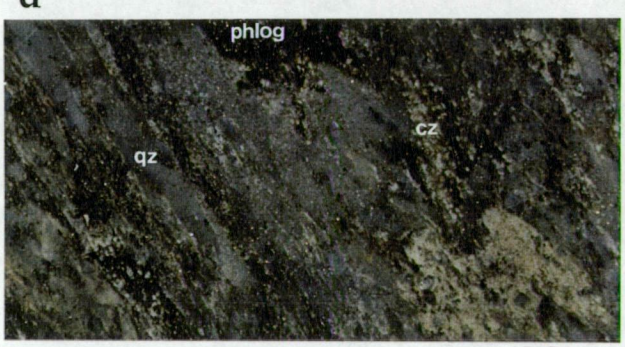
d
phlog
cz
qz
10 mm


e
QEV
cp
ep

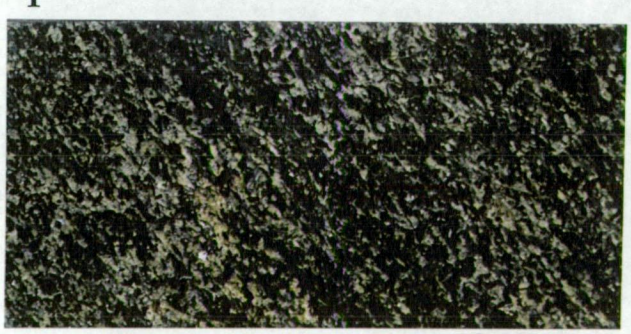
f
20 mm

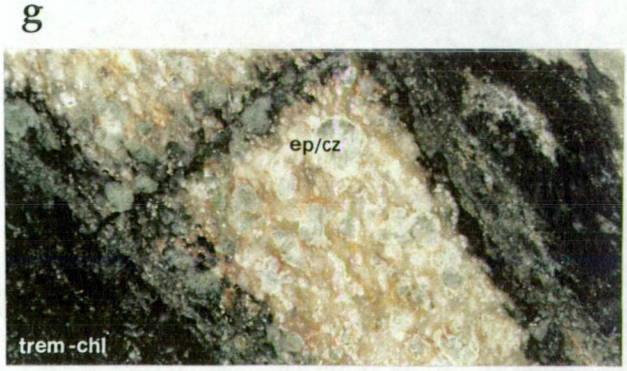
g
ep/cz
trem-chl
10 mm

assemblages. Quartz-muscovite-rich assemblages are present in the QEV units in Central Thalanga, and in QEV units that occur between the footwall and hangingwall massive sulphide lenses in East Thalanga. Epidote-actinolite-rich assemblages have overprinted QEV units in West Thalanga and are only present in minor amounts in East Thalanga.

Quartz-Muscovite Assemblages

The quartz-muscovite-rich QEV units (inferred to have been metamorphosed from quartz-sericite altered QEV) contain pyrite and minor sphalerite and chalcopyrite disseminations, blebs and veins that are subparallel to S_2 . The most quartz-muscovite-rich QEV directly overlies the thickest and most pyrite-chalcopyrite-rich parts of the footwall massive sulphide lens in East Thalanga (Fig. 6.10). The abundance of quartz-muscovite within the QEV decreases up-dip as the footwall massive sulphide lens gradually becomes thinner and contains more QFP and rhyolite clasts. The area of quartz-muscovite-rich QEV is similar in extent to the hangingwall ore lens, which also decreases in thickness and abundance of sulphides up-dip. Feldspars are not preserved in the most quartz-muscovite-rich QEV units in East Thalanga, resulting in an apparently quartz-only sandstone (Fig. 10.6c, top), but altered feldspars (now composed of muscovite ± calcite ± quartz) are present in the less-altered parts of the QEV. Irregular wisps of intergrown, fine grained muscovite and muscovite-rich QFP clasts (with apparent crystal enrichment) within the QEV are inferred to be altered pumice clasts (Chapter 4).

Where the QEV is overlain by massive sulphides in West Thalanga, the QEV contains abundant muscovite-phlogopite ± chlorite (Fig. 10.6c, bottom), suggesting that prior to metamorphism, these parts of the QEV had been overprinted by sericite-chlorite alteration. The discontinuous lenses of QEV in Central Thalanga vary from muscovite-rich with variable phlogopite, to siliceous with minor muscovite (Fig. 10.6d). Feldspar crystals are now composed of muscovite or zoisite, and pyrite is typically disseminated through the QEV matrix. In places, intense quartz-sericite alteration is inferred to have destroyed volcaniclastic textures, with quartz phenocrysts the only volcanic texture preserved within intergrown fine grained quartz and muscovite. Wispy domains of fine grained muscovite may be altered pumice clasts. Pyrite stringers and disseminated blebs of pyrite are common in the quartz-muscovite-rich QEV units in Central and West Thalanga.

Epidote-Actinolite Assemblages

Distribution: In West Thalanga there is a sharp contact between massive sulphides and the overlying QEV (Chapter 6). However, in most places, there is an epidote-actinolite-rich zone between the massive sulphides and the QEV, which has sharp contacts with the massive sulphides and gradational contacts with the QEV (Fig. 10.1a). Chalcopyrite veins within

the QEV units are enclosed by intergrown epidote-actinolite/tremolite (Fig. 10.6e). Epidote-actinolite-rich assemblages also occur at the few contacts between the QEV and underlying CTC assemblages, with domains of tremolite, or tremolite-chlorite and minor epidote, present between the epidote-actinolite and the CTC units. Where massive sulphide lenses are not present, epidote-rich QEV stratigraphically overlies, with gradational contacts over 20 cm, quartz-muscovite-pyrite-rich QEV (e.g. diamond drill hole TH249; Appendix A). Epidote-tremolite-chlorite-rich assemblages are present within parts of the QEV breccia units in East Thalanga, where they are typically associated with zones of abundant sulphides near the base of QEV breccia facies. Epidote-tremolite-chlorite-rich assemblages also occur as gangue in the mineralised upper rhyolite breccia.

Textures and Mineralogy: Areas of massive epidote-actinolite-rich assemblages vary from massive epidote-rich to massive actinolite/tremolite with minor epidote (Fig. 10.6f). Typically sheafs of acicular actinolite, anhedral epidote, minor phlogopite, traces of anhedral K-feldspar, and accessory apatite and sphene constitute the epidote-actinolite assemblages. Tremolite, rather than actinolite, is more common towards the stratigraphic base of domains of epidote-actinolite-rich QEV units in West Thalanga. Locally, clinozoisite rather than epidote is intergrown with actinolite, and anhedral clinozoisite typically has cores of subhedral epidote or zoisite. These assemblages are interpreted to have been produced by the metamorphism of chlorite-calcite-quartz-rich hydrothermal alteration assemblages (Chapter 3). Epidote-actinolite assemblages are inferred to have formed from units that contained Fe-rich chlorite, whereas clinozoisite-tremolite formed from units that contained Mg-rich chlorite (see Chapter 3 for possible reactions).

In the contact zones between weakly altered QEV units and regions of massive epidote, or massive tremolite with traces of epidote, the quartz and feldspar crystals (both in the QEV matrix and in QFP clasts) have been partly replaced by clinozoisite, albite, actinolite/tremolite, calcite and phlogopite (Fig. 10.6g). In most cases, this alteration is restricted to fractures and subgrain boundaries within the quartz crystals (Fig. 10.7a,b), but rare quartz crystals have been completely replaced by clinozoisite. The matrix between crystals, and groundmass of QFP clasts, has been variably replaced by chlorite, microcrystalline muscovite and epidote.

Similar textures are evident in the epidote-tremolite-chlorite-rich assemblages from East Thalanga, with zoisite or clinozoisite typically intergrown with tremolite and albite, and minor chlorite and calcite. Chalcopyrite and sphalerite are present along fractures in quartz and clinozoisite, in inclusions in tremolite and in inclusions in altered feldspar crystals. At the margin of some QFP clasts (particularly where in contact with pyrite-chalcopyrite-phlogopite veins), Ba-rich margarite (indicated by microprobe) is intergrown with

Figure 10.7 Composition and textures of altered quartz-feldspar-porphyry (QFP).

(a) Photomicrograph of partly clinozoisite-altered quartz phenocryst from QFP clast within the QEV. Clinozoisite and fibrous tremolite occur along subgrain boundaries within the quartz phenocryst and sphene and minor calcite have enclosed an anhedral zoisite grain within the quartz-muscovite-rich groundmass. Sample W2031ND07-61.6, West Thalanga. Plane light.

(b) Same as (a) under crossed nicols.

(c) Irregular to spherical domains of biotite within the chloritic groundmass of the stratigraphically lowest QFP sill in East Thalanga. Sample E3212SI18-46.

(d) Epidote-rich groundmass of the stratigraphically uppermost QFP sill in East Thalanga. Sample TH274-261.3.

(e) Pervasive silicification of QFP (30 cm sized clast located within, and near stratigraphic top of massive sulphide lens) in Central Thalanga. Sample CT-91-18. C860 Stope: 20 232 mN, 20 422 mE.

(f) Diffuse contact between typical dark grey, biotite-quartz-rich QFP and light grey, muscovite-rich QFP. In the muscovite-rich zone, the feldspar pseudomorphs are composed of biotite, fine grained muscovite, quartz, whereas in the biotite-rich zone, the feldspar pseudomorphs are composed of albite and quartz. Sample TH205-71, Central Thalanga.

(g) Albite-quartz altered feldspar phenocryst, with minor phlogopite. The groundmass contains abundant phlogopite and minor epidote. Sample TH205-71, Central Thalanga. Plane light.

(h) Same as (g) under crossed nicols.

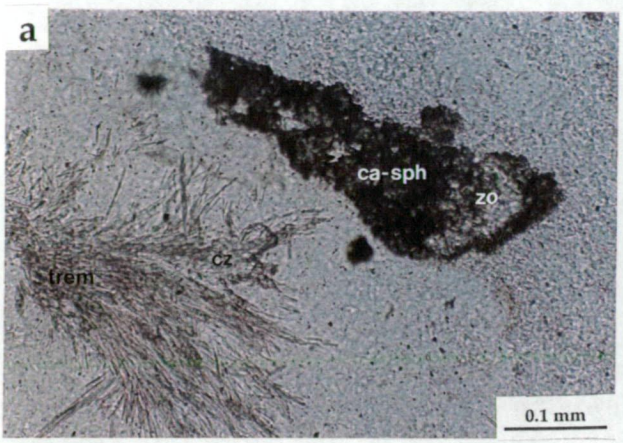
a
ca-sph
zo
cz
trem
0.1 mm

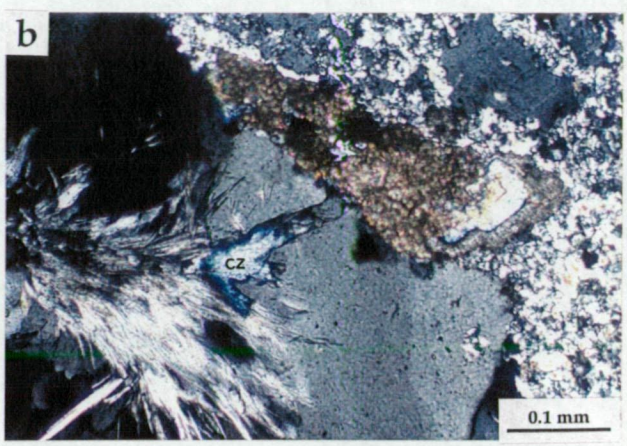
b
cz
0.1 mm

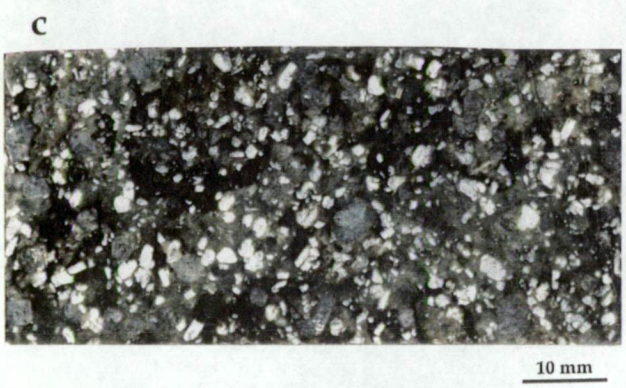
c
10 mm


d
10 mm


e
20 mm


f
20 mm

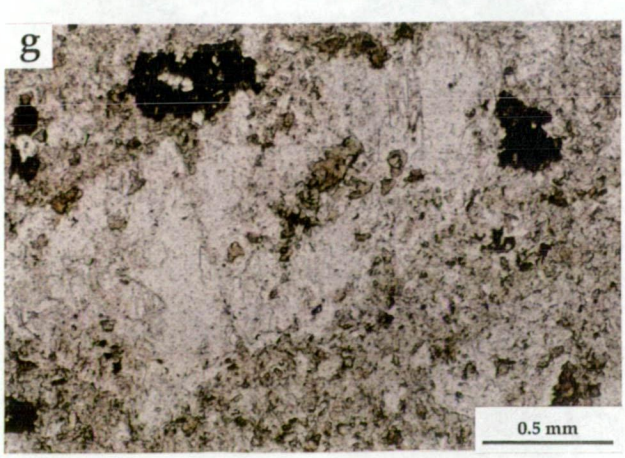
g
0.5 mm

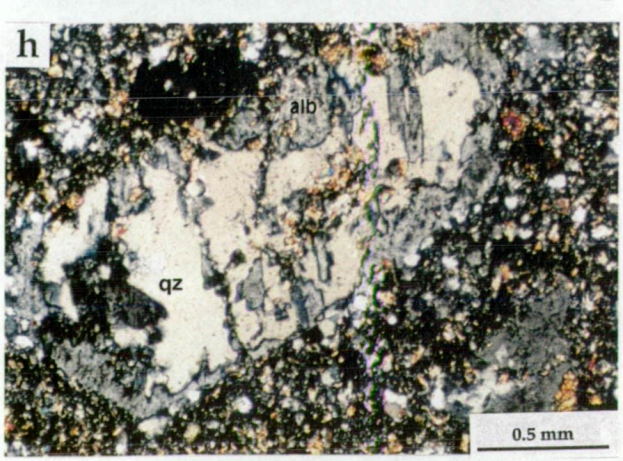
h
alb
qz
0.5 mm

plagioclase and has rimmed quartz crystals. The margarite has been partly replaced, along cleavage planes and grain boundaries, by chalcopyrite.

10.3.2 Alteration of the QFP

The stratigraphically lowest QFP sill in East Thalanga (Fig. 6.10) is moderately chloritic, with chlorite-biotite spots to disseminated chlorite present in the groundmass (Fig. 10.7c). Diffuse chlorite-quartz veins also cross cut the QFP in places. This differs from the overlying QFP units (located between the footwall and hangingwall ore lenses) that are typically siliceous, contain few to moderately abundant epidote-quartz veins and have irregular zones of albitised feldspars that are pink in hand specimen (Fig. 10.7d). Although single QFP clasts within the massive sulphide lenses are typically strongly silicified (Fig. 10.7e), the QFP mega-clasts in Central Thalanga have a groundmass almost completely replaced by fine grained muscovite (Fig. 10.7f). Feldspar phenocrysts in the QFP mega-clasts are now composed of phlogopite, or quartz and fine grained muscovite (Fig. 10.7g,h).

10.3.3 Carbonate- and Chlorite-rich (CTC) Units

Most of the sulphide lenses in West Thalanga are hosted by CTC assemblages (Chapter 6), yet similar carbonate- and chlorite-rich units are not present in East Thalanga. Calcite, dolomite, chlorite and tremolite are the main components of the CTC units at Thalanga, and the main types of CTC units are:

(i) carbonate-chlorite-tremolite assemblage: 5-50% calcite and dolomite, intergrown with chlorite and variable amounts of tremolite;

(ii) chlorite-tremolite assemblage: khaki to dark green chlorite with tremolite crystals (≤3 cm in length). Tremolite crystals are radial, or subparallel to the cleavage, and there is <5% carbonate; and

(iii) chlorite schist: foliated chlorite, dark green to black in hand specimen, contains minor muscovite, phlogopite and sphene and rare tremolite crystals.

Most CTC units are confined to the ore-horizon and are extensive in the West Thalanga lens, with minor occurrences in the western parts of Central Thalanga. Massive chlorite (chlorite schist) is common in West Thalanga, particularly underlying the thickest parts of the ore horizon (Fig. 10.1a-c). Carbonate-chlorite-tremolite and chlorite-tremolite assemblages occur within the ore-horizon, between the chlorite schist and the overlying QEV (Fig. 10.1a,b). The irregular to gradational contact between the carbonate-chlorite-tremolite and chlorite-tremolite assemblages is marked by the change in carbonate abundance, and carbonate-rich regions are more prevalent in the cores of chlorite-tremolite dominated assemblages (Herrmann, 1994).

Lenses and veins of polymetallic massive sulphides occur in the carbonate-chlorite-tremolite and chlorite-tremolite units, whereas pyrite ± chalcopyrite veins and disseminations are typically associated with chlorite schist (Chapter 6). The massive sulphides are up to 30 m thick adjacent to the major normal fault between West and Central Thalanga. Along strike from this position, the sulphides become thinner and more vein-like, and the carbonate-chlorite and chlorite-tremolite units predominate (Fig. 10.1b). Herrmann (1994) reported that CTC units do not extend more than 150 m beyond ore.

East Thalanga and the Vomacka Zone contain very little carbonate, with calcite present as a minor gangue phase in the footwall lens and the mineralised upper rhyolite breccia. Chlorite schist occurs at the contact between the quartz-muscovite ± pyrite altered rhyolitic volcanics and the intensely silicified rhyolite (silicification 1), and rarely at the stratigraphic top of the footwall (Fig. 6.10). Tremolite is a gangue mineral within the hangingwall ore lens in East Thalanga and parts of the ore lens in the Vomacka Zone. The petrology, textures and origins of the CTC units, as well as the paucity of CTC units in East Thalanga, compared with their abundance in the ore horizon of West Thalanga, are discussed in Chapter 11.

10.4 Hangingwall Alteration

10.4.1 Alteration of the HWF

Despite the abundant fine grained muscovite in the siltstone and sandy siltstone facies and matrix of rhyolite breccia units within the HWF, feldspar crystals are typically only weakly altered to muscovite. Most feldspars are now albite. Irregularly distributed domains of biotite-rich quartz-feldspar sandstone facies in the HWF, present in both West and East Thalanga, also contain minor anhedral barite. Although the biotite is inferred to be metamorphic in origin (Chapter 3), the barite may be related to waning hydrothermal alteration.

Irregular domains of intergrown fine grained phlogopite and muscovite, with feathered ends and abundant quartz and feldspar crystals, are interpreted to be altered pumice clasts (Chapter 4). These clasts are flattened parallel to cleavage and are therefore interpreted to have been altered prior to regional deformation. Silicified rhyolite clasts present within breccia facies of the HWF are inferred to have been altered prior to deposition as evidence of silicification does not extend beyond the clast margin. However, rare subvertical bands (<5 cm in thickness) of quartz, with diffuse margins have overprinted the sandstone facies of the HWF.

10.4.2 Alteration in the Dacite and Dacite Breccia Units

Quartz-Epidote Assemblages

Distinctive fracture-controlled to irregular patches of intergrown quartz-epidote are common within the dacite and andesite stratigraphically overlying the ore horizon at Thalanga (Fig. 10.8a-c). Locally, quartz-albite-chlorite, with variable epidote alteration may overprint the dacite (Fig. 10.8d). Only rare veins and diffuse patches of quartz-epidote are present in otherwise weakly altered feldspar-quartz-phyric rhyolite in the footwall. Typically, the quartz-epidote veins are <1 cm in thickness (Fig. 10.8a) and also contain minor chlorite, variable amounts of sulphides (chalcopyrite, sphalerite and galena in particular) and have chlorite ± actinolite ± epidote selvages. Strongly silicified alteration haloes around the veins also contain traces of hematite (pink colour in hand specimen) and, in places, disseminated epidote (Fig. 10.8b). Thin selvages of epidote also rim rare spherical inclusions (up to15 cm in diameter) of pink, sugary calcite (Fig. 10.8e), and veins of epidote-chlorite cross cut local dacite breccia with a pink calcite matrix (Fig. 10.8f). Rare pyrite veins (<2 mm thick) within the dacite have chloritic selvages and epidote-rich haloes.

Quartz-epidote assemblages are more common in the dacite units overlying the western half of Central Thalanga and parts of West Thalanga, than in East Thalanga or the Vomacka Zone. This may be partly due to the abundance of ENE-trending normal faults (D_3) in Central Thalanga, or possibly due to the presence of a larger area of exposure in the decline and the larger number of drill holes collared from within the dacite in Central and West Thalanga compared with East Thalanga. Alternatively, quartz-epidote assemblages within dacite may be more prevalent in Central Thalanga because locally the dacite directly overlies massive sulphide lenses, compared to East Thalanga, where 5-18 m of HWF is present between the sulphides and overlying dacite. Where dacite directly overlies the sulphide lenses it is strongly bleached and silicified, with veins of quartz-epidote and minor chlorite. This style of alteration is irregularly distributed, but is more abundant where associated with piercement veins and remobilised sulphides (Fig. 3.17f and Fig. 3.18a).

Stolz (1991) suggested that the quartz-epidote assemblage with the dacite at Thalanga may be hangingwall alteration associated with the continuation of hydrothermal alteration after sulphide mineralisation. Indeed, the presence of folded quartz-epidote veins, with axial planes parallel to S_2, and the random orientation of the quartz-epidote veins (Chapter 3) indicates that they (or their pre-metamorphic equivalents) formed prior to deformation. However, irregular zones of quartz-epidote are abundant (although not ubiquitous) adjacent to zones of faulting and sulphide remobilisation, suggesting that quartz-epidote assemblages may also have formed during deformation. Epidote is also disseminated in the groundmass of microdiorite dykes inferred to post-date regional deformation. These inconsistent timings of

Figure 10.8 Alteration within the dacite and dacite breccia.

(a) Epidote-quartz vein, containing traces of pyrite and chalcopyrite and without an alteration halo in the dacite, dips moderately west and is cross cut by ENE-trending normal fault to the east of this location.
Central Thalanga: 955 mRL, 20 210 mN, 20 600 mE.

(b) Two generations of epidote-rich veins in dacite; (1) epidote-quartz-chlorite vein, with minor pyrite and pink alteration halo in dacite, and (2) cross cutting epidote vein with traces of pyrite and minor pink alteration halo. Central Thalanga: 955 mRL, 20 210 mN, 20 432 mE.

(c) Irregular-shaped epidote-rich domain, with minor chlorite and patchy quartz. Traces of pyrite are also present. Central Thalanga: 955 mRL, 20 210 mE, 20 525 mE.

(d) Albite-chlorite-rich assemblage that has overprinted coherent dacite. Sample 2011NI12-23.8, West Thalanga.

(e) Spheroidal, calcite and quartz-filled inclusion in dacite, with rim of epidote-quartz-rich dacite. Pink, sugary calcite fills most of the inclusion, with anhedral quartz, and void-fill white to clear calcite filling the remainder. Sample 955-21, Central Thalanga.

(f) Pink, sugary calcite matrix to dacite breccia (partly jigsaw fit texture) is cross cut by chlorite-epidote veins that have an epidote alteration halo. Sample W2033NI15-44.3, West Thalanga.

(g) Zones of silicification in dacite: Top: patchy silicification of matrix between dacite clasts (jigsaw-fit texture) in monomict breccia at contact between coherent dacite and underlying HWF. Sample C2069ND40-27, Central Thalanga. Bottom: strongly silicified dacite in halo about vein of remobilised chalcopyrite and minor sphalerite. Sample C2037NH00-6.7, Central Thalanga.

(h) Photomicrograph of patchy chlorite alteration within perlitic dacite clasts which has resulted in pseudoclastic texture. Sample TH239-136, Central Thalanga. Plane light.

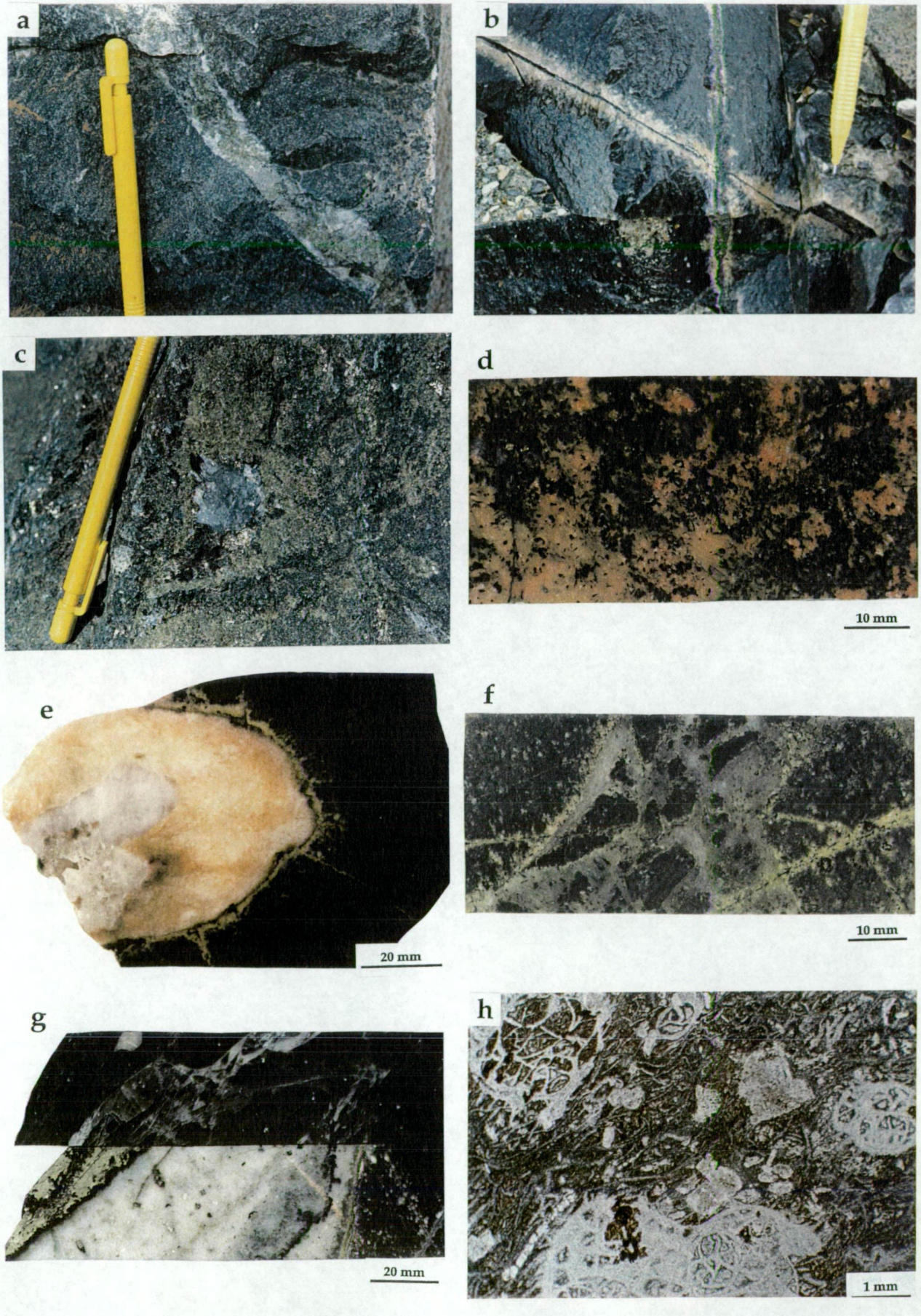
a
b
c
d
10 mm
e
20 mm
f
10 mm
g
20 mm
h
1 mm

quartz-epidote alteration may reflect multiple generations of formation. It is therefore interpreted that fracture-controlled and pervasive chlorite-calcite-quartz alteration of dacite occurred during the waning stages of hydrothermal alteration and was subsequently metamorphosed to quartz-epidote-rich assemblages. Local remobilisation during metamorphism may have concentrated the quartz-epidote adjacent to major structures.

Silicification

Localised silicification of the dacite breccia facies has produced pseudoclastic textures, comprising irregular to rounded 'clasts' of quartz (<5 cm in diameter) with diffuse margins. These patches of silicification overprint both dacite clasts and matrix (Fig. 10.8g, top). Quartz-filled amygdales within the dacite are further evidence of the local silicification of dacite units at Thalanga. Patchy to pervasive silicification (no epidote) has locally overprinted the dacite where it is cross-cut by piercement veins (Fig. 10.8g, bottom) directly overlies massive sulphide lenses.

Chlorite Alteration

Chlorite alteration within the dacite and dacitic breccia units varies from vein-style, disseminated and blotchy chlorite alteration in the coherent facies, to chlorite blotches in the volcaniclastic facies. Chlorite spots overprint the metamorphic biotite that is present along perlitic fractures in the dacite, and locally this has resulted in a pseudoclastic texture (Fig. 10.8h). Chlorite blotches and spots are more abundant in volcaniclastic facies in the hangingwall units and may be temporally related to similar chlorite spots in the HWF (which are interpreted to be retrogressive after cordierite; Chapter 3).

10.5 Alteration Geochemistry

10.5.1 Footwall Alteration

Whole-rock geochemical analyses were determined for 96 samples of the footwall rhyolitic volcanics and the results are listed in Appendix F. These analyses were subdivided on the basis of textural and mineralogical composition, stratigraphic location and SiO_2 content into 8 groups (Fig. 10.9; Table 10.1).

The samples determined to be the least altered from Thalanga, on the basis of the presence of weakly altered feldspar and low amounts of muscovite, chlorite and pyrite, clearly fall in a wide scatter about the group 9 rhyolites used by Herrmann (1994) as the least altered rhyolites for mass balance calculations (Fig. 10.9a-e). Rhyolite units (mostly sandstone and

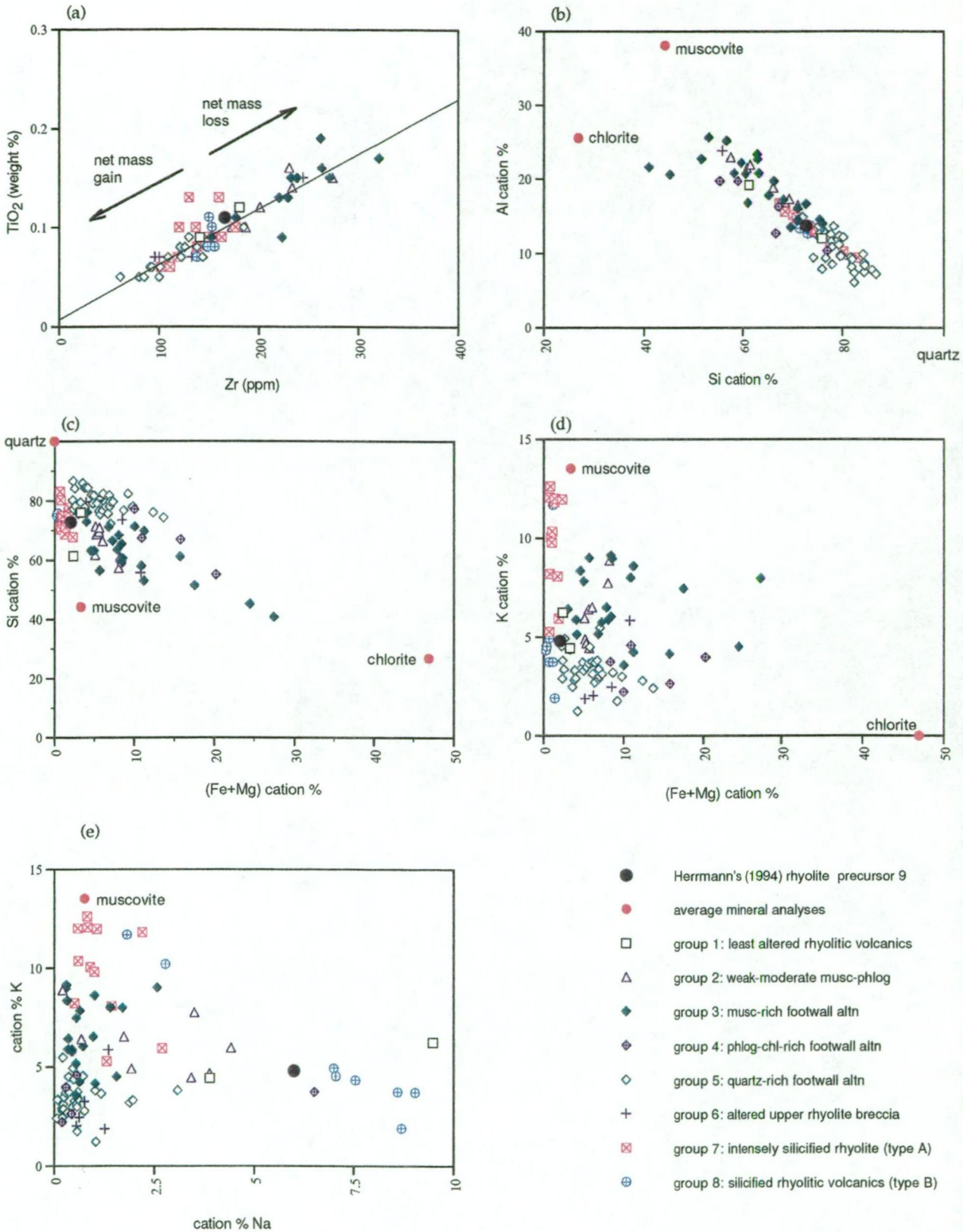

Figure 10.9 Geochemical variations between differing types of footwall alteration in the rhyolitic volcanics (Mount Windsor Volcanics) at Thalanga. (a) TiO_2 versus Zr. The line of best fit is y = 0.001x + 0.007. (b) Al versus Si, showing average compositions of chlorite and muscovite in the footwall (determined by microprobe). (c) Si versus (Fe+Mg). (d) K versus (Fe+Mg). (e) K versus Na. Abbreviations: altn = alteration, musc = muscovite, py = pyrite, phlog = phlogopite, qz = quartz.

breccia units) containing minor to moderate muscovite or phlogopite away from sulphide mineralisation were also collected into a separate group (group 2), and analyses of quartz-muscovite ± phlogopite ± chlorite ± pyrite-rich assemblages within the footwall rhyolitic volcanics (quartz-sericite ± chlorite ± pyrite alteration prior to metamorphism) were subdivided into three groups comprising samples containing abundant muscovite, phlogopite-chlorite and quartz (groups 3-5; Table 10.1). The samples of siliceous quartz-muscovite-pyrite assemblages possibly correlate to group 4 of Herrmann (1994) (Table 10.1). Analyses of clasts from the altered, upper rhyolite breccia in East Thalanga also constitute a single group (group 6; Table 10.1). Analyses of the intensely silicified (type A) rhyolite in East Thalanga were separated from analyses of type B silicified rhyolitic volcanics in West Thalanga (Table 10.1).

Table 10.1 Comparison between the classification scheme used in Figure 10.9 and that used for the rhyolites at Thalanga by Herrmann (1994).

Group	This classification	Group	Herrmann's classification
1	Least altered rhyolite: qz-fspr-phyric, medium-dark grey siliceous groundmass, weakly altered fspr phenocrysts, Na_2O <2 weight %, <1 % pyrite	1 6	Least-weakly altered rhyolite: weakly altered fspr phenocrysts, <1 % pyrite, Dark grey, siliceous qz-fspr-phyric rhyolite
2	Weak-moderately altered rhyolite: rhyolitic sandstone-breccia unit (qz & fspr crystals), variable muscovite & phlogopite, pseudofiamme textures weak-moderately altered fspr crystals, <1 % pyrite	7	Weak-moderately altered (chl-ser) rhyolite in hangingwall setting: low pyrite, wispy pseudofiamme fabrics
3-6	Typical qz-musc-chl-py assemblage: 3. muscovite-rich 4. phlogopite-chlorite-rich 5. quartz-rich 6. upper rhyolite breccia (qz-chl-phlog-musc-rich)	4 ?	Intensely altered (qz-ser-chl-py) rhyolitic volcanics: with pyrite stringers, <4 % pyrite
7	Intensely silicified rhyolite (type A): grey to white in hand specimen, qz-phyric, trace-minor muscovite rare pyrite stringers	5	Siliceous rhyolite in footwall setting: low Na, high K, low pyrite
8	Silicified rhyolitic volcanics (type B): grey to pink in hand specimen, typically rhyolitic sandstone-breccia (qz & fspr crystals), trace pyrite, trace muscovite	6	Siliceous qz-fspr-phyric rhyolite in hangingwall setting: variable Na & K, low pyrite

Abbreviations: chl = chlorite, fspr = feldspar, musc = muscovite, phlog = phlogopite, qz = quartz, ser = sericite

Barrett and MacLean (1991) demonstrated that variations along the line of best fit on a TiO_2 versus Zr diagram are due to mass increases or decreases during alteration. The muscovite- and chlorite-rich rhyolitic volcanics at Thalanga have higher TiO_2 and Zr contents compared with the precursor 9 (Fig. 10.9a), which indicates concentration of these elements due to mass loss during sericitisation and chloritisation (cf. Barrett and MacLean, 1991). Conversely,

samples with lower TiO_2 and Zr than the precursor 9 (Fig. 10.9a), have been diluted by mass gain during silicification. This is consistent with the results of Herrmann (1994), who demonstrated (using the methods of MacLean and Barrett, 1993) that most rhyolitic volcanics in the footwall at Thalanga have had significant addition of Si, Fe and S, and loss of Na. The upper rhyolite breccia (group 6) plots on both sides of the precursor 9 on the TiO_2-Zr diagram (Fig. 10.9a), which is consistent with the variable quartz-muscovite-chlorite ± phlogopite assemblages recognised in hand specimen.

Diagrams incorporating element concentration data expressed as cation % provide a useful method of comparing the whole rock composition of various alteration types with the composition of particular minerals in the alteration assemblage (e.g. Barrett and MacLean, 1991). The degree of Si loss or gain can be illustrated on a plot of Al (shown to be immobile at Thalanga by Herrmann, 1994) versus Si (Fig. 10.9b). The most siliceous quartz-muscovite ± pyrite-rich samples (group 5) have gained Si compared with the precursor 9, whereas the most muscovite- and chlorite-rich footwall rhyolitic volcanics (groups 3 and 4) have lost Si and trend towards the muscovite and chlorite compositions (Fig. 10.9b). Muscovite- and chlorite-rich samples of the quartz-muscovite ± pyrite assemblage also fall on separate parts of a plot of Si versus Fe + Mg compared to more siliceous quartz-muscovite ± pyrite samples, but all samples occur within the triangle defined by the quartz, chlorite and muscovite compositions (Fig. 10.9c).

The K versus (Fe+Mg) diagram (Fig. 10.9d) shows that rhyolites with type A silicification contain more K and trend towards the muscovite composition, compared with the type B silicified rhyolitic volcanics. The type A silicification also contains more K than the quartz-muscovite ± pyrite assemblages (groups 3-6). The clustering of most of the type B silicified rhyolitic volcanics around the precursor 9 position on the cation % diagrams (Fig. 10.9b-d) indicates that these samples are only weakly altered. This interpretation is also confirmed using a K versus Na diagram (Fig. 10.9e), on which most type B silicified rhyolitic volcanics contain similar Na to the precursor 9 samples of Herrmann (1994). On these cation % diagrams (Fig. 10.9b-c) the type A silicification has very similar Si, Ti and Zr contents to the precursor 9 composition, yet Herrmann (1994) showed that intensely silicified (type A) rhyolitic volcanics at Thalanga could be derived from a rhyolitic precursor by the addition of 35-50 g of Si per 100g of rock. Perhaps selection of a different precursor composition (e.g. group 1) would illustrate the difference in Si content. Herrmann (1994) also calculated that type A silicified rhyolitic volcanics could be derived from a rhyolitic precursor by the addition of 4-5 g of K per 100g of rock and major Na depletion, and this is supported by the position of samples of type A silicification with respect to the precursor 9 on Figures 10.9(d,e).

10.5.2 Calc-silicate Assemblages

Epidote-actinolite/tremolite-rich QEV units fall between the rhyolitic volcanics and QFP, similar to the position of weakly altered QEV, on a TiO_2-Zr diagram (Fig. 10.10). Massive epidote-actinolite also has a similar distribution on the TiO_2-Zr diagram (Fig. 10.10), and this supports the textural interpretation (section 10.3.1) that domains of epidote-actinolite (or tremolite) are pervasively altered and metamorphosed QEV units. Because the whole-rock geochemical compositions of QEV units are so variable (due to original mineralogical heterogeneities; Chapter 4), mass changes associated with formation of epidote-rich assemblages within QEV units were not calculated.

Herrmann (1994) found that the CTC units at Thalanga have similar immobile element ratios to the footwall rhyolitic volcanics and therefore inferred that the CTC units formed either by hydrothermal alteration of a rhyolitic precursor, or by addition of a rhyolitic detrital component to a calc-silicate exhalative deposit. In order to compare with Herrmann's (1994) results, the 20 310 mE cross section in West Thalanga was sampled at evenly-spaced intervals (1 to 3 m between 0.3-1.0 m length drill core samples) and whole-rock geochemical analyses were determined for the CTC units, partly mineralised CTC units and the host volcanic units. The relationships between Ti/Zr and geology (Fig. 10.11a-d) are:

(i) dacite has Ti/Zr ~ 12-15, the QEV has Ti/Zr ~ 5-8 and the rhyolitic volcanics have Ti/Zr ~ 2-3;

(ii) the Ti/Zr of the chlorite schist is similar to that of the underlying rhyolitic volcanics (Fig. 10.11a,c,d);

(iii) the carbonate-chlorite-tremolite and chlorite-tremolite units have Ti/Zr less than the footwall in places (Fig. 10.11a), but these samples have low Ti and Zr concentrations (Ti and Zr <70 ppm, detection limit = 10 ppm), which means there is some uncertainty in the Ti/Zr values. In other drill holes, the carbonate-chlorite-tremolite and chlorite-tremolite units also have Ti/Zr values comparable to those of the overlying QEV (Fig. 10.11c,d); and

(iv) the epidote-actinolite ± chlorite-rich domains and the QEV both have Ti/Zr > 5 (Fig. 10.11b,d).

These relationships suggest that the CTC assemblages may have overprinted the stratigraphic top of the rhyolitic volcanics and also partly replaced the QEV. Replacement of the QEV implies that formation of the massive sulphides (which replace the CTC units; Chapters 6 and 11) must post-date QEV deposition.

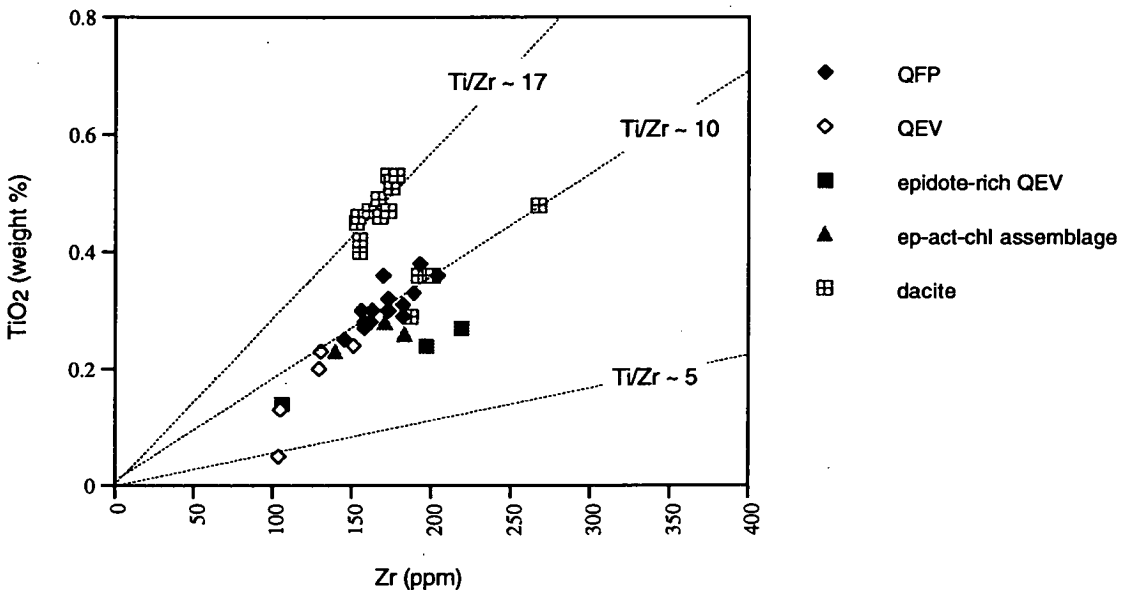

Figure 10.10 Comparison of TiO_2 and Zr values of QEV, QFP, and dacite with altered QEV and epidote-actinolite assemblages. Lines depict the Ti/Zr values for the rhyolitic volcanics (Ti/Zr < 5), dacite 1 and the QFP (Ti/Zr ~ 10), and dacite 2 (Ti/Zr ~ 17; see Chapter 5).

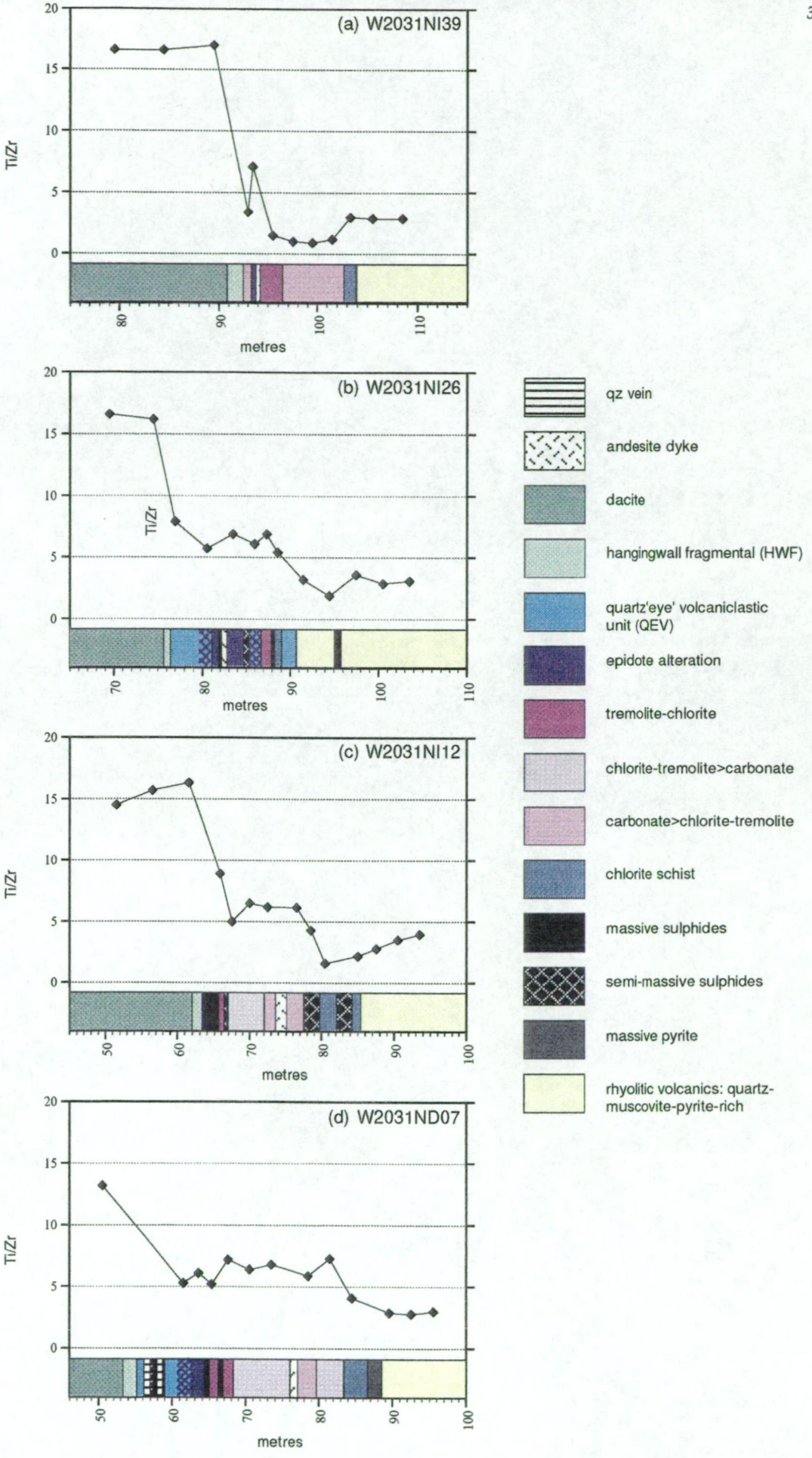

Figure 10.11 Comparison between Ti/Zr values of the volcanic units at Thalanga and the carbonate-chlorite-tremolite (CTC) assemblages within the ore horizon. Hatched pattern in QEV indicates that it contains patchy epidote-actinolite-rich assemblages.

10.5.3 Oxygen Isotopes in the Footwall

Green *et al.* (1983) demonstrated that whole rock O isotope ratios of the rocks underlying the Fukazawa massive sulphide deposit, in Japan, decrease towards the ore body. This distribution was interpreted to be the result of hydrothermal alteration (by seawater) at different temperatures, with the lowest $\delta^{18}O$ values in the zone directly underlying the massive sulphides corresponding to the zone of highest temperature hydrothermal alteration (Green *et al.*, 1983). This zonation in whole rock $\delta^{18}O$ values has been identified at ancient massive sulphide deposits, where it is also interpreted to indicate a temperature gradient (e.g. Amulet, Quebec; Beaty and Taylor, 1982; Mattagami, Quebec; Costa *et al.*, 1983; Corbet, Quebec; Hoy, 1993; and Kidd Creek, Ontario; Huston *et al.*, 1995c).

Whole rock oxygen isotopes were determined at the University of Tasmania on samples of variably altered rhyolitic volcanics collected by M. Jones and S. Halley, and the results have been presented in Miller (1996). The $\delta^{18}O_{whole\ rock}$ values of the rhyolitic volcanics range from 7.4 ‰ (underlying Central Thalanga) to 12.9 ‰ (east of East Thalanga, where massive sulphides are not present), with mean about 9 ‰ (Miller, 1996). Rhyolitic volcanics with $\delta^{18}O_{whole\ rock} < 9$ ‰ underlie the East Thalanga ore lenses and most parts of the massive sulphides in West and Central Thalanga, and zones with $\delta^{18}O_{whole\ rock} > 10$ ‰ are more common at the margins of the massive sulphides (Miller, 1996). However, the maximum relative temperatures of formation (about 170°C to 330°C) calculated by S. Halley, assuming $\delta^{18}O$ = 2-4 ‰ for the hydrothermal fluid, coincide with the massive sulphide lenses in East and Central Thalanga and may indicate the location of the main high temperature feeder zones in the footwall (see Miller, 1996). The recently discovered Orient ore lens, and the weak mineralisation in diamond drill hole TH45 west of West Thalanga, also coincide with zones of high calculated temperatures (see Miller, 1996).

10.6 Discussion

10.6.1 Pattern of Footwall-Style Alteration at Thalanga

The footwall at Thalanga is composed of both rhyolite breccia units and coherent perlitic rhyolite (Chapter 4) which would have been highly porous and permeable during alteration. The broad zone of quartz-muscovite ± chlorite ± pyrite-rich footwall rhyolitic volcanics at Thalanga is consistent with formation during hydrothermal alteration by diffuse flow of hydrothermal solutions through porous volcanic rocks (cf. Morton and Franklin, 1987; Large, 1992).

The only mineralogical zonation within the footwall at Thalanga occurs as subvertical zones that are oriented at a low angle to the ore horizon. Contacts between the footwall alteration types vary from gradational and irregular, to sharp and planar. Diffuse, gradational contacts may be more common where contacts between alteration types occur within a specific rhyolitic facies, whereas sharp alteration contacts may reflect variations in the precursor volcanic composition or facies textures. The occurrence of pyrite stringers and regions of quartz-muscovite-pyrite-rich rhyolite within sharply-bounded, subvertical zones that are subparallel to the ore horizon suggests that these may be present within volcaniclastic facies between coherent rhyolite domes or lavas. Alternatively, the orientation of the pyrite stringer zones may be controlled by a pre-existing fault that was rotated into its present position during D_2 deformation. Given that the location of the pyrite stringer zones can be related to the location of thick massive sulphide lenses (section 10.2.1), but not to the distribution of the thickest volcaniclastic and sedimentary units within the ore horizon (Chapter 3), then any structure that the pyrite stringer zones were formed along cannot have been a syn-volcanic growth fault.

Multiple stages of footwall alteration may be common in hydrothermal alteration systems and have been identified, on the basis of vein paragenesis, in several less metamorphosed VHMS deposits (e.g. Que River, Offler and Whitford, 1992; Hellyer, Gemmell and Large, 1992). At least two-stage alteration is suggested by some pseudoclastic textures within the footwall at Thalanga. However, except for remobilised chalcopyrite-rich veins, the quartz-muscovite-rich pyrite stringer zones are typically not overprinted by alteration. Rare pyrite-barite veins that overprint the pyrite veins are interpreted to have formed during the latest-stages of alteration and sulphide deposition.

The interpreted pre-deformation and metamorphism location of zones of typical footwall-style alteration, with respect to the massive sulphide lenses, in West and East Thalanga is summarised in Figure 10.12(a,b). The restriction of quartz-sericite ± chlorite alteration and pyrite stringer zones to the footwall rhyolitic volcanics, and small parts of the overlying QEV units, is consistent with alteration produced during formation of the massive sulphides on or near the seafloor prior to deposition of the HWF and dacite. Domains of phlogopite and Mg-rich chlorite within the footwall and ore horizon at Thalanga, are interpreted to be the products of metamorphism and retrogression of Mg-rich hydrothermal alteration assemblages. Mg-enrichment is common in the rocks that stratigraphically underlie massive sulphide deposits and is interpreted to indicate reaction between seawater and the footwall rocks during hydrothermal activity (e.g. Izawa *et al.*, 1978; Janecky and Seyfried, 1984; Schmidt, 1988). Therefore at Thalanga, mixing between ascending hydrothermal solutions and cold, Cambro-Ordovician seawater circulating in the porous facies of the footwall rhyolitic volcanics is likely to have resulted in Mg-rich alteration minerals (see also Chapter 11).

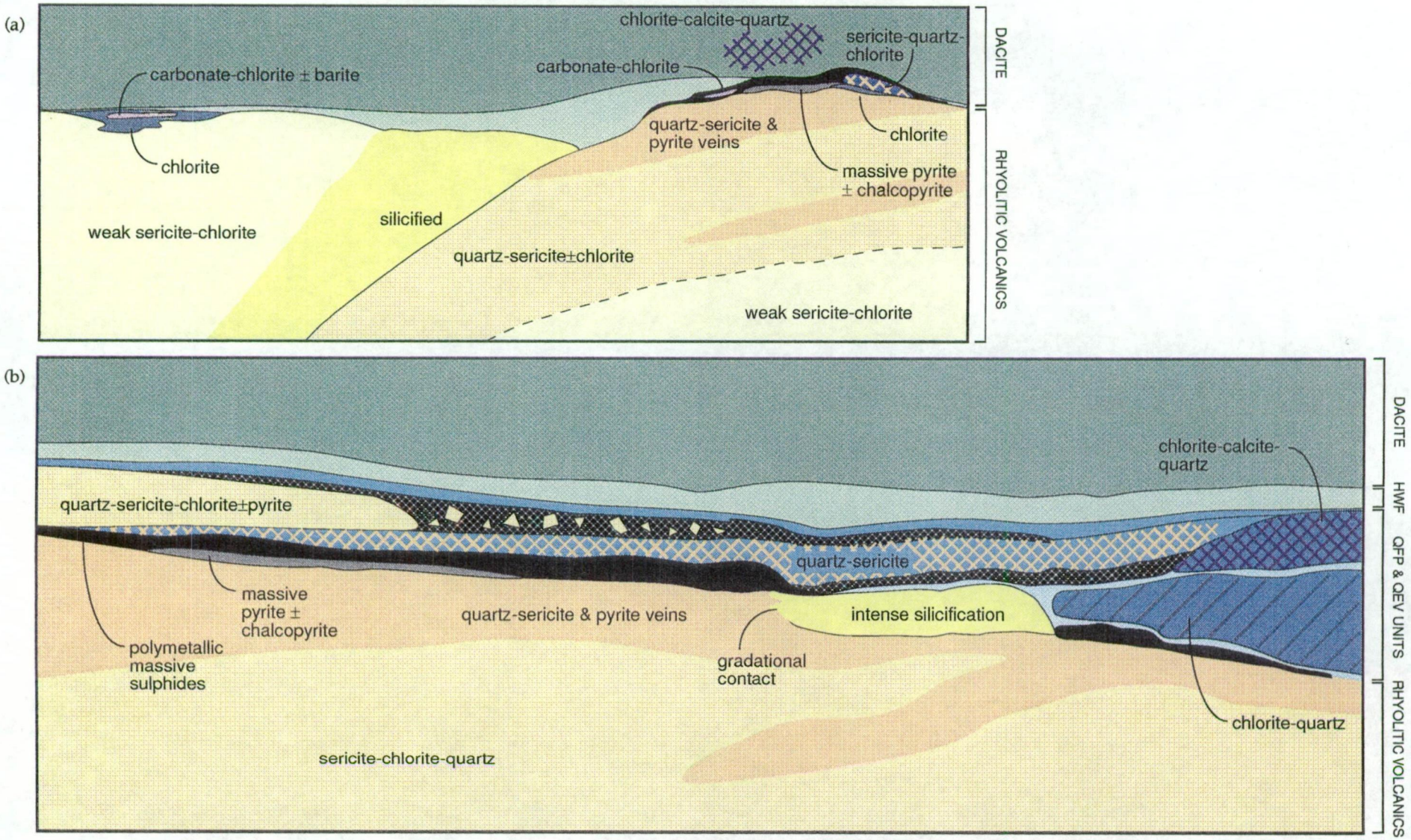

Figure 10.12 Schematic diagram showing the interpreted pre-deformation location of the various pre-metamorphic alteration types in the footwall, quartz 'eye' volcaniclastic unit and quartz-feldspar porphyry in (a) Central Thalanga, based on section 20 390 mE, and (b) East Thalanga, based on section 32 080 mE. See Figure 10.1a for geology legend.

The presence of footwall-style alteration in the QEV units between the footwall and hangingwall ore lenses in East Thalanga is consistent with deposition of the QEV prior to formation of the hangingwall lens. The similar up-dip extent of both the footwall and hangingwall ore lenses, and the area of strong quartz-sericite alteration of the QEV, may have resulted from deposition of the QEV prior to formation of the footwall lens (by replacement of the QEV; Chapter 12).

10.6.2 Origin of Hangingwall Alteration

Epidote-actinolite/tremolite is the main alteration assemblage present in units stratigraphically overlying the massive sulphide lenses at Thalanga. The restriction of these assemblages to units immediately overlying the massive sulphide lenses is consistent with hydrothermal alteration following formation of the massive sulphides and dacite deposition. These skarn-like assemblages may have formed during metamorphism of areas within the QEV units, QFP sills and dacite that were previously chlorite-calcite-quartz altered. Pan and Fleet (1992) reported a similar origin for the calc-silicate assemblages (that included clinopyroxene, garnet, Ca-amphibole, wollastonite, epidote, magnetite and calcite) associated with the Archaean Millroy and Geco VHMS deposits in Ontario, and suggested hydrothermal Ca and Cl enrichment occurred during sulphide deposition.

At younger, less metamorphosed VHMS deposits, alteration minerals present within the rocks that overlie the massive sulphide lenses are generally interpreted to have formed during the waning stages of hydrothermal activity following sulphide deposition. Common hangingwall alteration assemblages include sphalerite and calcite veins (Izawa *et al.*, 1978), clay minerals (smectic, illite, kaolin, montmorillonite), carbonates (dolomite, calcite), chlorite and disseminated hematite (Date *et al.*, 1983; Çagatay and Eastoe, 1995). At the Archaean Scuddles deposit, quartz, sericite, chlorite and carbonate are present in the hangingwall (Ashley *et al.*, 1988). Comparison with these deposits suggests that chlorite (or clay minerals), calcite and quartz are feasible pre-metamorphic alteration phases within the QEV, QFP and dacite at Thalanga.

In West Thalanga, the presence of epidote-actinolite altered QEV directly overlying massive sulphides, and grading upwards to less altered QEV, is consistent with continued hydrothermal alteration (chlorite-calcite-quartz formation) after formation of the massive sulphides and deposition of the QEV. The gradation between epidote-actinolite-rich assemblages, tremolite-chlorite ± epidote-rich assemblages and chlorite-tremolite units down stratigraphy in West Thalanga may be due to metamorphism, rather than a temporal relationship. There is no gradation between altered QEV units and the epidote-rich assemblages within the overlying dacite, and typically the HWF between the QEV and dacite is unaltered. However, local areas of biotite-garnet-epidote-magnetite-rich HWF

(Chapter 3) may occur where the hydrothermal solutions moved through the HWF into the overlying quartz-epidote-rich dacite.

In Central Thalanga, the spatial association between dacite in direct contact with the massive sulphides and abundant quartz-epidote assemblages is consistent with genesis of the quartz-epidote veins as late-stage hangingwall alteration following deposition of sulphides. However, domains of intense epidote alteration present in dacite not directly overlying the massive sulphides in both West and Central Thalanga may be related to chalcopyrite-filled piercement veins that formed during vertical extension of the ore horizon (D_2) or later ENE-trending normal faults that cross cut the ore horizon (D_3).

The lack of CTC assemblages and extensive chlorite schist within and underlying the ore horizon in East Thalanga and the Vomacka Zone may have been an important cause of the lack of epidote-actinolite/tremolite alteration in the hangingwall units in these areas (i.e. no pre-existing carbonate-rich alteration assemblages to dissolve calcite from). Alternatively, the hydrothermal system in East Thalanga and the Vomacka Zone may have shut down rapidly after sulphide formation and therefore did not produce the hangingwall-style alteration, or the hydrothermal solutions may have been diverted along strike, rather than penetrating the hangingwall.

10.7 Summary

1. At Thalanga, the mineralogy, distribution and abundance of metamorphic minerals is interpreted to reflect pre-metamorphic variations in hydrothermal alteration assemblages. Quartz-muscovite-pyrite-rich assemblages at the Thalanga deposit are confined to the rhyolitic volcanics and to parts of the QEV and QFP within the ore horizon, and are interpreted to be metamorphosed quartz-sericite-pyrite hydrothermal alteration associated with sulphide mineralisation. The lack of similar alteration minerals within the stratigraphically overlying HWF and dacite supports the interpretation that the rhyolitic volcanics were the footwall to sulphide mineralisation and that mineralisation occurred, and ceased, prior to deposition of the overlying dacite and HWF.

2. The pre-metamorphic equivalents of the epidote-actinolite-chlorite-rich assemblages within the QEV are interpreted to have been chlorite-calcite-quartz alteration that may have formed during the waning of hydrothermal activity after deposition of the QEV and formation of the massive sulphide lenses.

3. Vein-style to irregular zones of pervasive quartz-epidote within the dacite in West and Central Thalanga and the QFP in East Thalanga are probably related to the formation of

epidote within QEV units. The epidote-rich assemblages may be metamorphosed hangingwall chlorite-calcite-quartz alteration, which is inferred to occurred during the waning stages of hydrothermal alteration. However, quartz-epidote alteration of the dacite is locally associated with deformation and remobilised sulphides.

CHAPTER 11.

TEXTURES AND SIGNIFICANCE OF CARBONATE- AND CHLORITE-RICH ASSEMBLAGES IN THE ORE HORIZON

11.1 Introduction

A suite of carbonate-chlorite-tremolite rocks (CTC assemblages, after Herrmann, 1994) is associated with the sulphides in the West Thalanga ore lens, with chlorite schist at the footwall margin. Both carbonate and chlorite-rich assemblages are associated with several volcanic-hosted massive sulphide (VHMS) deposits in Australia and North America (Table 11.1). There is a wide range in carbonate compositions, and the assemblages have been interpreted as either of exhalative origin (e.g. Large and Both, 1980; McLeod and Stanton, 1984; Ashley *et al.*, 1988), or due to hydrothermal alteration associated with massive sulphide formation (e.g. Gemmell and Large, 1992; Khin Zaw and Large, 1992; Hill and Orth, 1994; Orth and Hill, 1994).

Carbonate is recognised as an important criteria in distinguishing the Mattabi-type from the Noranda-type VHMS deposits of Canada (Morton and Franklin, 1987). Iron-bearing carbonates, dolomite, and calcite are common components of poorly defined alteration pipes of the Mattabi-type deposits. In most cases, the carbonate is considered to be an alteration phase, possibly an early stage of the hydrothermal system (Franklin *et al.*, 1975; Larocque and Hodgson, 1993; Osterberg *et al.*, 1987; Schandl and Wicks, 1993). In some Canadian and Swedish deposits carbonate is an important component of the orebody, and many workers consider the carbonate to be hydrothermal and to have either been deposited before mineralisation, or co-precipitated with the massive sulphides (e.g. Carlon and Bleeker, 1988; Costa *et al.*, 1983; De Groot and Sheppard, 1988; Galley *et al.*, 1993). Alternatively, carbonate may post-date the massive sulphides, and could have been deposited from a cooling hydrothermal fluid (e.g. Khin Zaw, 1991; Khin Zaw and Large, 1992).

Wills (1985) and Gregory *et al.* (1990) interpreted all carbonate-bearing rocks at Thalanga, as well as massive chlorite, actinolite-tremolite units, massive sulphides, epidote-rich units, and silica-magnetite units, to be exhalative deposits. Recently Herrmann (1994) demonstrated that the CTC assemblages have immobile element concentrations and ratios similar to the altered footwall rhyolitic volcanics. He suggested that the CTC assemblages formed by variable Mg, Ca, Si, and CO_2 metasomatism of the rhyolitic volcanics. However, parts of the CTC units have immobile element ratios similar to the stratigraphically overlying QEV units (Chapter 10). The objectives of this study are to categorise the carbonate

overlying QEV units (Chapter 10). The objectives of this study are to categorise the carbonate units at Thalanga and determine the origin of the carbonate, using microscopy, cathodoluminescence, and carbon and oxygen isotopes.

Descriptions of carbonate textures are emphasised in this section because similar textures occur in carbonate units associated with other massive sulphide deposits. At Rosebery, spheroidal carbonate with concentric zonation were interpreted as ooids and the carbonate considered to be a seafloor deposit (Brathwaite, 1974; Dixon, 1980). Recent evidence from the Rosebery deposit (Hill and Orth, 1994; Orth and Hill, 1994) shows that many of the carbonate textures infact formed by primary replacement and open-space filling during sub-seafloor hydrothermal alteration. Similar concentric carbonate textures at Thalanga are documented in this section.

11.2 Petrology of the CTC Units

11.2.1 Types and Distribution

Wills (1985) divided the carbonate and chlorite units into three mains groups, describing them as shaley exhalite, carbonate exhalite, and actinolite exhalite. He also separated the carbonate and chlorite rocks using geochemistry and reported that the shaley exhalites contain moderate SiO_2 (80 weight %) and Mg/Fe + Mg ratios (0.89), whereas the carbonate and actinolite exhalites are low in SiO_2 (6 weight %) and have high Mg/Fe + Mg ratios (0.96). Wills (1985) considered the exhalites to be a single facies, and suggested that the carbonate exhalites may represent proximal exhalites and the quartz magnetite units their distal equivalents.

The carbonate and chlorite rocks were re-examined by Herrmann (1994) and subdivided according to proportions of mineral components. His five assemblages are:
i) carbonate > 50% > tremolite + chlorite,
ii) tremolite + chlorite(variable) + 5-50%carbonate,
iii) tremolite > chlorite + <5%carbonate,
iv) chlorite>tremolite + <5%carbonate, and
v) chlorite schist.

While this subdivision is useful in a detailed geochemical study, it would be unwieldy and repetitious to discuss the textures of each group. For the purposes of this discussion of textures and origins, the groupings of Herrmann (1994) are amalgamated into three main groups; i) carbonate-chlorite-tremolite, ii) chlorite-tremolite, and iii) chlorite schist. The distribution and composition of these groups were outlined in Chapter 10 (Fig. 10.1; section 10.3.3).

11.2.2 Carbonate - Chlorite - Tremolite Assemblage

Petrology

The carbonate-chlorite-tremolite unit is composed of variable proportions of dolomite and calcite in a matrix of chlorite with tremolite. Dolomite rhombs are usually zoned and composed of alternating clear and inclusion-rich bands. Boundaries between dolomite grains are irregular, and the zoned grains are truncated where in contact with the chlorite matrix. Undulose extinction is common in the dolomite grains at Thalanga. Calcite overprints dolomite and tremolite and typically occurs as mosaics of coarse, equant grains that have sharp planar boundaries and triple-point grain junctions. Calcite is slightly dustier and pinker in transmitted light than dolomite, and twinning is common to most calcite grains.

Colourless chlorite, 0.025-0.15 mm in length, with khaki to olive birefringence colours, forms the matrix to the intergrown calcite and dolomite. Chlorite defines the foliation in the carbonate-chlorite rocks, and is coarse grained in pressure shadow regions. Coarse blades of tremolite are poikiloblastic with irregular crystal boundaries, and randomly oriented often as radiating aggregates that post-date cleavage. Tremolite is associated with dolomite rhombs dispersed in the chlorite matrix, and rarely occurs in close-packed dolomite regions.

Interstitial quartz and feldspar are present in some samples, and accessory sphene and apatite grains are confined to the chlorite matrix. The colourless to pale brown sphene porphyroblasts are inclusion-rich and subhedral to rounded with irregular margins (Fig. 11.1a,b), and rare sphene porphyroblasts are rimmed with galena. Apatite occurs as euhedral to subhedral crystals within either bladed tremolite or the chlorite matrix (Fig. 11.1c). Rare apatite crystals are zoned and contain submicroscopic inclusions that are interpreted to be CO_2. Talc has been reported by Wills (1985) and Gregory *et al.* (1990) in the CTC units at Thalanga. However, only traces of talc are dispersed in the CTC units, either as isolated laths intergrown with dolomite and tremolite, or fringing tremolite blades (Fig. 11.1d).

Sulphide veins and disseminations within the carbonate-chlorite units have replaced dolomite and infilled fractures and spaces between dolomite rhombs (Fig. 11.1e,f). Disseminated euhedral pyrite is concentrated in the chlorite matrix, and coarse chlorite or sphalerite occur in pressure shadows around pyrite grains. In carbonate-rich domains, pyrite and other sulphides have overgrown the contact between dolomite and chlorite. Chalcopyrite, sphalerite and galena are interstitial to carbonate, chlorite and tremolite crystals. These sulphides cross-cut and replace dolomite rhombs, infill cleavage partings and fractures in tremolite crystals (Fig. 11.1g,h), and are interstitial to chlorite in pressure shadow regions. In many places chalcopyrite, sphalerite, and galena are intergrown with calcite.

Figure 11.1 Photomicrographs of minerals present in the carbonate-chlorite-tremolite unit at Thalanga.

(a) Irregular sphene porphyroblast, with rutile and chlorite inclusions and rimmed by galena, within the colourless chlorite matrix of a carbonate-chlorite-tremolite unit. Black ring is an ink mark. Sample TH139A-268.3, West Thalanga, plane light.

(b) Same sphene porphyroblast as (a) in crossed nicols. Typically, the chlorite matrix has anomalous grey to khaki birefringence. There is no cleavage within the chlorite domain in this specimen.

(c) Apatite crystals within metamorphic tremolite, minor talc. Sample TH245-499.5, West Thalanga, crossed nicols.

(d) Talc extends radially from the tremolite grain, and is sub-parallel to the cleavage in the chlorite matrix. Sample 2031ND07-69.7, West Thalanga, crossed nicols.

(e) Hand specimen of sulphides that have overprinted a carbonate-chlorite-tremolite assemblage. Spheroidal dolomite is preserved in places (arrow). Sample TH139A-268.3, West Thalanga.

(f) Hand specimen of pyrite-sphalerite vein that cross-cuts massive to rhombic dolomite. Sample TH230-108, Central Thalanga.

(g) Sulphides overprint metamorphic tremolite. The sulphides have probably filled cleavage partings and voids within the poikiloblastic tremolite, rather than replaced tremolite. Sample TH245-494.5, West Thalanga, crossed nicols.

(h) Same tremolite grain as (g) under reflected light. Galena, chalcopyrite, and minor sphalerite commonly cross-cut and infill tremolite, with rare euhedral pyrite intergrown with tremolite.

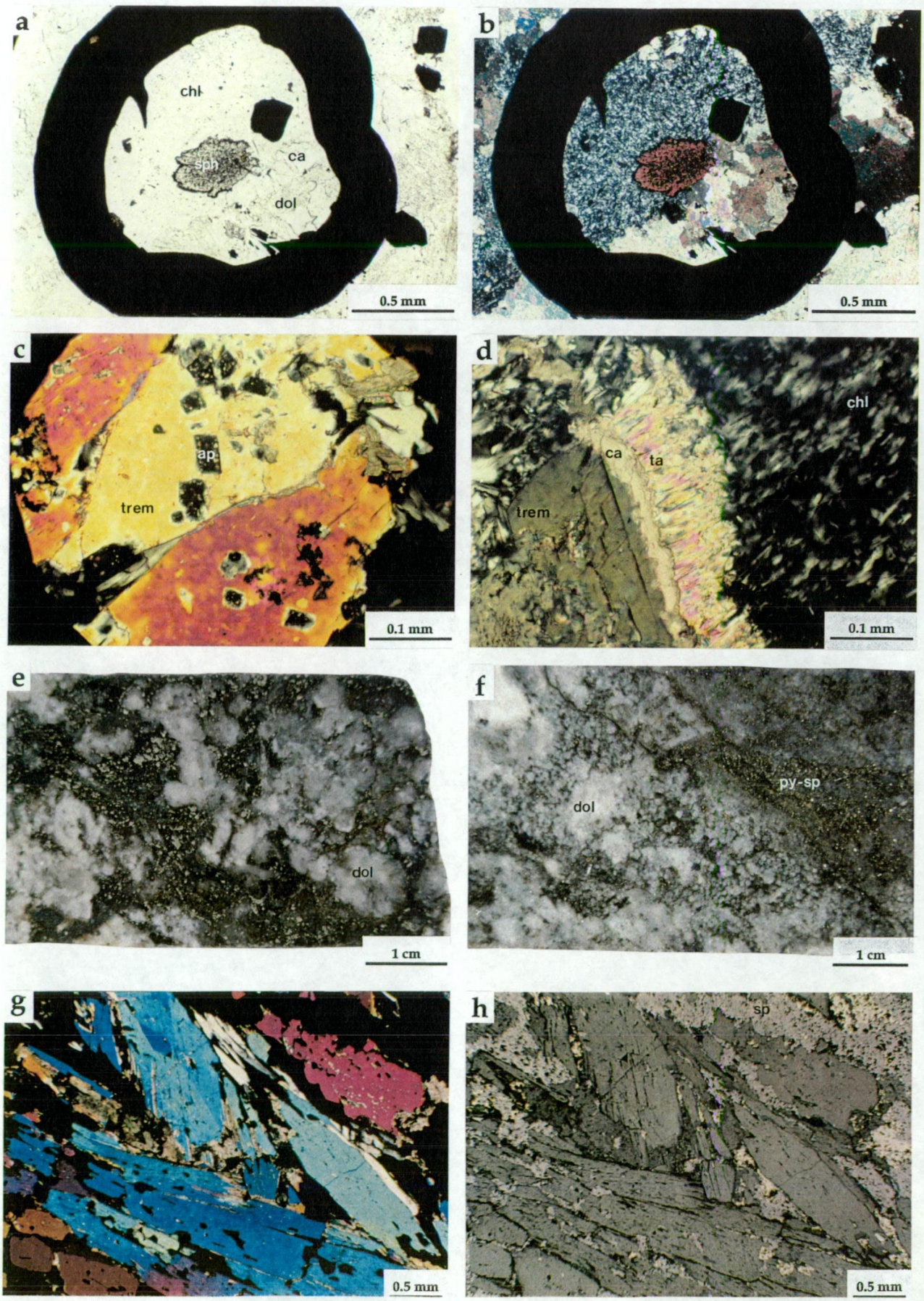
a
chl
sph
ca
dol
0.5 mm
b
0.5 mm
c
ap
trem
0.1 mm
d
chl
ca
ta
trem
0.1 mm
e
dol
1 cm
f
py-sp
dol
1 cm
g
0.5 mm
h
sp
0.5 mm

Irregular veins of coarse-grained, pink to white calcite cross-cut cleavage in the CTC units. Massive or semi-massive sulphides have a brecciated appearance where cross-cut by these irregular calcite veins. Coarse galena, chalcopyrite, and sphalerite are associated with the coarse calcite veins and commonly fill extensional sites within these calcite veins. *En echelon*, shallow-dipping clear to white calcite veins have cross-cut both the sulphides and pink calcite veins.

Carbonate Textures

Despite significant deformation, many examples of primary carbonate textures are preserved within discrete carbonate pods within the ore horizon. The carbonate pods (up to 5m wide) are bounded by either chlorite schist or massive sulphides. Strain is interpreted to have been partitioned into these contact zones; thus the pre-deformation textures of the carbonate zones were retained.

The contact between different textural types is diffuse, with one texture gradually becoming either more disseminated or more massive. The main textural categories of the carbonates are summarised in Table 11.2. All of these textures are recognisable in the ore-horizon in West and Central Thalanga, regardless of the presence of sulphides. Mesh-veined calcite that has overprinted the CTC units is the most common carbonate texture. In East Thalanga the small amount of carbonate occurs either as <20 cm wide regions of massive calcite within the massive sulphides, or as larger (<1 m wide) veins or zones of alteration within the mineralised upper rhyolite breccia that occurs down-dip in the East Thalanga ore horizon.

Table 11.2 Hand specimen-scale textures of the carbonates at Thalanga.

Texture	Description	Size	Abundance & Distribution
Rhombs	Euhedral dolomite rhombs, commonly zoned (Fig. 11.2a,b).	<3mm	Common from core to near stratigraphic base of CTC's.
Void-fill	Compositional banding and open-space crystal growth, common in pods of dolomite within massive sulphides (Fig. 11.2c).		Rare
Spheroids	Spherical aggregates of dolomite with rims of radial euhedral dolomite. Concentric zonation is typical (Fig. 11.2d,e,f).	<5mm	Rare, present within core of CTC unit.
Massive	Mosaic of anhedral to subhedral carbonate grains, to intergrown rhombs or spheroids with fine, irregular cross-cutting veins of chlorite (Fig. 11.2g).		Common, patchy distribution but mainly in core of CTC unit.
Pods	Irregular sized aggregates or blebs of carbonate grains. Typical shape of carbonate pods in massive sulphides (Fig. 11.2h).	<20 cm	Common in patches.
Mesh-veined	Network of irregular to mimetic calcite veins (< 10 mm thick) (Fig. 11.3a,b).		Common in core of CTC's, grades to massive carbonate
Banded	White calcite veins with minor chlorite (Fig. 11.3c)		Rare

Figure 11.2 Textures from the carbonate-chlorite-tremolite assemblages at Central and West Thalanga.

(a) White dolomite rhombs (arrow) and irregular pods of intergrown dolomite-calcite in chlorite matrix. Sample 2031NI12-75.5, West Thalanga.

(b) Photomicrograph of zoned dolomite rhombs in colourless chlorite matrix. Pyrite-tremolite vein cross-cuts the rhombs. Sample TH230-108, Central Thalanga, plane light.

(c) Zoned, euhedral dolomite crystals at core of void-fill dolomite, with remaining space filled with barite. Sample CT-91-1, Central Thalanga, crossed nicols.

(d) Close-packed dolomite spheroids. Concentric zonation is more prominent towards the rim of the spheroid. Such large and well preserved spheroids are uncommon at Thalanga. Sample APH76, West Thalanga.

(e) Photomicrograph of dolomite spheroids. Anhedral mosaic of dolomite grains in the core, with zoned, euhedral dolomite at the rim. Sample APH76, plane light.

(f) Spheroids typically display a radial extinction pattern under crossed nicols. Note truncation of zonation at arrow. Sample APH76.

(g) Massive dolomite with patches of closed-packed rhombs. Thin veins of chlorite cross-cut the dolomite. Sample TH245-499.5, West Thalanga.

(h) Irregular pod of massive dolomite and intergrown calcite within massive sulphides. Central Thalanga, 860 Stope. Hammer is approximately 30 cm in length, and the handle is orientated parallel to vertical.

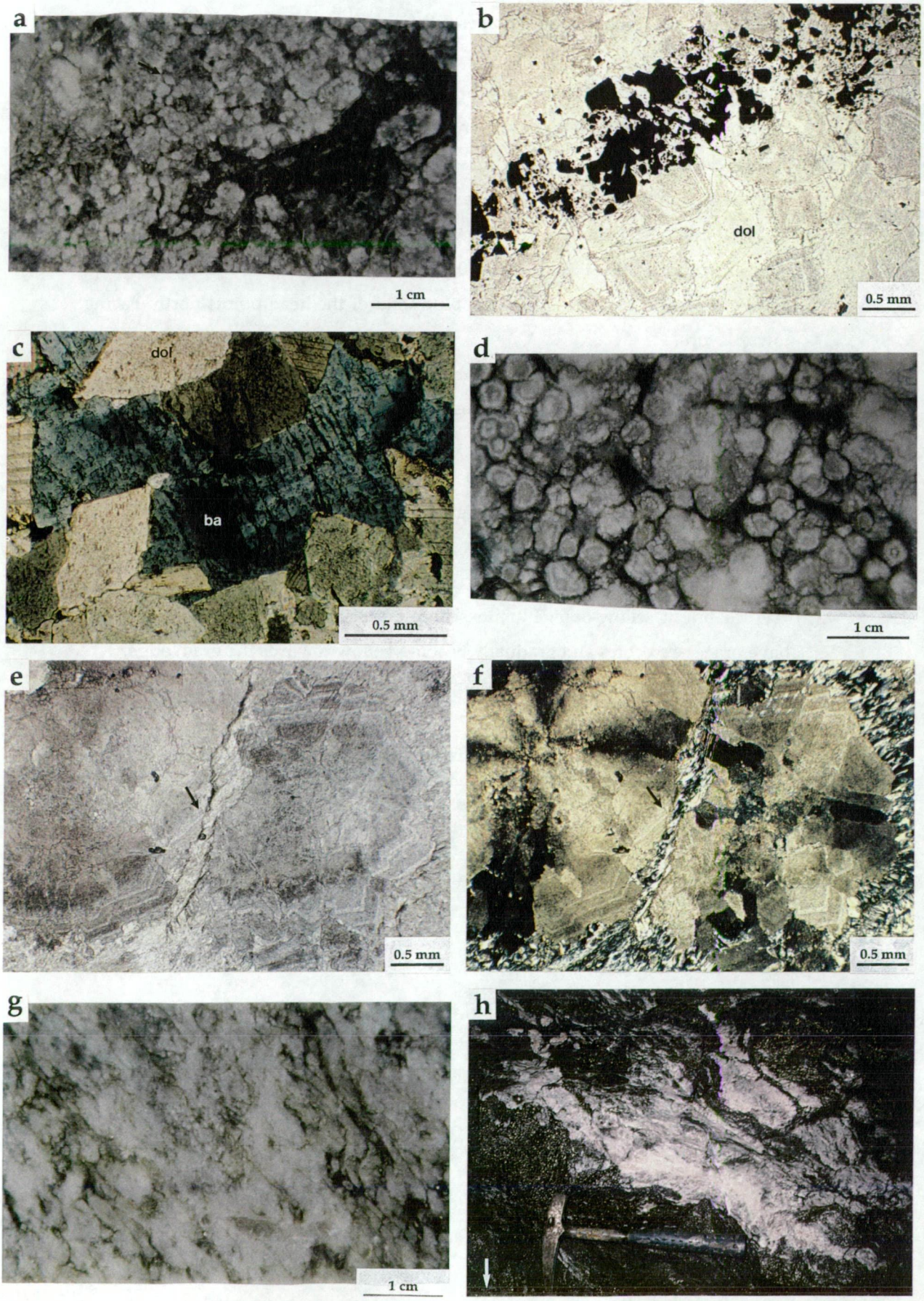
a
1 cm
b
dol
0.5 mm
c
dol
ba
0.5 mm
d
1 cm
e
0.5 mm
f
0.5 mm
g
1 cm
h

Figure 11.3 Textures of the carbonate-chlorite-tremolite assemblages in hand specimen, thin section and under cathodoluminescence.

(a) White, meshed veined calcite overprints spheroidal dolomite in a chlorite matrix. Sample 2031NI39-100.6, West Thalanga.

(b) White calcite veins cross cutting massive sulphides. Central Thalanga, 860W Stope, 20260 mN, 20408 mE. Pencil is parallel to vertical.

(c) Banded calcite-chlorite formed by parallel veins of white calcite in massive chlorite-tremolite. West Thalanga, 780 Stope, 20320 mN, 20230 mE. Hammer handle is parallel to vertical, and the blunt end of the head points north. Facing towards top.

(d) Radial clusters of elongate crystals (arrow) now composed of dolomite within a dolomitic matrix. Crystal shape suggests that dolomite may be pseudomorphing anhydrite or gypsum. Sample TH230-108.3, Central Thalanga.

(e) Photomicrograph of dolomite rhombs with colourless dolomite overgrowth that is parallel to cleavage and more abundant within pressure shadows. Sample TH230-108, Central Thalanga, plane light.

(f) Same sample as (e) under crossed nicols.

(g) Typical bright yellow-orange luminescence of calcite under CL. Some calcite grains have orange-red cores and gradually become yellow towards the grain edge, suggesting a change in the composition of the calcite. Sample TH263-128.7, East Thalanga.

(h) There is no evidence of any compositional variation in the same sample as (g) under plane light.

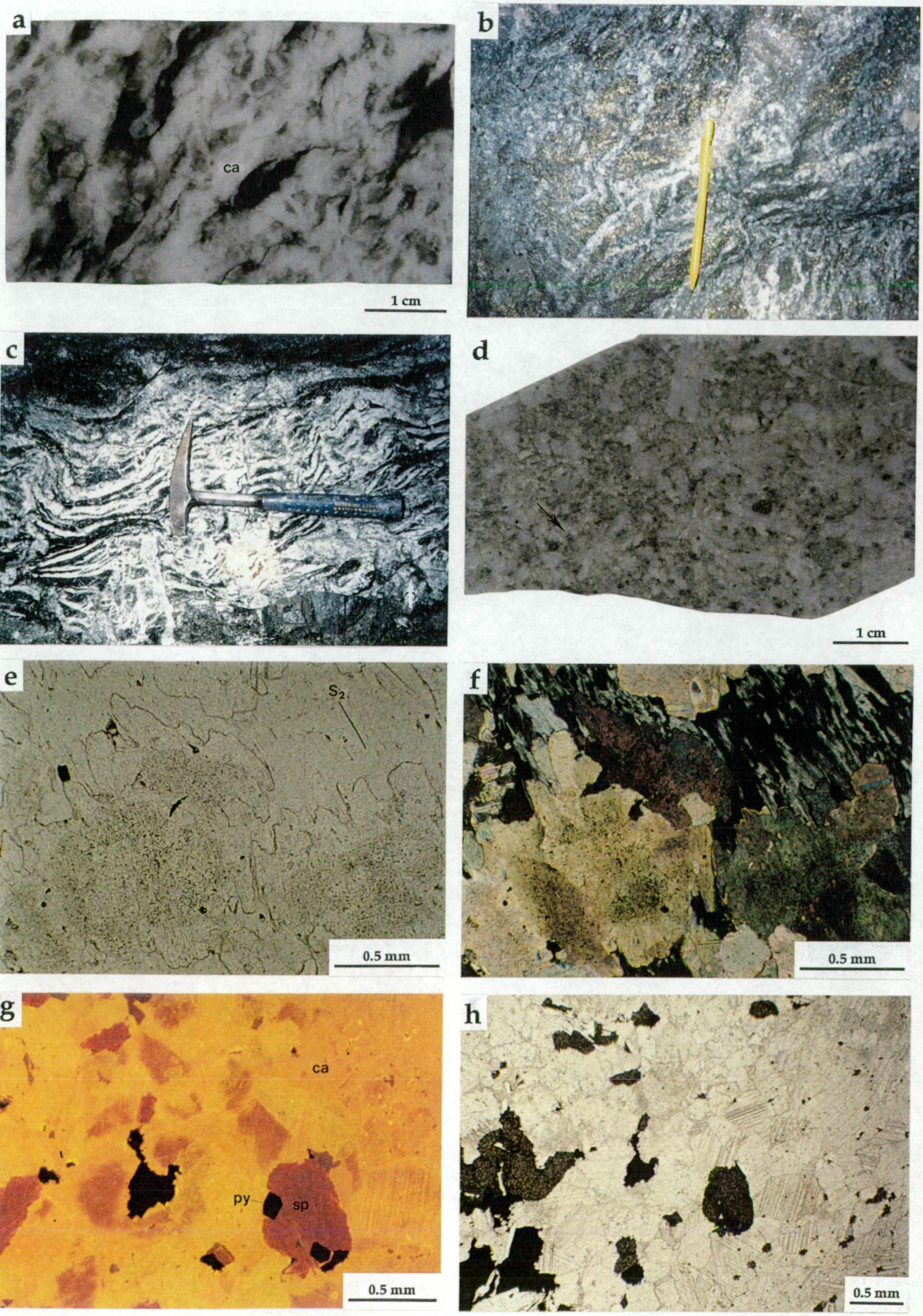
a
ca
1 cm
b
c
d
1 cm
e
S_2
0.5 mm
f
0.5 mm
g
ca
py
sp
0.5 mm
h
0.5 mm

Euhedral rhombs are the most common form of dolomite at Thalanga and thin section examination shows that some rhombs have inclusion-rich cores and clear rims, with two or three bands of inclusion-rich and clear dolomite at the rim of most rhombs. Clear dolomite, subparallel to the cleavage, fringes rhombs in Central Thalanga (Fig. 11.3e,f).

Typically the cores of spheroidal dolomite are large compared to the entire spheroid and are composed of small (<0.02 mm) dolomite grains in anhedral to nonplanar-S mosaics (cf. Tucker and Wright, 1990). Zonation in the coarse (0.4 mm) euhedral rims is recognised by alternating bands of clear and inclusion-rich dolomite. In some spheroids, elongate, dusty brown and inclusion-rich crystals, with irregular grain boundaries, extend radially from a small core to the zoned, euhedral rim (Fig. 11.2e,f). Undulose extinction within each crystal swings anticlockwise, similar to the radial cross extinction of the whole spheroid, as the microscope stage is rotated clockwise. Such undulose extinction is typical of baroque or saddle dolomite, which is recognised as a replacement product (Tucker and Wright, 1990).

Most carbonate textures occur in a matrix of massive to foliated chlorite. Within the massive sulphides, carbonate occurs as irregular, discontinuous bands and pods (Fig. 11.2h). Calcite is equigranular and white to faintly pink in hand specimen, and in many cases cross-cuts the sulphides, whereas dolomite is white and overprinted by the sulphides. Void-fill and spheroidal textures, easily recognised by thin section and CL examination, are preserved within some dolomite pods. The carbonate pods were stretched during deformation and coarse grained, dark, honey-coloured sphalerite and chalcopyrite in the necks between dolomite boudins.

An unusual texture of coarse (up to 1.5 cm in length) subhedral grains, now composed of carbonate, occurs in radial clusters within a carbonate>chlorite>tremolite matrix (Fig. 11.3d). The grain shapes suggest that carbonate has pseudomorphed gypsum or anhydrite. Both the matrix and the gypsum/anhydrite pseudomorphs are now composed of close-packed, microscopic dolomite rhombs, and in thin section, only interstitial chlorite and sulphides distinguishes the matrix from the radial pseudomorphs. This rare carbonate rock is <1 m in thickness, with gradational contacts to more typical rhombic dolomite-chlorite-tremolite assemblages, and is present at one locality at Central Thalanga, where it occurs within the pyrite and carbonate-rich ore lens.

Cathodoluminescence

Cathodoluminescence (CL) is useful in distinguishing calcite from dolomite and in determining microtextures of apparently recrystallised carbonate. Compositional differences between different generations of carbonate are also revealed using CL. Luminescence in carbonates is typically yellow-red-brown colours depending on the Fe and Mn content. Dark

colours under CL usually indicate that the carbonate is Fe-rich, whereas luminescence is bright when carbonate is Mn-rich (Pierson, 1981). The principles of CL and the methods used in this research are outlined in Appendix K.

The most prominent feature of the Thalanga carbonates is the bright yellow luminescence of calcite under CL, compared to the darker oranges, reds, and browns of the intensely zoned dolomites. Dark red-orange cores within some calcite grains have an irregular and diffuse contact with the yellow rims (Fig. 11.3g,h).

Zonation within the dolomite rhombs is similar to the zonation within the dolomite spheroids and void-fill textures, and prominent bands can be correlated in all carbonate textures (Table 11.3). CL reveals eight dolomite types, herein called dolomite (dol) 1 through 8, with dol 1 being the oldest. Typically the dolomites have a dull red to brown speckled core (dol 1 and 2) and notable colour zonation is restricted to the outer radial crystals (dol 4 to 7). The zone of finely alternating bright red and orange bands (dol 4) is a distinctive marker in rhombs, spheroids, and void-fill textures.

Table 11.3 Comparison of the zonation within carbonates under CL.

	Rhombs (Fig. 11.4a,b)	**Spheroids** (Fig. 11.4c,d)	**Void-fill** (Fig. 11.4e,f)
Core	dol 1) dull red speckled.	dol 1) medium red-brown to pink, speckled	dol 1) thick dull speckled red-brown,
	dol 2) dull red-brown speckled outer band.	dol 2) darker (red or pink) speckled outer band	dol 2) dull speckled dark brown outer band,
Rim	dol 3) series of mid-red speckled bands.	dol 3) medium red-brown to pink, speckled band; then darker (red or pink) speckled band; repeated once	dol 3) thin band of rich red-brown, speckled
	dol 4) thin band of finely alternating bright red and yellow bands	dol 4) finely alternating bright yellow-orange (or pink) and red bands	dol 4) finely zoned bright red and orange bands
	dol 5) dark red speckled bands	dol 5) medium dull red speckled band; then a dark speckled band; then a thin, very dark brown band	dol 5) dark brown speckled band
		dol 6) series of finely alternating bright red and orange bands	
		dol 7) dark brown speckled band	

dol = dolomite

One carbonate-chlorite ± tremolite sample contains very dark luminescing dolomite, suggesting that the dolomite contains significant levels of $FeCO_3$. This carbonate-chlorite, from within the ore horizon in Central Thalanga, is composed of close-spaced zoned dolomite rhombs in a chlorite matrix. The ore horizon in this location is pyrite-rich and pyrite veins cross-cut the carbonate-chlorite. The dolomite rhombs are smaller than those in other carbonate-chlorite-tremolite rocks from Thalanga and have been overgrown by dolomite (dol 8) that is clear in transmitted light and blood-red under CL (Fig. 11.4g). The contact between

Figure 11.4 Photomicrographs of carbonate textures under cathodoluminescence.

(a) Dolomite rhombs vary from brown to red and orange under CL, in contrast to the yellow calcite. CL shows that the rhomb is compositionally zoned and has been partly corroded and replaced by calcite. Dolomite growth in open space is suggested by the small rhombs extending from the rim of the large rhomb (arrow). These textures are not discernible in transmitted light. Chlorite and tremolite do not luminescence, but do appear a red-brown colour. Sample 2031NI12-75.5, West Thalanga.

(b) Ragged dolomite remnants and intensely corroded dolomite rhombs (red and brown bands) enclosed in calcite (yellow). The textural relationship between dolomite and calcite is unclear under transmitted light, yet obvious under CL. Sample TH139A-268.3.

(c) The large core of dolomite spheroids is speckled red and weakly zoned under CL, whereas the zoned euhedral rim is composed of several bands of reds and browns. Finely zoned dolomite at the edge of the spheroids appears to have formed in open spaces between spheroids. Veins of calcite have cross-cut the zoned spheroids. Sample 2031NI39-100.6, West Thalanga.

(d) The same dolomite spheroids as (c) under transmitted light. Spheroidal texture is difficult to distinguish in plane light (although radial extinction is visible under crossed nicols) and the surrounding dolomite displays no void-fill textures. Large calcite grains are easily noticed because they are twinned.

(e) Void-fill textures are conspicuous under CL, with speckled red-brown dolomite grading to finely zoned euhedral dolomite and then red-brown dolomite towards the centre of the void. CL shows that continuous dolomite deposition and corrosion forms some open spaces. Calcite has partly replaced the dolomite. Sample CT-91-1, Central Thalanga.

(f) The finely banded stage is partly replaced, with the banding preserved, by dolomite with blue luminescence. Same sample as (e). The colour difference between (e) and (f) is due to different film speeds.

(g) The colourless dolomite (dol 8) that overgrows zoned rhombs has blood-red luminescence under CL. The blood-red dolomite is weakly zoned. Note the dissolution surface (arrow) between zoned rhomb and zoned dolomite 8 overgrowth. Sample TH230-108, Central Thalanga.

(h) Dolomite 8 veins with blood-red luminescence cross cuts zoned, void-fill dolomite, but is overprinted by the yellow calcite. Sample CT-91-1, Central Thalanga.

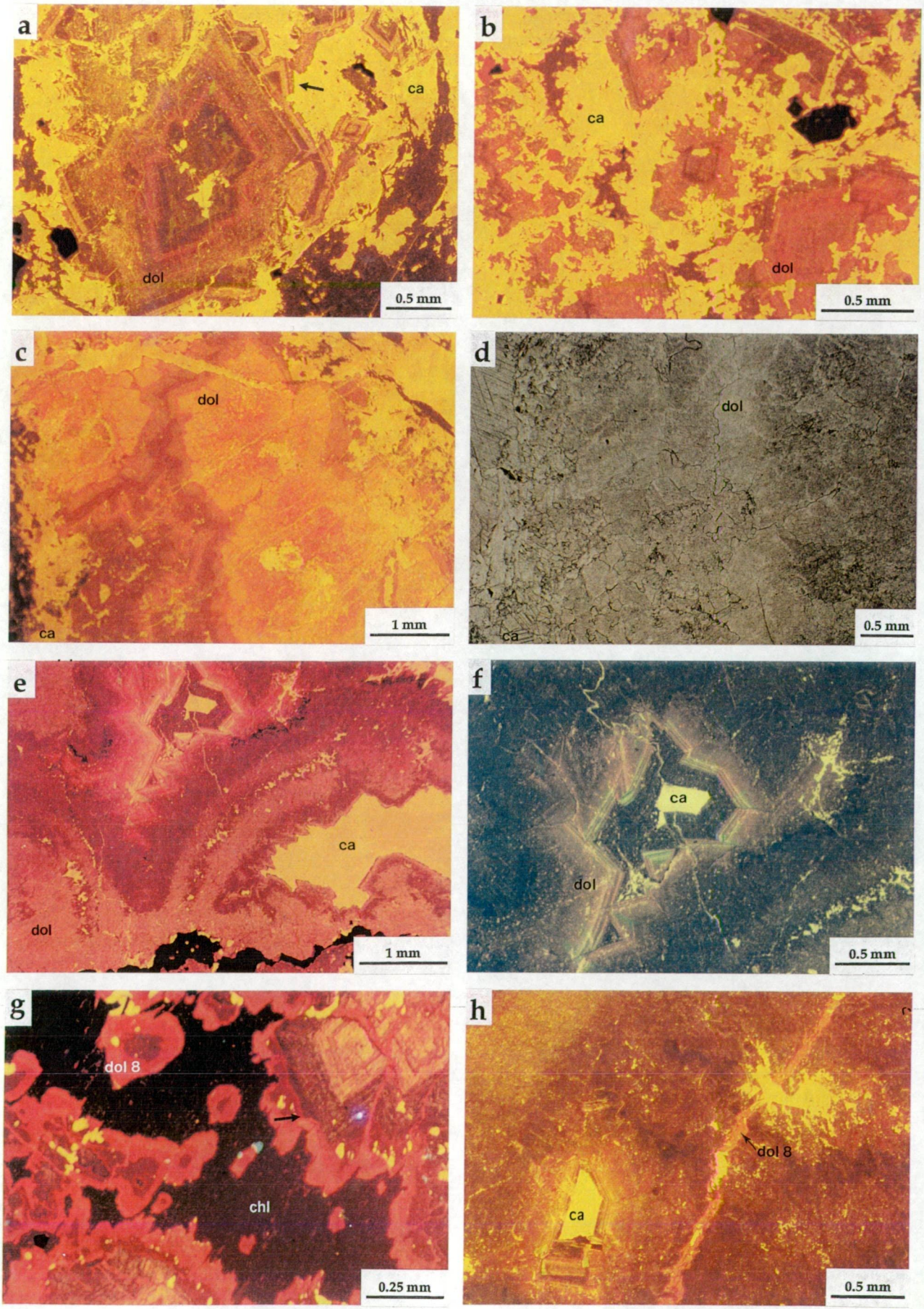
a
ca
dol
0.5 mm
b
ca
dol
0.5 mm
c
dol
ca
1 mm
d
dol
ca
0.5 mm
e
ca
dol
1 mm
f
ca
dol
0.5 mm
g
dol 8
chl
0.25 mm
h
dol 8
ca
0.5 mm

the zoned rhombs and the dolomite 8 overgrowth represents a dissolution surface (Fig. 11.4g). Similar dolomite, blood-red under CL, is widespread in most carbonate-chlorite-tremolite assemblages, where it occurs in irregular veins that cross-cut zoned dolomite (Fig. 11.4h). The blood-red dolomite 8 is also present as dolomite + sulphide veins that have infilled voids within zoned dolomite (Fig. 11.5a,b).

Spatially associated with the dark luminescing carbonate are the gypsum/anhydrite pseudomorphs that are now composed of dolomite rhombs. The dolomite rhombs are zoned and display bright orange-red luminescence under CL, with slightly irregular margins (Fig. 11.5c). Slight colour differences between the dolomite rhombs in the pseudomorphed grains and in the matrix were distinguished under CL. Rhombs in the matrix are typically coarser and more zoned than those making up the pseudomorphs. Dolomite rhombs at the rim of the gypsum pseudomorphs are coarser but less zoned than those in the core.

Corroded dolomite, replaced by calcite, is distinctive under CL, but almost impossible to distinguish in thin section (cf. Fig. 11.4c with 11.4d). In hand specimen, irregular carbonate blebs and pods are composed of grey-white calcite between white dolomite rhombs (Fig. 11.2a). The details are easily recognised in CL, with veins of bright yellow luminous calcite cross-cutting zoned dolomites, and massive calcite surrounding irregular and ragged dolomite rhombs and spheroids (Fig. 11.4a). This same calcite also fills fractures and cleavage partings in tremolite blades.

Interpretation of Cathodoluminescence

Table 11.3 shows that the same changes in luminescence colours are recorded in the rhombs, spheroids, and open space-fill dolomite. Coarse, euhedral dolomite is always finely banded under CL, whereas massive dolomite and the core of rhombs and spheroids are relatively unzoned. This suggests that the different textural forms of dolomite precipitated contemporaneously from a similar fluid, and that either the composition of that fluid, or the conditions of deposition, changed with time. Dolomite composition was determined by microprobe, and traverses across dolomite rhombs and spheroids revealed significant compositional zonation. The details of the compositional variation are discussed in section 11.4.

The differing dolomite habits may reflect differences in the number and distribution of nucleation sites. Fine-grained anhedral mosaics may have formed when there were abundant sites for dolomite nucleation, whereas coarse-grained euhedral dolomite may have resulted where the number of nucleation sites was low. The presence of fine compositional banding in euhedral dolomite in the centre of void-fill textures suggests that some euhedral dolomite

Figure 11.5 Carbonate textures under cathodoluminescence, and textures of the chlorite-tremolite and chlorite schist assemblages.

(a) CL clearly shows that sulphides have infilled voids and partly replace zoned dolomite. Sulphides are commonly associated with the blood-red dolomite, and in this example the blood-red dolomite occurs between the sulphides and the zoned dolomite rhombs. The yellowish colour of host dolomite under CL is due to almost complete replacement of dolomite by calcite. Sample TH230-110, Central Thalanga.

(b) Under plane light the textural relationships in the same sample as (a) are difficult to interpret. Sulphides appear to cross-cut and be intergrown with dolomite.

(c) Edge of a gypsum/anhydrite pseudomorph under CL (in left hand corner of photomicrograph). Both the pseudomorph and the matrix (right hand side) are composed of close-packed zoned dolomite rhombs. The rhombs are much yellower at the edge of the pseudomorph, suggesting that calcite has replaced dolomite at this position. Sample TH230-108.3, Central Thalanga.

(d) Hand specimen of chlorite-tremolite. Chlorite is dark green in hand specimen, and decussate tremolite blades are pale green. Sample WT-91-4, West Thalanga.

(e) Rectangular galena suggests that it completely replaced some pre-existing mineral. Sample APH105, West Thalanga, reflected light.

(f) Sample in (e) under crossed nicols. Chlorite in chlorite-tremolite assemblages is colourless in plane light with anomalous grey to khaki birefringence.

(g) Hand specimen of chlorite schist with cross cutting sphalerite-chalcopyrite-pyrite vein. Chlorite is dark green-black, and the shiny grey mineral is phlogopite. Sample TH239-139, Central Thalanga

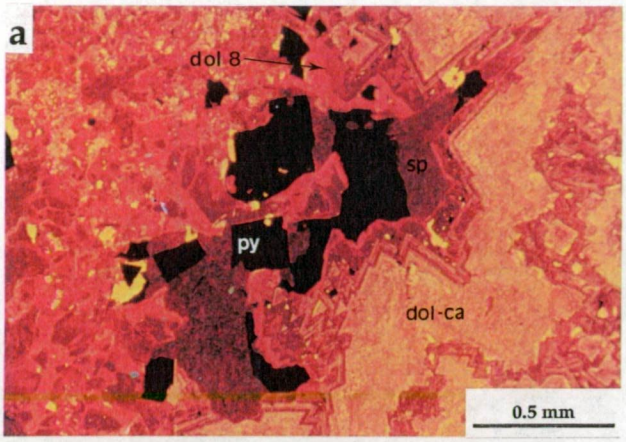
a
dol 8
sp
py
dol-ca
0.5 mm

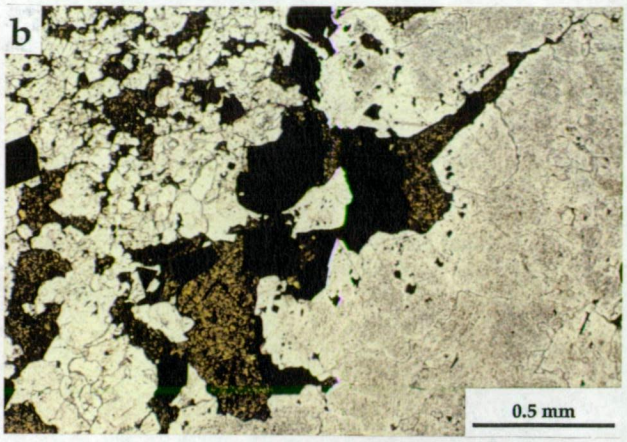
b
0.5 mm

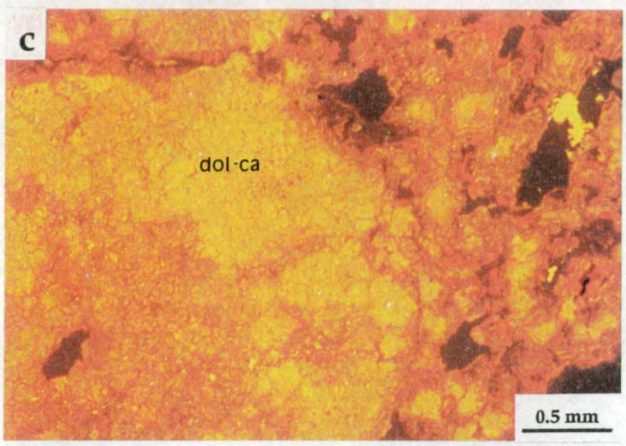
c
dol-ca
0.5 mm


d
chl
trem
10 mm

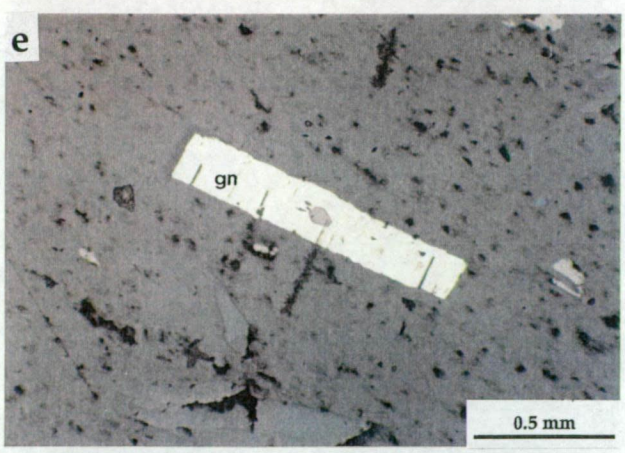
e
gn
0.5 mm

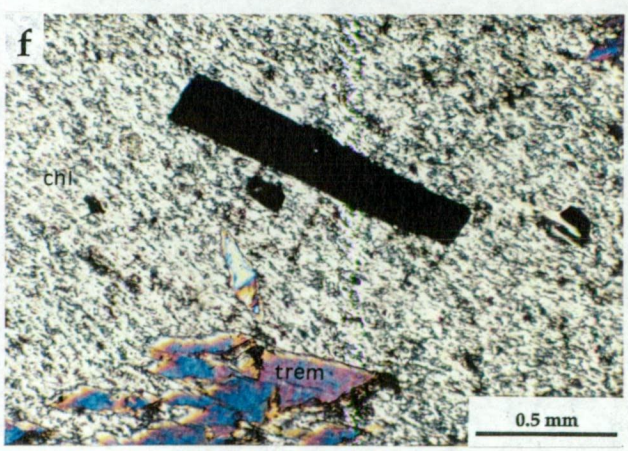
f
chl
trem
0.5 mm

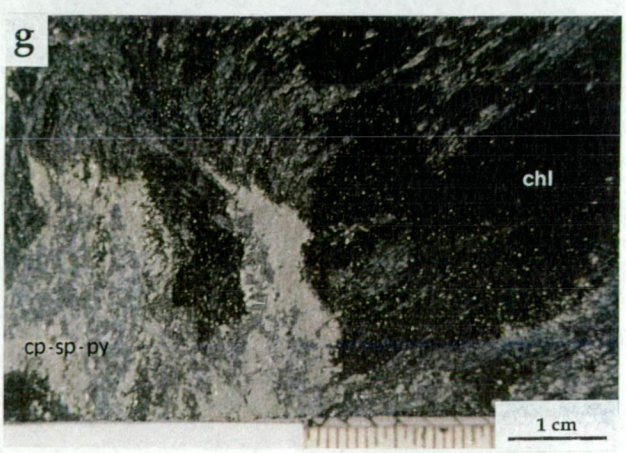
g
chl
cp-sp-py
1 cm

may have grown in open space. The significance of the high proportion of dolomite rhombs within the possible gypsum/anhydrite pseudomorphs is enigmatic.

Two calcite phases are recognised in hand specimen, a white-pink, equigranular calcite, and a later white calcite, common in veins. CL shows that the late white calcite is zoned and displays excellent void-fill textures, whereas the white-pink calcite is more uniform in composition. Subtle colour variations within individual grains of the white-pink calcite under CL suggests minor within-grain variation in calcite composition.

11.2.3 Chlorite - Tremolite Assemblage

Chlorite-tremolite-rich assemblages, with minor carbonate, commonly enclose the carbonate-chlorite-tremolite units within the ore horizon. The chlorite-tremolite unit is composed of fine grained, dark grey-green chlorite (colourless in thin section), with variable proportions of coarse, pale green to colourless tremolite (Fig. 11.5d). Tremolite has a radial to sheaf-like habit and is up to 5 cm in length.

Muscovite is uncommon, and apatite and sphene are accessory minerals. Sphene porphyroblasts are similar in size to those in the carbonate-chlorite-tremolite unit. Calcite both cross-cuts and is interstitial to tremolite blades. Clinozoisite and barium feldspar (celsian) were recognised in this assemblage by Wills (1985), who named it a tremolite exhalite.

The West Thalanga ore lens is partly composed of veins (up to 5 m thick) of banded sulphides that cross-cut the chlorite-tremolite units. Where poorly mineralised, sphalerite, pyrite, chalcopyrite, and galena are disseminated through the chlorite-tremolite assemblage, and are commonly intergrown with or enveloped by coarse grained chlorite and tremolite. In places, sulphides are intergrown with or rimmed by calcite. It is unclear what the galena has pseudomorphed in Figure 11.5(e,f).

Variations in the texture of the chlorite-tremolite unit are due to variations in the proportions of the main components. Chlorite is moderately to well foliated, with weakly developed crenulations of S_2, and tremolite crystals have overgrown the chlorite foliation. Very coarse blades of tremolite form radial sheafs where chlorite is more abundant than tremolite (e.g. Fig. 11.5d). Locally, the growth of tremolite has been controlled by pre-existing cleavage and tremolite blades extend radially along the plane of the foliation, but not into parallel cleavage planes. Where tremolite is abundant (about 80 %), the crystals are <1 cm in length, and there is no cleavage.

11.2.4 Chlorite Schist

Chlorite schist extends partly along the contact between the altered footwall rhyolitic volcanics and the CTC units in West Thalanga. In East Thalanga, chlorite schist is present at the stratigraphic top and within the footwall rhyolitic volcanics. The chlorite is dark grey-green to almost black in hand specimen (Fig. 11.5g) and colourless to pale green, with anomalous khaki interference colours, in thin section. Medium grained muscovite is disseminated throughout, with lensoid patches of phlogopite in places. Rare tremolite grains are disseminated in the chlorite.

Locally, bands of altered feldspar crystals or zoisite grains (<2 mm in size) are present within the chlorite schist. The altered feldspar crystals are now composed of intergrown plagioclase, zoisite, and coarse muscovite. Accessory sphene porphyroblasts are weakly zoned, with slightly rounded with irregular margins. Similar sphene porphyroblasts are rare in the underlying rhyolitic volcanics. Quartz grains and crystal fragments occur within some chlorite schists, and these may represent original volcaniclastic layers. Rare irregular to rounded blebs of quartz present as bands in the chlorite schist are partly internally fibrous in thin section (Fig. 11.6a,b), but are interpreted as silica alteration, rather than partly recrystallised spherulites.

Cross-cutting pyrite-chalcopyrite ± sphalerite veins are common in the chlorite schist. In the non-mineralised sections, minor euhedral pyrite is disseminated in the chlorite, and rare chalcopyrite, with traces of galena and sphalerite, is intergrown with chlorite.

11.3 Timing of CTC Components

11.3.1 Dolomite and Chlorite

The relative timing of components of the carbonate-chlorite unit is summarised in Figure 11.7(a-f). An extended phase of early dolomite formation is evident from CL studies (Table 11.3), and early-formed mosaics of anhedral dolomite (dol 1,2), either as massive dolomite or as spheroids, were overgrown by several bands of euhedral dolomite (dol 3,4), and bands of subhedral (dol 5,7) to euhedral dolomite (dol 6). The is no evidence of dissolution surfaces between dolomite 1 to 7, and formation of the dolomite probably occurred as one continuous event prior to and during the early stages of sulphide mineralisation. Late-stage colourless, but blood-red under CL, dolomite (dol 8) overgrew and cross-cut the zoned rhombs. Dolomite 8 is interpreted to have formed after corrosion of the zoned dolomite rhombs and spheroids (Fig. 11.4g).

Figure 11.6 Textures of the chlorite schist, and evidence of the relative timing of dolomite and sulphide formation.

(a) Photomicrograph of irregular to spherical quartz alteration within a tremolite-rich zone of the chlorite schist. Sample TH243-389.7, West Thalanga, plane light.

(b) The spherical quartz displays crude radial textures, and has been overprinted by calcite. Sample in (a) under crossed nicols.

(c) Photomicrograph of chlorite schist showing euhedral pyrite intergrown with tremolite. The chlorite is faintly green coloured in plane light. Pyrite cross cuts the cleavage. Sample 3208SD23-40, East Thalanga, plane light.

(d) Chlorite from the chlorite schists displays anomalous khaki green birefringence. Same sample as (c) under crossed nicols.

(e) Void-fill dolomite vein overprinting intergrown dolomite and sulphides. Sample 2039NI33-59.3, Central Thalanga, plane light.

(f) The vein displays compositional banding under CL, and is composed of dolomites 5, 6, and 7, with calcite in the remaining space. The sulphides are intergrown with dolomite 3.

(g) Photomicrograph of chalcopyrite at contact between corroded zoned dolomite rhomb and colourless dolomite overgrowth. Sample TH139A-268.3, West Thalanga, plane light.

(h) Same sample as (g) under crossed nicols. Note that calcite is twinned.

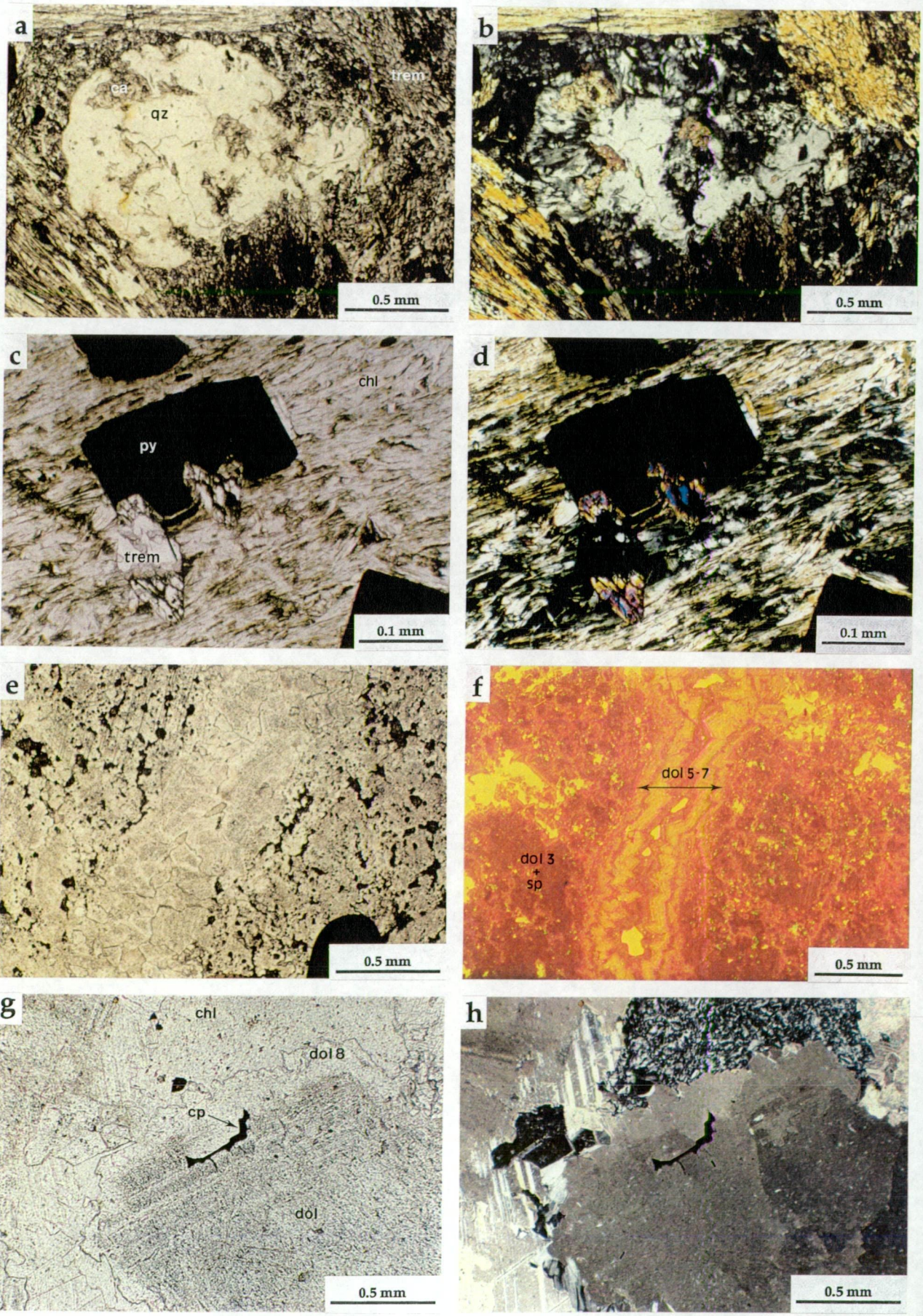
a
trem
ca
qz
0.5 mm
b
0.5 mm
c
chl
py
trem
0.1 mm
d
0.1 mm
e
0.5 mm
f
dol 5-7
dol 3
+
sp
0.5 mm
g
chl
dol 8
cp
dol
0.5 mm
h
0.5 mm

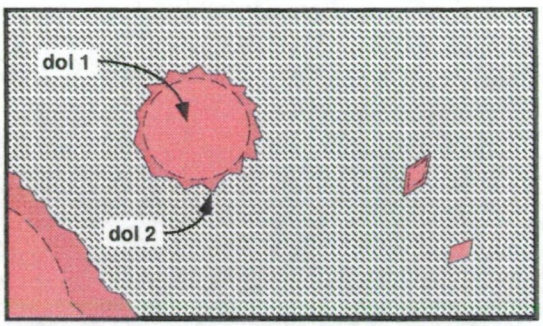

(a) Formation of anhedral mosiacs of dolomite 1 and 2 as spheroids, rhombs, and regions of massive dolomite. Dolomite probably nucleated on feldspars and glassy fragments. Grey area is clay or chloritised rhyolite.

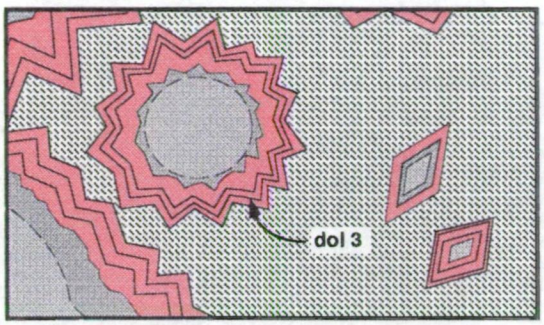

(b) Bands of euhedral dolomite 3 rim spheroids and rhombs, possibly forming in open-spaces.

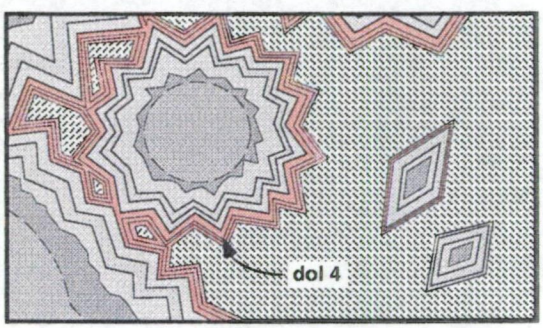

(c) Fine bands of euhedral dolomite 4 form in open-spaces. In some parts of the deposit, sulphide mineralisation replaces dolomite and fills voids after this stage.

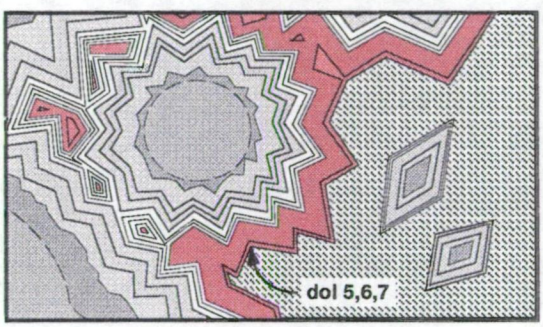

(d) Bands of euhedral dolomite 5, 6 and 7 form in remaining open-spaces and in veins that overprint earlier dolomite textures and sulphides.

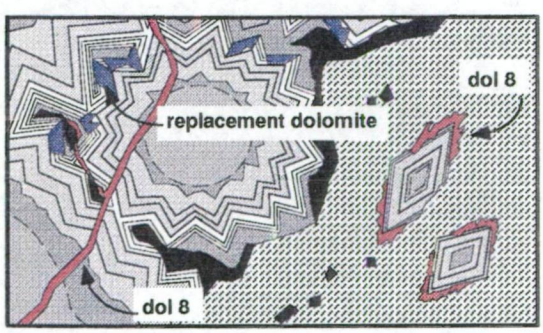

(e) During deformation and metamorphism, sulphides (black) are remobilised and partial dissolution of dolomite occurs prior to deposition of dolomite 8 veins and overgrowths. At some stage, parts of the finely zoned dolomite 4 are replaced by a blue luminescing dolomite.

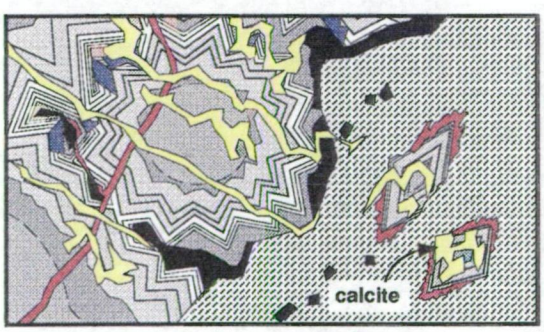

(f) Calcite overprinted all textures during the final stages of metamorphism.

Figure 11.7 Schematic diagram depicting the evolution of carbonate textures at Thalanga.

According to calculations by Herrmann (1994), dolomite formation was contemporaneous with chlorite formation, and dolomite spheroids and rhombs probably nucleated in a chlorite-rich matrix. In places, the zoned dolomites have been cross-cut by veins of chlorite (Fig. 11.2e,f). Dolomite 8 is intergrown with the chlorite matrix in the pressure shadows of some dolomite rhombs, indicating that dol 8 is associated with deformation. Crenulations of an earlier fabric (S_2) in the chlorite are recognised in some specimens, indicating that the chlorite pre-dates D_3 and metamorphism, and the association of sulphides with the chlorite-dolomite contact also suggests that the chlorite existed prior to deformation and mineralisation. Coarse grained chlorite in the pressure shadows of pyrite euhedra and calcite grains (Fig. 11.6c,d) suggests that chlorite recrystallisation post-dated deformation.

11.3.2 Sulphides

Sulphides have replaced the zoned dolomite (dol 1-7), and irregular pods of dolomite have been preserved within the massive to banded sulphides in Central and West Thalanga (Fig. 11.2h). In some places, remaining space around void-fill dolomite (dol 1 - 4) is infilled with barite and sulphides, suggesting that barite mineralisation post-dated dol 4 (Fig. 11.2c). In Central Thalanga, dolomite veins with void-fill textures (dol 5,6 and 7) have cross cut areas of massive dolomite (dol 3) with interstitial sulphides (Fig. 11.6e,f). These cross-cutting relationships are interpreted to indicate that sulphide mineralisation pre-dated formation of dolomite 5.

Figure 11.6(g,h) shows that chalcopyrite has partly replaced a dolomite rhomb, and is rimmed by dolomite 8. Chalcopyrite is interpreted to have been deposited following corrosion of the zoned dolomite, and subsequently overgrown by dolomite 8 during deformation and metamorphism. Elsewhere, dolomite 8 (blood red under CL) has pre-dated sulphides (e.g. Fig. 11.5a,b).

Sulphide minerals occur along cleavage partings in tremolite, in pressure shadow regions in the chlorite matrix, and locally, veins of tremolite-pyrite-sphalerite-galena-chalcopyrite cross-cut the zoned dolomite. The overprinting textures and coarse grainsize suggests that sulphides were remobilised and recrystallised during metamorphism. Pyrite must have recrystallised after the peak of deformation because most pyrite euhedra have overgrown the dominant cleavage in the chlorite-rich domains, and are intergrown with tremolite (Fig. 11.6c,d).

11.3.3 Tremolite, Talc and Calcite

Tremolite is randomly oriented and overprints the cleavage, indicating that it formed after the peak of deformation, and therefore is not an exhalative mineral as suggested by Wills

(1985) and Gregory *et al.* (1990). Corrosion and replacement of dolomite by calcite probably occurred during metamorphism. Calcite also fills spaces in metamorphic tremolite, is intergrown with remobilised sulphides, and forms a mesh of veins that overprint the dolomite-chlorite-tremolite assemblage. A simplified metamorphic paragenesis is (i) tremolite formation, (ii) sulphide remobilisation and recrystallisation, (iii) calcite and talc formation. Calcite has been overprinted by clear calcite veins and brittle factures.

Rivers (1985), Stolz (1991), and Herrmann (1994) suggested that tremolite and calcite formed by reaction between quartz and dolomite during regional metamorphism:

$$8SiO_2 + 5CaMg(CO_3)_2 + H_2O = Ca_2Mg_5Si_8O_{22}(OH)_2 + 3CaCO_3 + 7CO_2$$

Dolomite — Tremolite

This reaction will proceed between 350-450°C, at 2 kbars pressure, and at low to moderate activity of CO_2 (Rivers, 1985; Herrmann, 1994), and is reasonably consistent with the conditions of peak metamorphism determined in Chapter 3. The absence of quartz in the carbonate-chlorite-tremolite units indicates that all precursor quartz was consumed during metamorphism. Herrmann (1994) demonstrated that the rare diopside will form where quartz was in excess via:

$$SiO_2 + CaCO_3 + Ca_2Mg_5Si_8O_{22}(OH)_2 = CaMgSi_2O_6 + H_2O + CO_2$$

Tremolite — Diopside

Normative calculations by Herrmann (1994) demonstrate that there is no requirement for CO_2 addition during metamorphism, as all the calcite could have been derived from a pre-metamorphic quartz-chlorite-dolomite-(calcite) assemblage.

Talc is only a minor constituent of the CTC's and thus it is unlikely to have formed by reaction of quartz and dolomite during metamorphism. Radial talc overgrowths on tremolite crystals suggests that talc may be derived from tremolite during the later stages of metamorphism by reacting with dolomite, CO_2 and H_2O according to:

$$Ca_2Mg_5Si_8O_{22}(OH)_2 + CaMg(CO_3)_2 + CO_2 + H_2O = Mg_6Si_8O_{20}(OH)_4 + 3CaCO_3.$$

tremolite — dolomite — talc

11.4 Composition of Carbonate and Chlorite

11.4.1 Carbonate Composition

The composition of the carbonate at Thalanga was quantitatively determined using the Cameca SX50 Electron Microprobe in the Central Science Laboratory at the University of Tasmania, and the results are tabulated in Appendix B. Figure 11.8(a) shows that the carbonates at Thalanga are predominantly calcite or dolomite in composition, with minor variation in $MgCO_3$ and $MnCO_3$ content. Most calcite samples plot close to the $CaCO_3$ apex,

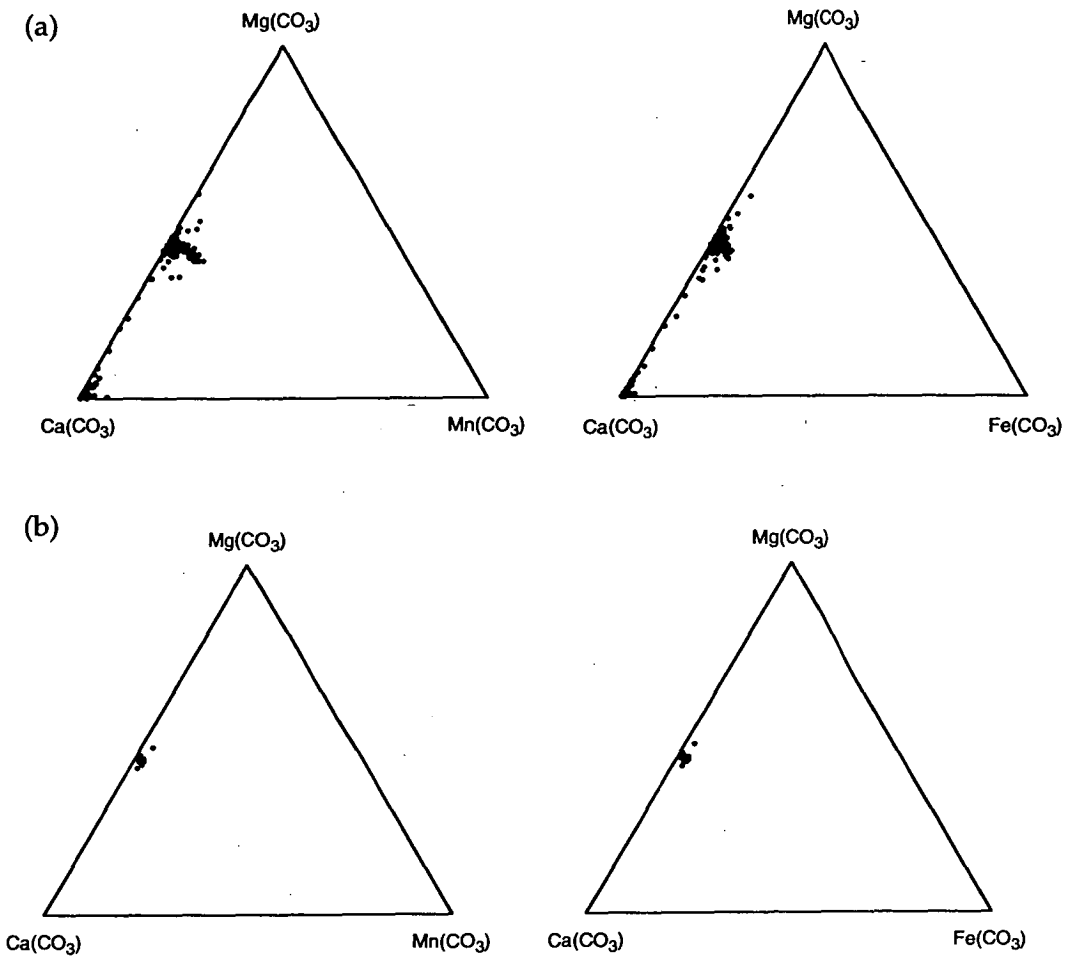

Figure 11.8 Composition of carbonate in the CTC units at Thalanga; (a) all carbonate, (b) overprinting blood-red dolomite.

with a few samples of high-Mg calcite present. The dolomite analyses are tightly clustered, with a spread in the $MnCO_3$ content that trends towards kutnohorite-rhodochrosite composition (0.1 - 10.9 weight % $MnCO_3$). There is no obvious spatial trend in the $MnCO_3$ content of dolomites within the ore horizon. The carbonates from Thalanga are relatively Mn-poor compared to Rosebery (Khin Zaw, 1991).

There is minor spatial variation in $FeCO_3$ content, and the average $FeCO_3$ content of dolomite in West and Central Thalanga increases from west to east along the ore horizon (Fig. 11.9). The most Fe-rich dolomite is the dark luminescent TH230-108 samples at 20430 mE (mine grid), with average $FeCO_3$ = 2.51 weight % and some bands of <10 weight % $FeCO_3$, whereas the westernmost samples contain mean $FeCO_3$ = 0.4-0.86 weight %. $ZnCO_3$, $SrCO_3$, and $BaCO_3$ contents of the dolomite are insignificant, with variations in these components less than 0.1 weight %. Average $ZnCO_3$ content of dolomite is about 0.3 weight % and typically $ZnCO_3$ > $SrCO_3$ > $BaCO_3$.

Several grains were traversed and regularly probed (20 to 50 μm spacing) in order to determine if the zonation recognised under CL is related to changes in composition. The grain traverses show that the $CaCO_3$ and $MgCO_3$ contents remain constant from the core to rim of most dolomite spheroids and rhombs, although in some examples, $MgCO_3$ content decreases slightly from core to rim (Fig. 11.10a,b). Despite overall low levels, $BaCO_3$, $SrCO_3$, and $ZnCO_3$ appear to occur in discrete bands within the rhombs or spheroids.

The most significant variations in colour under CL correspond to variations in $FeCO_3$ and $MnCO_3$ content (Fig. 11.10b,c). In general, the $MnCO_3$ content is greater than the $FeCO_3$ content, and consequently the dolomite is medium to bright red under CL (e.g. dol 3; Table 11.4). The brown and dark red-brown luminescent cores and bands contain more $FeCO_3$ than $MnCO_3$ (dol 1, 2, & 5; Table 11.4). The composition of fine bands in rhombs and spheroids (dol 4; Table 11.4) are unable to be accurately determined as most probe sites are too widely spaced, but element distribution maps show that the fine bands are due to variations in Mn content (Fig. 11.10c).

There is very little compositional difference between zoned dolomite (dol 1 to 7) and the overprinting blood-red dolomite 8 (Fig. 11.8a,b). Dolomite 8 contains 0.8 to 2.6 weight % $MnCO_3$, which is significantly higher than that of most rhomb cores (~0.4 weight % $MnCO_3$, ~0.8 weight % $FeCO_3$). $FeCO_3$ content of dolomite 8 is variable, with most analyses about 1.9 weight % $FeCO_3$. There is no consistent amount of $BaCO_3$, $SrCO_3$, or $ZnCO_3$ in the dolomite 8 overgrowth.

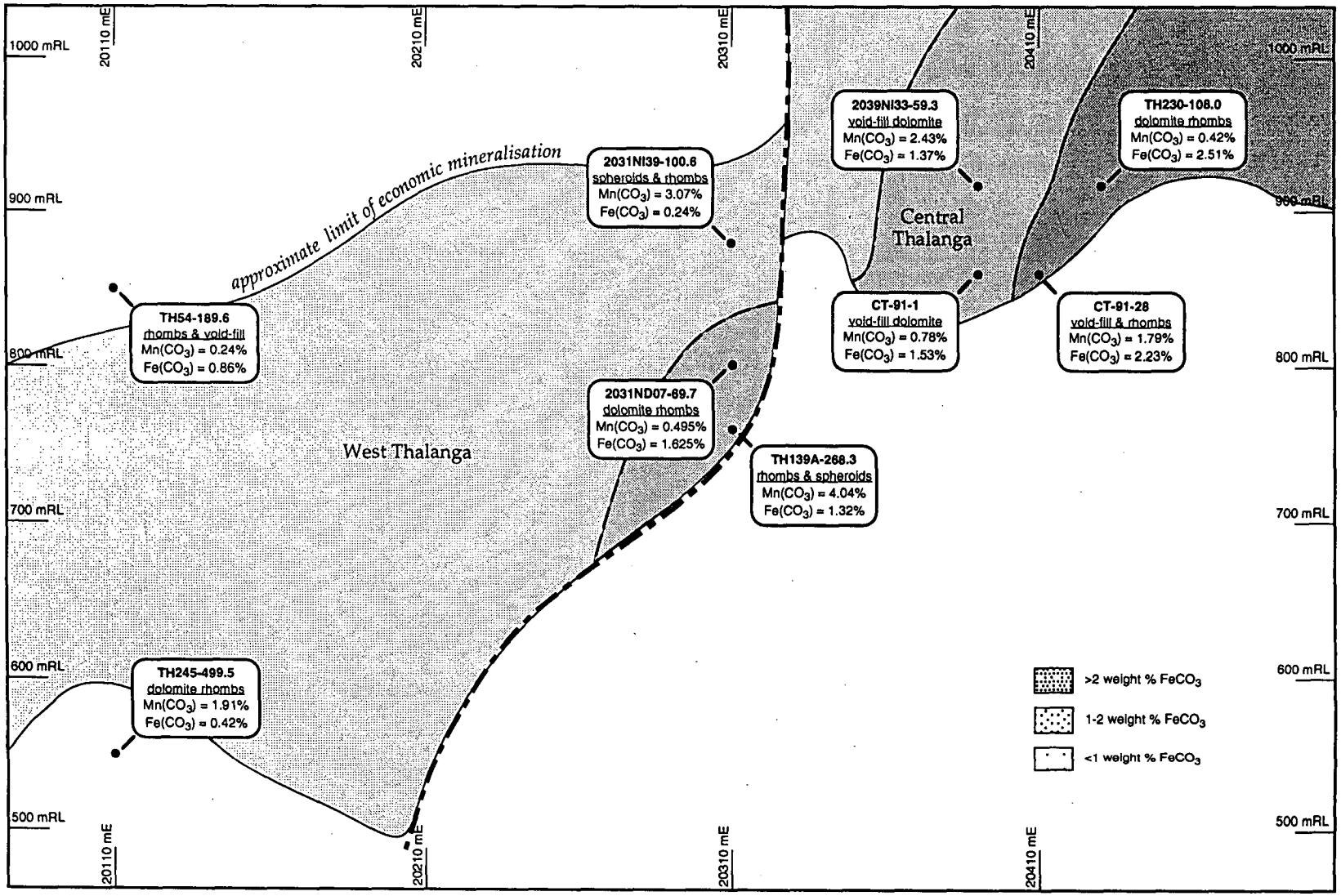

Figure 11.9 Long section of West and Central Thalanga depicting average $FeCO_3$ and $MnCO_3$ contents of dolomite.

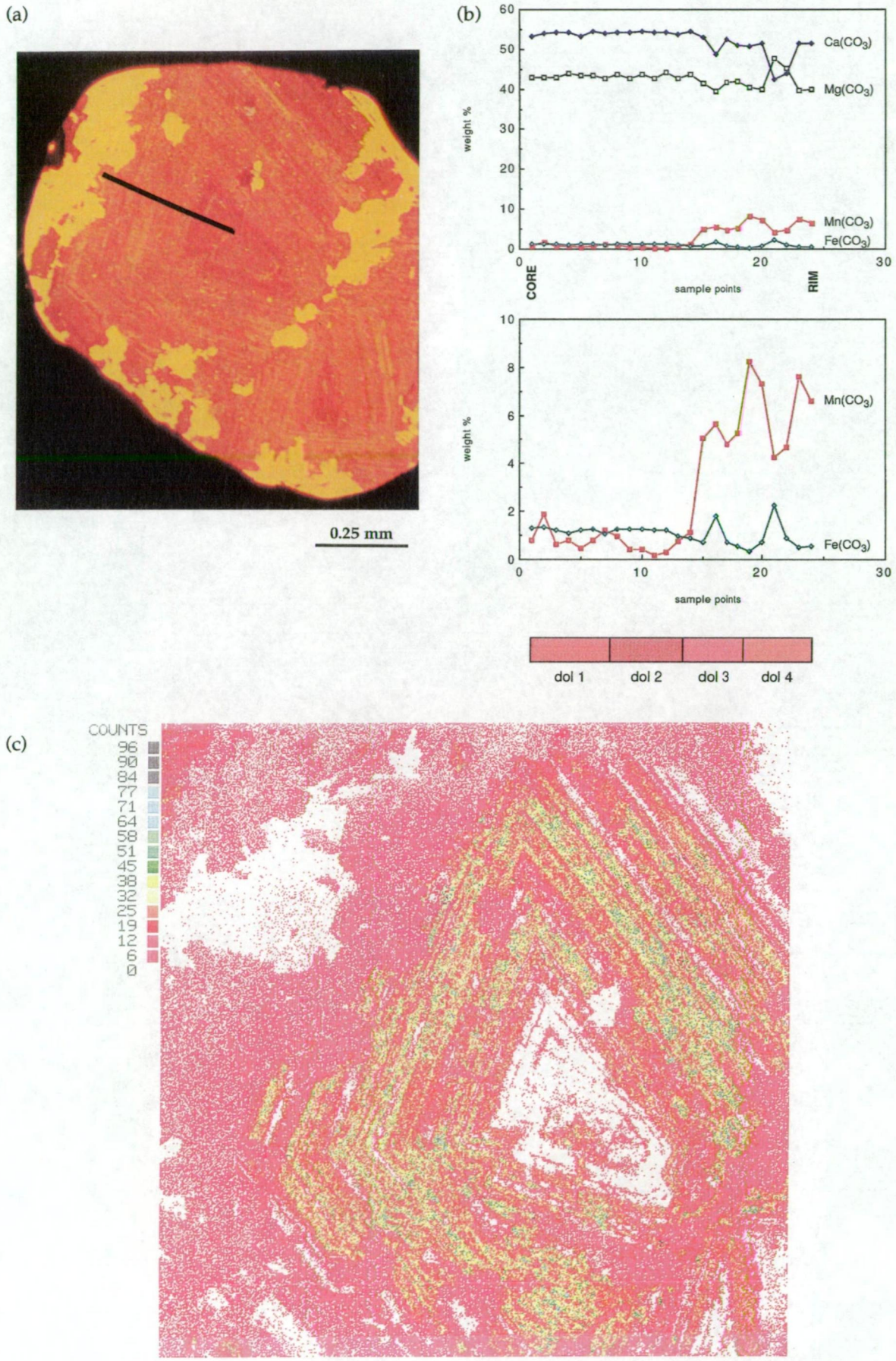

Figure 11.10. Relationship between colour of dolomite under CL and dolomite composition. (a) Dolomite rhomb from TH139A-268.3 under CL. Location of probe traverse in (b) shown by black line. (b) Composition from core to rim of rhomb. Electron microprobe sample sites are spaced about 17 μm apart. (c) X-ray map of part of the dolomite rhomb (1.024 mm^2), showing Fe and Mn concentrations. The core of the rhomb has Fe > Mn, and is therefore dark red under CL, and white in the x-ray map.

Table 11.4 Relationship between colour of dolomite under CL and its composition determined by microprobe. Dolomite numbers (e.g. dol 5) are the same as Table 11.3. Dol 6 and dol 7 were not analysed by microprobe.

	Colour under CL	Composition
Core	dol 1) dull-red to brown speckle	$FeCO_3$ = or >> $MnCO_3$
	dol 2) brown to red-brown	$FeCO_3$ >>>> $MnCO_3$
Rims	dol 3) medium red	$FeCO_3 \leq MnCO_3$
	dol 4) alternating bands	usually $FeCO_3 < MnCO_3$
	dol 5) dark red to brown	$FeCO_3$ >>>>>> $MnCO_3$
Overgrowth	dol 8) blood red	$FeCO_3$ >> $MnCO_3$

Key: (>>) = twice as much $FeCO_3$ and $MnCO_3$;

(>>>>) = four times as much $FeCO_3$ as $MnCO_3$;

(>>>>>>) = four to ten times as much $FeCO_3$ as $MnCO_3$

11.4.2 Relationship Between Dolomite Composition and Mineralisation

The initiation of sulphide mineralisation after dolomite 4 corresponds to changes in the Fe and Mn content of the dolomites (Fig. 11.10). In general, the Mn content of the dolomites at Thalanga reached a peak (in dol 3 and 4) immediately prior to sulphide deposition. Dolomite that was syn- or post-dated sulphide mineralisation (dol 5) contains four to ten times as much $FeCO_3$ as $MnCO_3$ (Table 11.4), and the gradual increase in redness under CL suggests that the Fe content of the dolomites gradually decreases in dolomites 6 to 11. Veins of dolomite 8 that post-date sulphide mineralisation generally contain twice as much $FeCO_3$ as $MnCO_3$ (Table 11.4).

The Mn content of carbonates at other styles of base-metal deposits has been shown to increase to a peak immediately prior to sulphide mineralisation. For example, the MnO content of the host dolomites and shales at the McArthur Deposit, in the Northern Territory, is elevated (0.5 to 1.9 %) in the rocks immediately underlying the sulphides, and sharply decreases in the rocks overlying the sulphides (Lambert and Scott, 1973). Lambert and Scott (1973) also report that away from the deposit, the MnO content of the laterally equivalent dolomites is moderately high.

In a regional study of Mississippi Valley-type (MVT) deposits in Missouri, Farr (1989) defined four zones of dolomite cements, each with disconformable contacts with each other, and reported that each zone was composed of a dull luminescent inner zone and an outer zone with multiple brightly luminescent bands. Correlation of CL studies with compositional analyses showed that the variation in colours under CL corresponded to decreasing Fe and Mn content towards the outer part of the zones (Farr, 1989). Anderson (1983) and Voss *et al.* (1989) correlated each dissolution surface in the dolomite cements with episodes of sulphide

precipitation. Thus in this example, both Fe and Mn in the carbonates decrease immediately prior to sulphide mineralisation and, similar to the dolomites at Thalanga, Fe content is elevated immediately after sulphide deposition. Farr (1989) regarded the Fe and Mn content of carbonates to reflect variations in the oxidation state, and to some extent pH, of the depositional fluids. In the MVT deposits, the fluids associated with sulphide mineralisation are interpreted to have been enriched in Fe (Hanor, 1979; Carpenter *et al.*, 1974), and therefore the subsequent carbonate cement was enriched in Fe (Farr, 1989).

11.4.3 Chlorite Composition

The colourless to pale green colour of the chlorite within the CTC units, in thin section, suggests that the chlorite is Fe-poor, and this was confirmed by microprobe analysis. Average spot analyses are tabulated in Appendix B, and are used in Figures 11.11, 11.12, and 11.13. Chlorite in the CTC assemblages is distinctive both optically and chemically from the green Fe-rich chlorite in the units that stratigraphically overlie the ore lenses at Thalanga (Chapter 3), and is similar in composition to hydrothermal chlorite from some other Australian deposits (Fig. 11.11). The structural formula of the chlorites at Thalanga were calculated on the basis of 36 oxygens, with all Si assigned to the tetrahedral sites and Al assumed to occupy the remaining tetrahedral positions. The surplus Al was assigned to the octahedral position along with Mg, Fe, and Mn. Chlorite in the CTC assemblages is classified as a clinochlore with compositional formula $(Mg_{10}Al_2)[(Si,Al)_8O_{20}](OH)_{16}$.

The greater MgO content of chlorite within the chlorite schists compared to chlorite within the overlying carbonate-chlorite-tremolite and chlorite-tremolite units at West Thalanga (Fig. 11.12a) is opposite to the variation in chlorite composition at Mt Chalmers, where the MgO/FeO ratio of the chlorite increases towards the top of the ore horizon (McLeod, 1987). There is no significant variation in chlorite composition laterally along the ore horizon at West and Central Thalanga (Fig. 11.13), although FeO values are slightly higher towards the west and with vertical height. The MgO, Al_2O_3 and MnO content of chlorite within the CTC assemblages is greater than that of chlorite disseminated within the underlying altered rhyolitic volcanics (Fig. 11.12a-c). This is the opposite trend to that reported from the Horne massive sulphide deposit in Quebec, where the zones of chlorite schist are composed of more Fe-rich chlorite than that disseminated within the footwall (MacLean and Hoy, 1991).

The Mg-number of carbonates in the Que River deposit is proportional to the Mg-number of co-existing phyllosilicates, suggesting that they are in chemical equilibrium (Offler and Whitford, 1992). However, there is no correlation between the Mg-number of dolomite and associated chlorite Thalanga (Appendix L), supporting the textural interpretation that dolomite formation predated formation of chlorite.

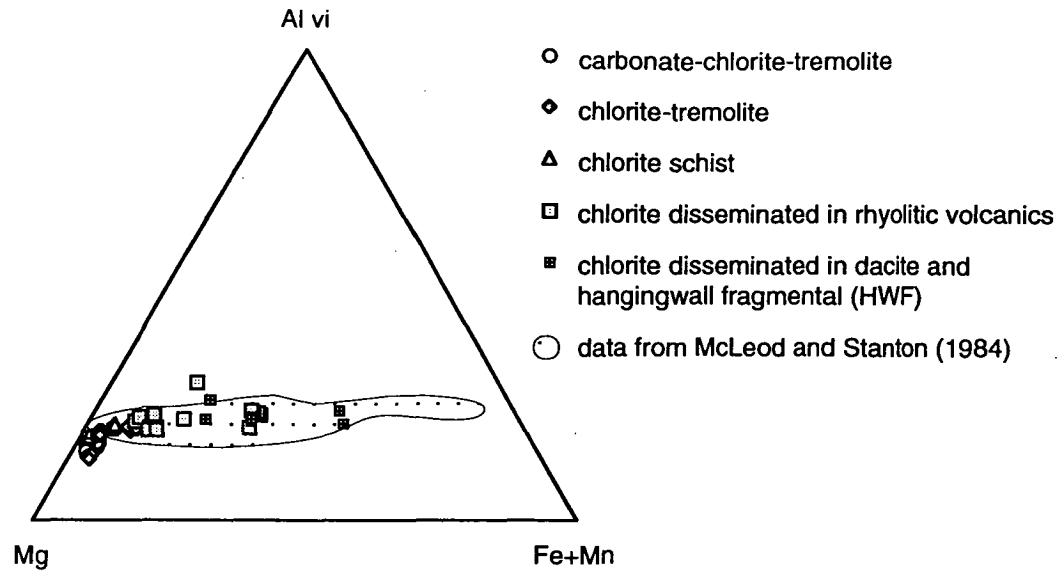

Figure 11.11 Comparison of the cations in octahedral sites between chlorite from the CTC units, chlorite disseminated in the stratigraphically overlying and underlying units at the Thalanga deposit, and chlorite from other Australian deposits.

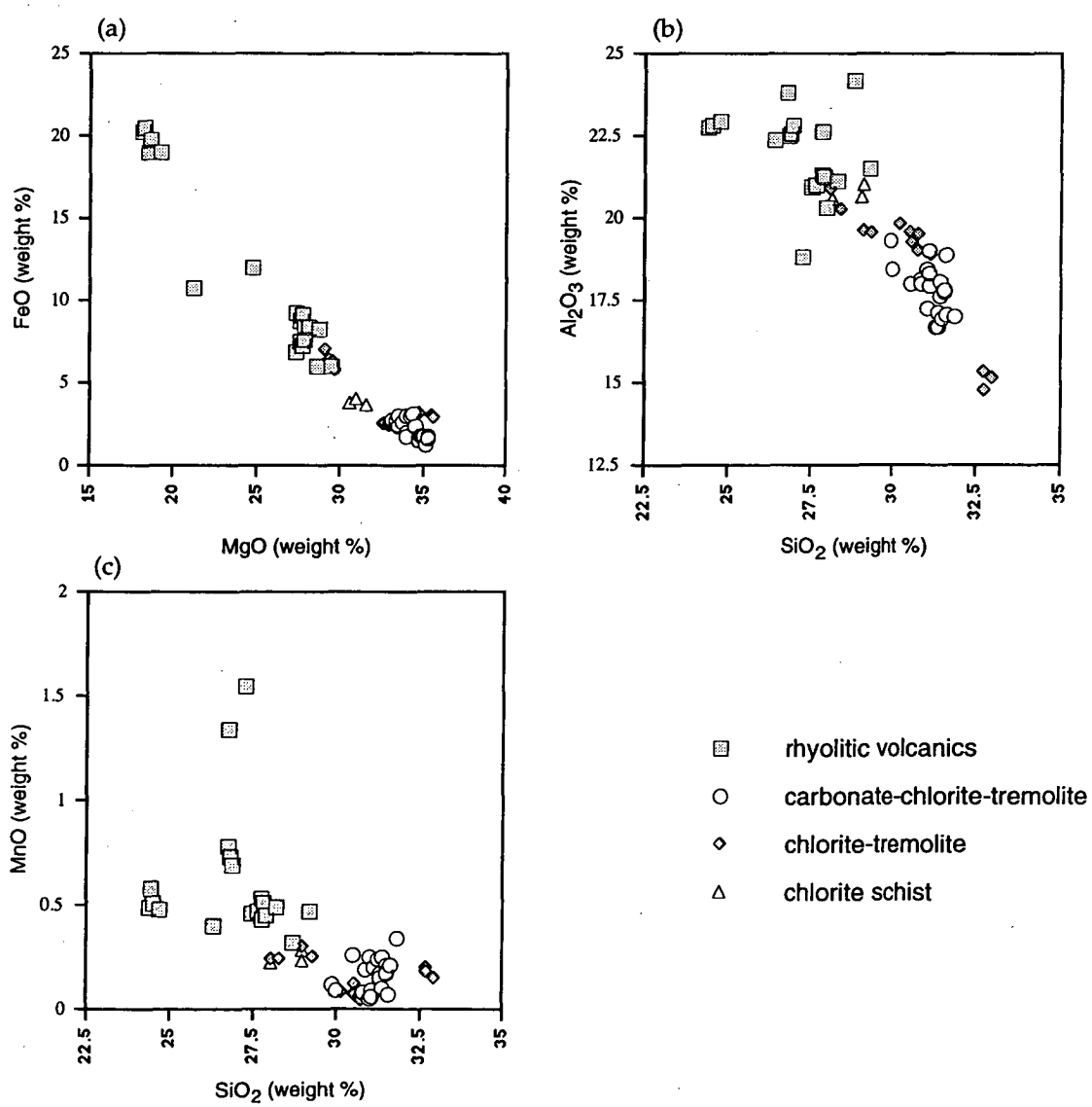

Figure 11.12 (a-c) Discrimination diagrams of the composition of chlorite from the CTC units at Thalanga, compared to the chlorite disseminated in the rhyolitic volcanics.

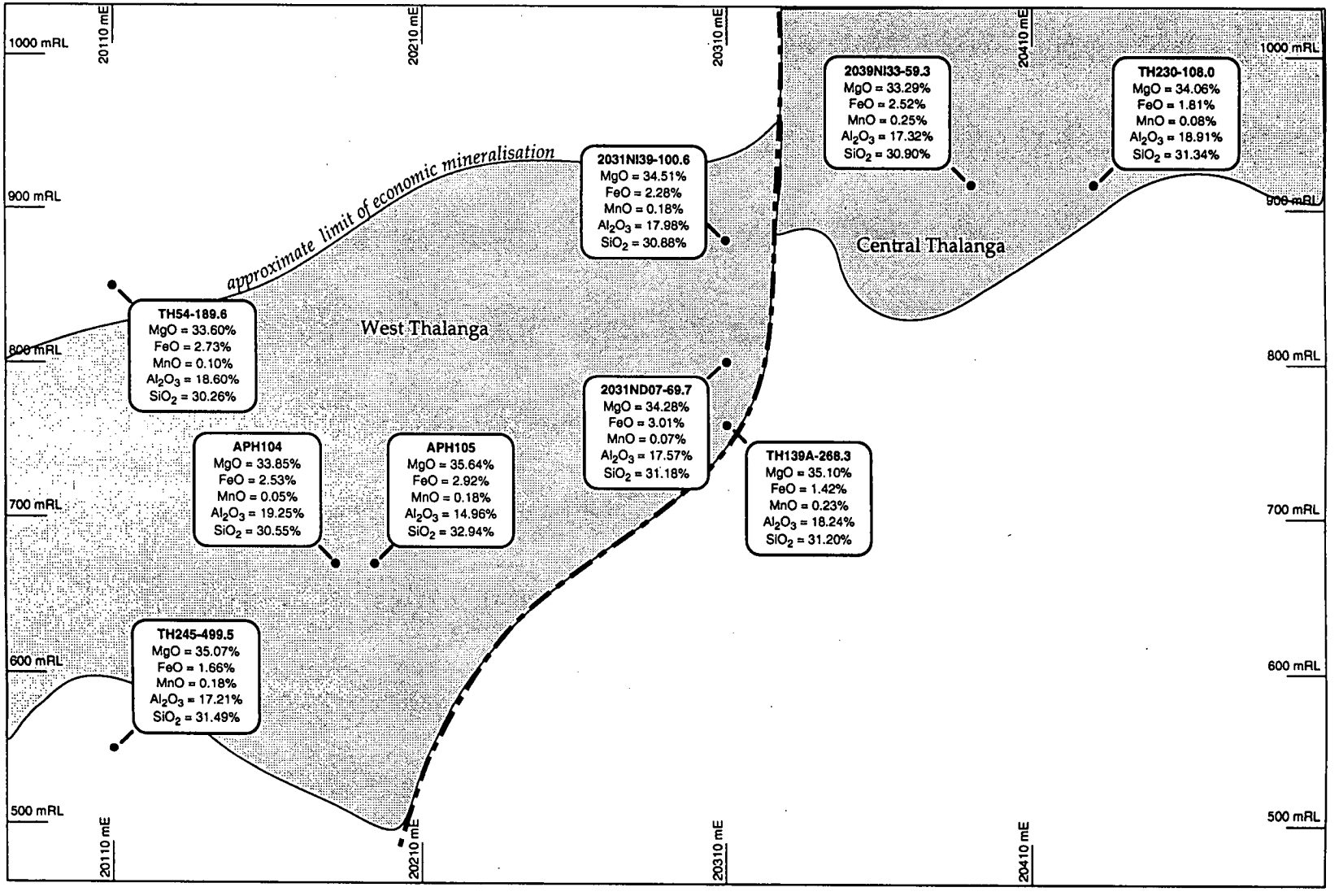

Figure 11.13 Long section of West and Central Thalanga depicting sample locations and average composition of chlorite from carbonate-chlorite-tremolite and chlorite-tremolite assemblages.

11.4.4 Composition of Other Minerals

Microprobe analyses of tremolite and talc from the CTC units at the Thalanga deposit are tabulated in Appendix B. Only a few grains of talc were analysed because of its paucity and fine grain size. Consequently, the presence or absence of variations in talc composition were not recognised. Those grains analysed (from two samples) are uniform in composition.

11.5 Carbon and Oxygen Isotopes

Carbon and oxygen isotope ratios were determined for calcite and dolomite in several CTC samples from Thalanga, in order to constrain the source hydrothermal fluids, and possibly to discriminate between hydrothermal carbonate and metamorphic carbonate. However, the results are treated with caution because, although carbon and oxygen isotopes remain stable in carbonates metamorphosed without H_20 to 400 °C (Rye and Ohmoto, 1974), at higher temperatures carbonates are depleted in ^{18}O due to decarbonation reactions and partial isotopic exchange between metamorphic fluids and the original carbonate (Sheppard and Schwarcz, 1970). Fractionation of C will also occur if C is available in the metamorphic solutions or if C is lost as CO_2 during metamorphic reactions. Therefore at Thalanga, where metamorphic temperatures are calculated to be 485 ± 23°C (Chapter 3), both the oxygen and carbon isotopes may have been homogenised during metamorphism.

Pure dolomite and calcite samples were drilled from hand specimens in order to minimise contamination. The samples most likely to contain carbonate with primary isotopic compositions are the regions of massive carbonate without metamorphic minerals. Therefore samples containing large dolomite rhombs or spheroids were analysed and dolomite was not sampled from specimens with abundant calcite replacement of dolomite. Chlorite contamination of the finely ground samples is very minor. Carbon and oxygen isotopes were determined using a VG Micromass 602D mass spectrometer in the Central Science Laboratory, University of Tasmania, using the method of McCrae (1950). Dolomite samples were reacted with phosphoric acid at 50° for 24 hours.

11.5.1 Results

Nine dolomite and ten calcite samples were analysed for $\delta^{18}O$ and $\delta^{13}C$ in this study, and the results, together with unpublished data collected by Penarroya, are tabulated in Appendix M. Despite extensive corrosion of dolomite and formation of calcite and tremolite during metamorphism, the $\delta^{13}C$ values of dolomite are tightly clustered and vary from -2.3 to 0.5 ‰, whereas the $\delta^{13}C$ of calcite ranges from +0.5 to -4 ‰ (Fig. 11.14a). $\delta^{18}O$ values of dolomite

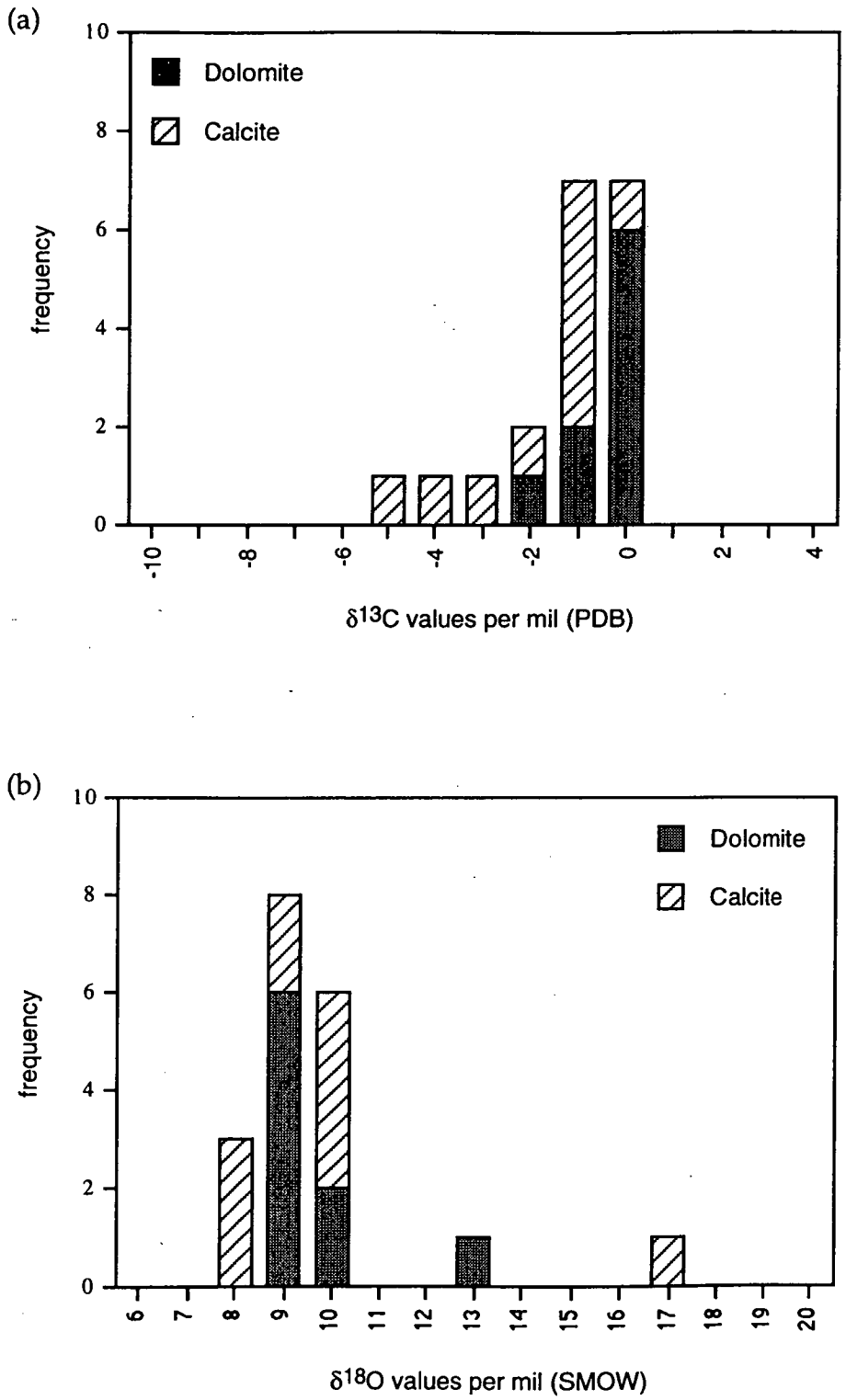

Figure 11.14 Histograms illustrating (a) $\delta^{13}C$ and (b) $\delta^{18}O$ values of carbonate minerals from Thalanga (rounded to nearest integer).

vary from 8.5 to 12.8 ‰, and are more clustered than the $\delta^{18}O$ values of calcite (Fig. 11.14b). White calcite associated with post-tectonic brittle faults has a significantly different O isotopic value compared to metamorphic calcite at Thalanga, with $\delta^{18}O = 17.0$ ‰ and $\delta^{13}C = -4.6$ ‰. The $\delta^{13}C$ and $\delta^{18}O$ values of the carbonate minerals at Thalanga are similar to those determined for the carbonate associated with sulphide mineralisation at Rosebery (Khin Zaw and Large, 1990; Khin Zaw, 1991).

11.5.2 Interpretation of C and O isotopes

There is no consistent correlation between dolomite texture and $\delta^{13}C$ and $\delta^{18}O$ values, although the spheroidal dolomite has slightly lighter $\delta^{13}C$ and $\delta^{18}O$ values than void-fill dolomite and some rhombs (Fig. 11.15a). This may reflect the interpretation from textural and CL studies that the dolomite spheroids, rhombs and void-fill textures formed from the same hydrothermal fluid, and that the cores of the spheroids formed prior to the rhombs and void-fill dolomite. A detailed examination of C and O isotopes of individual zones within dolomite rhombs and spheroids may clarify the variation between metamorphic and possibly primary carbonate isotopic compositions.

The overlap of dolomite and calcite isotopes at Thalanga is probably due to modification and homogenisation of the $\delta^{13}C$ and $\delta^{18}O$ values by metamorphism. The restricted range of $\delta^{13}C$ and $\delta^{18}O$ values of dolomite, compared to that of metamorphic calcite, may indicate that these are primary isotopic compositions of the dolomite. The $\delta^{13}C$ values of dolomite fall within the field of marine carbonates and may be similar to the original values (Fig. 11.15b). The $\delta^{18}O$ values of dolomite fall outside the field of marine carbonates (Fig. 11.15b) and may have decreased as a result of re-equilibration with water. Re-equilibration could have been accomplished by heating the carbonates in the presence of seawater. Subsequent re-equilibration with metamorphic or other water probably further lowered the $\delta^{18}O$ values. There is a weak $\delta^{13}C$ depletion towards igneous carbonate values, similar to trends identified from contact aureoles (Valley, 1986), and $\delta^{18}O$ values of 8 to 11 ‰ are consistent with igneous carbonates (Fig. 11.15b). However, mass balance calculations by Herrmann (1994) showed that CO_2 was not required to have been added during metamorphism in order to produce calcite at Thalanga.

It is evident from Figure 11.16(a) that there is no clear relationship between the $MnCO_3$ content and the C and O isotopic composition of the dolomite at Thalanga, although some dolomite samples with higher $MnCO_3$ have lighter $\delta^{13}C$ values. There is a weak positive linear correlation between Mg content and both $\delta^{13}C$ and $\delta^{18}O$ values (Fig. 11.16b). In comparison, $\delta^{18}O$ values increase, and become more variable, with increasing $MnCO_3$ content of the carbonates at Hercules, in Tasmania (Khin Zaw and Large, 1992).

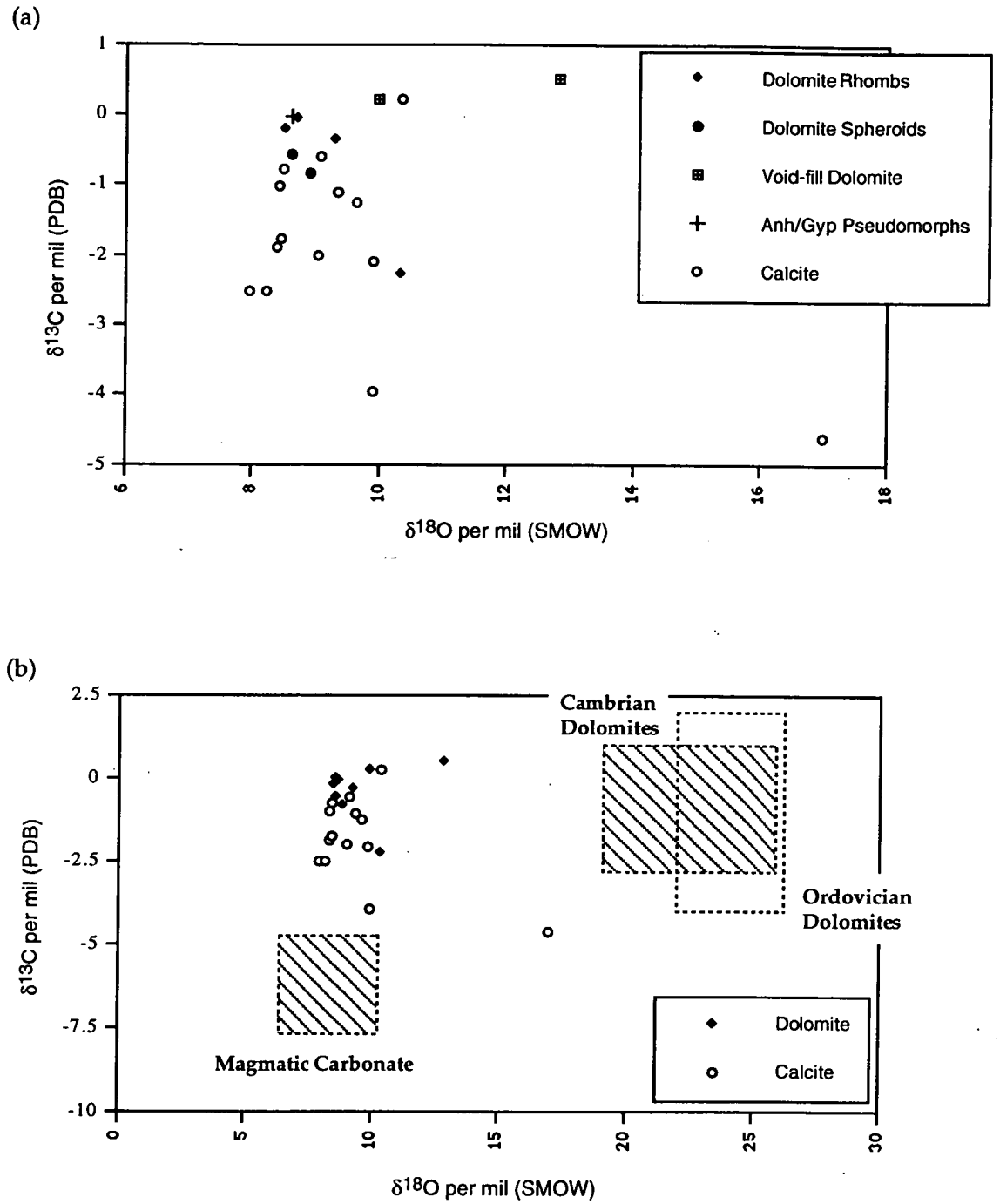

Figure 11.15 Carbon and oxygen isotope results from Thalanga. (a) Plot of $\delta^{13}C$ and $\delta^{18}O$ values of carbonates compared to textural classification. (b) Plot of $\delta^{13}C$ and $\delta^{18}O$ values of carbonates from Thalanga together with the fields of magmatic carbonate (Ohmoto, 1986; Hoefs, 1987) and marine carbonates (Veizer and Hoefs, 1976). Abbreviations: Anh = anhydrite, Gyp = gypsum.

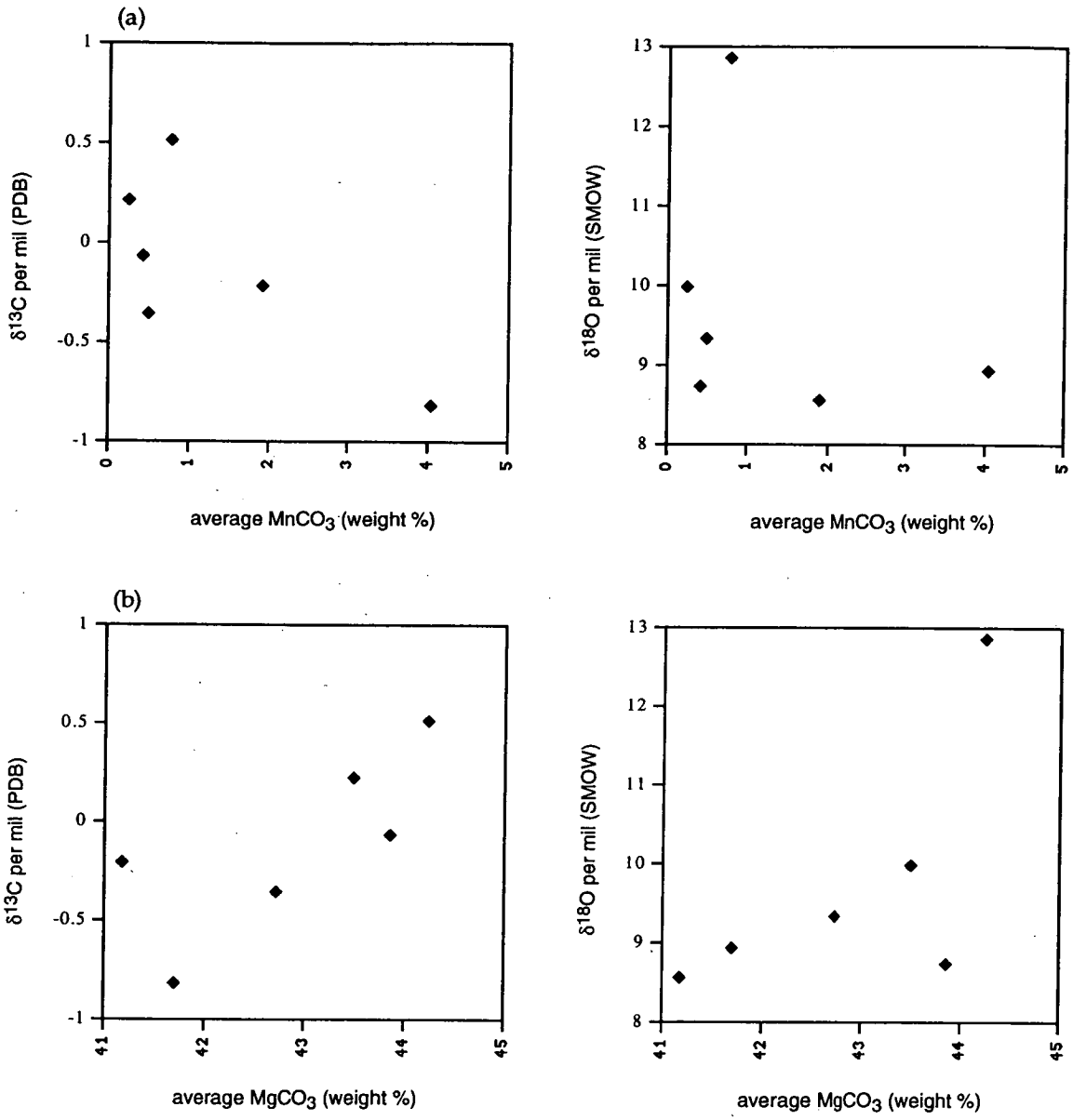

Figure 11.16 Comparison between $\delta^{13}C$ and $\delta^{18}O$ values and (a) average $MnCO_3$ content, and (b) average $MgCO_3$ content of dolomite at Thalanga.

Sources of Carbonate Ions

Carbonate present in modern and ancient hydrothermal systems is interpreted to have originated from mixing of various fluids sourced from dissolution of igneous calcite, degassing of CO_2-rich magmas, oxidation of organic carbonaceous material, dissolution of sedimentary carbonates, or metamorphism of carbonate-bearing material (Ohmoto and Rye, 1979). Seawater also contains minor dissolved CO_2 (present as HCO_3^-) and this bicarbonate is partitioned into magnesite in the recharge zones of hydrothermal systems (Seyfried, 1993), or is scavenged to form biogenic shells and tests.

For example, carbonate in nodules adjacent to an active seafloor hydrothermal vent in the Middle Valley is interpreted to have been sourced originally from seawater via diagenesis of biogenic carbonate sediments (foraminifera tests; Baker *et al.*, 1994). Limestone underlies the host volcanic units at the Afterthought-Ingot mine, California, and C isotopes of carbonate minerals associated with sulphide mineralisation (0 to -12 ‰) were interpreted to indicate mixing of marine carbonate with oxidised organic carbon (Eastoe and Nelson, 1988). Likewise, calcite in sulphide chimneys located in the Southern Trough of the Guaymas Basin, has $\delta^{13}C$ ~ -9.6 to -14 ‰, which is interpreted to indicate the mixing of carbon from oxidised biogenic material and dissolved marine carbonate (Peter and Scott, 1988). However, at the Helen siderite deposit, Morton and Nebel (1984) suggested that CO_2-rich hydrothermal fluids were derived from either diagenetic carbonate, or by the mixing of hydrothermal solutions with metamorphic CO_2-rich fluids.

The $\delta^{13}C$ and $\delta^{18}O$ values of the carbonate minerals at Thalanga indicate that the overlying Cambrian-Ordovician seawater was an important source of C and probably O. Alternative sources of HCO_3^- or CO_2 from reactions with organic matter dispersed in rocks lower in the stratigraphy (Puddler Creek Formation) are unsupported by the C and O isotopes. There is also no evidence of limestone lower down in the stratigraphy at Thalanga.

C and O isotopes from carbonate associated with mineralisation at Hercules in western Tasmania suggest that HCO_3^- or CO_2 could have been sourced from Cambrian seawater that was modified by circulation in the volcanic pile, and possibly mixed with some magmatic CO_2 (Khin Zaw and Large, 1992). The $\delta^{13}C$ and $\delta^{18}O$ values of the carbonate minerals at Thalanga are similar to those reported from Rosebery (Khin Zaw, 1991) and the weak trend towards magmatic $\delta^{13}C$ and $\delta^{18}O$ values (Fig. 11.15b) may indicate minor input of magmatic fluids into the hydrothermal solution.

11.6 Origin of Carbonate- and Chlorite-rich Units

Textural evidence, combined with the normative calculations by Herrmann (1994), demonstrates that dolomite-chlorite-quartz-(calcite) is a valid pre-metamorphic assemblage. Dolomite pre-dated sulphide deposition at Thalanga, similar to some other VHMS deposits (Large and Both, 1980; Gemmell and Large, 1992; Galley *et al.*, 1993; Hill and Orth, 1994; Orth and Hill, 1994), and because of its close spatial association with the massive sulphides, it is considered to represent an early stage of hydrothermal alteration. Large and Both (1980) suggested that carbonate zones represent a cooler temperature or distal equivalent to the massive sulphides. This may explain the absence of CTC assemblages in the eastern part of Central Thalanga and East Thalanga where extensive quartz-muscovite-pyrite-rich assemblages in the footwall and chalcopyrite-rich massive sulphides indicates that temperatures of hydrothermal alteration were high (Herrmann, 1994). The ore lenses in West Thalanga may have formed in a comparatively cooler part of the hydrothermal system, with a thinner and less pervasively pyritic quartz-sericite altered footwall (Herrmann, 1994). However, West Thalanga and Central Thalanga have overall higher Cu-grades than East Thalanga (Chapter 2), which is consistent with higher temperatures of sulphide formation in West Thalanga compared to East Thalanga.

Wills (1985) considered that the CTC units represent primary exhalites, and thought that the variation between mono-mineralic CTC units and all gradations between may have formed by mixing volcaniclastic with exhalative materials. Herrmann (1994) convincingly demonstrated that the immobile element ratios of the CTC units suggest a rhyolitic precursor. Chlorite-dominated assemblages could have formed from rhyolite by mass loss of Si and Na and gain of Mg. However, Herrmann (1994) was unable to clarify whether carbonate-chlorite-tremolite assemblages formed by either significant addition of Mg, Ca, and CO_2 to a rhyolitic precursor, or by addition of volcaniclastic material to a carbonate exhalite. Carbonate textures are useful in resolving this problem.

11.6.1 Significance of Dolomite Textures

Spheroidal, rhombic, and void-fill carbonate textures have been recognised in several VHMS deposits (Table 11.1). The similarity in carbonate textures from different deposits, despite varying metamorphic grades, suggests that these textures are primary and resist metamorphism.

Carbonate alteration at Rosebery in western Tasmania (chlorite grade, greenschist facies; Brathwaite, 1974) has textures similar to the carbonate at Thalanga. Yet primary volcanic textures have been preserved in the carbonate (Hill and Orth, 1994; Orth and Hill, 1994). The main carbonate textures are spheroids, blebs, pods, rhombs and massive carbonate (Table

11.5), with a gradation between all textures. Spheroid and rhomb cores are composed of fine grained anhedral carbonate, and are rimmed by coarse, euhedral radial carbonate (Hill and Orth, 1994; Orth and Hill, 1994), comparable to those at Thalanga.

Table 11.5 Hand specimen textures of the carbonate at Rosebery (from Hill and Orth, 1994; Orth and Hill, 1994).

Carbonate texture	Core	Rim
Spheroids:	Spherical to nodular shape, 0.2 - 20 mm diameter, Mosaic of anhedral grains	0.2-1 mm thick, Radial, euhedral, zoned grains
Blebs	Irregular shape, some rectangular - possibly carbonate after feldspar, Variable size up to 10 mm, Mosaic of fine anhedral grains	Rare rims of radial, euhedral carbonate rhombs
Pods	Irregular shape, Up to 100 mm in length, Mosaic of anhedral carbonate grains or intergrown spheroids	Irregular margins, no distinctive rim
Rhombs	Dusty, inclusion-rich in transmitted light	Zoned, <1.5 mm thick
Massive	Mosaic of anhedral to euhedral carbonate grains, or intergrown carbonate spheroids, Intergranular muscovite, quartz and chlorite are common	

Circular and arcuate shapes in the cores of spheroids or blebs were interpreted by Hill and Orth (1994) and Orth and Hill (1994) to be uncompacted pumice replaced and preserved by carbonate alteration. CL studies by Hill and Orth (1994) and Orth and Hill (1994) show that the carbonate at Rosebery is composed of several generations of carbonate, similar to Thalanga, and that it formed by initially nucleating on and replacing pumice fragments, then precipitating in remaining vesicles and open-spaces. Replacement of felsic glass by carbonate, commonly calcite, has been recognised in other volcanic sequences (Browne and Ellis, 1970), but only rarely are volcanic textures preserved (e.g. Carrigan and Cameron, 1991; Howells *et al.*, 1991).

Spheroidal carbonate textures are common in many diagenetic environments (e.g. Talbot and Kelts, 1986; Brown and Kingston, 1993; Gibson *et al.*, 1994; Sugitani *et al.*, 1995), and indicate that after nucleating on a point, the carbonate was able to either grow displacively outwards, or replace the matrix in a radial habit. Some authors have reported an association between carbonate concretions and coarse-grained sediments (e.g. Strakov, 1969; Curtis *et al.*, 1975; Pederson and Price, 1982), suggesting that porosity may be the critical factor in the habit of diagenetic or hydrothermal carbonate. Diagenetic carbonate associated with an active seafloor hydrothermal vent in the Middle Valley of Juan de Fuca Ridge forms spherical to elliptical nodules, some of which are concentrically zoned, preferentially in the coarse-grained basal turbidite sediments (Baker *et al.*, 1994). Uncompacted pumice textures

within the carbonate at Rosebery indicate that replacement occurred while the footwall pumiceous mass-flows were porous and therefore probably close to the seafloor (Hill and Orth, 1994; Orth and Hill, 1994).

Perhaps then, spheroidal dolomite at Thalanga indicates that dolomite grew in, and replaced, a porous host. At Thalanga, dolomite overgrowths on some dolomite rhombs have textures consistent with growth in open spaces (Fig. 11.4c), and domains of massive dolomite with undulose extinction are indicative of baroque dolomite which is interpreted to be a replacement product (Tucker and Wright, 1990). These varying dolomite textures may be related to varying porosity and number of nucleation sites, with regions of massive anhedral dolomite formed where nucleation sites were abundant. Zones of void-fill textures may indicate continuous circulation of carbonate-bearing solutions and the overprinting of massive dolomite with fracture-fill dolomite veins.

11.6.2 Formation of Dolomite

Dolomitisation of Calcite?

Dolomite formation may have occurred either by the direct precipitation of dolomite, or by the dolomitisation of pre-existing calcite. Modern models of dolomite formation involve the dolomitisation, or Mg-metasomatism, of meta-stable calcite (Carozzi, 1993). Calcite may have been deposited initially at Thalanga, and diagenetically altered during the early stages in the evolution of the hydrothermal system as the temperature of rising fluids increased. Indeed, Galley *et al.* (1993) proposed that carbonate associated with massive sulphides at the Chisel Lake deposit was precipitated as calcite on the seafloor (from the overlying seawater) and was dolomitised during hydrothermal alteration.

Cloudy-centred, clear-rimmed dolomite rhombs are a common textural feature indicative of dolomitisation (Carozzi, 1993), and similar rhombs (although more highly zoned) are present at Thalanga (Fig. 11.2b, 11.3e). Scattered zoned rhombs are evidence of incipient diagenetic dolomitisation, whereas mosaics of anhedral to subhedral crystals indicate complete dolomitisation (Carozzi, 1993). Thus, the zones of massive dolomite at Thalanga, with textures indicative of replacement, may have formed by the complete alteration of pre-existing calcite.

Bischoff and Seyfried (1978) showed experimentally that carbonates become more undersaturated as the temperature of seawater increases, and concluded that carbonates must form during low temperature alteration. This interpretation differs from Ellis (1963), who showed that calcite has reverse solubility and could precipitate directly from seawater oversaturated in $CaCO_3$ if rising high-temperature solutions mixed with and heated the

overlying seawater. Alternatively, calcite will be deposited in open spaces at elevated temperatures from acidic, HCO_3^- or CO_2-bearing hydrothermal solutions (Ellis, 1963; Holland and Malinin, 1979). As the carbonate textures at Thalanga are interpreted here to indicate replacement of a porous substrate rather than seafloor deposition, the latter scenario is favoured. In order to prevent dissolution of the calcite during cooling, there must be continuous input of HCO_3^- or CO_2 -bearing solutions because calcite solubility is also inversely proportional to available CO_2 (Browne, 1978).

At Thalanga, the early formed calcite may have been diagenetically altered to dolomite as the hydrothermal system evolved, either by rising hot Mg-rich fluids, or heating of circulating seawater. The textures of dolomite formed in this manner depend on the composition of the precursor, the grainsize and availability of dolomitisation nucleation sites, and the degree of saturation of the circulating solution with respect to the carbonate being replaced (Carozzi, 1993). Original fabrics are only preserved if the precursor was high-Mg calcite (Carozzi, 1993), and there were abundant nucleation sites. Even if the precursor calcite at Thalanga fulfilled these criteria, it is difficult to envisage the preservation of delicate compositional banding in rhombs, spheroids and void-fill textures in this model. Such fine compositional banding such as dolomite 4 (Table 11.3) must surely have only formed by the direct precipitation of dolomite. Therefore, it is interpreted that dolomite at Thalanga may have formed by the dolomitisation of calcite during the early stages of the hydrothermal alteration, with the majority of dolomite directly precipitated in remaining voids during later alteration.

Replacement of Anhydrite?

Chimneys or mounds around modern hydrothermal seafloor vents are commonly composed of porous sulphides with an outer margin or cap enriched in anhydrite (e.g. Janecky and Seyfried, 1984; Graham *et al.*, 1988; Paradis *et al.*, 1988; Fouquet *et al.*, 1991). Anhydrite is interpreted to precipitate due to heating of seawater, and mixing with the hydrothermal fluids, at the outer edge of chimneys and mounds (Ohmoto *et al.*, 1983; Janecky and Seyfried , 1984). Sulfur isotopes indicate that the SO_4^{2-} in anhydrite, formed at active seafloor hydrothermal centres, originated from seawater (Kusakabe *et al.*, 1982).

Anhydrite has also been noted within the subsurface at some modern seafloor settings, for example, calcite after anhydrite veins within pillow basalts (Alt *et al.*, 1986). The anhydrite in subsurface zones may have formed by (i) high temperature mixing of seawater and hydrothermal fluids at the top of the mixing zone in the vicinity of a hydrothermal vent, or (ii) initial seawater-basalt interaction in recharge zones. Alt *et al.* (1986) suggested that anhydrite veins in pillow basalts formed during earlier high temperature alteration, and were replaced by calcite during later, cooler alteration. Anhydrite is also replaced by

calcite in active chimneys in the Southern Trough of the Guaymas Basin as the temperature of the hydrothermal fluids increases (Peter and Scott, 1988).

Pre-existing anhydrite in the footwall at Thalanga may have either been dissolved by hydrothermal fluids, with carbonate precipitated higher in the stratigraphy, or carbonate may have directly replaced anhydrite that precipitated at the stratigraphic top of the rhyolitic volcanics. Direct replacement of anhydrite by calcite is interpreted to occur due to reaction with CO_2-or HCO_3^--rich hydrothermal fluids after sealing of the vent (Peter and Scott, 1988), and may proceed according to:

$$CaSO_4 + HCO_3^- + H^+ = CaCO_3 + H_2SO_4$$

The presence of rare bladed textures pseudomorphed by dolomite in the immediate footwall to ore at Thalanga may support this model (Fig. 11.3d).

Temperature of Dolomite Formation

Primary fluid inclusions are absent in mineral phases associated with carbonate at Thalanga. Consequently, precise estimates of the temperature of carbonate precipitation have not been determined. Domains of massive dolomite in the CTC's at Thalanga, composed of intergrown anhedral to subhedral grains, indicate that the temperature of dolomite formation was greater than 50°C (Gregg and Sibley, 1984). However, there is a wide range in estimations of the temperature of carbonate formation at both ancient and modern hydrothermal systems.

Fluid inclusion studies by Khin Zaw and Large (1992) showed that carbonate at Hercules precipitated between 150 and 250 °C, and could have been sourced from a hydrothermal fluid that evolved from seawater via circulation in the footwall volcanic units. At Rosebery, carbonate is interpreted to have formed from hydrothermal fluids of 200 °C to 250 °C (Dixon, 1980). Galley *et al.* (1993) suggest that at the Chisel Lake and North Chisel deposits in Manitoba, dolomitisation of early formed calcite occurred during mineralisation at temperatures of 350 - 450 °C, and that initial calcite precipitation occurred at lower temperatures. Active seafloor hydrothermal vents associated with anhydrite-calcite-barite chimneys and mounds in the Bering Sea are reported to vent fluids at 180 - 360°C (Sagalevich *et al.*, 1992), and fluid inclusions in calcite present in sulphide chimneys at the Southern Trough of the Guaymas Basin, indicate formation temperatures of 150 - 315 °C (Peter and Scott, 1988).

The similarity in carbonate textures and $\delta^{13}C$ and $\delta^{18}O$ values from the Rosebery (Dixon, 1980; Khin Zaw, 1991) and Thalanga deposits suggests that temperatures of formation could be similar. Therefore at Thalanga, initial calcite (or anhydrite) formation may have occurred at low temperatures (150-250°C), and may have been dolomitised as the temperature of the

hydrothermal solutions increased and sulphides were deposited (sphalerite-galena formed at 220-280°C; Large, 1992).

Sources of Cations

Solutions emanating from some modern seafloor hydrothermal vents are enriched in Ca^{2+} (Koski *et al.*, 1985; Von Damm *et al.*, 1985; Seyfried and Ding, 1993), and perhaps ancient seafloor hydrothermal vent fluids may have been similar in composition. Calcium is interpreted to have dissolved from plagioclase in the footwall rocks as warm, acidic hydrothermal fluids ascend to the seafloor. Alternatively Ca could be sourced from the overlying seawater, as in recharge zones Ca from seawater is partitioned into anhydrite (Seyfried, 1993). Subsurface zones of anhydrite may also have been a source of Ca for the carbonate at Thalanga.

Seawater is an obvious source of Mg for both the direct formation of dolomite and the metasomatism of calcite. Indeed, recent studies suggest that large-scale dolomitisation will only occur where continuous flushing of normal or slightly modified seawater is able to occur (Carozzi, 1993). Provided the underlying rhyolitic volcanics at Thalanga were porous, then seawater would have been able to circulate and mix with the hydrothermal fluids.

11.6.3 Formation of Chlorite

Sparse volcanic quartz crystals in the chlorite schist indicate a volcanic precursor. Herrmann (1994) regarded the chlorite schists as either of hydrothermal or metamorphic origin. He considered that with excess dolomite in the CTC's, quartz would be scavenged from the underlying quartz-sericite altered rhyolitic volcanics to produce tremolite during metamorphism, resulting in zones of silica depletion, now chlorite schist, at the boundary between the CTC assemblages and the rhyolitic volcanics. However, even without carbonate alteration or metamorphism, chlorite schists are commonly associated with footwall alteration at other VHMS deposits (e.g. Costa *et al.*, 1983; McLeod and Stanton, 1984; Schmidt, 1988; Large, 1992).

Lenses of Mg-rich chlorite associated with other VHMS deposits are considered to have formed either as chlorite or as a clay mineral precursor when seawater mixed with ascending hydrothermal solutions (Costa *et al.*, 1983; McLeod and Stanton, 1984; Offler and Whitford, 1992; Schmidt, 1988; Whitford *et al.*, 1989). McLeod (1987) suggested that Mg-rich chlorites and/or clays either precipitated on the seafloor or replaced volcanic glass. Chlorite could also form directly from high temperature ore-forming fluids during sulphide mineralisation (Schmidt, 1988), or the precursor clay minerals may have diagenetically altered to chlorite during sulphide mineralisation or regional metamorphism.

Experimental work (Bischoff and Seyfried, 1978) has shown that as normal seawater is heated to 350°C, its Mg content decreases as Mg-bearing minerals precipitate. Similarly, experimental reactions of seawater and rhyolite (Shiaki *et al.*, 1978) show that Mg is the first element to be removed from seawater. Urabe *et al.* (1983) used activity diagrams to demonstrate that substantial seawater is required to mix with ascending hydrothermal solutions in order to develop zones of intense Mg-rich enrichment. Modelling by Janecky and Seyfried (1984) also showed that Mg in hydrothermal fluids is derived from seawater, and that Mg metasomatism will occur in the sub-seafloor rocks as such fluids ascend. Therefore at Thalanga, the Mg-rich chlorite assemblages in the ore horizon probably formed either as chlorite or clays, when seawater interacted with hydrothermal solutions within a porous volcaniclastic zone at the stratigraphic top of the footwall rhyolitic volcanics.

Dolomitisation of early formed calcite or anhydrite may have occurred during formation of the Mg-rich chlorite or clays at Thalanga. Alternatively, Mg-rich clay formation may be contemporaneous with early calcite or anhydrite deposition. Dolomitisation of the primary calcite and diagenetic alteration of the neoformed clay to chlorite may have occurred during mineralisation.

Urabe *et al.* (1983) considered changing MgO/FeO ratios of chlorite to reflect a temperature gradient, with the most Fe-rich chlorites indicating the coolest temperatures of formation. Cathelineau and Nieva (1985) suggested that the Al occupancy of the tetrahedral site in chlorite increases with temperature, and therefore the Al content of chlorite can be used as geothermometer. Cathelineau (1988) and Bevins *et al.* (1991) suggested that the Al^{iv} content of chlorite also increases with temperature of metamorphism. However, the effect of high pressure on Al and Si substitution in chlorite is unknown and Kranidiotis and MacLean (1987) advised that the chlorite geothermometer may not be valid in high pressure metamorphic environments. They also suggested that chlorites recrystallised during metamorphism may be unsuitable for geothermometry. Therefore, estimation of the temperature of chlorite formation, using the chlorite geothermometer of either Walshe (1986) or Cathelineau and Nieva (1985), was not attempted as textural evidence indicates that the chlorite was recrystallised during upper greenschist facies metamorphism. Furthermore, Jiang *et al.* (1994) demonstrated that the apparent increase in Al^{iv} in chlorite with temperature is a function of decreasing abundances of mixed-layers and finely intergrown minerals.

Chlorite composition can be related to fS_2 and fO_2 if chlorite is in equilibrium with an alumino-silicate, magnetite, pyrite and/or pyrrhotite (Bryndzia and Scott, 1987a,b). If pyrite-pyrrhotite is stable, then fS_2 is high and the associated chlorite contains less Fe than chlorite in low fS_2 assemblages where pyrrhotite is stable (Bryndzia and Scott, 1987a,b). McLeod (1987) argued that the progressive Mg-enrichment in chlorites stratigraphically upwards within the ore zone, as occurs at Thalanga, reflects an increase in the cation-

exchange capacity of the precursor clays as conditions became more anoxic. In an increasingly anoxic environment, where total reduced sulphur is increasing, more Fe would be liberated from the clays to form pyrite (McLeod, 1987). Thus, increasingly Mg-rich chlorite should be associated with increasing pyrite, and given that all CTC chlorites are significantly enriched in Mg (Fig. 11.11a), the abundance of disseminated pyrite in the CTC units may reflect an anoxic depositional environment.

11.6.4 Model of CTC Formation

The interpreted requirements for carbonate-chlorite development at Thalanga were:
i) A porous footwall: Both carbonate and chlorite textures support Herrmann's (1994) interpretation that the CTC units formed by the alteration of the footwall rhyolitic volcanics. Evidence from Rosebery suggests that carbonate spheroids developed in porous volcaniclastic units (Hill and Orth, 1994; Orth and Hill, 1994). Zones of Mg-rich chlorite are considered to form when seawater is able to mix with ascending hydrothermal fluids in porous volcanic rocks (Urabe *et al.*, 1983). A porous footwall at Thalanga allowed both the upwards migration of hydrothermal fluids, the downward circulation of seawater, and the mixing of these two solutions in order to deposit both dolomite and chlorite, or precursor calcite and clays. Despite texturally destructive quartz-sericite-pyrite alteration in the footwall rhyolitic volcanics at Thalanga, there is evidence that parts of the footwall are composed of perlitic rhyolite and rhyolitic volcaniclastic units, which were porous and permeable prior to alteration (Chapter 4 and 10). Moreover, the dispersed nature of the footwall alteration zone reflects diffuse fluid flow through porous units, rather than focussed flow along fractures or faults (Chapter 10).

ii) An impermeable cap: An impermeable capping unit may have been required to prevent the exhalation of the hydrothermal solutions, and to trap the fluids in underlying porous rocks. Hill and Orth (1994) and Orth and Hill (1994) suggested that at Rosebery, either the upper part of the footwall pumiceous mass-flows, or the overlying pyritic black mudstone acted as a cap during the sub-seafloor carbonate alteration. Herrmann (1994) also considered an impermeable barrier necessary to force hydrothermal fluids to migrate laterally, but conceded that at Thalanga there is little evidence for such a cap rock. In West Thalanga, the most likely candidate is the overlying QEV. The matrix of the QEV in West Thalanga contains more silt than the QEV in East Thalanga, where the QEV is largely composed of porphyry clasts. Perhaps the more silty QEV in West Thalanga behaved as an impermeable capping unit, whereas the equivalent units in East Thalanga are more clast-supported in texture, and thus, were permeable. The deposition of the QEV units prior to formation of the CTC assemblages is consistent with the geochemical evidence that locally the CTC assemblages have Ti/Zr ratios similar to the overlying QEV units (Chapter 10).

Alternatively, early-formed anhydrite (temperatures = 150-250°C; Large, 1992) may have provided an excellent impermeable barrier and prevented venting of hydrothermal solutions. Either dolomite or calcite may have replaced the anhydrite, prior to sulphide mineralisation, as the temperature of the hydrothermal fluids increased. However, because of the geochemical evidence, the preferred interpretation is that the QEV units were the impermeable barrier.

iii) Cool hydrothermal fluids: Herrmann (1994) suggested that West Thalanga represents an area of cool temperature alteration and low fluid flow, and regarded East Thalanga as an area of high temperature and high hydrothermal fluid flow, and suggested that differences in temperature and fluid flow conditions during formation would account for the lack of CTC units in East Thalanga. Porous volcaniclastics in the footwall at West Thalanga would have allowed the circulation of seawater, thus decreasing the temperature of the hydrothermal solutions as the two mixed. The temperature of hydrothermal fluids in East Thalanga would have been elevated if either the hydrothermal fluids were unable to mix with seawater, or they were originally significantly hotter than those circulating in West Thalanga, or there was a much higher fluid flux in East Thalanga such that the effect of seawater was negligible (Herrmann, 1994).

iv) Glassy, felsic volcanic units? Herrmann (1994) presented compelling geochemical evidence that the CTC units at Thalanga have a rhyolitic precursor. Similarly, textural evidence suggests that the rocks were originally volcanic. It has been demonstrated that the footwall at Rosebery is composed of a series of pumiceous mass-flow deposits (Allen and Cas, 1990), and that this felsic glass has been replaced by carbonate similar in texture to that of Thalanga (Hill and Orth, 1994; Orth and Hill, 1994). Chlorite or precursor clays associated with VHMS mineralisation are also thought to have replaced glassy volcanic units in Kuroko deposits (Urabe *et al.*, 1983). Volcanic glass is thermodynamically unstable and therefore could easily and rapidly be altered during the mixing of hydrothermal fluids and seawater. The localised development of CTC units in West Thalanga could be interpreted to indicate that glassy volcaniclastics were restricted to the top of the footwall in West Thalanga. However, altered perlite indicates that glassy rhyolite are present at all levels in the footwall of both West and East Thalanga (Chapter 4), and porosity and localisation of fluids under an impermeable cap may have been a more important criteria for carbonate and chlorite alteration.

v) CO_2 or HCO_3^--bearing fluids: Isotopic studies suggest that the source of CO_2 or HCO_3^- -bearing hydrothermal fluids at Thalanga was Cambrian-Ordovician seawater. These solutions may have circulated through the Mount Windsor Volcanics and possibly mixed and re-equilibrated with magmatic water. The quartz-feldspar-porphyry (QFP) and QEV units at Thalanga are interpreted to be products of a volatile-rich magma chamber (Chapter 4),

and volatiles driven off this magma chamber and incorporated into the circulating hydrothermal solutions may have included CO_2 or HCO_3^-.

The model for carbonate- and chlorite-rich alteration at Thalanga is summarised in Figure 11.17. If an impermeable cap is required, then alteration must have commenced after deposition of the QEV, although diagenesis and possibly the first stages of carbonate and clay alteration may have begun when the seafloor was equivalent to the top of the footwall rhyolitic volcanics. Seawater was probably the source of the Mg in the clays, and perhaps calcite precipitated when the rising warm HCO_3^--bearing hydrothermal solutions encountered cool seawater, as the result of temperature and pH change (Fig. 11.17a). Glassy volcanic fragments and feldspar crystals probably provided suitable nucleation sites for spheroidal calcite formation, and early-formed anhydrite may have been replaced by calcite or dolomite.

With continuous influx of seawater and hydrothermal fluids, the early calcite was dolomitised, and perhaps the Mg-rich clays diagenetically altered to chlorite. Compositionally zoned dolomite grew in the remaining open spaces, possibly reflecting fluctuations in the dominance of seawater versus hydrothermal solutions. Intervals of clinozoisite-chlorite-tremolite within the footwall rhyolitic volcanics are more common in West and Central Thalanga than East Thalanga (Chapter 10), and are interpreted to be the metamorphosed equivalents of calcite-chlorite-quartz altered fluid pathways to the CTC assemblages in the ore horizon (cf. Rivers, 1985).

The influence of hydrothermal fluids is reflected in the zone of massive chlorite that directly overlies the quartz-muscovite ± pyrite-rich rhyolitic volcanics. The slightly lower MgO/FeO ratios of chlorite in this zone suggest that either seawater was less able to circulate, or hydrothermal solutions were more abundant at this position.

At some stage seawater was unable to circulate in the footwall. This may have occurred either as chlorite and carbonate alteration continued, and porosity eventually decreased, or because of the deposition of the impermeable QEV unit. Once seawater was not involved, and following the deposition of the most Mn-rich dolomite, metals were deposited from the rising hydrothermal solutions (Fig. 11.17b). Temperatures of 280-350°C are required for chalcopyrite deposition (Costa *et al.*, 1983; Pisutha-Arnond and Ohmoto, 1983; Large, 1992). Veins of sulphides have partly to completely replaced the chlorite-dolomite-quartz-(calcite) assemblage, with some sulphides possibly deposited on the seafloor.

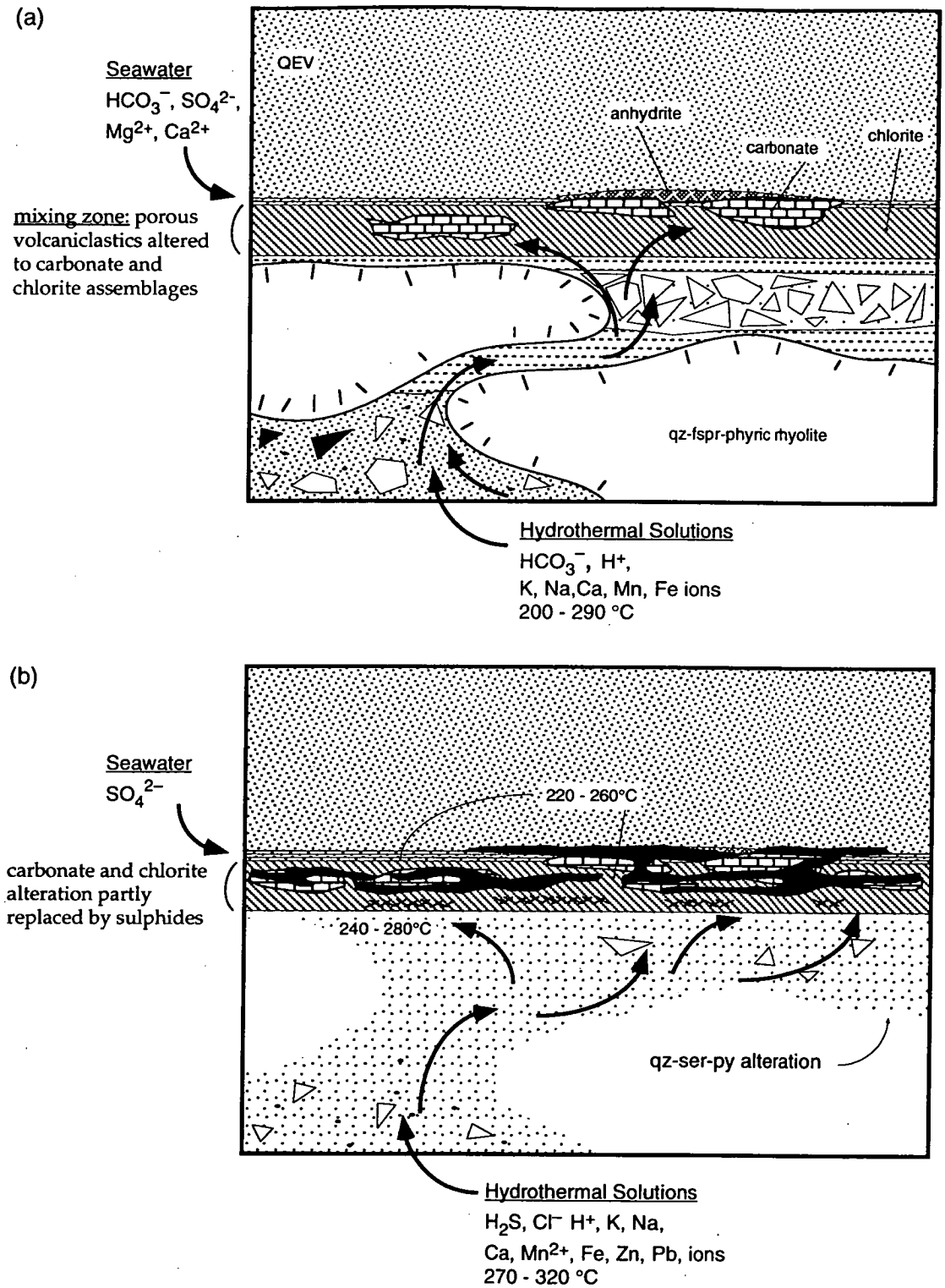

Figure 11.17 Sketches representing the formation of carbonate- and chlorite-rich assemblages at the stratigraphic top of the Mount Windsor Volcanics at Thalanga (adapted from Herrmann, 1994). (a) HCO_3^--bearing hydrothermal fluids circulate through the volcanic pile and mix with cool seawater in a porous and permeable unit beneath the seafloor position. The QEV stratigraphically overlies the incipient carbonate-chlorite alteration. (b) The volume of high temperature hydrothermal fluids increases, possibly as seawater is excluded, and sulphide minerals replace the carbonate-chlorite assemblages, with some sulphides precipitated on the seafloor. Primary volcanic textures in the rhyolitic footwall are overprinted by the quartz-sericite-pyrite alteration.

11.7 Summary

1. The main CTC assemblages are carbonate-chlorite-tremolite, chlorite-tremolite, and chlorite schist, and these are present at the stratigraphic top of the rhyolitic volcanics in West Thalanga and the western-most part of Central Thalanga.

2. Pre-metamorphic dolomite textures include spheroids, rhombs, void-fill, and massive dolomite, and strong zonation under CL reflects variation in Mn and Fe content of the dolomite. Spheroidal dolomite probably indicates growth in a porous substrate, and may have nucleated on and then replaced volcanic glass fragments. Dolomite rhombs with dusty, inclusion-rich cores and clear rims indicate the diagenetic dolomitisation of precursor calcite. Void-fill dolomite textures illustrate continuous dolomite dissolution and deposition. Rare dolomite pseudomorphs of rosettes of a bladed mineral suggest that dolomite may have replaced anhydrite in places.

3. C and O isotopic compositions of the dolomite at Thalanga suggest that the hydrothermal fluid was derived from Cambro-Ordovician seawater. Some CO_2 or HCO_3^- -bearing solutions may have been derived from the volatile-rich magma chamber that produced the QFP and QEV at Thalanga.

4. Chlorite in the CTC assemblages is Mg-rich, indicating circulation of seawater in the rhyolitic footwall and mixing with upwelling hydrothermal fluids. This supports the interpretation that the precursor rhyolite was porous and permeable, and therefore either volcaniclastic or composed of perlitic glass. It is not clear whether the chlorite represents Mg-rich clays diagenetically altered to chlorite during sulphide mineralisation, or directly precipitated chlorite.

5. The CTC assemblages are interpreted to be products of sub-seafloor replacement of rhyolitic material that occurred during the early stages of development of the hydrothermal system. Calcite formed initially when rising CO_2 or HCO_3^- -bearing fluids mixed with seawater in the porous rhyolitic volcanics. Calcite may have nucleated on and replaced feldspar crystals, glass fragments, and early-formed anhydrite. Diagenetic alteration of volcanic glass was probably co-incident with calcite formation, and resulted in the formation of Mg-rich clay minerals in spaces between volcanic fragments or in perlitic fractures. As the hydrothermal system continued to heat up (210-280°C), and seawater circulated through the porous volcaniclastics, the primary calcite was dolomitised, with further generations of dolomite precipitating in remaining open spaces. Primary clays may have altered to Mg-rich chlorite during this stage. Sulphides precipitated in remaining voids, partly corroding and replacing dolomite, following the deposition of the most Mn-rich dolomite.

6. The QEV units overlying the CTC units in West Thalanga are interpreted to have been deposited prior to CTC formation, and may have acted as an impermeable barrier, trapping hydrothermal solutions and restricting alteration to a narrow zone along the upper part of the rhyolitic volcanics.

CHAPTER 12.

CONTROLS ON THE GENESIS OF THALANGA

12.1 Syngenetic vs Epigenetic Mineralisation

12.1.1 Timing of Deformation and Metamorphism

At Thalanga, two main deformation events (D_2 and D_3) and at least one metamorphic event has been identified on the basis of overprinting relationships (Chapter 3). Despite the recognition of pre-D_2 structures elsewhere in the Mount Windsor subprovince (Berry *et al.*, 1992), there is no evidence of a D_1 deformation event in either the host stratigraphy or the massive sulphide lenses at Thalanga. The steeply, south-dipping bedding and subvertical S_2 cleavage are the most prominent manifestations of D_2 at Thalanga, and S_2 is typically strongly defined in the hydrothermally altered units stratigraphically underlying and within the ore horizon, and phyllosilicate-rich volcaniclastic units stratigraphically overlying the massive sulphides. Compositional banding within the massive sulphide lenses is subparallel to S_2, and locally parallel to S_3, and is therefore interpreted to have formed in response to D_2.

Subvertical extension during D_2 produced steeply-plunging mineral and clast elongation lineations, boudins with subhorizontal necks, and subhorizontal extension veins in units both within, underlying and overlying the ore horizon. Sulphides were remobilised into dilated areas during this extension, and were also remobilised during D_3 normal faulting. Remobilised sulphides are distinguished from non-remobilised sulphides by their substantially greater chalcopyrite content.

Textures such as the preferential development of S_2 cleavage in phyllosilicate-rich hydrothermally altered units, together with the presence of recrystallised quartz in pressure shadows (parallel to S_2 and S_3) around pyrite grains, provide unequivocal evidence that alteration associated with the formation of the Thalanga massive sulphide deposit pre-dated D_2. The presence of chalcopyrite-rich remobilised sulphides in pressure shadows, boudin necks and subhorizontal veins also indicates that the massive sulphide lenses must pre-date D_2 and regional metamorphism, and did not form by the syn-deformational replacement of the stratigraphy (cf. Aerden, 1991; 1993; 1994b).

12.1.2 Relationship Between Hydrothermal Alteration and Massive Sulphides

Distribution of Alteration Assemblages

At Thalanga, the most intense region of hydrothermal alteration is present in the rhyolitic volcanics that stratigraphically underlie the massive sulphide lenses. The texturally destructive alteration has been metamorphosed and is now composed of quartz-muscovite ± phlogopite ± chlorite ± pyrite-rich assemblages that are at least 200 m thick and extend along the strike length of the massive sulphide lenses. The pre-metamorphic assemblages are inferred to have been quartz-sericite ± Mg-rich chlorite ± pyrite. This blanket-style alteration pattern is consistent with the diffuse flow of ascending hydrothermal solutions through a porous and permeable footwall (cf. Morton and Franklin, 1987; Large, 1992).

Stringer zones, comprising 2-50 % pyrite veins (now folded with axial planes subparallel to S_2) in quartz-muscovite-rich footwall rhyolitic volcanics, are subparallel to stratigraphy and intersect the ore horizon at a low angle. This semi-conformable geometry is interpreted to indicate that mineralising solutions were channelled along favourably permeable units. Typically, the thickest and most massive parts of the sulphide lenses are located at the intersection of the pyrite stringer zones with the overlying ore horizon. QFP and QEV units underlying massive sulphides in East and Central Thalanga are also moderately to strongly altered, with quartz-muscovite-phlogopite assemblages and local pyrite and/or pyrite-sphalerite stringer veins.

Alteration of the units that stratigraphically overlie the ore horizon is significantly less pervasive, and more limited in extent, than the alteration of the footwall rhyolitic volcanics. Epidote ± tremolite ± chlorite ± quartz assemblages are present in the QEV, QFP and dacite in places, and vary from vein-controlled to irregular domains of pervasive alteration. The pre-metamorphic alteration assemblages are inferred to have mainly consisted of calcite, chlorite and quartz. This asymmetry to the distribution and composition of alteration associated with massive sulphide formation is interpreted to indicate that alteration and mineralisation was syn-volcanic, and occurred prior to deposition of the hangingwall fragmental and dacite (Chapter 10).

Further demonstration of the asymmetry of the alteration assemblages at Thalanga lies in comparison of the composition of biotite and chlorite from the units underlying the massive sulphides to those units overlying the massive sulphide lenses. Mg-rich phlogopite and Mg-rich chlorite are disseminated in the footwall rhyolitic volcanics and intergrown with the highly Mg-rich chlorite schist and carbonate-chlorite-tremolite (CTC) assemblages present within the ore horizon at West and Central Thalanga. Phlogopite is also disseminated in the QEV and QFP units within the ore horizon. In contrast, Mg-poor biotite is present in the HWF

and dacite overlying the massive sulphides at Thalanga, and also in the footwall rhyolitic volcanics at the outer margins of the hydrothermal alteration zone. This compositional variation is interpreted to reflect the bulk composition of the metamorphic precursor, indicating that the units underlying and associated with the massive sulphides were altered by Mg-rich hydrothermal solutions. Mg-rich alteration assemblages are considered to have formed in response to the mixing of abundant seawater with hot hydrothermal solutions (e.g. Schmidt, 1988), and therefore requires that the rhyolitic volcanics underlying Thalanga were sufficiently porous and permeable to allow the infiltration of cold Mg-bearing seawater, and mixing with rising, warmer, hydrothermal solutions.

Timing and Significance of Intense Silicification

Local areas of intense silicification at the stratigraphic top of the rhyolitic volcanics are typically not overlain by massive sulphides. Silicification is therefore interpreted to have occurred prior to sulphide deposition, and resulted in reduced permeability which blocked the ascent of hydrothermal solutions. This interpretation is supported by local gradational contacts between domains of intense silicification and regions of typical footwall quartz-muscovite-pyrite assemblages (although in some cases the margins of intensely silicified rhyolitic volcanics are sharply defined by brittle faults). These gradational contacts are interpreted to indicate that mineralising solutions, which could not pass through the thickest parts of intense silicification, were only able to overprint the limits of the intensely silicified domains before depositing sulphides at the stratigraphic top of the rhyolitic volcanics. Massive sulphide lenses overlying the margins of the intensely silicified rhyolitic volcanics in East Thalanga are thicker and have higher grades of Zn, Pb, Cu and Ag than massive sulphide lenses along strike, and this could be due to higher fluid flow rates at the margins of the intensely silicified rhyolitic volcanics (Chapter 8). Alternatively, the metal content of the ore lens in this region may also have been enriched by remobilisation into a macro-pressure shadow during D_2.

In less altered parts of the footwall rhyolitic volcanics, perlitic fractures have been replaced by muscovite, phlogopite and chlorite, and these altered perlite textures have been subsequently overprinted by fine grained, equant, anhedral quartz. This suggests that locally silicification post-dated weak sericite-chlorite alteration.

Origin of the Carbonate- and Chlorite-Rich Assemblages

Recent immobile element studies and mass balance calculations (Herrmann, 1994) have shown that the chlorite schist and the overlying CTC assemblages within the ore horizon at West and Central Thalanga are geochemically equivalent to strongly altered and metamorphosed rhyolitic volcanics. Comparison of immobile element ratios also suggests that parts of the

CTC units may be intensely altered QEV units (Chapter 10). This supports the interpretation that the QEV must have been deposited prior to formation of the chlorite schist and CTC units, and acted as a relatively impermeable barrier, allowing the low temperature alteration of the top of the rhyolitic volcanics (Chapter 11).

Initially calcite is inferred to have replaced glassy volcanic fragments, and Mg-rich chlorite (or neo-formed Mg-rich clay minerals) probably filled spaces between the clasts. These processes require the addition of Ca and CO_2 (or HCO_3^-) to the hydrothermal solutions. Cambrian-Ordovician seawater was the main source of HCO_3^- and some CO_2 may have been magmatic in origin. The Ca may have been leached from volcanic plagioclase crystals or from anhydrite which formed earlier by the low temperature (150-250°C) heating of seawater. The calcite is inferred to have been dolomitised as the temperature of the hydrothermal solutions increased (210-280°C). With increasing temperatures, or accompanying dolomitisation, sulphides filled remaining voids and formed as veins of massive to banded sulphides, subparallel to the seafloor, in the CTC assemblages (Chapter 11).

Extensive chlorite schist and CTC assemblages did not form at East Thalanga because the QEV had not been deposited prior to low temperature alteration or was too porous to allow concentration of the hydrothermal solutions at the stratigraphic top of the rhyolitic volcanics. The non-deposition of QEV in the Vomacka Zone may explain the lack of CTC assemblages and chlorite schist in this part of the ore horizon at Thalanga.

12.2 Importance of Volcanism at Thalanga

Observations concerning the relationship between massive sulphide lenses and volcanism at Thalanga are:

i) the massive sulphide lenses are located at the stratigraphic top of rhyolitic volcanics (Mount Windsor Volcanics; Ti/Zr ~ 2-5). Although in most places at Thalanga the original volcanic textures have been destroyed by alteration, evenly distributed quartz phenocrysts indicate that most parts of the footwall are composed of coherent rhyolite. The least altered parts of the footwall are composed of perlitic rhyolite lavas, domes, and/or sills, with rhyolite autobreccia, rhyolite hyaloclastite breccia, rhyolitic pumice-bearing breccia, and rhyolitic sandstone;

ii) the rhyolitic volcanics reach a maximum of about 1200 m in thickness at Thalanga, and decrease in thickness (to 500 m) within 6 km along strike. This increase in thickness may be partly due to structural repetition, but is also interpreted to be a primary feature;

iii) the massive sulphide lenses at Thalanga are spatially associated with, and have similar areal extent to, coarse quartz-bearing units that comprise the ore horizon. The QEV breccia, QEV sandstone and syn-volcanic QFP sills (Ti/Zr ~ 8-12) are located at the

base of the Trooper Creek Formation (although rare QFP sills are also present in units overlying the ore horizon; Paulick, 1996);

iv) units that stratigraphically overlie the ore horizon include the hangingwall fragmental (HWF; a quartz-feldspar siltstone to sandstone and graded breccia unit), dacite 1 lava with 5-10 % feldspar phenocrysts (Ti/Zr ~ 15-20), sparsely feldspar-phyric dacite 2 lava (Ti/ Zr ~9-12), polymict dacite-rhyolite breccia units, and syn-volcanic andesite sills. Dacite lava is not present along strike from the massive sulphide lenses. The nearest coherent dacite is located about 2 km along strike from Thalanga;

v) lenses of quartz-magnetite (metamorphosed, hydrothermal seafloor quartz-hematite deposits according to Duhig *et al.*, 1992) are present along strike from the massive sulphide lenses at Thalanga in stratigraphically equivalent positions, as well as at the stratigraphic base of the rhyolitic volcanics, and the stratigraphic top of both the QFP and dacite lavas in places.

These characteristics suggest that deposition of massive sulphides at Thalanga coincided with an abrupt change from rhyolitic volcanism to deposition of distinctive polymict, coarse quartz-bearing mass flow deposits (QEV) and emplacement of syn-volcanic sills (QFP), followed by the emplacement of dacite lavas and associated breccia units, and syn-volcanic andesite sills. There is no lithological evidence that the change in volcanic composition and formation of massive sulphides coincided with a major depositional hiatus (except for thin graded sandstone and siltstone units that locally underlie the footwall lens in East Thalanga). Quartz-magnetite lenses along strike from Thalanga indicated some period of hydrothermal alteration after the deposition of the rhyolitic volcanics, as well as following emplacement of the QFP and dacite.

Lithofacies variations show that most parts of the rhyolitic footwall to Thalanga would have been glassy, highly porous and permeable, and this is consistent with the diffuse, blanket-style distribution of the footwall alteration. The substantial thickness of the rhyolitic volcanics underlying Thalanga is attributed to the abundance of coherent rhyolitic units, with possibly some repetition due to faulting. It is therefore inferred that Thalanga is located at the stratigraphic top of a rhyolitic volcanic centre. Local feldspar- and quartz-bearing sandstone within the footwall rhyolitic volcanics is interpreted to have an extra-basinal source, and to have been emplaced by subaqueous mass flows (Chapter 4). This indicates that parts of Thalanga must have been a depocentre at times. Constructional volcanism during deposition of the Trooper Creek Formation (syn-volcanic QFP and andesite sills, dacite lavas) is also concentrated at Thalanga, rather than along strike from the massive sulphide lenses, suggesting that this area remained a volcanic centre during emplacement of the Trooper Creek Formation.

The QEV units contain rare altered QFP pumice clasts and abundant free quartz and feldspar crystals, which may have formed by the explosive eruption of a vesicular, porphyritic magma (Chapter 4). Other non-vesicular QFP, rhyolite, siltstone, and massive sulphide clasts were probably incorporated during transportation of the QEV by mass flows. An explosive eruption implies water depths of ≤1 km at the source vent (McBirney, 1963). If the thick underlying rhyolitic volcanics had created a topographic high, then in order for volcaniclastic components to have been deposited at Thalanga, the site of explosive eruption must have been near Thalanga. Alternatively, intense quench fragmentation of a partly pumiceous subaqueous QFP dome or lava may have generated both abundant crystals, and non-vesicular and pumiceous QFP clasts. Transportation to the sites of deposition at West and East Thalanga by mass flows may have followed gravitational collapse of the dome. The spherulitic QFP mega-clasts in Central Thalanga may be remnants of this dome. Some non-vesicular QFP clasts are inferred to be blocky peperite margins of QFP sills that intruded while the QEV was wet and unconsolidated (Chapter 4). This second interpretation is preferred because the QEV has lithofacies characteristics (poorly sorted, variable crystal concentration) consistent with a proximal setting and limited transport distances.

The location of a volcanic centre in the vicinity of Thalanga implies that there would have been high heat flux prior to and during the formation of the massive sulphides. Large-scale hydrothermal convection cells may have been generated due to the presence of a magma chamber at depth, allowing the circulation of seawater (see section 12.5) down through the rhyolitic volcanics and potentially the underlying sandstone and siltstone of the Puddler Creek Formation (section 12.6). As well as providing an important heat source, the magma chamber may also have contributed volatiles (e.g. CO_2 for carbonate formation), and potentially metals (see section 12.5) to the ascending hydrothermal solutions.

Perhaps the formation of massive sulphides at Thalanga was closely linked to the change in volcanic composition from rhyolitic through to dacitic and andesitic volcanic units. The intimate spatial and temporal association between the massive sulphide lenses and the QEV and QFP at Thalanga (see section 12.5) may indicate a genetic association. The Britannia prospect, within the Mount Windsor subprovince, is also spatially associated with coarse quartz bearing units (C.J. Kendall, pers. comm., 1996). The large size of the quartz crystals in the QFP and QEV units, indicates that the parent magma contained elevated volatile contents, and therefore could have provided some components to the mineralising solutions. Alternatively, the circulation and ascent of the hydrothermal solutions may have been driven by the parent magma chamber of the QEV and QFP units (and later dacite lavas).

12.3 Seafloor Sulphide Deposition vs Sub-seafloor Replacement

The mineralogical and metal zonation at Thalanga provides the best guide to the formation and growth of the massive sulphide deposit. Typically, massive to semi-massive pyrite ± chalcopyrite with Mg-rich chlorite gangue directly overlies the footwall rhyolitic volcanics, and is overlain by massive sphalerite-galena-pyrite ± chalcopyrite-rich sulphides, containing quartz, barite, chlorite, phlogopite and muscovite gangue. Barite-rich sulphides are present in the uppermost and more distal parts of the ore lenses, and quartz magnetite lenses are the distal equivalent of the massive sulphides (Duhig *et al.*, 1992). This distribution of sulphides is reflected in the metal zonation, whereby Zn, Pb, Ag and Ba are enriched at the stratigraphic top of the ore lenses (Chapter 8). The distribution of elevated Cu is partly controlled by stratigraphy (regions of high Cu associated with massive pyrite at the base of the ore lenses) and partly structurally controlled. High grades of Cu typically coincide with faults or zones of extension (especially at the stratigraphic top of the ore lenses). The gross zonation in sulphide and gangue distribution at Thalanga is comparable to the mineralogical zonation reported from other ancient less metamorphosed VHMS deposits (e.g. Hellyer, Rosebery, Woodlawn; Large, 1992) and from the Kuroko deposits of Japan (Eldridge *et al.*, 1983).

Possible mechanisms for the genesis of sheet-style massive sulphide deposits have been reviewed by Large (1992). The main models of sulphide deposition are (i) seafloor deposition from a dense brine (Sato, 1972; McDougall, 1984; Solomon *et al.*, 1990), (ii) seafloor deposition as a mound or series of coalesced mounds (Knuckey *et al.*, 1982; Eldridge *et al.*, 1983; Huston, 1988; Lydon, 1988; Large *et al.*, 1988; Large, 1992), and (iii) sub-seafloor replacement of favourable horizons (Williams, 1979; Goodfellow and Blaise, 1988; Goodfellow and Franklin, 1993; Franklin, 1990; Zierenberg *et al.*, 1993; Bodon and Valenta, 1995).

12.3.1 Brine Pool vs Mound Model of Sulphide Mineralisation

The cyclic compositional banding in the massive sulphides and stratified geometry of the ore lenses at Thalanga lead Gregory *et al.* (1990) to suggest that the massive sulphides were deposited from a dense brine, and the location of the ore lenses within basins at the top of the rhyolitic Mount Windsor Volcanics, as defined by the location of QEV units, supports the brine pool model. So do the locations of QFP sills (partially, but not consistently, antithetic to massive sulphides; Chapter 4), whereby topography created by emplacement of QFP sills controlled the location of local basins and thus the site of sulphide deposition from a dense brine (cf. Boulter, 1993). Alternatively, QFP sills may have blocked the ascent of hydrothermal fluids, which probably then vented and deposited sulphides laterally from the sill.

The lack of primary fluid inclusions within the massive sulphides at Thalanga and evidence for the high salinities required to form a dense brine (cf. McKay and Walshe, 1990; Solomon *et al.*, 1990) means that the brine pool model cannot be adequately tested at the Thalanga massive sulphide deposit. However, the position of the QEV units at Thalanga does provide evidence of the location of basins at the time of QEV deposition, and given that QEV deposition was syn-sulphide mineralisation (see section 12.3.2), then dense brines capable of forming massive sulphides would also concentrate in these areas. The lack of QEV units in the Vomacka Zone is interpreted to indicate that this part of the ore horizon was a topographic high during QEV deposition (Chapter 4). Therefore, deposition of the barite-rich sulphide lens in the Vomacka Zone must also have occurred on a topographic high and is unrelated to brine pool development.

In parts of the hangingwall lens in East Thalanga, barite-rich massive sulphides and polymetallic massive sulphide lenses occur at the same stratigraphic location (e.g. the hangingwall lens, East Thalanga; Chapter 6). The proximity of these sulphides with differing composition is more consistent with a mound model (rather than brine pool model) of sulphide formation, because in modern seafloor hydrothermal vents, high temperature fluids emanate from polymetallic sulphide chimneys and mounds (black smokers) while adjacent low temperature barite-silica-sulphide chimneys (white smokers) simultaneously vent cooler hydrothermal fluids (Lydon, 1988; Fouquet *et al.*, 1993). The gross mineralogical zonation, from pyrite ± chalcopyrite at the base of the massive sulphide lenses, to sphalerite-galena-pyrite ± barite-rich sulphides at the top, may support the zone-refining processes thought to operate in the mound model of sulphide deposition (Eldridge *et al.*, 1983; Huston and Large, 1989; Large, 1992).

However, the gradation up- and down-dip within the sulphide lenses in all parts of Thalanga, from massive sulphides, to semi-massive sulphides, to no sulphides is more consistent with a replacement origin than a mound model of sulphide formation. Furthermore, the brine pool model does not explain the gradational contact between the massive sulphide lenses and the stratigraphically overlying QEV units in East Thalanga, nor is it consistent with the vein-style massive sulphide lenses in West Thalanga.

12.3.2 Evidence for Syn-volcanic Replacement Origin of the Massive Sulphides

Critical evidence of the timing between deposition of the host sequences and the massive sulphide lenses is:

i) clasts of QFP and rhyolite are present in massive sulphides in Central Thalanga and the footwall lens in East Thalanga. Single QFP clasts within the footwall massive sulphide lens are unlikely to have been deposited during formation of the sulphides, and it is more probable that the coarse grained base of the QEV breccia facies was replaced during

sulphide mineralisation. The rhyolite clasts are interpreted to be either relicts of the footwall rhyolite between coalesced sulphide veins or else part of the QEV breccia;

ii) massive sulphide clasts occur within the QEV in both West and East Thalanga. This is interpreted to indicate that massive sulphide lenses were exposed on the seafloor and were eroded and deposited with the QEV breccia. Given that the QEV breccia is inferred to be a proximal volcaniclastic deposit, then the source of the massive sulphide clasts must have been close to Thalanga;

iii) gradation down-dip in the footwall lens in East Thalanga, from minor disseminated sulphides in QEV, to semi-massive sulphides hosted in the QEV breccia facies, to massive sphalerite-pyrite-rich sulphides, to massive pyrite ± chalcopyrite-rich sulphides, to semi-massive sulphides in footwall rhyolitic volcanics. This gradation is interpreted to be the result of replacement along the base of the QEV. However, domains of massive sulphides that do not contain QFP clasts are not considered to have formed by the total replacement of the QEV (unless there had been a precursor alteration stage), and may represent regions of seafloor sulphide deposition;

iv) massive sulphide veins are present between QFP clasts at the base of the QEV that stratigraphically overlies the footwall lens in East Thalanga. These veins are interpreted to have formed during the migration of mineralising solutions through the QEV breccia and represent partial replacement of the base of the QEV;

v) quartz-muscovite ± phlogopite ± pyrite-rich QEV units, with thin subvertical pyrite and pyrite-sphalerite stringer veins, are present between the footwall ore lens and the overlying hangingwall ore lens in East Thalanga and occur with the ore lenses in Central Thalanga. These assemblages are typical of metamorphosed footwall-style alteration and are interpreted to indicate that deposition of these units pre-dated massive sulphide formation, and that hydrothermal solutions ascended through the QEV;

vi) the hangingwall lens in East Thalanga partly comprises semi-massive sulphides in the matrix of the upper rhyolite breccia, but grades to massive barite with minor sulphides or massive sulphides up-dip, and then to semi-massive sulphides hosted in the coarse grained base of QEV sandstone units. This relationship is interpreted to be consistent with replacement of the upper rhyolite breccia and possibly partial seafloor deposition. The concentration of sulphides at the base of graded QEV sandstone units is probably the result of replacement rather than simultaneous deposition of sandstone and sulphides;

vii) in the Vomacka Zone there is a gradation within the ore lens up-dip from weakly mineralised rhyolite breccia, to sulphide-barite veins in rhyolite or polymict rhyolite breccia, to massive sulphides ± barite. The requirement of a seawater source of sulphate for barite formation (as determined by sulphur isotopic ratios; Chapter 9) is evidence that barite-rich massive sulphide lenses were deposited on the seafloor. The presence of sulphide-barite veins within the matrix of breccia down-dip from the barite-rich sulphides indicates that both sub-seafloor and seafloor sulphide deposition occurred simultaneously;

viii) the ore lens in Central Thalanga grades up-dip from weakly disseminated to vein style sulphides in the footwall rhyolitic volcanics, to massive sulphides, with patchy semi-massive sulphides in CTC units. Massive sulphide lenses may have been deposited on the seafloor in Central Thalanga. Locally the HWF does not overlie the massive sulphides (Chapter 3 and 4), implying that the massive sulphides had formed as a topographic high or mound in places. However, both the up- and down-dip margins are interpreted to have formed by the replacement of the footwall rhyolitic volcanics or the CTC units;

ix) in West Thalanga, the ore lens grades up-dip from weakly disseminated and vein-style sulphides in footwall rhyolitic volcanics, to massive sulphides, to anastomosing massive sulphide veins in CTC alteration assemblages, to semi-massive sulphides in CTC units, to weakly disseminated sulphides in thin CTC units. This gradation is interpreted to be consistent with sulphide replacement and veining in the earlier-formed CTC units;

x) a QFP unit is interpreted to have intruded into wet and unconsolidated QEV breccia in East Thalanga (Chapter 4). Typically, the QFP sills in East Thalanga are only weakly altered (metamorphosed to patchy chlorite-quartz- or epidote-quartz-rich assemblages) and the hangingwall lens is not present overlying QFP sills.

12.4 Structure at the Time of Mineralisation

There is no evidence of highly focussed fluid flow in the footwall at Thalanga, other than the semi-conformable pyrite stringer zones, which may have formed as mineralising solutions were concentrated along more permeable breccia units between coherent rhyolite. Lenses of massive pyrite ± chalcopyrite underlie polymetallic sulphide lenses in the eastern part of West Thalanga, in most parts of Central Thalanga and in the down-dip parts of East Thalanga (Chapter 6 and 8). The massive pyrite is interpreted to have formed above the main zones of hydrothermal discharge.

When restored to pre-deformation geometry, the sulphide lenses and QEV units are located within two elongate basins that pitch shallow-moderately east on long section (Chapter 8). The distribution of massive pyrite and other possible feeder zones (identified on the basis of coincident high Cu ratios and low Zn ratios) is subparallel to the pitch of the pre-deformational orebodies (Chapter 8). This geometry may have been controlled by a major, similarly-oriented structure that was overprinted during alteration and mineralisation. The asymmetric distribution of massive pyrite within the West and Central Thalanga orebody is consistent with the eastern part of Central Thalanga being located at the major zone of hydrothermal discharge (Chapter 8).

Barite-rich sulphides typically occur at the margins and tops of massive sulphide deposits, and are interpreted to form during the waning of the hydrothermal system (cf. Eldridge *et al.*,

1983; McArthur and Dronseika, 1990; Large, 1992). Massive barite and barite-rich sulphides in the ore lenses at Thalanga are therefore interpreted to have formed from lower temperature (and oxidised) hydrothermal solutions either at the top or side margins of the deposit. Thus the barite-rich Vomacka Zone may be the western margin of the East Thalanga ore lens. The lack of continuity of ore lenses from the Vomacka Zone to Central Thalanga (as determined from available drill holes) supports the interpretation that the East Thalanga ore lens was fed from a separate hydrothermal vent to West and Central Thalanga.

12.5 Composition and Origin of Mineralising Solutions

12.5.1 Composition of Hydrothermal Solutions

No primary fluid inclusions have been preserved in either sphalerite or quartz within the massive sulphide lenses at Thalanga due to the multiple deformation and metamorphic events. Therefore the composition of the ore-forming fluids and physicochemical conditions cannot be precisely determined. However, a reasonable estimate of the composition of the ore-solutions can be made by comparing the sulphide and gangue mineralogy of the massive sulphide lenses, and the composition of the footwall and hangingwall alteration with those of less deformed massive sulphide deposits (e.g. deposits in the Hokuroko district of Japan, Eldridge *et al.*, 1983; Pisutha-Arnond and Ohmoto, 1983; and Hellyer and Millenbach deposits, Huston and Large, 1989). The morphology of the massive sulphide lenses at Thalanga, with massive pyrite ± chalcopyrite at the base overlain by sphalerite-galena-pyrite-rich sulphides and barite-rich sulphides at the stratigraphic top, is consistent with deposition of the sulphides from a slightly acidic VHMS fluid (pH = 4, salinity = 1 molal NaCl, $a_{H_2S} = 10^{-2.5}$, $SO_4^{2-}/H_2S = 10^{-1}$, $fO_2 = 10^{-35}$ atm at 300°C and in equilibrium with pyrite; Large, 1992).

The temperature of the mineralising solutions would have changed throughout the deposition of sulphides (see section 12.6), and such changes are manifest in the distribution of pyrite and chalcopyrite at the base, compared to sphalerite, galena and barite at the stratigraphic top of the ore lenses. Although textural evidence indicates that magnetite has replaced sphalerite and chalcopyrite in parts of the massive sulphide lenses (Chapter 7), the restriction of most of the minor magnetite to the pyrite stringer zones and lenses of massive pyrite is consistent with deposition of these sulphides from a moderately oxidised fluid. The presence of barite in the upper parts and lateral extremities of the ore lenses indicates that the mineralising solutions became more oxidised with time (due to mixing with seawater).

12.5.2 Source of Sulphur

The sulphur isotopic composition of pyrite disseminated in the altered rhyolitic volcanics (7.6-17.3 ‰) is consistent with the formation of pyrite from hydrothermal solutions containing a mixture of dissolved igneous sulphur and Cambro-Ordovician seawater that had been inorganically reduced during hydrothermal convection. The $\delta^{34}S$ values of pyrite increase towards the stratigraphic top of the footwall and are interpreted to indicate mixing between the ascending hot, hydrothermal solutions with partially reduced, cold seawater near the top of footwall (Chapter 9). The $\delta^{34}S$ values of barite (27.6-32.4 ‰) are consistent with a direct seawater source of sulphate.

12.5.3 Source of Metals

The main models for the origin of metals within hydrothermal solutions associated with the formation of massive sulphide deposits are: 1) convection of seawater (driven by heat from an underlying magma chamber) and leaching of metals from the volcanic pile; 2) direct input of metals exsolved from subvolcanic magma chambers; and 3) a mixture of both sources of fluids (e.g. Franklin *et al.*, 1981; Large, 1992). Interpretation of S, O and H isotopes, and trace element data from VHMS deposits in the Hokuroko district in Japan, in North America, and in western Tasmania has suggested that seawater was the main source of hydrothermal solutions and that metals within massive sulphide deposits were leached from the underlying rocks by circulating, contemporaneous seawater (Sangster, 1968; Solomon, 1976; Green *et al.*, 1981; Hutchinson, 1982; Ohmoto *et al.*, 1983; Pisutha-Arnond and Ohmoto, 1983; Solomon *et al.*, 1988; Gemmell and Large, 1992; Stolz and Large, 1992).

However, Sawkins and Kowalik (1981) and Stanton (1985, 1991) have argued that the volume of rock required to be leached is unrealistically large (Solomon (1976) estimated volumes of 49-100 km^3 in order to generate Rosebery and Mount Lyell; Stolz and Large (1992) estimated a volume of about 70 km^3 in order to generate Hellyer), and that metals within VHMS deposits are more easily derived from magmatic fluids. Furthermore, salinities of fluid inclusions within the Kuroko deposits have been interpreted to support a magmatic contribution to hydrothermal solutions (Urabe and Sato, 1978; Bryndzia *et al.*, 1983), as have S isotopes (Ishihara and Sasaki, 1978).

However, most proponents of the magmatic model agree that the contribution of seawater to the hydrothermal solutions that formed VHMS deposits is important, and consequently a model involving both a seawater and magmatic input to the hydrothermal solutions has been suggested (Sawkins, 1986; Stanton, 1985, 1991; Large, 1992). Sawkins (1986) and Stanton (1985, 1991) have argued that small volumes of magmatic solutions, with high concentrations of metals, may mix with large volumes of seawater in the upper part of the volcanic pile prior

which metals may have been sourced from both magmatic fluids and leaching of the volcanic pile by seawater, and proposed that soluble metals (Zn, Pb, Ba, Ag, and traces of As, Sb, Hg, and Tl) may have been leached from the volcanic pile during hydrothermal convection (T = 100-250 °C), and that less soluble metals (Cu, and traces of Bi, Sn, Mo, and Te) may be derived directly from magmatic sources. Consequently, Large (1992) also suggested that proximity to the magmatic centre may be reflected by the metal content of the massive sulphide deposit, and that Cu-Au-rich deposits may have been close to the magmatic source (e.g. Mount Lyell, Mount Morgan), whereas Zn-Pb-Cu-rich deposits were located further from the magmatic centre (e.g. Rosebery, Woodlawn).

A similar relationship between metal content of the massive sulphide deposits in eastern Australia and source of metals has been suggested by Huston *et al.* (1995b) on the basis of the Se content of pyrite. These workers showed that the Se content of pyrite is a reasonable indicator of the source of the hydrothermal solutions, and concluded that elevated Se in pyrite indicates a magmatic hydrothermal input. Huston *et al.* (1995b) concluded that i) low temperature Zn-rich, Cu-poor massive sulphide deposits have low Se levels and therefore formed from fluids with Se/S ratio consistent with evolved seawater; and ii) high temperature, Cu-rich massive sulphide deposits have high Se levels (particularly within the stringer zones and base of massive sulphide lenses) and formed from solutions with Se/S ratio consistent with magmatic fluids.

The source of ore metals at Thalanga has not been constrained, although sulphur isotopic ratios are consistent with a significant seawater component. The recent studies summarised above have indicated that many recent and ancient VHMS deposits may have formed from hydrothermal solutions that contained metals derived directly from a magmatic source and from the volcanic pile which had been leached by contemporaneous seawater. Metals within the ore lenses at Thalanga could have been leached from the underlying rhyolitic volcanics (Mount Windsor Volcanics) and sandstone and siltstone of the underlying Puddler Creek Formation during hydrothermal convection of Cambro-Ordovician seawater (with convection driven by a sub-volcanic magma chamber). A sub-volcanic magma chamber may also have provided metals to the circulating (seawater-rich) hydrothermal solutions, and the presence of coarsely quartz-phyric units (the QEV and QFP) within the ore horizon are interpreted to indicate the residence of a hydrous parent magma at depth.

12.6 Ore Genesis

The possible formation of the host stratigraphy and evolution of the Thalanga massive sulphide deposit is described as follows (and summarised in Fig. 12.1a-d):

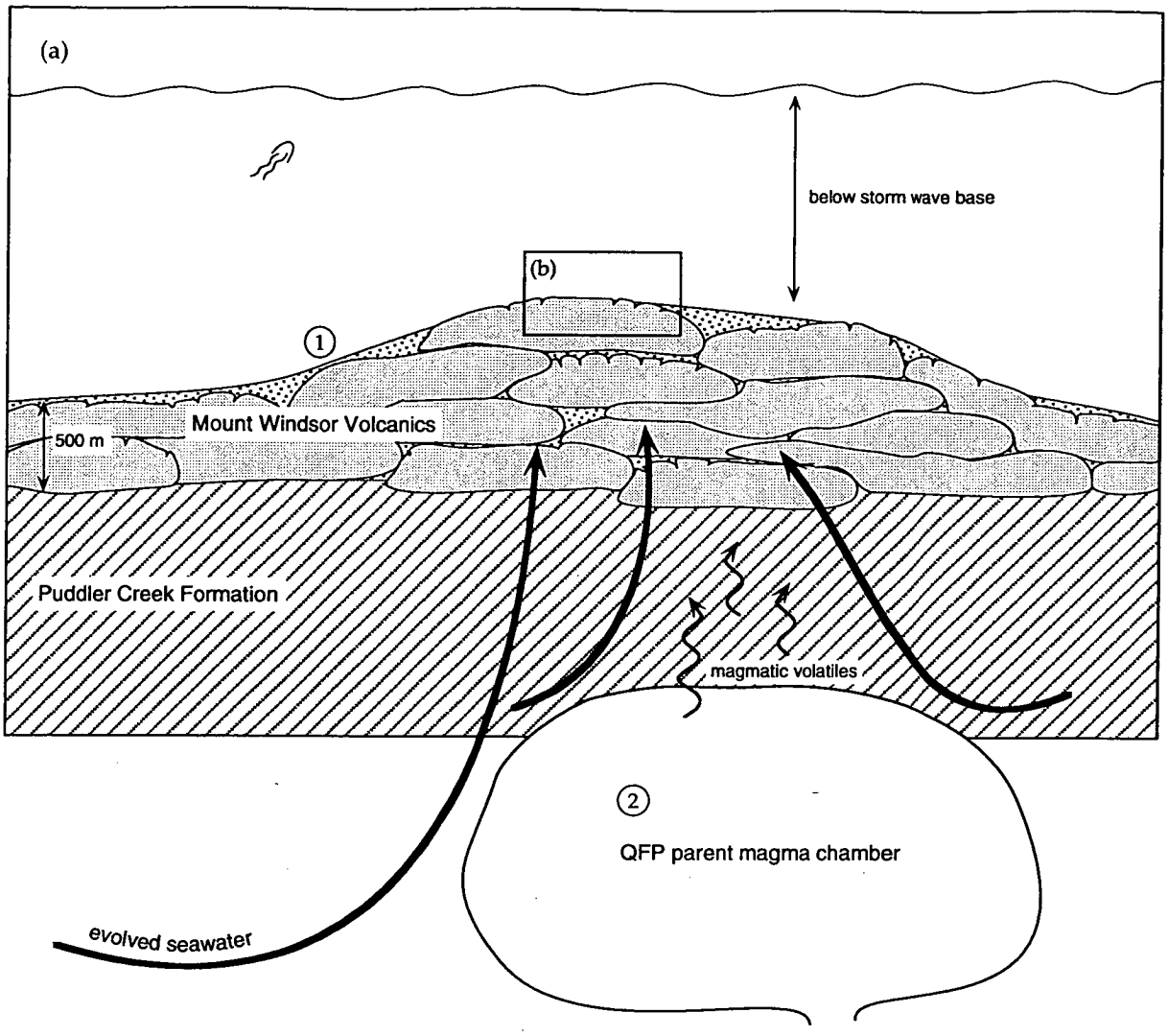

Figure 12.1 Evolution of Thalanga. (a) Hydrothermal convection initiated by emplacement of sub-volcanic magma chamber:

(1.) Subaqueous emplacement of Mount Windsor Volcanics (mainly rhyolite domes, lavas or sills) stratigraphically overlying continental-derived sandstone and siltstone (Puddler Creek Formation).

(2.) During final stages of rhyolitic volcanism, sub-volcanic magma chamber was emplaced (inferred to be the source of QFP and dacite) and initiated hydrothermal convection of Cambro-Ordovician seawater.

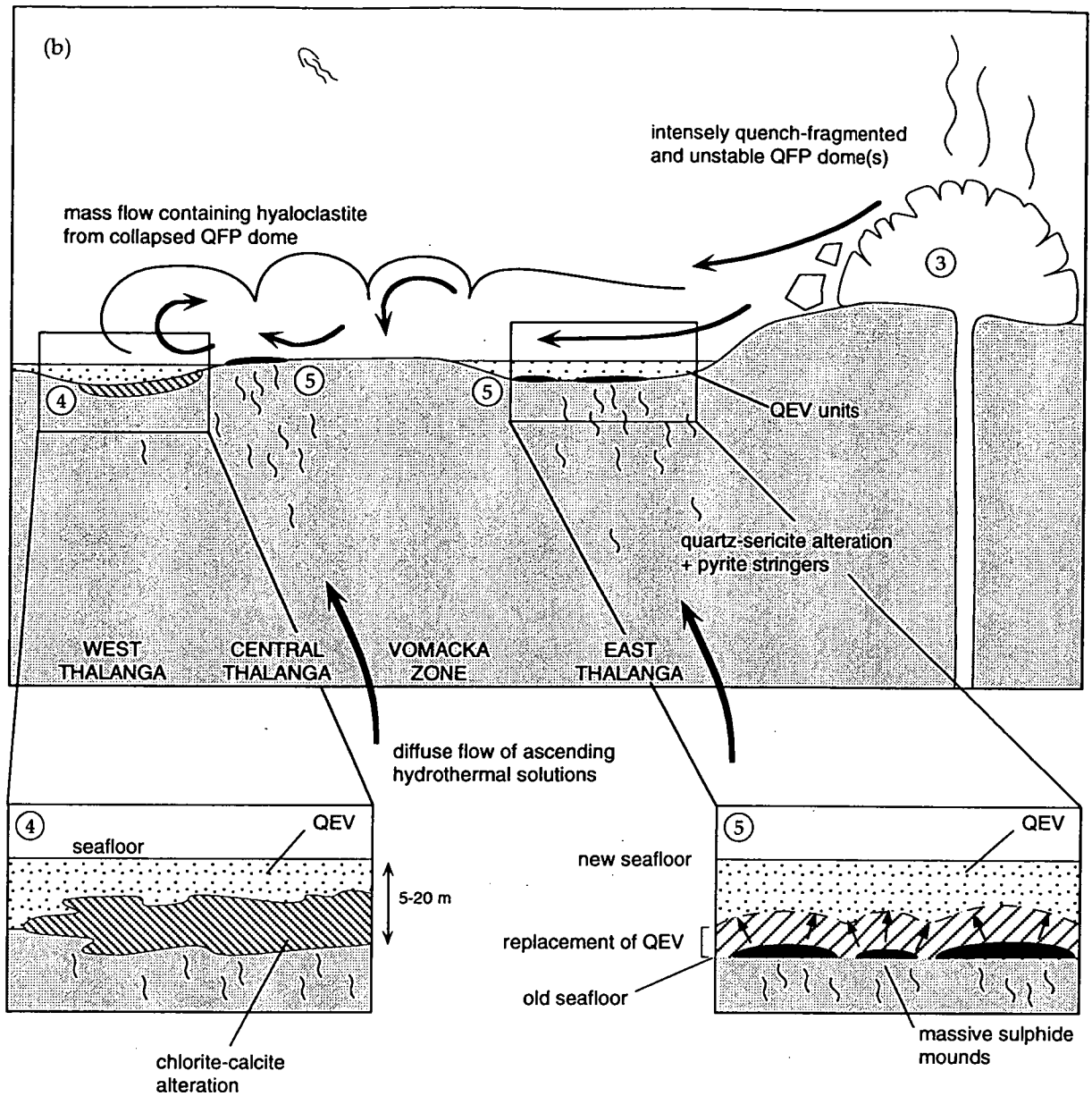

Figure 12.1 (b) Sulphide mineralisation interupted by deposition of QEV. Horizontal distance across large diagram is 3-4 km:

(3.) Subaqueous emplacement of QFP dome (probably located north of Central Thalanga, rather than east of East Thalanga as shown here), followed by intense quench fragmentation, gravitational collapse, and mass wasting, which resulted in transportation and resedimentation of quartz and feldspar crystals and QFP clasts (pumiceous and non-vesicular) into local basins (West and East Thalanga) to form the QEV units.

(4.) Rhyolitic volcanics underlying QEV units in West Thalanga (and parts of the QEV) are altered to chlorite and calcite assemblages by low temperature, CO_2-bearing hydrothermal solutions.

(5.) Formation of massive sulphide mounds may have begun in parts of Central and East Thalanga as temperature of hydrothermal solutions increased.

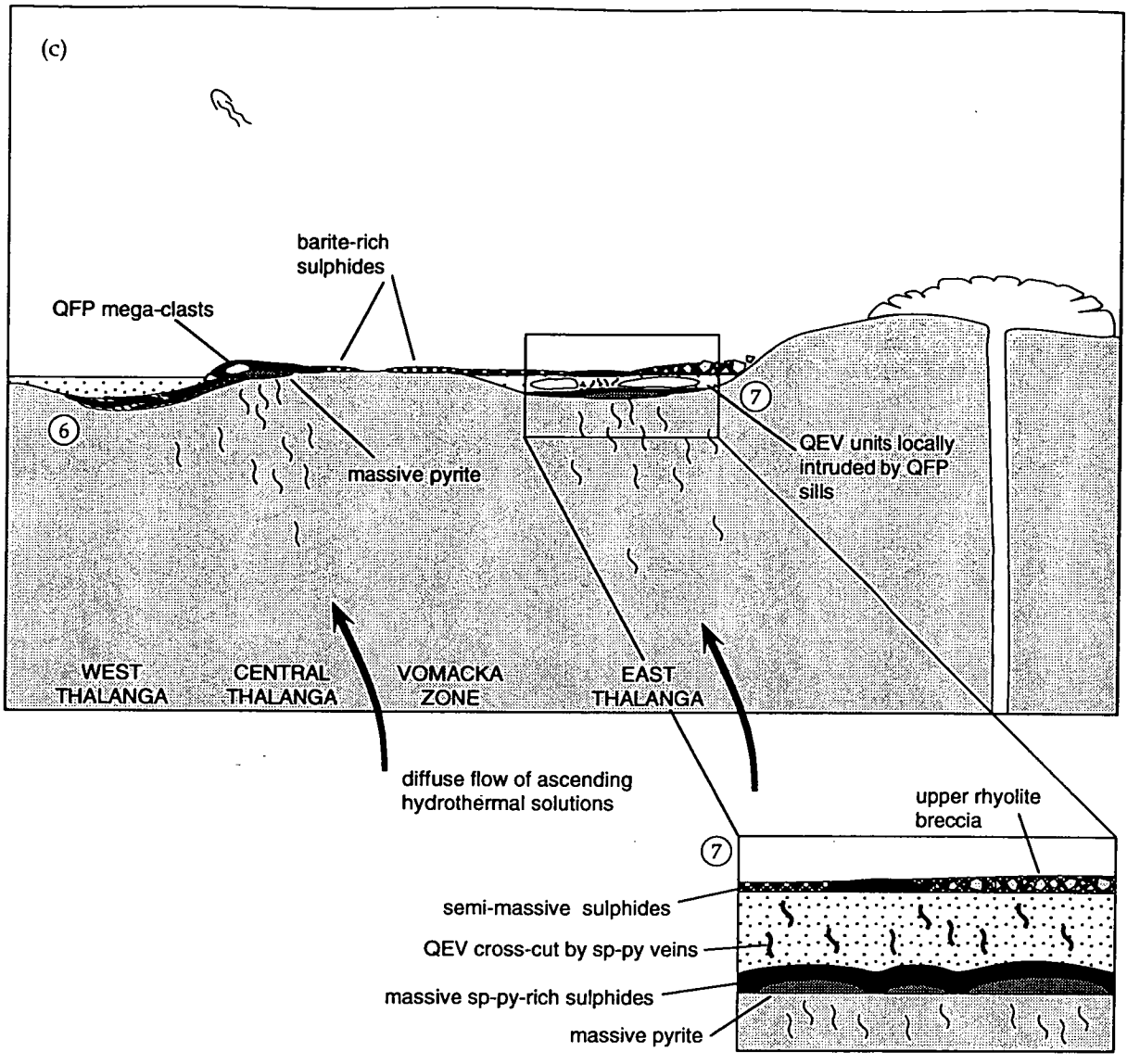

Figure 12.1 (c) Growth of local sulphide mounds and replacement of selected units:

(6.) The temperature of the hydrothermal solutions increased, and chlorite-calcite alteration assemblages in West Thalanga are altered to chlorite-dolomite and are replaced by sulphides. A mound of massive sulphides is constructed in Central Thalanga, with the base of the polymetallic sulphides replaced by pyrite ± chalcopyrite (which also occurred in eastern parts of West Thalanga).

(7.) The base of the QEV in East Thalanga is partly replaced by polymetallic sulphides, and these are replaced by pyrite ± chalcopyrite in locations directly overlying main zone of hydrothermal fluid flow. Mineralising solutions alter overlying QEV and eventually replace an overlying rhyolite breccia (upper rhyolite breccia), the coarse grained bases of overlying QEV sandstone units, and possibly locally form massive sulphides on the seafloor.

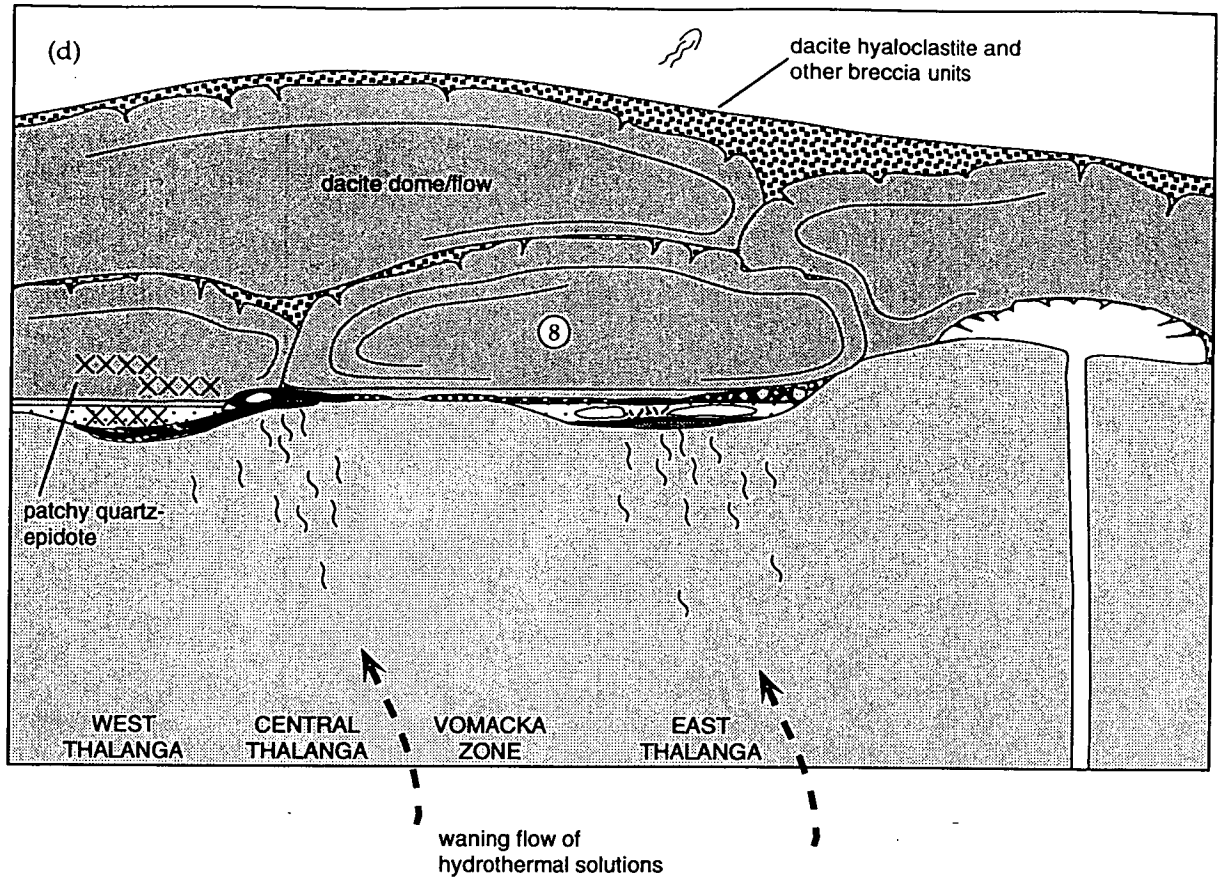

Figure 12.1 (d) Cessation of hydrothermal activity:

(8.) Deposition of HWF siltstone and sandstone following cessation of sulphide formation. Dacite flows then emplaced, and locally altered during waning stages of hydrothermal activity (chlorite, quartz, calcite: metmorphosed to quartz-epidote-rich assemblages). QEV and QFP units are similarly altered where they overlie carbonate-rich assemblages within the ore horizon.

1. Formation of the Mount Windsor Volcanics at Thalanga involved emplacement of rhyolite domes or lavas, and possibly syn-volcanic intrusions, and deposition of associated autobreccia and hyaloclastite units in a sub-basin within a regional-scale back-arc basin. Constructional volcanism was concentrated at Thalanga and local basins trapped rhyolitic pumice breccia and other subaqueously transported units (Fig. 12.1a)). Initiation of the hydrothermal system at Thalanga probably occurred during the final stages of rhyolitic volcanism (as rhyolite breccia units partly host massive sulphides in the hangingwall lens in East Thalanga) and is interpreted to have been caused by the emplacement of the QFP parent magma (Fig. 12.1a). Metals may have been leached from the Puddler Creek Formation and the Mount Windsor Volcanics and may have been sourced directly from the magma chamber, which was volatile-rich (Fig. 12.1a).

2. Subaqueous emplacement, intense quench fragmentation, and gravitational collapse of a QFP dome or lava at Thalanga (Fig. 12.1b), resulted in the redeposition of the hyaloclastite, by mass flows, into local basins at West and East Thalanga, and parts of Central Thalanga (QEV units). Shallow, syn-volcanic QFP sills locally intruded the QEV units while they were unconsolidated (Fig. 4.19; Chapter 4). Volatiles associated with the QFP parent magma may have contributed to the hydrothermal solutions that were ascending through the permeable perlitic rhyolite lavas and rhyolitic breccia units at this stage. The porosity and permeability of the rhyolitic footwall allowed infiltration of cold seawater, which mixed with the warm hydrothermal solutions and produced Mg-rich chlorite. Pervasive Mg-rich chlorite alteration is associated with carbonate alteration of the rhyolitic volcanics and QEV in West Thalanga (Fig. 12.1b, inset 4). Carbonate and chlorite alteration may have been promoted by the mixing between cold seawater and warm CO_2 or HCO_3^--bearing hydrothermal solutions (sourced from seawater and possibly partly from the QFP magma) in porous glassy, rhyolitic volcanics that were overlain by more impermeable QEV units.

3. Sulphide mineralisation may have preceded QEV deposition in parts of Central and East Thalanga, and the preferred interpretation is that the QEV was deposited on top of clusters of evolving sulphide mounds in these regions (Fig. 12.1b, inset 5). Deposition of the QEV interrupted seafloor sulphide formation, and continuation of sulphide formation resulted in the partial replacement of the coarse base of the QEV, as the mineralising solutions travelled laterally along the permeable base of the QEV. Eventually the hydrothermal solutions were able to ascend through the QEV (producing quartz-sericite alteration assemblages and pyrite stringer veins) and either vented at the seafloor, where a second group of barite-rich massive sulphide mounds and quartz magnetite lenses formed, or partly replaced a monomict rhyolite breccia and the coarse base of the QEV sandstone facies (Fig. 12.1c, inset). Immobile element ratios indicate that the monomict rhyolite breccia (the upper rhyolite breccia) may represent the final eruption of rhyolite of the underlying Mount Windsor Volcanics.

4. In West Thalanga, the sulphide lenses are veins of massive sulphides that cross cut the CTC assemblages. The sulphides are interpreted to have replaced the CTC units (Fig. 12.1c), when the hydrothermal system reached temperatures high enough to allow sulphide deposition (150-250°C; Large, 1992). The lack of sulphide lenses overlying the QEV in West Thalanga is interpreted to indicate either the cessation of hydrothermal activity prior to deposition of the QEV, or that the mineralising solutions were not able to pass through the QEV in this area (i.e. the QEV in West Thalanga was more impermeable than the QEV in East Thalanga). Perhaps the epidote-actinolite-chlorite assemblage within the QEV, and locally the overlying dacite, represents the metamorphic equivalent of late-stage, post sulphide mineralisation hydrothermal alteration.

5. Deposition of sulphides in West Thalanga was probably due to changes in pH and fO_2 conditions of the mineralising solutions when they ascended through the CTC alteration assemblages. In East Thalanga, deposition of sulphides may have been due to a sudden change in pH, fO_2 and pressure (lithostatic) as the mineralising solutions moved from the rhyolitic footwall to the highly porous and permeable base of the QEV breccia facies. The sulphide lenses at Thalanga are interpreted to have evolved in a similar process to the mound-building and zone-refining processes outlined by Eldridge *et al.* (1983), Huston and Large (1989) and Large (1992), whereby as the temperature of the hydrothermal solution increased to 300-350°C, early-formed sphalerite-galena assemblages in the CTC or QEV are replaced by pyrite ± chalcopyrite in areas overlying hydrothermal feeder zones, and are re-precipitated at the upper and lateral margins of the sulphide lens. During the waning stages of the hydrothermal system barite-rich sulphides were precipitated at the top of the sulphide lens. In East Thalanga, barite-rich sulphides are inferred to have been deposited at the seawater-QEV interface.

6. Deposition of rhyolite breccia grading to quartz-feldspar sandstone and silty sandstone (the HWF) is interpreted to have post-dated sulphide mineralisation (Chapter 4). Emplacement of multiple dacite lavas followed, with the first dacite partly foundering into wet and unconsolidated HWF in Central and East Thalanga. Hydrothermal activity had almost ceased after dacite deposition, but local epidote-rich assemblages are interpreted to indicate continued hydrothermal activity (Fig. 12.1d).

7. The main deformation (D_2) of Thalanga occurred during the Early Ordovician and produced east-west trending upright folds. This event is interpreted to have resulted in the formation of compositional banding within the sulphide lenses parallel to the subvertical S_2 direction (Chapter 3 and 6). Sulphides were remobilised into extension sites that also formed during this subvertical extension.

8. Repetition of the ore horizon along the steeply north-dipping normal faults during the Silurian-Devonian (D_3) resulted in structural thickening of the massive sulphide lenses, and local remobilisation of sulphides (Chapter 3). Peak metamorphism is inferred to post-date S_3 formation, and resulted in the strong coarsening and recrystallisation of sulphides and gangue minerals at Thalanga.

12.7 Synthesis: Controls on the Location of Massive Sulphides

The most important features that are interpreted to control the location and abundance of massive sulphide lenses at Thalanga (and are therefore likely to be useful exploration criteria within the Mount Windsor subprovince) are:

1. The abundance of proximal volcanism. This suggests that there was a major magma chamber at depth which drove the circulation of hydrothermal convention cells in the footwall rhyolitic volcanics, and was also a possible source of some of the hydrothermal solutions.

2. In the absence of growth faults to channel mineralising fluids, abundant porous and permeable volcanic units (perlitic fractures in coherent units, breccia facies) within the footwall allowed the flow of hydrothermal solutions to the stratigraphic top of the rhyolitic volcanics.

3. The presence of a favourable horizon. The intimate association between the massive sulphides and the CTC and QEV units at Thalanga suggests that the right chemical change may have been critical in promoting deposition of sulphides from the mineralising fluid. Such a favourable horizon is critical in an active volcanic environment that contains little evidence of a major volcanic hiatus (and therefore little time to deposit massive sulphides on the seafloor) in order for sulphide mineralisation to have occurred in a sub-seafloor position. Gradation from semi-massive to massive sulphides within the ore horizon at Thalanga is interpreted to be consistent with the lateral migration of hydrothermal solutions, and deposition of sulphides by replacement along a favourable horizon.

4. Coarse quartz-bearing QEV and QFP units within the favourable horizon. These volcanic units are interpreted to have formed in a volatile-rich magma and the time required to crystallise the distinctive large quartz crystals may have led to the initiation of a hydrothermal convection cell in the overlying rhyolitic volcanics. Volatiles from the magma may also have been released to ascend and mix with the convecting seawater.

CHAPTER 13.

CONCLUSIONS

Massive sulphide lenses at Thalanga are associated with poorly sorted, polymict breccia and quartz sandstone units (QEV), syn-volcanic quartz-feldspar porphyry (QFP) sills, and local carbonate- and chlorite-rich (CTC) alteration assemblages that stratigraphically overlie rhyolitic volcanics, and are collectively known as the ore horizon. Bedding is now subvertical and faces south, and Thalanga is interpreted to occur on the northern limb of a northwest striking syncline.

The massive sulphides are interpreted to be syn-volcanic in origin because:

i) the massive sulphide and hydrothermal alteration assemblages have the same generations of tectonic structures as the host volcanic units;

ii) the largest and most extensive area of hydrothermal alteration is present in the rhyolitic volcanics stratigraphically underlying the massive sulphide lenses;

iii) there is a strong stratigraphic control on the location of massive sulphides (at the stratigraphic top of the Mount Windsor Volcanics and intercalated with the lowermost volcanic units of the overlying Trooper Creek Formation).

Two significant deformation events (D_2 and D_3) are inferred to have overprinted the host stratigraphy and the massive sulphide lenses at Thalanga. Both of these may have been associated with metamorphism. However, textural evidence indicates that peak metamorphism (485 ± 23°C and 2.5 ± 1.5 kbars) at Thalanga post-dated S_3. Remobilisation of sulphides is interpreted to have occurred during both D_2 and D_3. The main structures are:

D_2: Ordovician age, regional-scale east-west vertical folds, possibly associated with regional metamorphism. The pervasive axial planar cleavage (S_2) is defined by metamorphic biotite, phyllosilicate alteration minerals, and compositional banding in the sulphide lenses. Formerly irregularly-oriented pyrite veins in footwall stringer zones are folded with axial planes parallel to S_2. Steep, NE- to E-plunging mineral and clast elongation lineations indicate subvertical extension during D_2. Chalcopyrite-rich sulphides (± quartz) have been remobilised into dilation sites associated with subvertical extension, including the subhorizontal boudin necks in CTC assemblages, pressure shadows around clasts (cm- to m-scale) and phenocrysts, and subhorizontal tension gashes and piercement veins at the upper and lower contacts of massive sulphide lenses.

D_3: Silurian-Devonian age, ENE-striking normal faults and weakly bifurcating crenulation cleavage (S_3). The normal faults have cross-cut and truncated the ore horizon at depth,

structurally thicken the massive sulphide lens in places, and partly control the separation of the semi-continuous ore lens into four main lenses. Sulphides have been remobilised adjacent to the faults and parallel to S_3. Late-stage strike-slip displacement has also occurred along these faults.

Syn-volcanic structures may have controlled the location and geometry of the local basin in which massive sulphides and the QEV were deposited, but unequivocal evidence of their presence has been overprinted by hydrothermal alteration. The semi-conformable pyrite stringer zones are interpreted to reflect original permeability contrasts within the footwall rhyolitic volcanics, which are composed of perlitic rhyolite domes or sills, rhyolite breccia and sandstone, and local rhyolite pumice breccia units.

Evidence that Thalanga was formed in the vicinity of an active volcanic centre includes:

i) the rhyolitic volcanics reach a maximum stratigraphic thickness at Thalanga, which gradually decreases along strike;

ii) QEV is locally intruded by co-magmatic QFP sills with peperitic margins at Thalanga;

iii) minor rhyolite eruption continued after QEV and QFP emplacement;

iv) dacite lavas and syn-volcanic andesite sills overlie the ore horizon, but dacite is not present within 2 km along strike from Thalanga. The similarity between immobile element ratios and REE contents of the QFP sills and the first erupted dacite suggests that both may have had the same parent magma;

v) there is no evidence of extended ambient basin (terrigenous) sedimentation, until deposition of the overlying Rollston Range Formation, that would indicate periods of volcanic quiescence.

The QEV is interpreted to have either:

i) been sourced from an explosively erupted QFP magma at an unknown vent which liberated abundant quartz and feldspar crystals. This would probably have occurred at water depths of ≤1 km (McBirney, 1963). If the thickest parts of the underlying rhyolitic volcanics correspond to a regional-scale, topographic high, then the vent was probably located near Thalanga; or

ii) formed by intense quench fragmentation, gravitational collapse and mass wasting of one or more QFP domes. This interpretation is consistent with the variable crystal concentrations and poorly sorted components of the QEV.

Quartz and feldspar crystal and crystal fragments, non-vesicular QFP clasts and pumiceous QFP clasts from the collapsed domes or explosive eruption are interpreted to have been transported and redeposited by a sub-aqueous mass-flow into local basins at Thalanga, interrupting incipient seafloor massive sulphide formation. The QEV was not deposited in the Vomacka Zone and eastern parts of Central Thalanga, indicating that these areas were

topographic highs at that time. Locally, non-vesicular QFP sills were emplaced while the QEV was wet and unconsolidated.

The large sizes of the phenocryst and crystal component of the QFP and QEV units indicates that the parent magma was volatile-rich and had remained in the magma chamber for sufficient time to grow large crystals. This magma chamber is interpreted to have been the heat source required to drive the circulation of hydrothermal solutions, which as well as comprising evolved seawater (as indicated by sulphur isotopes), may also have contained volatiles and metals released from the fluid-rich QFP parent magma.

The major conclusions about the composition and origin of the massive sulphides at Thalanga are:

i) the sulphide lenses comprise massive to banded lenses of sphalerite-galena-pyrite ± chalcopyrite-rich sulphides, with minor tetrahedrite-tennantite and arsenopyrite. These sulphide lenses stratigraphically overlie massive pyrite ± chalcopyrite ± minor magnetite lenses;

ii) barite-rich sulphides are present at the stratigraphic top and lateral margins of the ore lenses, and in places are associated with quartz-magnetite lenses. In East Thalanga barite-rich sulphides overlie the QEV breccia facies;

iii) the sulphides are coarse-grained, strongly annealed and any evidence of deformation has been obliterated by recrystallisation during metamorphism. Banding is defined by alternative bands of pyrite-rich and sphalerite-rich sulphides, and is interpreted to be metamorphic in origin;

iv) the gradation from semi-massive to massive sulphides at Thalanga is consistent with the lateral migration of hydrothermal solutions and deposition of sulphides (probably due to changes in pH and fO_2) by replacement of favourable units. Massive sulphide veins and disseminations have replaced CTC alteration assemblages in West and parts of Central Thalanga, and massive sulphides have replaced the poorly sorted, coarse-grained base of the QEV breccia facies, the coarse grained base of the overlying QEV sandstone facies and the upper rhyolite breccia unit in East Thalanga. Local formation of sulphide mounds on the seafloor is interpreted to have occurred in Central Thalanga and parts of East Thalanga;

v) barite-rich sulphides may have formed on the seafloor in East Thalanga, but in the Vomacka Zone, barite-sulphide veins have replaced a polymict rhyolite breccia that overlies the footwall rhyolitic volcanics;

vi) metal zonation within the ore lenses is poorly developed and is interpreted to reflect widespread remobilisation and repetition of the normally zoned massive sulphide lenses along normal faults during D_3;

vii) $\delta^{34}S$ of pyrite disseminated in the footwall indicates that sulphur is sourced from hydrothermal solutions containing a mixture of dissolved igneous sulphur and Cambro-

Ordovician seawater that was inorganically reduced during circulation. Progressive mixing with partly reduced seawater is interpreted to have occurred as the hydrothermal solutions ascended through the permeable rhyolitic volcanics.

viii) $\delta^{34}S$ of barite is consistent with sulphate derived from the overlying Cambro-Ordovician seawater and deposition of barite on or immediately below the seafloor.

The important types and distribution of metamorphosed hydrothermal alteration assemblages at Thalanga are:

i) quartz-muscovite ± pyrite ± phlogopite ± chlorite-rich assemblages are concentrated in the rhyolitic volcanics underlying the massive sulphide lenses at Thalanga. The pre-metamorphic hydrothermal alteration assemblage is inferred to have been quartz-sericite ± chlorite ± pyrite. Except for quartz phenocrysts, most original volcanic textures have been destroyed by this alteration and pseudoclastic textures are common within the footwall rhyolitic volcanics. Quartz-muscovite-phlogopite-rich assemblages (metamorphosed quartz-sericite ± chlorite alteration) and pyrite ± sphalerite veins have overprinted the QFP and QEV units that are overlain by massive sulphides;

ii) semi-conformable pyrite stringer zones in the rhyolitic volcanics comprise 5-50 % irregular pyrite veins, now subparallel to S_2, in quartz-muscovite-rich intervals. Minor amounts of chalcopyrite are present in stringer zones closest to the ore horizon. The thickest lenses of massive sulphides are present where the stringer zones intersect the ore horizon;

iii) intervals of intense silicification in the footwall rhyolitic volcanics contain only traces of muscovite and few pyrite veins, are typically not overlain by massive sulphides, and are therefore considered to have formed prior to sulphide formation and acted as a barrier to hydrothermal solutions. This interpretation explains the local gradational contacts with quartz-muscovite-pyrite-rich rhyolitic volcanics;

iv) domains of clinozoisite-chlorite-tremolite near the stratigraphic top of the rhyolitic volcanics in West and Central Thalanga are interpreted to be metamorphosed zones of calcite-chlorite-quartz alteration, and may have been feeder zones to the CTC assemblages within the overlying ore horizon;

v) chlorite schist has replaced the stratigraphic top of the rhyolitic volcanics in places and typically contains disseminated pyrite and is closely associated with massive pyrite lenses;

vi) CTC units within the ore horizon are interpreted have formed by the low temperature replacement of a rhyolitic precursor and the QEV in places. The QEV is interpreted to have been deposited prior to alteration and acted as mostly impermeable barrier, allowing low temperature hydrothermal solutions (containing marine HCO_3^- and possibly minor CO_2 from the QFP parent magma) to mix with cold seawater in porous rhyolitic volcanics at the top of the footwall. Calcite is interpreted to have nucleated on and replaced glassy rhyolite fragments, and chlorite precipitated in pore spaces. Calcite was dolomitised as the hydrothermal system evolved and heated up.

vi) epidote-actinolite- and epidote-quartz-rich assemblages are common in the QEV and dacite that overlie CTC units, and are considered to be the metamorphosed equivalents of calcite-chlorite-quartz alteration that formed during the waning stages of the hydrothermal system.

REFERENCES

Adamson, R.G., and Teichmann, R.F.H., 1986. The Matchless cupreous pyrite deposit. *In* Anhaeusser, C. R., and Maske, S., eds. *Ore Deposits of Southern Africa.* Geological Society of South Africa Special Publication, 1755-1760.

Aerden, D.G.A.M., 1990. Formation of a massive sulphide orebody by syn-deformational host rock replacement in a ductile shear zone, Rosebery, Tasmania [abs.]: Tenth Australian Geological Convention, Gondwana: Terranes and Resources, Hobart, Geological Society of Australia, 174-175.

Aerden, D.G.A.M., 1991. Foliation boudinage control on the formation of the Rosebery Pb-Zn orebody, Tasmania. *Journal of Structural Geology* **13**, 759-775.

Aerden, D.G.A.M., 1993. Formation of massive sulfide lenses by replacement of folds: the Hercules Pb-Zn mine, Tasmania. *Economic Geology* **88**, 377-396.

Aerden, D.G.A.M., 1994a. Formation of the Rosebery and Hercules ore deposits, Tasmania by syntectonic mobilization of metals and wallrock replacement about structural traps [abs.]: Contentious issues in Tasmanian geology: a symposium, Hobart, Geological Society of Australia, Tasmania Division, 83-88.

Aerden, D.G.A.M., 1994b. Microstructural timing of the Rosebery massive sulphides, Tasmania: evidence for a metamorphic origin through mobilization of disseminated base metals. *Journal of Metamorphic Geology* **12**, 505-522.

Allen, R.L., 1988. False pyroclastic textures in altered silicic lavas, with implications for volcanic-associated mineralization. *Economic Geology* **83**, 1424-1446.

Allen, R.L., 1992. Reconstruction of the tectonic, volcanic, and sedimentary setting of strongly deformed Zn-Cu massive sulfide deposits at Benambra, Victoria. *Economic Geology* **87**, 825-854.

Allen, R.L., 1994. Synvolcanic, subseafloor replacement model for Rosebery and other massive sulphide ores [abs.]: Contentious Issues in Tasmanian geology: a symposium, Hobart, Geological Society of Australia, Tasmania Division, 89-91.

Allen, R.L., and Cas, R.A.F., 1990. The Rosebery controversy: Distinguishing prospective submarine ignimbrite-like units from true subaerial ignimbrites in the Rosebery-Hercules Zn-Cu-Pb massive sulphide district, Tasmania [abs.]: Tenth Australian Geological Convention, Gondwana: Terranes and Resources, Hobart, Geological Society of Australia, 31-32.

Alt, J.C., Honnorez, J., Laverne, C., and Emmermann, R., 1986. Hydrothermal alteration of a 1 km section through the upper crust, Deep Sea Drilling Project hole 504B: mineralogy, chemistry, and evolution of seawater-basalt interactions. *Journal of Geophysical Research* **91**, 10309-10335.

Amcoff, Ö., 1976. The solubility of silver and antimony in galena. *Neues Jahrbuch Mineralogie Monatsh.* **6**, 247-261.

Amcoff, Ö., 1984. Distribution of silver in massive sulfide ores. *Mineralium Deposita* **19**, 63-69.

Anderson, G.M., 1983. Some geochemical aspects of sulfide precipitation in carbonate rocks [abs.]: International conference on Mississippi Valley-type lead-zinc deposits, University of Missouri – Rolla, 61-76.

Ashley, P.M., Dudley, R.J., Lesh, R.H., Marr, J.M., and Ryall, A.W., 1988. The Scuddles Cu-Zn prospect, and Archean volcanogenic massive sulfide deposit, Golden Grove district, Western Australia. *Economic Geology* **83**, 918-951.

Atkinson, B.K., 1974. Experimental deformation of polycrystalline galena, chalcopyrite and pyrrhotite. *Institute of Mining and Metallurgy Transactions, Section B* **83**, 19-28.

Atkinson, B.K., 1975. Experimental deformation of polycrystalline pyrite: effects of temperature, confining pressure, strain rate, and porosity. *Economic Geology* **70**, 473-487.

Baker, J.H., and De Groot, P.A., 1983. Proterozoic seawater-felsic volcanics interaction W. Bergslagen, Sweden. Evidence for high REE mobility and implication for 1.8 Ga seawater compositions. *Contributions to Mineralogy and Petrology* **82**, 119-130.

Baker, P.A., Cross, S.L., and Burns, S.J., 1994. Geochemistry of carbonate nodules and cements and implications for hydrothermal circulation, Middle Valley, Juan de Fuca Ridge. *Proceedings of the Ocean Drilling Program, Scientific Results* **139**, 313-328.

Barrett, T.J., and MacLean, W.H., 1991. Chemical, mass and oxygen isotope changes during extreme hydrothermal alteration of an Archean rhyolite, Noranda, Quebec. *Economic Geology* **86**, 406-414.

Barrett, T.J., and MacLean, W.H., 1994. Mass changes in hydrothermal alteration zones associated with VMS deposits of the Noranda area. *Exploration and Mining Geology* **3**, 131-160.

Barton, P.B., Jr, and Bethke, P.M., 1987. Chalcopyrite disease in sphalerite: pathology and epidemiology. *American Mineralogist* **72**, 451-467.

Barton, P.B., Jr, and Toulmin, P. III, 1966. Phase relations involving sphalerite in the Fe-Zn-S system. *Economic Geology* **61**, 815-849.

Beams, S.D., 1993. Polymetallic massive sulphide exploration case histories Mt Windsor volcanic belt, north Queensland. *In* Henderson, R.A., ed. *Guide to the Economic Geology of the Charters Towers Region, northeastern Queensland.* Geological Society Australia, Queensland division, Townsville. 75-79.

Beams, S.D., Laing, W.P., and O'Neill, D.M., 1989. The exploration history and geology of the polymetallic Reward deposit, Mount Windsor volcanic belt, north Queensland [abs.]: North Queensland Gold '89 Conference, Townsville, Queensland, 95-102.

Beams, S.D., Laurie, J.P., and O'Neill, D.M., 1990. Reward polymetallic sulphide deposit. *In* Hughes, F. E., ed. *Geology of the Mineral Deposits of Australia and Papua New Guinea.* Australasian Institute of Mining and Metallurgy, Monograph 14, 1539-1543.

Beaty, D.W. and Taylor, H.P.,Jr, 1982. Some petrologic and oxygen isotope relationships in the Amulet mine, Noranda, Quebec, and their bearing on the origin of Archean massive sulfide deposits. *Economic Geology* **77**, 95-108.

Bell, T.H., 1980. The deformation history of northeastern Queensland - a new framework. *In* Henderson, R. A., and Stephenson, P.J., eds. *The geology and geophysics of northeastern Australia,* Geological Society Australia, Queensland division, Brisbane. 307-313.

Bente, K., and Doering, T., 1993. Solid-state diffusion in sphalerites: an experimental verification of the "chalcopyrite disease". *European Journal of Mineralogy* **5**, 465-478.

Berman, R.G., 1990. Mixing properties of Ca-Mg-Fe-Mn garnets. *American Mineralogist* **75**, 328-344.

Berry, R.F., 1989. Structure of the Mount Windsor Subprovince - initial report. Centre for Ore Deposit and Exploration Studies, University of Tasmania, Mount Windsor Project - Research Report No. 1, 51-73, (unpubl.).

Berry, R.F., 1990. The structure of the Rosebery mine sequence, Western Tasmania [abs.]: Tenth Australian Geological Convention, Hobart, Geological Society of Australia, 278.

Berry, R.F., 1991. Structure of the Mount Windsor Subprovince. Centre for Ore Deposit and Exploration Studies, University of Tasmania, Mount Windsor Project - Research Report No. 2, 1-22, (unpubl.).

Berry, R.F., Huston, D.L., Stolz, A.J., Hill, A.P., Beams, S.D., Kuronen, U., and Taube, A., 1992. Stratigraphy, structure, and volcanic-hosted mineralization of the Mount Windsor subprovince, north Queensland, Australia. *Economic Geology* **87**, 739-763.

Bevins, R.E., Robinson, D., and Rowbotham, C., 1991. Compositional variations in mafic phyllosilicates from the regional low-grade metabasites and application of the chlorite geothermometer. *Journal of Metamorphic Geology* **9**, 711-721.

Bhattacharya, A., Mohanty, L., Maji, A., Sen, S.K., and Raith, M., 1992. Non-ideal mixing in the phlogopite-annite binary: constraints from experimental data on Mg-Fe partitioning and a reformulation of the biotite-garnet geothermometer. *Contribution of Mineralogy and Petrology* **111**, 87-93.

Bierlein, F.P., Ashley, P.M., and Plimer, I.R., 1995. Sulphide mineralisation in the Olary Block, South Australia — Evidence for syn-tectonic to late-stage mobilisation. *Mineralium Deposita* **30**, 424-438.

Binns, R.A., and Scott, S.D., 1993. Actively forming polymetallic sulfide deposits associated with felsic volcanic rocks in the eastern Manus back-arc basin, Papua New Guinea. *Economic Geology* **88**, 2226-2236.

Bischoff, J.L., and Seyfried, W.E., 1978. Hydrothermal chemistry of seawater from 25° to 350°C. *American Journal of Science* **278**, 838-869.

Bishop, J.R., and Lewis, R.J.G., 1992. Geophysical signatures of Australian volcanic-hosted massive sulfide deposits. *Economic Geology* **87**, 913-930.

Bodon, S.B., and Valenta, R.K., 1995. Primary and tectonic features of the Currawong Zn-Cu-Pb(-Au) massive sulfide deposit, Benambra, Victoria: implications for ore genesis. *Economic Geology* **90**, 1694-1721.

Bortnikov, N.S., Genkin, A.D., Dobrovol'skaya, M.G., Muravitskaya, G.N., and Filimonava, A.A., 1991. The nature of chalcopyrite inclusions in sphalerite: exsolution, co-precipitation, or "disease"? *Economic Geology* **86**, 1070-1082.

Bortnikov, N.S., Genkin, A.D., and Troneva, N.V., 1993. Tennantite decomposition: evidence from the Kedabek copper deposit, Azerbaijan. *Mineralogy and Petrology* **47**, 171-181.

Boulter, C.A., 1993. High-level peperitic sills at Rio Tinto, Spain: implications for stratigraphy and mineralization. *Transactions Institution of Mining and Metallurgy* **B 102**, 30-38.

Brathwaite, R.L., 1974. The geology and origin of the Rosebery ore deposit, Tasmania. *Economic Geology* **69**, 1086—1101.

Brooker, D.D., Craig, J.R., and Rimstidt, J.D., 1987. Ore metamorphism and pyrite porphyroblast development at the Cherokee mine, Ducktown, Tennessee. *Economic Geology* **82**, 72-86.

Brown, D., 1994. Low temperature, low pressure deformation and metamorphism of the Vangorda massive sulphide orebody, Yukon, Canada. *Mineralium Deposita* **29**, 330-340.

Brown, D., and McClay, K.R., 1993. Deformation textures in pyrite from the Vangorda Pb-Zn-Ag deposit, Yukon, Canada. *Mineralogical Magazine* **57**, 55-66.

Brown, G.H., and Kingston, D.M., 1993. Early diagenetic spherulitic siderites from Pennsylvanian palaeosols in the Boss Point Formation, Maritime, Canada. *Sedimentology* **40**, 467-474.

Brown, G., and Taylor, B., 1988. Sea-floor mapping of the Sumisu Rift, Izu-Ogasawara (Bonin) island arc. *Bulletin of the Geological Survey of Japan* **39**, 23-38.

Browne, P.R.L., 1978. Hydrothermal alteration in active geothermal fields. *Annual Reviews of Earth and Planetary Science* **6**, 229-250.

Browne, P.R.L., and Ellis, A.J., 1970. The Ohaki-Broadlands hydrothermal area, New Zealand: Mineralogy and related geochemistry. *American Journal of Science* **269**, 97-131.

Bryant, W.R., Bennett, R.H., and Katherman, Ch.F., 1981. Shear strength, consolidation, porosity and permeability of oceanic sediments. *In* Emiliani, C., ed. *The oceanic lithosphere. The sea.* J. Wiley and Sons, New York. 1555-1616

Bryndzia, L.T., and Scott, S.D., 1987a. The composition of chlorite as a function of sulfur and oxygen fugacity: An experimental study. *American Journal of Science* **287**, 50-76.

Bryndzia, L.T., and Scott, S.D., 1987b. Application of chlorite-sulfide-oxide equilibria to metamorphosed massive sulfide ores, Snow Lake area, Manitoba. *Economic Geology* **82**, 963-970.

Bryndzia, L.T., Scott, S.D., and Farr, J.E., 1983. Mineralogy, geochemistry, and mineral chemistry of siliceous ore and altered footwall rocks in the Uwamuki 2 and 4 deposits, Kosaka mine, Hokuroko district, Japan. *Economic Geology Monograph* **5**, 507-522.

Bryndzia, L.T., Scott, S.D., and Spry, P.G., 1988. Sphalerite and hexagonal pyrrhotite geobarometer: experimental calibration and application to the metamorphosed sulfide ores of Broken Hill, Australia. *Economic Geology* **83**, 1193-1204.

Bryndzia, L.T., Scott, S.D., and Spry, P.G., 1990. Sphalerite and hexagonal pyrrhotite geobarometer: correction in calibration and application. *Economic Geology* **85**, 408-411.

Bubela, B., and McDonald, J.A., 1969. Formation of banded sulphides: metal ion separation and precipitation by inorganic and microbial sulphide sources. *Nature* **221**, 465-466.

Busby-Spera, C.J., 1984. The lower Mesozoic continental margin and marine intra-arc sedimentation at mineral king, California. *In* Crouch, J.K. and Bachman, S.B., eds. *Tectonics and Sedimentation along the California Margin, Field Trip Guidebook - Pacific Section.* 38, Society of Economic Palaeontologists and Mineralogists, 135-155.

Busby-Spera, C.J., and White, J.D.L., 1987. Variation in peperite textures associated with differing host-sediment properties. *Bulletin of Volcanology* **49**, 765-775.

Çagatay, M.N. and Eastoe, C.J., 1995. A sulfur isotope of volcanogenic massive sulfide deposits of the Eastern Black Sea province, Turkey. *Mineralium Deposita* **30**, 55-66.

Campbell, I.H., Lesher, C.M., Coad, P., Franklin, J.H., Gorton, M.P., and Thurston, P.C., 1984. Rare-earth element mobility in alteration pipes below massive Cu-Zn sulfide deposits. *Chemical Geology* **45**, 181-202.

Cann, J.R., 1970. Rb, Sr, Y, Zr, and Nb in some ocean-floor basaltic rocks. *Earth and Planetary Science Letters* **10**, 7-11.

Carlon, C.J., and Bleeker, W., 1988. The geology and structural setting of the Håkansboda Cu-Co-As-Sb-Bi-Au deposit and associated Pb-Zn-Ag-Sb mineralisation, Bergslagen, central Sweden. *Geologie en Mijnbouw* **67**, 279-292.

Carmichael, I.S.E., Turner, F.J., and Verhoogen, J., 1974. *Igneous Petrology.* McGraw-Hill, New York, 739p.

Carozzi, A.V., 1993. *Sedimentary Petrography.* Prentice-Hall Inc., New Jersey, 263p.

Carpenter, A.B., Trout, M.L., and Pickett, E.E., 1974. Preliminary report on the origin and chemical evolution of lead- and zinc-rich brines in central Mississippi. *Economic Geology* **69**, 1191-1206.

Carr, G.R., Dean, J.A., Suppel, D.W., and Heithersay, P.S., 1995. Precise lead isotope fingerprinting of hydrothermal activity associated with Ordovician to Carboniferous metallogenic events in the Lachlan fold belt of New South Wales. *Economic Geology* **90**, 1467-1505.

Carrigan, W.J., and Cameron, E.M., 1991. Petrological and stable isotope studies of carbonate and sulfide minerals from the Gunflint Formation, Ontario: evidence for the origin of early Proterozoic iron-formation. *Precambrian Research* **52**, 347-380.

Cas, R., 1978. Silicic lavas in Paleozoic flyschlike deposits in New South Wales, Australia: behaviour of deep subaqueous silicic flows. *Geological Society of America Bulletin* **89**, 1708-1714.

Cas, R.A.F., 1983. Submarine 'crystal tuffs': their origin using a Lower Devonian example from southeastern Australia. *Geological Magazine* **120**, 471-486.

Cas, R.A.F., 1992. Submarine volcanism: eruption styles, products, and relevance to understanding the host-rock successions to volcanic-hosted massive sulfide deposits. *Economic Geology* **87**, 511-541.

Cas, R.A.F., Allen, R.L., Bull, S.W., Clifford, B.A., and Wright J.V., 1990. Subaqueous, rhyolitic dome-top tuff cones: a model based on the Devonian Bunga Beds, southeastern Australia and a modern analogue. *Bulletin of Volcanology* **52**, 159-174.

Cathelineau, M., 1988. Cation site occupancy in chlorites and illites as a function of temperature. *Clay Minerals* **23**, 471-485.

Cathelineau, M., and Nieva, D., 1985. A chlorite solid solution geothermometer: The Los Azufres (Mexico) geothermal system. *Contributions to Mineralogy and Petrology* **91**, 235-244.

Clarke, D.E., 1971. Geology of the Ravenswood 1-mile Sheet area, Queensland. Geological Survey Queensland, Report, 53, (unpubl.).

Clarke, J.W., 1984. The core of the Blue Ridge anticlinorium in northern Virginia. *Geological Society of America Special Paper* **194**, 155-160.

Clark, B.R., and Kelly, W.C., 1973. Sulfide deformation studies: I. Experimental deformation of pyrrhotite and sphalerite to 200 bars and 500°C. *Economic Geology* **68**, 332-352.

Clark, B.R., and Kelly, W.C., 1978. Experimental deformation of common sulphide minerals. *In* Strens, R. G. J., ed. *Physics and Chemistry of Minerals and Rocks*, Wiley, New York. 51-69

Claypool, G.E., Holser, W.T., Kaplan, I.R., Sakai, H., and Zak, I., 1980. The age curves of sulfur and oxygen isotopes in marine sulfate and their mutual interpretation. *Chemical Geology* **28**, 199-260.

Coblieg, T., Zolensky, M.E., and Sylvester, P.J., 1986. Why is blue quartz blue? *Geological Society of America, Abstracts with Programs* **18**, 567.

Coleman, M., and Moore, M.P., 1978. Direct reduction of sulfates to sulfur dioxide for isotopic analysis. *Analytical Chemistry* **50**, 1594-1598.

Cook, N.J., Klemd, R., and Okrusch, M., 1994. Sulphide mineralogy, metamorphism and deformation in the Matchless massive sulphide deposit, Namibia. *Mineralium Deposita* **29**, 1-15.

Costa, U.R., Barnett, R.L., and Kerrich, R., 1983. The Mattagami Lake mine Archean Zn-Cu sulfide deposit, Quebec: Hydrothermal coprecipitation of talc and sulfides in a sea-floor brine pool — evidence from geochemistry, $^{18}O/^{16}O$, and mineral chemistry. *Economic Geology* **78**, 1144-1203.

Cox, S.F., 1987. Flow mechanisms in sulphide minerals. *Ore Geology Reviews* **2**, 133-171.

Cox, S.F., Etheridge, M.A., and Hobbs, B.E., 1981. The experimental ductile deformation of polycrystalline and single crystal pyrite. *Economic Geology* **76**, 2105-2117.

Craig, J.R., and Vokes, F.M., 1993. The metamorphism of pyrite and pyritic ores. *Mineralogical Magazine* **57**, 3-18.

Crawford, A.J., Corbett, K.D., and Everard, J.L., 1992. Geochemistry of the Cambrian volcanic-hosted massive sulfide-rich Mount Read Volcanics, Tasmania, and some tectonic implications. *Economic Geology* **87**, 597-619.

Curtis, C.D., Pearson, M.J., and Somogyi, V.A., 1975. Mineralogy, chemistry, and origin of a concretionary siderite sheet (clay-ironstone band) in the Westphalian of Yorkshire. *Mineralogical Magazine* **40**, 385-393.

Date, J., Watanabe, Y., and Saeki, Y., 1983. Zonal alteration around the Fukazawa Kuroko deposits, Akita Prefecture, northern Japan. *Economic Geology Monograph* **5**, 365-386.

Daux, V., Crovisier, J.L., Hemond, C., and Petit, J.C., 1994. Geochemical evolution of basaltic rocks subjected to weathering; fate of the major elements, rare earth elements, and thorium. *Geochimica et Cosmochimica Acta* **58**, 4941-4954.

Davidson, G.J., Eggins, S.M., and McCulloch, M.T., 1993. Detailed rare earth (REE) geochemical anatomy of an ancient ferruginous chert lens, northern Australia: a preliminary report [abs.]: RIDGE Theoretical Institute, workshop and short course,

Day, R.W., Murray, C.G., and Whitaker, W.G., 1978. The eastern part of the Tasman Orogenic Zone. *Tectonophysics* **48**, 327-364.

Day, R.W., Whitaker, W.G., Murray, C.G., Wilson, I.H., and Grimes, R.G., 1983. Queensland geology. Geological Survey Queensland, 383, (unpubl.).

Deer, W.A., Howie, R.A., and Zussman, J., 1966. An Introduction to the Rock-Forming Minerals. Longman, Harlow,528p.

De Caritat, P. and Braun, J., 1991. Extension/collision cyclicity and the convergent margin history of outboard Gondwana (eastern Australia) [abs.]. *EOS* **72**, 300.

De Groot, P.A., and Sheppard, S.M.F., 1988. Carbonate rocks from W. Bergslagen, central Sweden: isotopic (C,O,H) evidence for marine deposition and alteration by hydrothermal processes. *Geologie en Mijnbouw* **67**, 177-188.

De Long, S.E., and Long, L.E., 1976. Petrology and Rb-Sr age of Precambrian rhyolite dikes, Llano County, Texas. *Geological Society of America Bulletin* **87**, 275-280.

Dietrich, R.V., 1965. The general absence of blue quartz in sedimentary rocks of the "Folded Appalachians" of southwestern Virginia. *Southeastern Geology* **7**, 1-8.

Dixon, G.H., 1980. Geological, geochemical and stable isotope studies of the carbonates at Rosebery. B.Sc. Honours thesis, University of Tasmania, (unpubl.).

Douglas-Brown, C., 1975. Report on reconnaissance of Hodgkinson Basin and Charters Towers areas. Le Nickel (Aust) Exploration Pty Ltd, North Queensland Project, (unpubl.).

Doyle, M.G., 1994. Facies architecture of a submarine felsic volcanic centre: Highway-Reward, Mount Windsor Volcanics, Cambro-Ordovician, Northern Queensland [abs.]: New Developments in Geology and Metallogeny: Northern Tasman Orogenic Zone, Townsville, EGRU Contribution, 149-150.

Doyle, M.G., and McPhie, J., 1994. A silicic submarine syn-sedimentary intrusive-dome-hyaloclastite host sequence to massive sulphide mineralisation: Mount Windsor Volcanics, Cambro-Ordovician, Australia [abs.]: IAVCEI International Volcanological Congress, Ankara, Turkey.

Duhig, N. C. 1991. The Geology of East Waddys Mill and the Geochemical and Textural Aspects of Ironstone near Thalanga, North Queensland. B.Sc. Honours thesis, University of Tasmania, (unpubl.).

Duhig, N.C., Stolz, J., Davidson, G.J., and Large, R.R., 1992. Cambrian microbial and silica gel textures in silica iron exhalites from the Mount Windsor Volcanic Belt, Australia: their petrography, chemistry and origin. *Economic Geology* **87**, 764-784.

Duckworth, R.C., and Rickard, D., 1993. Sulphide mylonites from the Renström VMS deposit, northern Sweden. *Mineralogical Magazine* **57**, 83-91.

Duffield, W.A., and Dalrymple, G.B., 1990. The Taylor Creek Rhyolite of New Mexico: a rapidly emplaced field of larva domes and flows. *Bulletin of Volcanology* **52**, 475-487.

Eastoe, C.J., and Nelson, S.E., 1988. A Permian Kuroko-type hydrothermal system, Afterthought-Ingot area, Shasta County, California: Lateral and vertical sections, and geochemical evolution. *Economic Geology* **83**, 588-605.

Ehlers, E.G., and Blatt, H., 1982. *Petrology: igneous, sedimentary, and metamorphic.* W.H. Freeman and Company, San Francisco, 732p.

Ehlers, K., Powell, R., and Stüwe, K., 1994. Cooling rate histories garnet + biotite equilibrium. *American Mineralogist* **79**, 737-744.

Einsele, G., 1986. Interaction between sediments and basalt injections in young Gulf of California-type spreading centers. *Geologische Rundschau* **75**, 197-208.

Einsele, G., Gieskes, J.M., Curray, J., Moore, D.M., Aguayo, E., Aubry, M-P., Fornari, D., Guerrero, J., Kastner, M., Kelts, K., Lyle, M., Matoba, Y., Molina-Cruz, A., Niemitz, J., Rueda, J., Saunders, A., Schrader, H., Simoneit, B., and Vacquier, V., 1982. Intrusion of basaltic sills into highly porous sediments, and resulting hydrothermal activity. *Nature* **283**, 441-445.

Eldridge, C.S., Barton, P.B.Jr, and Ohmoto, H., 1983. Mineral textures and their bearing on formation of the Kuroko orebodies. *Economic Geology Monograph* **5**, 241-281.

Ellis, A.J., 1963. The solubility of calcite in sodium chloride solutions at high temperatures. *American Journal of Science* **261**, 259-267.

Ewart, A., 1979. A review of the mineralogy and chemistry of Tertiary-Recent dacitic, latitic, rhyolitic and related salic volcanic rocks. *In* Barker, F., ed. *Trondhjemites, dacites and related rocks.* Elsevier, Amsterdam. 13-121.

Farr, M.R., 1989. Compositional zoning characteristics of late dolomite cement in the Cambrian Bonneterre Formation, Missouri: implications for parent fluid migration pathways. *Carbonates and Evaporites* **4**, 177-194.

Ferry, J.M., and Spear, F.S., 1978. Experimental calibration of the partitioning of Fe and Mg between biotite and garnet. *Contributions to Mineralogy and Petrology* **66**, 113-117.

Fink, J.H., and Manly, C.R., 1987. Origin of pumiceous and glassy textures in rhyolitic flows and domes.*Geological Society of America Special Paper* **212**, 77-88.

Fouquet, Y., von Stackelberg, U., Charlou, J.L., Donval, J.P., Foucher, J.P., Erzinger, J., Herzig, P., Mühe, R., Wiedicke, M., Soakai, S., and Whitechurch, H., 1991. Hydrothermal activity in the Lau back-arc basin: sulfides and water chemistry. *Geology* **19**, 303-306.

Fouquet, Y., von Stackelberg, U., Charlou, J.L., Erzinger, J., Herzig, P., Mühe, R., and Wiedicke, M., 1993. Metallogenesis in back-arc environments: the Lau basin example. *Economic Geology* **88**, 2154-2181.

Franklin, J.M., 1990. Volcanogenic massive sulphide deposits, ancient and modern [abs.]: Tenth Australian Geological Convention, Hobart, Geological Society of Australia, 11-13.

Franklin, J.M., Kasarda, J., and Poulsen, K.H., 1975. Petrology and chemistry of the alteration zone of the Mattabi massive sulphide deposit. *Economic Geology* **70**, 63-79.

Franklin, J.M., Sangster, D.M., and Lydon, J.W., 1981. Volcanic-associated massive sulphide deposits. *Economic Geology 75th Anniversary Volume*, 485-627.

Frater, K.M., 1983. Geology of the Golden Grove prospect, Western Australia: a volcanogenic massive sulfide-magnetite deposit. *Economic Geology* **78**, 875-919.

Frater, K.M., 1985a. Mineralization at the Golden Grove deposit, Western Australia. I: Premetamorphic textures of the opaque minerals. *Canadian Journal of Earth Sciences* **22**, 1-14.

Frater, K.M., 1985b. Mineralization at the Golden Grove Cu-Zn deposit, Western Australia. II: Deformation textures of the opaque minerals. *Canadian Journal of Earth Sciences* **22**, 15-26.

Fritz, P., Drimmie, R.J., and Nowocki, V.K., 1974. Preparation of sulfur dioxide for mass spectrometer analyses by combustion of sulfides with copper oxide. *Analytical Chemistry* **46**, 164-166.

Galley, A.G., Bailes, A.H., and Kitzler, G., 1993. Geological setting and hydrothermal evolution of the Chisel Lake and North Chisel Zn-Pb-Cu-Ag-Au massive sulfide deposits, Snow Lake, Manitoba. *Exploration and Mining Geology* **2**, 271-295.

Ganguly, J., and Saxena, S.K., 1984. Mixing properties of aluminosilicate garnets: constraints from natural and experimental data, and applications to geothermobarometry. *American Mineralogist* **69**, 88-97.

Gemmell, J.B., and Large, R.R., 1990. Geologic evolution of the stringer zone underlying the Hellyer volcanogenic sulphide deposit, Tasmania [abs.]: Pacific Rim Conference, Gold Coast, Queensland, Australia, 385-392.

Gemmell, J.B., and Large, R.R., 1992. Stringer system and alteration zones underlying the Hellyer volcanic-hosted massive sulfide deposit, Tasmania, Australia. *Economic Geology* **87**, 620-649.

Gemmell, J.B., and Large, R.R., 1993. Evolution of a VHMS hydrothermal system, Hellyer deposit, Tasmania, Australia: sulphur isotope evidence. *Resource Geology Special Issue* **17**, 108-119.

Gibson, P.J., Shaw, H.F., and Spiro, B., 1994. The nature and origin of sideritic ironstone bands in the Tertiary Lowmead and Duaringa Basins, Queensland. *Australian Journal of Earth Sciences* **41**, 255-263.

Gilligan, L.B., and Marshall, B., 1987. Textural evidence for remobilization in metamorphic environments. *Ore Geology Reviews* **2**, 205-229.

Gimeno, D., 1994. Genesis of crystal-rich epiclastic rocks from subaqueous silicic lava domes: role of thermal shock on quartz phenocrysts. *Sedimentary Geology* **90**, 33-47.

Goldman, D.S., and Albee, A.L., 1977. Correlation of Mg/Fe partitioning between garnet and biotite with $^{18}O/^{16}O$ partitioning between quartz and magnetite. *American Journal of Science* **277**, 750-767.

Goodfellow, W.D., and Blaise, B., 1988. Sulfide formation and hydrothermal alteration of hemipelagic sediment in Middle Valley, northern Juan de Fuca Ridge. *Canadian Mineralogist* **26**, 675-696.

Goodfellow, W.D., and Franklin, J.M., 1993. Geology, mineralogy, and chemistry of sediment-hosted clastic massive sulfides in shallow cores, Middle Valley, northern Juan de Fuca Ridge. *Economic Geology* **88**, 2037-2068.

Graham, U.M., Bluth, G.J., and Ohmoto, H., 1988. Sulfide-sulfate chimneys on the East Pacific Rise, 11° and 13° latitudes. Part 1: mineralogy and paragenesis. *Canadian Mineralogist* **26**, 487-504.

Green, G.R., 1983. The geological setting and formation of the Rosebery volcanic-hosted massive sulfide orebody, Tasmania. Ph.D. thesis, University of Tasmania, (unpubl.).

Green, G.R., Solomon, M., and Walshe, J.L., 1981. The formation of the volcanic-hosted massive sulfide ore deposit at Rosebery, Tasmania. *Economic Geology* **76**, 304-338.

Green, G.R., Ohmoto, H., Date, J., and Takahashi, T., 1983. Whole-rock oxygen isotope distribution in the Fukazawa-Kosaka area, Hokuroku district, Japan, and its potential application to mineral exploration. *Economic Geology Monograph* **5**, 395-411.

Gregg, J.M., and Sibley, D.F., 1984. Epigenetic dolomitization and the origin of xenotopic dolomite texture. *Journal of Sedimentary Petrology* **54**, 908-931.

Gregory, P.W., and Hartley, J.S., 1982. The Thalanga zinc-lead-copper-silver deposit [abs.]: Field Conference 1982, Charters Towers-Greenvale Area, Geological Society of Australia, Queensland Division, 12-21.

Gregory, P.W., Hartley, J.S., and Wills, K.J.A., 1987. The Thalanga massive sulphide deposit [abs.]: Pacific Rim Congress '87,Gold Coast, Queensland, 573-577.

Gregory, P.W., Hartley, J.S., and Wills, K.J.A., 1990. Thalanga zinc-lead-copper-silver deposit. *In* Hughes, F. E., ed. *Geology of the Mineral Deposits of Australia and Papua New Guinea.* Australasian Institute Mining Metallurgy, Monograph 14, 1527—1537.

Guidotti, C.V., 1984. Micas in metamorphic rocks. *In* Bailey, S.W., ed. *Micas.* Mineralogical Society of America, 357-467.

Hackler, R.T., and Wood, B.J., 1989. Experimental determination of Fe and Mg exchange between garnet and olivine and estimation of Fe-Mg garnet mixing properties. *American Mineralogist* **74**, 994-999.

Hall, W.D.M., 1981. Structural geology of the Thalanga area, North Queensland. Report to BHP, Minerals Division, Exploration Department, (unpubl.).

Hannington, M.D., and Scott, S.D., 1987. Sulfidation equilibria as guides to gold mineralization in volcanogenic massive sulfides [abs.]: *Geological Society of America Abstracts with Programs* **19**, 692.

Hannington, M.D., Peter, J.M., and Scott, S.D., 1986. Gold in sea-floor polymetallic sulfide deposits. *Economic Geology* **81**, 1867-1883.

Hanor, J.S., 1979. The sedimentary genesis of hydrothermal fluids. *In* Barnes, H.L., ed. *Geochemistry of hydrothermal ore deposits.* Wiley Intersciences, New York. 127-132.

Hanson, R.E., 1991. Quenching and hydroclastic disruption of andesitic to rhyolitic intrusions in a submarine island-arc sequence, northern Sierra Nevada, California. *Geological Society America Bulletin* **103**, 804-819.

Hanson, R.E., and Wilson, T.J., 1991. Submarine rhyolitic volcanism in a Jurassic proto-marginal basin; southern Andes, Chile and Argentina. *Geological Society of America, Special Paper* **265**, 13-27.

Hanson, R.E., and Wilson, T.J., 1993. Large-scale rhyolitic peperites (Jurassic, southern Chile). *Journal of Volcanology and Geothermal Research* **54**, 247-264.

Hartley, J.S., 1984. Thalanga - exploration history [abs.]: Seventh Australian Geological Convention, Sydney, New South Wales, Australian Geological Society, 216-218.

Hartley, J.S., Peters, S.G., and Beams, S.D., 1989. Current developments in Charters Towers geology and gold mineralisation [abs.]: North Queensland Gold '89 Conference, Townsville, Queensland, 7-14.

Hartley, J.S., Peters, S.G., and Beams, S.D., 1993. Geological context and concepts of mineralisation in the Charters Towers region. *In* Henderson, R.A., ed. *Guide to the economic geology of the Charters Towers region, northeastern Queensland.* 1993 Field Conference, Geological Society Australia, Queensland division, 49-59.

Henderson, R.A., 1980. Structural outline and summary geological history for northeastern Australia. *In* Henderson, R.A., and Stephenson, P.J., eds. *The geology and geophysics of northeastern Australia.* Geological Society Australia, Queensland division, Brisbane. 1-26.

Henderson, R.A., 1983. Early Ordovician faunas from the Mount Windsor Subprovince, northeastern Queensland. *Memoirs Association Australasian Palaeontologists* **1**, 145-175.

Henderson, R.A., 1986. Geology of the Mt Windsor Subprovince—a Lower Palaeozoic volcano-sedimentary terrane in the northern Tasman Orogenic Zone. *Australian Journal of Earth Sciences* **33**, 343-364.

Herrmann, W., 1994. Immobile element geochemistry of altered volcanics and exhalites at the Thalanga Deposit, north Queensland. M. Econ. Geol. thesis, University of Tasmania, (unpubl.).

Herz, N., and Force, E., 1984. Rock suites in Grenvillian terrane of the Roseland district, Virginia. Part 1. Lithological relations. *Geological Society of America Special Paper* **194**, 187-200.

Hill, A.P., 1992. Geology of the Thalanga Range. Pancontinental Mining Ltd, 92/9, (unpubl.).

Hill, A.P., 1993. Synchronous felsic volcanism and sea-floor base-metal sulphide mineralisation at East Thalanga, north Queensland, Australia [abs.]: General Assembly: Ancient Volcanism and Modern Analogues, Canberra, International Association of Volcanology and Chemistry of the Earth's Interior, 48.

Hill, A.P., and Orth, K., 1994. Textures and origin of carbonate associated with some Australian VHMS deposits [abs.]: AMF Symposium, Australian Research on Ore Genesis, Adelaide, 25.1– 25.3.

Hillenbrand, J.M., 1990. The Potato Sandstone – southern California; implications for displacement of San Andreas Fault. M. Sc. Thesis, University of California, (unpubl.).

Hoefs, J., 1987. *Stable isotope geochemistry.* Springer-Verlag, Berlin, 241p.

Holland, H.D., and Malinin, S.D., 1979. The solubility and occurrence of non-ore minerals. *In* Barnes, H.L., ed. *Geochemistry of hydrothermal ore deposits.* John Wiley, New York. 461-508.

Howells, M.F., Reedman, A.J., and Cambell, S.D.G., 1991. *Ordovician (Caradoc) marginal basin volcanism on Snowdonia (northwest Wales).* HMSO for the British Geological Survey, London, 191p.

Hoy, L.D., 1993. Regional evolution of hydrothermal fluids in the Noranda district, Quebec: evidence from $d^{18}O$ values from volcanogenic massive sulfide deposits. *Economic Geology* 88, 1526-1541.

Humphries, S.E., 1984. The mobility of rare earth elements in the crust. *In* Henderson, P., ed. *Rare Earth Element Geochemistry (Developments in Geochemistry, 2).* Elsevier, Amsterdam. 315-341.

Huston, D.L., 1988. Aspects of the geology of massive sulphide deposits from the Balcooma district, northern Queensland and Rosebery, Tasmania: implications for ore genesis. Ph.D. thesis, University of Tasmania, (unpubl.).

Huston, D.L., 1989. Preliminary investigations on the mineralogy of gold at the Thalanga deposit, north Queensland. Centre for Ore Deposit and Exploration Studies, University of Tasmania, Mount Windsor Project – Research Report No. 1, 75-83, (unpubl.).

Huston, D.L., 1990. The stratigraphic and structural setting of the Balcooma volcanogenic massive sulphide lenses, north Queensland. *Australian Journal of Earth Sciences* **37**, 423-440.

Huston, D.L., 1991. Distribution and mineralogical occurrence of gold and silver in the Thalanga volcanogenic massive sulphide deposit. Centre for Ore Deposit and Exploration Studies, University of Tasmania, Mount Windsor Project — Research Report No.2, 85-108, (unpubl.).

Huston, D.L., 1993. The effect of alteration and metamorphism on wall rocks to the Balcooma and Dry River South volcanic-hosted massive sulfide deposits, Queensland, Australia. *Journal of Geochemical Exploration* **48**, 277-307.

Huston, D.L. and Large, R.R., 1987. Genetic and exploration significance of the zinc ratio (100Zn/[Zn + Pb]) in massive sulfide systems. *Economic Geology* **82**, 1521-1539.

Huston, D.L., and Large, R.R., 1988. Distribution, mineralogy, and geochemistry of gold and silver in the north end orebody, Rosebery, Tasmania. *Economic Geology* **83**, 1181-1192.

Huston, D.L., and Large, R.R., 1989. A chemical model for the concentration of gold in volcanogenic massive sulphide deposits. *Ore Geology Reviews* **4**, 171-200.

Huston, D.L., Bottrill, R.S., Creelman, R.A., Khin Zaw, Ramsden, T.R., Rand, S.W., Gemmell, J.B., Jablonski, W., Sie, S.H., and Large, R.R., 1992a. Geologic and geochemical controls on the mineralogy and grain size of gold-bearing phases, eastern Australian volcanic-hosted massive sulfide deposits. *Economic Geology* **87**, 542-563.

Huston, D.L., Taylor, T., Fabray, J., and Patterson, D.J., 1992b. Comparison of the geology and mineralization of the Balcooma and Dry River South volcanic-hosted massive sulfide deposits, northern Queensland. *Economic Geology* **87**, 785-811.

Huston, D.L., Sie, S.H., Suter, G.F., and Ryan, C.G., 1993. The composition of pyrite in volcanogenic massive sulfide deposits as determined with the proton microprobe. *Nuclear Instruments and Methods of Physical* Research, Series **B75**, 531-534.

Huston, D.L., Kuronen, U., and Stolz, J., 1995a. Waterloo, and Agincourt prospects, northern Queensland: contrasting styles of mineralization within the same volcanogenic hydrothermal system. *Australian Journal of Earth Sciences* **42**, 203-221.

Huston, D.L., Sie, S.H., Suter, G.F., Cooke, D.R. and Both, R.A., 1995b. Trace elements in sulfide minerals from eastern Australian volcanic - hosted massive sulfide deposits: Part I. Proton microprobe analyses of pyrite, chalcopyrite, and sphalerite, and Part II. Selenium levels in pyrite: comparison with $\delta^{34}S$ values and implications for the source of sulfur in volcanogenic hydrothermal system. *Economic Geology* **90**, 1167-1196.

Huston, D., Talyor, B., Bleeker, W., Stewart, B., Cook, R., and Koopman, E.R., 1995c. Isotope mapping around the Kidd Creek deposit, Ontario: application to exploration and comparison with other geochemical indicators. *Exploration and Mining Geology* **4**, 175-185.

Hutchinson, R.W., 1982. Syn-depositional hydrothermal processes and Precambrian sulphide deposits. *In* Hutchinson, R.W., Spence, C.D. and Franklin, J.M., eds. *Precambrian Sulphide Deposits, H.S. Robinson Memorial Volume.* Geological Association of Canada Special Paper 25, 761-791.

Hutchinson, M.N., and Scott, S.D., 1981. Sphalerite geobarometry in the Cu-Fe-Zn-S system. *Economic Geology* **76**, 143-153.

Hutton, L.J., and Crouch, S.B.S., 1993. New and revised igneous units in the Charters Towers 1:100 000 Sheet areas. Queensland Government Mining Journal, (unpubl.).

Hutton, L.J., Rienks, I.P., and Wyborn, D., 1990. A reinterpretation of the Ravenswood Batholith, north Queensland [abs.]: Pacific Rim Congress '90, Proceedings, 179-185.

Hutton, L.J., Rienks, I.P., and Wyborn, D., 1992. Granites of the Ravenswood Batholith, northern Australia [abs.]: The second Hutton Symposium on the origin of granites and related rocks, *Transactions Royal Society Edinburgh, Earth Sciences* 83,492.

Hutton, L.J., Hartley, J.S., and Rienks, I.P., 1993. Geology of the Charters Towers region. *In* Henderson, R.A., ed. *Guide to the economic geology of the Charters Towers region, northeastern Queensland.* 1993 Field Conference, Geological Society Australia, Queensland division, 1-12.

Hutton, L.J., Rienks, I.P., Woods, K.T., Hartley, J.S., and Crouch, S.B.S., 1994. A geochemically and structurally based reinterpretation of the Ravenswood Batholith, North Queensland [abs.]: New Developments in Geology and Metallogeny: Northern Tasman Orogenic Zone, Townsville, EGRU Contribution, 3-5.

Irvine, R.J., 1987. Drillhole TEM surveys at Thalanga, Queensland. *Bulletin of the Australian Society of Exploration Geophysics* **18**, 285-293.

Ishihara, S., and Sasaki, A., 1978. Sulfur of Kuroko deposits – a deep seated origin? *Mining Geology* **28**, 361-367.

Izawa, E., Yoshida, T. and Saito, R., 1978. Geochemical characteristics of hydrothermal alteration around the Fukazawa Kuroko deposit, Akita, Japan. *Mining Geology* **28**, 325-335.

Jack, D.J., 1989. Hellyer host rock alteration. M. Sc. thesis , University of Tasmania, (unpubl.).

Janecky, D.R., and Seyfried, W.E., 1984. Formation of massive sulfide deposits on oceanic ridge crests: incremental reaction models of mixing between hydrothermal solutions and seawater. *Geochimica et Cosmochimica Acta* **48**, 2723-2738.

Jeppsson, M., 1987. Mineral chemistry of silver in antimony and bismuth rich sulfide ores in Bergslagen, central Sweden. *Neues Jahrbuch Mineralogie Monatsh* **H5**, 205-216.

Jiang, W.T., Peacor, D.R., and Buseck, P.R., 1994. Chlorite geothermometry - contamination and apparent octahedral. *Clays and Clay Minerals* **42**, 593-605.

Kay, J.R., 1987. The Highway gold mine, Charters Towers—submarine volcanogenic gold-barite stringer mineralization, modified by lateritic weathering. *University of Queensland, Department of Geology Paper* **12**, 111-125.

Kajiwara, Y., 1971. Sulfur isotope study of the Kuroko-ores of the Shakanai No.1 deposits, Akita Prefecture, Japan. *Geochemical Journal* **4**, 157-181.

Kano, K., Takeuchi, K., Yamamoto, T., and Hoshizumi, H., 1991. Subaqueous rhyolite block lavas in the Miocene Ushikiri Formation, Shimane Peninsula, SW Japan. *Journal of Volcanology and Geothermal Research* **46**, 241-253.

Kelly, W.C., and Clark, B.R., 1975. Sulfide deformation studies: III. Experimental deformation of chalcopyrite to 2000 bars and 500°C. *Economic Geology* **70**, 431-435.

Khin Zaw, 1991. The effect of Devonian metamorphism and metasomatism on the mineralogy and geochemistry of the Cambrian VMS deposits in the Rosebery-Hercules district, western Tasmania. Ph.D. thesis, University of Tasmania, (unpubl.).

Khin Zaw, and Large, R.R., 1990. ^{18}O and ^{13}C isotopic variation of hydrothermal carbonates from the Rosebery, Hercules and South Hercules deposits, western Tasmania: Interplay of Cambrian vs Devonian systems [abs.]: Seventh International Conference Geochronology, Cosmochronology and Isotope Geology, Canberra, Geological Society of Australia, 114.

Khin Zaw, and Large, R.R., 1992. The precious metal-rich South Hercules mineralisation, western Tasmania: A possible subsea-floor replacement volcanic-hosted massive sulfide deposit. *Economic Geology* **87**, 931—952.

Kirkegaard, A.G., 1974. Structural elements in the northern part of the Tasman Geosyncline. *In* A.K. Denmead, G.W.T., and A.F. Wilson, eds. *The Tasman Geosyncline—a symposium.* Geological Society Australia, Queensland division, Brisbane. 47-64.

Kleemann, U., and Reinhardt, J., 1994. Garnet-biotite thermometry revisited: the effect of AL^{VI} and Ti in biotite. *European Journal of Mineralogy* **6**, 925-941.

Knuckey, M.J., Comba, C.D.A., and Riverin, G., 1982. Structure, metal zonation and alteration at the Millenbach deposit, Noranda, Quebec. *In* Hutchinson, R.W., Spence, C.D., and Franklin, J.M., eds. *Precambrian Sulphide Deposits, H.S. Robinson Memorial Volume.* Geological Association of Canada Special Paper 25 , 255-295.

Kokelaar, B.P., 1982. Fluidization of wet sediments during the emplacement and cooling of various igneous bodies. *Journal of the Geological Society London* **139**, 21-33.

Kokelaar, P., 1986. Magma-water interactions in subaqueous and emergent basaltic volcanism. *Bulletin of Volcanology* **48**, 275-289.

Koski, R.A., Lonsdale, P.F., Shanks, W.C., Berndt, M.E., and Howe, S.S., 1985. Mineralogy and geochemistry of a sediment-hosted hydrothermal sulfide deposit from the Southern Trough of Guaymas Basin, Gulf of California. *Journal of Geophysical Research* **90**, 6695-6707.

Kranidiotis, P., and MacLean, W.H., 1987. Systematic of chlorite alteration at the Phelps Dodge massive sulfide deposit, Matagami, Quebec. *Economic Geology* **82**, 1898-1911.

Kretschmar, U., and Scott, S.D., 1976. Phase relations involving arsenopyrite in the system Fe-As-S and their application. *Canadian Mineralogist* **14**, 364-386.

Kurokawa, A., 1991. Formation of felsic pumiceous hyaloclastites: a case study from Tadami district, Fukushima Prefecture, Japan. *Journal of Mineralogy, Petrology and Economic Geology (in Japanese)* **86**, 439-458.

Kusakabe, M., Chiba, H., and Ohmoto, H., 1982. Stable isotopes and fluid inclusion study of anhydrite from the East Pacific Rise at 21°N. *Geochemical Journal* **16**, 89-95.

Kushiro, I., 1976. Changes in viscosity and structure of melt of $NaAlSi_2O_6$ composition at high pressures. *Journal of Geophysical Research* **81**, 6347-6350.

Kushiro, I., 1978. Density and viscosity of hydrous calc-alkaline andesite magma at high pressures. Carnegie Institute Washington, Yearbook 77, 675-677.

Kushiro, I., 1980. Viscosity, density and structure of silicate melts at high pressures, and their petrological applications. *In* Hargraves, R.B., ed. *Physics of magmatic processes.* Princeton University Press, Princeton, New Jersey. 93-120.

Kushiro, I., Yoder, H.S. Jnr, and Mysen, B.O., 1976. Viscosities of basalt and andesite melts at high pressures. *Journal of Geophysical Research* **81**, 6351-6356.

Lacroix, J., Daigneault, R., Chartrand, F., and Guha, J., 1993. Structural evolution of the Grevet Zn-Cu massive sulfide deposit, Lebel-sur-Quévillon area, Abitibi subprovince, Quebec. *Economic Geology* **88**, 1559-1577.

Laing, W.P., 1984. The structural environment of the Thalanga ore deposit. Report to Penarroya (Aust) Pty Ltd, (unpubl.).

Lambert, I.B., and Scott., K.M., 1973. Implications of geochemical investigations of sedimentary rocks within and around the McArthur zinc-lead-silver deposit, Northern Territory. *Journal of Geochemical Exploration* **2**, 307-330.

Large, R.R., 1977. Chemical evolution and zonation of massive sulfide deposits in volcanic terrains. *Economic Geology* **72**, 549-572.

Large, R.R., 1992. Australian volcanic-hosted massive sulfide deposits: features, styles and genetic models. *Economic Geology* **87**, 471—510.

Large, R.R., and Both R.A., 1980. The volcanogenic sulfide ores at Mount Chalmers, eastern Queensland. *Economic Geology* **75**, 992—1009.

Large, R.R., McGoldrick, P.J., Berry, R.F., and Young, C.H., 1988. A tightly folded, gold-rich, massive sulfide deposit: Que River mine, Tasmania. *Economic Geology* **83**, 681-693.

Larocque, A.C.L., and Hodgson, C.J., 1993. Carbonate-rich footwall alteration at the Mobrun mine, a possible Mattabi-type VMS deposit in the Noranda camp. *Exploration and Mining Geology* **2**, 165-169.

Larocque, A.C.L., and Hodgson, C.J., 1995. Effects of greenschist-facies metamorphism and related deformation on the Mobrun massive sulfide deposit, Québec, Canada. *Mineralium Deposita* **30**, 439-448.

Larocque, A.C.L., Hodgson, C.J., and Lafleur, P-J., 1993. Gold distribution in the Mobrun volcanic-associated massive sulfide deposit, Noranda, Quebec: a preliminary evaluation of the role of metamorphic remobilization. *Economic Geology* **88**, 1443-1459.

Larocque, A.C.L., Hodgson, C.J., Cabri, L.J., and Jackman, J.A., 1995. Ion-microprobe analysis of pyrite, chalcopyrite and pyrrhotite from the Mobrun VMS deposit in northwestern Quebec: evidence for metamorphic remobilization of gold. *The Canadian Mineralogist* **33**, 373-388.

Levingston, K.R., 1981. *Geological evolution and economic geology of the Burdekin River region, Queensland.* Bureau Mineral Resources, Geology and Geophysics, Bulletin 208.

Lianghat, S., and MacLean, H., 1995. Lithogeochemistry of altered rocks at the New Insco VMS deposit, Noranda, Quebec. *Journal of Geochemical Exploration* **52**, 333-350.

Lonsdale, P., and Hawkins, J., 1985. Silicic volcanism at an off-axis geothermal field in the Mariana Trough back-basin. *Geological Society of America Bulletin* **96**, 940-951.

Lusk, J., and Crockett, J.H., 1969. Sulfur isotope fractionation in co-existing sulfides from the Heath Steele B-1 orebody, New Brunswick, Canada. *Economic Geology* **64**, 147-155.

Lydon, J.W., 1988. Volcanogenic massive sulphide deposits, Part 2: Genetic models. *In* Roberts, R.G., and Sheahan, P.A., eds. *Ore Deposit Models.* Geoscience Canada, 43-65.

Machel, H.G., 1985. Cathodoluminescence in calcite and dolomite and its chemical interpretation. *Geoscience Canada* **12**, 139-147.

MacLean, W.H., 1988. Rare earth element mobility at constant inter-REE ratios in the alteration zone at the Phelps Dodge massive sulfide deposit, Matagami, Quebec. *Mineralium Deposita* **23**, 231-238.

MacLean, W.H., and Barrett, T.J., 1993. Lithogeochemical techniques using immobile elements. *Journal of Geochemical Exploration* **48**, 109-133.

MacLean, W.H., and Hoy, L.D., 1991. Geochemistry of hydrothermally altered rocks at the Horne mine, Noranda, Quebec. *Economic Geology* **86**, 506-528.

MacLean, W.H., and Kranidiotis, P., 1987. Immobile elements as monitors of mass transfer in hydrothermal alteration: Phelps Dodge massive sulfide deposit, Matagami, Quebec. *Economic Geology* **82**, 951-962.

Maiden, K.J., Chimimba, L.R., and Smalley, T.J., 1986. Cuspate ore rock interfaces, piercement structures and the localization of some sulfide deposits. *Economic Geology* **81**, 1464-1472.

Marshall, B., and Gilligan, L.B., 1987. An introduction to remobilization: information from ore-body geometry and experimental considerations. *Ore Geology Reviews* **2**, 87-131.

Marshall, B., and Gilligan, L.B., 1989. Durchbewegung structure, piercement cusps, and piercement veins in massive sulphide deposits: formation and interpretation. *Economic Geology* **84**, 2311-2319.

Marshall, B., and Gilligan, L.B., 1993. Remobilization, syn-tectonic processes and massive sulphide deposits. *Ore Geology Reviews* **8**, 39-64.

McArther, G.J., and Dronseika, E.V., 1990. Que River and Hellyer zinc-lead deposits. *Australasian Insititute of Mining and Metallurgy Monograph* **15**, 1331-1339.

McBirney, A.R., 1963. Factors governing the nature of submarine volcanism. *Bulletin of Volcanology* **26**, 455-469.

McBirney, A.R., 1980. Mixing and unmixing of magmas. *Journal of Volcanology and Geothermal Research* **7**, 357-371.

McBirney, A.R., and Murase, T., 1970. Factors governing the formation of pyroclastic rocks. *Bulletin of Volcanology* **34**, 372-384.

McClay, K.R., 1983. Structural evolution of the Sullivan Fe-Pb-Zn-Ag orebody, Kimberley, British Columbia, Canada. *Economic Geology* **78**, 1398-1424.

McClay, K.R., and Ellis, P.G., 1984. Deformation of pyrite. *Economic Geology* **79**, 400-403.

McConnell, K.I., and Costello, J.O., 1984. Basement-cover rock relationships along the western edge of the Blue Ridge thrust sheet in Georgia. *Geological Society of America Special Paper* **194**, 263-280.

McCrea, J.M., 1950. The isotope chemistry of carbonates and a paleotemperature scale. *Journal of Chemical Physics* **18**, 849-857.

McDonald, J.A., 1967. Metamorphism and its effects on sulphide assemblages. *Mineralium Deposita* **2**, 200-220.

McDougall, T.J., 1984. Fluid dynamic implications for massive sulphide deposits of hot saline fluid flowing into a submarine depression from below. *Deep-Sea Research* **31**, 145-170.

McKay, W.J., and Hazeldene, R.K., 1987. Woodlawn Zn-Pb-Cu sulfide deposit, New South Wales, Australia: an interpretation of ore formation from field observations and metal zoning. *Economic Geology* **82**, 141–164.

McKay, W.J., and Walshe, J.L., 1990. Environment and mechanism of formation of the Woodlawn massive sulphide deposit, NSW [abs.]: Tenth Australian Geological Convention, Hobart, Geological Society of Australia, 5.

McLeod, R.L., 1987. Alteration associated with volcanogenic sulphide ores at Mount Chalmers, Queensland, Australia. *Transactions of the Institution of Mining and Metallurgy, Section B* **96**, 117-127.

McLeod, R.L., and Stanton, R.L., 1984. Phyllosilicates and associated minerals in some Paleozoic stratiform sulfide deposits of southeastern Australia. *Economic Geology* **79**, 1-22.

McPhie, J., 1993. The Tennant Creek porphyry revisited: a synsedimentary sill with peperitic margins, Early Proterozoic, Northern Territory. *Australian Journal of Earth Sciences* **40**, 545-558.

McPhie, J., and Allen, R.L., 1992. Facies architecture of mineralized submarine volcanic sequences: Cambrian Mount Read Volcanics, western Tasmania. *Economic Geology* **87**, 587—596.

McPhie, J., Doyle, M., and Allen, R.L., 1993. *Volcanic textures: a guide to the interpretation of textures in volcanic rocks.* CODES Key Centre, University of Tasmania, Hobart, 196p.

Menzies, J.C., 1979. Geology and geochemistry of the Thalanga Range area and Thalanga massive sulphide. B.Sc. Honours thesis, James Cook University, (unpubl.).

Miller, C.R., 1996. Geological and geochemical aspects of the Liontown VHMS deposit, north eastern Queensland. M. Econ. Geol., University of Tasmania, (unpubl.).

Miller, J., 1988. Cathodoluminescence microscopy. *In* Tucker, M.E., ed. *Techniques in Sedimentology.* Blackwell Scientific Publications, Oxford. 174-190.

Mookherjee, A., 1964. Thermal metamorphism of the sulphide minerals at Zawar Mines, Rajasthan, India. *Economic Geology* **59**, 498-501.

Mookherjee, A., 1976. Ores and metamorphism. *In* Wolf, K.H., ed. *Handbook of Stratabound and Stratiform Ore Deposits.* 4, Elsevier, Amsterdam. 204-260.

Mookherjee, A., and Mishra, B., 1984. 'Derived' and observed sulphosalt-sulphide phase assemblages compared - a case study from Rajpura-Dariba, India. *Mineralium Deposita* **19**, 112-117.

Morrison, G.W., 1988. Palaeozoic gold deposits of northeast Queensland [abs.]: Bicentennial Gold 1988, Geological Society Australia, 91-101.

Morton, R.L., and Franklin, J.M., 1987. Two-fold classification of Archean volcanic-associated massive sulfide deposits. *Economic Geology* **82**, 1057-1063.

Morton, R.L., and Nebel, M.L., 1984. Hydrothermal alteration of felsic volcanic rocks at the Helen siderite deposit, Wawa, Ontario. *Economic Geology* **79**, 1319-1333.

Mulholland, I.R., 1991. The geology, petrology and alteration geochemistry of the Magpie volcanogenic massive sulfide deposit, north Queensland, Australia. *Economic Geology* **86**, 1387-1400.

Munoz, J.L., 1984. F-OH and Cl-OH exchange in micas with applications to hydrothermal ore deposits. *In* Bailey, S.W., ed. *Micas.* Mineralogical Society of America, 469-493.

Murray, C.G., 1986. Metallogeny and tectonic development of the Tasman Fold Belt in Queensland. *Ore Geology Reviews* **1**, 315-400.

Murray, C.G., 1990. Tasman fold belt in Queensland. *In* Hughes, F.E., ed. *Geology of the Mineral Deposits of Australia and Papua New Guinea.* Australasian Institute Mining Metallurgy, 1431-1450.

Murray, C.G., and Kirkegaard, A.G., 1978. The Thompson Orogen of the Tasman Orogenic Zone. *Tectonophysics* **48**, 299-325.

Nickel, E., 1978. The present status of cathode luminescence as a tool in sedimentology. *Minerals Science and Engineering* **10**, 73-100.

Norrish, K., and Chappell, B.W., 1977. X-ray fluorescence spectrometry. *In* Zussman, J., ed. *Physical Methods in Determinative Mineralogy.* Academic Press, London. 201-272.

Offler, R., and Whitford, D.J., 1992. Wall-rock alteration and metamorphism of a volcanic-hosted massive sulfide deposit at Que River, Tasmania: petrology and mineralogy. *Economic Geology* **87**, 686-705.

Ohmoto, H., 1972. Systematics of sulfur and carbon isotopes in hydrothermal ore deposits. *Economic Geology* **67**, 551-578.

Ohmoto, H., 1986. Stable isotope geochemistry of ore deposits. *In* Valley, J.W., Taylor, H.P., and O'Neil, J.R., eds. *Stable Isotopes in High Temperature Geological Processes.* Mineralogical Society of America, 491-560.

Ohmoto, H. and Lasaga, A., 1982. Kinetics of reactions between aqueous sulfates and sulfides in hydrothermal systems. *Geochimica et Cosmochimica Acta* **46**, 1727-1745.

Ohmoto, H., and Rye, R.O., 1979. Isotopes of sulfur and carbon. *In* Barnes, H.L., ed. *Geochemistry of Hydrothermal Ore Deposits.* John Wiley and Sons, New York. 509-567.

Ohmoto, H., Mizukami, M., Drummond, S.E., Eldridge, C.S., Pisutha-Arnond, V., and Lenagh, T.C., 1983. Chemical processes of Kuroko formation. *Economic Geology Monograph* **5**, 570-604.

Orth, K.O., and Hill, A.P., 1994. Textures and origins of carbonate associated with the Rosebery VHMS deposit [abs.]: Contentious issues in Tasmanian geology, Hobart, Geological Society of Australia, 105.

Osterberg, S.A., Morton, R.L., and Franklin, J.M., 1987. Hydrothermal alteration and physical volcanology of Archean rocks in the vicinity of the Headway-Coulee massive sulfide occurrence, Onaman area, northwestern Ontario. *Economic Geology* **82**, 1505-1520.

Osterman, C., and Hutchinson, R.W., 1994. Sulfide piercement structures in the Selebi-Phiwe nickel-copper deposits, Botswana. *Exploration and Mining Geology* **3**, 285-295.

Paine, A.G.L., Harding, R.R., and Clarke, D.E., 1971. *Geology of the northeastern part of the Hughenden 1:250 000 Sheet area, Queensland.* Bureau Mineral Resources, Geology and Geophysics Australia, Report 126.

Paine, A.G.L., Clarke, D.E., and Gregory, C.M., 1974. *Geology of the northern half of the Bowen 1:250,000 Sheet area, Queensland, (with additions to the geology of the southern half).* Bureau Mineral Resources, Geology and Geophysics Australia, Report 145.

Pan, Y. and Fleet, M., 1992. Mineralogy and genesis of calc-silicates associated with Archean volcanogenic massive sulphide deposits at the Manitouwadge mining camp, Ontario. *Canadian Journal of Earth Science* **29**, 1375-1388.

Paradis, S., Jonasson, I.R., Le Cheminant, G.M, and Watkinson, D.H., 1988. Two zinc-rich chimneys from the plume site, southern Juan de Fuca Ridge. *Canadian Mineralogist* **26**, 637-654.

Paulick, H., 1996. Facies architecture, alteration and metamorphism of the volcanic host rock sequence at the Thalanga massive sulphide deposit, north Queensland, Australia. CODES: AMIRA Project P439 — Studies of VHMS-related alteration: geochemical and mineralogical vectors to ore, Report 2, 147-153, (unpubl.).

Pearce, J.A., and Cann, J.R., 1971. Ophiolite origin investigated by discriminant analysis using Ti, Zr and Y. *Earth and Planetary Science Letters* **12**, 339-349.

Pearce, J.A., and Cann, J.R., 1973. Tectonic setting of basic volcanic rocks determined using trace element analyses. *Earth and Planetary Science Letters* **19**, 290-300.

Pederson, T.F., and Price, N.B., 1982. The geochemistry of manganese carbonate in Panama Basin sediments. *Geochimica et Cosmochimica Acta* **40**, 413-423.

Perchuk, L.L., and Lavrent'eva, I.V., 1983. Experimental investigation of the exchange equilibria in the system cordierite-garnet-biotite. *In* Saxena, S.K., eds. *Kinetics and Equilibrium in Mineral Reactions; Advances in Physics and Geochemistry.* 3, Springer, New York. 199-239.

Perkins, C., and Walshe, J.L., 1993. Geochronology of the Mount Read Volcanics, Tasmania, Australia. *Economic Geology* **88**, 1176-1197.

Perkins, C., McDougall, I., and Walshe, J.L., 1993. Isotopic dating of precious and base metal deposits and their host rocks in eastern Australia, final report. Australian Mineral Industries Research Association Ltd, Project P334, (unpubl.).

Pesquera, A., and Velasco, F., 1993. Ore metamorphism in sulfide mineralizations from the Cinco Villas massif (western Pyrenees, Spain). *Economic Geology* **88**, 266-282.

Peter, J.M., and Scott, S.D., 1988. Mineralogy, composition, and fluid inclusion microthermometry of seafloor hydrothermal deposits in the Southern Trough of the Guaymas Basin, Gulf of California. *Canadian Mineralogist* **26**, 567-587.

Petit, J.P., 1987. Criteria for the sense of movement on fault surfaces in brittle rocks. *Journal of Structural Geology* **9**, 597-608.

Pierson, B.J., 1981. The control of cathodoluminescence in dolomite by iron and manganese. *Sedimentology* **28**, 601-610.

Pichler, H., 1965. Acid hyaloclastites. *Bulletin of Volcanology* **28**, 293-310.

Pisutha-Arnond, V., and Ohmoto, H., 1983. Thermal history, and chemical and isotopic compositions of the ore-forming fluids responsible for the kuroko massive sulfide deposits in the Hokuroko district of Japan. *Economic Geology Monograph* **5**, 523-558.

Pitt, M.A., 1988. Nature and origin of the Campaspe Formation: a Pliocene continental sedimentary assemblage from north Queensland. B.Sc. Honours, James Cook University of North Queensland, (unpubl.).

Plimer, I.R., 1980. Hydrothermal mobilization of silver during retrograde metamorphism at Broken Hill, Australia. *Neues Jahrbuch Mineralogie Monatsh* **H10**, 433-439.

Poitrasson, F., Pin, C., and Duthou, J.L., 1995. Hydrothermal remobilization of rare earth elements and its effect on Nd isotopes in rhyolite and granite. *Earth and Planetary Science Letters* **130**, 1-11.

Powell, R., and Holland, T.J.B., 1990. An enlarged and updated internally consistent thermodynamic data set with uncertainties and correlations: the system K_2O-Na_2O-CaO-MgO-MnO-FeO-Fe_2O_3-Al_2O_3-TiO_2-SiO_2-C-H_2-O_2. *Journal of Metamorphic Geology* **8**, 89-124.

Purvis, A.H., 1989. The geology and development of the Thalanga massive sulphide deposit [abs.]: Base Metal Update: Some Australian Base Metal Projects — Exploration and Recent Developments, Sydney, New South Wales Department of Minerals and Energy, and Sydney Mineral Exploration Discussion Group, 21-23.

Ramdohr, P., 1980. *Ore Minerals and their Intergrowth.* Pergamon Press, Oxford, 1174p.

Ramsay , J.G., and Huber, M.I., 1987. *The Techniques of Modern Structural Geology, Volume 2: Folds and Fractures.* Academic Press, London, 700p.

Raymond, O.L., 1992. Geology and mineralisation of the southern Prince Lyell Deeps, Queenstown, Tasmania. M. Sc. Thesis, University of Tasmania, (unpubl.).

Richards, D.N.G., 1980. Palaeozoic granitoids of northeastern Australia. *In* Stephenson, P.J. and Henderson R.A., eds. *The geology and geophysics of northeastern Australia.* Geological Society Australia, Queensland division, Brisbane. 229-246.

Rienks, I.P., 1991. Geology of the southern portion of the Mingela 1:100 000 Sheet area. Queensland Resource Industries, Record 1991/13, (unpubl.).

Riverin, G., and Hodgson, C.J., 1980. Wall-rock alteration at the Millenbach Cu-Zn mine, Noranda, Quebec. *Economic Geology* **75**, 424-444.

Rivers, C.J., 1985. An investigation of the effects of hydrothermal alteration in the footwall rocks of the Thalanga volcanogenic massive sulphide deposit, north Queensland. B. Sc. (Hons) thesis, James Cook University, (unpubl.).

Rollinson, H.R., 1993. *Using Geochemical Data: Evaluation, Presentation, Interpretation.* Longman Scientific and Technical, Essex, England, 352p.

Robinson, B.W. and Kusakabe, M., 1975. Quantitative preparation of SO_2 for $^{34}S/^{32}S$ analyses from sulfides by combustion with cupreous oxide. *Analytical Chemistry* **47**, 1179-1181.

Roscoe, W.E., 1975. Experimental deformation of natural chalcopyrite at temperatures up to 300°C over the strain rate range 10^{-2} to 10^{-6} sec^{-1}. *Economic Geology* **70**, 454-472.

Rye, R.O., and Ohmoto, H., 1974. Sulfur and carbon isotopes and ore genesis: a review. *Economic Geology* **69**, 826-842.

Sagalevich, A.M., Torokhov, P.V., Matveyenkov, V.V., Galkin, S.V., and Moskalev, L.I., 1992. Hydrothermal manifestations at Piyp submarine volcano, Bering Sea. *International Geology Review* **34**, 1200-1209.

Salmon, B.C., Clark, B.R., and Kelly, W.C., 1974. Sulfide deformation studies II. Experimental deformation of galena to 2000 bars and 400°C. *Economic Geology* **69**, 1-16.

Sangster, D.F., 1968. Relative sulphur isotope abundances of ancient seas and stratabound sulphide deposits. *Geological Association of Canada Proceedings* **17**, 79-91.

Sangster, D.F., 1972. Precambrian volcanogenic massive sulphide deposits in Canada. Geological Survey of Canada Paper 72-22, 44p.

Sato, T., 1972. Behaviours of ore-forming solutions in seawater. *Mining Geology* **22**, 31-42.

Savard, M.M., Veizer, J., and Hinton, R., 1995. Cathodoluminescence at low Fe and Mn concentrations - a SIMS study of zones of natural calcites. *Journal of Sedimentary Research* **65**, 208-213.

Sawkins, F.J., 1986. Some thoughts on the genesis of kuroko-type deposits. *Geology in the Real World — the Kingsley Dunham Volume.* London Institute of Mining and Metallurgy, 387-394.

Sawkins, F.J., and Kowalik, J., 1981. The source of ore metals at Buchans: magmatic versus leaching models. *In* Swanson, E.A., Strong, D.F. and Thurlow, J.G., eds. *The Buchans Orebodies: Fifty Years of Geology and Mining.* Geological Association of Canada Special Paper 22, 255-267.

Schade, J., Cornell, D.H., and Theart, H.F.J., 1989. Rare earth element and isotopic evidence for the genesis of the Prieska massive sulfide deposit, South Africa. *Economic Geology* **84**, 49-63.

Schandl, E.S., and Wicks, F.J., 1993. Carbonate and associated alteration of ultramafic and rhyolitic rocks at the Hemingway property, Kidd Creek Volcanic Complex, Timmins, Ontario. *Economic Geology* **88**, 1615-1635.

Scheepers, R., and Rozendaal, A., 1993. Redistribution and fractionation of U, Th and Rare-earth elements during weathering of subalkaline granites in SW Cape Province, South Africa. *Journal of African Earth Sciences and the Middle East* **17**, 41-50.

Schmidt, J.M., 1988. Mineral and whole-rock compositions of seawater-dominated hydrothermal alteration at the Artic volcanogenic massive sulfide prospect, Alaska. *Economic Geology* **83**, 822-842.

Schroeder, N.A.M., Kulm, L.D., and Muehlberg, G.E., 1987. Carbonate chimneys on the outer continental shelf: evidence for fluid venting on the Oregon margin. *Oregon Geology* **49**, 91-98.

Schwarcz, H.P., and Burnie, S.W., 1973. Influence of sedimentary environments on sulfur isotope ratios in clastic rocks: a review. *Mineralium Deposita* **8**, 264-277.

Scott, S.D., 1973. Experimental calibration of the sphalerite geobarometer. *Economic Geology* **68**, 466-474.

Scott, S.D., 1976. Application of the sphalerite geobarometer to regionally metamorphosed terrains. *American Mineralogist* **61**, 661-670.

Scott, S.D., 1983. Chemical behaviour of sphalerite and arsenopyrite in hydrothermal and metamorphic environments. *Mineralogical Magazine* **47**, 427-435.

Scott, S.D., and Barnes, H.L., 1971. Sphalerite geothermometry and geobarometry. *Economic Geology* **66**, 653-669.

Scott, S.D., Both, R.A., and Kissin, S.A., 1977. Sulfide petrology of the Broken Hill region, New South Wales. *Economic Geology* **72**, 1410-1425.

Seyfried, W., 1993. Chemical processes in subseafloor hydrothermal systems: experimental and theoretical constraints [abs.]: Workshop and Short Course, Physical, Chemical, Biological and Geological Interactions within Seafloor Hydrothermal Systems, RIDGE Theoretical Institute, Section E.

Seyfried, W.E., and Ding, K., 1993. The effect of redox on the relative solubilities of copper and iron in Cl-bearing aqueous fluids at elevated temperatures and pressures: an experimental study with application to subseafloor hydrothermal processes. *Geochimica et Cosmochimica Acta* **57**, 1905-1917.

Shanks, W.C., III,, Bischoff, J.L., and Rosenbauer, R.J., 1981. Seawater sulfate reduction and sulfur isotope fractionation in basaltic systems: interactions of seawater with fayalite and magnetite at 200-350°C. *Geochimica et Cosmochimica Acta* **45**, 1977-1995.

Sharpe, R., 1991. The distribution, mineralogy and paragenesis of the Hellyer baritic and siliceous caps. B.Sc. Honours, University of Tasmania, (unpubl.).

Shaw, S.E., and Flood, R.H., 1981. The New England batholith, eastern Australia: geochemical variations in time and space. *Journal of Geophysical Research* **86**, 10530-10544.

Sheppard, S.M.F., and Schwarcz, H.P., 1970. Fractionation of carbon and oxygen isotopes and magnesium between coexisting metamorphic calcite and dolomite. *Contributions to Mineralogy and Petrology* **26**, 161-198.

Shiraki, R., Sakai, H., Kishima, K., and Tazaki, K., 1978. Hydrothermal reaction experiments on the system rhyolite-seawater [abs.]: Geochimica Society of Japan Annual Meeting Abstracts **1**, 191.

Solomon, M., 1976. "Volcanic" massive sulphide deposits and their host rocks — a review and an explanation. *In* Wolfe, K.A., ed. *Handbook of Strata-bound and Stratiform Ore Deposits, II, Regional studies and Specific Deposits.* Elsevier, Amsterdam. 21-50.

Solomon, M., 1981. Introduction to the geology and metallic ore deposits of Tasmania. *Economic Geology* **76**, 194-208.

Solomon, M. & Groves, D. I. 1994. The Geology and Origin of Australia's Mineral Deposits. Oxford University Press, Oxford, 951p.

Solomon, M., Eastoe, C.J., Walshe, J.L., and Green, G.R., 1988. Mineral deposits and sulfur isotope abundances in the Mount Read Volcanics between Que River and Mount Darwin, Tasmania. *Economic Geology* **83**, 1307-1328.

Solomon, M., Walshe, J.L., and Heinrich, C.A., 1990. The formation of Rosebery-type, volcanogenic massive sulphide deposits [abs.]: Tenth Australian Geological Convention, Hobart, Geological Society of Australia, 6.

Sommer, S.E., 1972. Cathodoluminescence of carbonates, 2. Geological applications. *Chemical Geology* **9**, 257-273.

Stalder, H.A., 1966. Two unusual quartz occurrences in the Swiss Alps; blue quartz and ferruginous quartz. **46**, 697-702.

Stanton, R.L., 1965. Mineral interfaces in stratiform ores. *Transactions of the Institute of Mining and Metallurgy* **74**, 45-79.

Stanton, R.L., 1972. *Ore Petrology.* McGraw-Hill, New York, 713p.

Stanton, R.L., 1985. Stratiform ores and geological processes. *Journal and Proceedings Royal Society of New South Wales* **118**, 77-100.

Stanton, R.L., 1991. Understanding volcanic massive sulfides — past, present, and future. *Economic Geology Monograph* **8**, 82-95.

Stolz, A.J., 1991. Stratigraphy and geochemistry of the Mt Windsor Volcanics and associated exhalites. Centre for Ore Deposit and Exploration Studies, University of Tasmania, Mount Windsor Project – Research Report No. 2, 23-83 (unpubl.).

Stolz, A.J., 1995. Geochemistry of the Mt Windsor Volcanics: implications for the tectonic setting of Cambro-Ordovician VHMS mineralisation in northeastern Australia. *Economic Geology* **90**, 1080-1097.

Stolz, J., 1989. Stratigraphic relationships and geochemistry of the Mt Windsor Volcanics. Centre for Ore Deposit and Exploration Studies, University of Tasmania, Mount Windsor Project – Research Report No. 1, 1-50, (unpubl.).

Stolz, J., and Large, R.R., 1992. Evaluation of the source-rock control on precious metal grades in volcanic-hosted massive sulfide deposits from western Tasmania. *Economic Geology* **87**, 720-738.

Strakhov, N.M., 1969. *Principles of Lithogenesis.* Oliver and Boyd, Edinburgh, 609p.

Subramanain, A.P., 1967. Charnockites and granulites of southern India; a review. **17**, 473-493.

Sugitani, K., Sugisaki, R., and Adachi, M., 1995. Authigenic carbonate concretions and host shales from the Shimanto Belt, southwestern Japan: implications for carbonate precipitation. *Journal of Sedimentary Research* **A65**, 531-540.

Sundblad, K., Zachrisson, E., Smeds, S-A., Berglund, S., and Ålinder, C., 1984. Sphalerite geobarometry and arsenopyrite geothermometry applied to metamorphosed sulfide ores in the Swedish Caledonides. *Economic Geology* **79**, 1660-1668.

Talbot, M.R., and Kelts, K., 1986. Primary and diagenetic carbonates in the anoxic sediments of Lake Bosumtwi, Ghana. *Geology* **14**, 912-916.

Tarantov, A.S., and Garvilina, K.S., 1969. On a decomposition of fahlore with the formation of arsenopyrite. *In* Knristoforov, B.S., ed. *Metody izuchnia Vestchestvennogo Sostava ikh Primenenie.* Nauka, Siberian Branch, Novosibirsk. 104.

Taylor, S.R., and Gorton, M.P., 1977. Geochemical applications of spark-source mass spectrography, III. Element sensitivity, precision and accuracy. *Geochimica et Cosmochimica Acta* **41**, 1375-1380.

Toulmin, P., III, Barton, P.B., Jr, and Wiggins, L.B., 1991. Commentary on the sphalerite geobarometer. *American Mineralogist* **76**, 1038-1051.

Tourigny, G., Doucet, D., and Bourget, A., 1993. Geology of the Bousquet 2 mine: an example of a deformed, gold-bearing, polymetallic sulfide deposit. *Economic Geology* **88**, 1578-1597.

Tucker, M.E., and Wright, V.P., 1990. *Carbonate Sedimentology.* Blackwell Scientific Publications, Oxford, 482p.

Urabe, T., and Sato, T., 1978. Kuroko deposits of the Kosaka mine, northeast Honshu, Japan — products of submarine hot springs on Miocene seafloor. *Economic Geology* **76**, 161-179.

Urabe, T., Scott, S.D., and Hattori, K., 1983. A comparison of footwall-rock alteration and geothermal systems beneath some Japanese and Canadian volcanogenic massive sulfide deposits. *Economic Geology Monograph* **5**, 345-364.

Valley, J.W., 1986. Stable isotope geochemistry in metamorphic rocks. *In* Valley, J.W., Taylor, H.P., and O'Neil, J.R., eds. *Stable Isotopes in High Temperature Geological Processes.* Mineralogical Society of America, 445-489.

Valley, J.W., Petersen, E.U., Essene, E.J., and Bowman, J.R., 1982. Fluorophlogopite and fluorotremolite in Adirondack marbles and calculated C-O-H-F compositions. *American Mineralogist* **67**, 545-557.

Van Hook, H.J., 1960. The ternary system Ag_2S-Bi_2S_3-PbS. *Economic Geology* **55**, 759-788.

Veizer, J., and Hoefs, J., 1976. The nature of O^{18}/O^{16} and C^{13}/C^{12} secular trends in sedimentary carbonate rocks. *Geochimica et Cosmochimica Acta* **40**, 1387-1395.

Vivallo, W., 1985. Subseafloor hydrothermal alteration during the early Proterozoic at Garpenberg, central Sweden. *Mineralium Deposita* **20**, 33-42.

Vokes, F.M., and Craig, J.R., 1993. Post-recrystallisation mobilisation phenomena in metamorphosed stratabound sulphide ores. *Mineralogical Magazine* **57**, 19-28.

Von Damm, K.L., Edmond, J.M., Measures, C.I., and Grant, B., 1985. Chemistry of submarine hydrothermal solutions at Guaymas Basin, Gulf of California. *Geochimica et Cosmochimica Acta* **49**, 2221-2237.

Voss, R.L., Hagni, R.D., and Gregg, J.M., 1989. Sequential deposition of zoned dolomite and its relationship to sulfide mineral paragenetic sequence in the Viburnum Trend, southeast Missouri. *Carbonates and Evaporites* **4**, 195-209.

Walker, G., 1985. Mineralogical applications of luminescence techniques. *In* Berry, F.J. and Vaughan, D.J., eds. *Chemical bonding and spectroscopy in mineral chemistry.* Chapman and Hall, London. 103-140.

Walshe, J.L., 1986. A six-component chlorite solid solution model and the conditions of chlorite formation in hydrothermal and geothermal systems. *Economic Geology* **81**, 681-703.

Walshe, J.L., Heithersay, P.S, and Morrison, G.W., 1995. Towards an understanding of the metallogeny of the Tasman fold belt system. *Economic Geology* **90**, 1382-1401.

Warland, I.R., 1995. The Thalanga Geology Resource Summary. Pancontinental Resources Ltd, (unpubl.).

Webb, A.W., 1969. Metallogenic epochs in eastern Queensland. *Australasian Institute Mining Metallurgy Proceedings* **230**, 29-37.

Webb, A.W., 1970. Appendix—Isotopic age determinations from the Townsville 1:250 000 Sheet area. *In* Wyatt, D.H., Paine, A.G.L., Clarke, D.E., and Harding, R.R., eds. *Geology of the Townsville 1:250 000 Sheet area, Queensland.* Bureau Mineral Resources, Geology and Geophysics Australia, Report 127.

Webb, A.W., 1971a. Appendix—Isotopic dating of the Lolworth Complex, Hughenden and Charters Towers Sheet areas. *In* Paine, A.G.L., Harding, R.R., and Clarke, D.E., eds. *Geology of the northeastern part of the Hughenden 1:250 000 Sheet area, Queensland.* Bureau Mineral Resources, Geology and Geophysics Australia, Report 126.

Webb, A.W., 1971b. Appendix 2—Isotopic age determinations. *In* Wyatt, D.H., Paine, A.G.L., Clarke, D.E., Gregory, C.M., and Harding, R.R., eds. *Geology of the Charters Towers 1:250 000 Sheet area, Queensland.* Bureau Mineral Resources, Geology and Geophysics Australia, Report 137.

Wellman, P., 1995. Tasman orogenic system: a model for its subdivision and growth history based on gravity and magnetic anomalies. *Economic Geology* **90**, 1430-1442.

Whitford, D.J., Korsch, M.J., Porritt, P.M., and Craven, S.J., 1988. Rare-earth element mobility around the volcanogenic polymetallic massive sulfide deposit at Que River, Tasmania, Australia. *Chemical Geology* **68**, 105-119.

Whitford, D.J., McPherson, W.P.A., and Wallace, D.B., 1989. Geochemistry of the host rocks to the volcanogenic massive sulfide deposit at the Que River, Tasmania. *Economic Geology* **84**, 1-21.

Wiggins, L.B., and Craig, J.R., 1980. Reconnaissance of the Cu-Fe-Zn-S system: sphalerite phase relationships. *Economic Geology* **75**, 742-751.

Williams, H., and McBirney, A.R., 1979. *Volcanology.* Freeman, Cooper, San Francisco, 397p.

Williams, N., 1979. The timing and mechanisms of formation of the Proterozoic stratiform Pb-Zn and related Mississippi Valley-type deposits at McArthur River, N.T., Australia [abs.]: Society of Economic Geologists—AIME Joint Meeting, New Orleans, 15.

Wills, K.J.A., 1985. Thalanga comprehensive study - final report. Penarroya (Australia) P/L, No:1551/10, (unpubl.).

Winchester, J.A., and Floyd, P.A., 1977. Geochemical discrimination of different magma series and their different products using immobile elements. *Chemical Geology* **20**, 325-343.

Winkler, H.G.F., 1979. *Petrogenesis of Metamorphic Rocks.* Springer — Verlag, New York. 347p.

Withnall, I.W., Black, L.P. and Harvey, K.J., 1991. Geology and geochronology of the Balcooma area: part of an early Palaeozoic magmatic belt in north Queensland. *Australian Journal of Earth Sciences* **38**, 15-29.

Wood, D.L., and Ballman, A.A., 1966. Blue synthetic quartz. *American Mineralogist* **51**, 216-220.

Wormald, P.J., Orr, T.O.R., and Hodkinson, I.P., 1993. The Mount Leyshon Gold Mine (NE Queensland), an intrusive breccia and igneous complex. *In* Henderson, R.A., ed. *Guide to the economic geology of the Charters Towers region, northeastern Queensland.* 1993 Field Conference, Geological Society Australia, Queensland division, 61-74.

Wyatt, D.H., Paine, A.G.L., Clarke, D.E., Gregory, C.M., and Harding, R.R., 1971. *Geology of the Charters Towers 1:250 000 Sheet area, Queensland.* Bureau Mineral Resources, Geology and Geophysics Australia, Report 137.

Yamagishi, H., 1987. Studies on the Neogene subaqueous lavas and hyaloclastites in southwest Hokkaido. *The Geological Survey of Hokkaido Report* **59**, 55-117.

Yamamoto, T., Soya, T., Suto, S., Uto, K., Takada, A., Sakaguchi, K., and Ono, K., 1991. The 1989 submarine eruption off eastern Izu Peninsula, Japan: ejecta and eruption mechanisms. *Bulletin of Volcanology* **53**,

Yardley, B.W.D., 1989. *An Introduction to Metamorphic Petrology.* Longman Scientific and Technical, New York, 248p.

Yui, S., 1983. Textures of some Japanese Besshi-type ores and their implications for kuroko deposits. *Economic Geology Monograph* **5**, 231-240.

Yui, S., and Ishitoya, K., 1983. Some textures of the ores from the Ezuri kuroko deposits, Akita prefecture, Japan. *Economic Geology Monograph* **5**, 224-230.

Zierenberg, R.A., Koski, R.A., Morton, J.L., Bouse, R.M., and Shanks, W.C. III, 1993. Genesis of massive sulfide deposits on a sediment-covered spreading centre, Escanaba trough, southern Gorda Ridge. *Economic Geology* **88**, 2069-2098.

Zolensky, M.E., Sylvester, P.J., and Paces, J.B., 1988. Origin and significance of blue coloration in quartz from Llano rhyolite (llanite), north-central Llano County, Texas. *American Mineralogist* **73**, 313-323.